Design funktionalisierter TATA- und TOTA-Plattformen für die Aufklärung eines goldvermittelten katalytischen Mechanismus

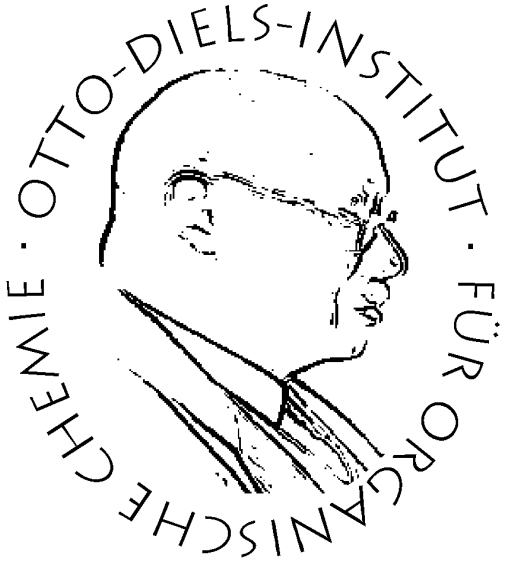

Dissertation

zur Erlangung des Doktorgrades

der Mathematisch-Naturwissenschaftlichen-Fakultät

der Christian-Albrechts-Universität

zu Kiel

vorgelegt von

Roland Löw

Otto Diels-Institut
Christian-Albrechts-Universität zu Kiel
September 2019

Referent: Prof. Dr. Rainer Herges
Korreferent: Prof. Dr. Ulrich Lüning

Tag der mündlichen Prüfung: 24.10.2019
Zum Druck genehmigt: 08.11.2019

gez. Prof. Dr. F. Kempken, Dekan

Die vorliegende Arbeit wurde unter Anleitung von
Prof. Dr. Rainer Herges
am Otto Diels-Institut für Organische Chemie
der Christian-Albrechts-Universität
im Zeitraum von Dezember 2015 bis September 2019 angefertigt.

Teile dieser Arbeit entstanden im Rahmen des
Sonderforschungsbereich 677 „Funktion durch Schalten“.

Eidesstattliche Erklärung

Hiermit erkläre ich, Roland Löw, an Eides statt, dass ich die vorliegende Doktorarbeit selbstständig und nur mit den angegebenen Quellen und Hilfsmitteln angefertigt habe. Diese Dissertation ist nach Inhalt und Form, abgesehen von der Beratung durch meinen Betreuer Herrn Prof. Dr. Rainer Herges, durch mich eigenständig nach den Regeln guter wissenschaftlicher Praxis der Deutschen Forschungsgemeinschaft verfasst worden. Sie hat weder in Auszügen noch in ganzer Form einer anderen Stelle im Rahmen eines Prüfungsverfahrens vorgelegen. Es handelt sich um meinen ersten Promotionsversuch und mir wurde auch kein akademischer Grad entzogen.

Kiel, 10.09.2019

_____

Roland Löw

Danksagung

Als erstes danke ich Herrn Prof. Dr. Rainer Herges für die Bereitstellung des äußerst interessanten und ergiebigen Arbeitsthemas. In der Zeit meiner Doktorarbeit hat er mich mit seinem Forschungseifer motiviert und hat sich stets die Zeit für Diskussionen genommen, um neue Lösungsansätze zu entwickeln. Weiterhin danke ich ihm für die Ermöglichung, auf mehreren internationalen Konferenzen teilgenommen zu haben.

Weiterhin danke ich Herrn Prof. Dr. Olaf Magnussen und Prof. Dr. Felix Tuczek für die sehr produktive Zusammenarbeit unserer Arbeitsgruppen. Ein besonderer Dank gebührt meinen Kooperationspartnern Talina und Alexander. Mit unserer gemeinsamen Arbeit, gegenseitigen Unterstützung und angenehmen Arbeitsweise konnten die Projekte ergebnisreich abgeschlossen werden.

Der gesamten Arbeitsgruppe sei für die schöne Arbeitsatmosphäre und die große Hilfsbereitschaft gedankt. Mir werden die ausgiebigen Schnack- und Trainingseinheiten im FIZ und die Mittagsstammtische in Erinnerung bleiben. Mein Dank gilt auch Stephan Kienitz, Tobias Moje, Tobias Ketzel und Niklas Petersen für ihre motivierte Unterstützung meiner Forschungsarbeit in ihren Bachelorarbeiten bzw. F3-Praktikum.

Den nicht-wissenschaftlichen Mitarbeitern als auch der spektroskopischen Abteilung des Otto Diels-Instituts danke ich für die durchgeführte Analytik, sowie für die Bereitstellung von Chemikalien und Laborgeräten.

Eine große Hilfe beim Schreiben dieser Doktorarbeit waren die nützlichen Korrekturen von Pascal, Fabian, Torsten und Claus.

Besonders möchte ich meiner Familie danken, die mir in schwierigen Momenten zur Seite stehen und mir den Weg zum Abschluss dieser Doktorarbeit ebneten. Weiterhin sind sie meine Vorbilder, deren Lebensrat ich niemals missen möchte.

Mein größter Danke gilt meiner Freundin Jasna Brekalo, die mich in jeden Lebenslagen unterstützt und mich immer aufmuntert und motiviert. Ich freue mich auf die kommenden Lebensherausforderungen mit dir an meiner Seite. Uvijek me usrećuje i nasmijava.

Kurzzusammenfassung

In dieser Arbeit wurden Photoschalter mithilfe eines modularen Systems auf Goldoberflächen adsorbiert und der Einfluss des Goldes auf das thermische Schaltverhalten untersucht. Mit passenden Verknüpfungseinheiten zwischen einer molekularen Plattform und funktionellen Molekülen werden diese Moleküle räumlich von der Oberfläche getrennt, ohne die elektronische Kopplung zum Gold zu reduzieren. Azobenzole, die mithilfe des modularen Systems auf Goldoberflächen aufgebracht werden, weisen beschleunigte thermische *cis*→*trans*-Isomerisierungen auf. Die Aufklärung der Wirkungsweise dieses Prozesses war das Ziel dieser Arbeit. Für eine umfassende Untersuchung dieses Prozesses wurden geeignete Photoschalter über molekulare Plattformen auf Goldoberflächen funktionalisiert und auf beschleunigte thermische Isomerisierungen überprüt. In dieser Arbeit wurden Triazatriangulenium- (TATA) und Trioxatringulenium- (TOTA) Plattformen mit Azobenzolen, Diazocinen und Norbornadienen funktionalisiert und charakterisiert. Kopplungseinheiten in Form von Biphenyleinheiten wurden zwischen Azobenzol und TATA-Plattform eingefügt, die die Konjugation von der Azofunktion zur TATA-Plattform bzw. die elektronische Kopplung zur Goldoberfläche über systematisch steigende Verdrillungswinkel schrittweise reduzieren, um einen elektronischen Einfluss des Goldes zu untersuchen. Mit einem isolierenden Bizyklus wurde die Konjugation weitestgehend unterbrochen. Die Untersuchung der Kinetik als Funktion der elektronischen Kopplung des über die TATA-Plattform mit der Goldoberfläche verknüpften Azobenzols klärte einen nicht adiabatischen Mechanismus auf, der das quantenmechanische Verbot des Intersystem-Crossings zwischen der Singulett- und Tripletthyperfläche des Azobenzols aufhebt. Daraus resultiert die Aufhebung der Aktivierungsbarriere der thermischen *cis*→*trans*-Isomerisierung und die Reaktionsgeschwindigkeit wird ausschließlich von der quantenmechanischen Übergangsgeschwindigkeit kontrolliert. Um einen Anwendungsbereich für diesen Mechanismus definieren zu können wurden Diazocine über eine zur Azofunktion in *para*- bzw. *meta*-ständigen Acetylenbrücke mit der TATA-Plattform verknüpft. Diese unterschiedlichen Substitutionsmuster regulieren die Konjugation und somit die elektronische Kopplung der Diazocine mit der Plattform. Über die Verknüpfung von Norbornadienen auf TATA-Plattformen mit Verknüpfungseinheiten, die unterschiedlich hohe Konjugationen realisieren, soll überprüft werden, ob der nicht adiabatischen Mechanismus die thermisch verbotene [2+2]-Cycloreversion beschleunigt. Mit der Funktionalisierung eines Norbornadiens auf der TOTA-Plattform wird die unzersetzte Deponierung durch Sublimation im Ultrahochvakuum auf Au(111) ermöglicht. Weiterhin wurden in dieser Arbeit nicht schaltbare Arylsysteme auf Plattformen etabliert, die über die Variation von Kopfgruppen Erkenntnissse über das Verhalten der Monolagenausbildung auf Au(111)-Oberflächen geben.

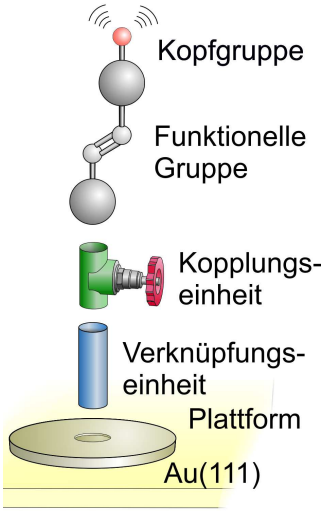

Abstract

In this thesis photoswitches were adsorbed on gold surfaces with the help of modular systems to investigate the influence of gold on their thermal switching behavior. This modular system enables the formation of ordered monolayers on atomically flat metal surfaces, on which molecules can be mounted upright. With suitable spacer units, the corresponding molecules are spatially removed from the surface without reducing the electronic coupling to a gold surface. Azobenzenes, which are using the modular system to be mounted on gold surfaces, demonstrate accelerated thermal *cis*→*trans* isomerizations. The clarification of this effect was the aim of this thesis. For a comprehensive investigation of this process, suitable photoswitches were functionalized with the molecular platforms on gold surfaces and investigated for rate accelerations. In this thesis triazatriangulenium (TATA) and trioxatriangulenium (TOTA) platforms were functionalized with azobenzenes, diazocines, and norbornadienes and have been characterized. Linking units in form of biphenyl units were added between azobenzene and TATA-platform, which gradually reduce the conjugation of the azo function to the TATA platform and therefore the electronic coupling to the gold surface via systematically increasing twist angles to investigate an electronic influence of the gold surface. With an insulating bicyclus, the conjugation was mostly interrupted. The investigation of kinetic as a function of the electronic coupling of the gold surface and the azobenzene, which is connected with the surface over the TATA platform, elucidated a non-adiabatic mechanism, which revoke the quantum mechanical forbbidance of the intersystem crossing between the singlet and triplet surface of the azobenzene. This results in a revocation of the activation barrier of the *cis*→*trans* isomerization and the reaction rate is only controlled of the quantum mechanical transition probability. To gain a comprehensive understanding of this mechanism, diazocines have been functionalized on the TATA platform via acetylene spacers at the *para* or *meta* position with respect to the azo function. The conjugation and following the electronic coupling of the azo function to the platform is regulated by this different substitution pattern. Norbornadienes are attached on the TATA platform via linking units that realize different levels of conjugation, to check if the non-adiabatic mechanism accelerate the thermally forbidden [2+2] cycloreversion. The functionalization of a norbornadiene on the TOTA platform enables the nondestructively deposition by sublimation under ultrahigh-vacuum conditions on gold surfaces. Furthermore, in this work, arylic non-switchable systems were introduced on platforms, which provided insight into the behavior of monolayer formation on Au (111) surfaces by varying the headgroup.

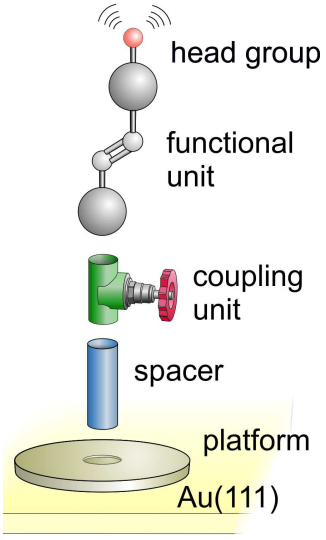

Inhaltsverzeichnis

1 Einleitung

Seit dem industriellen Zeitalter übernehmen Maschinen in nahezu jedem Bereich Arbeitsprozesse. Moleküle werden auf mikroskopischer Ebene als Maschinen verstanden, wenn sie maschinelle Funktionen, wie beispielsweise gerichtete Bewegungen, durch externe Stimuli ausführen.[1] Die Entwicklung von molekularen Maschinen dient der Grundlagenforschung und der Weiterentwicklung von Nanotechnologien. Ein Konzept von FERINGA ist der molekulare Transport mit einem molekularen Auto auf Oberflächen, der durch Tunnelelektronen aus der STM Spitze angetrieben wurde.[2] Ein weiteres Konzept, das den Transport von Partikeln durch das Nachahmen der Schlagbewegung eines Flimmerepithels ermöglichen soll, ist die Funktionalisierung von Oberflächen mit photoschaltbaren Molekülen wie Azobenzol.[3–5] Dabei bietet sich die Funktionalisierung auf Oberflächen über selbst organisierende Monolagen (self-assembled monolayers (SAMs)) an,[6] bei denen die Bindung der Azobenzole auf Goldoberflächen über Alkylthiole erfolgt.

1.1 Selbstorganisierende Monolagen mit Alkylthiolen

SAMs sind geordnete Monolagen von Atomen oder Molekülen, die sich durch Adsorption oder über eine kovalente Bindung auf einer Oberfläche von selbst ausbilden.[7] Thiolfunktionalisierte Alkylketten, die auf Goldoberflächen binden, stellen eine Gruppe dieser Moleküle dar.[8–14] Durch die hohe Packungsdichte sind die Thiolketten nahezu aufrecht ausgerichtet.[9] Untersuchungen können mit verschiedenen analytischen Methoden wie der Rastertunnelmikroskopie, Transmissionselektronenmikroskopie, Kontaktwinkelbestimmung, Infrarot-Reflektions-Absorptions-Spektroskopie, Röntgenphotoelektronenspektroskopie und elektrochemisch erfolgen.[8–10,15–17] Das Konzept zur Ausbildung von Monolagen bietet sich für die Untersuchung von schaltbaren Molekülen an, bei denen ein direkter Kontakt zur Goldoberfläche durch den Abstand vermittelt durch die Alkylketten vermieden werden soll. Dabei konnten bereits mit Alkanthiolen funktionalisierte Azobenzole auf Goldoberflächen gebunden werden (Abb. 1.1). Allerdings konnte keine Isomerisierung oder nur moderate Schalteffizienzen nachgewiesen werden, was aus der hohen Packungsdichte resultiert.[6,18,19] Durch die Reduktion des sterischen Einflusses,[20] mit Hilfe von kooperativem Schalten[21] oder durch die Krümmung der Goldoberfläche in Nanopartikeln[22] kann das Schaltverhalten verbessert werden. Mit der Einführung einer zweiten kürzeren Komponente in den SAMs, die als Abstandshalter dienen, wird ein größerer Raum für die Isomerisierung gewährleistet (Abb. 1.1).[6,19,22,23] Die Abstandshalter in den gemischten SAMs bieten zusätzlich die Möglichkeit, die Isomerisierung der Azobenzole in der Rastertunnelmikroskopie nachzuweisen.[23] Dabei wird die unterschiedliche relative Höhe, die von der eigentlichen Höhe und der Leitfähigkeit der Aufbauten abhängt, des *cis*- und *trans*-Azobenzols mit der definierten Höhe der Abstandshalter verglichen.

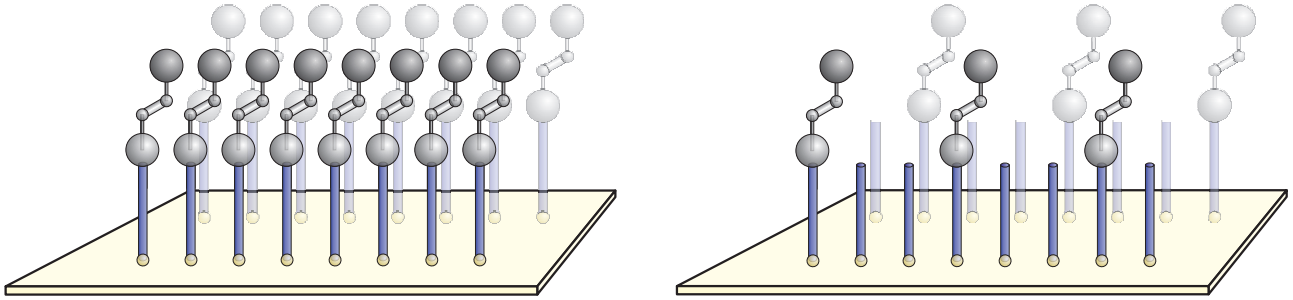

Abb. 1.1: Links: Schematische Darstellung von Azobenzol SAMs, die kovalent über Thiole auf einer Au(111)-Oberfläche gebunden sind. Die dichte Packung des SAMs verhindert eine Isomerisierung der *trans*-Azobenzole in das *cis*-Isomer. Rechts: Die Einführung von kurzen Alkanthiolen ohne Kopfgruppe erhöht den lateralen Abstand der Azobenzole, wodurch die Isomerisierung ohne intermolekulare Hinderung stattfinden kann.

Häufig auftretende Separationen der beiden Komponenten in den Monolagen verhindern jedoch die Reduktion der Packungsdichte der Azobenzole,[24–26] wodurch die Verbesserung der Isomerisierung nicht ermöglicht werden kann. Aus diesem Grunde wurden neue Funktionalisierungsmethoden entwickelt, mit denen unter anderem verbesserte Isomerisierungseffizienzen ermöglicht werden sollten.[27–29]

1.2 Das Plattformkonzept zur Ausbildung von SAMs

Das Plattformkonzept, das von der Arbeitsgruppe HERGES etabliert wurde, eignet sich hervorragend für die Funktionalisierung von atomar flachen Metalloberflächen mit funktionellen Molekülen wie dem Azobenzol.[29] Im Plattformkonzept dient ein Triazatrianguleniumion (TATA) als molekularer Sockel, das ein zentrales Carbokation enthält, welches mit verschiedenen Molekülen über Verknüpfungseinheiten, wie Ethinyl- oder Phenylgruppen funktionalisiert werden kann (Abb. 1.2).[30] Bei der Funktionalisierung von Trioxatrianguleniumionen (TOTA) kann auf Verknüpfungseinheiten verzichtet werden, da die funktionelle Einheit direkt mit dem kationischen Zentrum der Plattform funktionalisiert werden kann. Zudem haben diese TOTA-Plattformsysteme eine höhere Stabilität zwischen Plattform und Aufbau, sodass sie über ein Elektrosprayverfahren unter Ultrahochvakuumbedingungen auf Metalloberflächen adsorbiert werden können.[31–33] Untersuchungen der TATA-Plattformen auf Au(111) legen nahe, dass die Phenylringe als auch die Stickstoffatome jeweils ein Goldatom „on-top“ besetzen.[34] Das Plattformkonzept hat gegenüber der Funktionalisierung von Photoschaltern über Alkylthiole auf Metalloberflächen mehrere Vorteile. Der Abstand zwischen den Plattformen auf Au(111)-Oberflächen kann über die Länge der Alkylketten, die an den Stickstoffatomen angebracht sind, eingestellt werden.[34,35] Zusätzlich wurde die hohe Variabilität der Funktionalisierung mit verschiedenen Photoschaltern und weiteren funktionellen Molekülen gezeigt. Dabei wurden bereits Azobenzole,[29,30,36] Porphyrine,[37,38] Diazocine,[39] Imine,[40] Komplexe[41] und weitere phenylische Aufbauten[42] auf TATA-Plattformen etabliert. Die SAMs der azobenzolfunktionalisierten TATA-Plattformen auf Au(111) konnten mit der Rastertunnelmikroskopie,[29,35,43] der oberflächenverstärkten Raman-Spektroskopie[44] und der Röntgen-Nahkanten-Absorptions-Spektroskopie[45] untersucht und

weiterhin deren Isomerisierung mittels UV/Vis-Spektroskopie,[46] Infrarot-Reflexions-Absorptions-Spektroskopie,[47] Chronoamperometrie und Cyclovoltammetrie[48] analysiert werden.

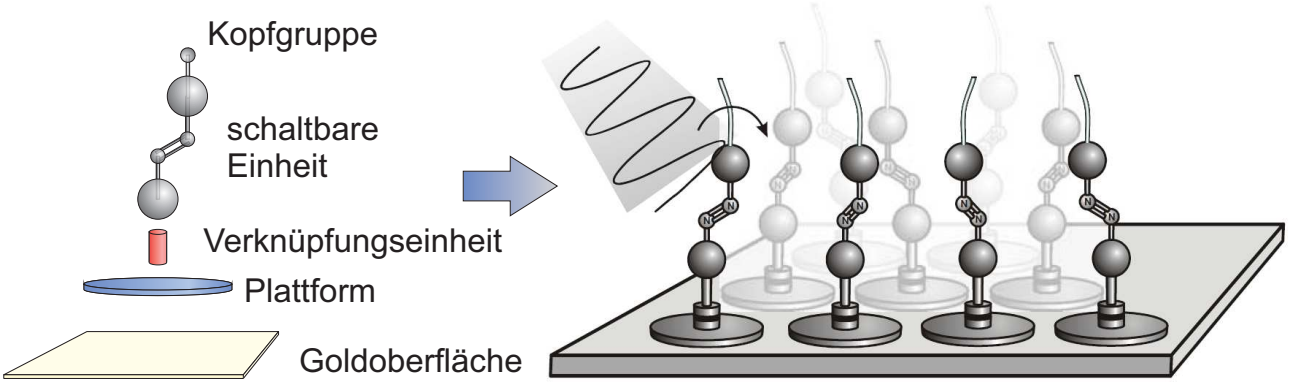

Abb. 1.2: Links: Darstellung des Plattformkonzepts mit den einzelnen Komponenten. Rechts: Schema der adsorbierten TATA-Plattformen mit schaltbarer Einheit auf einer Metalloberfläche, die mit der Bestrahlung von Licht isomerisieren.[49]

Um die Isomerisierung der Azobenzoleinheiten auf der Oberfläche nachzuweisen, muss eine Spektroskopie angewendet werden, die die Unterscheidung der beiden Azobenzol-Isomere (*cis*/*trans*) ermöglicht. Dazu ist die Infrarot-Reflexions-Absorptions-Spektroskopie (IRRAS) prinzipiell geeignet. Verstärkt wird der Unterschied der IRRAS-Spektren des *cis*- und des *trans*-Azobenzols durch die Einführung einer Methoxygruppe in 4-Position der terminalen Phenylgruppe der Azobenzol-Einheit.[47] Die photophysikalischen Eigenschaften der auf Au(111) adsorbierten Azobenzol-TATA-Plattformen sind mit Ausnahme der thermischen Halbwertszeit vergleichbar mit den Eigenschaften des Systems in Lösung.[47,48] In den Untersuchungen mehrerer Arbeitsgruppen konnte eine um mehrere Größenordnungen beschleunigte *cis*→*trans*-Isomerisierung beobachtet werden, wobei der Mechanismus, der zu dieser Beschleunigung führt, bisher nicht aufgeklärt werden konnte.[47,48,50,51]

1.3 Katalyseprozesse auf Goldoberflächen

Die Beschleunigung der thermischen *cis*→*trans*-Isomerisierung könnte über eine katalytische Beeinflussung des Goldes über eine elektronische Kopplung zwischen Azobenzol und Goldoberfläche erfolgen, die durch die vollständige Konjugation zwischen TATA-Plattform und Azoeinheit ermöglicht wird. Die beschleunigte *cis*→*trans*-Isomerisierung ist unerwartet, da Gold als reaktionsarmes Element gilt[52] und nur wenige Beispiele bekannt sind, in denen Gold heterogener Katalysator[53] dient. In der heterogenen Katalyse konnten beispielsweise Reaktionen nachgewiesen werden, die sowohl von Goldatomen[54–61] als auch von reinen Goldkristallen katalysiert wurden. Beispiele für Reaktionen auf Goldkristallen sind Oxidationen adsorbierter Moleküle[62–64] als auch Kupplungsreaktionen wie von Methyliodid zu Ethan[65] und weiteren Alkylhalogeniden[66,67] sowie von Phenyliodid zu Biphenyl.[68] Neben der beschleunigten thermischen *cis*→*trans*-Isomerisierung des Azobenzols, das auf einer TATA-Plattform gebunden ist und mithilfe der Plattform auf Goldoberflächen adsorbiert, wurde

weiterhin die Reduktion der Aktivierungsenergie der thermischen *cis*→*trans*-Isomerisierung eines Azobenzols, das direkt auf Au(111)-Oberflächen adsorbiert, nachgewiesen. Eine Erklärung dieses Prozesses für ein Azobenzol war nicht möglich.[50,51] Die Schwierigkeit der Analyse dieser Mechanismen auf Goldoberflächen ist die aufwendige Untersuchung mit oberflächensensitiven Messmethoden.[69]

1.4 Untersuchungsmethoden von Oberflächen

Für die Untersuchung von Atomen oder Molekülen und deren Eigenschaften auf Oberflächen sowie der Aufklärung katalytischer Prozesse bieten sich verschiedene oberflächensensitive Methoden an. In der Rasterkraftmikroskopie (Atomic Force Microscopy (AFM)) werden sowohl leitende als auch nichtleitende Oberflächen unter Ultrahochvakuum mit einer Spitze mechanisch abgefahren. Mit dieser Technik kann sowohl die Oberflächentopografie mit einer lateralen Auflösung von bis zu 6 Å als auch mechanische Kräfte im Bereich von 18 N untersucht werden.[70–72] Die oberflächenverstärkte Raman-Spektroskopie (Surface-enhanced Raman spectroscopy (SERS)) ist eine Technik, die die Ramanstreuung von Molekülen, die auf rauen Oberflächen adsorbieren, verstärkt. Die daraus resultierende Verbesserung des Signal-zu-Rausch-Verhältnisses ermöglicht die Detektion der Ramanstreuung von adsorbierten Molekülen.[73–75] Mit der Röntgen-Nahkanten-Absorptions-Spektroskopie (Near edge X-ray absorption fine structure (NEXAFS)) werden kernnahe Elektronen mit weicher Röntgenstrahlung in unbesetzte Orbitale (π*, σ*) angeregt, woraus Informationen über die elektronische Struktur und die Orientierung von Molekülen bzw. Molekülfragmenten auf Oberflächen gewonnen werden können.[76–78] Weiterhin sind die Rastertunnelmikroskopie (STM) und die Infrarot-Reflektions-Absorptions-Spektroskopie (IRRAS) etablierte oberflächensensitive Methoden, die sich sehr gut für die Untersuchung adsorbierter Azobenzole auf Goldoberflächen anbieten.

1.4.1 Die Rastertunnelmikroskopie

Die Rastertunnelmikroskopie (scanning tunneling microscopy (STM)) wurde anfang der 1980er Jahre von BINNIG und ROHRER etabliert.[79,80] Dazu wird eine aus Wolfram oder Platin-Iridium gefertigte Spitze auf 3-5 Å der zu untersuchenden Metalloberfläche angenähert, sodass eine Überlappung zwischen den Wellenfunktionen der Atome der Spitze und Oberfläche auftritt. Bei einer definierten Vorspannung können Elektronen von der Spitze in die Oberfläche tunneln (Abb. 1.3).[81] Dabei wird die Spitze rasterartig mittels drei orthogonalen piezoelektrischen Wandlern über die Oberfläche gefahren. Der gemessene Tunnelstrom ist exponentiell vom Abstand zwischen Spitze und Oberfläche abhängig, wodurch das Höhenprofil einzelner Atome auf den Oberflächen den Tunnelstrom beeinflusst.[81] Zusätzlich wird der Tunnelstrom und somit das gemessene Höhenprofil durch die Leitfähigkeit der adsorbierten Moleküle beeinflusst.[82] Das STM kann sowohl mit konstanter Höhe als auch mit konstantem Tunnelstrom betrieben werden. Beim Modus mit konstantem Tunnelstrom wird der gemessene Tunnelstrom mit einem Referenzwert verglichen und liefert einen Rückkopplungskreis mit der Oberfläche. Bei einer Höhenänderung führt eine Korrekturspannung zur Auslenkung der Spitze, wodurch

der konstante Tunnelstrom unverändert bleibt. Die Informationen aus der Korrekturspannung oder dem Rückkopplungssignal als Funktion der seitlichen Spitzenposition während des Abrasterns der Oberfläche ergibt die Oberflächentopografie.[81]

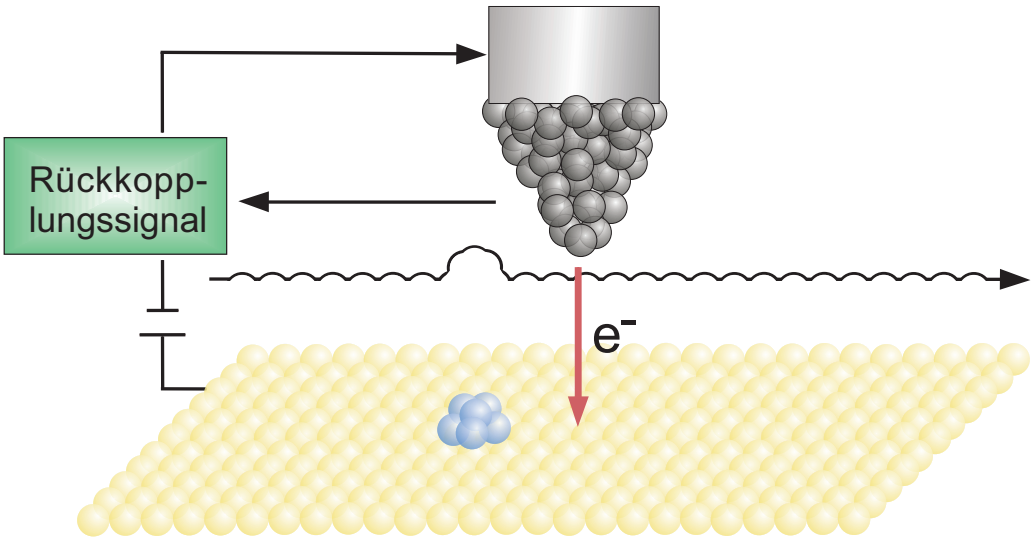

Abb. 1.3: Schematische Darstellung des Aufbaus eines Rastertunnelmikroskops und die Vorgehensweise für die Aufnahme der Oberflächentopografie.[81,83]

Diese Methode bietet sich vor allem für den Nachweis der hochgeordneten Monolagen der funktionalisierten Plattformen an.[29,35,43] Für die Untersuchung der Isomerisierung von Photoschaltern bietet sich die Infrarot-Reflexions-Absorptions-Spektroskopie an.

1.4.2 Die Infrarot-Reflexions-Absorptions-Spektroskopie

Die Infrarot-Reflexions-Absorptions-Spektroskopie (IRRAS, auch: Reflektion-Absorption-Infrarot-Spektroskopie (RAIRS)) wurde von GREENLER 1966 etabliert.[84] Die Bedeutung der Infrarotspektroskopie wie der IRRA-Spektroskopie für die Aufklärung katalytischer Prozesse konnte BADDOUR aufzeigen, indem er die Verbreiterung einer C-O-Schwingungsbande auf der katalytisch aktiven Palladiumoberfläche nachwies.[85,86] Diese oberflächensensitive Technik eignet sich für die Untersuchung von Monolagen bzw. Submonolagen auf reflektierenden Metalloberflächen.[87] Dabei wird die einfallende IR-Strahlung von auf Metalloberflächen adsorbierten Molekülen absorbiert. Die Strahlung wird an der Oberfläche reflektiert, wodurch das Substrat zweimal durchtreten und die Signalintensität erhöht wird. Senkrecht zur Oberfläche polarisierte (s-polarisierte) Strahlung führt zu destruktiver und parallel zur Oberfläche polarisierte (p-polarisierte) Strahlung zu konstruktiver Interferenz (Abb. 1.4). Für eine gute Wechselwirkung der einfallenden Strahlung mit den adsorbierten Molekülen sind hohe Einstrahlwinkel von in der Regel 80 ° der p-polarisierten Strahlung nötig.[86,88–90] Durch die Entwicklung der IRRA-Spektroskopie, bei der ein photoelastischer Modulator (PEM) eingesetzt wird (PM-IRRAS),[91–94] kann das Signal-zu-Rausch-Verhältnis erhöht werden.[90] Dabei führt die p-polarisierte Strahlung zur Erhöhung der Intensität der detektierten Dipole, die senkrecht zur Oberfläche ausgerichtet sind,

während die s-polarisierte Strahlung die Intensität der Dipole, die parallel zur Oberfläche ausgerichtet sind, auf nahezu Null reduziert.[95] Zusätzlich werden durch den PEM atmosphärische Interferenzen reduziert.[90] Ein wichtiger Aspekt ist die Oberflächenauswahlregel (surface selection rule).[96] Diese Regel resultiert aus der Eigenschaft, dass Dipole auf Metalloberflächen ein Ebenbild mit gleichem Abstand im Metall generieren. Dipole, die parallel zur Oberfläche ausgerichtet sind, haben Dipole mit umgedrehten Vorzeichen in der Metalloberfläche, wodurch die Partialladungen ausgeglichen werden. Dipole, die senkrecht zur Oberfläche ausgerichtet sind, haben einen entsprechenden Dipol mit gleicher Ausrichtung in der Metalloberfläche (Abb. 1.4).[96]

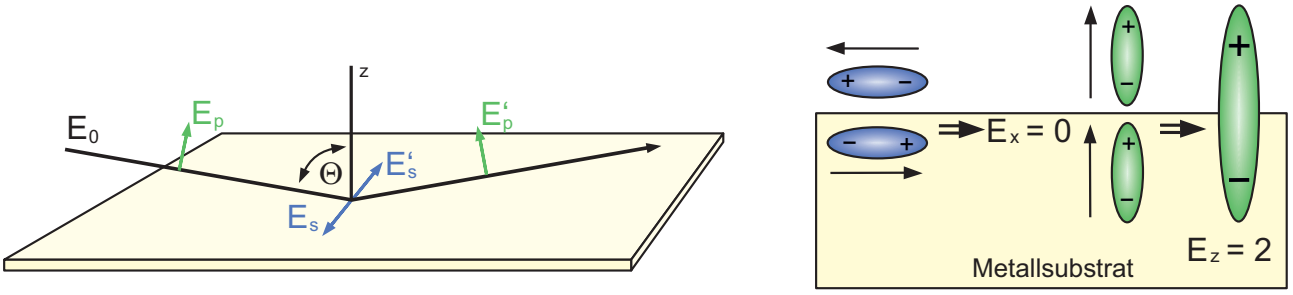

Abb. 1.4: Links: Darstellung der einfallenden Strahlung E_0 mit deren elektrischen Vektoren der s- (E_s) und p-Anteilen (E_p) und der reflektierten Strahlung (E_s', E_p') auf einer Metalloberfläche. Rechts: Erklärung der Oberflächenauswahlregel für die Detektierbarkeit von Dipolen auf Metalloberflächen, bei der parallel zur Oberfläche ausgerichtete Dipole ausgelöscht und orthogonal zur Oberfläche ausgerichtete Dipole verstärkt werden.[97,98]

Daraus resultiert, dass nur senkrecht zur Oberfläche orientierte Dipole in der IRRA-Spektroskopie detektiert werden können.[90] Mithilfe dieser Eigenschaften kann bei einer flachen Metalloberfläche und bekannter Molekülstruktur die IRRA-Spektroskopie Informationen über die Molekülausrichtung auf Oberflächen geben.[89] Daraus bietet sich die Möglichkeit, das *cis*- und *trans*-Isomer eines Azobenzols über unterschiedlich ausgerichtete Dipole dieser Isomere zu detektieren.[47]

1.5 Kopplungskontrolle

Um den von der Goldoberfläche ausgehenden Katalysemechanismus, der die beschleunigte thermische *cis*→*trans*-Isomerisierung hervoruft, aufklären zu können, bietet es sich an, eine mögliche elektronische Kopplung nachzuweisen. Die hohe Variabilität der Funktionalisierung von Plattformen bietet die Möglichkeit, die Konjugation zwischen Azobenzol und TATA-Plattform über eine Reduktion bzw. vollständige Unterbrechung der Konjugation über die Verknüpfungseinheit zu regulieren. Eine Reduktion der Konjugation kann über systematisch steigende Verdrillungen von Biphenyleinheiten realisiert werden.[99,100] Dieses Verhalten wurde bereits von WANDLOWSKI belegt und in den Forschungsarbeiten von HECHT zur schrittweisen Entkopplung von Azobenzolen genutzt.[99–101]

1.6 Photoschaltbare Moleküle

Neben der Analyse des Azobenzols auf Goldoberflächen durch mehrere oberflächensensitiven Untersuchungsmethoden und der Reduktion der elektronischen Kopplung bietet es sich weiterhin an, den katalytischen Mechanismus ausgehend vom Gold in thermischen Isomerisierungen weiterer Photoschalter nachzuweisen bzw. aufzuklären. In der Literatur werden mehrere spinverbotene Reaktionen diskutiert, die durch ein Intersystem-Crossing katalysiert werden.[102–110] Darauf aufbauend können potentielle Photoschalter untersucht werden, deren thermische Isomerisierung über ein mögliches Intersystem-Crossing beschleunigt werden. Zusätzlich sollten die unterschiedlichen Isomere in oberflächensensitiven Messmethoden detektierbar sein. Potentielle Photoschalter und deren Eigenschaften werden in den folgenden Abschnitten diskutiert.

1.6.1 Spiropyran

Die photochemischen Eigenschaften des Spiropyrans wurden als erstes von HIRSHBERG und FISHER am Anfang der 1950er Jahre untersucht.[111] Das Spiropyran, das in einer neutralen Form vorliegt, isomerisiert über die Absorption von Licht zwischen 320-400 nm in die Merocyanin-Form. Dieses kann lösungsmittelabhängig in einer ionischen oder neutralen Form vorliegen (Abb. 1.5).[112–116] Die Rückisomerisierung des thermodynamisch metastabilen Isomers kann thermisch oder photochemisch erfolgen.[112,117]

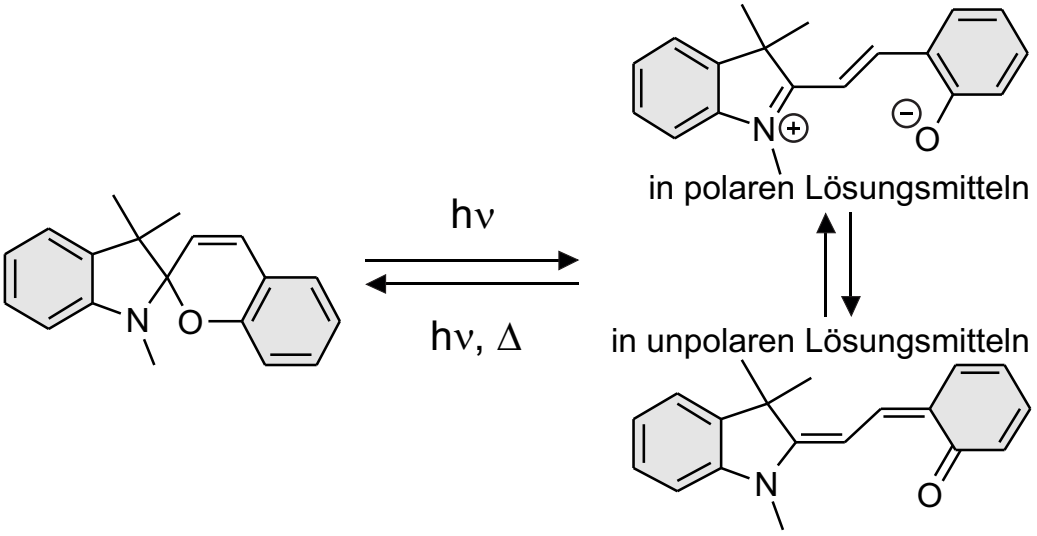

Abb. 1.5: Isomerisierung zwischen dem thermodynamisch stabilen Spiropyran (links) und dem metastabilen Merocyanin (rechts) in dem zwitterionischen Mesomer bzw. chinoiden neutralen Mesomer.[116]

Der Mechanismus der thermischen Isomerisierung ist lösungsmittelabhängig und kann über zwei Wege ablaufen. Das chinoide Merocyanin durchläuft einen intramolekularen elektrozyklischen Prozess, bei dem die Ratenkonstante nur von elektrostatischen und sterischen Abstoßungen abhängt. In der zwitterionischen Form wird eine *trans*→*cis*-Isomerisierung durchlaufen, bei der die ionischen

Ladungen in räumliche Nähe kommen und über eine Anion-Kation-Rekombination das Spiropyran bilden. Die Energiebarriere dieser Isomerisierung zu dem Spiropyran wird von der *trans*→*cis*-Rotation bestimmt, die eine Aktivierungsbarriere von 272 kJ/mol hat.[118] Es ist davon auszugehen, dass das Merocyanin, adsorbiert auf Goldoberflächen, in der neutralen Form vorliegt, da Einflüsse fehlen sollten, die die ionische Form stabilisieren. In dieser Form sollte die thermische Rekombination vom Gold unbeeinflusst bleiben.

1.6.2 Stilben

Die Photoisomerisierung zwischen dem *trans*- und *cis*-Isomer des Stilbens ist eine der am besten verstandenen photochemischen Reaktionen (Abb. 1.6).[119] Die *trans*→*cis*-Isomerisierung kann nach unterschiedlichen Mechanismen ablaufen.[120] In substituierten Stilbenen wird ein Triplett-Mechanismus über ein Intersystem-Crossing durchlaufen, bei der die Singuletthyperfläche von der Tripletthyperfläche durchschnitten bzw. nahezu durchschnitten wird.[120–122]

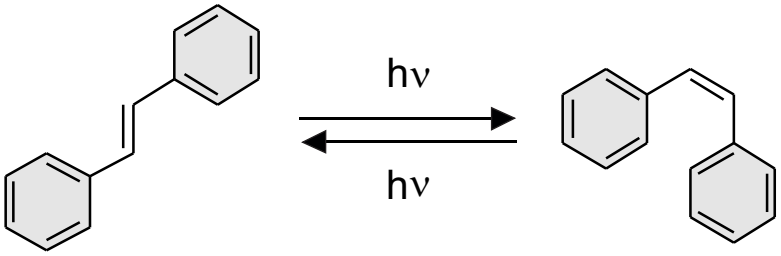

Abb. 1.6: Isomerisierung zwischen dem *trans*- (links) und dem *cis*-Stilben (rechts).[119,123]

Der allgemein ablaufende Mechanismus erfolgt über eine Drehung der Ethylenbindung im ersten angeregten Zustand über die Torsionsenergieoberfläche.[123,124] Der Abfall dieses angeregten Zustands in den Grundzustand führt zu einem nahezu gleichen Verhältnis von *trans*- und *cis*-Stilben.[125] Die thermische *cis*→*trans*-Isomerisierung erfolgt über den Rotationsmechanismus mit einer Aktivierungsenergie von 192.6 kJ/mol in Lösung[126,127] bzw. 178.4-179.2 kJ/mol in der Gasphase,[126,128] weshalb bei Raumtemperatur keine thermische Isomerisierung statt findet. Aufgrund dieser hohen Energien ist es unklar, ob eine vom Gold ausgehende mögliche Reduktion der Aktivierungsenergie ausreicht, um eine thermische *cis*→*trans*-Isomerisierung eines auf Goldoberflächen adsorbierten Stilbens zu beobachten.

1.6.3 Diarylethen

Die Photoisomerisierung von Diarylethenen wurde erstmals Ende der 1980er Jahre nachgewiesen. Dabei kann das Diarylethen photochemisch mit einer Bestrahlung von 331 nm (Cyclisierung) bzw. 552 nm (Ringöffnung) zwischen der offenen und der cyclisierten Form isomerisieren (Abb. 1.7).[129,130]

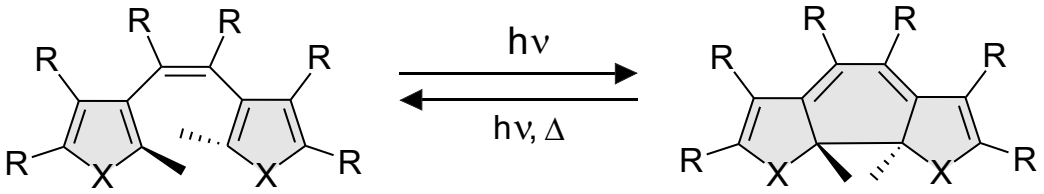

Abb. 1.7: Die Isomerisierung zwischen der offenen (links) und der cyclisierten Form (rechts) ist gezeigt.[129,131–133]

Die thermische Stabilität des geschlossenen Isomers ist von der Aromatenstabilisationsenergie,[129,133] den Substituenten an den Arylgruppen[134] und der sterischen Hinderung[135] abhängig. Die Aktivierungsenergie für die thermische Rückisomerisierung eines Diarylethens mit Thiophenringen liegt bei 139 kJ/mol.[132] Aus der geringen Geometrieänderung sind die Isomere in oberflächensensitiven Messmethoden aufwendig zu unterscheiden, weswegen sich die Untersuchung von Diarylethenen auf Goldoberflächen nicht anbietet. Ein bereits gut verstandener Photoschalter ist das Norbornadien, das für eine Untersuchung auf Goldoberflächen geeignet ist.

1.6.4 Norbornadien

Das Norbornadien (NBD) ist aus einem Cyclohexadien, das in 1 und 7 Position mit einer Methyleneinheit verbrückt ist, aufgebaut. Über eine photochemische [2+2]-Cycloaddition kann das Quadricyclan (QC) erhalten werden und ebenfalls photochemisch über eine [2+2]-Cycloreversion zurück zum Norbornadien isomerisieren (Abb. 1.8). Weiterhin kann die [2+2]-Cycloreversion sowohl katalytisch als auch thermisch bei höheren Temperaturen ablaufen.[136,137]

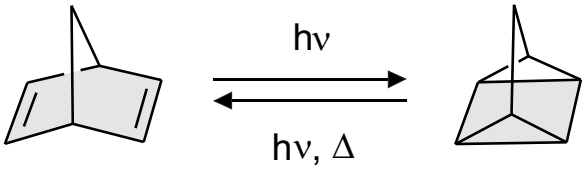

Abb. 1.8: Isomerisierung zwischen dem thermodynamisch stabilen Norbornadien (links) und dem metastabilen Quadricyclan (rechts) über eine [2+2]-Cycloaddition bzw. [2+2]-Cycloreversion.[136,137]

Für die [2+2]-Cycloaddition im Norbornadien liegen zwei mögliche Isomerisierungsmechanismen vor. Im ersten Mechanismus wird das Norbornadien in einen Singulett-Zustand angeregt und isomerisiert direkt zum Quadricyclan, wobei diese Isomerisierung ineffizient abläuft. Im zweiten Mechanismus erfolgt ein Intersystem-Crossing des ersten angeregten Singulett-Zustands zu einem Triplett-Zustand, wodurch in hohem Maße Quadricyclan gebildet wird.[138] Dies ist mit der unsymmetrischen Tripletthyperfläche zu erklären, deren Minimum auf der Seite des Quadricyclans im Grundzustand liegt (Abb. 1.9).[139] Das Minimum des ersten angeregten Zustands (S_1) auf der Energieoberfläche entspricht einem Biradikal, bei dem zwei Radikale in 2- und 3-Position vorliegen. Diese Form wird durch zwitterionische Beiträge stabilisiert. Die Umwandlung von diesem angeregten Biradikal in den Grundzustand (S_0)

begünstigt die Bildung des Norbornadiens. Dem gegenüber liegt im Minimum des ersten angeregten Triplettzustands (T_1) ein Biradikal vor, dessen Radikale in 3- und 5-Position lokalisiert sind. Über ein weiteres Intersystem-Crossing in den Grundzustand (S_0) wird dieses Biradikal begünstigt in das Quadricyclan überführt.[123,140]

Eine bathochrome Verschiebung der Absorption des Norbornadiens kann durch die Erweiterung des Grundgerüsts erfolgen.[136,137] Mit der Einführung von Arylcarbamoyl- oder Arylimidgruppen konnte die Absorption in den sichtbaren Bereich verschoben werden. Allerdings liegen in diesen Systemen sehr geringe Quantenausbeuten ($\phi_{NBD\rightarrow QC} = 0.13$) vor.[141] Mit der Einführung von Donor-Akzeptor-Chromophoren kann die Absorption ebenfalls bis in den sichtbaren Bereich ($\lambda_{max} = 400\,\text{nm}$) gebracht werden, indem der Elektronendonor die Energie des HOMOs anhebt und der Elektronenakzeptor die Energie des LUMOs herabsetzt. Weiterhin werden in diesem Fall hohe Quantenausbeuten gewährleistet. Allerdings nimmt die thermische Stabilität des Quadricyclans mit der Einführung von arylischen Donoren ab.[142,143] Mit der Einführung dieser push-pull-Substituenten werden zusätzlich die Topografien der Hyperflächen der S_1- und T_1-Zustände verändert, wodurch sich die favorisierten Isomerisierungsmechanismus ändern. Während im Stammsystem die [2+2]-Cycloaddition über einen $S_1 \rightarrow T_1 \rightarrow S_0$ Mechanismus, der über ein Intersystem-Crossing erfolgt, abläuft,[144] wird der direkte $S_1 \rightarrow S_0$ Mechanismus durch die push-pull-Stubstituenten begünstigt.[139]

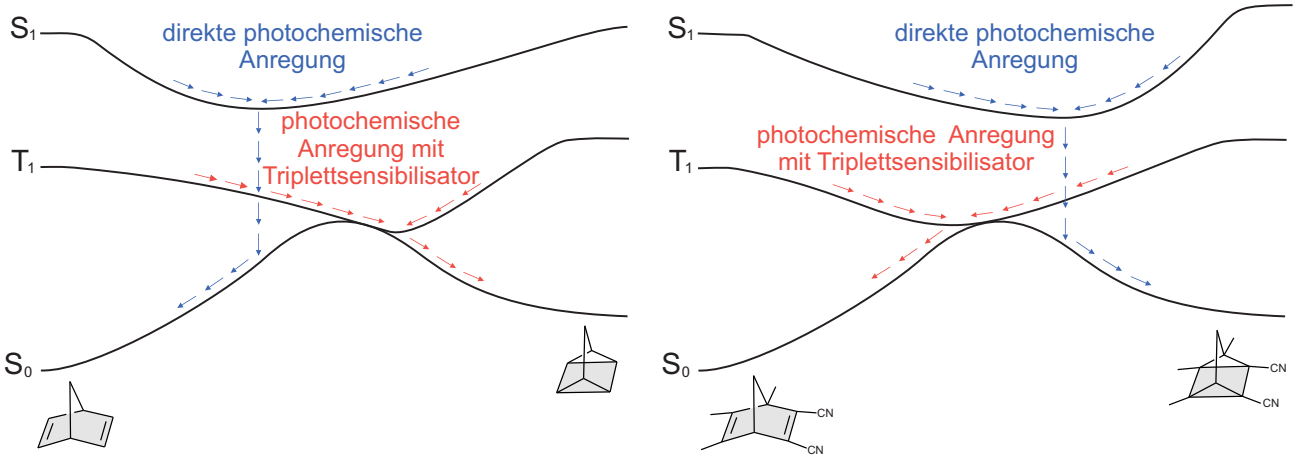

Abb. 1.9: Postulierte Topografie der Energiehyperflächen (S_0, T_1, S_1) des Stammsystems des Norbornadiens und Quadricyclans (links) und mit elektronenziehenden und elektronenschiebenden Substituenten des Norbornadiens bzw. Quadricyclans (rechts). Die unterschiedlichen Reaktionsverläufe aus den angeregten Zuständen (T_1 = rot, S_1 = blau) sind für beide Systeme gezeigt.[139]

Die photochemische [2+2]-Cycloreversion läuft im Stammstystem ebenfalls über einen radikalischen Mechanismus ab.[145] Das Quadricyclanstammsystem ist gegenüber der thermischen Cycloreversion, die eine Aktivierungsenergie von 140.3 kJ/mol hat, bei milden Bedingungen stabil.[123] Mit verschiedenen Katalysatoren, die Übergangsmetalle wie Silber,[146] Cobalt,[147] Rhodium,[148] Nickel, Palladium oder Platin[141] enthalten, ist eine effiziente katalytische Cycloreversion realisierbar. Zudem können auch Oxidationsmittel oder ein Triplettsensibilisator, wie beispielsweise photochemisch angeregtes

Benzophnenon,[149,150] die Cycloreversion begünstigen. Bei der Cycloreversion wird eine Enthalpie von 100 kJ/mol frei, weswegen das Norbornadien-Quadricyclansystem in der Literatur als geeignete schaltbare Einheit zu Speicherung von Sonnenenergie diskutiert wird.[151,152] Da die Cycloreversion mit verschiedenen Katalysatoren beschleunigt wird, bietet sich das Norbornadien zur Analyse der nicht aufgeklärten katalytischen Beeinflussung des Goldes an. Ein ebenfalls weitestgehend gut verstandener Photoschalter ist das Azobenzol, dessen beschleunigte *cis*→*trans*-Isomersierung zwar bereits nachgewiesen[50,51] allerdings noch nicht vollends verstanden wurde.

1.6.5 Azobenzol

Das Azobenzol wurde erstmals 1834 beschrieben[153] und von HARTLEY[154] auf die Schalteigenschaften untersucht. Die photochemische Isomerisierung kann nach zwei Mechanismen ablaufen. Dem Inversionsmechanismus,[155,156] bei dem die π-Bindung der Azobrücke intakt bleibt und dem Rotationsmechanismus,[157,158] bei dem die π-Bindung gebrochen wird. Nach welchem Mechanismus die photochemische Isomerisierung abläuft, konnte bis heute nicht eindeutig geklärt werden.[159] Weiterhin besteht die Möglichkeit, dass die Isomerisierung nach einem gemischten Hula-Twist-Mechanismus abläuft.[160] Des Weiteren ist nicht eindeutig geklärt, nach welchem Mechanismus die thermische *cis*→*trans*-Isomerisierung abläuft (Abb. 1.10).[161]

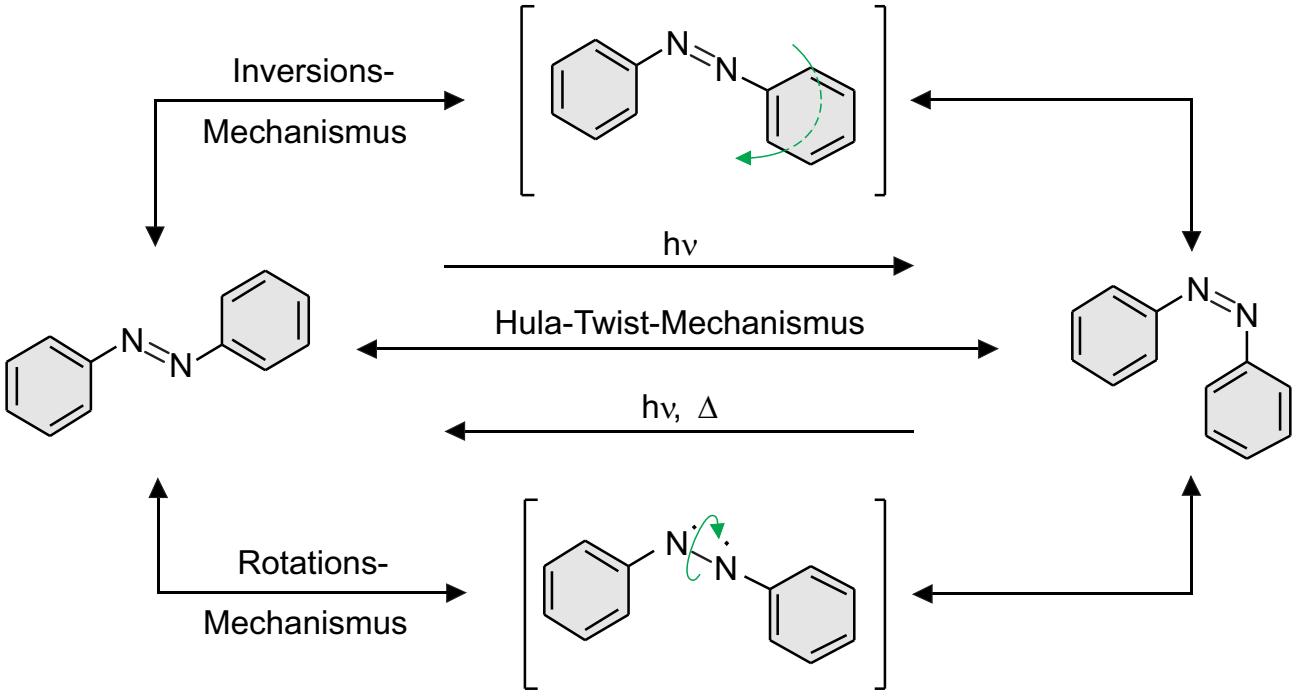

Abb. 1.10: Die Isomerisierung zwischen dem thermodynamisch stabilen *trans*-Azobenzol (links) und dem metastabilen *cis*-Azobenzol (rechts) kann nach einem Inversions- oder Rotationsmechanismus ablaufen. Weiterhin wird die Möglichkeit eines Hula-Twist-Mechanismus diskutiert, bei dem die Inversion und Rotation gemischt ablaufen.[5,160,161]

Das Absorptionsspektrum des *trans*-Azobenzols zeigt eine schwache Bande im sichtbaren Bereich mit einem Maximum bei 432 nm (ε_{max} = 400 L/mol·cm),[159] die dem niedrigsten Singulett-Zustand S_1 mit nπ*-Natur zugeordnet werden kann. Eine zweite Absorption ist im UV-Bereich mit einem Maximum bei 318 nm (ε_{max} = 22300 L/mol·cm), die dem S_2 Übergang mit $\pi\pi$*-Charakter zugewiesen wird.[161] Im *cis*-Azobenzol liegen zwei nahezu identische Banden im Bereich von 440 nm und 260 nm, die ähnliche Übergangswahrscheinlichkeiten wie das *trans*-Azobenzol aufweisen.[159] Aufgrund dieser Absorptionsspektren wird die photochemische *trans*→*cis*-Isomerisierung in der Regel mit einer Wellenlänge von $\lambda \approx$ 365 nm durchgeführt, wobei in die $\pi\pi$*-Bande eingestrahlt wird.[159] Der Energieunterschied zwischen dem *trans*- und *cis*-Isomer liegt bei ca. 50 kJ/mol[162] mit einer Aktivierungsenergie von 95-105 kJ/mol in Lösung[163–165] und 131 kJ/mol im Feststoff.[166] Die Berechnung der *cis*→*trans*-Isomerisierung über einen Rotationsmechanismus wurde auf 293 kJ/mol und über einen Inversionsmechanismus auf 137 kJ/mol bestimmt.[167] Im *cis*-Isomer liegt aufgrund der sterischen Abstoßung der beiden Phenylringe eine verdrillte Struktur im Vergleich zur planaren Struktur des *trans*-Isomers vor.[168] Diese Geometrieänderung bietet sich für die Untersuchung beider Isomere in oberflächensensitiven Messmethoden wie der IRRA-Spektroskopie an, um die beschleunigte Isomerisierung auf Goldoberflächen besser zu verstehen. Über eine zusätzliche *ortho*-Ethylenverbrückung beider Phenylringe des Azobenzols wird das Diazocin gebildet, das einen weiteren interessanten Photoschalter darstellt.

1.6.6 Diazocin

Das Diazocin wurde von DUVAL entwickelt,[169] allerdings erst knapp 100 Jahre später auf seine photochemischen Isomerisierungseigenschaften untersucht.[170] Mithilfe einer photochemischen Anregung bei $\lambda \approx$ 370-400 nm wird das *cis*-Diazocin mit einem Anteil von über 90 % in das metastabile twist-*trans*-Diazocin überführt und isomerisiert mit einer Wellenlänge von $\lambda \approx$ 480-550 nm vollständig zurück in das *cis*-Isomer (Abb. 1.11). Die Quantenausbeuten sind beim Diazocin höher als im Vergleich zu Azobenzol.[171,172] Bei der Isomerisierung resultiert eine Farbänderung von gelb zu rot durch die bathochrome Verschiebung der Absorption des nπ*-Übergangs von λ_{max} = 404 nm (*cis*) zu λ_{max} = 490 nm (*trans*).[170]

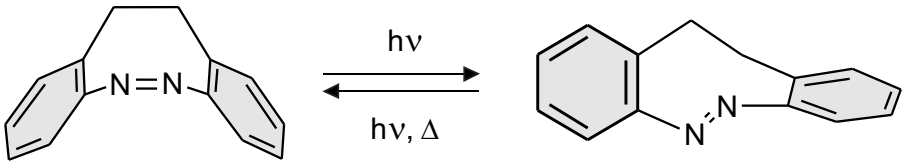

Abb. 1.11: Isomerisierung zwischen dem thermodynamisch stabilen *cis*-Diazocin (links) und dem metastabilen twist-*trans*-Diazocin (rechts).[170]

Der Achtring des Diazocins lässt das *cis*-Isomer des Diazocins als thermodynamisch stabile Form vorliegen.[170,173] Die thermische Isomerisierung ist mit $t_{1/2}$ = 4.5 h (28.5 °C) kürzer als beim Azobenzol mit $t_{1/2}$ = 119 h (25 °C).[165,170] Mit der inversen thermischen Isomerisierung im Vergleich

zu Azobenzol bietet sich das Diazocin zur Untersuchung auf Goldoberflächen an, um eine mögliche Beschleunigung in der *trans*→*cis*-Isomerisierung nachzuweisen.

2 Aufgabenstellung

Die katalytische Beschleunigung von Reaktionen von direkt adsorbtierten Molekülen auf Metalloberflächen kann durch eine direkte, chemische Beteiligung der Metallatome erfolgen[50,51] oder durch einen nicht-klassischen Effekt, der durch die elektronische Kopplung der Moleküle mit dem Metallsubstrat vermittelt wird.[47,48] Das Plattformkonzept erlaubt die getrennte Betrachtung der elektronischen Kopplung mit dem Substrat, da das reagierende Molekül räumlich von der Oberfläche getrennt, allerdings weiterhin elektronisch über einen durchgehenden Konjugationspfad mit der Oberfläche gekoppelt ist.[29,69] Diese Dissertation befasst sich mit der schrittweisen Variation der elektronischen Kopplung zwischen dem Azobenzol und der Goldoberfläche, die über die Einführung von Regulierungseinheiten erfolgen soll, um systematisch den Einfluss der elektronischen Kopplung mit dem Metall auf die *cis*→*trans*-Isomerisierung zu untersuchen (Abb. 2.1).

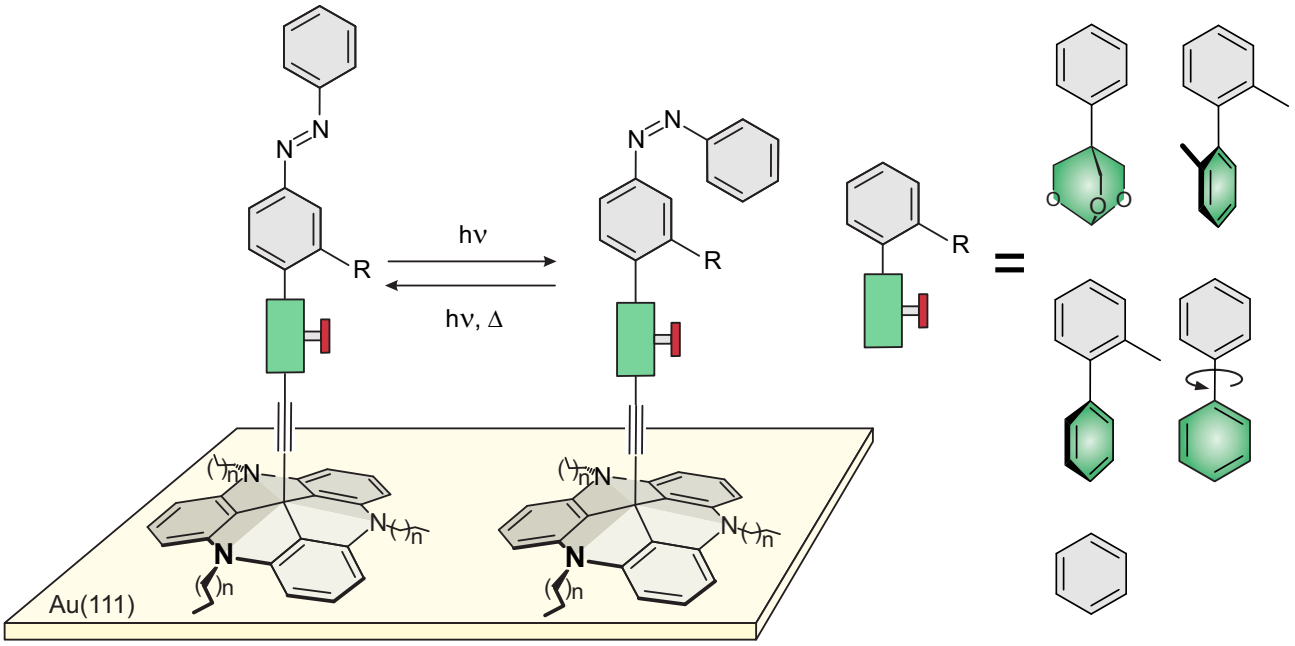

Abb. 2.1: Schematische Darstellung der Isomerisation eines Azobenzols funktionalisiert auf einer TATA-Plattform. Die Regulierungseinheit (grün) steuert die Konjugation zwischen Azofunktion und Goldoberfläche.

Dabei bieten sich substituierte Biphenyle als Regulierungseinheiten an, die über einen stetig steigenden Verdrillungswinkel die Konjugation zwischen Azobenzol und TATA-Plattform und damit die elektronische Kopplung zwischen Goldoberfläche und Azofunktion systematisch reduzieren. Mit einem cyclischen Orthoester soll die Konjugation vollständig unterbrochen werden.
Zusätzlich ist es für ein besseres Verständnis essentiell, Photoschalter auf Plattformen zu funktionalisieren, die in weiteren Isomerisierungsvarianten in die thermodynamisch stabile Form isomerisieren. Mithilfe dieser Isomerisierungen kann der Katalysemechanismus ausgehend vom Gold genauer un-

tersucht werden. Dafür bietet sich das Diazocin als Azobenzolderivat (Abb. 2.2) an. Der aus der Ethylenverbrückung der beiden Phenylringe gebildete Achtring führt dazu, dass das *cis*-Isomer als thermodynamisch stabile Form vorliegt und somit kann eine mögliche Beschleunigung der thermischen *trans*→*cis*-Isomerisierung auf Au(111)-Oberflächen nachgewiesen werden.[169,170]

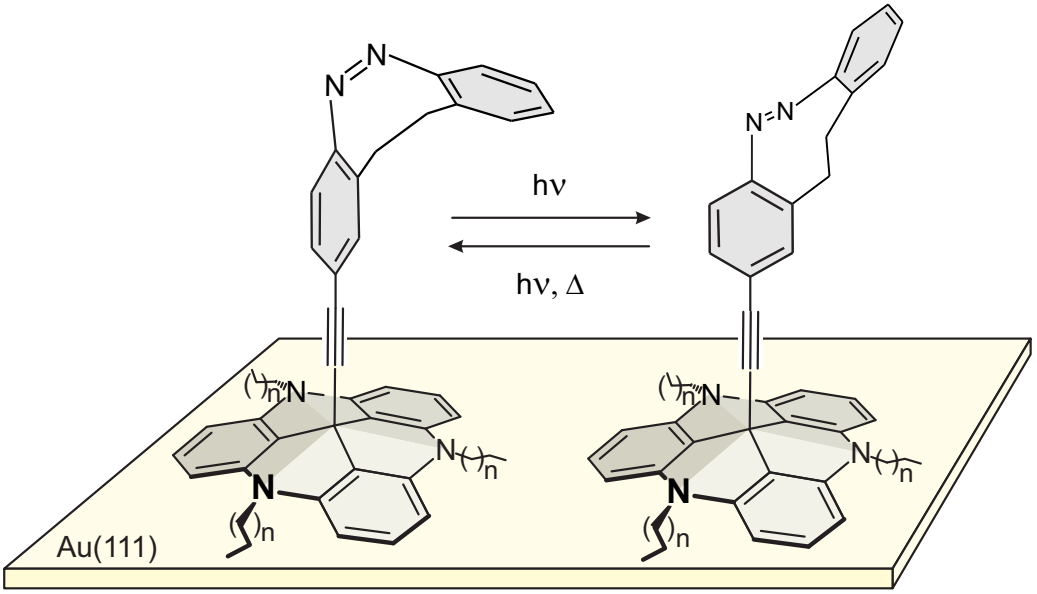

Abb. 2.2: Schematische Darstellung des Diazocins im thermodynamisch stabilen *cis*- (links) und *trans*-Isomer (rechts) funktionalisiert über eine Acetyleneinheit auf einer TATA-Plattform, die auf einer Au(111) Oberfläche adsorbiert.

Zusätzlich wird durch die Ethylenverbrückung die Rotation um die Azobrücke verhindert, wodurch die Regulierungseinheit in *para*- und *meta*-Position zur Azofunktion etabliert werden kann, während die orthogonale Ausrichtung des oberen Phenylrings im *trans*-Isomer bzw. horizontale Ausrichtung im *cis*-Isomer zur Plattform erhalten bleibt. Mit dieser Variabilität wird über die *para*-Funktionalisierung des Acetylens zur Azobrücke am Diazocin eine hohe Konjugation zwischen Azogruppe und Plattform gewährleistet, während die *meta*-Funktionalisierung die Konjugation nahezu unterbricht. Damit kann im Diazocinsystem die Konjugation allein über das Substitutionsmuster der Verknüpfungseinheit variiert werden, während das vertikal ausgerichtete *trans*-Isomer bzw. das horizontal ausgerichtete *cis*-Isomer weiterhin in IRRAS Messungen detektierbar sein sollte.
Die von der Goldoberfläche ausgehende katalytische Beeinflussung von Azobenzolen und potentiell bei Diazocinen erfolgt in beiden Fällen über eine Beschleunigung der thermischen Isomerisierung zwischen dem *cis*- und *trans*-Isomer. Für eine umfassende Analyse des bisher unbekannten Mechanismus ist ein Nachweis der Isomerisierungsbeschleunigung in weiteren Systemen notwendig. Dafür bietet sich das Quadricyclan an, das thermisch über eine [2+2]-Cycloreversion in das thermodynamisch stabile Norbornadien isomerisieren soll (Abb. 2.3).[136,137]

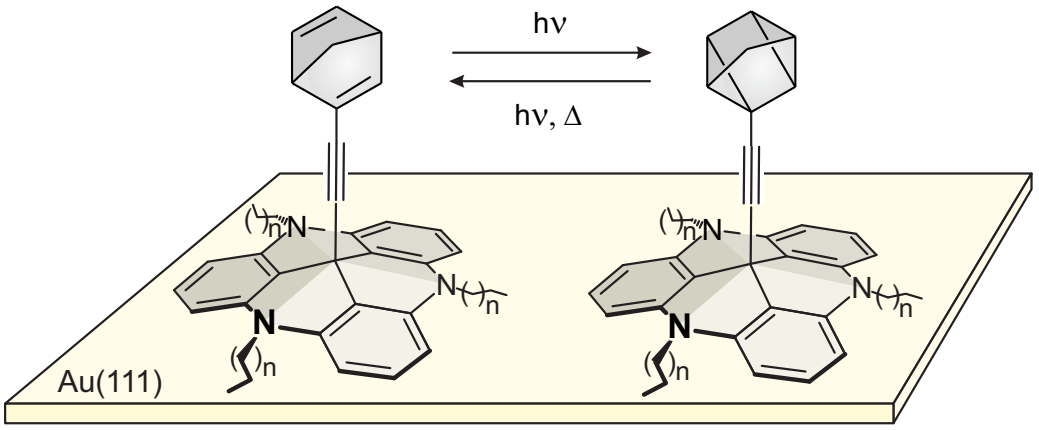

Abb. 2.3: Schematische Darstellung des thermodynamisch stabilen Norbornadiens (links), welches über eine Acetyleneinheit auf einer TATA-Plattform funktionalisiert ist. Photochemisch kann das Norbornadien über eine [2+2]-Cycloaddition in das metastabile Quadricyclan (rechts) sowie photochemisch als auch thermisch über eine [2+2]-Cycloreversion zurück zum Norbornadien isomerisieren.

Bisher ist die Detektion der photochemischen und thermischen Isomerisierung von Azobenzolen auf Au(111)-Oberflächen, die auf TATA-Plattformen funktionalisiert wurden, ausschließlich über oberflächensensitive Messmethoden wie der UV/Vis- bzw. IRRA-Spektroskopie möglich. Die Untersuchung der Isomerisierung von Photoschaltern kann prinzipiell mittels Rastertunnelmikroskopie über die Änderung der relativen Höhe erfolgen. Allerdings ist dafür eine Referenz mit definierter unveränderbarer relativer Höhe in den Monolagen essentiell. Mit der Entwicklung von TATA-Plattformen, die mit systematischen Aufbauten funktionalisiert werden, könnten definierte relative Höhen in STM-Messungen erhalten werden. Mithilfe dieser Referenz-Plattformen könnten die Isomere von Photoschaltern in STM-Messungen unterscheidbar sein, sodass die Isomerisierung der Photoschalter und somit der Einfluss des Goldes auf die thermische Isomerisierung mit dem STM untersucht werden kann.

3 Publikationen und deren Zusammenfassungen

3.1 Ratenverkürzung durch Goldoberflächen über eine lange Distanz

Mit dem Nachweis der beschleunigten thermischen Isomerisierung von Azobenzolen auf Au(111)-Oberflächen[50] liegt der Fokus in der detaillierten Untersuchung und vollständigen Aufklärung dieses Mechanismus. Problematisch in der Untersuchung von direkt auf Au(111)-Oberflächen adsorbierten Azobenzolen ist die eingeschränkte Variabilität, die Stärke des Einflusses des Goldes auf die thermische Isomerisierung mit verschiedenen Parametern zu steuern. Das modulare Plattformkonzept bietet sich für die Aufklärung dieses Mechanismus im besonderem Maße an und ermöglichte bereits den Nachweis der beschleunigten thermischen *cis*→*trans*-Isomerisierung des Azobenzols auf Goldoberflächen (Abb. 3.1).[46–48] Der Photoschalter ist dabei kovalent über eine Acetyleneinheit mit der Plattform verknüpft, sodass die hohe Konjugation mit der Plattform erhalten bleibt, die selbst wiederum planar auf der Goldoberfläche adsorbiert.

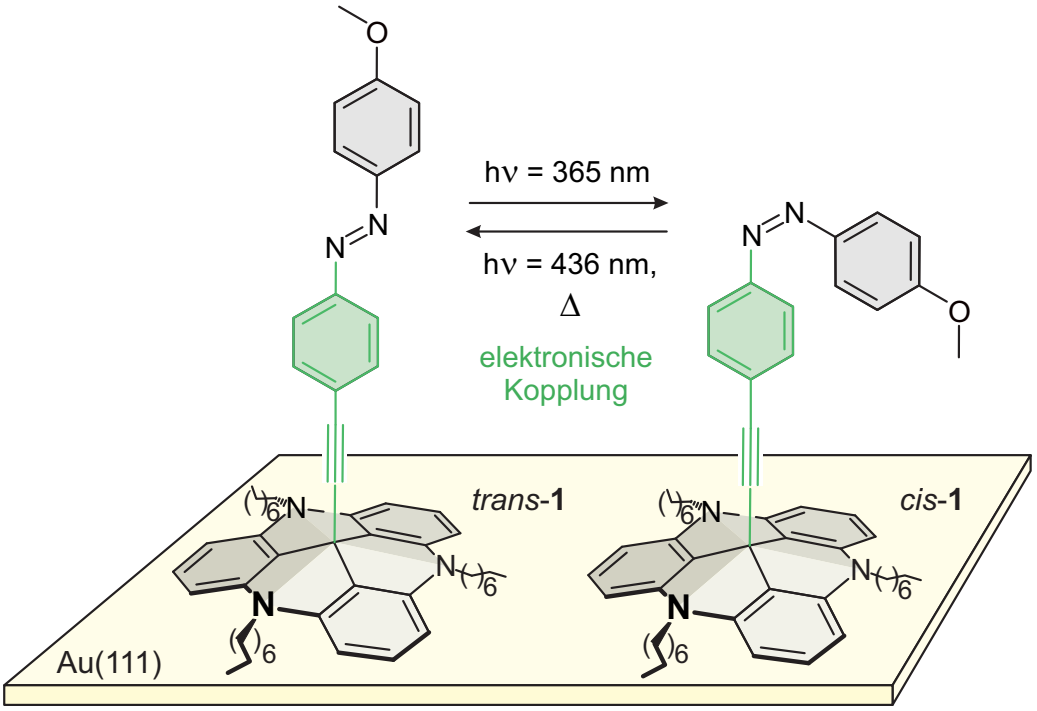

Abb. 3.1: Darstellung des Azobenzols funktionalisiert über eine Acetylenspacereinheit auf einer Octyl-TATA-Plattform **1**, die auf einer Au(111)-Oberfläche adsorbiert. Die Methoxykopfgruppe dient zur Detektion beider Isomere in IRRAS-Messungen.

Diese Beobachtung grenzt die Art der Wirkungsweise der Goldoberfläche ein. Als wahrscheinlichste Art der Beeinflussung des Goldes gilt die elektronische Kopplung der Goldoberfläche mit dem π-System des Azobenzols. Die hohe Konjugation über die Acetylenspacereinheit sollte mit der Einführung von Biphenyleinheiten, die unterschiedlich hohe Verdrillungswinkel haben, schrittweise reduziert werden können und über die unterschiedlich hohe Beschleunigung der thermischen *cis*→*trans*-Isomerisierung die postulierte elektronische Kopplung untersucht werden.

3.1.1 Long-Distance Rate Acceleration by Bulk Gold

Alexander Schlimm, Roland Löw, Talina Rusch, Fynn Röhricht, Thomas Strunskus, Tobias Tellkamp, Frank Sönnichsen, Uwe Manthe, Olaf Magnussen, Felix Tuczek, Rainer Herges

Angew. Chem. Int. Ed. **2019**, *56*, 6574-6578.
DOI:10.1002/anie.201814342

Eigenanteil: Die Synthesen aller Zielmoleküle mit Ausnahme der Synthesen aus der Syntheseroute von **1a** und **6a** und die photochemischen Messungen von allen Verbindungen in Lösung wurden von Roland Löw durchgeführt. Die Synthesen der Syntheseroute von **6a** wurde von Tobias Tellkamp durchgeführt. Die Untersuchungen der Zielmoleküle auf Goldoberflächen wurden von Talina Rusch und Alexander Schlimm durchgeführt. Die DFT-Rechnungen wurden von Fynn Röhricht angefertigt. Das Manuskript wurde von Prof. Dr. Rainer Herges verfasst.

3.1.2 Zusammenfassung

In dieser Publikation wird die Aufklärung des Mechanismus der thermischen Isomerisierungsbeschleunigung des Azobenzols durch Gold beschrieben. Dabei werden Triazatriangulenium-Plattformen ausgenutzt, um das Azobenzol räumlich von der Goldoberfläche zu entfernen und die elektronische Kopplung zwischen Goldoberfläche und Azofunktion mithilfe verschiedener Regulierungseinheiten systematisch zu reduzieren. Die Variation dieser Einheiten ist das zentrale Forschungskonzept dieser Publikation zur Aufklärung des vom Gold ausgehenden Mechanismus (Abb. 3.2). Die bereits etablierte Acetyleneinheit in **2a**, **2b**, die eine hohe Konjugation von der Azofunktion zur Plattform und dadurch eine hohe elektronische Kopplung zur Goldoberfläche zulässt, wird durch einen Phenylring in **3a**, **3b** erweitert, um die Konjugation über die Verdrillung des erhaltenen Biphenyls schrittweise zu reduzieren. Die Erhöhung der Verdrillung wird durch die Einführung von einer bis zwei Methylgruppen in **4a**, **4b**, **5a** und **5b** erreicht. Mit dem Austausch des zusätzlichen Phenylrings durch einen isolierenden cyclischen Orthoester in **6a** und **6b** wird die Konjugation vollständig unterbrochen und die elektronische Kopplung zwischen Azofunktion und Goldoberfläche nahezu unterbunden.

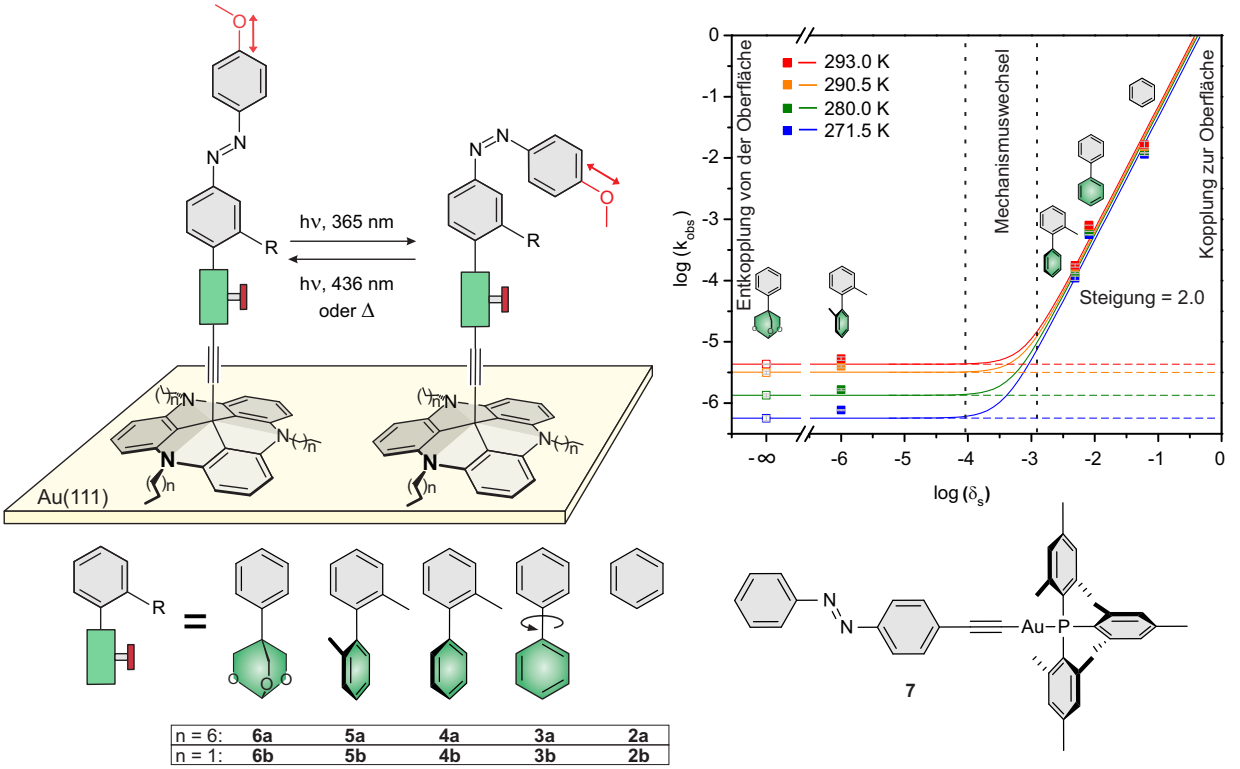

Abb. 3.2: Azobenzole funktionalisiert über verschiedene Regulierungseinheiten auf TATA-Plattformen, die die Konjugation zwischen Azofunktion und TATA-Plattform schrittweise reduzieren. Weiterhin ist ein mit einem Goldatom funktionalisiertes Azobenzol **7** gezeigt. Zusätzlich ist die Auftragung der logarithmischen Ratenkonstante der thermischen Isomerisierung (k_{obs}) als Funktion der logarithmischen Spindichte des Orbitals der Azofunktion unterhalb der Regulierungseinheit (δ_s) gezeigt.

Mit den unterschiedlichen thermischen Isomerisierungbeschleunigungen in Abhängigkeit der Stärke der elektronischen Kopplung der Azofunktion zur Goldoberfläche konnte der nicht adiabatische Mechanismus aufgeklärt werden. Dabei wird bei Azobenzolen, die mit dem Leitungsband des Goldes elektronisch koppeln, das quantenmechanische Verbot des Intersystem Crossings aufgehoben. Dadurch wird die Reaktionsgeschwindigkeit ausschließlich von der quantenmechanischen Übergangswahrscheinlichkeit kontrolliert. Diese Aufhebung resultiert in verkürzten Halbwertszeiten von Sekunden bis zu einer Stunde auf Gold verglichen zu mehreren Stunden in Lösung. Mit der Auftragung der logarithmischen Ratenkonstante (k_{obs}) der thermischen Isomerisierung als Funktion der logarithmischen Spindichte des Orbitals der Azofunktion unterhalb der Regulierungseinheit (δ_s), wurde der nicht adiabatische Mechanismus des Goldes und der klassische Mechanismus graphisch verglichen. Mit Regulierungseinheiten, die die elektronische Kopplung zwischen Azofunktion und Goldoberfläche zulassen, ist die Temperaturabhängigkeit der Ratenkonstanten vernachlässigbar gering, während die Ratenkonstanten bei der elektronischen Entkopplung der Azofunktion von der Goldoberfläche nach den Gesetzen der Thermodynamik beschrieben werden können. Zwischen beiden Mechanismen wurde ein Bereich postuliert, in dem der Verdrillungswinkel der Biphenyleinheit die elektronische Kopplung soweit reduziert, dass die thermische Isomerisierung von beiden Mechanismen abhängig ist. Dabei muss der Verdrillungswinkel größer als 51° wie im Fall von **4** und kleiner als 84 ° wie im Fall von **5** sein. Mit dem Vergleich der Ratenkonstanten dieser Azobenzole auf Octyl- und Propyl-TATA-Plattformen auf Au(111)-Oberflächen konnte ein signifikanter intermolekularer sterischer Einfluss auf die thermische *cis*→*trans*-Isomerisierung ausgeschlossen werden. Die Ergebnisse belegen, dass der geringere Freiraum im Fall der Propyl-TATA-Plattformen die Ratenkonstanten nur geringfügig verkürzt und im Fall der Octyl-TATA-Plattformen eine intermolekulare sterische Beeinflussung auf die Isomerisierung vernachlässigbar ist. Mit der Untersuchung eines Azobenzols **7** mit einem einzelnen kovalent gebundenen Goldatom in Lösung konnte ein Schweratomeffekt (Spin-Bahn-Kopplung), der ein Intersystem-Crossing begünstigen würde, als Ursprung dieses Mechanismus ausgeschlossen werden.

Reaction Kinetics

International Edition: DOI: 10.1002/anie.201814342
German Edition: DOI: 10.1002/ange.201814342

Long-Distance Rate Acceleration by Bulk Gold

Alexander Schlimm, Roland Löw, Talina Rusch, Fynn Röhricht, Thomas Strunskus, Tobias Tellkamp, Frank Sönnichsen, Uwe Manthe, Olaf Magnussen, Felix Tuczek,* and Rainer Herges**

Abstract: *We report on a very unusual case of surface catalysis involving azobenzenes in contact with a Au(111) surface. A rate acceleration of the cis–trans isomerization on gold up to a factor of 1300 compared to solution is observed. By using carefully designed molecular frameworks, the electronic coupling to the surface can be systematically tuned. The isomerization kinetics of molecules with very weak coupling to the metal is similar to that found in solution. For their counterparts with strong coupling, the relaxation rate is shown to depend on the spin-density distribution in the triplet states of the molecules. This suggests that an intersystem crossing is involved in the relaxation process. Aside from their impact on catalytic processes, these effects could be used to trigger reactions over long distances.*

The majority of chemical processes in nature and in industry involve catalysis. Often, there is no other way to form stable products from stable reactants under mild conditions. Most technologically relevant reactions employ heterogeneous catalysis, where the reacting molecules interact with atoms or ions on surfaces, forming intermediates.[1] This opens up reaction pathways with lower barriers and faster reaction rates than in the uncatalyzed processes. A number of reactions on surfaces have been studied and their mechanisms have been elucidated in detail.[1,2] Here, we report on a very unusual case of surface catalysis involving azobenzene units in contact with a Au(111) surface. We observe a drastic rate acceleration (up to a factor of 1300 compared to solution) of *cis–trans* isomerization on gold, even though the reacting N=N double bonds are located 14 Å above and are separated by eleven covalent bonds from the Au(111) surface. To elucidate this extraordinary long-range acceleration of the reaction rate, we employ carefully designed molecular frameworks.[3] The modularity of this unique system allows a precise adjustment of intermolecular distances and coupling.[4,5] Furthermore, the electronic coupling to the surface is systematically tuned by changing the π-conjugation of the coupling unit, while the distance between the gold surface and the azobenzene unit remains almost the same. Surprisingly, the isomerization kinetics of molecules with strong coupling to the metal follows a different mechanism than the one observed for their counterparts with no or very weak coupling. Specifically, activation energies drop to very low values and frequency factors become explicitly dependent on an electronic matrix element that can be correlated with the spin-density distribution in the triplet states of the molecules. Besides their impact on catalytic processes, these effects could be used to trigger chemical reactions over a long distance. Similar remote effects have not been considered in catalytic processes so far. However, they could be operative in a number of reactions on metallic surfaces or nanoparticles.

Catalysts increase the rates of chemical reactions by creating a new and energetically more favorable reaction path with lower activation energies. In heterogeneous catalysis, this new path involves the adsorption of reactants at a surface, where chemical bonds within the molecule are broken and new bonds with surface atoms are formed. Although the majority of chemical reactions follow the Eyring theory or RKKM-type transition state theories, there are a few examples of chemical reactions that substantially deviate from the theoretically predicted behavior.[6] Their reaction rates mainly depend on quantum-mechanical transition probabilities and not the height of an energy barrier. Characteristic features are apparently small frequency factors and low activation energies, corresponding to reaction rates that are almost temperature-independent. Such processes have mostly been observed at low temperatures (< 50 K).[7] Herein, we show that bulk gold can mediate similar phenomena at temperatures around 300 K. Moreover, by modifying the electronic coupling between the reaction center and the Au surface, we are able to shift the isomerization kinetics from a classical, solution-like behavior to a new regime involving a drastically lowered barrier and increased reaction rates.

In our studies, we employ azobenzene-functionalized TATA (azo-TATA) molecules (Figure 1, top). The *cis–trans*

[*] A. Schlimm, Prof. Dr. F. Tuczek
Christian Albrechts University Kiel, Institute of Inorganic Chemistry
Max-Eyth-Str. 2, 24118 Kiel (Germany)
E-mail: ftuczek@ac.uni-kiel.de
R. Löw, F. Röhricht, Dr. T. Tellkamp, Prof. Dr. F. Sönnichsen, Prof. Dr. R. Herges
Christian Albrechts University Kiel, Institute of Organic Chemistry
Otto-Hahn-Platz 4, 24118 Kiel (Germany)
E-mail: rherges@oc.uni-kiel.de
T. Rusch, Prof. Dr. O. Magnussen
Christian Albrechts University Kiel
Institute of Experimental and Applied Physics
Leibnizstr. 19, 24118 Kiel (Germany)
E-mail: magnussen@physik.uni-kiel.de
Dr. T. Strunskus
Christian Albrechts University Kiel, Institute for Materials Science
Kaiserstr. 2, 24143 Kiel (Germany)
Prof. Dr. U. Manthe
University of Bielefeld, Institute of Theoretical Chemistry
Universitätsstr. 25, 33501 Bielefeld (Germany)
Supporting information and the ORCID identification number(s) for the author(s) of this article can be found under: https://doi.org/10.1002/anie.201814342.

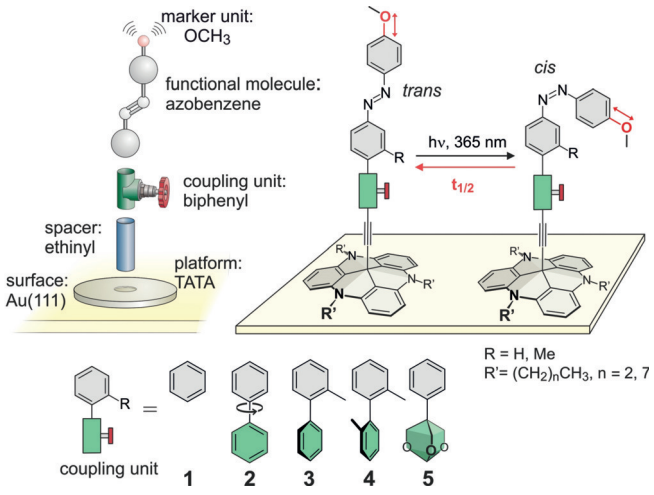

Figure 1. Modular design to tune the electronic coupling of azobenzene units with the metal surface: TATA platforms define the intermolecular distances on the surface (by the size of the side chain: a = octyl, b = propyl) and ethinyl spacers provide a freestanding upright orientation of the reacting azobenzene molecules. Coupling units (green) control the electronic coupling of azobenzenes with the surface. Methoxy groups allow to identify the configuration of the azobenzene (*cis* or *trans*) by IRRAS.

isomerization kinetics of **1a** and **2a** have recently been investigated in solution and for adsorbed monolayers, finding that the thermal *cis*-to-*trans* relaxation of the molecules adsorbed on bulk Au(111) is considerably faster than in solution.[8–10] Assuming that this rate acceleration involves electronic coupling to the metal,[8] we synthesized three new azo-TATA compounds with different coupling units inserted between the TATA platform and the azobenzene unit (Figure 1 and Supporting Information). Biphenyl groups were chosen to tune the electronic coupling of the azo group to the surface, because 4,4′-substituted biphenyls retain the upright alignment of the azobenzene with respect to the surface and, most importantly, upon addition of an increasing number of methyl groups ($n = 0$–4) in *ortho* position, the phenyl groups are twisted out of coplanarity, which decreases their conductivity (Supporting Information, Figure S124).[11] To shut off π-conjugation completely, we inserted a trioxabicyclo[2,2,2] unit which separates the π-systems of azobenzene and the ethinyl spacer with sp^3-hybridized C and O atoms. The new compounds (**3a**–**5a**, **1b**, **2b**, **5b**) were completely characterized in solution and bulk material with NMR, UV/Vis, and vibrational spectroscopy (see Supporting Information). Scanning Tunneling Microscopy (STM) shows that, in agreement with previous results,[3,4,12] optimized self-assembly conditions result in monolayers of **1a**–**5a** with $(\sqrt{19} \times \sqrt{19})$ R23.4° superstructures and low defect densities (see Figures 2 and S125). X-ray spectroscopy studies (XPS, NEXAFS) prove that the adlayers are of high purity with the molecules being oriented perpendicular to the surface, as shown in Figure 2 (Figures S126 and S127). The vertical alignment of the azobenzene with respect to the surface has

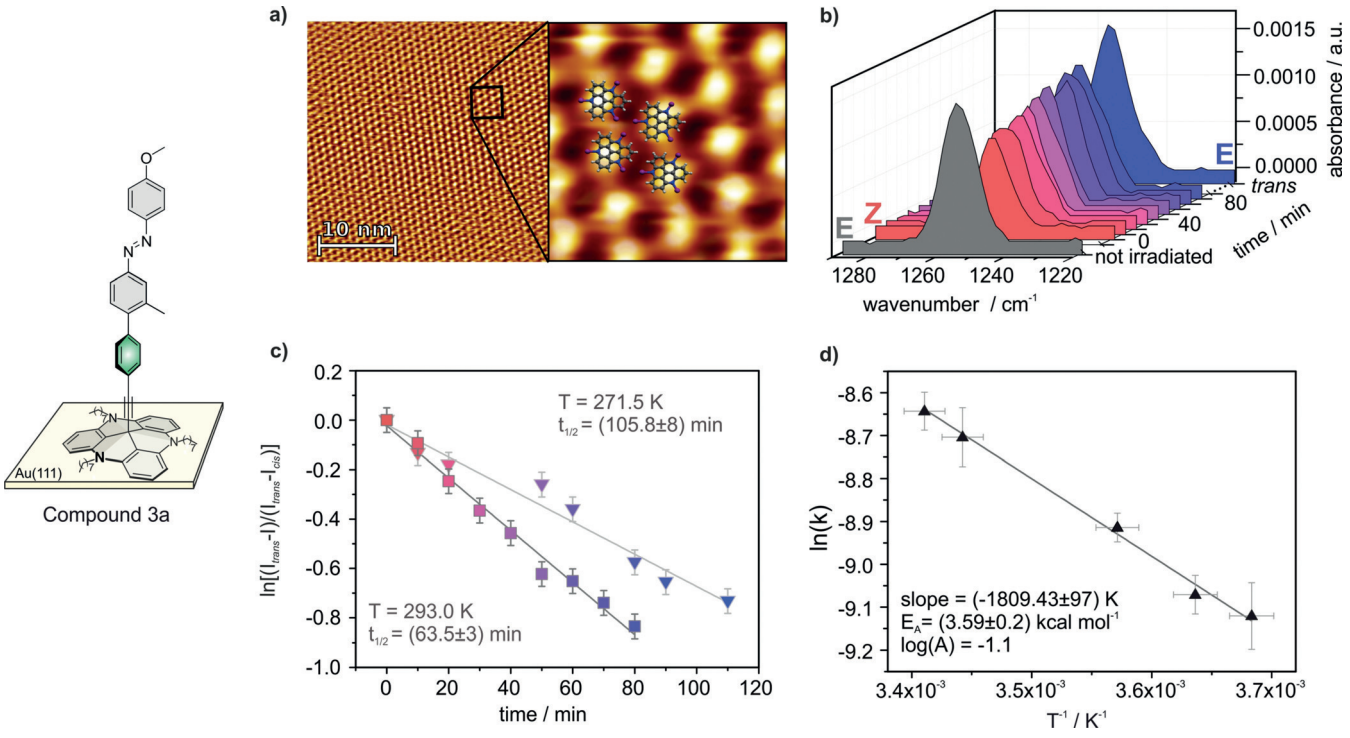

Figure 2. a) STM image and model of a monolayer of azo-TATA **3a** on Au(111). The molecules exhibit an intermolecular distance of 12.6 Å. b) PM-IRRAS signal of the C–O stretching vibration region before irradiation (gray) and after irradiation with light of 365 nm as a function of time (red to blue). The blue spectrum was obtained after irradiation with 440 nm light. In both cases, the irradiation time was 10 min. c) PM-IRRAS intensity of the C–O stretching vibration as a function of time at two different temperatures (271.5 K and 293.0 K). Half-lives ($t_{1/2}$) are derived by a linear regression. d) Arrhenius plot of reaction rates *k* at five different temperatures. The activation barrier E_a and the frequency factor *A* are derived by a linear regression.

been confirmed in previous studies as well (tilt angle: 6 ± 16°).[12]

The well-defined molecular orientation together with the surface selection rule allows to monitor the photochemical (365 nm) *trans*-to-*cis* isomerization as well as the ensuing thermal *cis*-to-*trans* relaxation by Infrared Reflection Absorption Spectroscopy (IRRAS).[13] The relaxation leads to orientational changes of the C_{phenyl}–$O_{methoxy}$ bond relative to the surface and thus, temporal changes in the intensity of the corresponding band in the IRRA spectrum. The rates of the thermal *cis*-to-*trans* relaxation were determined at five different temperatures (Figures 2 and S129). From these data, activation energies and frequency factors were obtained for compounds **1a**–**5a** (Figures 3 and S128). For adsorbate layers of compounds **1a**, **2a**, and **3a** on Au(111), the rates show only small changes in the investigated temperature range. Correspondingly, the activation energies and frequency factors are exceptionally small and typical for non-adiabatic reactions, where the rates are controlled by quantum-mechanical transition probabilities rather than classical energy barriers. On the contrary, the largely decoupled compounds **4a** and **5a** show a significantly stronger temperature dependence of the reaction rate, close to the rates observed in solution. The combined surface-kinetic data thus show that at a fixed temperature, the half-life of the adsorbed species can be changed by up to four orders of magnitude through adjusting the electronic coupling between the platform and the azo unit. In contrast, the half-lives of the five compounds in solution vary only slightly with the coupling unit.

The fundamental change in the *cis*-to-*trans* reaction observed across compounds **1a**–**5a** can be correlated with the degree of electronic coupling to the surface. Particularly remarkable is the change in kinetics between compounds **3a** and **4a** (Figure 3, right). Since both are structurally closely related and only differ in a methyl group, the kinetic data in solution are very similar. Absorbed on the metal surface, however, their half-lives ($t_{1/2}$), frequency factors (A), and activation energies (E_A) differ drastically (Figure 3). Electronic coupling to the metal surface is still operative in **3a**, whereas the almost orthogonal arrangement of the phenyl rings in **4a** interrupts π-conjugation and electronic coupling. The change from non-standard kinetics in **3a** to classical Arrhenius behaviour in **4a** is thereby clearly related to the breakdown of molecule–substrate coupling. The different activation energies of the compounds **4a**–**5a** in solution and adsorbed on a surface can be explained by the dissimilar environments.

Different hypotheses for the acceleration of *cis*-to-*trans* relaxation processes in molecular adsorbates were discussed. It is known that dense monolayers of azobenzenes on surfaces exhibit increased *cis*-to-*trans* isomerization rates, because intermolecular steric repulsion is larger in the bent *cis* than in the more straight *trans* configuration.[14] Even though this is unlikely to account for the large rate accelarations, we performed further experiments to probe this hypothesis. The large octyl side groups at the TATA platform were replaced by smaller propyl groups (**1b**, **2b**, **5b**), which results in a smaller intermolecular distance in the self-assembled

Parameter \ Molecule		1	2	3	4	5	6
In solution	$t_{1/2}$ (290.5 K)	18.7 h	25.6 h	37.9 h	49.9 h	64.8 h	15.3 h
	k_{obs} (290.5 K)	$1.03\cdot10^{-5}$ s^{-1}	$7.52\cdot10^{-6}$ s^{-1}	$5.08\cdot10^{-6}$ s^{-1}	$3.85\cdot10^{-6}$ s^{-1}	$2.97\cdot10^{-6}$ s^{-1}	$1.26\cdot10^{-5}$ s^{-1}
	E_A (kcal/mol)	24.1	22.6	21.7	21.2	21.5	23.5
	log(A)	13.12	14.02	11.04	10.58	10.67	11.70
On Au(111)	$t_{1/2}$ (290.5 K)	45.3 s	14.9 min	69.6 min	48.4 h	61.6 h	
	k_{obs} (290.5 K)	$1.53\cdot10^{-2}$ s^{-1}	$7.73\cdot10^{-4}$ s^{-1}	$1.66\cdot10^{-4}$ s^{-1}	$3.97\cdot10^{-6}$ s^{-1}	$3.13\cdot10^{-6}$ s^{-1}	
	E_A (kcal/mol)	2.5	2.6	3.6	13.7	14.7	
	log(A)	0.1	-1.2	-1.1	4.9	5.6	
spin density (δ_S)		$6.1\cdot10^{-2}$	$8.1\cdot10^{-3}$	$4.9\cdot10^{-3}$	$1.0\cdot10^{-6}$	$-3.4\cdot10^{-5}$	

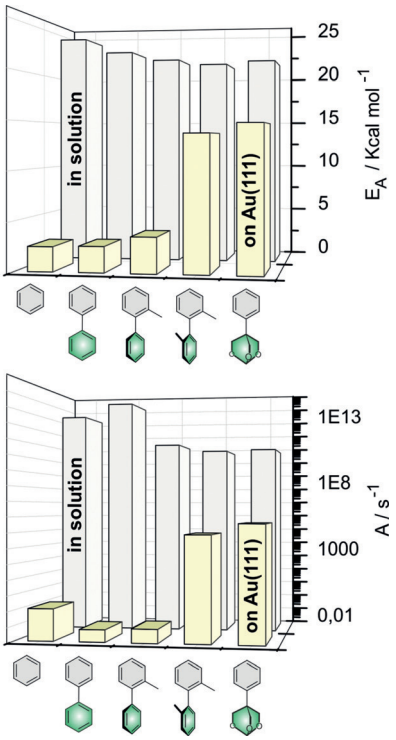

Figure 3. Kinetic data of the *cis–trans* isomerization of compounds 1a–5a and 6 in solution and adsorbed on Au(111). Half-lives ($t_{1/2}$), observed rates (k_{obs}), activation energy (E_a), and frequency factors (A) for azo-TATA compounds (sorted by decreased coupling between platform and azobenzene) are determined in solution (gray), and adsorbed on Au(111) (yellow). Spin densities (δ_s) of **1a**–**5a** in the triplet state are calculated with DFT (M08HX/def2-TZVP) and integrated over all atoms within the platform unit and the ethinyl spacer. For compound **6**, $t_{1/2}$, E_a, and A are presented in solution. More data points and error margins are given in the Supporting Information (Figure S129).

monolayers on Au(111) (octyl: 12.6 Å vs. propyl 10.4 Å).[3–5,10] However, the measured rate accelerations on gold are similar (Figure S129). Steric constraints can therefore be excluded. Moreover, steric confinement would not explain the very low barriers and frequency factors. Traces of absorbed water are also not responsible for the rate acceleration.[15] On the contrary, coincidental water on adsorbed azobenzenes decreases the relaxation rate.[16] Added water also slows down the reaction rates in solution (Figure S133). It is known that charge transfer can accelerate the *cis–trans* isomerization rates of azobenzenes. Azobenzenes that are either oxidized to the corresponding radical cations or reduced to the radical anions exhibit very fast thermal isomerization rates.[17] The low *cis–trans* activation barriers of azobenzenes directly absorbed on gold nanoparticles[18,19] or lying flat on Au(111)[20] or Bi(111)[21] surfaces have been explained by a transfer of electron density from the azobenzene to the metal.[19] To investigate if such a charge transfer would be operative in our system, we synthesized azobenzene **6**, where an Au^+ ion is directly connected to the ethinyl group (Scheme S5). According to the NBO analysis of **6**, the azoethinyl group carries approximately half an elementary charge ($-0.508\,e$). Kinetic analysis, however, reveals that the activation energy (20.3 kcal mol^{-1}) and the frequency factor ($\log(A/s^{-1}) = 13.78$; see Figure 3, right) are in the usual range expected for undisturbed azobenzenes.[22] The strongest argument against static charge transfer is the fact that the IR vibrational frequencies of the *cis* and the *trans* azo-TATA molecules in solution and absorbed on the surface are virtually identical (Figure S123).

The appearance of two different regimes in Figure 3 suggests the existence of two distinct mechanisms. It will be shown that the delocalization of the electronic wavefunction of the azobenzene unit over the entire molecule into the gold plays a key role in this context. A convenient measure of the delocalization is the spin density δ_s at the TATA platform computed for the triplet state (Figure S124): the wavefunction amplitude localized in the bulk gold is approximately proportional to the square root of δ_s for the triplet (T_1) as well as for the singlet (S_0) electronic state (see Supporting Information, Section 1). The plot of $\log(k_{obs})$ vs. $\log(\delta_s)$ shown in Figure 4 reveals that the observed rate constant k_{obs} can be written as a sum of a rate constant k, which is associated with a thermally activated process exhibiting standard Arrhenius-type behaviour, and a rate constant k', which additionally depends upon the square of the spin density at the TATA platform:

The parameters A ($10^{5.6}\ s^{-1}$) and E_A (14.7 kcal mol^{-1}) for the regime associated with k are taken from compound **5a**, serving as a reference system for a surface-deposited azo-TATA molecule with an electronically decoupled azobenzene unit (Figure 3). For k', a significantly reduced apparent barrier height E_A' of 2.7 ± 0.1 kcal mol^{-1} and a prefactor A' of $894 \pm 110\ s^{-1}$ are found by fitting our data to Equation (1) (Figures S130 and S131).

$$k_{obs} = k + k' = A\ exp\left(\frac{-E_A}{RT}\right) + \delta_s^2\ A'\ exp\left(\frac{-E_A'}{RT}\right) \quad (1)$$

The described findings strongly suggest that an electronic transition mediated by the bulk gold is involved in the

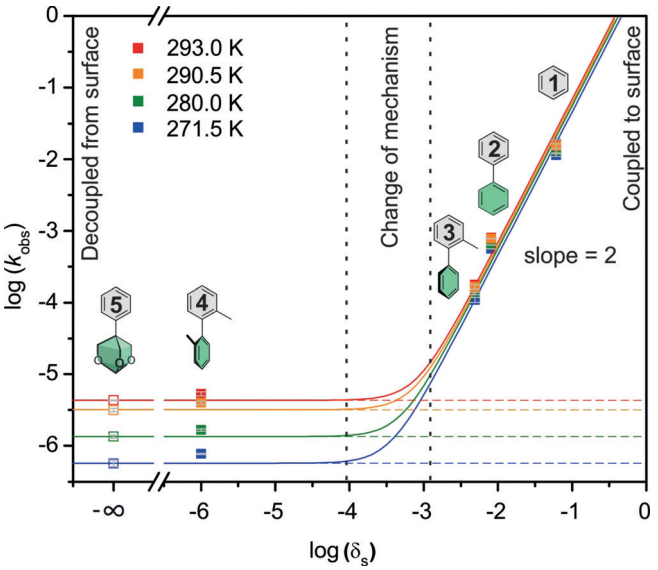

Figure 4. Log(k_{obs}) as a function of log(δ_s) for compounds **1a**–**5a**. δ_s is the spin density of the triplet state of **1a**–**5a** integrated over all atoms of the platform and the ethinyl spacer, calculated with DFT (M08HX/def2-TZVP). Compound **5** serves as a reference molecule without electronic coupling to the surface and a very small value for δ_s (dashed lines). Continuous lines are fitted according to Equation (1).

reaction mechanism associated with the rate constant k'. Two different mechanisms can be imagined: a gold-mediated intersystem crossing (ISC) between the singlet (S_0) and triplet (T_1) states of the azobenzene or a transient charge transfer (CT) between the gold and azo-TATA. By considering the coupling between the different electronic states to be a weak perturbation, k' can be assumed to be proportional to the square of the coupling element that enables the electronic transition (see Supporting Information, Section 1). Since the ISC as well as the CT are enabled by the coupling to the bulk gold, the value of the coupling element is determined by the respective wavefunction amplitudes localized in the bulk gold. The coupling matrix element for the ISC involves the S_0 and T_1 wavefunctions and is thus proportional to δ_s. In contrast, the coupling matrix element for the CT involves the S_0 wavefunction and the wavefunction of the CT state and is proportional to the square root of δ_s (see Supporting Information, Section 1). Thus, only the ISC mechanism is consistent with the observed quadratic δ_s dependence of k'.

The rate enhancement induced by bulk gold described above represents a new type of catalysis. Unlike in conventional heterogeneous catalysis, there is no direct chemical involvement of the surface (no chemical bonds to the surface are made or broken). Instead, the bulk metal opens an alternative pathway with almost vanishing barriers by the mixing of molecular states with the quantum states of gold. Particularly exceptional is the fact that the state transitions occur at room temperature, without photochemical activation, and over a large distance (14 Å, 11 bonds). We used a well-defined, controllable environment to investigate these non-classical effects systematically and propose that a change in spin state is responsible for the drastic rate acceleration. It is quite likely that similar effects are operative in a number of

catalytic processes where molecules react at metal surfaces. Likewise, the controlled coupling of molecules to the conducting band of materials could open new ways to trigger reactions with spatiotemporal control. Such effects may also be exploited to efficiently catalyze chemical reactions or to remote-control molecular machines on surfaces.[23]

Acknowledgements

We thank the Deutsche Forschungsgemeinschaft (SFB 677) for funding this research, the Helmholtz-Zentrum Berlin for the supply of beamtime at the HE-SGM beamline (XPS and NEXAFS measurements), and Martin Kirk for fruitful discussions.

Conflict of interest

The authors declare no conflict of interest.

Keywords: azobenzene · catalysis · self-assembled monolayers · surface spectroscopy · vibrational spectroscopy

How to cite: *Angew. Chem. Int. Ed.* **2019**, *58*, 6574–6578
Angew. Chem. **2019**, *131*, 6646–6650

[1] G. Ertl, H. Knözinger, F. Schüth, J. Weitkamp, *Handbook of Heterogeneous Catalysis*, Wiley-VCH, Weinheim, **2008**.
[2] G. Ertl, *Angew. Chem. Int. Ed.* **2008**, *47*, 3524; *Angew. Chem.* **2008**, *120*, 3578.
[3] B. Baisch, D. Raffa, U. Jung, O. M. Magnussen, C. Nicolas, J. Lacour, J. Kubitschke, R. Herges, *J. Am. Chem. Soc.* **2009**, *131*, 442.
[4] S. Lemke, S. Ulrich, F. Claußen, A. Bloedorn, U. Jung, R. Herges, O. M. Magnussen, *Surf. Sci.* **2015**, *632*, 71.
[5] S. Kuhn, B. Baisch, U. Jung, T. Johannsen, J. Kubitschke, R. Herges, O. Magnussen, *Phys. Chem. Chem. Phys.* **2010**, *12*, 4481.
[6] B. G. Gowenlock, *Q. Rev. Chem. Soc.* **1960**, *14*, 133.
[7] a) A. Hauser, *Coord. Chem. Rev.* **1991**, *111*, 275; b) J. N. Harvey, *Phys. Chem. Chem. Phys.* **2007**, *9*, 331; c) P. R. Schreiner, H. P. Reisenauer, F. C. Pickard, A. C. Simmonett, W. D. Allen, E. Mátyus, A. G. Császár, *Nature* **2008**, *453*, 906.
[8] U. Jung, C. Schütt, O. Filinova, J. Kubitschke, R. Herges, O. Magnussen, *J. Phys. Chem. C* **2012**, *116*, 25943.
[9] N. R. Krekiehn, M. Müller, U. Jung, S. Ulrich, R. Herges, O. M. Magnussen, *Langmuir* **2015**, *31*, 8362.
[10] H. Jacob, S. Ulrich, U. Jung, S. Lemke, T. Rusch, C. Schütt, F. Petersen, T. Strunskus, O. Magnussen, R. Herges, et al., *Phys. Chem. Chem. Phys.* **2014**, *16*, 22643.
[11] a) A. Mishchenko, L. A. Zotti, D. Vonlanthen, M. Bürkle, F. Pauly, J. C. Cuevas, M. Mayor, T. Wandlowski, *J. Am. Chem. Soc.* **2011**, *133*, 184; b) A. Mishchenko, D. Vonlanthen, V. Meded, M. Bürkle, C. Li, I. V. Pobelov, A. Bagrets, J. K. Viljas, F. Pauly, F. Evers, et al., *Nano Lett.* **2010**, *10*, 156; c) M. L. Kirk, D. A. Shultz, D. E. Stasiw, G. F. Lewis, G. Wang, C. L. Brannen, R. D. Sommer, P. D. Boyle, *J. Am. Chem. Soc.* **2013**, *135*, 17144.
[12] S. Ulrich, U. Jung, T. Strunskus, C. Schütt, A. Bloedorn, S. Lemke, E. Ludwig, L. Kipp, F. Faupel, O. Magnussen, et al., *Phys. Chem. Chem. Phys.* **2015**, *17*, 17053.
[13] a) X. Yu, Z. Wang, M. Buchholz, N. Füllgrabe, S. Grosjean, F. Bebensee, S. Bräse, C. Wöll, L. Heinke, *Phys. Chem. Chem. Phys.* **2015**, *17*, 22721; b) R. G. Greenler, *J. Chem. Phys.* **1966**, *44*, 310.
[14] a) M. Kaneta, T. Honda, K. Onda, M. Han, *New J. Chem.* **2017**, *41*, 1827; b) S. D. Evans, S. R. Johnson, H. Ringsdorf, L. M. Williams, H. Wolf, *Langmuir* **1998**, *14*, 6436.
[15] A. Muždalo, P. Saalfrank, J. Vreede, M. Santer, *J. Chem. Theory Comput.* **2018**, *14*, 2042.
[16] T. Moldt, D. Przyrembel, M. Schulze, W. Bronsch, L. Boie, D. Brete, C. Gahl, R. Klajn, P. Tegeder, M. Weinelt, *Langmuir* **2016**, *32*, 10795.
[17] a) A. Goulet-Hanssens, M. Utecht, D. Mutruc, E. Titov, J. Schwarz, L. Grubert, D. Bléger, P. Saalfrank, S. Hecht, *J. Am. Chem. Soc.* **2017**, *139*, 335; b) X. Tong, M. Pelletier, A. Lasia, Y. Zhao, *Angew. Chem. Int. Ed.* **2008**, *47*, 3596; *Angew. Chem.* **2008**, *120*, 3652.
[18] G. L. Hallett-Tapley, C. D'Alfonso, N. L. Pacioni, C. D. McTiernan, M. González-Béjar, O. Lanzalunga, E. I. Alarcon, J. C. Scaiano, *Chem. Commun.* **2013**, *49*, 10073.
[19] E. Titov, L. Lysyakova, N. Lomadze, A. V. Kabashin, P. Saalfrank, S. Santer, *J. Phys. Chem. C* **2015**, *119*, 17369.
[20] S. Hagen, P. Kate, M. V. Peters, S. Hecht, M. Wolf, P. Tegeder, *Appl. Phys. A* **2008**, *93*, 253.
[21] C. Bronner, P. Tegeder, *New J. Phys.* **2014**, *16*, 053004.
[22] P. Bortolus, L. Flamigni, S. Monti, M. Bolte, G. Guyot, *J. Chem. Soc. Faraday Trans.* **1991**, *87*, 1303.
[23] a) T. Kudernac, N. Ruangsupapichat, M. Parschau, B. Maciá, N. Katsonis, S. R. Harutyunyan, K.-H. Ernst, B. L. Feringa, *Nature* **2011**, *479*, 208; b) R. A. van Delden, M. K. J. ter Wiel, M. M. Pollard, J. Vicario, N. Koumura, B. L. Feringa, *Nature* **2005**, *437*, 1337.

Manuscript received: December 18, 2018
Revised manuscript received: January 30, 2019
Accepted manuscript online: February 22, 2019
Version of record online: April 12, 2019

Angewandte Chemie
Eine Zeitschrift der Gesellschaft Deutscher Chemiker

Supporting Information

Long-Distance Rate Acceleration by Bulk Gold

Alexander Schlimm, Roland Löw, Talina Rusch, Fynn Röhricht, Thomas Strunskus, Tobias Tellkamp, Frank Sönnichsen, Uwe Manthe, Olaf Magnussen, Felix Tuczek,* and Rainer Herges**

anie_201814342_sm_miscellaneous_information.pdf

Author Contributions

R.H. Conceptualization: Lead; Data curation: Supporting; Formal analysis: Supporting; Funding acquisition: Equal; Investigation: Supporting; Methodology: Supporting; Project administration: Lead; Resources: Supporting; Supervision: Equal; Visualization: Equal; Writing—original draft: Lead; Writing—review & editing: Lead
A.S. Data curation: Equal; Formal analysis: Supporting; Investigation: Supporting; Methodology: Supporting; Validation: Supporting; Visualization: Supporting; Writing—original draft: Supporting; Writing—review & editing: Supporting; NEXAFS, XPS, IRRAS, evaluation of data: Lead
R.L. Data curation: Supporting; Formal analysis: Supporting; Investigation: Supporting; Methodology: Supporting; Validation: Supporting; Writing—original draft: Supporting; Writing—review & editing: Supporting; Synthesis of the compounds: Lead
T.R. Data curation: Supporting; Formal analysis: Supporting; Methodology: Equal; Writing—original draft: Supporting; Writing—review & editing: Supporting; STM measurements and interpretation: Lead
F.R. Data curation: Supporting; Formal analysis: Supporting; Validation: Supporting; Writing—review & editing: Supporting; theoretical calculations DFT: Lead
T.S. Data curation: Supporting; Investigation: Supporting; Methodology: Supporting; Validation: Supporting; NEXAFS, XPS: Supporting
T.T. synthesis: Supporting
F.S. Data curation: Supporting; Formal analysis: Supporting; Methodology: Supporting; Validation: Supporting; Writing—original draft: Supporting; Writing—review & editing: Supporting; NMR: Lead
U.M. Conceptualization: Supporting; Formal analysis: Supporting; Writing—original draft: Supporting; Writing—review & editing: Supporting; theoretical part, non-adiabatic analysis of the data: Lead
O.M. Conceptualization: Supporting; Data curation: Supporting; Formal analysis: Supporting; Funding acquisition: Supporting; Investigation: Supporting; Methodology: Equal; Supervision: Supporting; Validation: Supporting; Writing—original draft: Supporting; Writing—review & editing: Supporting; supervision of the STM part: Lead
F.t. Conceptualization: Supporting; Data curation: Supporting; Formal analysis: Supporting; Funding acquisition: Equal; Investigation: Supporting; Methodology: Supporting; Project administration: Equal; Supervision: Equal; Validation: Supporting; Writing—original draft: Supporting; Writing—review & editing: Equal; supervised the NEXAFS, XPS, IRRAS measurements, kinetic analysis: Lead.

Content

1. Theoretical considerations

Within rigorous quantum theory, the thermal rate constant of a chemical reaction can be written as[1]

$$k(T) = \frac{1}{Q_r(T)} \lim_{t\to\infty} tr\left(e^{\frac{i}{\hbar}\hat{H}t}\, h\, e^{-\frac{i}{\hbar}\hat{H}t}\, e^{-\frac{\hat{H}}{k_B T}}\, \hat{F} \right) = \frac{1}{Q_r(T)} tr\left(\hat{P}_{prod} e^{-\frac{\hat{H}}{k_B T}}\, \hat{F} \right) \quad 1$$

where $\hat{H}$ is the system's Hamiltonian, $\hat{F}$ an operator measuring the flux through a dividing surface separating reactants and product, *h* a heavyside function which equals unity for products and vanishes for reactants, $Q_r(T)$ the partition function of the reactant, and k_B the Boltzmann constant. Note that the dividing surfaces used in $\hat{F}$ and *h* can be chosen independently and that the resulting *k(T)* is independent of the specific choices. The operator

$$\hat{P}_{prod} = \lim_{t\to\infty} e^{\frac{i}{\hbar}\hat{H}t}\, h\, e^{-\frac{i}{\hbar}\hat{H}t} \quad 2$$

present in Eq.(2) has an intuitive interpretation: it projects onto wavefunction components which will become products in the infinite future. Thus, the thermal rate constant is given by the thermally averaged flux through a dividing surface which will turn into product in the infinite future.

We now consider a reaction system with two electronic states as schematically depicted in Fig.1. Here reactants and products are in the same electronic state, state 1. The reaction can proceed either by remaining in state one and passing a higher reaction barrier or via a lower energy pathway which includes an intermediate transition to state 2. The Hamiltonian of the system can written as

$$\hat{H} = \hat{H}_1 + \hat{H}_2 + \hat{H}_{12} \quad 3$$

where $\hat{H}_1$ describes the nuclear motion in the electronic state 1, $\hat{H}_2$ the nuclear motion in the electronic state 2, and $\hat{H}_{12}$ the electronic transitions.

If the coupling between the two electronic states is sufficently weak, the reaction proceeds entirely in the electronic state 1 and the full Hamiltonian $\hat{H}$ can be replaced by $\hat{H}_1$ in Eq.(1). Positioning the dividing surface used in $\hat{F}$ and *h* at the top of the barrier (x_0 in Fig.S1), ignoring quantum effects, and invoking the no-recrossing approximation, the classical transition state theory expression for the thermal rate constant can obtained.

Alternatively, one can consider the case that the reaction barrier in the electronic state 1 is very high and reaction occurs only via an intermediate electronic transition. Assuming that electronic transitions are rare, the identity

$$e^{-\frac{i}{\hbar}\hat{H}t} = e^{-\frac{i}{\hbar}(\hat{H}_1+\hat{H}_2)t} + \frac{1}{i\hbar}\int_0^t dt'\, e^{-\frac{i}{\hbar}\hat{H}(t-t')}\hat{H}_{12} e^{-\frac{i}{\hbar}(\hat{H}_1+\hat{H}_2)t'} \quad 4$$

can be favorably employed. Positioning the dividing surface used in $\hat{F}$ at the first crossing point x_1 and the dividing surface used in *h* at the second crossing point x_2, Eq.(1) then takes the form

$$k(T) = \frac{1}{Q_r(T)} \frac{1}{\hbar^2} \int_0^\infty dt' \int_0^\infty dt'' \, tr \left(e^{\frac{i}{\hbar}\hat{H}_1 t'} \hat{H}_{12}^\dagger \, e^{-\frac{i}{\hbar}\hat{H} t'} \, \hat{P}_{prod} \, e^{\frac{i}{\hbar}\hat{H} t''} \hat{H}_{12} \, e^{-\frac{i}{\hbar}\hat{H}_1 t''} \, e^{-\frac{\hat{H}}{k_B T}} \hat{F} \right). \qquad 5$$

This expression again can be interpreted intuitively: The thermally averaged flux passing through the first dividing surface undergoes a transition from electronic state 1 to electronic state 2 after a time *t''*. Then one measures whether products are formed before the back-propagation is started. Assuming that after the electronic transition from state 1 to state 2 the process continues towards products (the analog of the no recrossing approximation used in transition state theory), the leading term in a perturbative expansion in $\hat{H}_{12}$ for the rate constant reads

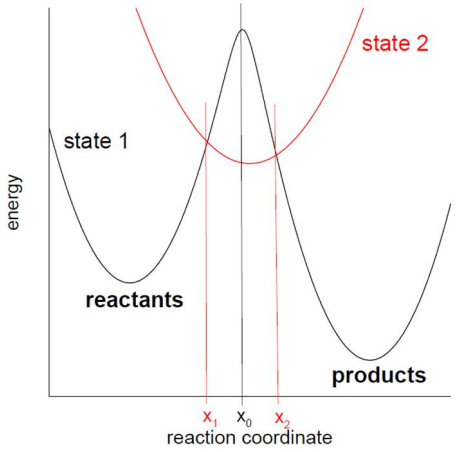

Figure S1. Schematic representation of reaction system with a second electronic state which enhances reactivity (see text for details).

$$k(T) = \frac{1}{Q_r(T)} \frac{1}{\hbar^2} \int_0^\infty dt' \int_0^\infty dt'' \, tr \left(e^{\frac{i}{\hbar}\hat{H}_1 t'} \hat{H}_{12}^\dagger \, e^{-\frac{i}{\hbar}\hat{H}_2 (t'-t'')} \, \hat{H}_{12} \, e^{-\frac{i}{\hbar}\hat{H}_1 t''} \, e^{-\frac{\hat{H}}{k_B T}} \hat{F} \right). \qquad 6$$

Thus, for weak coupling between the two electonic states the thermal rate constant will generally be proportional to the square of the coupling operator $\hat{H}_{12}$.

Employing a semiclassical approach, transition theory-type formulas for the rate constants of reactions with electronic transitions have been derived (see, e.g., Refs. 2, 3 and references therein for recent work on the subject). The resulting formulae combine squared matrix elements of $\hat{H}_{12}$ with a Arrhenius-type $exp\left(-\frac{E_{crossing}}{k_B T}\right)$ factor, where $E_{crossing}$ is the (minimal) energy of the crossing of the two potential energy surfaces (in Fig.1 this would be the energy at the coordinate values x_1). Thus, the energy at the crossing point takes the role of an apparent barrier height in the Arrhenius factor.

Rate constants where the leading term depends on the fourth power of the coupling operator $\hat{H}_{12}$ can only appear when the system after the electronic transition from state 1 to state 2 does not continue to form products but mainly transfers back to the reactant region of state 1. A dominant back transfer is statistically improbable and only occurs under special circumstances.

It is typically observed if the passage through state 2 can only be facilitated via a narrow resonance. Then all compentents of the incoming wavepacket which do match the resonance condition are reflected since they only give rise to a short lived virtual population of state 2 and do not continue towards products.

In the adsorbed azobenzene-TATA system studied in this work, two different types of electronic transitions have to be discussed. First, reaction via an intermediate transfer to the triplet state. Then state 2 in Fig. S1 represents the T_1 triplet state of the adsorbed azobenzene and state 1 its S_0 state. The coupling operator $\hat{H}_{12}$ describes transitions between the two electronic states. Since the S_0-T_1 conversion is facilitated by the coupling to the bulk gold, the electronic transition matrix element $<S_0|\hat{H}_{12}|T_1>$ is proportional to the component of S_0 electronic wavefunction localized in the bulk gold. It is also proportional to the component of T_1 electronic wavefunction localized in the bulk gold. Assuming that the electronic wavefunction component localized in the bulk gold is proportional to the electronic wavefunction component localized in the TATA group, the spin density in the TATA group can be employed to monitor the size of the coupling.

In the T_1 state, one unpaired electron is present at each of the two nitrogens of the azo group. Since the N-N-bond is twisted at the equilibrium geometry of the T_1 state, only the unpaired electron on the nearer N atom, called N1 in the following, is coupled to the TATA fragment. The electronic wavefunction for the electron mainly localized on N1 thus reads

$$\psi_1 = c_1 \cdot \psi_{N1} + \lambda \cdot \psi_{TATA} + \ldots \quad (7)$$

while the wavefunction for the electron mainly localized on N2 reads

$$\psi_2 = c_2 \cdot \psi_{N2} + \ldots \quad (8)$$

Here ψ_{N1}, ψ_{N2}, and ψ_{TATA} denote wavefunctions localized at atom N1, atom N2, and the TATA group, respectively, and c_1, c_2, and λ denote coefficients characterizing the magnitude of the wavefunction amplitude at the respective group or atom. Combining both one-electron wavefunctions to the two-electron wavefunction describing the T_1 state, one finds that the resulting spin density δ_s on the TATA fragment is

$$\delta_s = \lambda^2. \quad (9)$$

Furthermore, one finds that the (two-electron) wavefunction amplitude present at the TATA fragment is proportional to λ for the T_1 as well as for the S_0 state. Consequently, the matrix element $<S_0|\hat{H}_{12}|T_1>$ is proportional to λ^2 and, equivalently, proportional to δ_s. Thus, for the $S_0 \rightarrow T_1 \rightarrow S_0$ process the experimentially observed δ_s^2-dependence of the rate constant is perfectly compatible with our expectations discussed in context of Eq.(6).

We now consider the alternative mechanism which involves a charge transfer between the azo group and the bulk gold. Then state 2 actually does not represent a single electronic state but

a continuum of electronic states associated with the charged azo group and the hole or electron generated in the bulk gold. The corresponding coupling matrix element for the electronic transition is $< S_0 | \widehat{H}_{12} | CTstate >$ and only linearly depends on λ. Thus, for the CT process the experimentially observed δ_s^2-dependence of the rate constant is only compatible with a theoretical rate constant expression which show a quartic dependence on $\widehat{H}_{12}$.

Quartic dependencies of the rate on $\widehat{H}_{12}$ typically require the existence of narrow resonances which support the reaction processes. While such scenarios appear in process involving “pure” electron transfer, like electron transfer through a bridging ligand or a molecule located in a break junction, they are hardly imaginable for processes involving large amplitude motion of nuclei.[4] The time scale of the movement of large molecular groups, like the phenyl ring in the present system, is typically much larger than the time scale of relaxation processes which destroy the required quantum coherence.

2. Syntheses

All Azo-TATA compounds have been synthesized with octyl (a) and propyl (b) side chains. But only the compounds with octyl side chains have been exhaustively investigated adsorbed on a gold surface because the obtained adlayers had a higher reproducibility than for the propyl compounds (b). Moreover all octyl compounds (a) showed the same superstructure with higher intermolecular distances than for the propyl compounds (b). In this way, we made sure that the azobenzene has enough space for the *cis*/*trans* isomerization.

Materials and Methods

Most reagents were purchased from Acros Organics, Alfa Aesar, Chempur, Matrix Scientific, Merck, Sigma Aldrich or TCI and were used as received. Solvents for extraction and chromatography were technical grade. Most solvents used in reactions were extra dried (abs.) or used as received. Analytical TLC was performed with Polygeram® SilG/UV254 (Macherey Nagel, 0.2 mm paricle size) and visualization was accomplished by UV light. Flash chromatography was carried out using 0.040-0.063 nm silica gel (Merck). Solvents for spectroscopic studies were of spectrophotometric grade (Deutero). NMR spectra were recorded on Bruker (ARX300), Bruker (DRX 500) and Bruker (AV 600) spectrometers. Chemical shifts are denoted in parts per million (ppm) relative to the residual solvent peak (acetone-d_6: ^{1}H δ = 2.05 ppm, ^{13}C δ = 29.84 ppm, $CDCl_3$: ^{1}H δ = 7.26 ppm, ^{13}C δ = 77.16 ppm, C_6D_6: ^{1}H δ = 7.16 ppm, ^{13}C δ = 128.06 ppm, DMSO-d_6: ^{1}H δ = 2.50 ppm, ^{13}C δ = 29.52 ppm) or to the residual peak of tetramethylsilane. The splitting parameters are designated as follows: s = singlet, d = doublet, t = triplet, q = quartet, m = multiplet, dd = doublet of doublets, ddd = doublet of doublet of doublets. High-resolution mass spectrometry (EIMS) was performed on an AccuTOF GCv 4G (Joel) spectrometer with EI ionization and (ESIMS) was performed on a Thermo Scienific™ Q Exactive™ Plus spectrometer with ESI ionization. Matrix-assisted Laser Desorption/Ionization (MALDI) mass spectra were measured with a Biflex III by co. Bruker. Infrared spectra were measured on a Perkin-Elmer 1600 Series FT-IR spectrometer with an A531-G Golden-Gate-Diamond-ATR-unit. Signals were abbreviated with w, m, s and vs for weak, medium, strong and very strong intensities. Broad signals were additionally labeled with br. The following compounds were prepared according to procedures described in the literature: 4-(2-trimethylsilyl)ethynyl-aniline, (*E*)-1-(4-methoxyphenyl)-2-(4-((trimethylsilyl)-ethynyl)phenyl)diazene, (*E*)-12*c*-[4-(4-methoxyphenyldiazenyl)phenyl]ethynyl-4,8,12-tri-*n*-octyl-4,8,12-triazatriangulene, 4-iodo-4‘-nitro-1,1‘-biphenyl, 4‘-iodo-[1,1‘-biphenyl]-4-amine, 4-Amino-4‘-((trimethylsilyl)ethynyl)biphenyl, 1-bromo-4-[2-(trimethylsilyl)ethynyl]-benzene, 4,4,5,5-tetramethyl-2[-4-[2-(trimethylsilyl)ethynyl]phenyl]-1,3,2-dioxaborolane, 1-bromo-4-iodo-methyl-benzene, 1-bromo-2-methyl-4-[2-(trimethylsilyl)ethynyl]-benzene, trimethyl(3,3,3-

triethoxyprop-1-in-1-yl)silane, 2-(hydroxymethyl)-2-(4-nitrophenyl)propane-1,3-diol, 2-(4-aminophenyl)-2-(hydroxymethyl)propane-1,3-diol, 1-(4-ethynylphenyl)-2-phenyl-diazene.

2.1 Synthesis of compound 1a and 1b:

The azo ethynyl TATA platforms with octyl or propyl side chains were synthesized in 4 steps and the methoxy azobenzene **9**, the TATA platforms **7**/**8** and **1a** were synthesized as reported in literature.[5] The azobenzene **9** was functionalized at the central carbo cation of the platforms **7** and **8** to obtain the final products **1a** and **1b**.

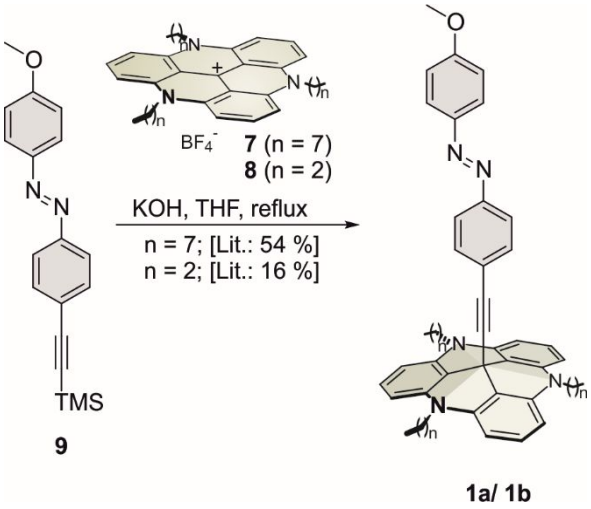

Scheme S1: Synthesis route of compound **1a** and **1b**.

Synthesis of (*E*)-12*c*-[4-(4-methoxyphenyldiazenyl)phenyl]ethynyl-4,8,12-tri-*n*-octyl-4,8,12-triazatriangulene (1a):
In tetrahydrofuran (abs., 50 mL) (*E*)-1-(4-methoxyphenyl)-2-(4-((trimethylsilyl)-ethynyl)phenyl)diazene (178 mg, 528 µmol) was dissolved under nitrogen atmosphere, octyl-TATA-BF_4 (400 mg, 647 µmol) and crushed potassium hydroxide (203 mg, 3.63 mmol) were added and the mixture was refluxed for 24 h. The solution was poured onto H_2O (50 mL) and the aqueous phase was extracted with diethylether (4x 50 mL). The combined organic layers were dried over magnesium sulfate and the solvent was removed under reduced pressure. The crude product was purified via column chromatography (alox basic, diethylether) to obtain an orange solid (379 mg, 443 µmol, 69%).

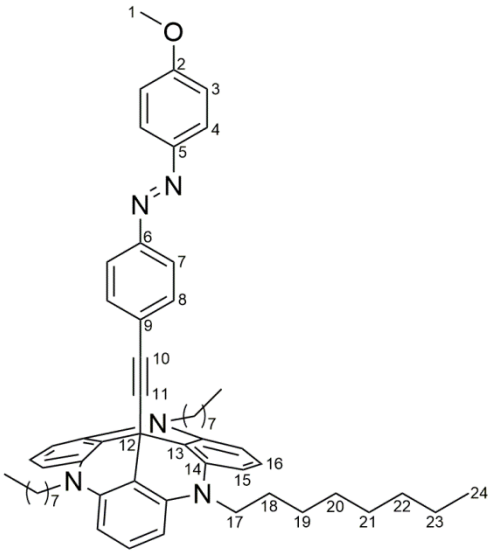

^{1}H-NMR (500.1 MHz, acetone-d_6, 300 K, TMS): δ = 7.87 (d, ^3J = 9.2 Hz, 2 H, *H*-4), 7.70 (d, ^3J = 8.8 Hz, 2 H, *H*-7), 7.25-7.19 (m, 5 H, *H*-8, *H*-16), 7.08 (d, ^3J = 9.2 Hz, 2 H, *H*-3), 6.69 (d, ^3J = 8.3 Hz, 6 H, *H*-15), 4.03 (t, ^3J = 7.6 Hz, 6 H, *H*-17), 3.89 (s, 3 H, *H*-1), 1.85 (ps. quint., 6 H, *H*-18), 1.51 (ps. quint., 6 H, *H*-19), 1.38 (ps. quint., 6 H, *H*-20), 1.32-1.18 (m, 18 H, *H*-21, *H*-22, *H*-23), 0.84 (ps. t, 9 H, *H*-24) ppm.
^{13}C-NMR (125.8 MHz, acetone-d_6, 300 K, TMS): δ = 163.54 (s, *C*-2), 152.32 (s, *C*-6), 147.70 (s, *C*-5), 141.49 (s, *C*-14), 132.94 (s, *C*-8), 129.46 (s, *C*-16), 125.58 (s, *C*-4), 123.18 (s, *C*-7), 115.28 (s, *C*-3), 111.04 (s, *C*-13), 106.17 (s, *C*-15), 84.18 (s, *C*-10), 56.07 (s, *C*-1), 46.70 (s, *C*-17), 32.63 (s, *C*-22), 30.21 (s, *C*-20), 30.10 (s, *C*-21), 27.53 (s, *C*-19), 26.84 (s, *C*-18), 23.32 (s, *C*-23), 14.39 (s, *C*-24) ppm.

Synthesis of (*E*)-12*c*-[4-(4-methoxyphenyldiazenyl)phenyl]ethynyl-4,8,12-tri-*n*-propyl-4,8,12-triazatriangulene (1b):
In tetrahydrofuran (abs., 60 mL) (*E*)-1-(4-methoxyphenyl)-2-(4-((trimethylsilyl)-ethynyl)phenyl)diazene (100 mg, 324 µmol) was dissolved under nitrogen atmosphere, propyl-TATA-BF_4 (177 mg, 357 µmol) and crushed potassium hydroxide (109 mg, 1.94 mmol) were

added and the mixture was refluxed for 16 h. The solution was poured onto saturated sodium chloride solution (50 mL) and was extracted with diethylether (3x 70 mL). The combined organic layers were dried over magnesium sulfate and the solvent was removed under reduced pressure. The crude product was purified via column chromatography (alox basic, diethylether) to obtain an orange solid (34.0 mg, 52.8 µmol, 16%).

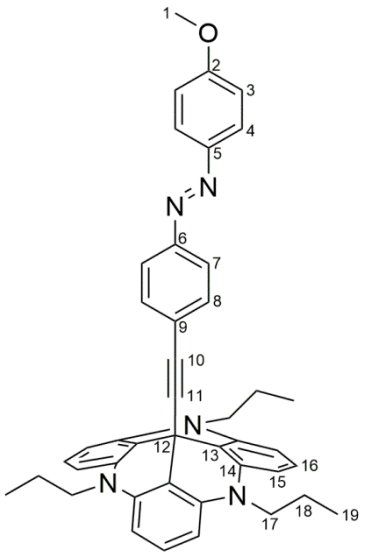

^{1}H-NMR (500.1 MHz, $CDCl_3$, 300 K, TMS): δ = 7.85 (m, 2 H, *H*-4), 7.63 (m, 2 H, *H*-7), 7.23-7.17 (m, 5 H, *H*-8, *H*-16), 6.97 (m, 2 H, *H*-3), 6.55 (d, ^{3}J = 8.3 Hz, 6 H, *H*-15), 3.93-3.87 (m, 6 H, *H*-17), 3.87 (s, 3 H, *H*-1), 1.92-1.82 (m, 6 H, *H*-18), 1.05 (ps. t, 9 H, *H*-19) ppm.

^{13}C-NMR (125.8 MHz, $CDCl_3$, 300 K, TMS): δ = 162.08 (s, *C*-2), 151.27 (s, *C*-6), 147.02 (s, *C*-5), 140.55 (s, *C*-14), 132.30 (s, *C*-8), 128.23 (s, *C*-16), 126.21 (s, *C*-9), 124.73 (s, *C*-4), 122.06 (s, *C*-7), 114.19 (s, *C*-3), 110.10 (s, *C*-13), 105.01 (s, *C*-15), 95.85 (s, *C*-11), 83.56 (s, *C*-12), 55.57 (s, *C*-1), 48.08 (s, *C*-17), 19.16 (s, *C*-18), 11.19 (s, *C*-19) ppm.

MS (Maldi-TOF, Cl-CCA): m/z = 643.7 $[M]^+$.

m.p. = 223.2 °C

IR: $\tilde{\nu}$ = 2955.2 (w), 2155.9 (m), 1599.5 (m), 1497.6 (m), 1244.9 (s), 1140.3 (m), 1030.2 (m), 836.4 (vs), 756.9 (s), 561.0 (s) cm^{-1}.

2.2 Synthesis of Compound 2a, 2b, 3a, 3b, 4a, 4b

The compounds **2**-**4** were synthesized in 6 or 7 steps from commercially available chemicals. The azo benzenes **22**, **23** and **24** as the precursor molecules were connected to platforms with octyl or propyl sidechains in yields between 87-96 %. Compounds **10**, **11** and **16** were

synthesized as described in the literature.[6] Compound **12** was synthesized analogously to the literature.[7]

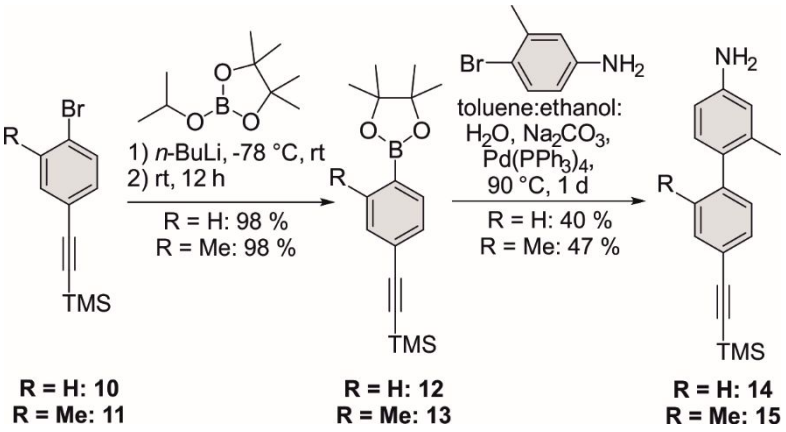

Scheme S2: Synthesis routes of different substituted amino biphenyls **14** and **15**.

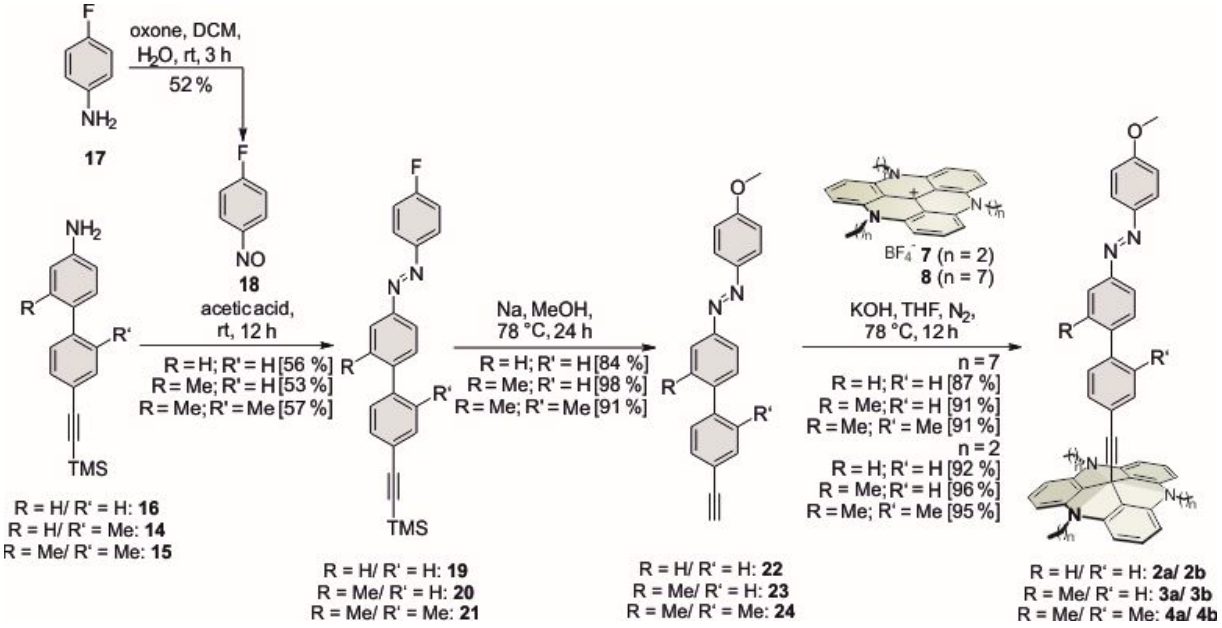

Scheme S3: Synthesis routes out of subtituted amino biphenyls for the preparation of compound **2a**, **2b**, **3a**, **3b**, **4a** and **4b**.

Synthesis of (*E*)-1-(4-fluorophenyl-2-(4-(4-((trimethylsilyl)ethynyl)phenyl)-phenyl) diazene (19):

To the solution of 4-amino-4'-((trimethylsilyl)ethynyl)biphenyl (500 mg, 1.89 mmol) in acetic acid (30 mL) 1-fluoro-4-nitrosobenzene (536 mg, 429 mmol) was added and stirred for 22 h at room temperature. The solid was filtered and recrystallized from ethanol to obtain an orange solid (395 g, 1.06 mmol, 56%).

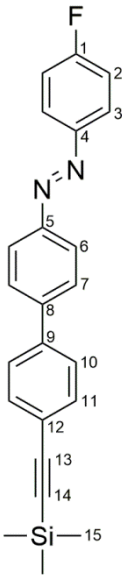

^{1}H-NMR (500.1 MHz, $CDCl_3$, 300 K, TMS): δ = 8.02-7.93 (m, 4 H, *H*-6, *H*-3), 7.74 (d, ^{3}J = 7.4 Hz, 2 H, *H*-7), 7.61 (d, ^{3}J = 8.5 Hz, 2 H, *H*-10), 7.56 (d, ^{3}J = 8.5 Hz, 2 H, *H*-11), 7.21 (m, 2 H, *H*-2), 0.28 (s, 9 H, *H*-15) ppm.

^{13}C-NMR (125.8 MHz, $CDCl_3$, 300 K, TMS): δ = 164.71 (d, ^{1}J = 252.0 Hz, *C*-1), 151.92 (s, *C*-5), 149.43 (s, *C*-4), 142.95 (s, *C*-8), 140.18 (s, *C*-9), 132.66 (s, *C*-11), 127.84 (s, *C*-7), 127.05 (s, *C*-10), 125.02 (s, *C*-3), 123.55 (s, *C*-6), 122.89 (s, *C*-12), 116.13 (s, *C*-2), 104.93 (s, *C*-13), 95.62 (s, *C*-14), 0.13 (s, *C*-15) ppm.

^{19}F-NMR (470.6 MHz, $CDCl_3$, 300 K, TMS): δ = 109.26 ppm.

^{29}Si-NMR (99.4 MHz, $CDCl_3$, 300 K, TMS): δ = -17.63 ppm.

MS (EI, 70eV): m/z = 372.19 $[M]^+$.

IR: $\tilde{\nu}$ = 2961.4 (w), 2158.8 (m), 1590.7 (m), 1485.6 (m) , 1246.4 (m), 1217.0 (m), 838.2 (vs), 823.4 (vs), 759.4 (s) cm^{-1}.

m.p.: 202.3 °C.

Elemental analysis: $C_{23}H_{21}FN_2Si$ Calc.: C 74.16, H 5.68, N 7.52,

Found: C 71.95, H 5.88, N 7.28.

Synthesis of (*E*)-1-(4-methoxyphenyl-2-(4-(4-(ethynyl)phenyl)-phenyl)diazene (22):

In methanol (190 mL) sodium (10.3 g, 449 mmol) was dissolved at room temperature and (*E*)-1-(4-fluorophenyl-2-(4-(4-((trimethylsilyl)ethynyl)phenyl)-phenyl)diazene (644 mg, 1.88 mmol) was added. The suspension was refluxed for 21 h. Water (100 mL) was added to the solution and aqueous phase was extracted with dichloromethane (3x 150 mL). The combined organic layers were dried over magnesium sulfate and the solvent was removed under reduced pressure. The crude product was purified via column chromatography (silica gel, dichloromethane) to obtain an orange solid (480 mg, 1.56 mmol, 84%).

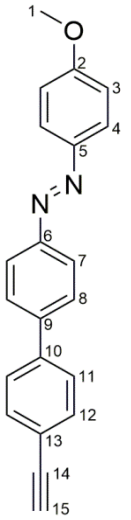

^{1}H-NMR (500.1 MHz, $CDCl_3$, 300 K, $CHCl_3$) δ = 7.99-7.92 (m, 4 H, *H*-4, *H*-7), 7.73 (d, ^{3}J = 8.7 Hz, 2 H, *H*-8), 7.63 (d, ^{3}J = 8.4 Hz, 2 H, *H*-11), 7.59 (d, ^{3}J = 8.4 Hz, 2 H, *H*-12), 7.03 (d, ^{3}J = 9.03 Hz, 2 H, *H*-3), 3.91 (s, 3 H, *H*-1), 3.16 (s, 1 H, *H*-15) ppm.

^{13}C-NMR (125.8 MHz, $CDCl_3$, 300 K, $CHCl_3$) δ = 162.17 (s, *C*-2), 152.15 (s, *C*-6), 147.13 (s, *C*-5), 141.99 (s, *C*-9), 140.64 (s, *C*-10), 132.64 (s, *C*-12), 127.65 (s, *C*-8), 127.00 (s, *C*-11), 124.83 (s, *C*-4), 123.15 (s, *C*-7), 121.49 (s, *C*-13), 114.26 (s, *C*-3), 83.45 (s, *C*-14), 78.09 (s, *C*-15), 55.60 (s, *C*-1) ppm.

MS (EI, 70eV): m/z (%) = 312.12 $[M]^{+}$.

IR: $\tilde{\nu}$ = 3255.6 (w), 1580.5 (m), 1485.6 (m), 1398.2 (w), 1243.5 (s), 1140.1 (m), 1105.6 (m), 1026.1 (s), 1026.1 (s), 839.5 (vs), 825.5 (vs) cm^{-1}.

m.p.: 222.8 °C.

Elemental analysis: $C_{21}H_{16}N_2O$ Calc.: C 80.75, H 5.16, N 8.97,
Found: C 80.37, H 5.29, N 8.76.

Synthesis of (*E*)-12c-(4-(4-(methoxyphenyldiazenyl)phenyl)phenyl)ethynyl-4,8,12-tri-*n*-octyl-4,8,12-triazatriangulene (2a):

In tetrahydrofuran (abs., 80 mL) (*E*)-1-(4-methoxyphenyl-2-(4-(4-(ethynyl)phenyl)-phenyl)diazene (100 mg, 320 µmol) was dissolved under nitrogen atmosphere, octyl-TATA-BF_4 (249 mg, 352 µmol) and crushed potassium hydroxide (193 mg, 3.44 mmol) were added and the mixture was refluxed for 18 h. The reaction mixture was poured onto half saturated sodium chloride solution (100 mL). The organic layer was washed with water (100 mL) and the water layer was extracted with diethylether (3x 100 mL). The combined organic layers were dried over magnesium sulfate and the solvent was removed under reduced pressure. The crude product was purified via column chromatography (alox basic, diethylether) to obtain an orange solid (258 mg, 277 µmol, 87%).

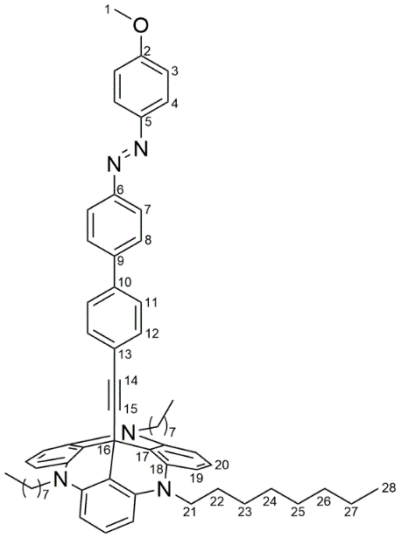

^{1}H-NMR (600.1 MHz, acetone-d_6, 300 K, acetone) δ = 7.93 (m, 4 H, *H*-4, *H*-7), 7.78 (d, ^3J = 8.6 Hz, 2 H, *H*-8), 7.60 (d, ^3J = 8.3 Hz, 2 H, *H*-11), 7.22 (t, ^3J = 8.3 Hz, 3 H, *H*-20), 7.19 (d, ^3J = 8.3 Hz, 2 H, *H*-12), 7.12 (d, ^3J = 9.0 Hz, 2 H, *H*-3), 6.69 (d, ^3J = 8.4 Hz, 6 H, *H*-19), 4.03 (t, ^3J = 7.6 Hz, 6 H, *H*-21), 3.91 (s, 3 H, *H*-1), 1.86 (ps. quint., 6 H, *H*-22), 1.53 (ps. quint., 6 H, *H*-23), 1.39 (ps. quint., 6 H, *H*-24), 1.32-1.21 (m, 18 H, *H*-25, *H*-26, *H*-27), 0.84 (ps. t, 9 H, *H*-28) ppm.

^{13}C-NMR (150.9 MHz, acetone-d_6, 300 K, acetone) δ = 163.41 (s, *C*-2), 152.77 (s, *C*-6), 147.79 (s, *C*-5), 142.76 (s, *C*-9), 141.44 (s, *C*-18), 139.88 (s, *C*-10), 132.64 (s, *C*-12), 129.33 (s, *C*-20), 128.25 (s, *C*-8), 127.44 (s, *C*-11), 125.50 (s, *C*-4), 123.83 (s, *C*-7), 115.24 (s, *C*-3), 111.19 (s, *C*-17), 106.09 (s, *C*-19), 84.09 (s, *C*-14), 56.03 (s, *C*-1), 46.66 (s, *C*-21), 32.57 (s, *C*-26), 30.50 (s, *C*-25), 30.47 (s, *C*-24), 27.48 (s, *C*-23), 26.80 (s, *C*-22), 23.27 (s, *C*-27), 14.31 (s, *C*-28) ppm.

MS (Maldi-TOF, Cl-CCA): m/z = 929.6 $[M]^+$.

IR: $\tilde{\nu}$ = 2922.1 (m), 2852.0 (m), 1599.5 (s), 1578.4 (vs), 1482.2 (vs), 1454.4 (vs), 1392.0 (s), 1255.1 (vs), 1244.0 (vs), 1167.0 (m), 1138.5 (m), 1025.1 (m), 837.8 (s), 821.8 (s), 756.8 (vs), 716.0 (vs) cm^{-1}.

m.p.: 134.9 °C.

Elemental analyis: $C_{64}H_{75}N_5O$ Calc.: C 82.63, H 8.13, N 7.53,
Found: C 82.53, H 8.24, N 7.31.

Synthesis of (*E*)-12c-(4-(4-(methoxyphenyldiazenyl)phenyl)phenyl)ethynyl-4,8,12-tri-*n*-propyl-4,8,12-triazatriangulene (2b):

In tetrahydrofuran (abs., 50 mL) (*E*)-1-(4-methoxyphenyl-2-(4-(4-(ethynyl)phenyl)-phenyl)diazene (110 mg, 352 µmol) was dissolved under nitrogen atmosphere, octyl-TATA-BF_4 (192 mg, 388 µmol) and crushed potassium hydroxide (196 mg, 3.50 mmol) were added and the mixture was refluxed for 19 h. The reaction mixture was poured onto water. The layers were separated and the water layer was extracted with diethylether (3x je 50 mL). The combined organic layers were dried over magnesium sulfate and the solvent was removed under reduced pressure. The crude product was purified via column chromatography (alox basic, diethylether) to obtain an orange solid (233 mg, 324 µmol, 92%).

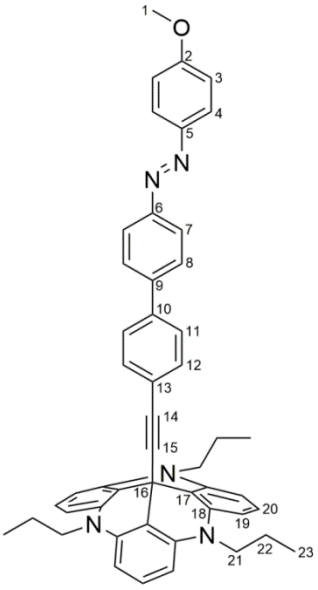

^{1}H-NMR (500.1 MHz, $CDCl_3$, 300 K, TMS) δ = 7.91 (d, ^3J = 8.9 Hz, 2 H, *H*-4), 7.89 (d, ^3J = 8.5 Hz, 2 H, *H*-7), 7.61 (d, ^3J = 8.5 Hz, 2 H, *H*-8), 7.41 (d, ^3J = 8.3 Hz, 2 H, *H*-11), 7.21-7.16 (m, 5 H, *H*-12, *H*-20), 7.00 (d, ^3J = 9.0 Hz, 2 H, *H*-3), 6.54 (d, ^3J = 8.2 Hz, 2 H, *H*-19), 3.90 (ps. t, 6 H, *H*-21), 3.88 (s, 3 H, *H*-1), 1.87 (ps. sext., 6 H, *H*-22), 1.06 (ps. t, 9 H, *H*-23) ppm.

^{13}C-NMR (125.8 MHz, $CDCl_3$, 300 K, TMS) δ = 162.06 (s, *C*-2), 151.87 (s, *C*-6), 147.12 (s, *C*-5), 142.31 (s, *C*-9), 140.54 (s, *C*-18), 138.91 (s, *C*-10), 132.03 (s, *C*-12), 128.17 (s, *C*-20), 127.44 (s, *C*-8), 126.36 (s, *C*-11), 124.75 (s, *C*-4), 123.56 (s, *C*-13), 123.03 (s, *C*-7), 114.22 (s, *C*-3), 110.26 (s, *C*-17), 104.99 (s, *C*-19), 94.65 (s, *C*-15), 83.38 (s, *C*-14), 55.58 (s, *C*-1), 48.07 (s, *C*-21), 19.17 (s, *C*-22), 11.20 (s, *C*-23) ppm.

MS (Maldi-TOF, Cl-CCA): m/z = 720.7 $[M+H]^+$.

IR: $\tilde{\nu}$ = 3254.3 (w), 2960.2 (w), 1597.7 (s), 1580.0 (vs), 1482.5 (s), 1454.2 (s), 1230.1 (vs), 1167.9 (m), 1133.9 (s), 1027.1 (m), 824.7 (vs), 755.3 (s), 711.6 (m) cm^{-1}.

m.p.: 206.1 °C.

Elemental analysis: $C_{49}H_{45}N_5O$ Calc.: C 81.75, H 6.30, N 9.73,
Found: C 81.17, H 6.32, N 9.37.

Synthesis of 4,4,5,5-tetramethyl-2[-4-[2-(trimethylsilyl)ethynyl]phenyl]-1,3,2-dioxaborolane (12):

In tetrahydrofuran (abs., 120 mL) bromo-4-trimethylsilylacetylene (4.00 g, 15.9 mmol) was dissolved under nitrogen atmosphere and cooled to -78 °C. Afterwards *n*-butyllithium (8.27 mL, 20.6 mmol, 2.5 M in *n*-hexane) was added over 15 min and the reaction was stirred for 0.5 h at -78 °C. To the reaction mixture isopropoxyborylane (10.3 mL , 50.8 mmol), which was cooled to -20 °C, was added over 3 min and the reaction solution was warmed up slowly to room temperature and stirred for 22 h. Afterwards 1 M HCl solution (120 mL) was added and the mixture was stirred for 5 min at room temperature. The layers were separated and the aqueous phase was extracted with diethylether (3x 150 mL). The combined organic layers were washed with water (2x 100 mL) and saturated sodium chloride solution (100 mL). The combined organic layers were dried over magnesium sulfate and the solvent was removed under reduced pressure. The crude product was purified via column chromatography (silica gel, diethylether) to obtain a white solid (4.67 g, 15.6 mmol, 98%; Lit.:90%).

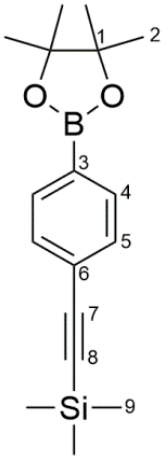

^{1}H-NMR (500.1 MHz, $CDCl_3$, 300 K, $CHCl_3$) δ = 7.73 (d, ^3J = 8.30 Hz, 2 H, *H*-4), 7.46 (d, ^3J = 8.30 Hz, 2 H, *H*-5), 1.34 (s, 12 H, *H*-2), 0.25 (s, 9 H, *H*-9) ppm.

^{13}C-NMR (125.8 MHz, $CDCl_3$, 300 K, $CHCl_3$) δ = 134.59 (*C*-4), 131.25 (*C*-5), 125.91 (*C*-6), 105.32 (*C*-7), 95.70 (*C*-8), 84.10 (*C*-1), 25.03 (*C*-2), 0.09 (*C*-9) ppm.

Synthesis of 2-methyl-4-amino-4'-((trimethylsilyl)ethynyl)biphenyl (14):

In a solution of toluene (180 mL), ethanol (45 mL) and H_2O (9 mL) 4,4,5,5-tetramethyl-2[-4-[2-(trimethylsilyl)ethynyl]phenyl]-1,3,2-dioxaborolane (3.00 g, 9.99 mmol), 3-methyl-4-bromo-

aniline (1.68 g, 9.00 mmol), $Pd(PPh_3)_4$ (231 mg, 200 µmol) and Na_2CO_3 (1.41 g, 20.0 mmol) were suspended under nitrogen atmosphere and refluxed for 24 h. To the reaction mixture water was added (150 mL) and the layers were separated. The aqueous phase was extracted with dichloromethane (3x 150 mL) and the combined organic layers were dried over magnesium sulfate. The solvent was removed under reduced pressure and the crude product was purified via column chromatography (silica gel, cyclohexane/ ethyl acetate, 2:1) to obtain a beige coloured solid (1.11 g, 3.97 mmol, 40%).

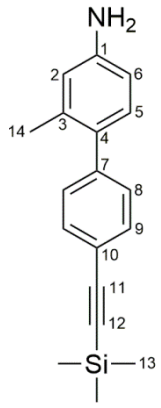

^{1}H-NMR (500.1 MHz, $CDCl_3$, 300 K, TMS) δ = 7.47 (d, ^{3}J = 8.2 Hz, 2 H, *H*-9), 7.23 (d, ^{3}J = 8.2 Hz, 2 H, *H*-8), 7.01 (d, ^{3}J = 8.0 Hz, 1 H, *H*-5), 6.59 (d, ^{4}J = 2.4 Hz, 1 H, *H*-2), 6.57 (ddd, ^{3}J = 8.0 Hz, ^{4}J = 2.3 Hz, ^{5}J = 0.5 Hz, 1 H, *H*-6), 4.66 (s, 2 H, NH_2), 2.19 (s, 3 H, *H*-14), 0.26 (s, 9 H, *H*-13) ppm.

^{13}C-NMR (125.8 MHz, $CDCl_3$, 300 K, TMS) δ = 145.76 (s, *C*-3), 142.31 (s, *C*-7), 136.27 (s, *C*-4), 131.74 (s, *C*-1), 131.58 (s, *C*-9), 130.67 (s, *C*-5), 129.29 (s, *C*-8), 121.37 (s, *C*-10), 117.07 (s, *C*-2), 113.06 (s, *C*-6), 106.30 (s, *C*-11), 94.24 (s, *C*-12), 20.77 (s, *C*-14), 0.06 (s, *C*-13) ppm.

^{29}Si-NMR (99.4 MHz, $CDCl_3$, 300 K, TMS) δ = -17.85 ppm.

MS (EI, 70eV): m/z (%) = 279.11 $[M]^+$.

IR: $\tilde{\nu}$ = 3478.7 (w), 3376.3 (w), 2956.1 (w), 2155.1 (m), 1615.9 (m), 1488.5 (s), 1244.3 (m), 937.7 (vs), 815.4 (vs), 758.7 (s), 695.5 (m), 577.3 (m), 561.8 (m) cm^{-1}.

m.p.: 87.4 °C.

Elemental analysis: $C_{18}H_{21}NSi$ calc.: C 77.36, H 7.57, N 5.01,
found: C 77.03, H 7.66, N 4.90.

Synthesis of (*E*)-1-(4-fluorophenyl)-2-(3-methyl-4-(4-((trimethylsilyl)ethynyl)phenyl)-phenyl) diazene (20):

In acetic acid (45 mL) 2-methyl-4-amino-4'-((trimethylsilyl)ethynyl)biphenyl (800 mg, 2.87 mmol) and nitroso-4-fluoroaniline (563 mg, 4.50 mmol) were dissolved and stirred for 16 h at room temperature. The solution was poured in water (450 mL) and extracted with ethyl acetate (3x 300 mL). The organic layer was washed with water (3x 300 mL) and dried over magnesium sulfate. The solvent was removed and the crude product was purified via column chromatography (silica gel, cyclohexane/ ethyl acetate, 1:1) to obtain an orange solid (574 mg, 1.49 mmol, 52%).

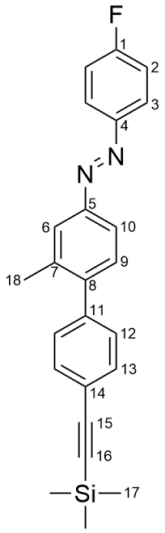

^{1}H-NMR (500.1 MHz, $CDCl_3$, 300 K, TMS) δ = 7.98-7.92 (m, 2 H, *H*-3), 7.81 (d, ^{4}J = 1.5 Hz, 1 H, *H*-6), 7.77 (dd, ^{3}J = 8.1 Hz, ^{4}J = 2.0 Hz, 1 H, *H*-10), 7.54 (d, ^{3}J = 8.1 Hz, 2 H, *H*-13), 7.35 (d, ^{3}J = 8.1 Hz, 1 H, *H*-9), 7.30 (d, ^{3}J = 8.0 Hz, 2 H, *H*-12), 7.23-7.17 (m, 2 H, *H*-2), 2.35 (s, 3 H, *H*-18), 0.28 (s, 9 H, *H*-17) ppm.

^{13}C-NMR (125.8 MHz, $CDCl_3$, 300 K, TMS) δ = 164.38 (d, ^{1}J = 251.8 Hz, *C*-1), 151.70 (s, *C*-5), 149.27 (d, ^{4}J = 3.0 Hz, *C*-4), 143.97 (s *C*-8), 141.30 (s, *C*-11), 136.39 (s, *C*-7), 131.84 (s, *C*-13), 130.48 (s, *C*-9), 128.99 (s, *C*-12), 124.85 (d, ^{3}J = 8.9 Hz, *C*-3), 124.71 (s, *C*-6), 122.09 (s, *C*-14), 120.43 (s, *C*-10), 116.07 (d, ^{2}J = 22.9 Hz, *C*-2), 104.86 (s, *C*-15), 94.87 (s, *C*-16), 20.59 (s, *C*-18), 0.00 (s, *C*-17) ppm.

^{19}F-NMR (470.6 MHz, $CDCl_3$, 300 K, TMS) δ = -109.87 ppm.
^{29}Si-NMR (99.4 MHz, $CDCl_3$, 300 K, TMS) δ = -17.64 ppm.

MS (EI, 70eV): m/z (%) = 386.16 (60) $[M]^+$.

IR: $\tilde{\nu}$ = 2960.4 (w), 2154.2 (w), 1592.9 (m), 1497.3 (m), 1483.6 (m), 1249.2 (m), 1226.2 (m), 1135.2 (w), 862.0 (m), 838.5 (vs), 823.5 (vs), 759.0 (m), 642.3 (w), 539.4 (m) cm^{-1}.

m.p.: 113.5 °C.

Elemental analysis: $C_{24}H_{23}FN_2Si$ Calc.: C 74.57, H 6.00, N 7.25,
Found: C 74.56, H 6.12, N 7.31.

Synthesis of (*E*)-1-(4-methoxyphenyl-2-(4-(4-(ethynyl)phenyl)-phenyl)diazene (23):

In methanol (130 mL) sodium (5.94 g, 258 mmol) was dissolved and (*E*)-1-(4-fluorophenyl)-2-(3-methyl-4-(4-((trimethylsilyl)ethynyl)phenyl)-phenyl)diazene (513 mg, 1.33 mmol) was added and refluxed for 19 h. Water (100 mL) was added to the solution and extracted with ethyl acetate (3x 100 mL). The combined organic layers were dried over magnesium sulfate and the solvent was removed under reduced pressure. The crude product was purified via column chromatography (silica gel, dichloromethane) to obtain an orange solid (464 mg, 1.30 mmol, 98%).

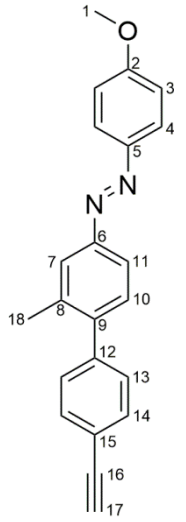

^{1}H-NMR (500.1 MHz, acetone-d_6, 300 K, acetone) δ = 7.95 (d, ^{3}J = 9.1 Hz, 2 H, *H*-4), 7.83 (d, ^{4}J = 1.5 Hz, 1 H, *H*-7), 7.78 (dd, ^{3}J = 8.1 Hz, ^{4}J = 2.1 Hz, 1 H, *H*-11), 7.61 (d, ^{3}J = 8.4 Hz, 2 H, *H*-14), 7.45 (d, ^{3}J = 8.5 Hz, 2 H, *H*-13), 7.41 (d, ^{3}J = 8.1 Hz, 1 H, *H*-10), 7.14 (d, ^{3}J = 9.1 Hz, 2 H, *H*-3), 3.93 (s, 3 H, *H*-1), 3.72 (s, 1 H, *H*-17), 2.39 (s, 3 H, *H*-18) ppm.

^{13}C-NMR (125.8 MHz, acetone-d_6, 300 K, acetone) δ = 163.43 (*C*-2), 152.89 (s, *C*-6), 147.84 (*C*-5), 144.10 (s, *C*-9), 142.60 (s, *C*-12), 137.20 (s, *C*-8), 132.75 (s, *C*-14), 131.34 (s, *C*-10), 130.17 (s, *C*-13), 125.54 (d, *C*-4), 125.54 (d, *C*-7), 122.22 (s, *C*-15), 120.71 (s, *C*-11), 115.30 (s, *C*-3), 84.03 (s, *C*-16), 79.70 (s, *C*-17), 56.09 (s, *C*-1), 20.69 (s, *C*-18) ppm.

MS (EI, 70eV): m/z = 326.11 $[M]^{+}$.

IR: $\tilde{\nu}$ = 2955.9 (w), 2924.4 (w), 2852.3 (w), 2154.8 (m), 1602.9 (m), 1579.3 (m), 1487.4 (s), 1392.7 (w), 1245.5 (vs), 1226.4 (s), 1134.2 (m), 838.3 (vs), 815.2 (s), 758.1 (s), 696.1 (m) cm^{-1}.

m.p.: 119.2 °C.

Elemental analysis: $C_{22}H_{18}N_2O$ Calc.: C 80.96, H 5.56, N 8.58,
Found: C 80.74, H 6.12, N 7.95.

Synthesis of (*E*)-12c-(4-(4-(methoxyphenyldiazenyl)-2-methylphenyl)phenyl)ethynyl-4,8,12-tri-*n*-octyl-4,8,12-triazatriangulene (3a):

In tetrahydrofuran (abs., 80 mL) (*E*)-1-(4-methoxyphenyl-2-(4-(4-(ethynyl)phenyl)-phenyl)diazene (100 mg, 307 µmol) was dissolved under nitrogen atmosphere, octyl-TATA-BF_4 (260 mg, 368 µmol) and crushed potassium hydroxide (172 mg, 3.07 mmol) was added and the mixture was refluxed for 21 h. The mixture was poured onto half saturated sodium chloride solution (100 mL) and the layers were separated. The aqueous layer was extracted with diethylether (3x 100 mL) and the combined organic layers were dried over magnesium sulfate. The solvent was removed under reduced pressure and the crude product was purified via column chromatography (alox basic, diethylether) to obtain an orange solid (263 mg, 279 µmol, 91%).

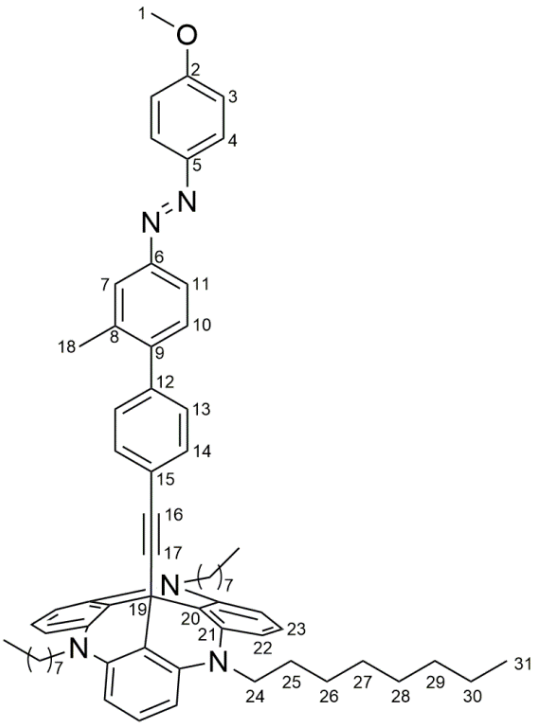

^{1}H-NMR (500.1 MHz, acetone-d_6, 300 K, acetone) δ = 7.92 (d, ^3J = 9.1 Hz, 2 H, *H*-4), 7.76 (d, ^4J = 1.4 Hz, 1 H, *H*-7), 7.71 (dd, ^3J = 8.2 Hz, ^4J = 1.9 Hz, 1 H, *H*-11), 7.27 (d, ^3J = 8.2 Hz, 1 H, *H*-10), 7.24-7.19 (m, 5 H, *H*-13, *H*-23), 7.15 (d, ^3J = 8.5 Hz, 2 H, *H*-14), 7.11 (d, ^3J = 9.1 Hz, 2 H, *H*-3), 6.68 (d, ^3J = 8.3 Hz, 6 H, *H*-22), 4.02 (t, ^3J = 7.6 Hz, 6 H, *H*-24), 3.91 (s, 3 H, *H*-11), 2.28 (s, 3 H, *H*-18), 1.86 (ps. quint., 6 H, *H*-25), 1.52 (ps. quint., 6 H, *H*-26), 1.44-1.35 (ps. quint., 6 H, *H*-27), 1.34-1.21 (m, 18 H, *H*-28, *H*-29, *H*-30), 0.86 (ps. t, 9 H, *H*-31) ppm.

^{13}C-NMR (125.8 MHz, acetone-d_6, 300 K, acetone) δ = 163.37 (s, *C*-2), 152.71 (s, *C*-6), 147.81 (s, *C*-5), 144.19 (s, *C*-9), 141.47 (s, *C*-21), 141.34 (s, *C*-12), 137.08 (s, *C*-8), 131.98 (s, *C*-14), 131.21 (s, *C*-10), 129.75 (s, *C*-13), 129.38 (s, *C*-23), 125.49 (s, *C*-7), 125.48 (s, *C*-4), 123.52 (s, *C*-15), 120.64 (s, *C*-11), 115.27 (s, *C*-3), 111.21 (s, *C*-20), 106.12 (s, *C*-22), 95.46 (s, *C*-17), 84.22 (s, *C*-16), 56.07 (s, *C*-1), 46.75 (s, *C*-24), 32.61 (s, *C*-29), 30.18 (s, *C*-27), 30.08 (s, *C*-28), 27.52 (s, *C*-26), 26.83 (s, *C*-25), 23.32 (s, *C*-30), 20.66 (s, *C*-18), 14.38 (s, *C*-31) ppm.

MS (ESI): m/z = 929.4 $[M]^+$.

IR: $\tilde{\nu}$ = 2922.5 (m), 2850.2 (m), 1614.9 (s), 1580.9 (vs), 1484.6 (vs), 1456.5 (vs), 1395.2 (s), 1373.9 (m), 1248.7 (vs), 1168.2 (s), 1139.8 (m), 1025.0 (w), 840.0 (m), 828.0 (m), 759.5 (m), 714.7 (m), 437.4 (m) cm^{-1}.

m.p.: 110.4 °C.

Elemental analysis: $C_{65}H_{77}N_5O$ Calc.: C 82.67, H 8.22, N 7.42
Found: C 82.36, H 8.21, N 7.30

Synthesis of (*E*)-12c-(4-(4-(methoxyphenyldiazenyl)-2-methylphenyl)phenyl)ethynyl-4,8,12-tri-*n*-propyl-4,8,12-triazatriangulene (3b):

In tetrahydrofuran (abs., 120 mL) (*E*)-1-(4-methoxyphenyl-2-(4-(4-(ethynyl)phenyl)-phenyl)diazene (120 mg, 368 µmol) was dissolved under nitrogen atmosphere, propyl-TATA-BF_4 (219 mg, 442 µmol) and crushed potassium hydroxide (207 mg, 3.68 mmol) were added and the mixture was refluxed for 17 h. The reaction mixture was poured onto half saturated sodium chloride solution (100 mL) and the layers were separated. The aqueous layer was extracted with diethylether (3x 100 mL) and the combined organic layers were dried over magnesium sulfate. The solvent was removed under reduced pressure and the crude product was purified via column chromatography (alox basic, diethylether) to obtain an orange solid (259 mg, 354 mol, 96%).

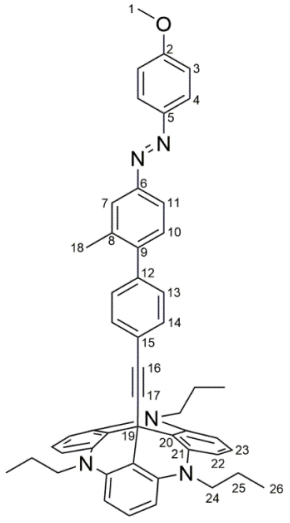

^{1}H-NMR (500.1 MHz, acetone-d_6, 300 K, acetone) δ = 7.92 (d, ^3J = 9.1 Hz, 2 H, *H*-4), 7.76 (d, ^4J = 1.4 Hz, 1 H, *H*-7), 7.71 (dd, ^3J = 8.2 Hz, ^4J = 2.0 Hz, 1 H, *H*-11), 7.28 (d, ^3J = 8.2 Hz, 1 H, *H*-10), 7.23 (d, ^3J = 8.2 Hz, 2 H, *H*-13), 7.22 (t, ^3J = 8.3 Hz, 3 H, *H*-23), 7.15 (d, ^3J = 8.2 Hz, 2 H, *H*-14), 7.11 (d, ^3J = 9.0 Hz, 2 H, *H*-3), 6.67 (d, ^3J = 8.3 Hz, 6 H, *H*-22), 3.99 (ps. t, 6 H, *H*-24), 3.91 (s, 3 H, *H*-1), 2.28 (s, 3 H, *H*-18), 1.88 (ps. sext, 6 H, *H*-25), 1.08 (ps. t, 9 H, *H*-26) ppm.

^{13}C-NMR (125.8 MHz, acetone-d_6, 300 K, acetone) δ = 163.37 (s, *C*-2), 152.71 (s, *C*-6), 147.81 (s, *C*-5), 144.19 (s, *C*-9), 141.47 (s, *C*-21), 141.38 (s, *C*-12), 137.11 (s, *C*-8), 131.89 (s, *C*-14), 131.23 (s, *C*-10), 129.82 (s, *C*-13), 129.44 (s, *C*-23), 125.47 (s, *C*-4), 125.47 (s, *C*-7), 123.48 (s, *C*-20), 120.64 (s, *C*-11), 115.27 (s, *C*-3), 111.01 (s, *C*-20), 106.11 (s, *C*-22), 95.42 (s, *C*-17), 84.23 (s, *C*-16), 56.07 (s, *C*-1), 48.41 (s, *C*-24), 20.62 (s, *C*-16), 19.94 (s, *C*-25), 11.31 (s, *C*-26) ppm.

MS (ESI): m/z = 733.3 $[M]^+$.

IR: $\tilde{\nu}$ = 3376.5 (w), 2956.0 (w), 2154.9 (m), 1604.7 (m), 1487.8 (m), 1245.2 (s), 838.9 (vs), 815.2 (s), 758.2 (s), 696.4 (w) cm^{-1}.

m.p. = 194.7 °C.

Elemental analysis: $C_{50}H_{47}N_5O$ Calc.: C 81.82, H 6.45, N 9.54,
Found: C 81.38, H 6.92, N 8.83.

Synthesis of of 2-[2-methyl-4-[2-(trimethylsilyl)ethynyl]phenyl]-4,4,5,5-tetramethyl-1,3,2-dioxaborolane (13):

Under nitrogen atmosphere 1-bromo-2-methyl-4-(2-(trimethylsilyl)ethynyl)-benzene (7.30 g, 27.3 mmol) was dissolved in tetrahydrofuran (abs., 200 mL) and cooled to -78 °C. To this solution *n*-butyllithium (2.5 M in *n*-Hexan, 14.2 mL, 35.5 mmol) was slowly added and the reaction mixture was stirred for 30 min. Afterwards 2-Isopropoxy-4,4,5,5-tetramethyl-1,3,2-dioxaborolane (16.6 mL, 82.9 mmol), which was cooled to -20 °C, was added and the reaction mixture was warmed up slowly to room temperature and stirred for 12 h. The reaction was quenched with 1 M hydrochloric acid (200 mL) and the layers were separated. The aqueous layer was extracted with diethylether (3x 100 mL) and the combined organic layers were washed with water (100 mL) and brine (100 mL). The combined organic layers were dried over magnesium sulfate and the solvent was removed under reduced pressure. The crude product was purified via column chromatography (silica gel, diethylether) to obtain a beige coloured solid (7.65 g, 24.4 mmol, 89%).

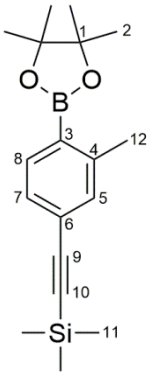

^{1}H-NMR (500.1 MHz, acetone-d_6, 300 K, acetone) δ = 7.68 (d, ^{3}J = 7.6 Hz, 1 H, *H*-8), 7.26-7.22 (m, 2 H, *H*-7, *H*-5), 2.49 (s, 3 H, *H*-12), 1.35 (s, 12 H, *H*-2), 0.23 (s, 9 H, *H*-11) ppm.

^{13}C-NMR (125.8 MHz, acetone-d_6, 300 K, acetone) δ = 145.7 (s, *C*-4), 136.7 (s, *C*-8), 133.6 (s, *C*-5), 128.7 (s, *C*-7), 126.2 (s, *C*-6), 106.1 (s, *C*-9), 95.5 (s, *C*-10), 84.5 (s, *C*-1), 25.2 (s, *C*-2), 22.1 (s, *C*-12), 0.00 (s, *C*-11) ppm.

^{11}B-NMR (160.5 MHz, acetone-d_6, 300 K, acetone) δ = 30.9 ppm.

^{29}Si-NMR (99.4 MHz, acetone-d_6, 300 K, acetone) δ = -17.8 ppm.

MS (EI, 70eV): m/z = 314.18 $[M]^+$.

IR: $\tilde{\nu}$ = 2980 (w), 2151 (w), 1603 (w), 1392 (m), 1372 (m), 1340 (s), 1317 (m), 1250 (m), 1141 (s),
1064 (m), 945 (w), 837 (vs), 758 (s), 659 (s), 453 (w) cm^{-1}.

m.p. = 81.2 °C.

Elemental analysis: $C_{18}H_{27}BO_2Si$ Calc.: C 68.78, H 8.66,
Found: C 67.74, H 8.76.

Synthesis of 2-methyl-4-amino-2'-methyl-4'-((trimethylsilyl)ethynyl)biphenyl (15):

In a solution of toluene (340 mL), ethanol (113 mL) and water (22.5 mL) 2-[2-methyl-4-[2-(trimethylsilyl)ethynyl]phenyl]-4,4,5,5-tetramethyl-1,3,2-dioxaborolane (2.66 g, 14.3 mol), $Pd(PPh_3)_4$ (735 mg, 636 µmol) and sodium carbonate (3.37 g, 31.8 mmol) were suspended under nitrogen atmosphere and stirred for 20 h at 95 °C. To the mixture water (300 mL) was added and the layers were separated. The water layer was extracted with dichloromethane (3x 300 mL) and the combined organic layers were dried over magnesium sulfate. The solvent was removed under reduced pressure and the crude product was purified via column chromatography (silica gel, cyclohexane/ethyl acetate, 2:1) to obtain a brown oil (2.19 g, 7.48 mmol, 52%).

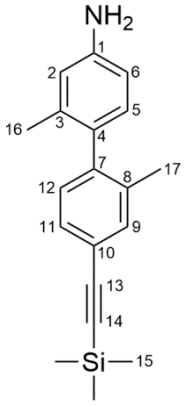

^{1}H-NMR (500.1 MHz, acetone-d_6, 300 K, acetone) δ = 7.35 (s, 1 H, *H*-9), 7.28 (dd, ^{3}J = 7.8 Hz, ^{4}J = 1.3 Hz, 1 H, *H*-11), 7.03 (d, ^{3}J = 7.8 Hz, 1 H, *H*-12), 6.74 (d, ^{3}J = 8.0 Hz, 1 H, *H*-5), 6.70 (d, ^{4}J = 1.9 Hz, 1 H, *H*-2), 6.55 (dd, ^{3}J = 8.0 Hz, ^{4}J = 2.3 Hz, 1 H, *H*-6), 4.57 (s, 2 H, NH_2), 2.04 (s, 3 H, *H*-17), 1.90 (s, 3 H, *H*-16), 024 (s, 9 H, *H*-15) ppm.

^{13}C-NMR (125.8 MHz, acetone-d_6, 300 K, acetone) δ = 148.67 (s, *C*-1), 144.00 (s, *C*-7), 137.74 (s, *C*-8), 136.53 (s, *C*-3), 133.83 (s, *C*-9), 131.10 (s, *C*-12), 130.39 (s, *C*-5), 130.08 (s, *C*-4), 129.68 (s, *C*-11), 122.21 (s, *C*-10), 116.55 (s, *C*-2), 112.75 (s, *C*-6), 106.45 (s, *C*-13), 93.75 (s, *C*-14), 20.04 (s, *C*-16), 19.87 (s, *C*-17), 0.07 (s, *C*-15) ppm.

^{29}Si-NMR (99.4 MHz, acetone-d_6, 300 K, acetone) δ = -18.09 ppm.

MS (EI, 70eV): m/z = 293.07 $[M]^+$.

IR: $\tilde{\nu}$ = 3370.0 (w), 2958.0 (w), 2147.7 (w), 1665.6 (w), 1623.0 (m), 1483.1 (m), 1248.7 (s), 838.5 (vs), 758.7 (m), 627.9 (m) cm^{-1}.

Elemental analysis: $C_{19}H_{23}N_2Si$ calc.: C 77.76, H 7.90, N 4.77,
Found: C 76.47, H 7.91, N 4.95.

Synthesis of (*E*)-1-(4-fluorphenyl)-2-(3-methyl-4-(3-methyl-4-((trimethylsilyl)ethynyl)-phenyl)-phenyl)diazene (21):

In acetic acid (43 mL) 2-methyl-4-amino-2‘-methyl-4‘-((trimethylsilyl)ethynyl)biphenyl (1.17 g, 3.98 mmol) and 1-nitroso-4-fluoroaniline (595 mg, 4.76 mmol) were dissolved and stirred for 18 h at room temperature. To the solution water (250 mL) was added and the layers were separated. The aqueous layer was extracted with ethyl acetate (3x 250 mL) and the combined organic layers were dried over magnesium sulfate. The solvent was removed under reduced pressure and the crude product was purified via column chromatography (silica gel, cyclohexane/ ethyl acetate, 2:1) to obtain an orange solid (905 mg, 2.26 mmol, 57%).

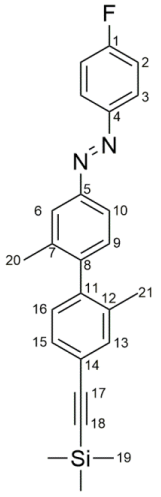

^{1}H-NMR (500.1 MHz, acetone-d_6, 300 K, acetone) δ = 8.05-8.00 (m, 2 H, *H*-3), 7.87 (dd, ^{4}J = 1.4 Hz, ^{5}J = 0.7 Hz, 1 H, *H*-6), 7.81 (dd, ^{3}J = 8.1 Hz, ^{4}J = 2.0 Hz, 1 H, *H*-10), 7.45-7.38 (m, 1 H, *H*-13), 7.40-7.35 (m, 2 H, *H*-2, *H*-15), 7.29 (d, ^{3}J = 8.0 Hz, 1 H, *H*-9), 7.15 (d, ^{3}J = 7.8 Hz, 1 H, *H*-16), 2.16 (s, 3 H, *H*-20), 2.09 (s, 3 H, *H*-21), 0.26 (s, 9 H, *H*-19) ppm.

^{13}C-NMR (125.8 MHz, acetone-d_6, 300 K, acetone) δ = 165.34 (d, ^{1}J = 250.5 Hz, *C*-1), 152.71 (s, *C*-5), 150.27 (d, ^{4}J = 3.1 Hz, *C*-4), 144.88 (s, *C*-8), 142.28 (s, *C*-11), 137.85 (s, *C*-7), 136.94 (s, *C*-12), 134.18 (s, *C*-13), 130.91 (s, *C*-9), 130.05 (s, *C*-15), 130.02 (s, *C*-16), 125.79 (d, ^{3}J = 9.1 Hz, *C*-3), 125.23 (s, *C*-6), 123.31 (s, *C*-14), 120.94 (s, *C*-10), 117.04 (d, ^{2}J = 23.2 Hz, *C*-2), 106.01 (s, *C*-17), 94.47 (s, *C*-18), 19.98 (s, *C*-20), 19.70 (s, *C*-21), 0.04 (s, *C*-19) ppm.

^{19}F-NMR (470.6 MHz, acetone-d_6, 300 K, TMS) δ = -109.94 ppm.

^{29}Si-NMR (99.4 MHz, acetone-d_6, 300 K, TMS) δ = -17.68 ppm.

MS (EI, 70eV): m/z = 400.08 $[M]^+$.

IR: $\tilde{\nu}$ = 3479.8 (w), 3376.4 (w), 2955.6 (w), 2154.7 (m), 1615.2 (w), 1488.5 (m), 1245.2 (m), 838.2 (vs), 815.4 (s), 758.6 (s), 696.3 (m), 561.7 (m) cm^{-1}.

m.p. = 88.6 °C.

Elemental analysis: $C_{25}H_{25}FN_2Si$ Calc.: C 74.96, H 6.29, N 6.99,
Found: C 74.69, H 6.50, N 7.12.

Synthesis of (*E*)-1-(4-methoxyphenyl)-2-(3-methyl-4-(3-methyl-4-(ethynyl)phenyl)-phenyl)diazene (24):

In methanol (165 mL) sodium (7.08 g, 308 mmol) was dissolved, (*E*)-1-(4-fluorphenyl)-2-(3-methyl-4-(3-methyl-4-((trimethylsilyl)ethynyl)phenyl)-phenyl)diazene (616 mg, 1.54 mmol) was added and the solution was refluxed for 18 h. To the solution water (300 mL) and saturated sodium chloride solution (100 mL) were added and the layers were separated. The aqueous layer was extracted with ethyl acetate (3x 400 mL) and the combined organic layers were dried over magnesium sulfate. The solvent was removed under reduced pressure and the crude product was purified via column chromatography (silica gel, dichloromethane/ ethyl acetate, 4/1) to obtain an orange solid (478 mg, 1.40 mmol, 91%).

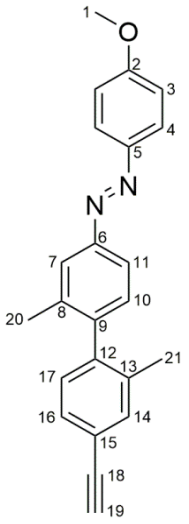

^{1}H-NMR (500.1 MHz, acetone-d_6, 300 K, acetone) δ = 7.95 (d, ^3J = 9.1 Hz, 2 H, *H*-4), 7.83 (d, ^4J = 1.3 Hz, 1 H, *H*-7), 7.78 (dd, ^3J = 8.0 Hz, ^4J = 2.0 Hz, 1 H, *H*-11), 7.49-7.46 (m, 1 H, *H*-14), 7.41 (dd, ^3J = 7.8 Hz, ^4J = 1.3 Hz, 1 H, *H*-16), 7.27 (d, ^3J = 8.1 Hz, 1 H, *H*-10), 7.16 (d, ^3J = 7.8 Hz, 1 H, *H*-17), 7.14 (d, ^3J = 9.0 Hz, 1 H, *H*-3), 3.93 (s, 3 H, *H*-1), 3.66 (s, 1 H, *H*-19), 2.15 (s, 3 H, *H*-20), 2.09 (s, 3 H, *H*-21) ppm.

^{13}C-NMR (125.8 MHz, acetone-d_6, 300 K, acetone) δ = 163.39 (s, *C*-2), 152.98 (s, *C*-6), 147.83 (s, *C*-5), 144.03 (s, *C*-7), 142.53 (s, *C*-21), 137.64 (s, *C*-8), 137.03 (s, *C*-13), 134.29 (s, *C*-14), 130.79 (s, *C*-10), 130.20 (s, *C*-16), 130.15 (s, *C*-17), 125.49 (s, *C*-4), 124.93 (s, *C*-7), 122.49 (s, *C*-15), 120.65 (s, *C*-11), 115.30 (s, *C*-3), 84.19 (s, *C*-18), 79.07 (s, *C*-19), 56.08 (s, *C*-1), 20.00 (s, *C*-20), 19.73 (s, *C*-21) ppm.

MS (EI, 70eV): m/z = 340.15 $[M]^+$.

IR: $\tilde{\nu}$ = 3282.0 (w), 1738.5 (w), 1598.8 (m), 1579.5 (m), 1497.4 (w), 1438.8 (w), 1245.9 (s), 1137.5 (m), 1027.3 (m), 887.5 (m), 837.0 (vs), 633.7 (m), 609.8 (s), 451.7 (m) cm^{-1}.

m.p. = 122.7 °C.

Elemental analysis: $C_{23}H_{20}N_2O$ Calc.: C 81.15, H 5.92, N 8.23,
Found: C 80.71, H 5.93, N 8.11.

Synthesis of (*E*)-12c-(3-methyl-4-(4-(methoxyphenyldiazenyl)-2-methylphenyl)-phenyl)ethynyl-4,8,12-tri-*n*-octyl-4,8,12-triazatriangulene (4a):

In tetrahydrofuran (abs., 80 mL) (*E*)-1-(4-methoxyphenyl)-2-(3-methyl-4-(3-methyl-4-(ethynyl)phenyl)-phenyl)diazene (120 mg, 352 µmol) was dissolved under nitrogen atmosphere, octyl-TATA-BF_4 (298 mg, 422 µmol) and crushed potassium hydroxide (197 mg, 3.52 mmol) were added and the mixture was refluxed for 24 h. The reaction was poured onto half saturated sodium chloride solution (100 mL) and the layers separated. The aquous layer was extracted with diethyl ether (3x 100 mL) and the combined organic layers were dried over magnesium sulfate. The solvent was removed under reduced pressure and the crude product was purified via column chromatography (alox basic, diethyl ether) to obtain an orange solid (336 mg, 351 µmol, 99%).

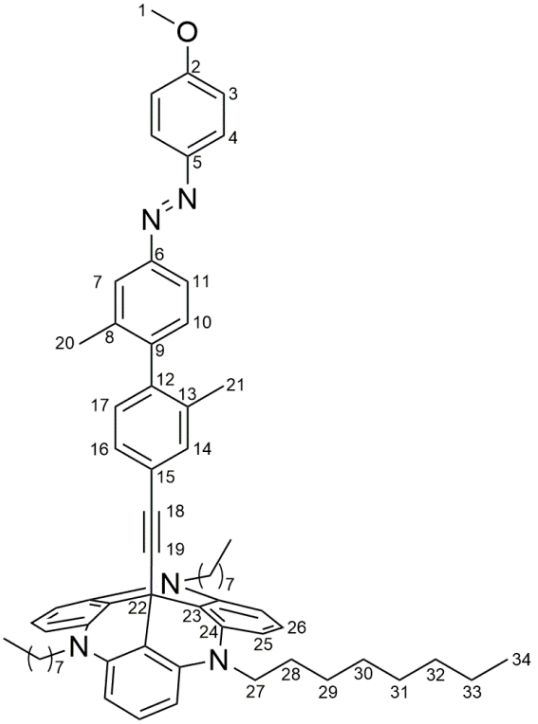

^{1}H-NMR (600.1 MHz, $CDCl_3$, 300 K, $CHCl_3$) δ = 7.91 (d, ^3J = 9.1 Hz, 2 H, *H*-4), 7.72 (d, ^4J = 1.5 Hz, 1 H, *H*-7), 7.68 (dd, ^3J = 8.2 Hz, ^4J = 1.8 Hz, 1 H, *H*-11), 7.19 (t, ^3J = 8.3 Hz, 3 H, *H*-26), 7.09 (d, ^3J = 8.0 Hz, 1 H, *H*-10), 7.06-7.05 (m, 1 H, *H*-14), 7.03-6.98 (m, 3 H, *H*-2, *H*-16), 6.87 (d, ^3J = 7.9 Hz, 1 H, *H*-17), 6.55 (d, ^3J = 8.4 Hz, 6 H, *H*-25), 3.94 (t, ^3J = 7.9 Hz, 6 H, *H*-27), 3.89 (s, 3 H, *H*-1), 2.02 (s, 3 H, *H*-20), 1.90 (s, 3 H, *H*-21), 1.85 (ps. quint., 6 H, *H*-28), 1.47 (ps. quint., 6 H, *H*-29), 1.38 (ps. quint., 6 H, *H*-30), 1.34-1.22 (m, 18 H, *H*-31, *H*-32, *H*-33), 0.88 (ps. t, 9 H, *H*-34) ppm.

^{13}C-NMR (150.9 MHz, $CDCl_3$, 300 K, $CHCl_3$) δ = 162.13 (s, *C*-1), 152.14 (s, *C*-6), 147.27 (s, *C*-5), 143.65 (s, *C*-9), 140.63 (s, *C*-24), 140.26 (s, *C*-12), 136.93 (s, *C*-8), 135.36 (s, *C*-13), 133.14 (s, *C*-14), 130.07 (s, *C*-10), 129.09 (s, *C*-16), 128.66 (s, *C*-17), 128.27 (s, *C*-26), 124.81 (s, *C*-4), 123.69 (s, *C*-7), 123.19 (s, *C*-15), 120.17 (s, *C*-11), 114.36 (s, *C*-3), 110.39 (s, *C*-23),

105.02 (s, *C*-25), 93.48 (s, *C*-19), 83.64 (s, *C*-18), 55.73 (s, *C*-1), 46.68 (s, *C*-27), 32.00 (s, *C*-32), 29.56 (s, *C*-30), 29.47 (s, *C*-31), 28.09 (s, *C*-22), 27.17 (s, *C*-29), 26.02 (s, *C*-28), 22.79 (s, *C*-33), 19.92 (s, *C*-20), 19.54 (s, *C*-21), 14.25 (s, *C*-34) ppm.

MS (Maldi-TOF, Cl-CCA): m/z = 957.4 $[M]^+$.

IR: $\tilde{\nu}$ = 2960.6 (w), 2354.5 (w), 2316.7 (w), 1740.6 (w), 1598.9 (m), 1578.1 (s), 1500.1 (m), 1483.2 (m), 1456.3 (s), 1393.7 (s), 1308.3 (s), 1252.6 (s), 1229.9 (vs), 1139.4 (s), 1013.2 (vs), 965.4 (s), 843.0 (s), 755.8 (s), 722.5 (m), 563.5 (m) cm^{-1}.

m.p. = 118.5 °C.

Elemental analysis: $C_{66}H_{79}N_5O$ Calc.: C 82.71, H 8.31, N 7.31,
Found: C 82.56, H 8.27, N 7.23.

Synthesis of (*E*)-12c-(3-methyl-4-(4-(methoxyphenyldiazenyl)-2-methylphenyl)phenyl) ethynyl-4,8,12-tri-*n*-propyl-4,8,12-triazatriangulene (4b):

In tetrahydrofuran (abs., 80 mL) (*E*)-1-(4-methoxyphenyl)-2-(3-methyl-4-(3-methyl-4-(ethynyl)phenyl)-phenyl)diazene (120 mg, 352 µmol) was added under nitrogen atmosphere, propyl-TATA-BF_4 (209 mg, 422 µmol) and crushed potassium hydroxide (197 mg, 3.52 mmol) were added and the mixture was refluxed for 18 h. The reaction mixture was poured onto water (150 mL) and the layers were separated. The aqueous layer was extracted with diethylether (3x 100 mL) and the combined organic layers were dried over magnesium sulfate. The solvent was removed under reduced pressure and the crude product was purified via column chromatography (alox basic, diethylether) to obtain an orange solid (216 mg, 289 µmol, 82%).

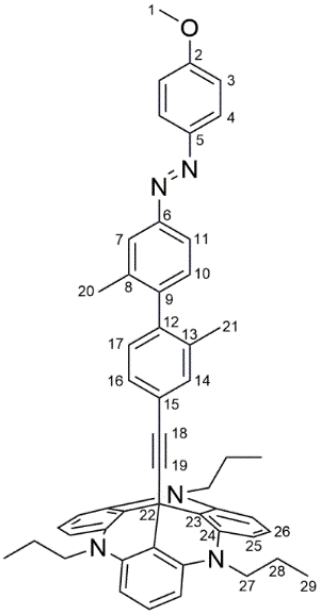

^{1}H-NMR (500.1 MHz, $CDCl_3$, 300 K, $CHCl_3$) δ = 7.91 (d, ^{3}J = 9.1 Hz, 2 H, *H*-4), 7.72 (d, ^{4}J = 1.5 Hz, 1 H, *H*-7), 7.68 (dd, ^{3}J = 8.1 Hz, ^{4}J = 1.9 Hz, 1 H, *H*-11), 7.19 (t, ^{3}J = 8.2 Hz, 3 H, *H*-26), 7.10 (d, ^{3}J = 8.1 Hz, 1 H, *H*-10), 7.07-7.05 (m, 1 H, *H*-14), 7.03-6.99 (m, 3 H, *H*-3, *H*-16), 6.88 (d, ^{3}J = 6.9 Hz, 1 H, *H*-17), 6.55 (d, ^{3}J = 8.3 Hz, 6 H, *H*-25), 3.91 (ps. t, 6 H, *H*-27), 3.89 (s, 3 H, *H*-1), 2.03 (s, 3 H, *H*-20), 1.91 (s, 3 H, *H*-21), 1.89 (ps. sext., 6 H, *H*-28), 1.07 (ps. t, 9 H, *H*-29) ppm.

^{13}C-NMR (125.8 MHz, $CDCl_3$, 300 K, $CHCl_3$) δ = 161.98 (s, *C*-2), 151.99 (s, *C*-6), 147.12 (s, *C*-5), 143.47 (s, *C*-9), 140.53 (s, *C*-24), 140.13 (s, *C*-12), 136.78 (s, *C*-8), 135.26 (s, *C*-13), 132.98 (s, *C*-14), 129.93 (s, *C*-10), 128.81 (s, *C*-16), 128.57 (s, *C*-17), 128.12 (s, *C*-26), 124.66 (s, *C*-4), 123.55 (s, *C*-7), 123.04 (s, *C*-15), 120,02 (s, *C*-11), 114.21 (s, *C*-3), 110.28 (s, *C*-23), 104.94 (s, *C*-25), 93.38 (s, *C*-19), 83.47 (s, *C*-18), 55.57 (s, *C*-1), 48.11 (s, *C*-27), 27.97 (s, *C*-22), 19.79 (s, *C*-20), 19.43 (s, *C*-21), 19.17 (s, *C*-28), 11.21 (s, *C*-29) ppm.

MS (Maldi-TOF, Cl-CCA): m/z = 747.1 $[M]^+$.

IR: $\tilde{\nu}$ = 2958.4 (w), 1738.4 (w), 1602.8 (s), 1580.5 (vs), 1482.2 (s), 1454.8 (vs), 1392.4 (m), 1379.4 (m), 1231.6 (vs), 1165.9 (m), 1140.6 (s), 1023.0 (m), 842.4 (m), 776.0 (m) cm^{-1}.

m.p. = 224.1 °C.

Elemental analysis: $C_{51}H_{49}N_5O$ Calc.: C 81.89, H 6.60, N 9.36,
Found: C 81.30, H 6.58, N 9.02.

2.3 Synthesis of compound 5a and 5b

The azo benzene cage platforms **5a** and **5b** were synthesized in 6 steps from commercially available chemicals. Compounds **25** and **28** were synthesized as reported in the literature.[8]

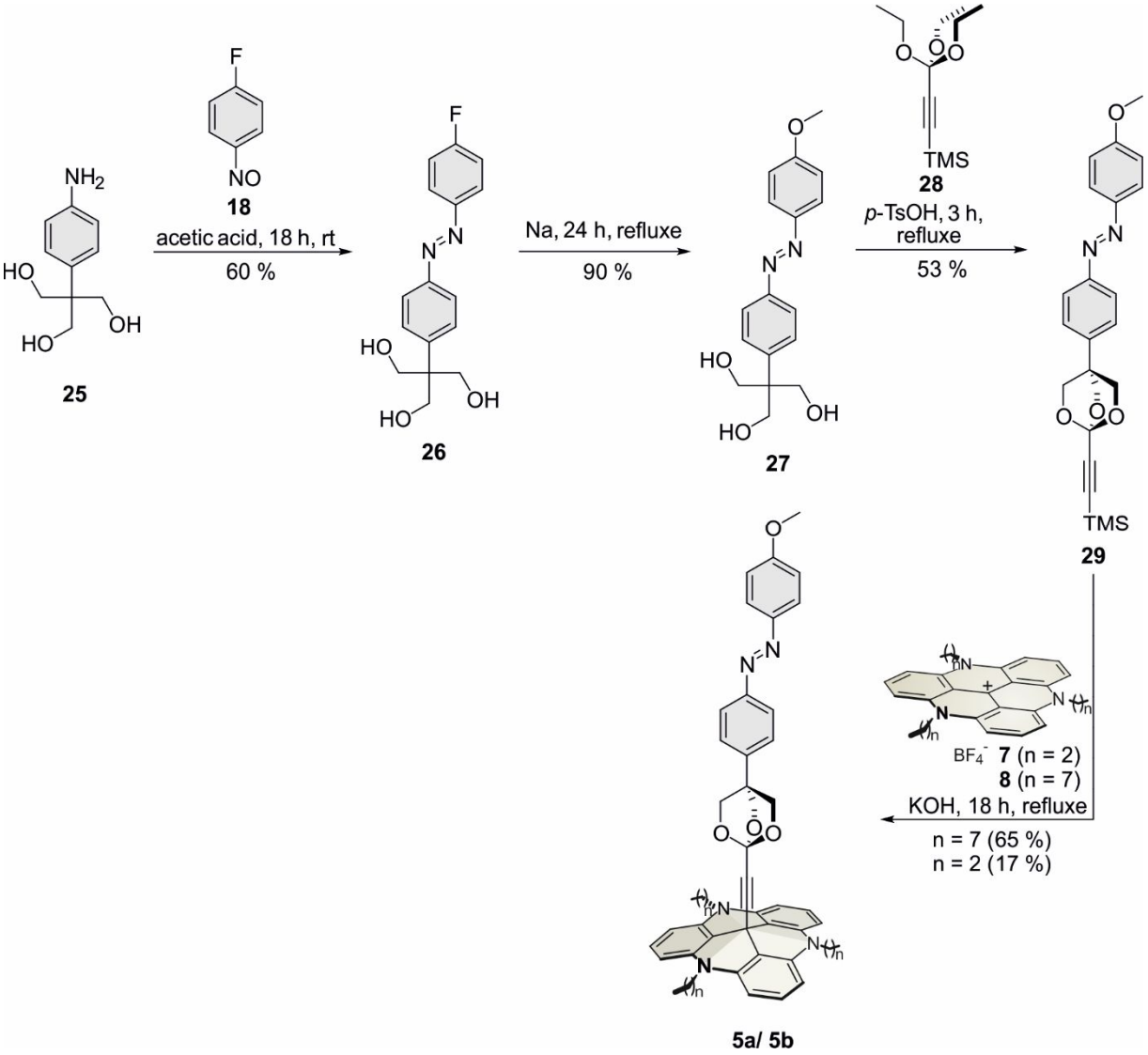

Scheme S4: Synthesis route of compound **5a** and **5b**.

Synthesis of (*E*)-2-(4-((4-fluorophenyl)diazenyl)phenyl)-2-(hydroxymethyl)-propane-1,3-diol (26):

In acetic acid (10 mL) 2-(4-aminophenyl)-2-(hydroxymethyl)propane-1,3-diol (200 mg, 1.01 mmol) and *p*-fluoronitrosobenzene (138 mg, 1.1 mmol) were dissolved and stirred for 18 h at room temperature. To the solution water (50 mL) was added and extracted with ethylacetate (3x 50 mL). The organic layer was dried over magnesium sulfate and the solvent was removed under reduced pressure. The crude product was purified via column chromatography (silica gel, dichloromethan/ methanol, 9:1) to obtain an orange solid (185 mg, 608 µmol, 60%).

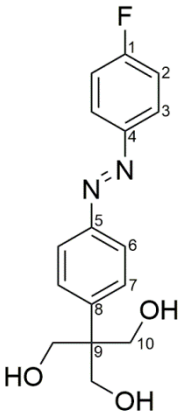

^{1}H-NMR (500.1 MHz, DMSO-d_6, 300 K, TMS) δ = 7.98-7.92 (m, 2 H, *H*-3), 7.80 (d, ^{3}J = 8.5 Hz, 2 H, *H*-6), 7.65 (d, ^{3}J = 8.6 Hz, 2 H, *H*-7), 7.42 (ps. t, 2 H, *H*-2), 4.51 (s, 3 H, O*H*), 3.76 (s, 6 H, *H*-10) ppm.

^{13}C-NMR (500.8 MHz, DMSO-d_6, 300 K, TMS) δ = 163.53 (d, ^{1}J = 249.5 Hz, *C*-1), 149.86 (s, *C*-5), 148.80 (s, *C*-4), 147.52 (s, *C*-8), 128.81 (s, *C*-7), 124.72 (d, ^{3}J = 9.2 Hz, *C*-3), 121.72 (s, *C*-6), 116.39 (d, ^{2}J = 23.0 Hz, *C*-2), 63.18 (s, *C*-10), 49.8 (s, *C*-9) ppm.

^{19}F-NMR (470.6 MHz, DMSO-d_6, 300 K, TMS) δ = 109.15 ppm.

MS (ESI-TOF): *m*/*z* = 327 (100) $[M+Na]^+$.

IR: $\tilde{\nu}$ = 3227 (br. m), 2949 (w), 1592 (m), 1495 (m), 1404 (w), 1229 (m), 1140 (w), 1074 (m), 1046 (m), 1005 (m), 925 (w), 842 (s), 709 (w), 560 (s), 515 (w) cm^{-1}.

m.p. = 161 °C.

Elemental analysis: $C_{16}H_{17}FN_2O_3$ calc.: C 63.15, H 5.63, N 9.21,
found: C 63.35, H 5.65, N 9.30.

Synthesis of (*E*)-2-(hydroxymethyl)-2-(4-((4-methoxyphenyl)diazenyl)phenyl)-propane-1,3-diol (27):

In methanol (297 mL) sodium (16.2 g, 707 mmol) was dissolved, (*E*)-2-(4-((4-fluorophenyl)diazenyl)phenyl)-2-(hydroxymethyl)-propane-1,3-diol (1.01 g, 3.62 mmol) was added and refluxed for 13 h. To the solution water (600 mL) was added and extracted with ethyl acetate (3x 300 mL). The combined organic layers were dried over magnesium sulfate and the solvent was removed under reduced pressure. The crude product was purified via column chromatography (silica gel, dichloromethane/ methanol, 9:1) to obtain an orange solid (1.03 g, 3.27 mmol, 90%).

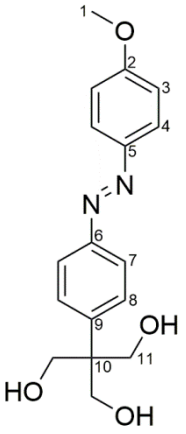

^{1}H-NMR (500.1 MHz, DMSO-d_6, 300 K, TMS) δ = 7.88 (d, ^{3}J = 9.0 Hz, 2 H, *H*-4), 7.76 (d, ^{3}J = 8.6 Hz, 2 H, *H*-7), 7.62 (d, ^{3}J = 8.6 Hz, 2 H, *H*-8), 7.12 (d, ^{3}J = 9.0 Hz, 2 H, *H*-3), 4.50 (t, ^{3}J = 5.2 Hz, 3 H, O*H*), 3.86 (s, 3 H, *H*-12), 3.76 (d, ^{3}J = 5.2 Hz, 6 H, *H*-11) ppm.

^{13}C-NMR (125.8 MHz, DMSO-d_6, 300 K, TMS) δ = 161.78 (s, *C*-2), 150.07 (s, *C*-6), 146.60 (s, *C*-9), 146.29 (s, *C*-5), 128.69 (s, *C*-8), 124.38 (s, *C*-4), 121.42 (s, *C*-7), 114.57 (s, *C*-3), 63.23 (s, *C*-11), 55.64 (s, *C*-12) ppm.

MS (ESI-TOF): *m*/*z* = 317 $[M+H]^+$.

IR: $\tilde{\nu}$ = 3235 (br. w), 2941 (w), 1600 (m), 1581 (m), 1497 (m), 1415 (w), 1295 (w), 1246 (s), 1136 (m), 1019 (m), 838 (m), 771 (w), 655 (w), 582 (w), 552 (w), 529 (w) cm^{-1}.

m.p. = 201 °C.

Elemental analysis: $C_{17}H_{20}N_2O_4$ calc.: C 64.54, H 6.37, N 8.86,
found.: C 64.30, H 6.33, N 8.88.

Synthesis of (*E*)-1-(4-methoxyphenyl)-2-(4-(1-((trimethylsilyl)ethynyl)-2,6,7-trioxabicyclo[2.2.2]octane-4-yl)phenyl)diazene (29):

In toluene (80 mL) (*E*)-2-(hydroxymethyl)-2-(4-((4-methoxyphenyl)diazenyl)phenyl)-propane-1,3-diol (296 mg, 937 µmol) was dissolved and trimethyl(3,3,3-triethoxyprop-1-in-1-yl)silane (230 mg, 944 µmol) and *p*-toluene sulfonic acid (500 µg, 2.90 µmol) were added. Toluene was added and the mixture was destilled for 3 h. Triethylamine (1 mL) was added and the solution was washed with saturated sodium carbonate solution (3x 150 mL). The combined organic layers were dried over magnesium sulfate and the solvent was removed under reduced pressure. The crude product was purified via column chromatography (silica gel, dichloromethane) to obtain an orange solid (196 mg, 465 µmol, 53%).

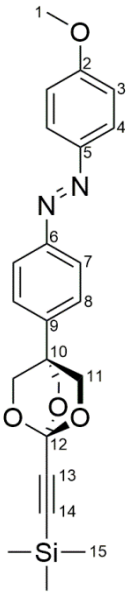

^{1}H-NMR (500.1 MHz, $CDCl_3$, 300 K, TMS) δ = 7.92 (d, ^{3}J = 9.1 Hz, 2 H, *H*-4), 7.87 (d, ^{3}J = 8.8 Hz, 2 H, *H*-7), 7.26 (d, ^{3}J = 8.5 Hz, 2 H, *H*-8), 7.02 (d, ^{3}J = 9.0 Hz, 2 H, *H*-3), 4.44 (s, 6 H, *H*-11), 3.90 (s, 3 H, *H*-1), 0.23 (s, 9 H, *H*-15) ppm.

^{13}C-NMR (125.8 MHz, $CDCl_3$, 300 K, TMS) δ = 162.43 (s, *C*-2), 152.36 (s, *C*-6), 146.90 (s, *C*-5), 137.04 (s, *C*-9), 125.97 (s, *C*-8), 124.97 (s, *C*-4), 123.21 (s, *C*-7), 114.28 (s, *C*-3), 101.64 (s, *C*-12), 96.63 (s, *C*-13), 88.45 (s, *C*-14), 71.92 (s, *C*-11), 55.63 (s, *C*-1), 36.74 (s, *C*-10), -0.58 (s, *C*-15) ppm.

^{29}Si-NMR (99.4 MHz, $CDCl_3$, 300 K, TMS) δ = -15.43 ppm.

MS (EI, 70eV): m/z = 422 $[M]^+$.

IR: $\tilde{\nu}$ = 2950 (w), 2900 (w), 1599 (w), 1581 (w), 1497 (w), 1292 (m), 1244 (m), 1137 (m), 1084 (m), 1008 (m), 965 (m), 840 (s), 757 (m), 656 (m), 564 (m), 517 (w) cm^{-1}.

m.p. = 276 °C.

Elemental analysis: $C_{23}H_{26}N_2O_4Si$ calc.: C 65.38, H 6.20, N 6.63,
found: C 65.76, H 6.41, N 6.01.

Synthesis of (*E*)-12c-((4-(4-((4-methoxyphenyl)diazenyl)phenyl)-2,6,7-trioxabicyclo [2.2.2]octane-1-yl)ethynyl)-4,8,12-tri-*n*-octyl-4,8,12-triazatriangulene (5a):

In tetrahydrofuran (abs., 50 mL) (*E*)-1-(4-methoxyphenyl)-2-(4-(1-((trimethylsilyl)ethynyl)-2,6,7-trioxabicyclo[2.2.2]octane-4-yl)phenyl)diazene (248 mg, 587 µmol) was dissolved under nitrogen atmosphere, octyl-TATA-BF_4 (424 mg, 601 µmol) and crushed potassium hydroxide (220 mg, 3.92 mmol) were added and the reaction mixture was refluxed for 18 h. The solution was poured onto saturated sodium chloride solution (100 mL) and diethylether (100 mL) was added. The layers were separated, the combined organic layers were washed with diluted sodium chloride solution (3x 100 mL) and dried over magnesium sulfate. The solvent was removed under reduced pressure and the crude product was purified via column chromatography (alox basic, diethylether) and recrystalization from ethanol to obtain a yellow solid (370 mg, 382 µmol, 65%).

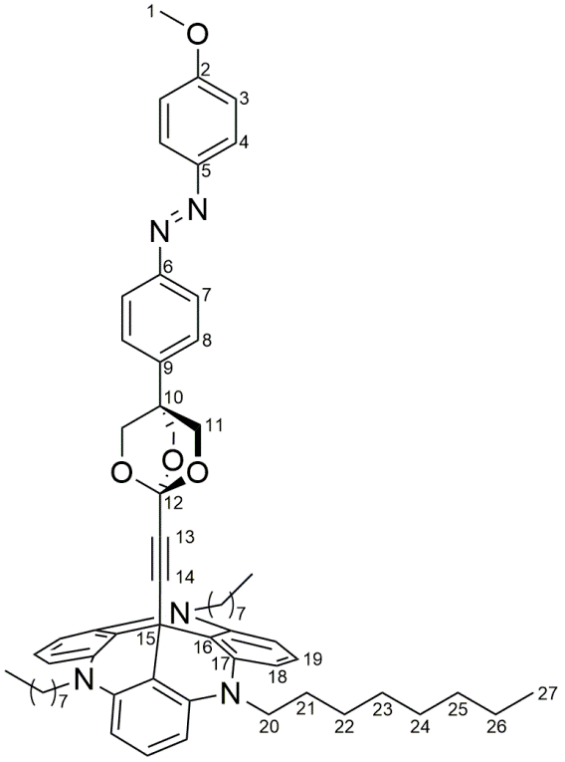

^{1}H-NMR (500.1 MHz, acetone-d_6, 300 K, TMS) δ = 7.90 (d, ^3J = 9.1 Hz, 2 H, *H*-4), 7.83 (d, ^3J = 8.6 Hz, 2 H, *H*-7), 7.39 (d, ^3J = 8.6 Hz, 2 H, *H*-8), 7.23 (t, ^3J = 8.3 Hz, 3 H, *H*-19), 7.10 (d, ^3J = 9.2 Hz, 2 H, *H*-3), 6.67 (d, ^3J = 8.3 Hz, 6 H, *H*-18), 4.19 (s, 6 H, *H*-11), 3.98 (ps. t, 6 H, *H*-20), 3.91 (s, 3 H, *H*-1), 1.84 (ps. quint., 6 H, *H*-21), 1.54 (ps. quint., 6 H, *H*-22), 1.48-1.28 (m, 24 H, *H*-23, *H*-24, *H*-25, *H*-26), 0.89 (ps. t, 9 H, *H*-27) ppm.

^{13}C-NMR (125.8 MHz, acetone-d_6, 300 K, TMS) δ = 163.57 (s, *C*-2), 152.82 (s, *C*-6), 147.65 (s, *C*-5), 141.34 (s, *C*-17), 139.27 (s, *C*-9), 129.64 (s, *C*-18), 127.36 (s, *C*-8), 125.61 (s, *C*-4), 123.63 (s, *C*-7), 115.29 (s, *C*-3), 109.51 (s, *C*-16), 106.02 (s, *C*-18), 103.30 (s, *C*-12), 71.85 (s, *C*-11), 56.08 (s, *C*-15), 47.01 (s, *C*-20), 37.27 (s, *C*-10), 32.65 (s, *C*-25), 30.17 (s, *C*-23), 30.08 (s, *C*-24), 27.52 (s, *C*-22), 26.34 (s, *C*-21), 23.36 (s, *C*-26), 14.40 (s, *C*-27) ppm.

MS (MALDI-TOF, Cl-CCA): m/z = 968 $[M]^+$.

IR: $\tilde{\nu}$ = 2963 (w), 2876 (w), 1608 (w), 1577 (w), 1515 (s), 1443 (m), 1353 (s), 1190 (w), 1151 (w), 1089 (w), 1032 (w), 960 (w), 854 (m), 783 (m), 751 (m), 710 (m), 666 (m), 561 (m), 530 (w) cm^{-1}.

m.p. = 131 °C

Elemental analysis: $C_{63}H_{77}N_5O_4$ x 2 H2O calc.: C 75.34, H 8.13, N 6.97, found: C 75.35, H 7.84, N 6.97.

Synthesis of (*E*)-12c-((4-(4-((4-methoxyphenyl)diazenyl)phenyl)-2,6,7-trioxabicyclo [2.2.2]octane-1-yl)ethynyl)-4,8,12-tri-*n*-octyl-4,8,12-triazatriangulene (5b):

In tetrahydrofuran (abs., 85 mL) (*E*)-1-(4-methoxyphenyl)-2-(4-(1-((trimethylsilyl)ethynyl)-2,6,7-trioxabicyclo[2.2.2]octane-4-yl)phenyl)diazene (100 mg, 237 µmol) was dissolved under nitrogen atmosphere, octyl-TATA-BF_4 (129 mg, 261 µmol) und crushed potassium hydroxide (97.0 mg, 1.73 mmol) were added and the mixture was sonificated for 5 h at room temperature. The mixture was poured onto saturated sodium chloride solution (100 mL) and extracted with diethylether (3x 100 mL). The combined organic layers were dried over magnesium sulfate and the solvent was removed under reduced pressure. The crude product was purified via column chromatography (alox basic, diethylether) to obtain an orange solid (32.0 mg, 42.3 µmol, 18%).

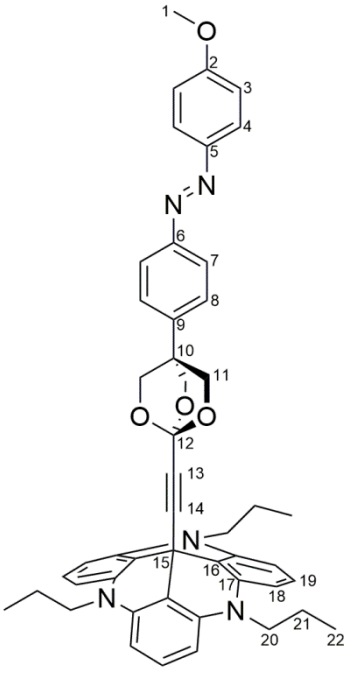

^{1}H-NMR (500.1 MHz, C_6D_6, 300 K, C_6H_6) δ = 8.04 (d, ^3J = 9.0 Hz, 2 H, *H*-4), 7.73 (d, ^3J = 8.6 Hz, 2 H, *H*-7), 7.14 (t, ^3J = 8.2 Hz, 3 H, *H*-19), 6.72 (d, ^3J = 9.1 Hz, 2 H, *H*-3), 6.43 (d, ^3J = 8.3 Hz, 6 H, *H*-18), 6.29 (d, ^3J = 8.6 Hz, 2 H, *H*-8), 3.68 (s, 6 H, *H*-11), 3.48 (ps. t, 6 H, *H*-20), 3.16 (s, 3 H, *H*-1), 1.70 (m, 6 H, *H*-21), 0.80 (ps. t, 9 H, *H*-22) ppm.

^{13}C-NMR (125.8 MHz, C_6D_6, 300 K, C_6H_6) δ = 162.76 (s, *C*-2), 152.28 (s, *C*-9), 147.58 (s, *C*-5), 141.02 (s, *C*-17), 138.38 (s, *C*-6), 128.67 (s, *C*-19), 126.19 (s, *C*-7), 125.35 (s, *C*-4), 123.16 (s, *C*-8), 114.62 (s, *C*-3), 109.87 (s, *C*-16), 105.47 (s, *C*-18), 103.38 (s, *C*-12), 71.18 (s, *C*-11), 55.01 (s, *C*-1), 48.28 (s, *C*-20), 36.53 (s, *C*-10), 19.17 (s, *C*-21), 11.16 (s, *C*-22) ppm.

MS (Maldi-TOF, Cl-CCA): m/z = 757.7 $[M]^+$.

m.p. = 231.5 °C

IR: $\tilde{\nu}$ = 2956 (w), 2876 (w), 1599 (s), 1578 (vs), 1457 (vs), 1394 (vs), 1308 (vs), 1255 (vs), 1229 (vs), 1141 (s), 1093 (s), 1013 (s), 964 (s), 843 (s), 756 (vs), 722 (s), 563 (m) cm^{-1}.

2.4 Synthesis of (*E*)-1-phenyl-2-(4-(((tris(2,4,6-trimethylphenyl)-phosphine)-(9Cl)-gold)-ethynyl)phenyl)diazene

Compound **6** was synthesized in 5 steps from commercial aviable compounds. Compound **30** was synthesized as described in the literature.[9]

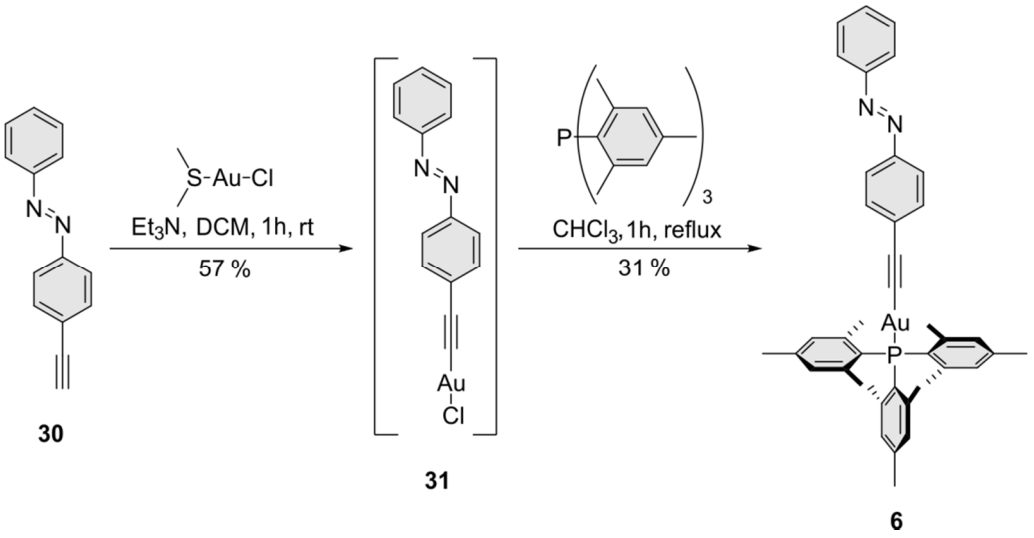

Scheme S5: Synthetic route of compound **6**.

Synthesis of (*E*)-1-phenyl-2-(4-(((tris(2,4,6-trimethylphenyl)-phosphine)-(9Cl)-gold) ethynyl)phenyl)diazene (6):

In dichloromethane (20 mL) 1-(4-ethynylphenyl)-2-phenyl-diazene (350 mg, 1.70 mmol) was dissolved and triethylamine (1.00 mL, 7.21 mmol) and chloro(dimethylsulfide)gold(I) (500 mg, 1.70 mmol) was added successively. The mixture was stirred for 1 h at room temperature. The solid was filtered and washed with dichloromethane to obtain an unsoluble green solid (465 mg).

In chloroform (6 mL) chloro[(phenyl-2-phenyl-diazene)ethynyl]-(9Cl)-aurate(I) (40.0 mg, 91.5 µmol) and tris(2,4,6-trimethylphenyl)-phosphine (53.3 mg, 137 µmol) were suspended and refluxed for 3 h. The reaction mixture was filtered over magnesium sulfate and the solvent was removed under reduced pressure. The crude orange solid was dissolved in methanol (10 mL) and stirred for 0.5 h at room temperature. The precipitated solid was filtered and washed with less methanol to obtain the product as an orange solid (28.0 mg, 35.4 µmol, 39%).

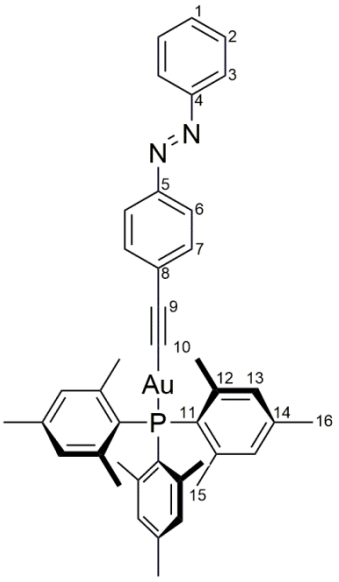

^{1}H-NMR (500.1 MHz, $CDCl_3$, 300 K, TMS) δ = 7.87 (d, ^{3}J = 7.9 Hz, 2 H, *H*-3), 7.78 (d, ^{3}J = 8.4 Hz, 2 H, *H*-6), 7.56 (d, ^{3}J = 8.5 Hz, 2 H, *H*-7), 7.49 (t, ^{3}J = 7.4 Hz, 2 H, *H*-2), 7.43 (t, ^{3}J = 7.1 Hz, 1 H, *H*-1), 6.87 (s, 6 H, *H*-13), 3.32-1.60 (m, 27 H, *H*-15, *H*-16) ppm.

^{13}C-NMR (125.8 MHz, $CDCl_3$, 300 K, TMS) δ = 152.82 (s, *C*-4), 150.62 (s, *C*-5), 140.72 (d, ^{4}J = 2.3 Hz, *C*-14), 132.98 (d, ^{5}J = 1.1 Hz, *C*-7), 131.54 (d, ^{2}J = 8.8 Hz, *C*-12), 130.69 (s, *C*-1), 129.02 (s, *C*-2), 128.69 (s, ^{4}J = 2.9 Hz, *C*-8), 126.04 (d, ^{1}J = 47.9 Hz, *C*-11), 122.75 (s, *C*-3), 122.63 (s, *C*-6), 103.44 (s, *C*-9), 20.88 (m, *C*-15, *C*-16) ppm.

^{31}P-NMR (202.5 MHz, $CDCl_3$, 300 K, TMS) δ = 10.17 ppm.

MS (ESI): m/z = 791 $[M+H]^+$.

IR: $\tilde{\nu}$ = 2921 (br. w), 2111 (br. w), 1712 (w), 1593 (m), 1437 (s), 1222 (w), 1030 (w), 846 (vs), 688 (m), 631 (vs), 554 (vs) cm^{-1}.

3. NMR Spectra

3.1 Synthesis Compound 1

(*E*)-12*c*-[4-(4-methoxyphenyldiazenyl)phenyl]ethynyl-4,8,12-tri-*n*-octyl-4,8,12-triazatriangulene:

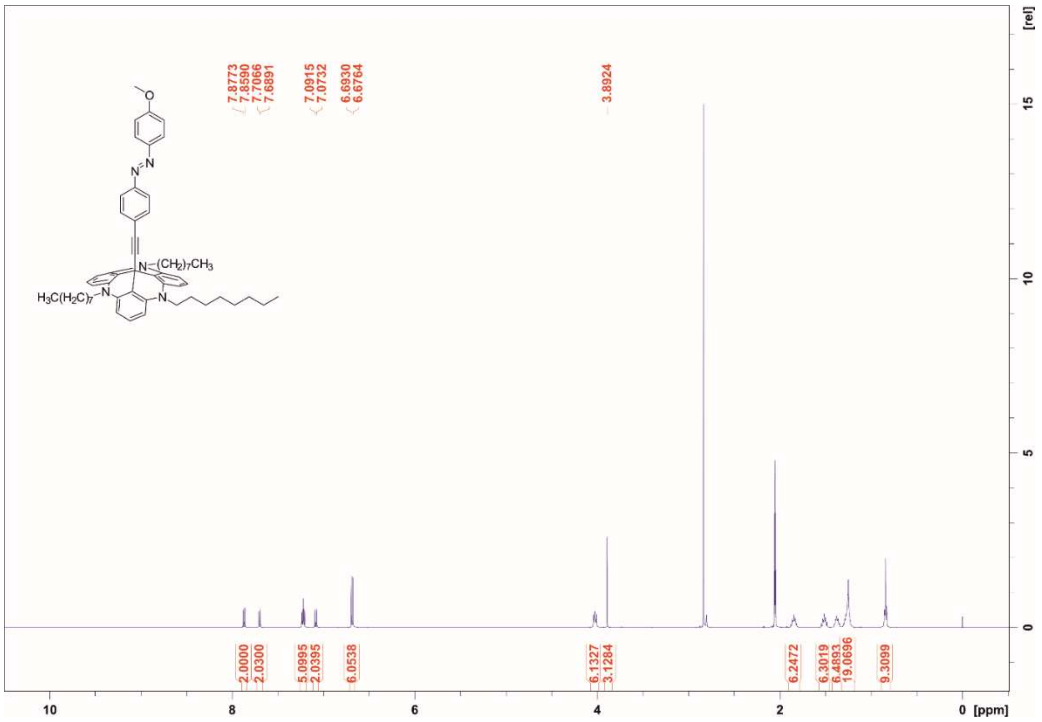

Figure S2. ^{1}H-NMR spectrum (500 MHz, acetone-d_6) of compound **1a**.

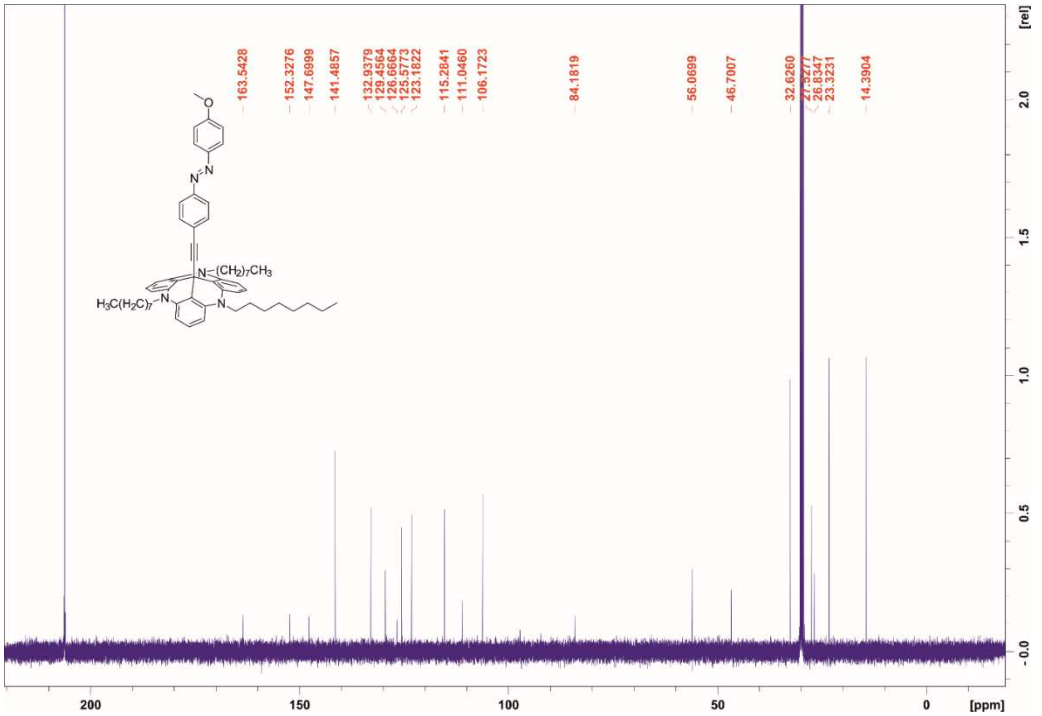

Figure S3. ^{13}C-NMR spectrum (126 MHz, acetone-d_6) of compound **1a**.

(*E*)-12*c*-[4-(4-methoxyphenyldiazenyl)phenyl]ethynyl-4,8,12-tri-*n*-propyl-4,8,12-triazatriangulene:

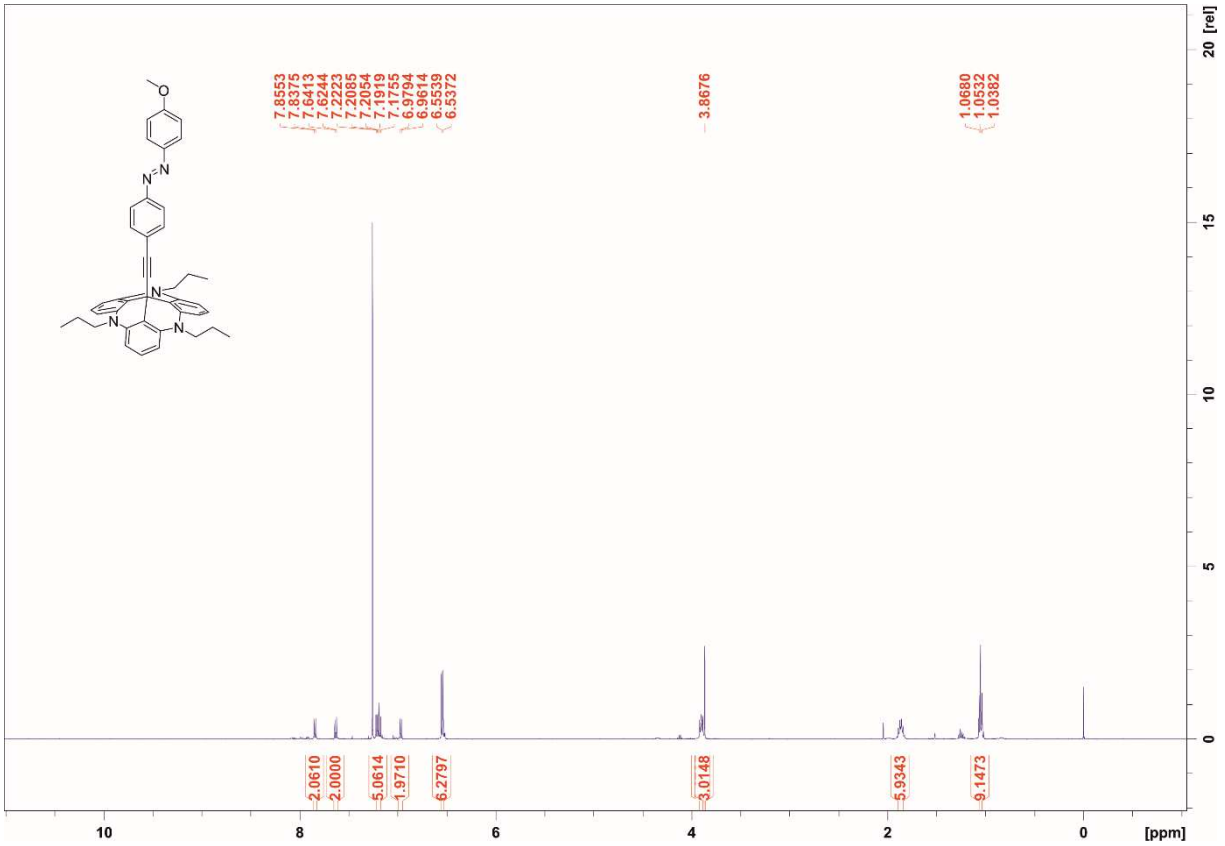

Figure S4. ^{1}H-NMR (500 MHz, $CDCl_3$) of compound **1b**.

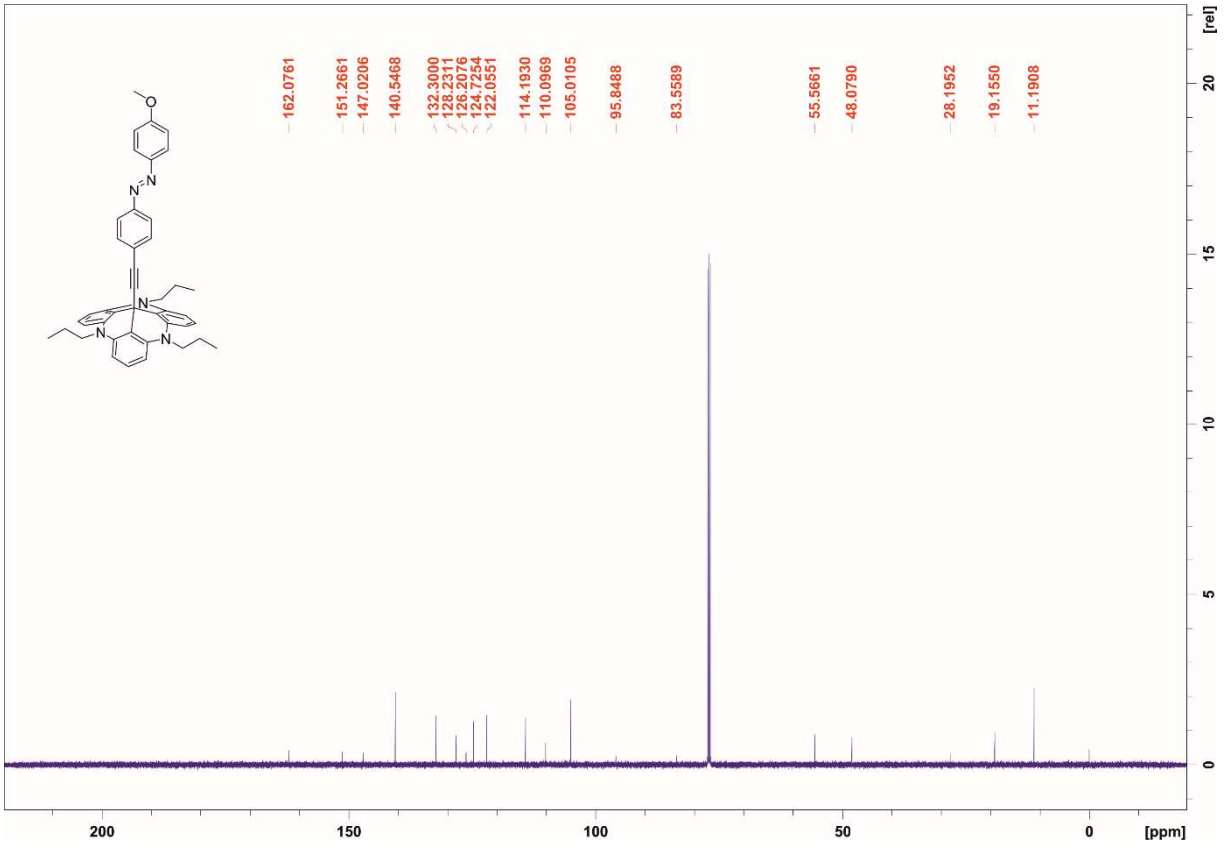

Figure S5. ^{13}C-NMR (126 MHz, $CDCl_3$) of compound **1b**.

3.2 Synthesis Compound 2

(*E*)-1-(4-fluorophenyl-2-(4-(4-((trimethylsilyl)ethynyl)phenyl)-phenyl)diazene:

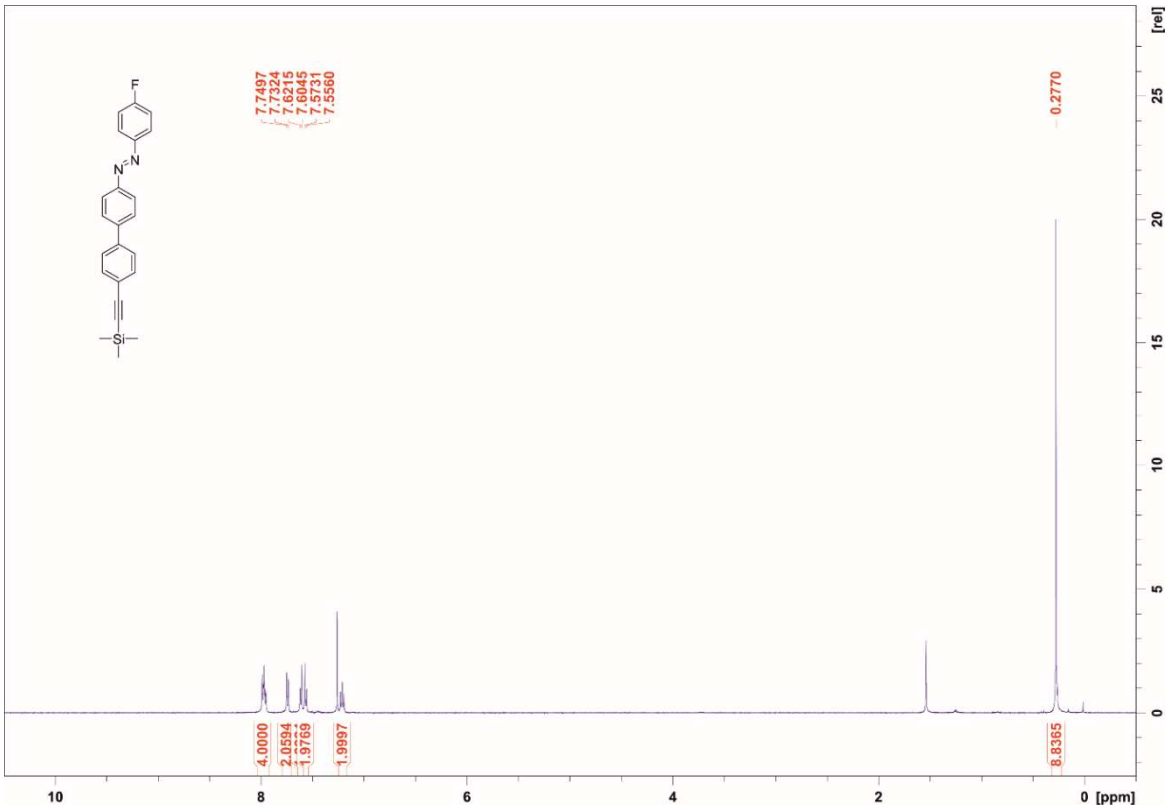

Figure S6. ^{1}H-NMR spectrum (500 MHz, $CDCl_3$) of compound **19**.

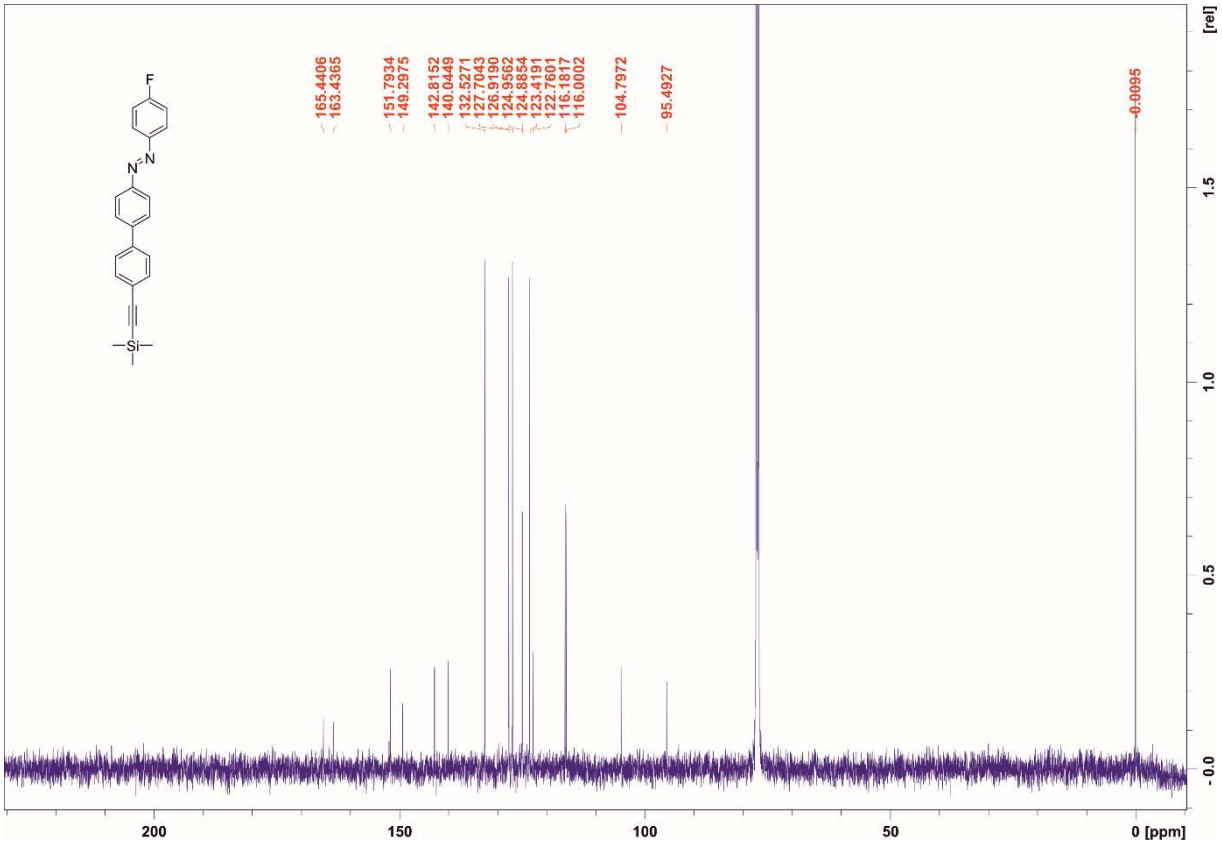

Figure S7. ^{13}C-NMR spectrum (126 MHz, $CDCl_3$) of compound **19**.

(*E*)-1-(4-methoxyphenyl-2-(4-(4-(ethynyl)phenyl)-phenyl)diazene:

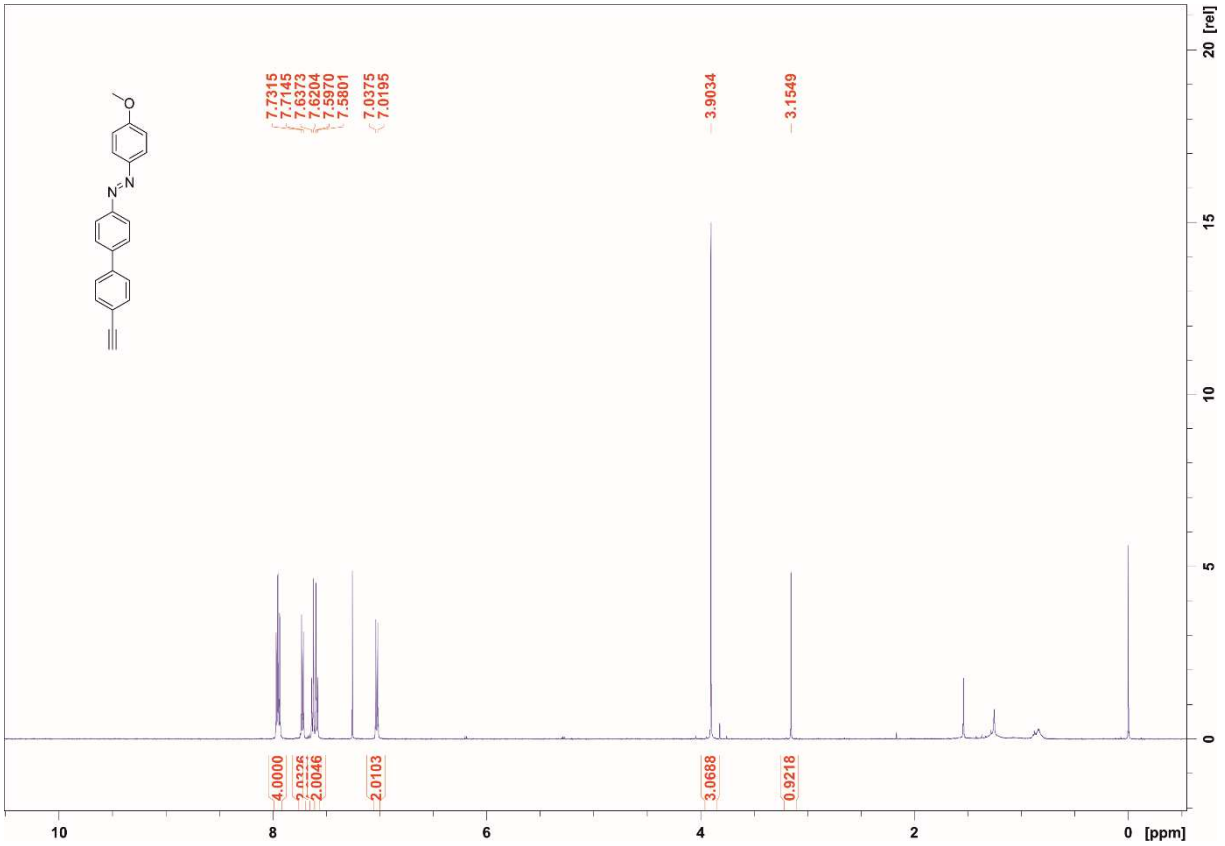

Figure S8. ^{1}H-NMR spectrum (500 MHz, $CDCl_3$) of compound **22**.

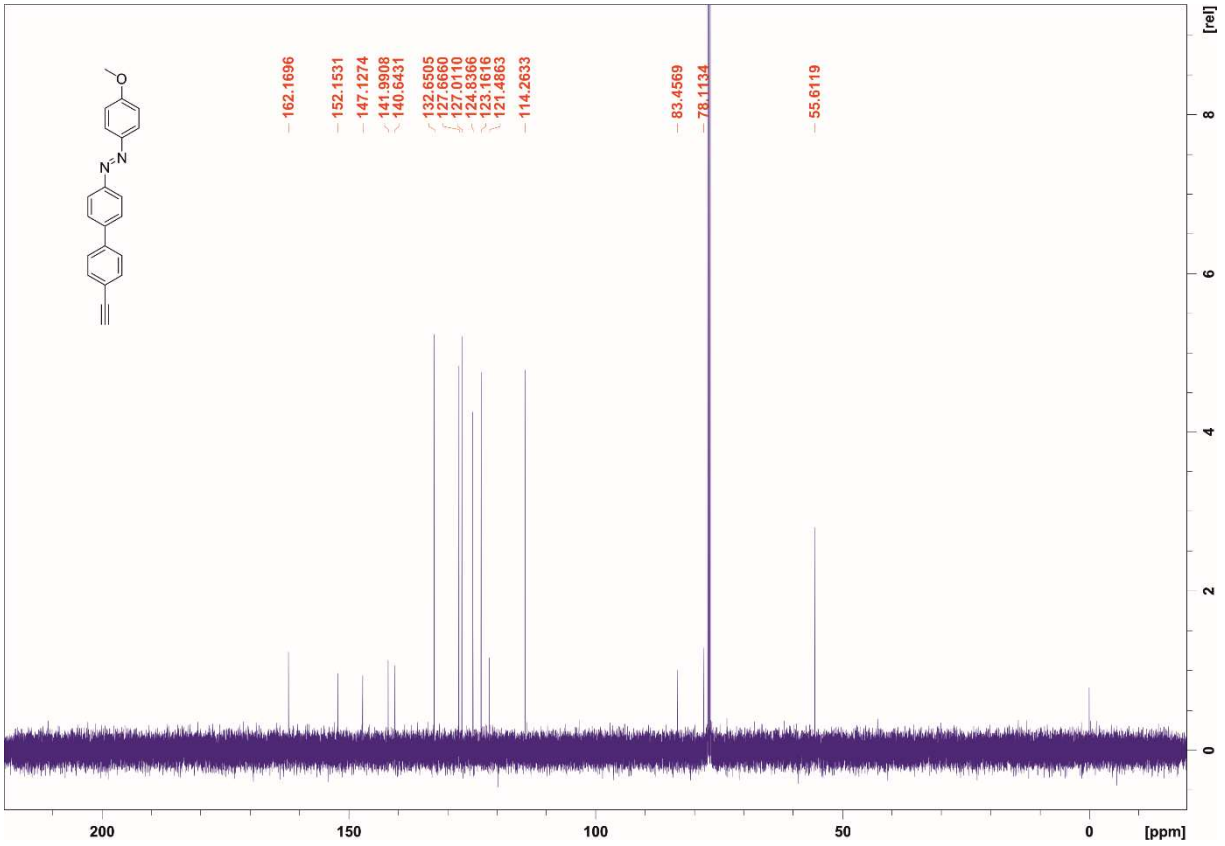

Figure S9. ^{13}C-NMR spectrum (126 MHz, $CDCl_3$) of compound **22**.

(*E*)-12c-(4-(4-(methoxyphenyldiazenyl)phenyl)phenyl)ethynyl-4,8,12-tri-*n*-octyl-4,8,12-triazatriangulene:

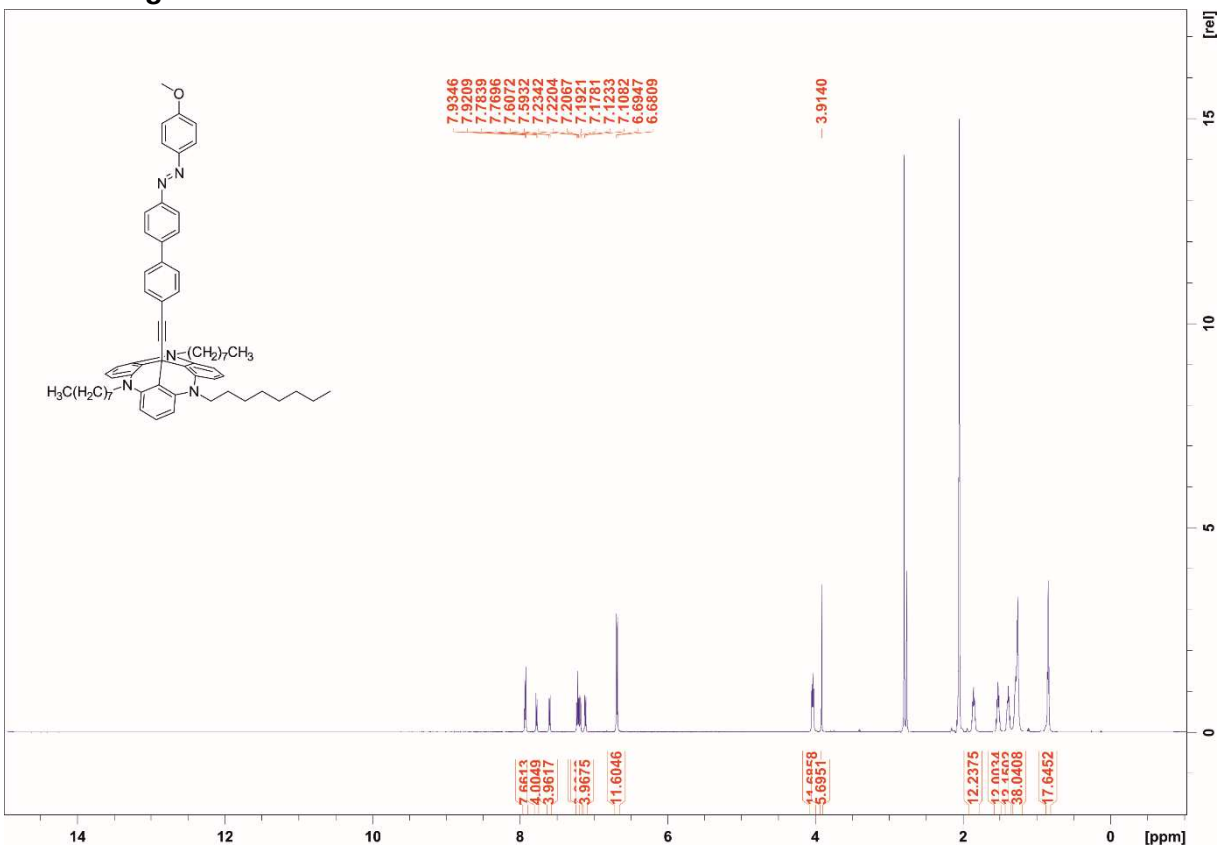

Figure S10. ^{1}H-NMR (600 MHz, acetone-d_6) of compound **2a**.

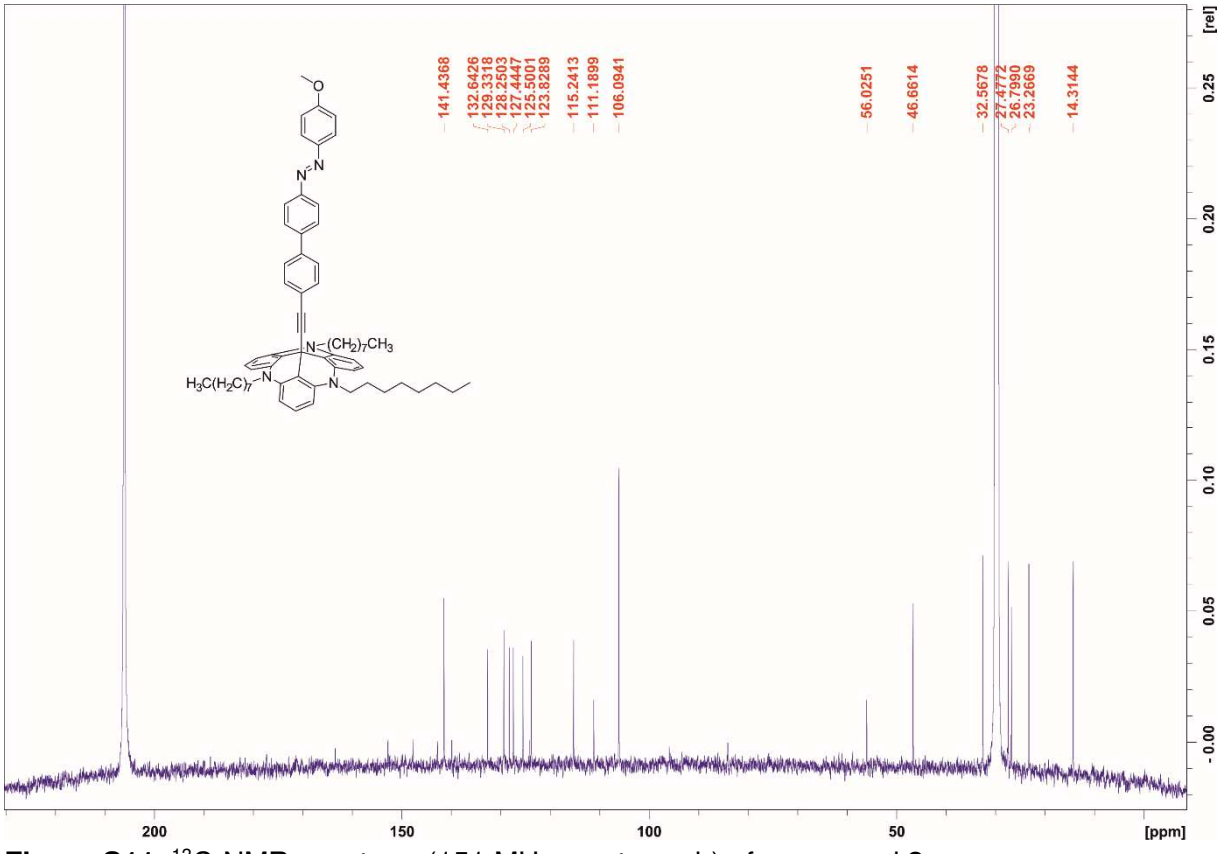

Figure S11. ^{13}C-NMR spectrum (151 MHz, acetone-d_6) of compound **2a**.

(*E*)-12c-(4-(4-(methoxyphenyldiazenyl)phenyl)phenyl)ethynyl-4,8,12-tri-*n*-propyl-4,8,12-triazatriangulene:

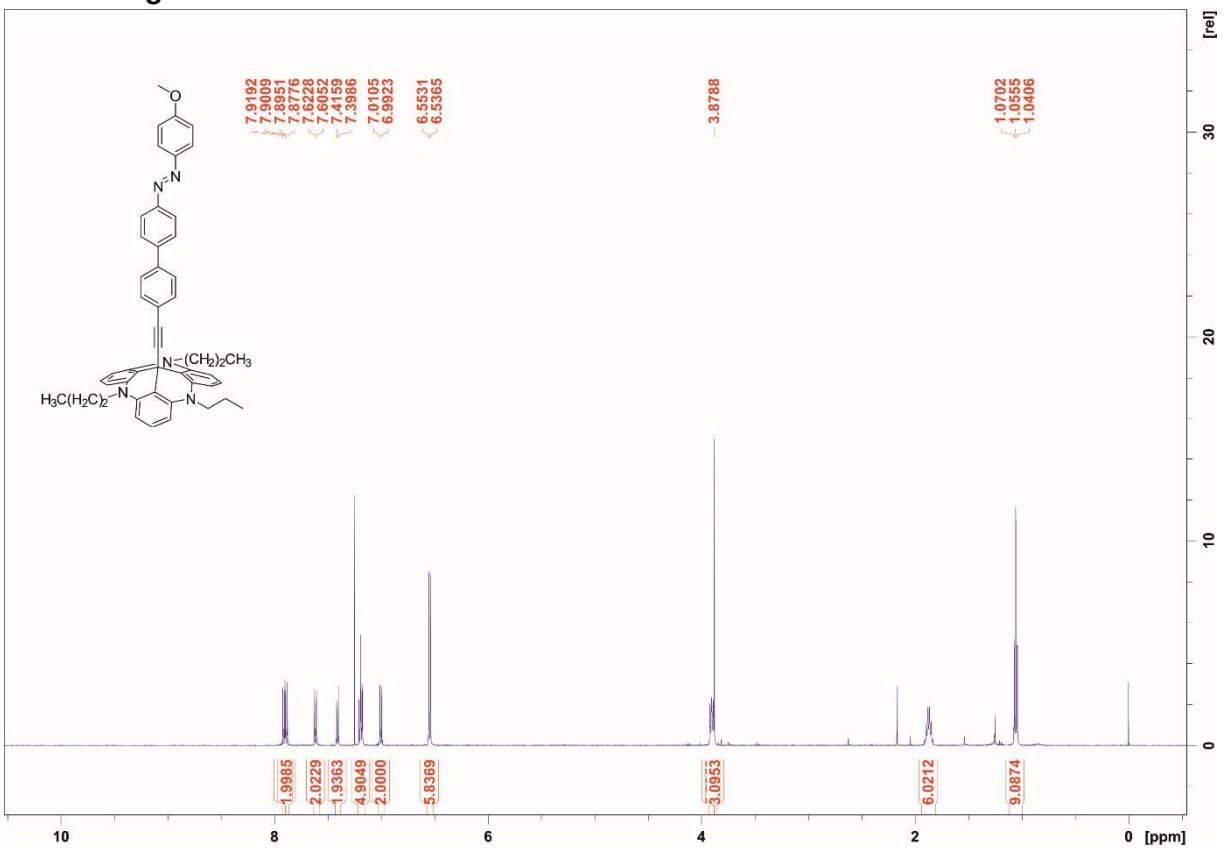

Figure S12. ^{1}H-NMR spectrum (500 MHz, $CDCl_3$) of compound **2b**.

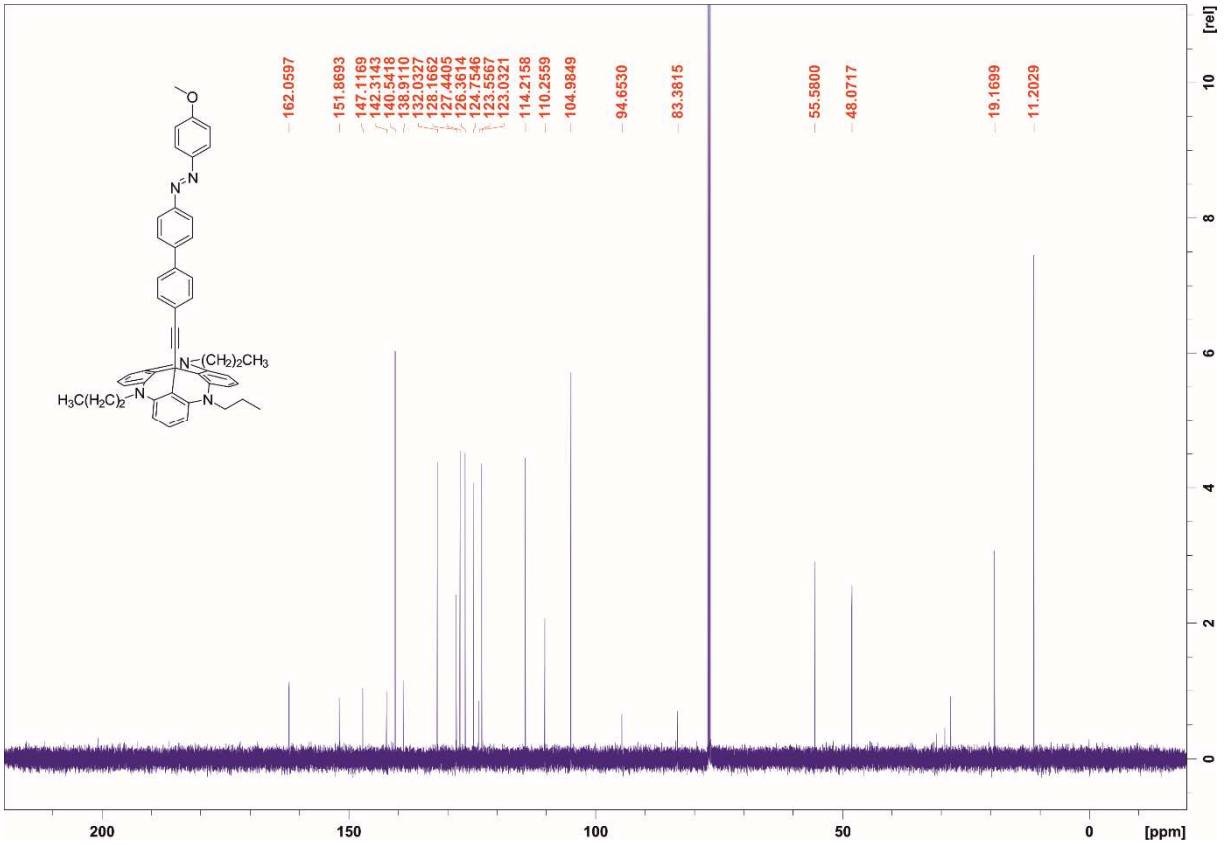

Figure S13. ^{13}C-NMR spectrum (126 MHz, $CDCl_3$) of compound **2b**.

3.3 Synthesis Compound 3

4,4,5,5-tetramethyl-2[-4-[2-(trimethylsilyl)ethynyl]phenyl]-1,3,2-dioxaborolane:

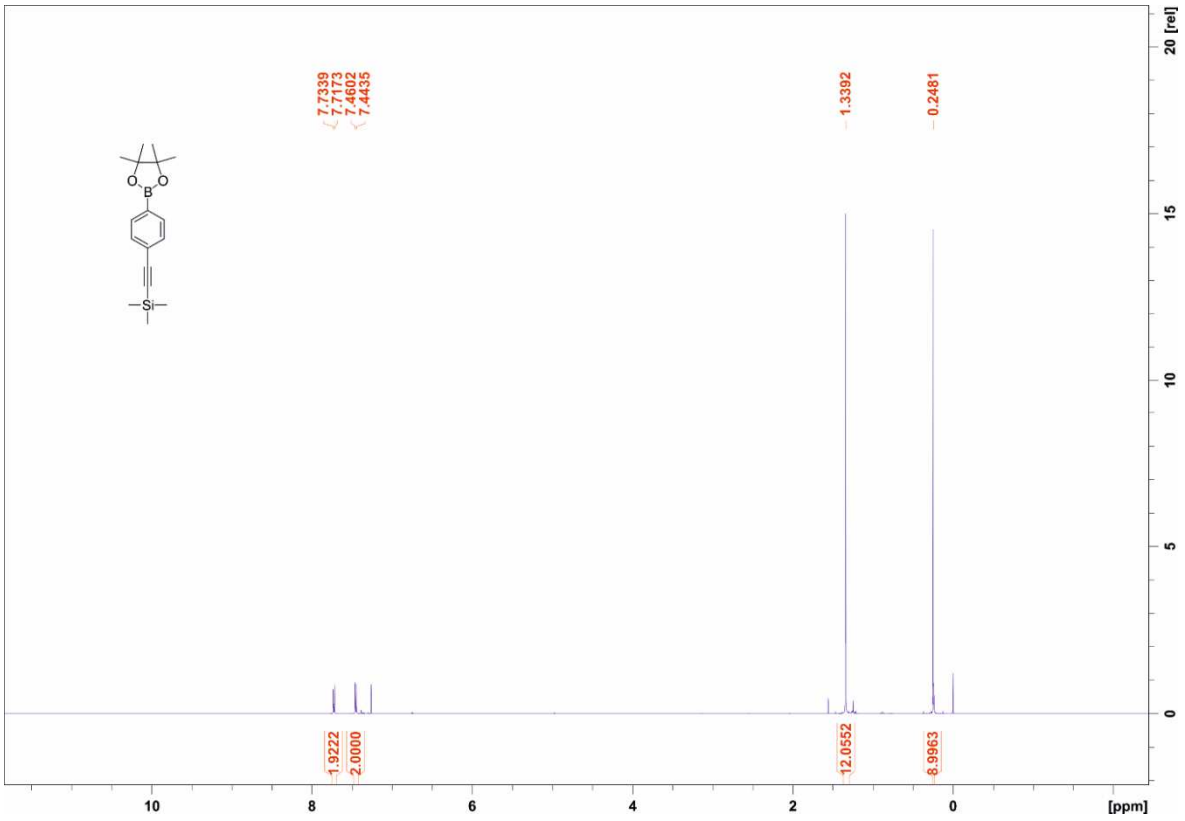

Figure S14. ^{1}H-NMR spectrum (500 MHz, $CDCl_3$) of compound **12**.

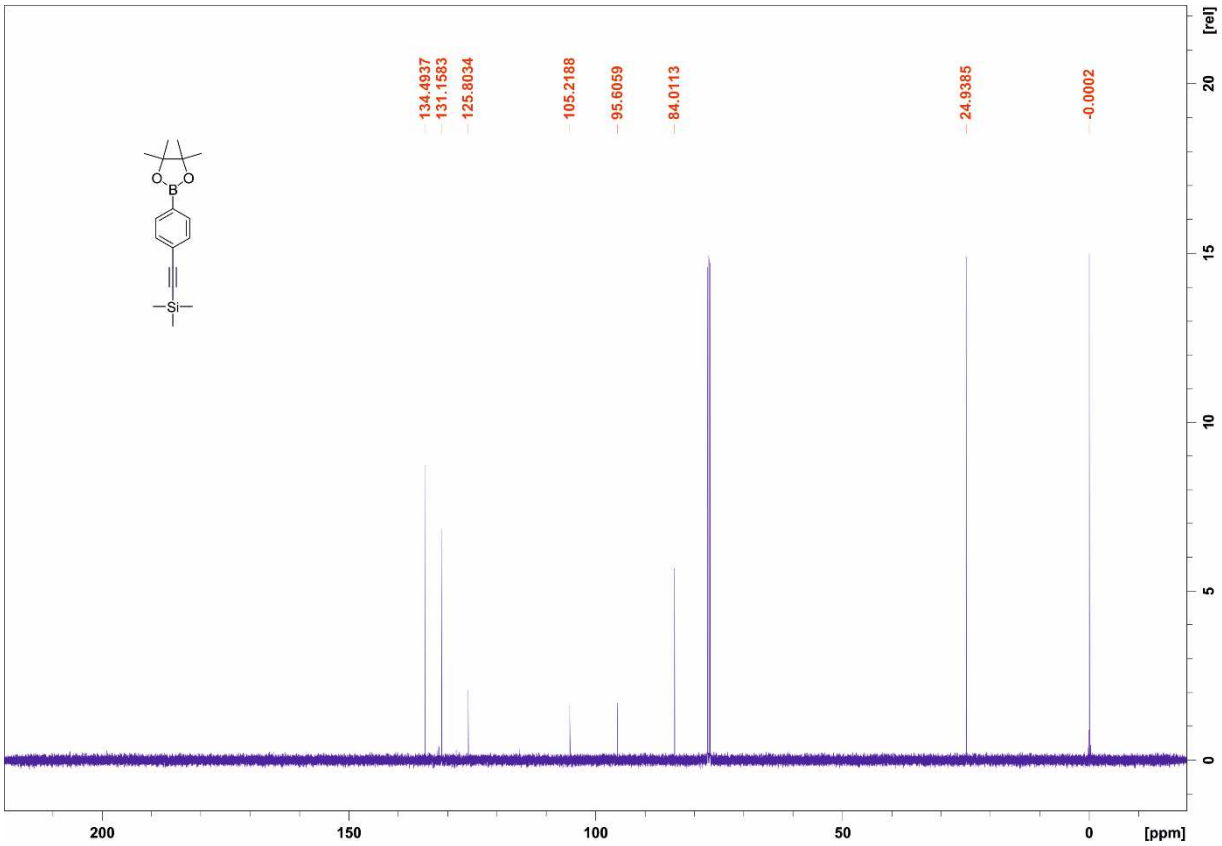

Figure S15. ^{13}C-NMR spectrum (126 MHz, $CDCl_3$) of compound **12**.

2-methyl-4-amino-4‘-((trimethylsilyl)ethynyl)biphenyl:

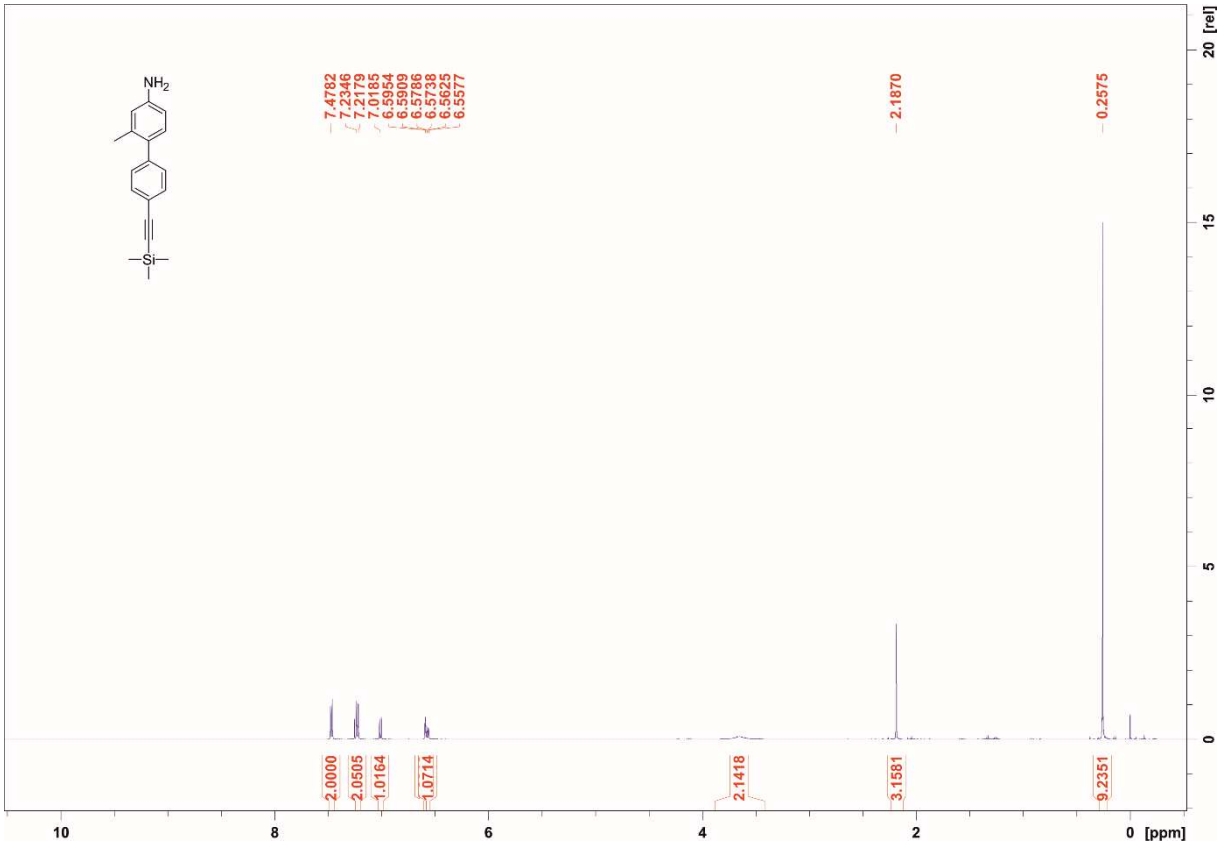

Figure S16. ^{1}H-NMR spectrum (500 MHz, $CDCl_3$) of compound **14**.

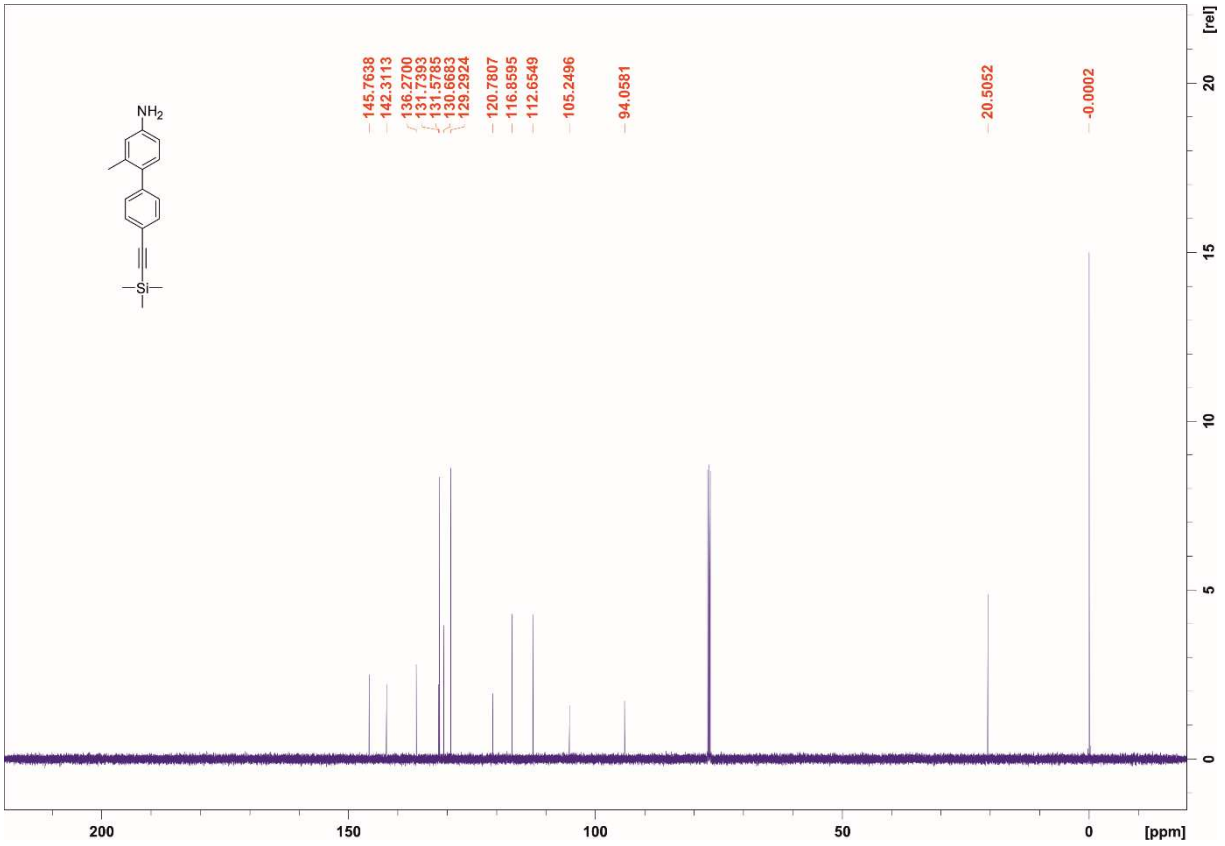

Figure S17. ^{13}C-NMR spectrum (126 MHz, $CDCl_3$) of compound **14**.

(*E*)-1-(4-fluorophenyl)-2-(3-methyl-4-(4-((trimethylsilyl)ethynyl)phenyl)-phenyl)diazene:

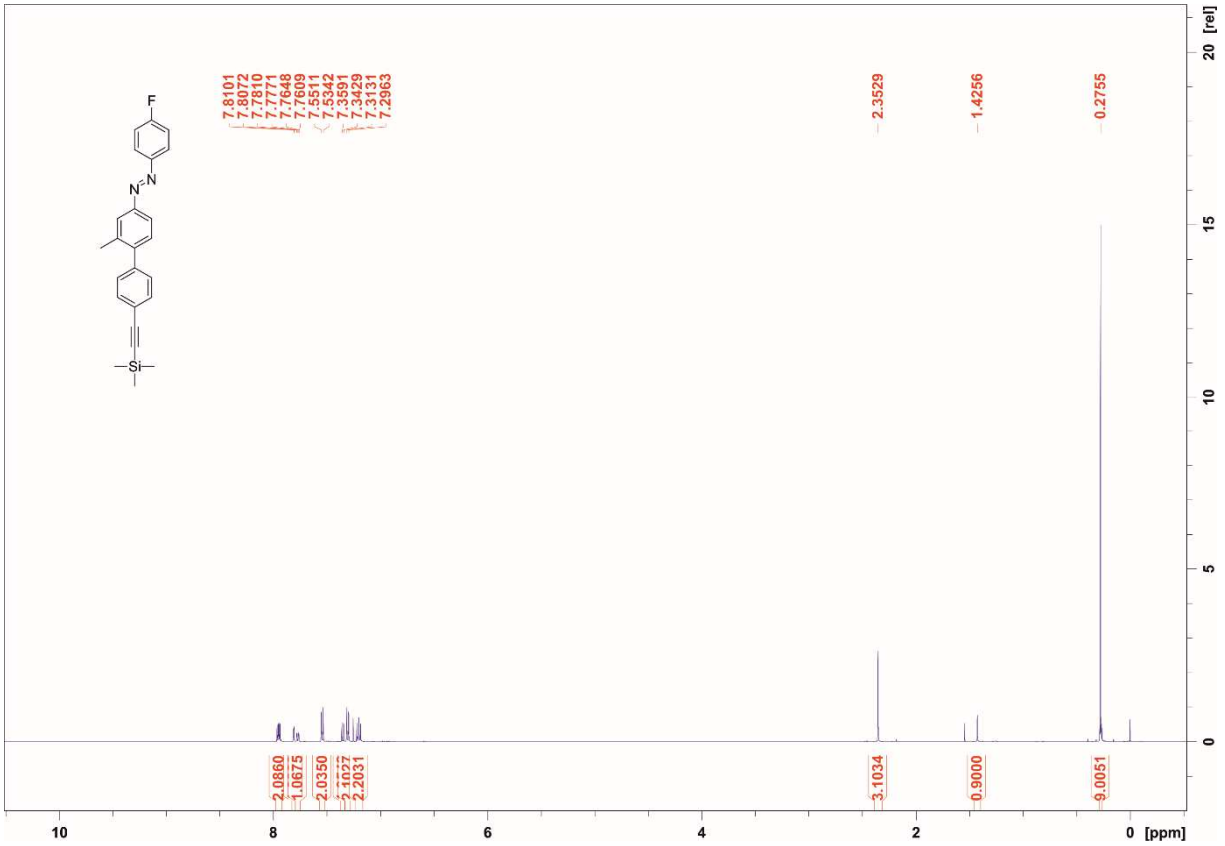

Figure S18. ^{1}H-NMR spectrum (500 MHz, $CDCl_3$) of compound **20**.

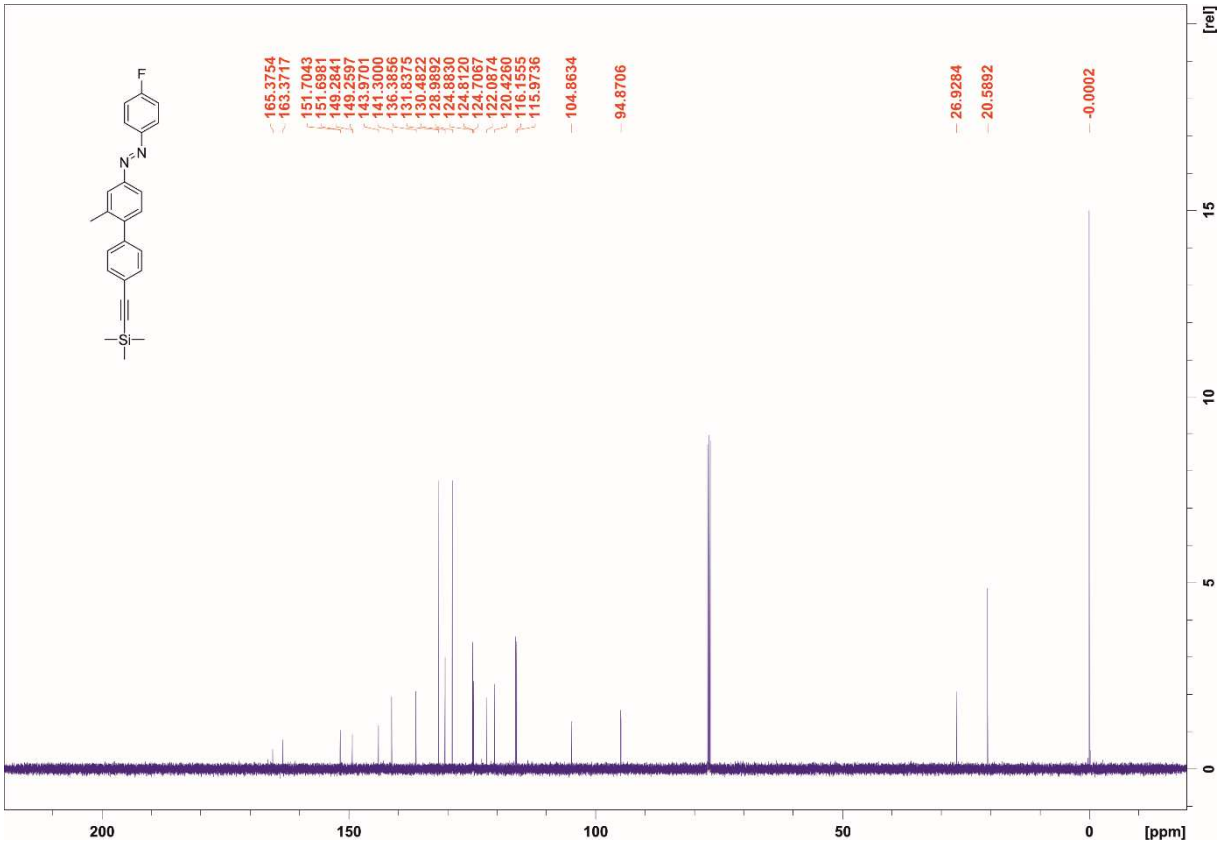

Figure S19. ^{13}C-NMR spectrum (126 MHz, $CDCl_3$) of compound **20**.

(*E*)-1-(4-methoxyphenyl-2-(4-(4-(ethinyl)phenyl)-phenyl)diazene:

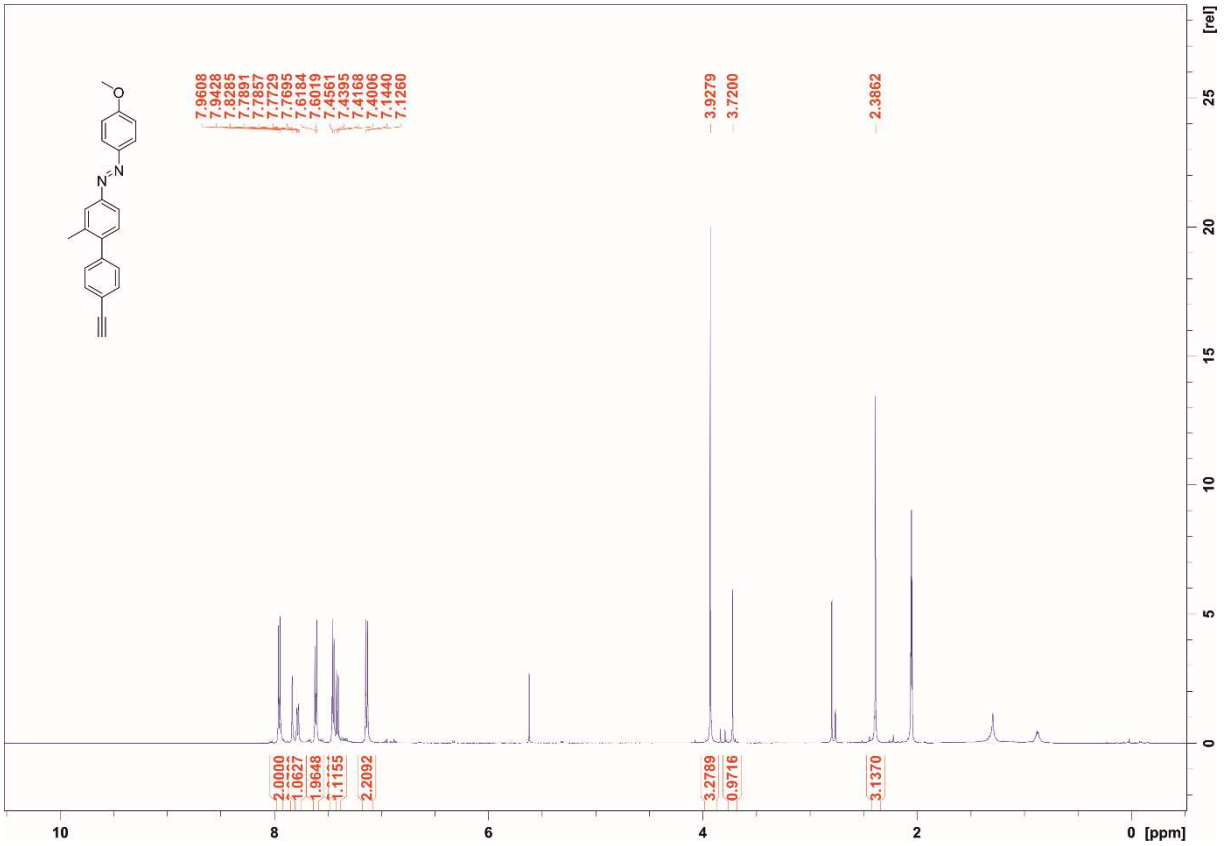

Figure S20. ^{1}H-NMR spectrum (500 MHz, acetone-d_6) of compound **23**.

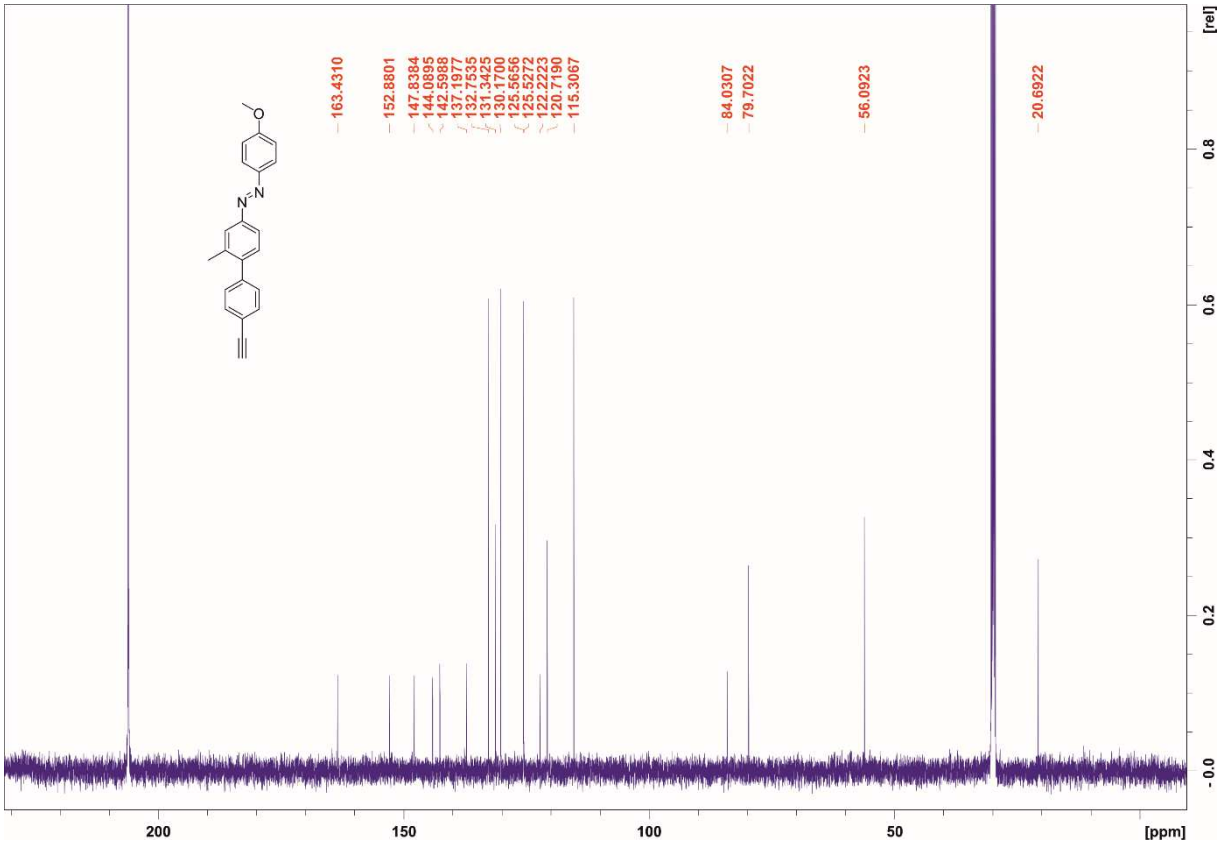

Figure S21. ^{13}C-NMR spectrum (126 MHz, acetone-d_6) of compound **23**.

(*E*)-12c-(4-(4-(methoxyphenyldiazenyl)-2-methylphenyl)phenyl)ethinyl-4,8,12-tri-*n*-octyl-4,8,12-triazatriangulene:

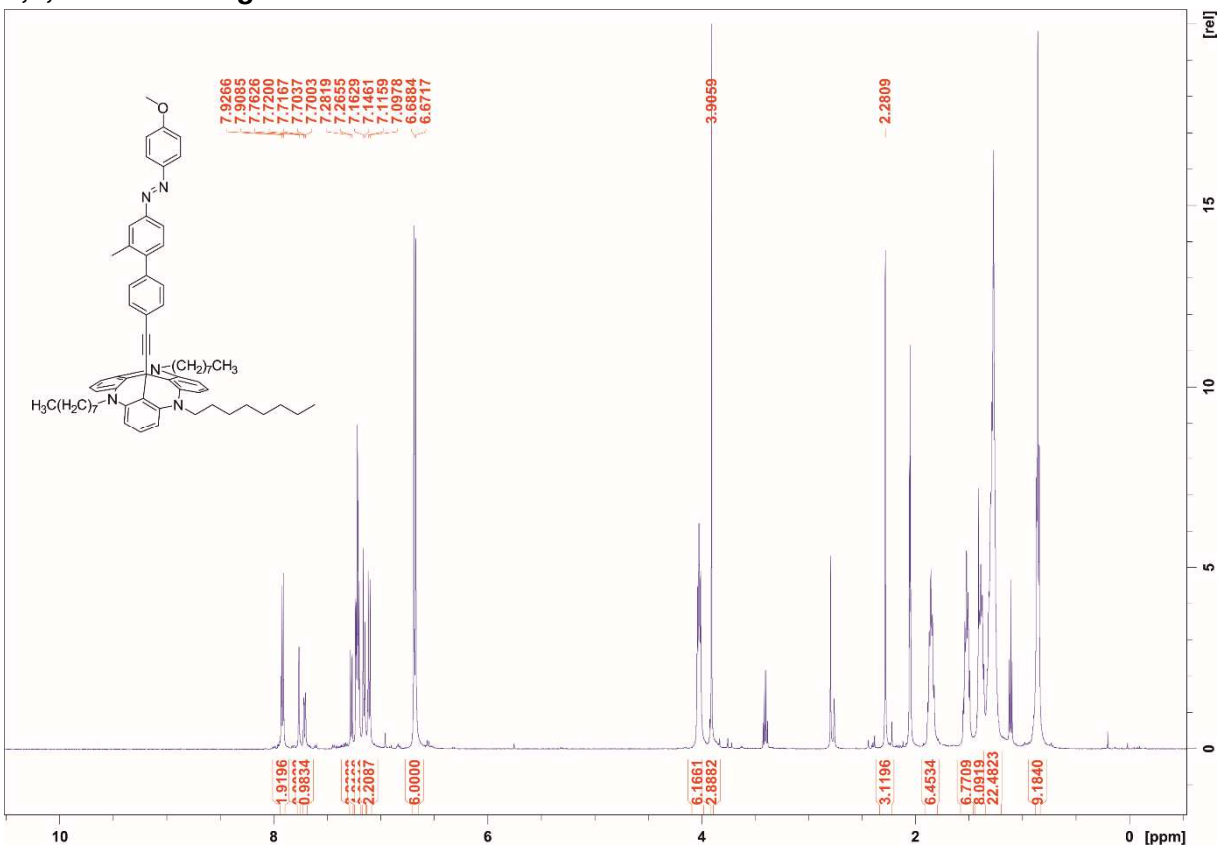

Figure S22. ^{1}H-NMR spectrum (500 MHz, acetone-d_6) of compound **3a**.

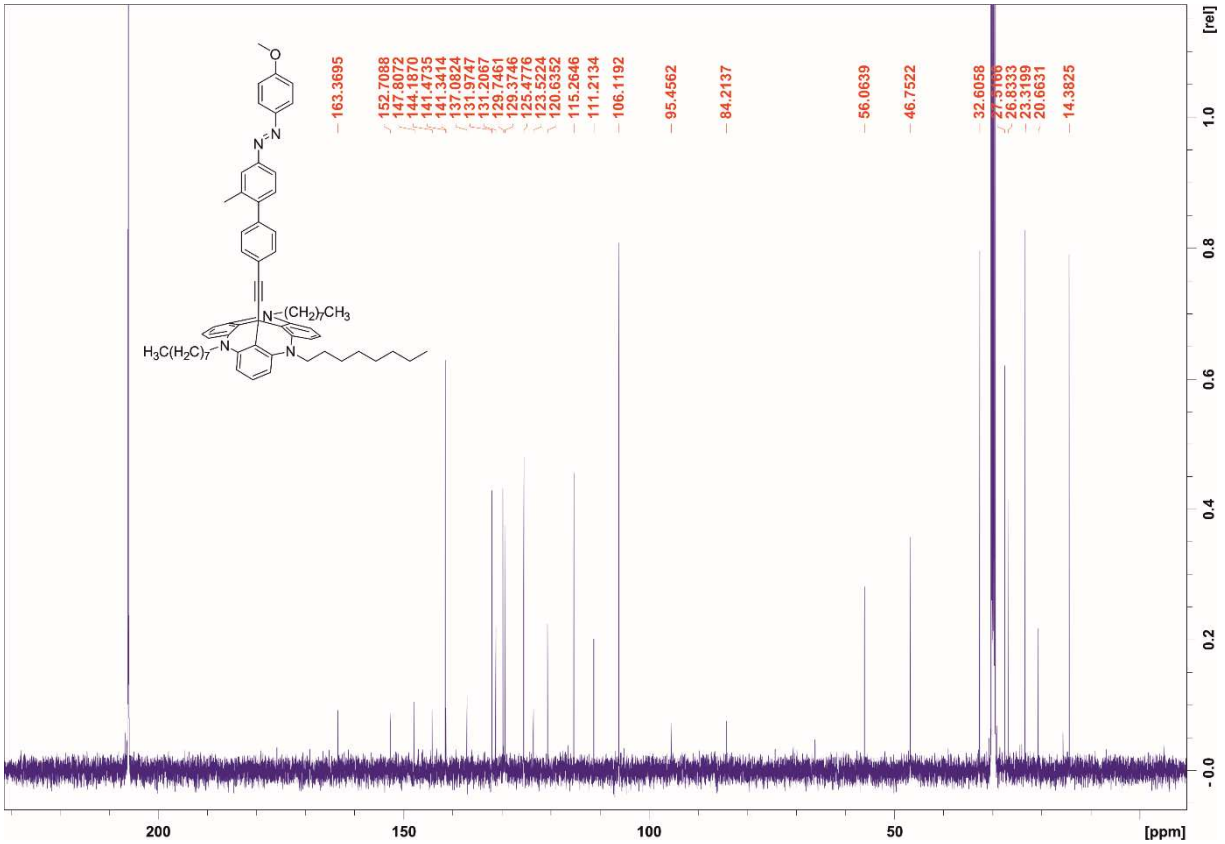

Figure S23. ^{13}C-NMR spectrum (126 MHz, acetone-d_6) of compound **3a**.

(*E*)-12c-(4-(4-(methoxyphenyldiazenyl)-2-methylphenyl)phenyl)ethynyl-4,8,12-tri-*n*-propyl-4,8,12-triazatriangulene:

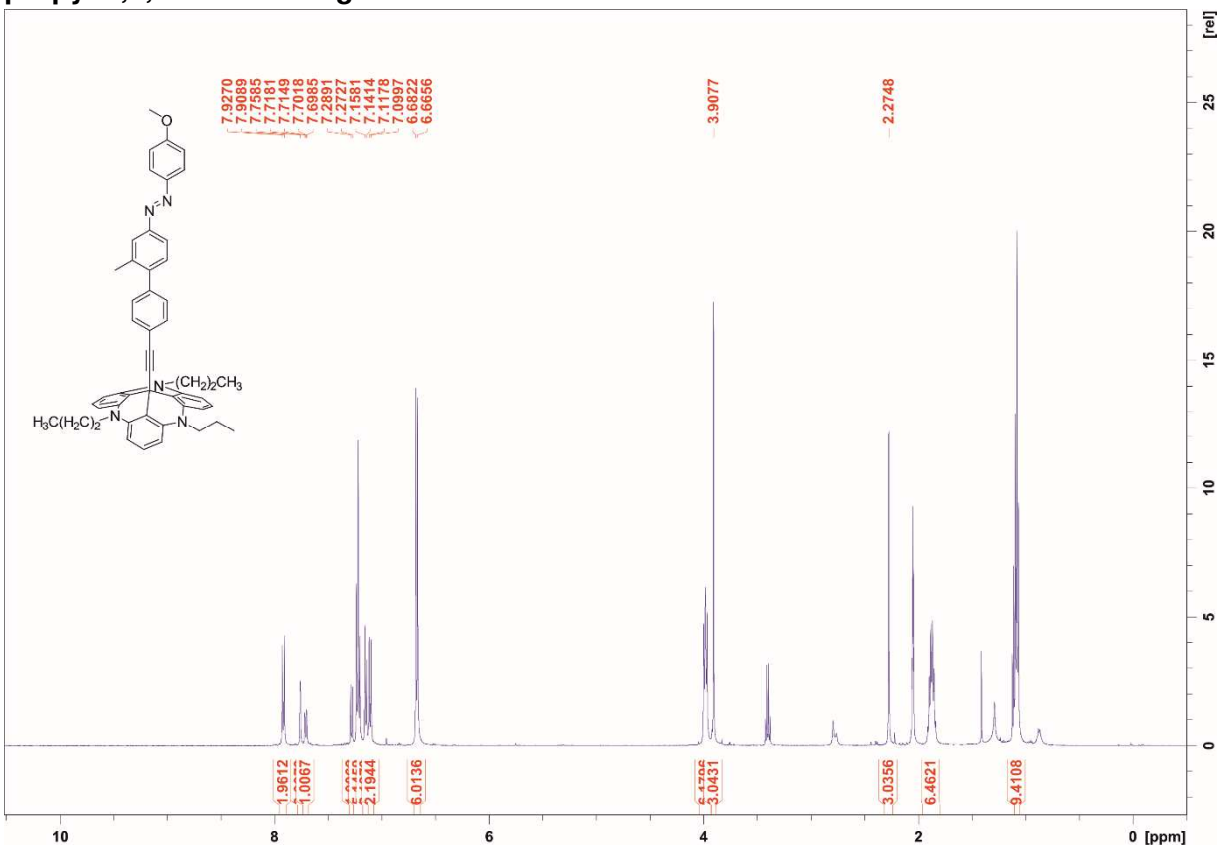

Figure S24. ^{1}H-NMR spectrum (500 MHz, acetone-d_6) of compound **3b**.

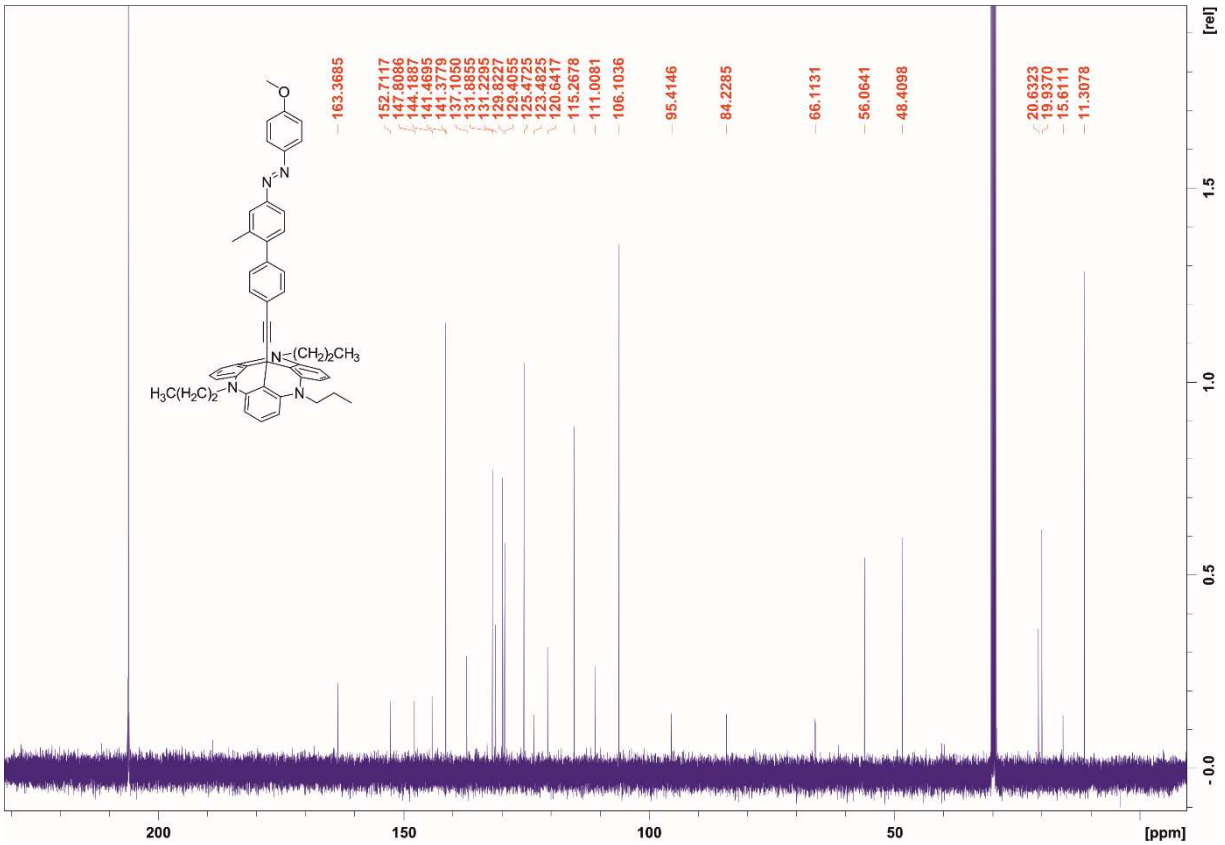

Figure S25. ^{13}C-NMR spectrum (126 MHz, acetone-d_6) of compound **3b**.

3.4 Synthesis Compound 4

2-[2-methyl-4-[2-(trimethylsilyl)ethynyl]phenyl]-4,4,5,5-tetramethyl-1,3,2-dioxaborolane:

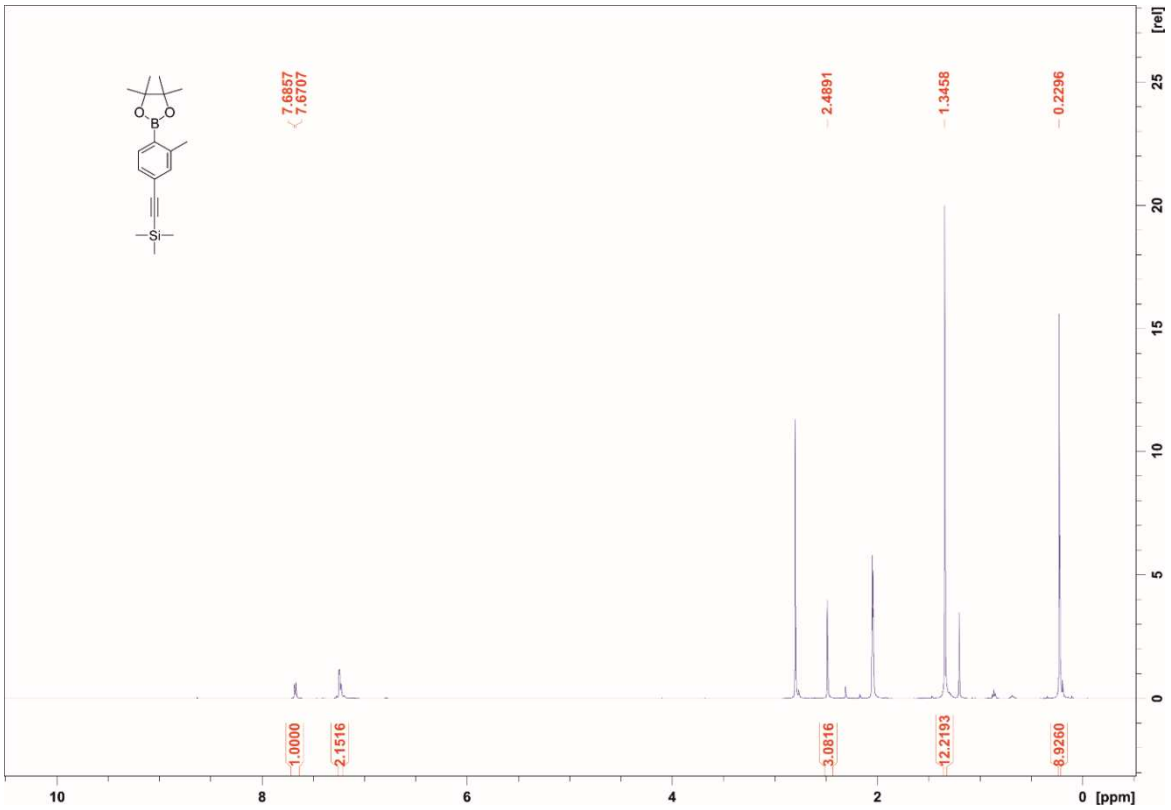

Figure S26. ^{1}H-NMR spectrum (500 MHz, acetone-d_6) of compound **13**.

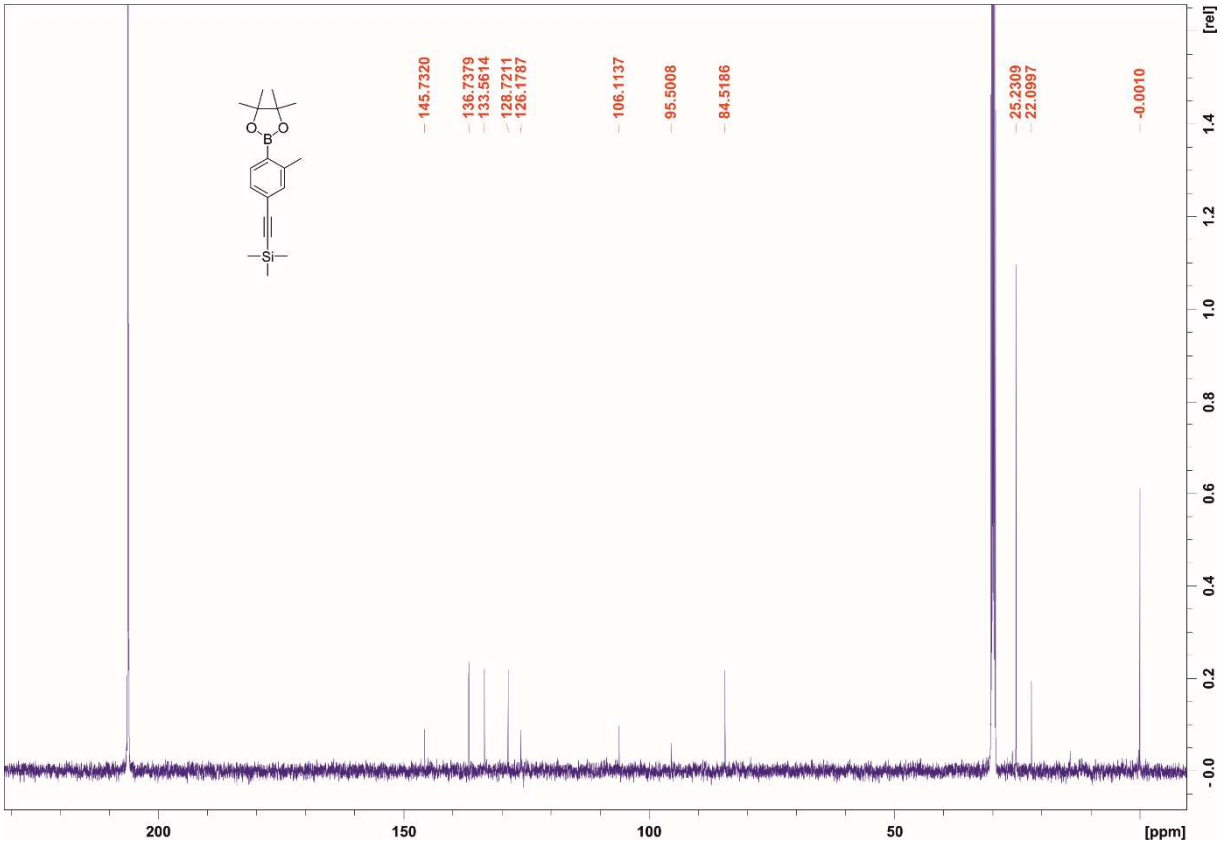

Figure S27. ^{13}C-NMR spectrum (126 MHz, acetone-d_6) of compound **13**.

2-methyl-4-amino-2‘-methyl-4‘-((trimethylsilyl)ethynyl)biphenyl:

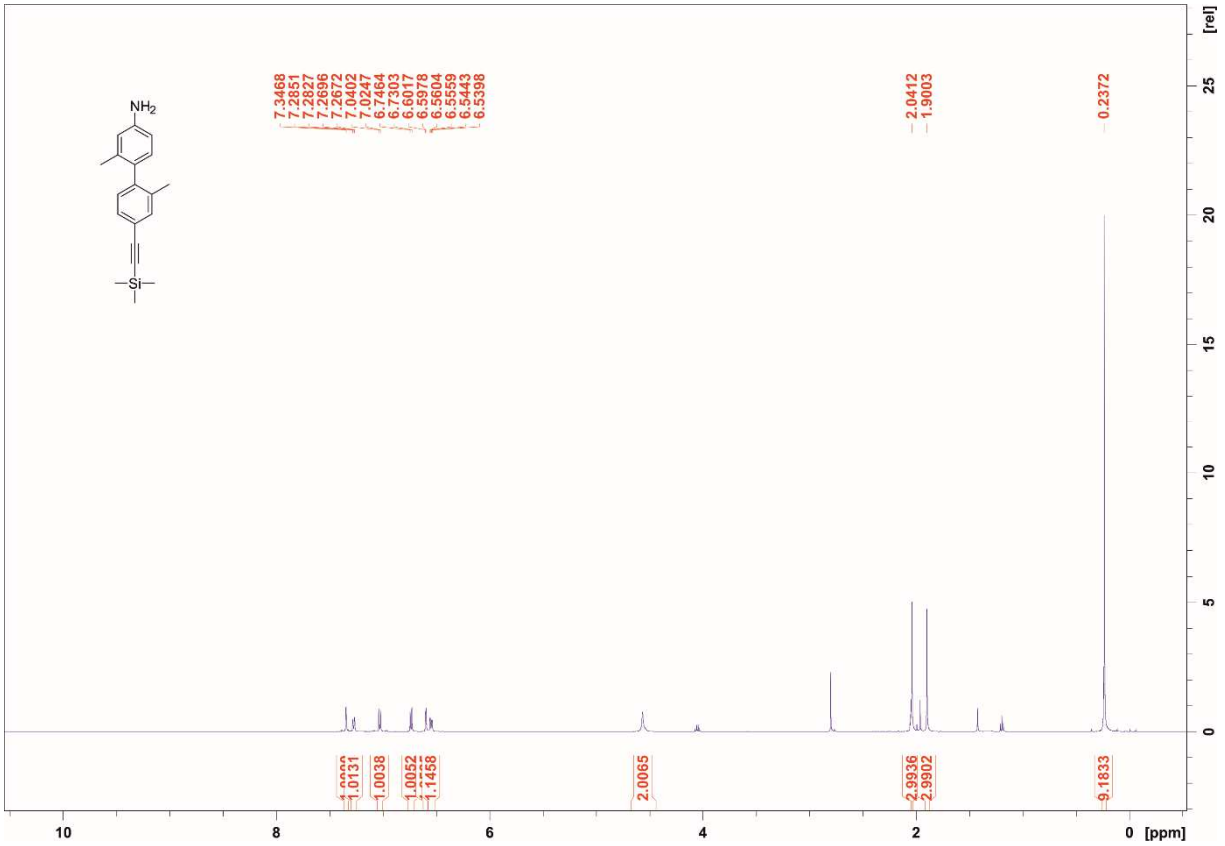

Figure S28. ^{1}H-NMR spectrum (500 MHz, acetone-d_6) of compound **15**.

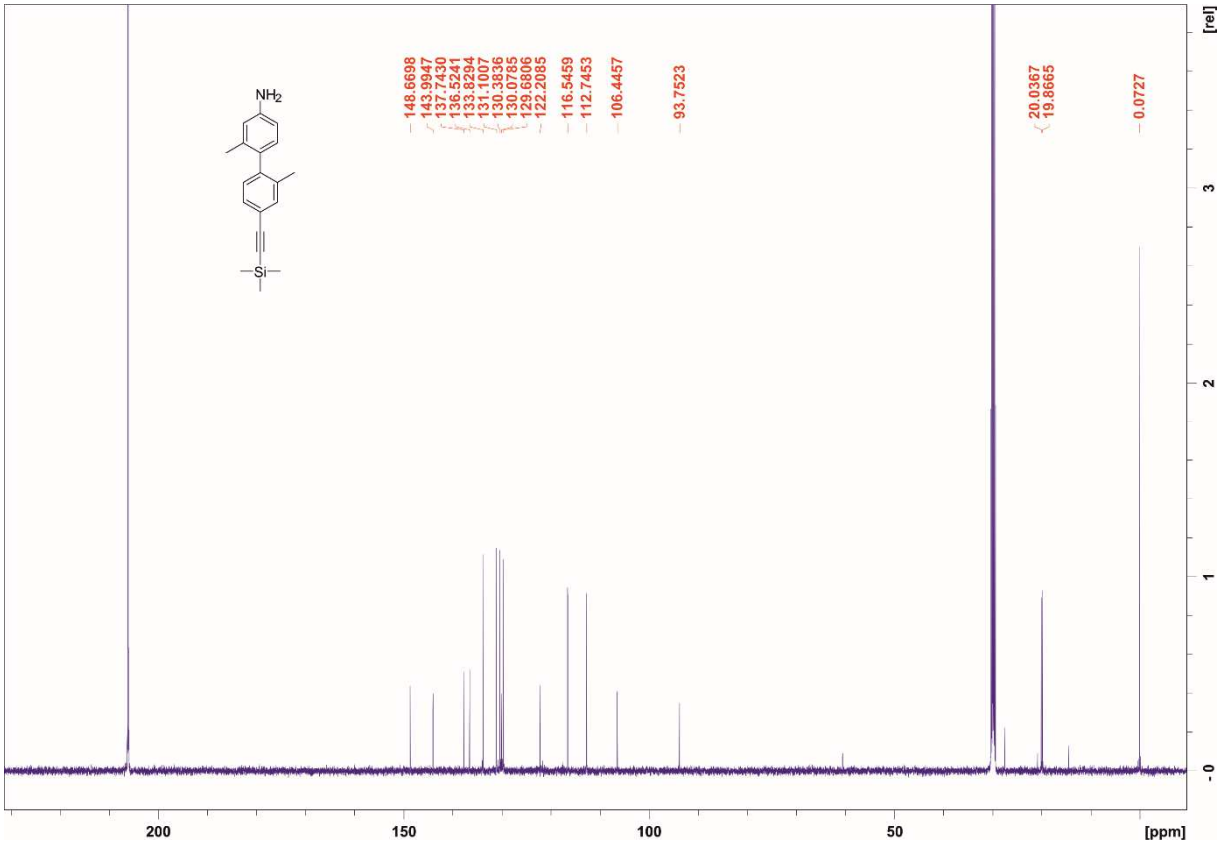

Figure S29. ^{13}C-NMR spectrum (126 MHz, acetone-d_6) of compound **15**.

(*E*)-1-(4-fluorphenyl)-2-(3-methyl-4-(3-methyl-4-((trimethylsilyl)ethynyl)phenyl)-phenyl)diazene:

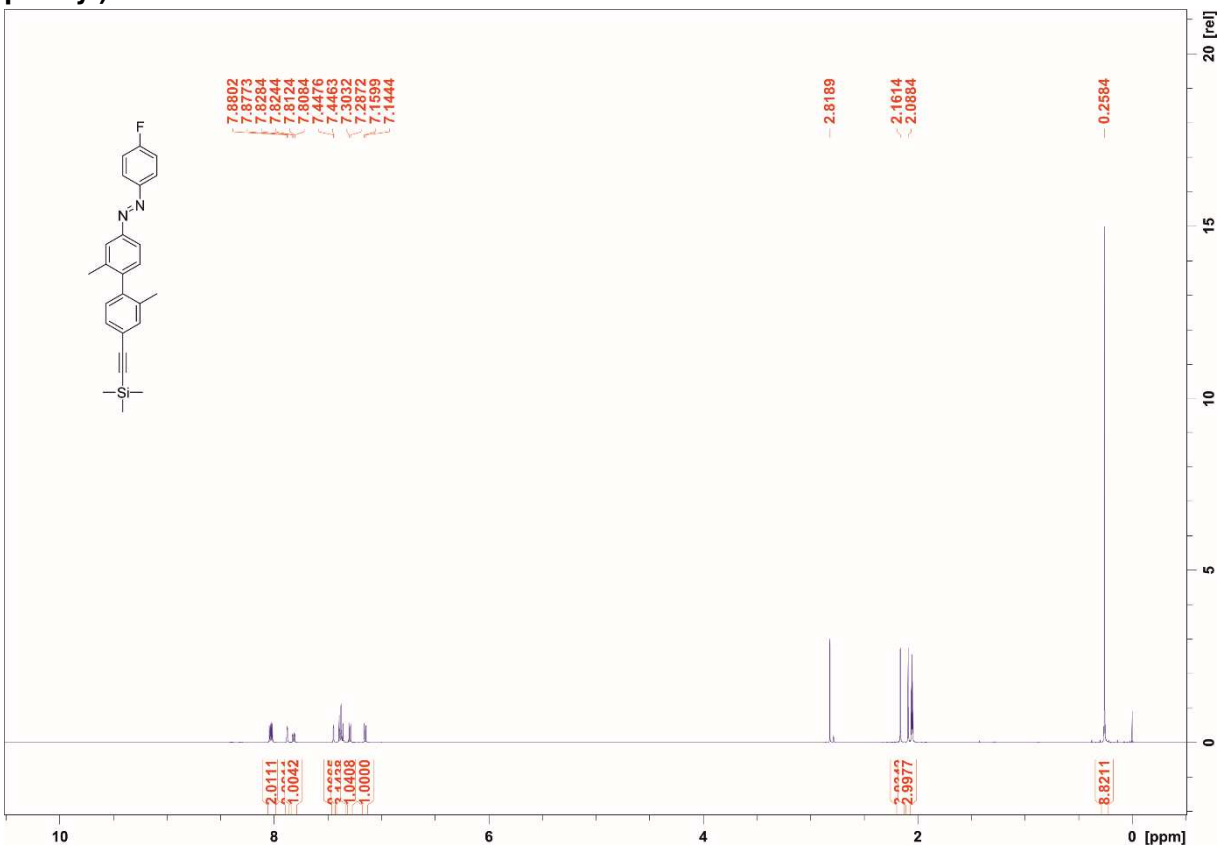

Figure S30. ^{1}H-NMR spectrum (500 MHz, acetone-d_6) of compound **21**.

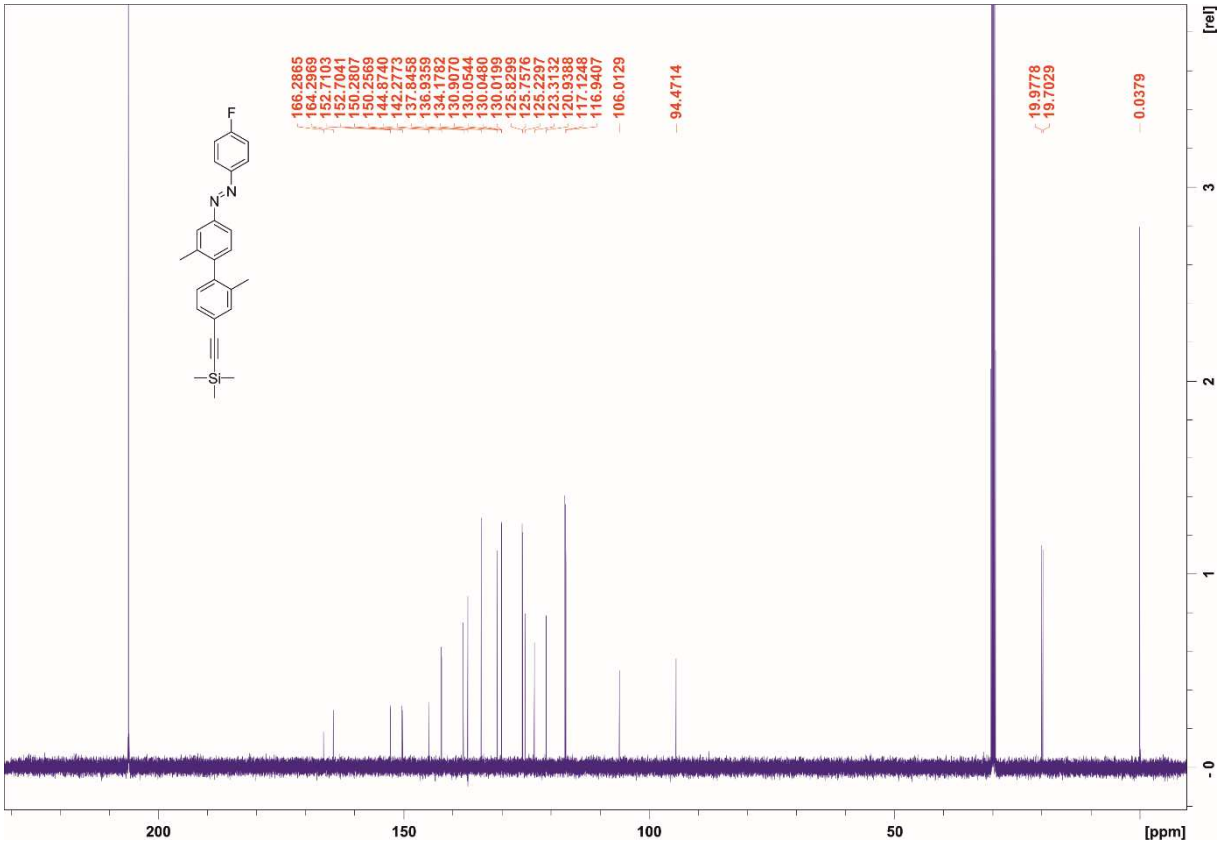

Figure S31. ^{13}C-NMR spectrum (126 MHz, acetone-d_6) of compound **21**.

(*E*)-1-(4-methoxyphenyl)-2-(3-methyl-4-(3-methyl-4-(ethynyl)phenyl)-phenyl)diazene:

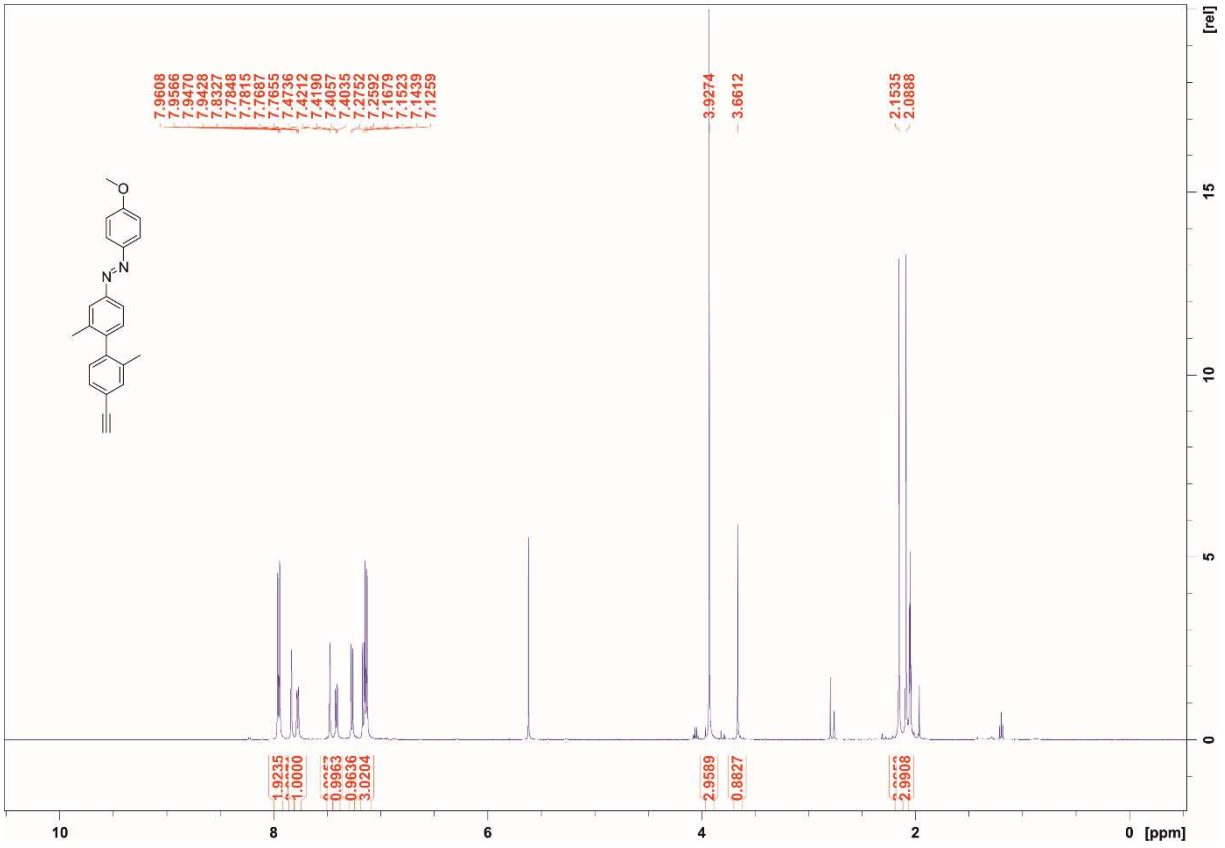

Figure S32. ^{1}H-NMR spectrum (500 MHz, acetone-d_6) of compound **24**.

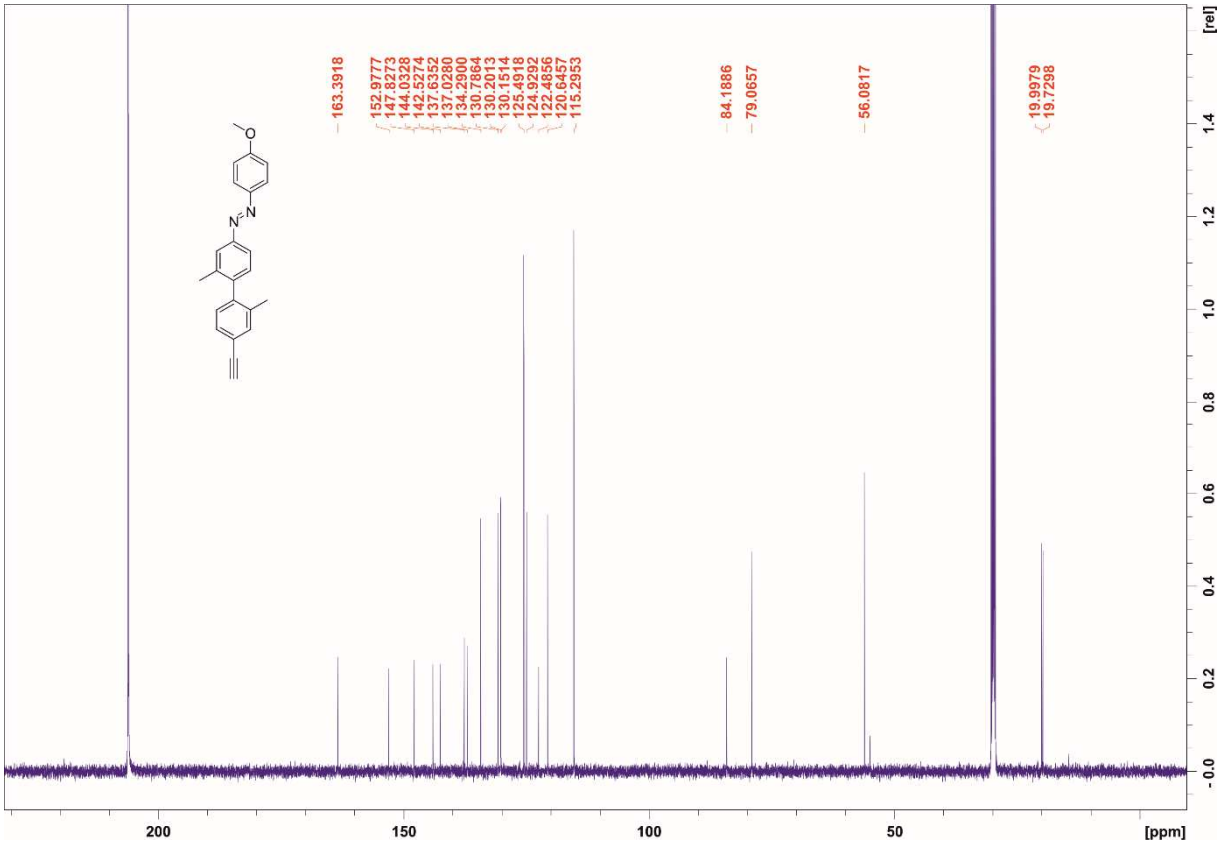

Figure S33. ^{13}C-NMR spectrum (126 MHz, acetone-d_6) of compound **24**.

(*E*)-12c-(3-methyl-4-(4-(methoxyphenyldiazenyl)-2-methylphenyl)phenyl)ethynyl-4,8,12-tri-*n*-octyl-4,8,12-triazatriangulene:

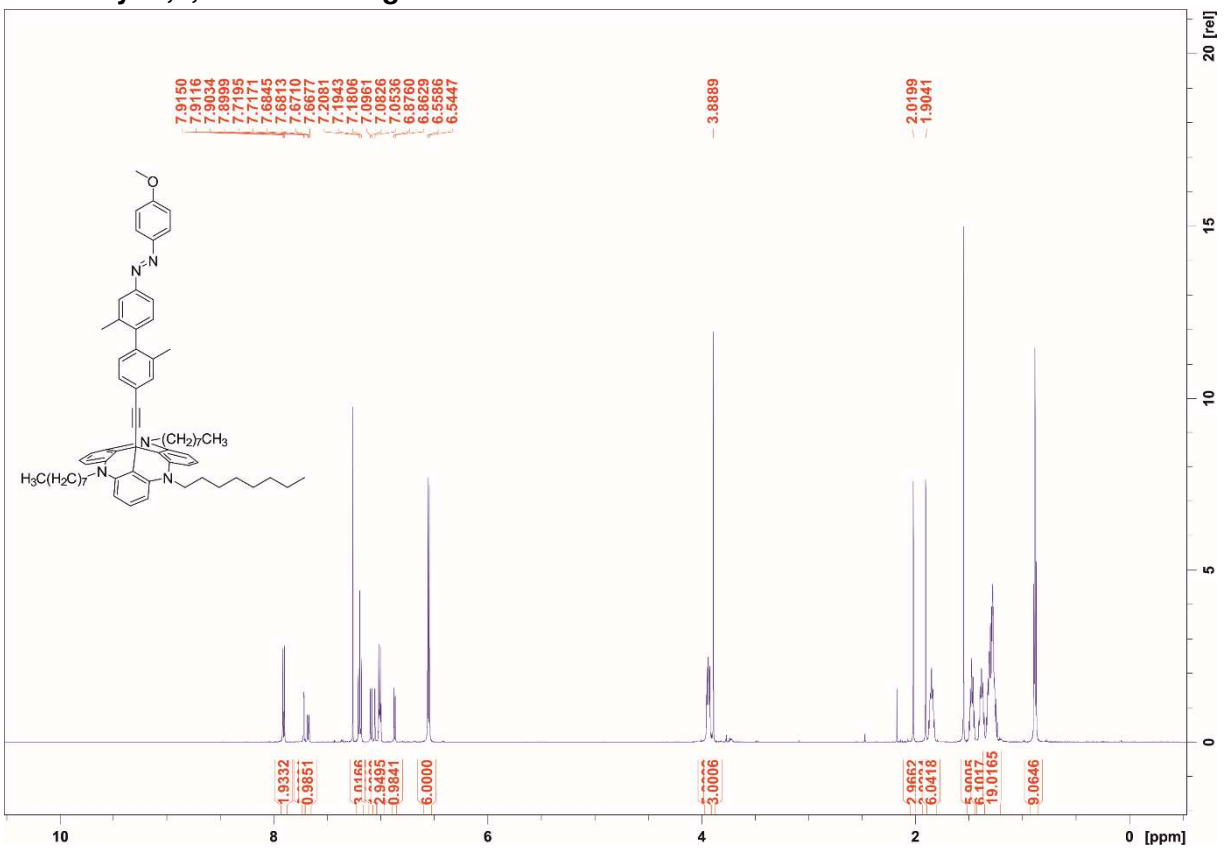

Figure S34. ^{1}H-NMR spectrum (600 MHz, $CDCl_3$) of compound **4a**.

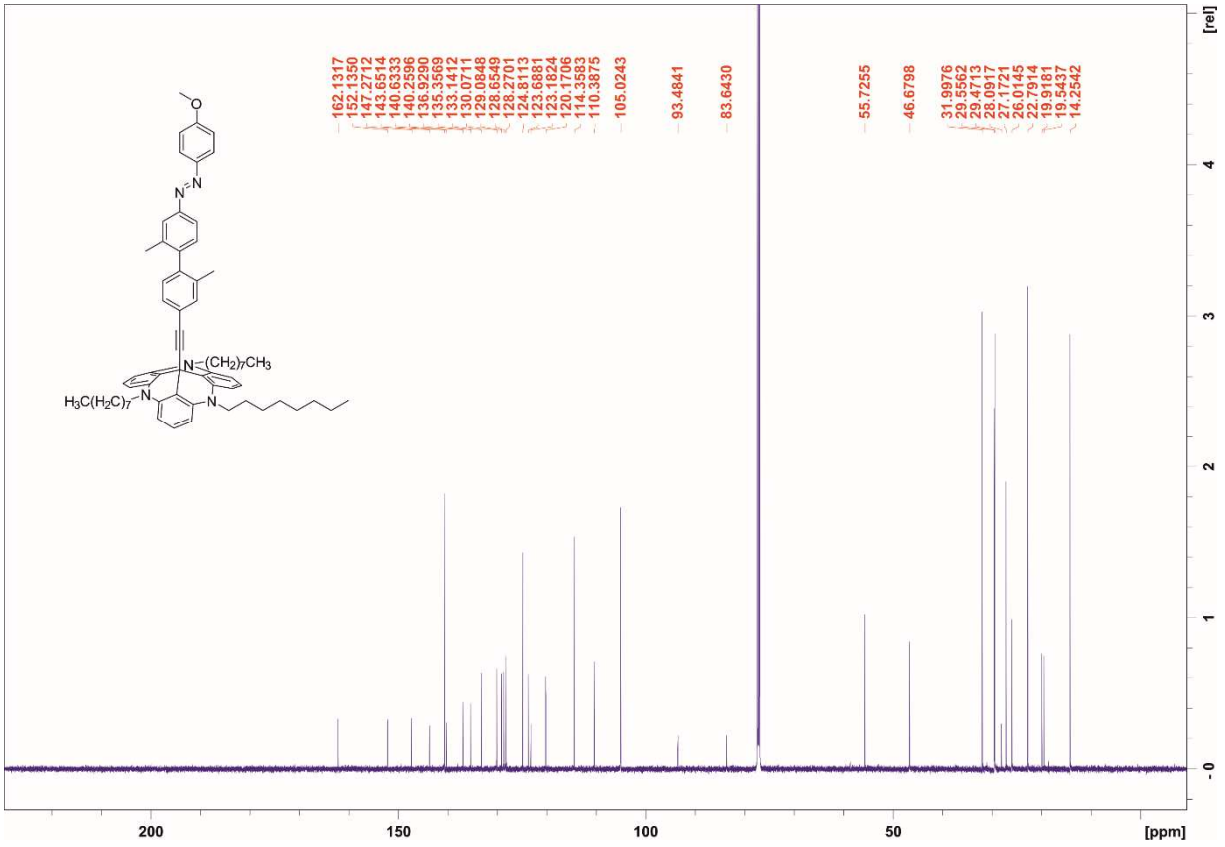

Figure S35. ^{13}C-NMR spectrum (151 MHz, $CDCl_3$) of compound **4a**.

(*E*)-12c-(3-methyl-4-(4-(methoxyphenyldiazenyl)-2-methylphenyl)phenyl)ethynyl-4,8,12-tri-*n*-propyl-4,8,12-triazatriangulene:

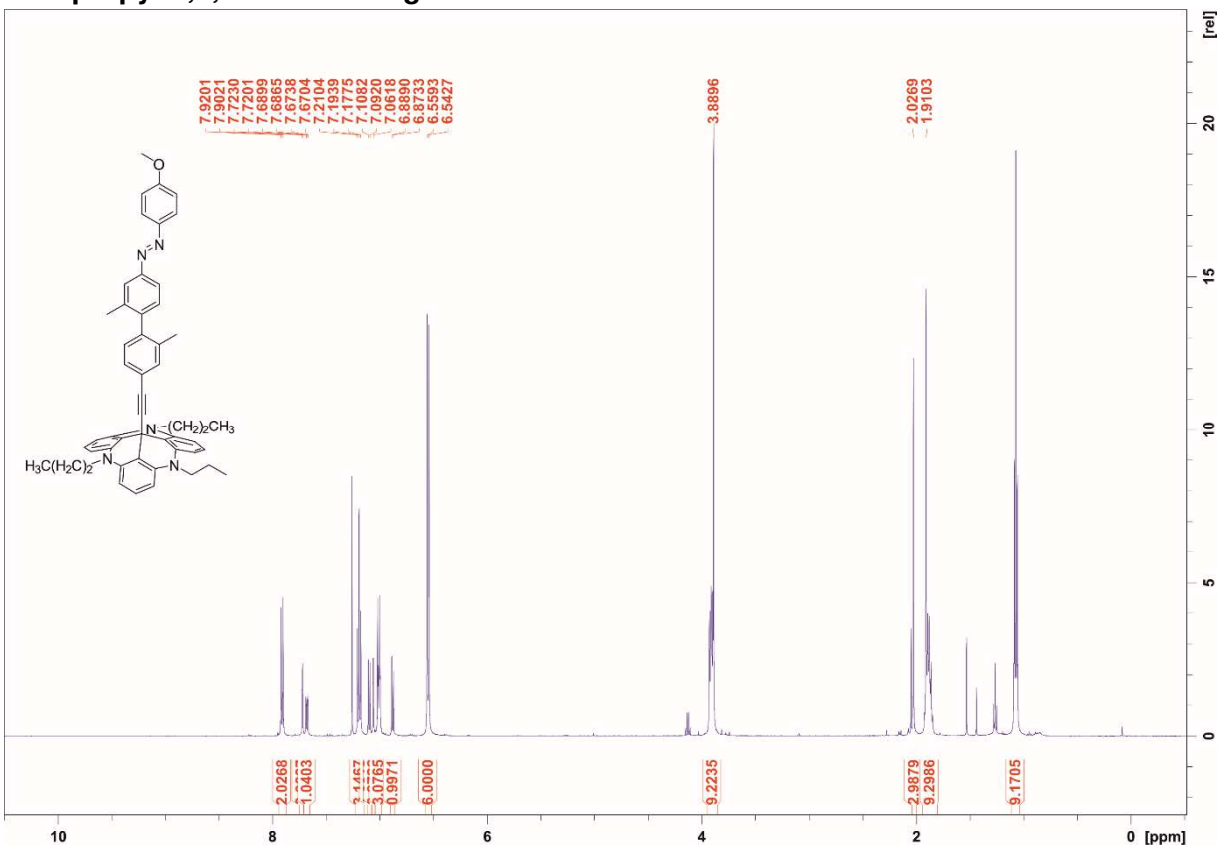

Figure S36. ^{1}H-NMR spectrum (500 MHz, $CDCl_3$) of compound **4b**.

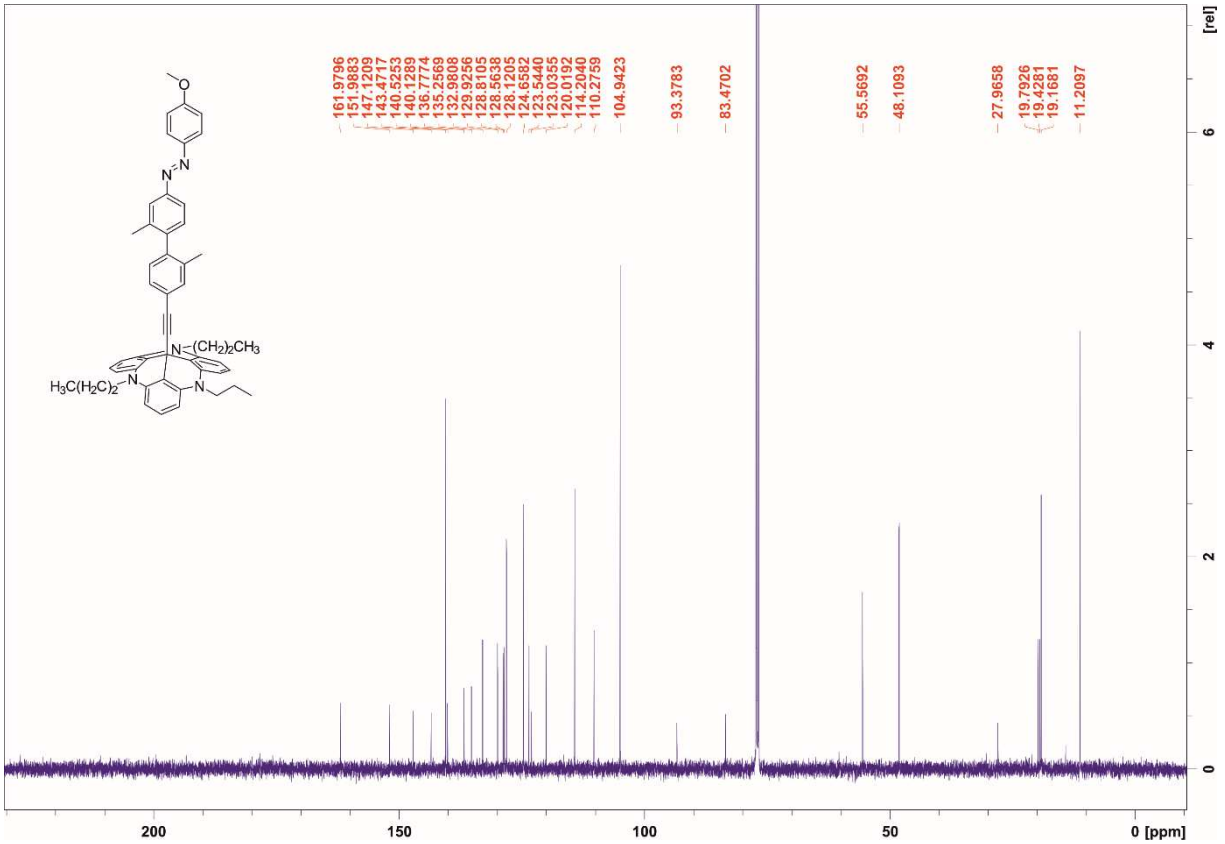

Figure S37. ^{13}C-NMR spectrum (126 MHz, $CDCl_3$) of compound **4b**.

3.5 Synthesis Compound 5

(*E*)-2-{4-[(4-fluorophenyl)diazenyl]phenyl}-2-(hydroxymethyl)-propane-1,3-diol:

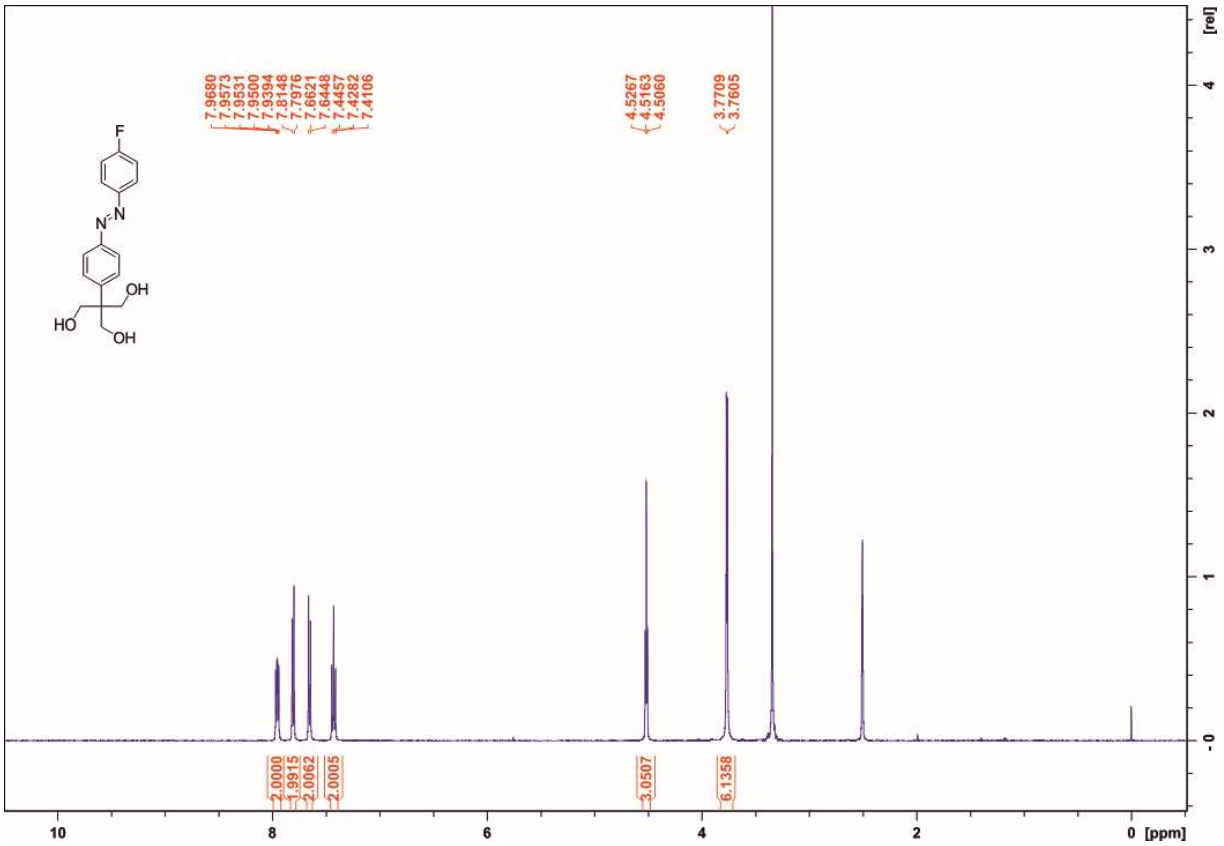

Figure S38. ^{1}H-NMR spectrum (500 MHz, DMSO-d_6) of compound **26**.

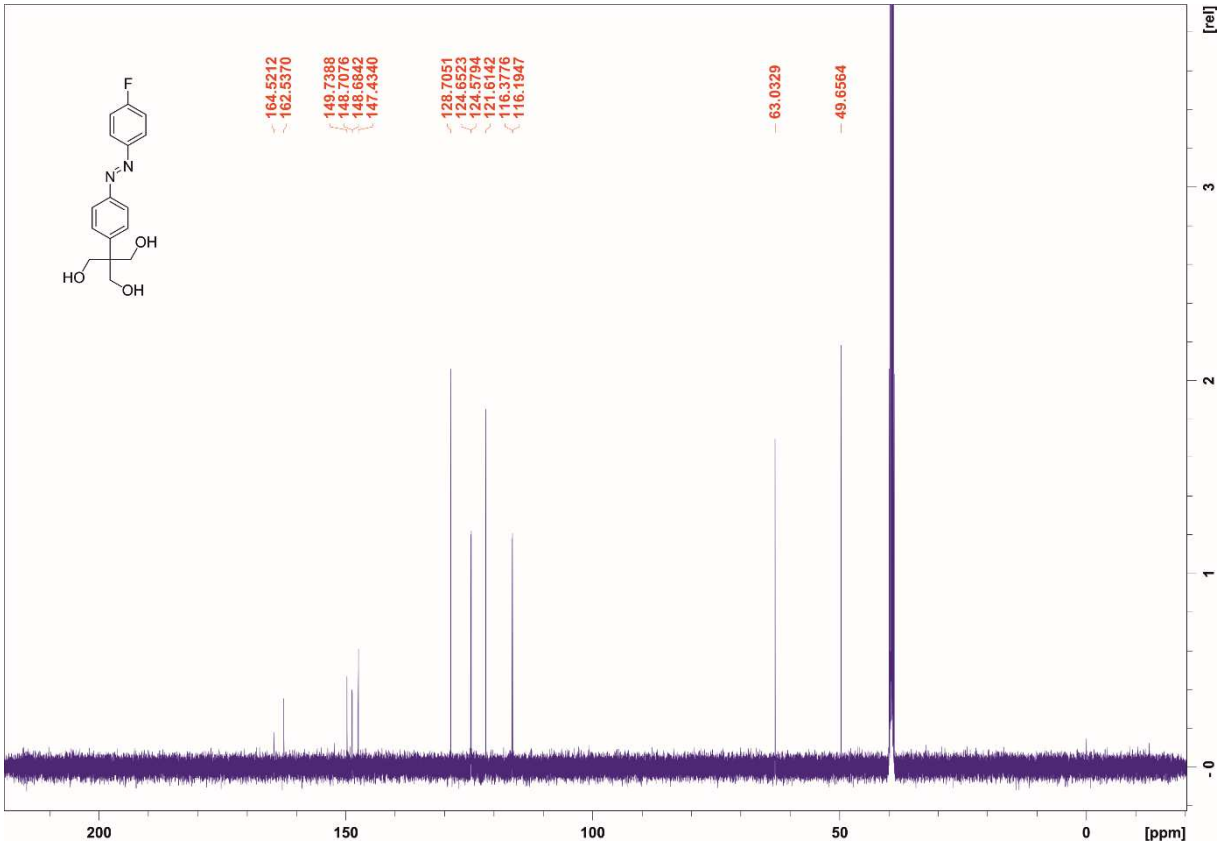

Figure S39. ^{13}C-NMR spectrum (126 MHz, DMSO-d_6) of compound **26**.

(*E*)-2-(hydroxymethyl)-2-{4-[(4-methoxyphenyl)diazenyl]phenyl}-propane-1,3-diol:

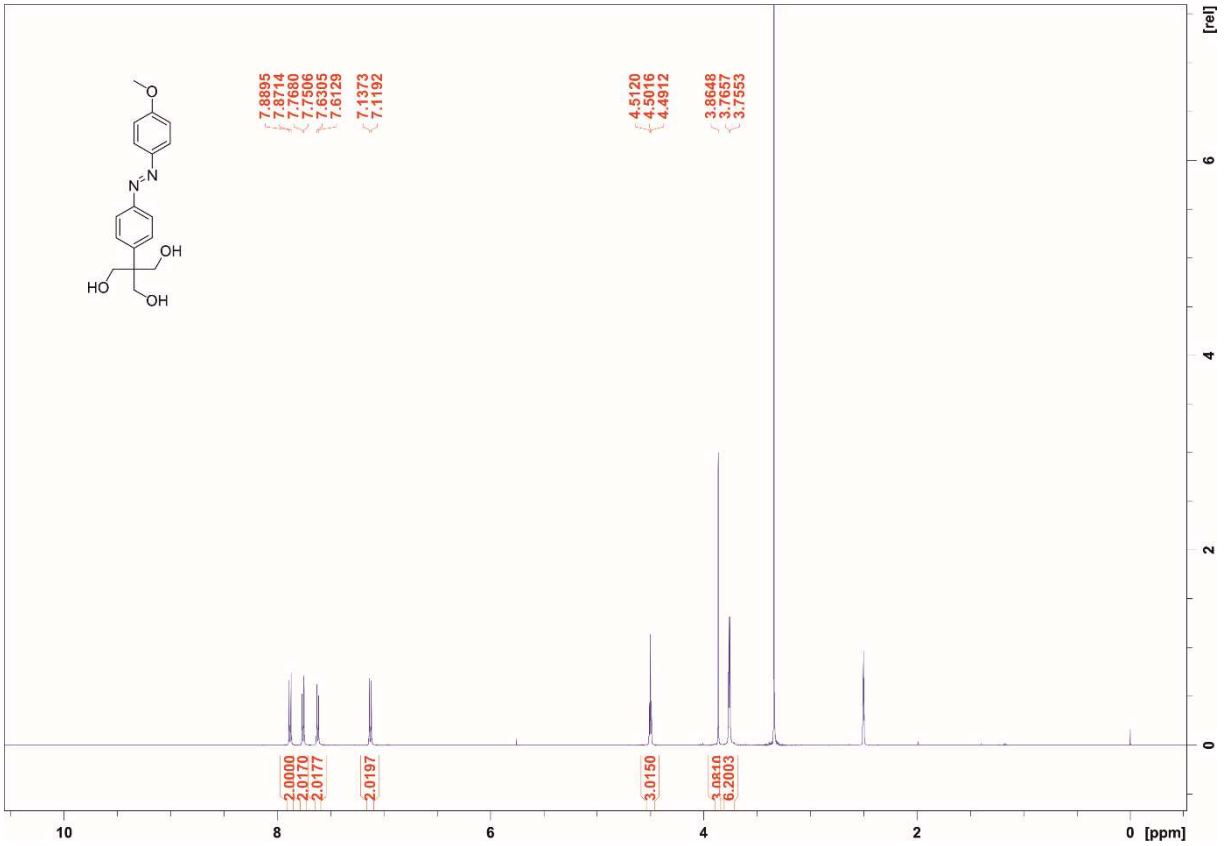

Figure S40. ^{1}H-NMR spectrum (500 MHz, DMSO-d_6) of compound **27**.

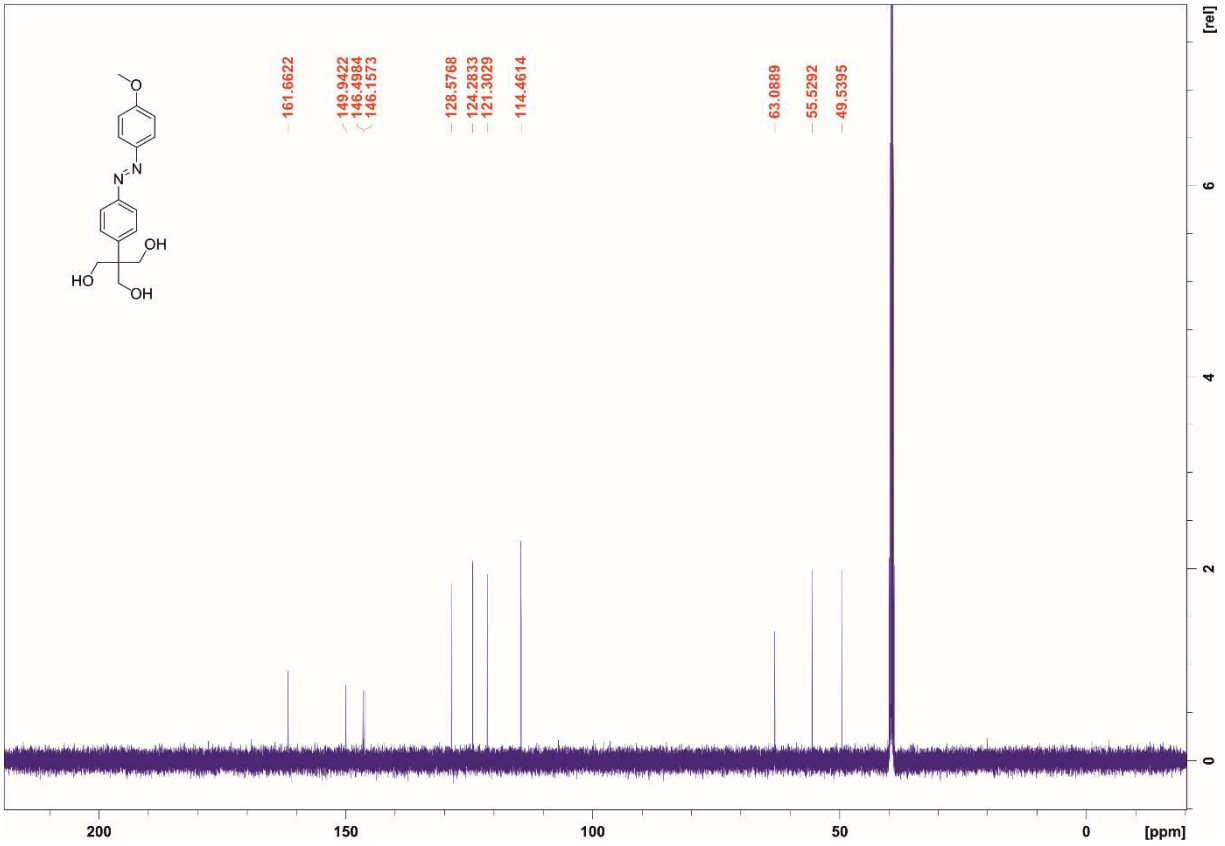

Figure S41. ^{13}C-NMR spectrum (126 MHz, DMSO-d_6)of compound **27**.

(*E*)-1-(4-methoxyphenyl)-2-(4-{1-[(trimethylsilyl)ethynyl]-2,6,7-trioxabicyclo[2.2.2] octane-4-yl}phenyl)diazene:

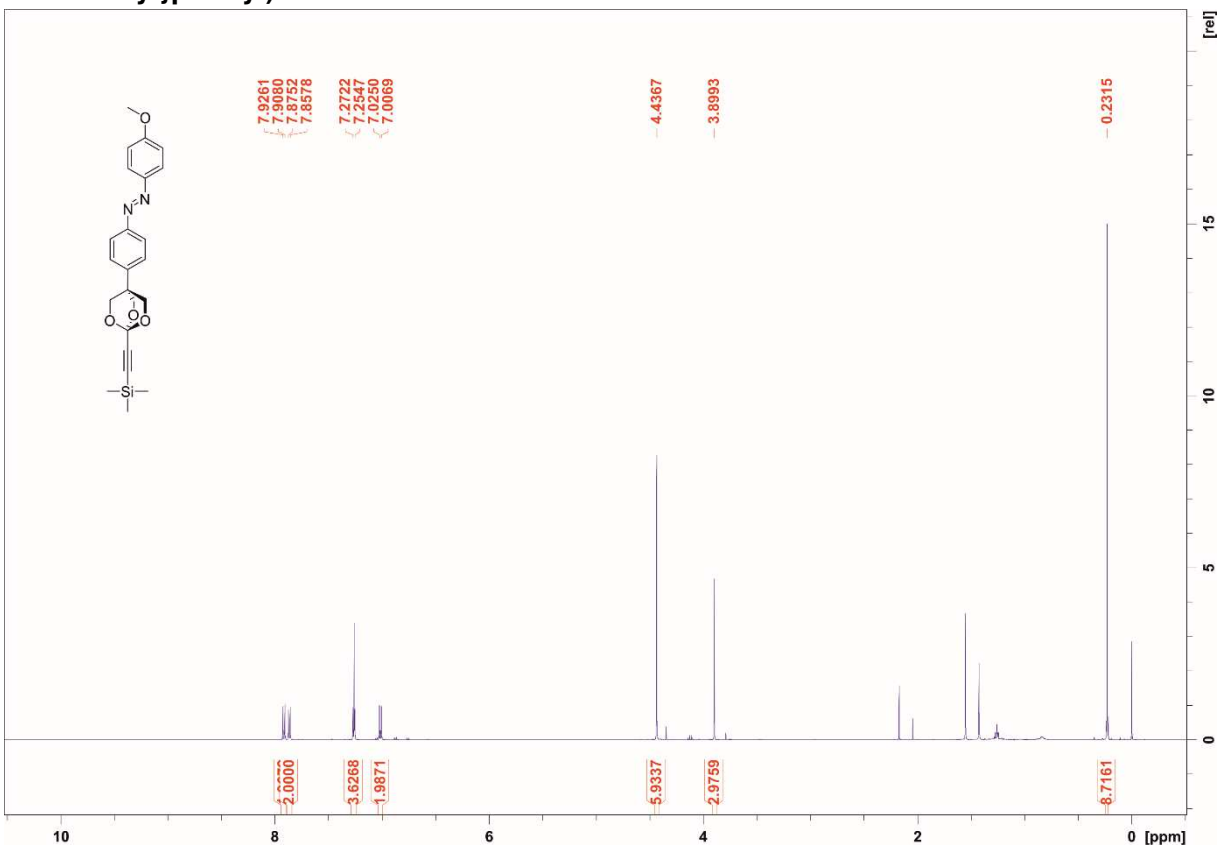

Figure S42. ^{1}H-NMR spectrum (500 MHz, $CDCl_3$) of compound **29**.

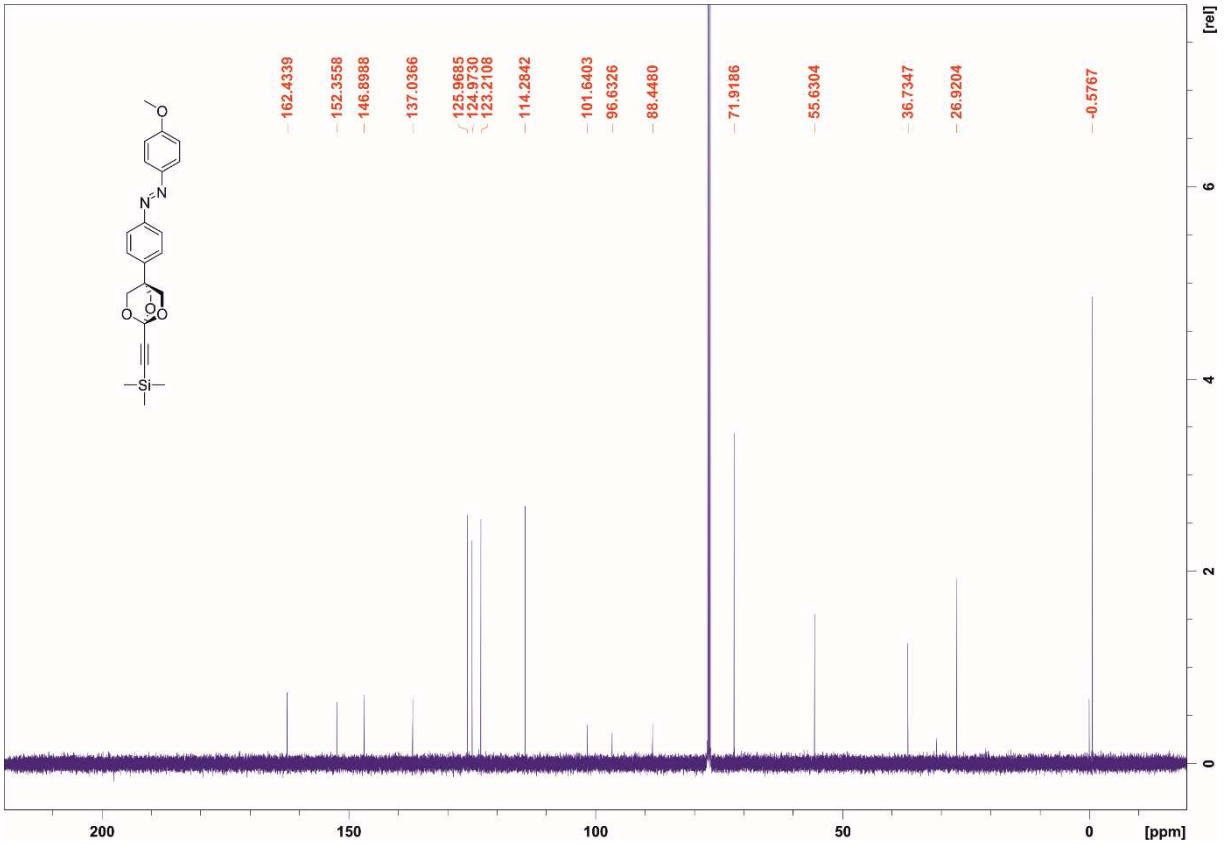

Figure S43. ^{13}C-NMR spectrum (126 MHz, $CDCl_3$) of compound **29**.

(*E*)-12c-[(4-{4-[(4-methoxyphenyl)diazenyl]phenyl}-2,6,7-trioxabicyclo[2.2.2]octane-1-yl)ethynyl]-4,8,12-tri-*n*-octyl-4,8,12-triazatriangulene:

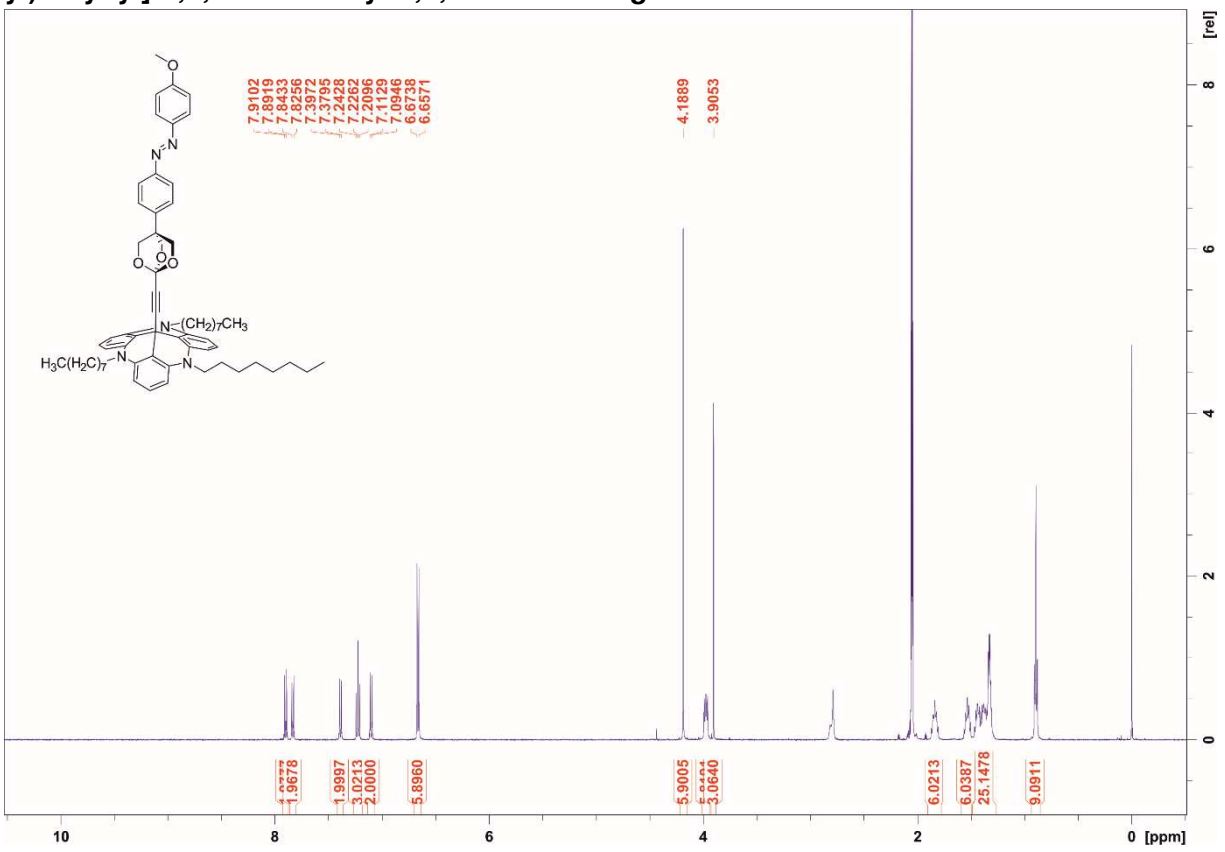

Figure S44. ^{1}H-NMR spetrum (500 MHz, acetone-d_6) of compound **5a**.

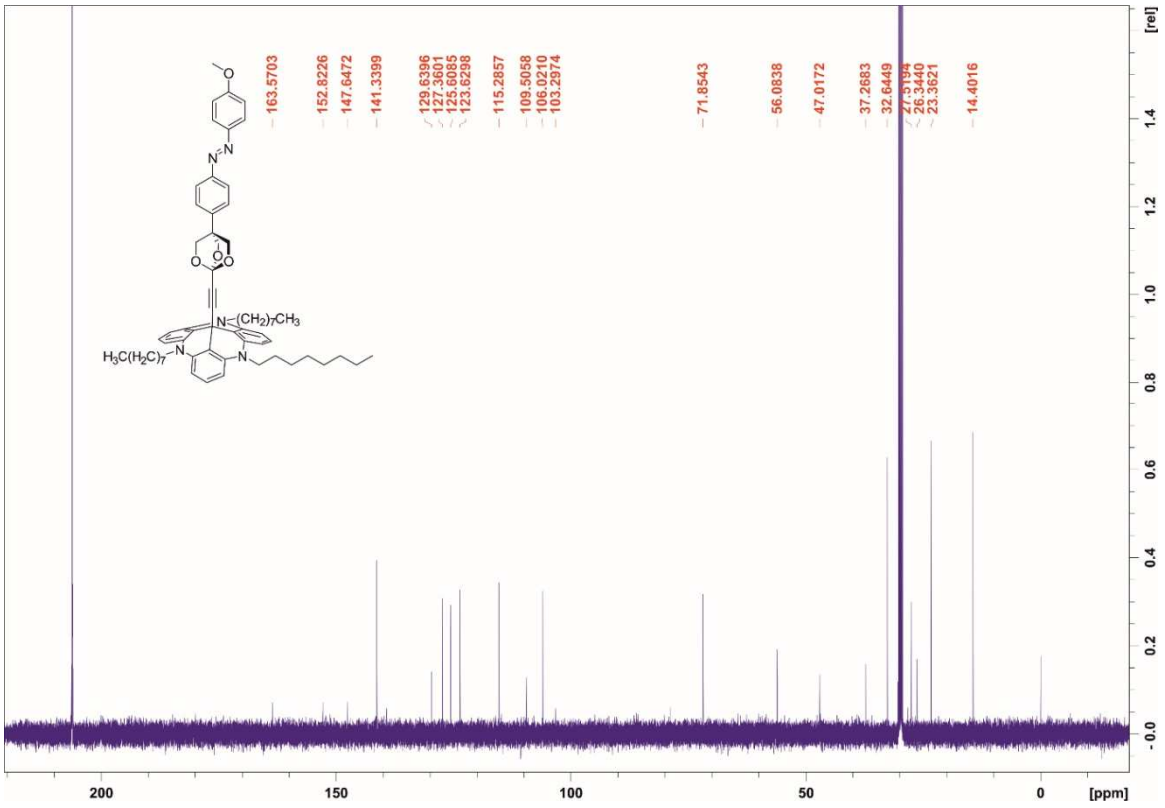

Figure S45. ^{13}C-NMR spectrum (126 MHz, acetone-d_6) of compound **5a**.

(*E*)-12c-[(4-{4-[(4-methoxyphenyl)diazenyl]phenyl}-2,6,7-trioxabicyclo[2.2.2]octane-1-yl)ethynyl]-4,8,12-tri-*n*-octyl-4,8,12-triazatriangulene:

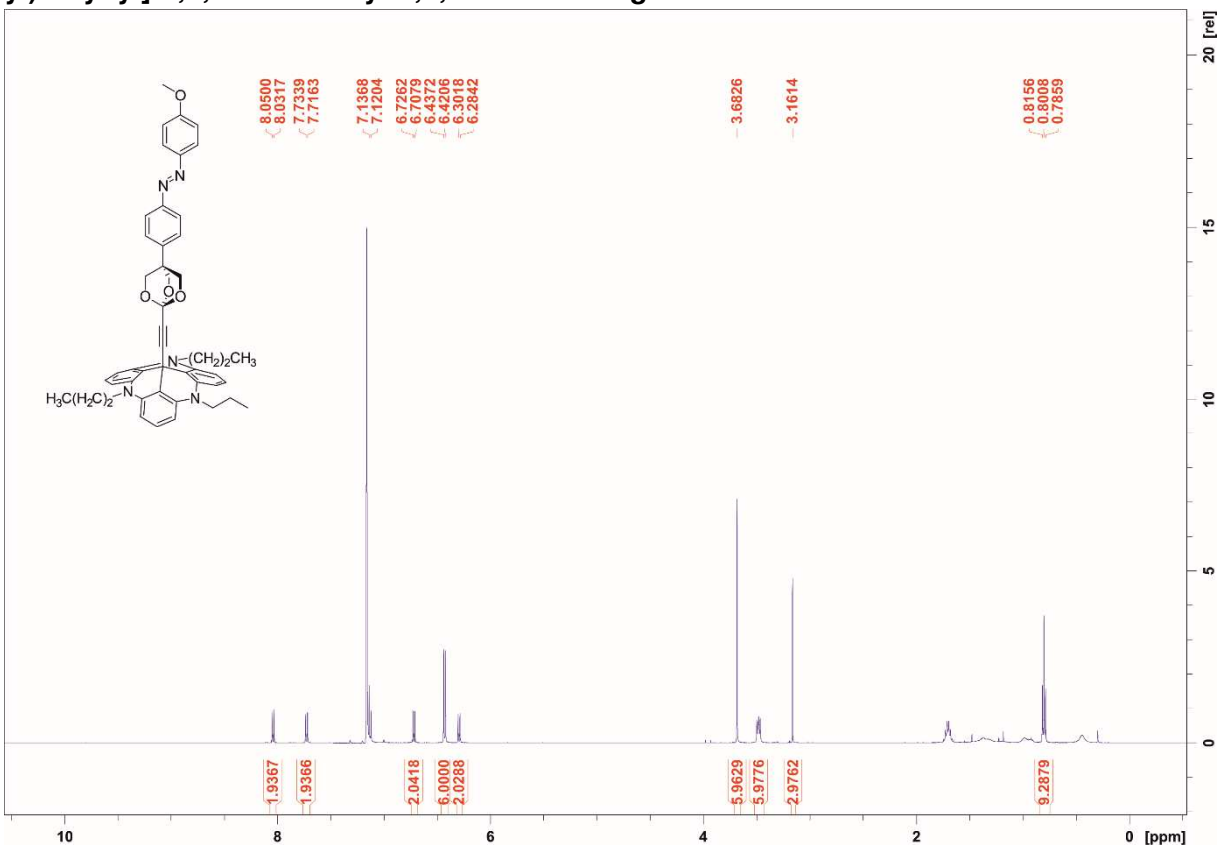

Figure S46. ^{1}H-NMR spectrum (500 MHz, C_6D_6) of compound **5b**.

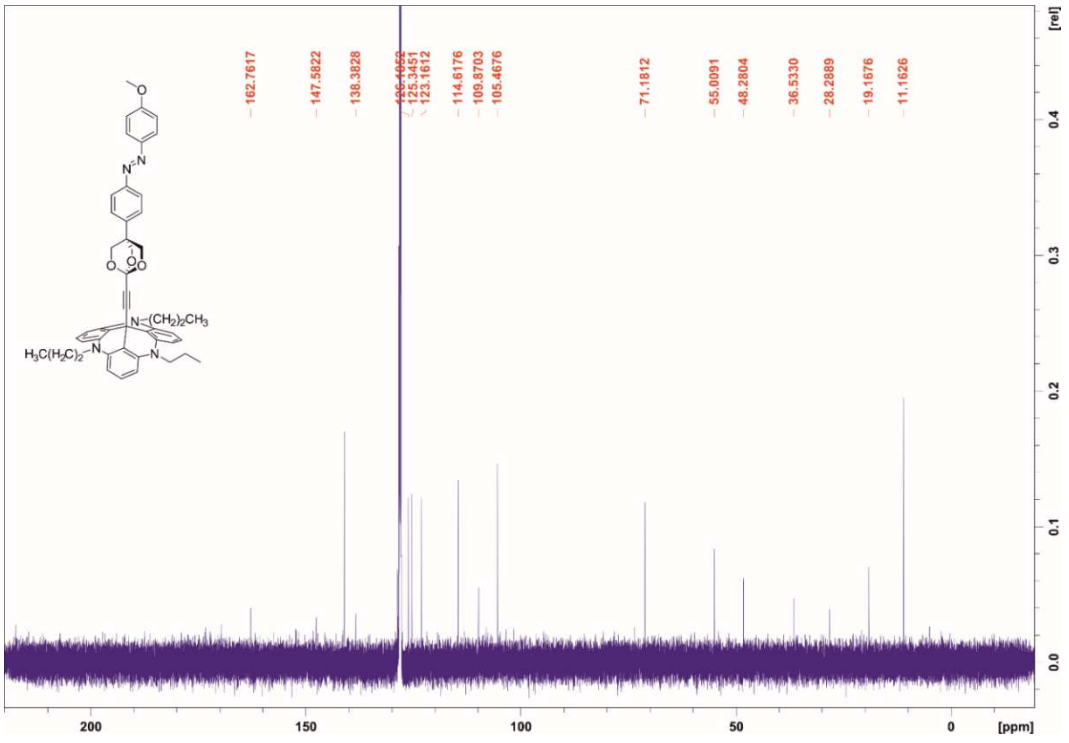

Figure S47. ^{13}C-NMR spectrum (126 MHz, C_6D_6) of compound **5b**.

3.6 Synthesis Compound 6

(*E*)-1-phenyl-2-(4-(((tris(2,4,6-trimethylphenyl)-phosphin)-(9Cl)-gold)-ethynyl) phenyl)diazene

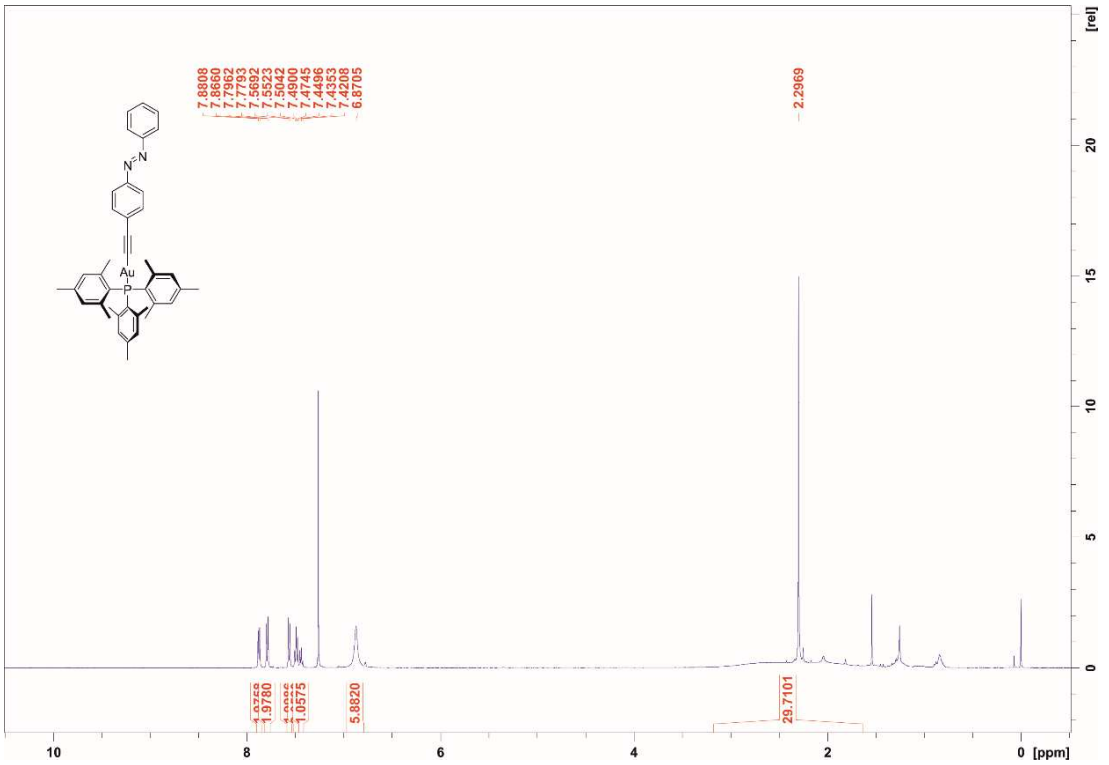

Figure S48. ^{1}H-NMR spectrum (500 MHz, $CDCl_3$) of compound **6**.

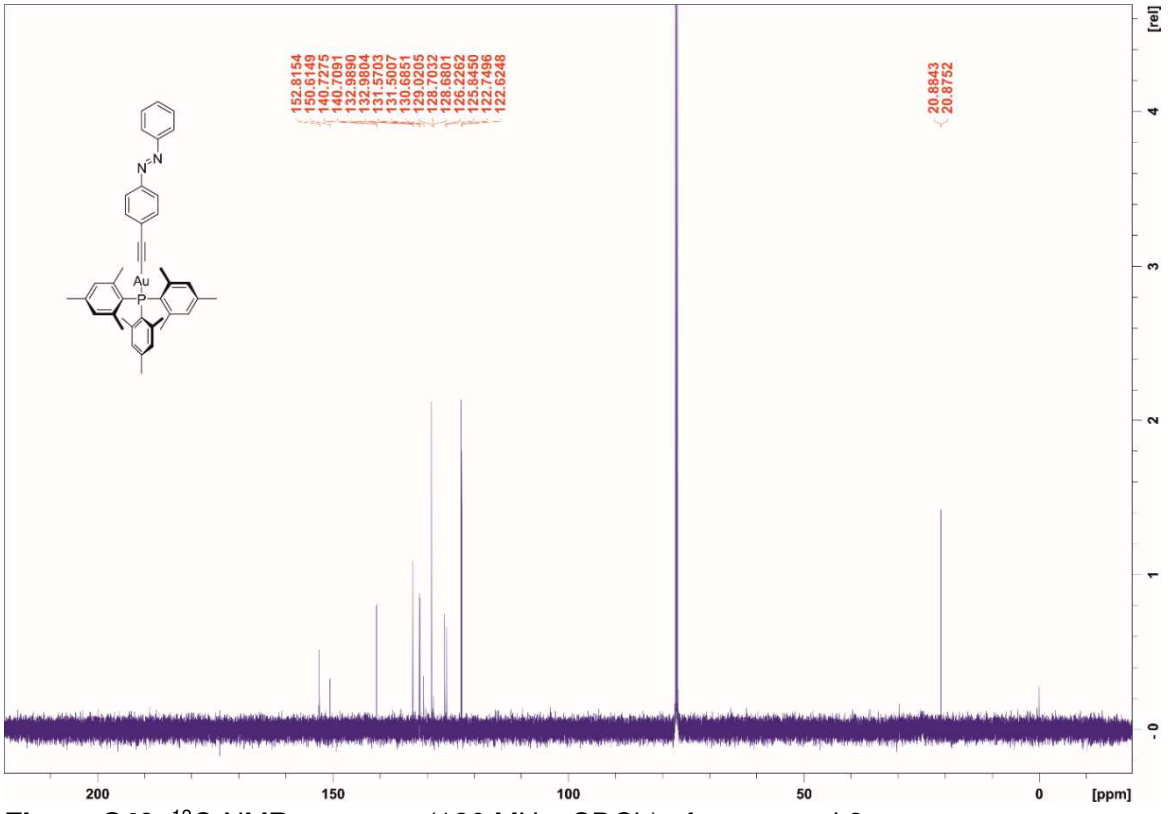

Figure S49. ^{13}C-NMR spectrum (126 MHz, $CDCl_3$) of compound **6**.

4. UV/Vis absorption spectra

4.1 Methods

UV-vis spectra were recorded on a Cary 5000 (Agilent Technologies) Photospectrometer in a 1 cm path length quartz cuvette. Irradiation of UV-vis samples was carried out at 25 °C using a self built LED positioned at a distance of 1 cm from the sample.

4.2 UV/Vis Spectra

Compound 1a: (*E*)-12*c*-[4-(4-methoxyphenyldiazenyl)phenyl]ethynyl-4,8,12-tri-*n*-octyl-4,8,12-triazatriangulene

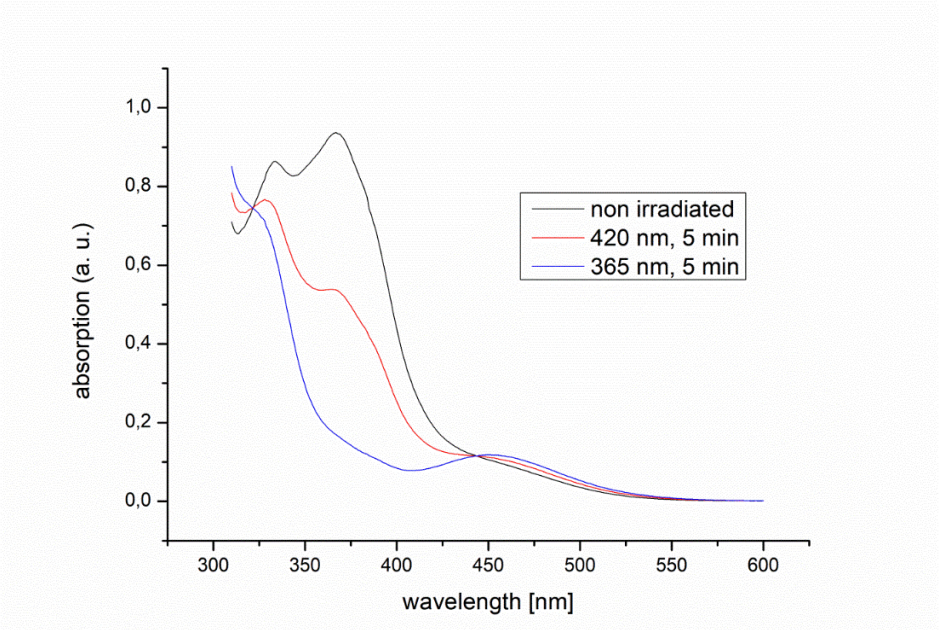

Figure S50. UV/Vis spectra of compound **1a** in toluene at room temperature. Upon irradiation with UV light (365 nm) the π- π* transition band decreases and the n-π* transition band increases in intensity.

Compound 1b: (*E*)-12*c*-[4-(4-methoxyphenyldiazenyl)phenyl]ethynyl-4,8,12-tri-*n*-propyl-4,8,12-triazatriangulene

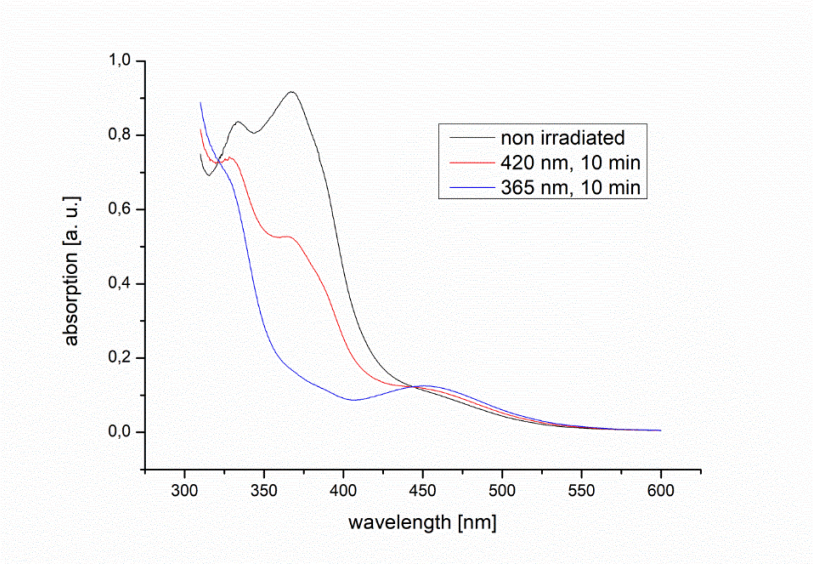

Figure S51. UV/Vis spectra of compound **1b** in toluene at room temperature. Upon irradiation with UV light (365 nm) the π-π* transition band decreases and the n-π* transition band increases in intensity.

Compound 2a: (*E*)-12c-(4-(4-(methoxyphenyldiazenyl)phenyl)phenyl)ethynyl-4,8,12-tri-*n*-octyl-4,8,12-triazatriangulene

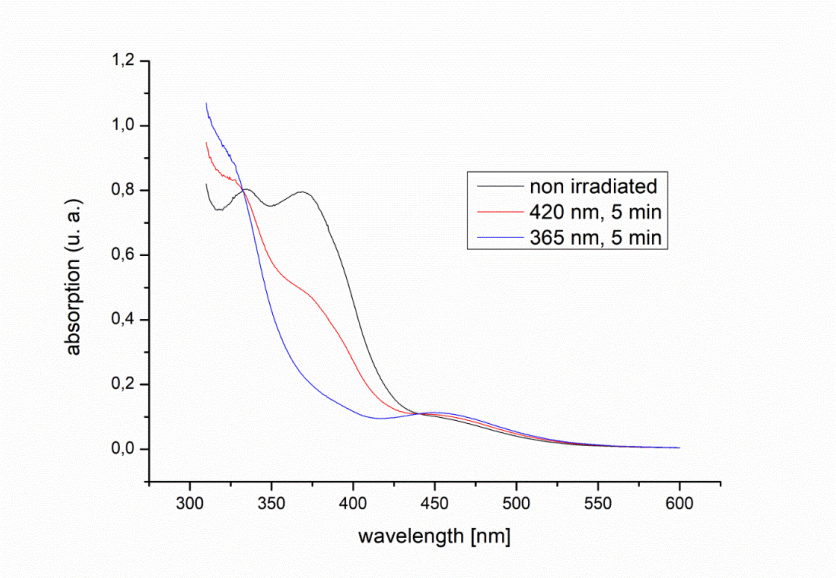

Figure S52. UV/Vis spectra of compound **2a** in toluene at room temperature. Upon irradiation with UV light (365 nm) the π-π* transition band decreases and the n-π* transition band increases in intensity.

Compound 2b: (*E*)-12c-(4-(4-(methoxyphenyldiazenyl)phenyl)phenyl)ethynyl-4,8,12-tri-*n*-propyl-4,8,12-triazatriangulene

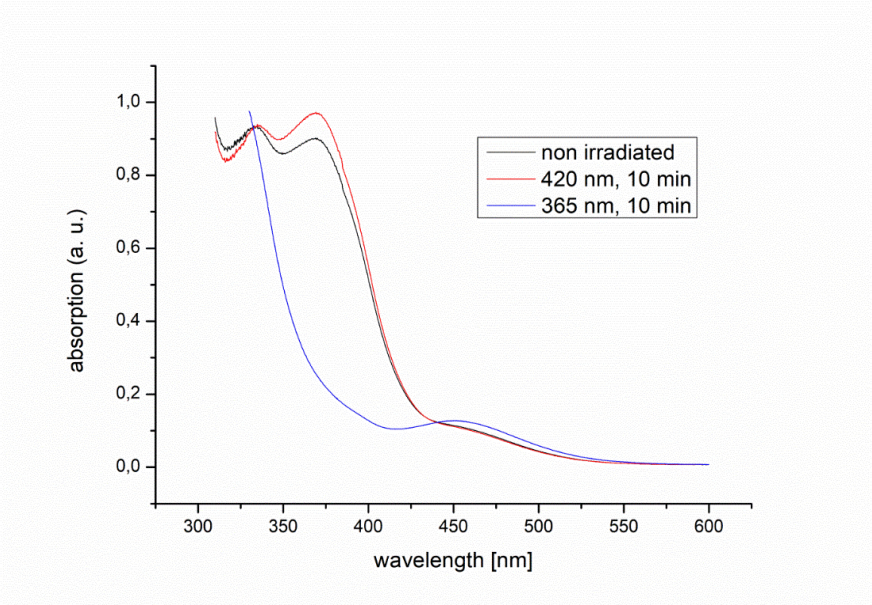

Figure S53. UV/Vis spectra of compound **2b** in toluene at room temperature. Upon irradiation with UV light (365 nm) the π-π* transition band decreases and the n-π* transition band increases in intensity.

Compound 3a: (*E*)-12c-(4-(4-(methoxyphenyldiazenyl)-2-methylphenyl)phenyl)ethynyl-4,8,12-tri-*n*-octyl-4,8,12-triazatriangulene

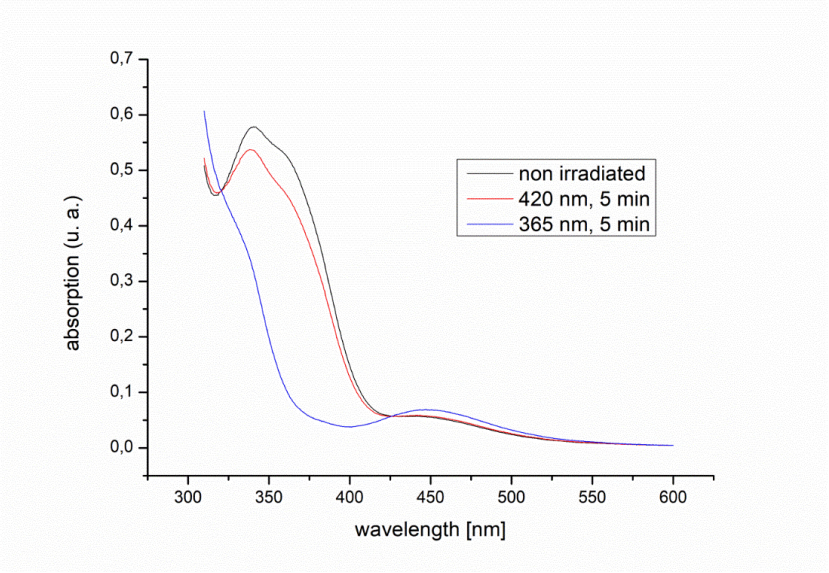

Figure S54. UV/Vis spectra of compound **3a** in toluene at room temperature. Upon irradiation with UV light (365 nm) the π-π* transition band decreases and the n-π* transition band increases in intensity.

Compound 3b: (*E*)-12c-(4-(4-(methoxyphenyldiazenyl)-2-methylphenyl)phenyl)ethynyl-4,8,12-tri-*n*-propyl-4,8,12-triazatriangulene

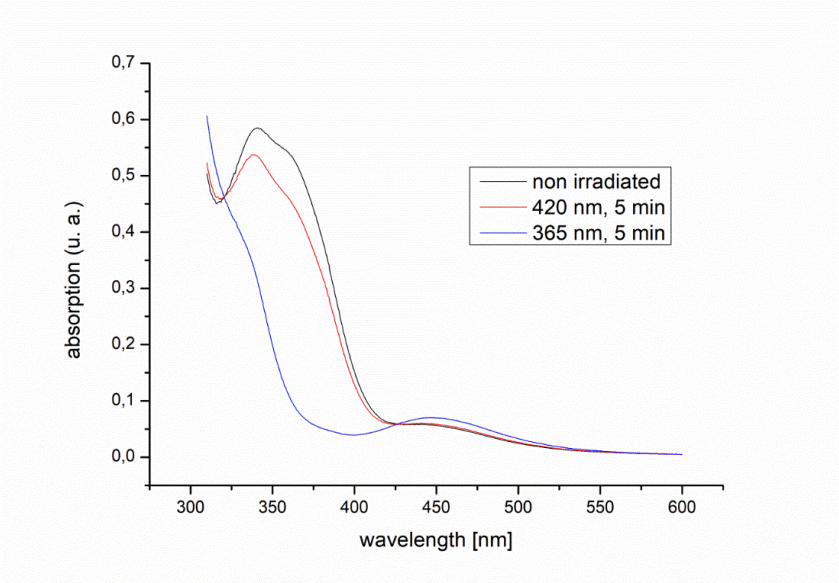

Figure S55. UV/Vis spectra of compound **3b** in toluene at room temperature. Upon irradiation with UV light (365 nm) the π-π* transition band decreases and the n-π* transition band increases in intensity.

Compound 4a: (*E*)-12c-(3-methyl-4-(4-(methoxyphenyldiazenyl)-2-methylphenyl)phenyl)ethynyl-4,8,12-tri-*n*-octyl-4,8,12-triazatriangulene

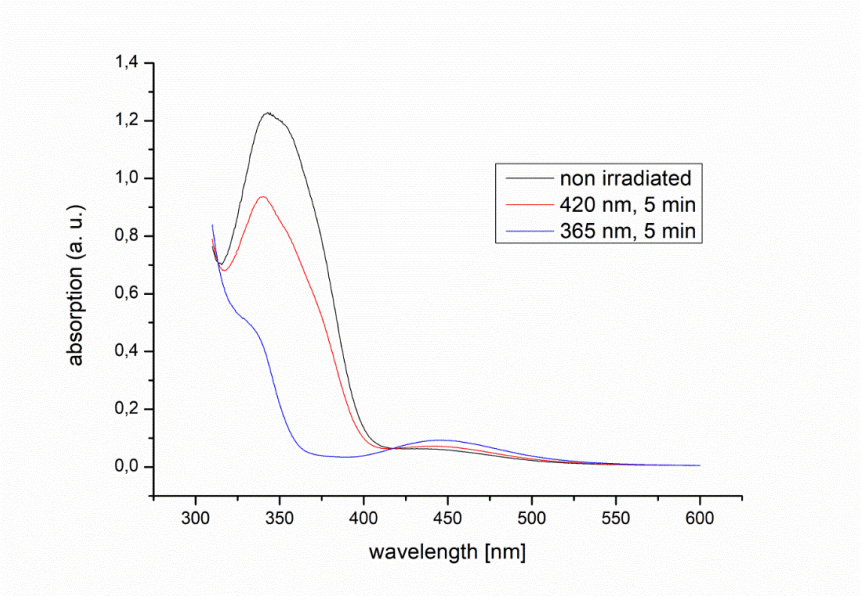

Figure S56. UV/Vis spectra of compound **4a** in toluene at room temperature. Upon irradiation with UV light (365 nm) the π-π* transition band decreases and the n-π* transition band increases in intensity.

Compound 4b: (*E*)-12c-(3-methyl-4-(4-(methoxyphenyldiazenyl)-2-methylphenyl) phenyl)ethynyl-4,8,12-tri-*n*-propyl-4,8,12-triazatriangulene

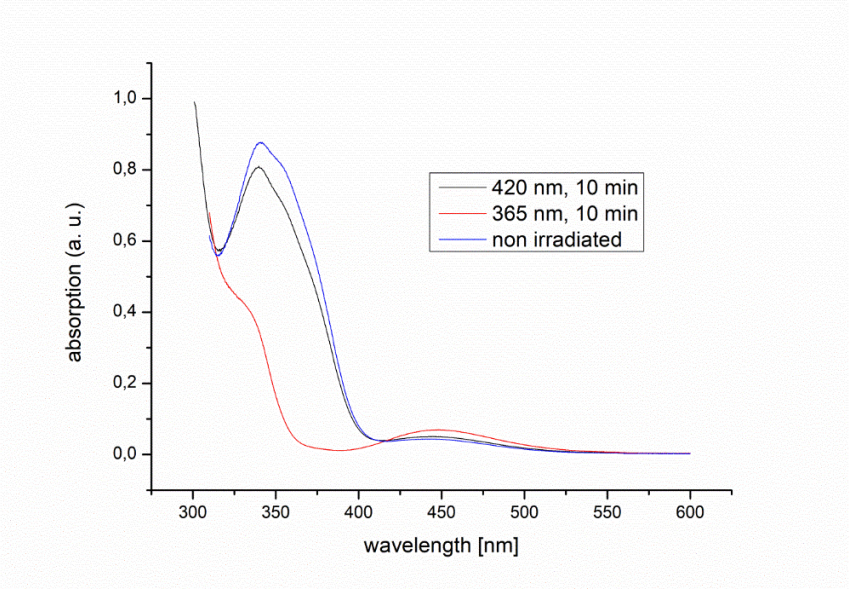

Figure S57. UV/Vis spectra of compound **4b** in toluene at room temperature. Upon irradiation with UV light (365 nm) the π-π* transition band decreases and the n-π* transition band increases in intensity.

Compound 5a: (*E*)-12c-[(4-{4-[(4-methoxyphenyl)diazenyl]phenyl}-2,6,7-trioxabicyclo [2.2.2]octane-1-yl)ethynyl]-4,8,12-tri-*n*-octyl-4,8,12-triazatriangulene

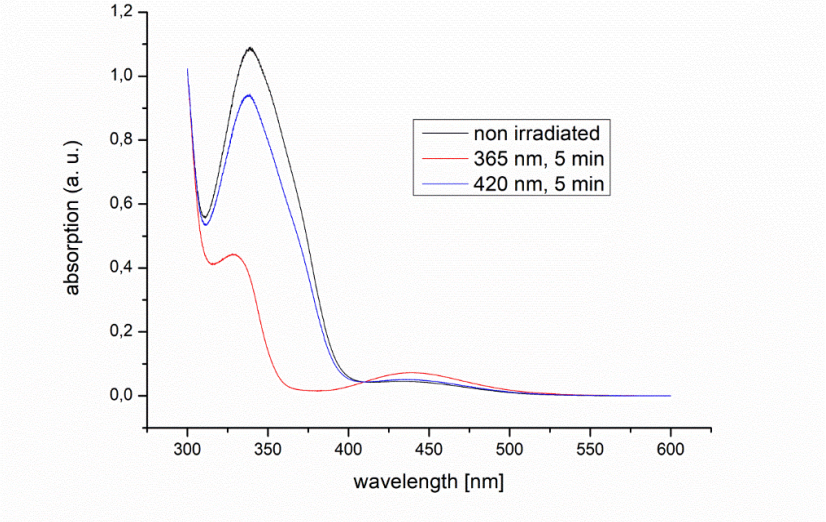

Figure S58. UV/Vis spectra of compound **5a** in toluene at room temperature. Upon irradiation with UV light (365 nm) the π-π* transition band decreases and the n-π* transition band increases in intensity.

Compound 5b: (*E*)-12c-[(4-{4-[(4-methoxyphenyl)diazenyl]phenyl}-2,6,7-trioxabicyclo [2.2.2]octane-1-yl)ethynyl]-4,8,12-tri-*n*-octyl-4,8,12-triazatriangulene

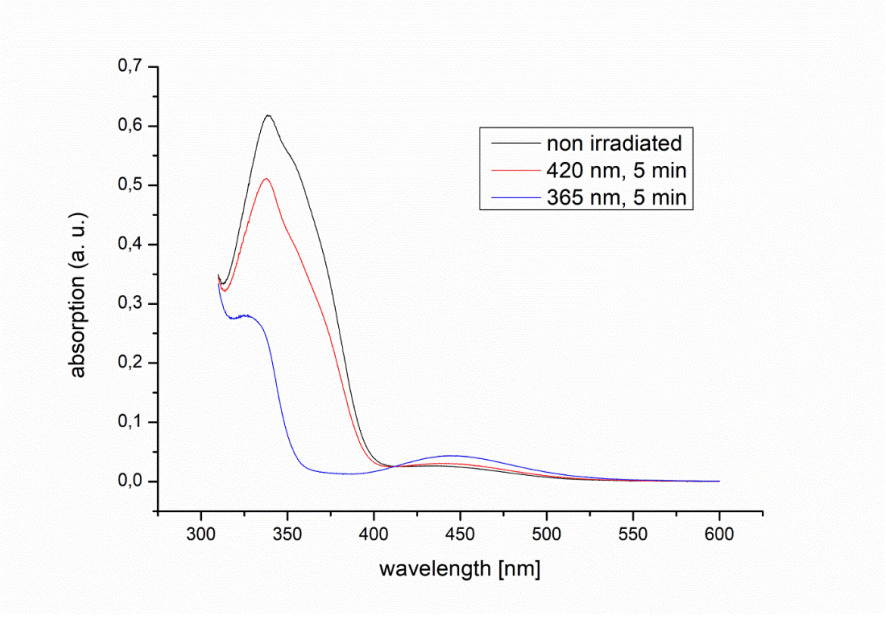

Figure S59. UV/Vis spectra of compound **5b** in toluene at room temperature. Upon irradiation with UV light (365 nm) the π-π* transition band decreases and the n-π* transition band increases in intensity.

Compound 6: (*E*)-1-phenyl-2-(4-(((tris(2,4,6-trimethylphenyl)-phosphin)-(9Cl)-gold)ethynyl) phenyl)diazene

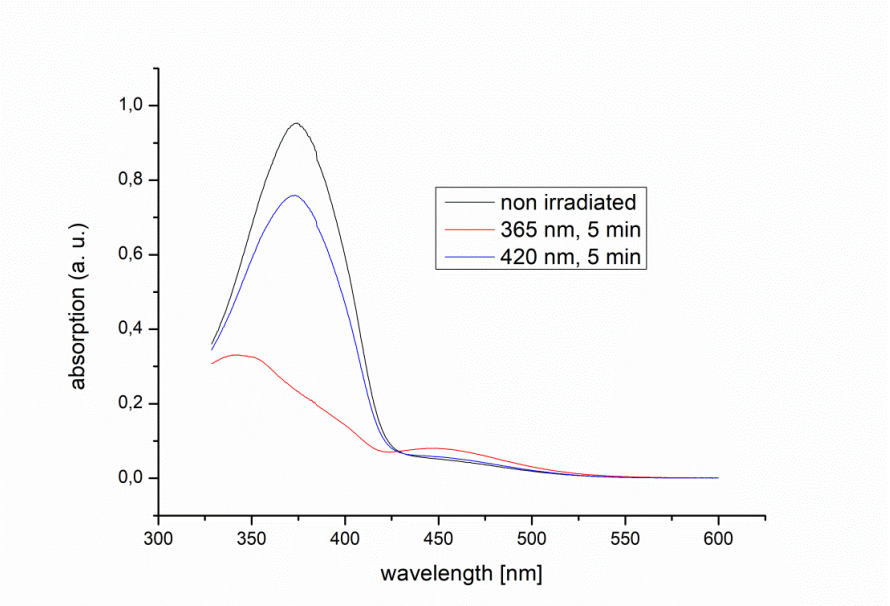

Figure S60. UV/Vis spectra of compound **6** in toluene at room temperature. Upon irradiation with UV light (365 nm) the π-π* transition band decreases and the n-π* transition band increases in intensity.

5. Kinetic studies in solution by ^{1}H-NMR spectroscopy

5.1 Relaxation measurements by ^{1}H-NMR

5.1.1 Compound 1a: (*E*)-12*c*-[4-(4-methoxyphenyldiazenyl) phenyl]ethynyl-4,8,12-tri-*n*-octyl-4,8,12-triazatriangulene

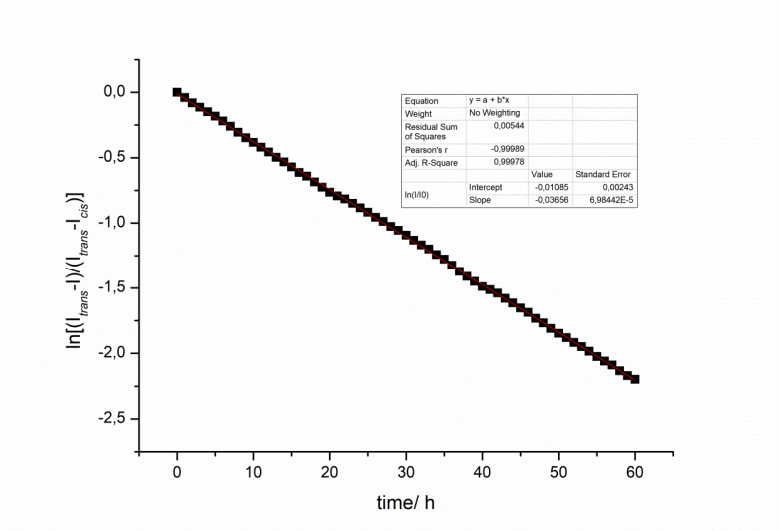

Figure S61. Plot of $\ln[(I_\infty - I)/(I_\infty - I_0)]$ vs. time of compound **1a** in toluene at 290.5 K, which shows a monoexponential decay of *cis* to *trans* with half-life of 18.7 h.

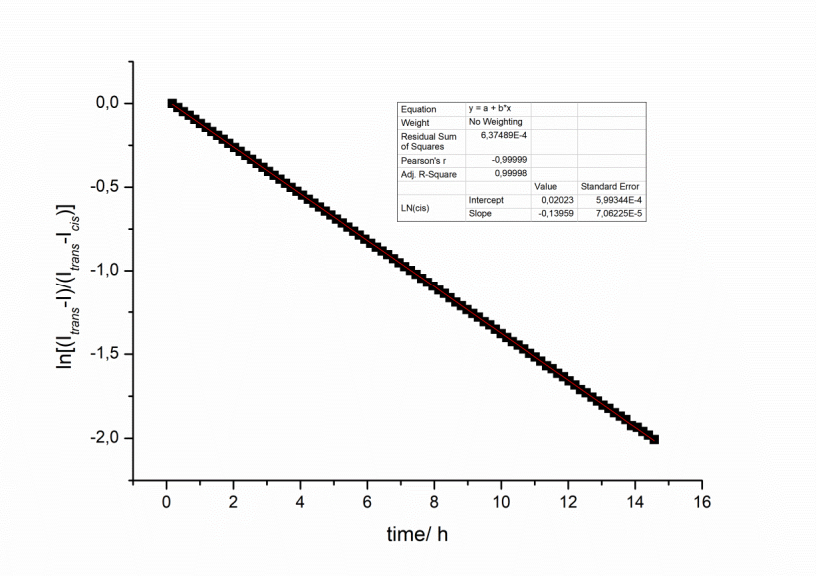

Figure S62. Plot of $\ln[(I_\infty - I)/(I_\infty - I_0)]$ vs. time of compound **1a** in toluene at 300 K, which shows a monoexponential decay of *cis* to *trans* with half-life of 4.97 h.

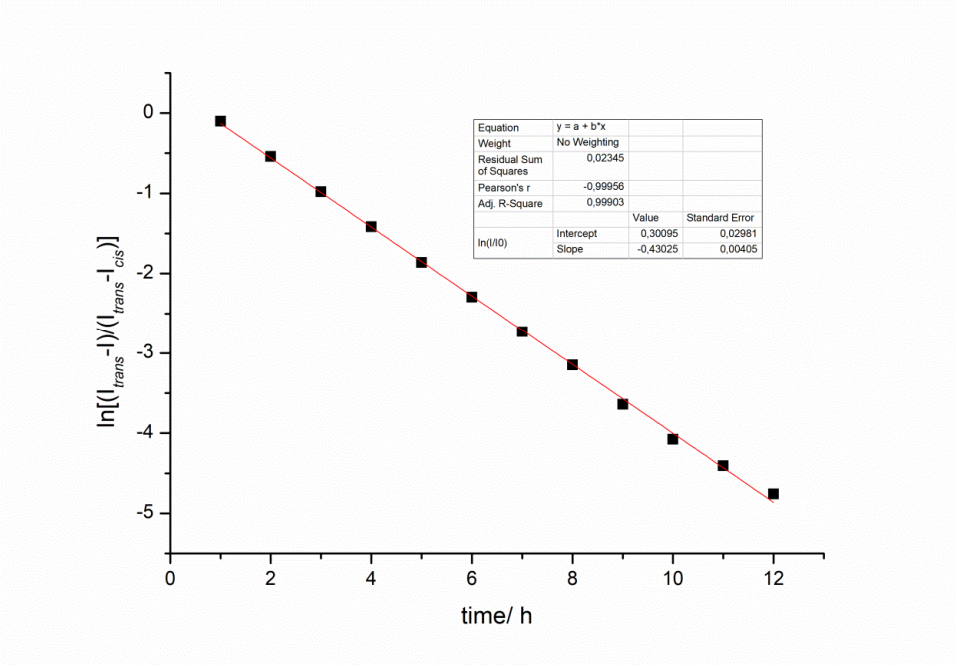

Figure S63. Plot of $\ln[(I_\infty - I)/(I_\infty - I_0)]$ vs. time of compound **1a** in toluene at 309.5 K, which shows a monoexponential decay of *cis* to *trans* with half-life of 1.60 h.

5.1.2 Compound 1b: (*E*)-12*c*-[4-(4-methoxyphenyldiazenyl)phenyl]ethynyl-4,8,12-tri-*n*-propyl-4,8,12-triazatriangulene

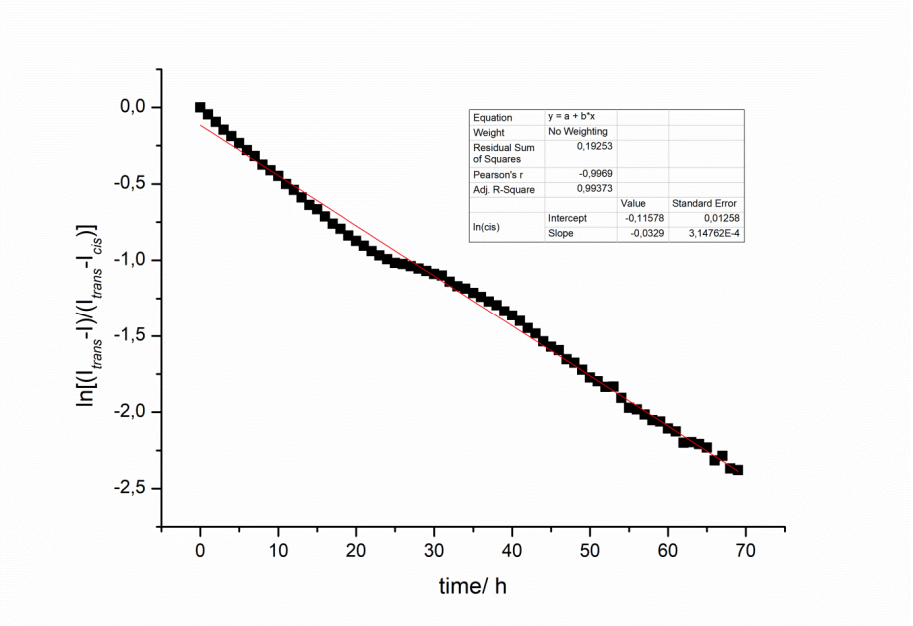

Figure S64. Plot of $\ln[(I_\infty - I)/(I_\infty - I_0)]$ vs. time of compound **1b** in toluene at 297 K, which shows a monoexponential decay of *cis* to *trans* with half-life of 15.9 h.

5.1.3 Compound 2a: (*E*)-12c-(4-(4-(methoxyphenyldiazenyl)phenyl) phenyl)ethynyl-4,8,12-tri-*n*-octyl-4,8,12-triazatriangulene

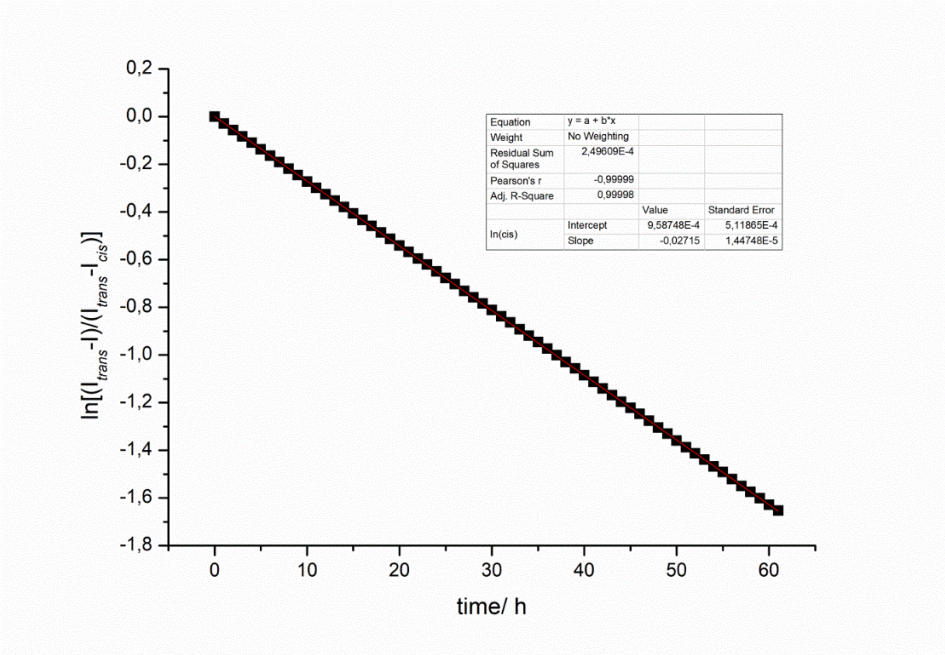

Figure S65. Plot of $\ln[(I_\infty - I)/(I_\infty - I_0)]$ vs. time of compound **2a** in toluene at 290.5 K, which shows a monoexponential decay of *cis* to *trans* with half-life of 25.6 h.

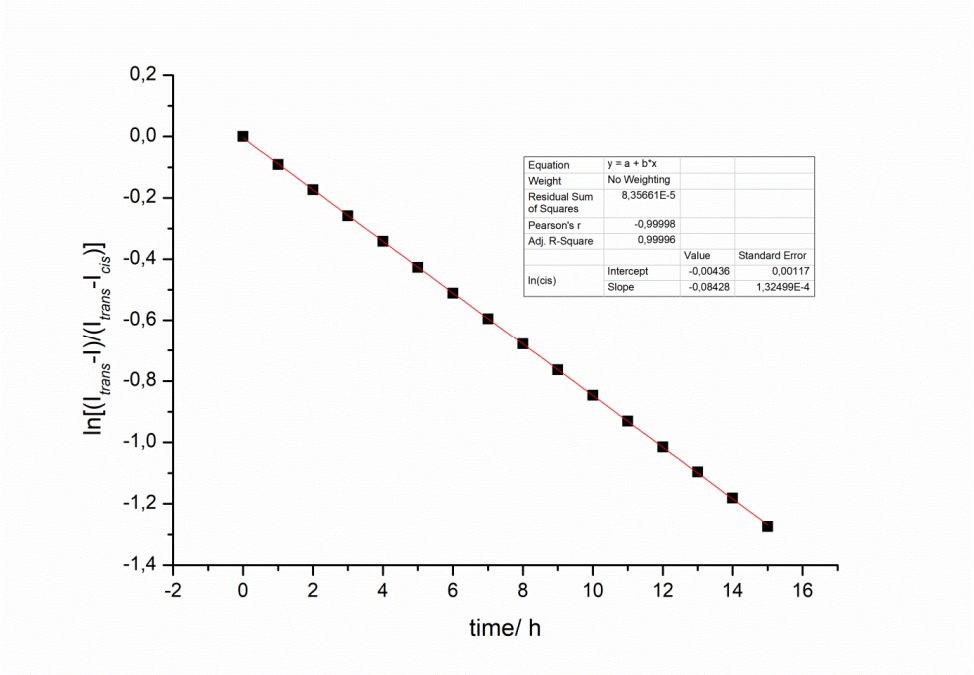

Figure S66. Plot of $\ln[(I_\infty - I)/(I_\infty - I_0)]$ vs. time of compound **2a** in toluene at 298 K, which shows a monoexponential decay of *cis* to *trans* with half-life of 8.22 h.

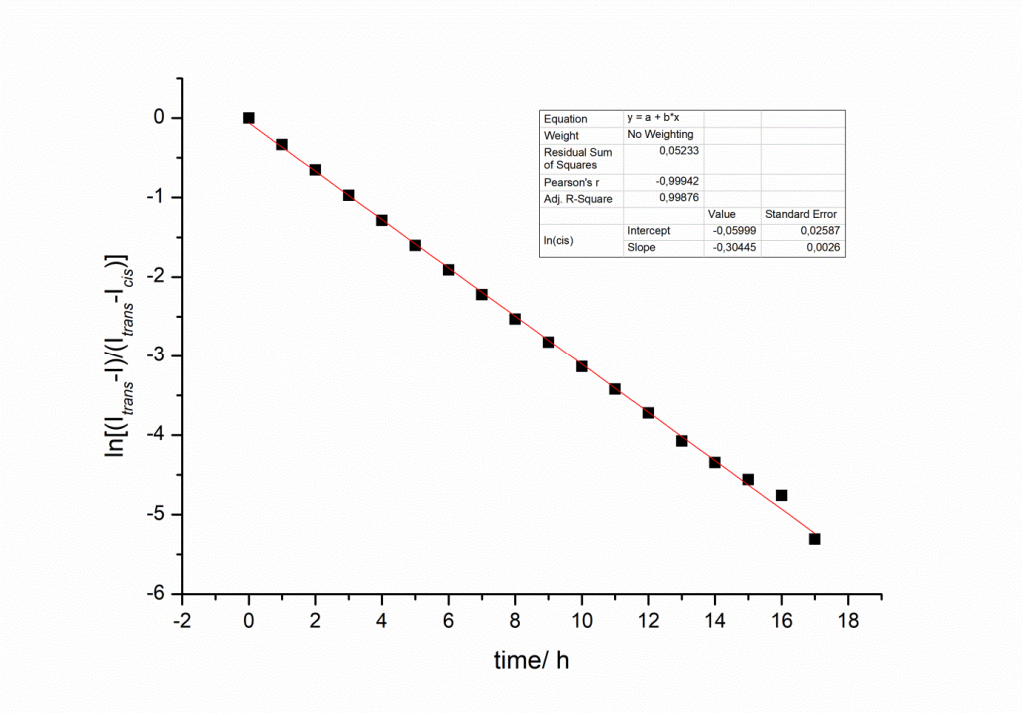

Figure S67. Plot of $\ln[(I_\infty - I)/(I_\infty - I_0)]$ vs. time of compound **2a** in toluene at 309.5 K, which shows a monoexponential decay of *cis* to *trans* with half-life of 2.28 h.

5.1.4 Compound 2b: (*E*)-12c-(4-(4-(methoxyphenyldiazenyl)phenyl) phenyl)ethynyl-4,8,12-tri-*n*-propyl-4,8,12-triazatriangulene

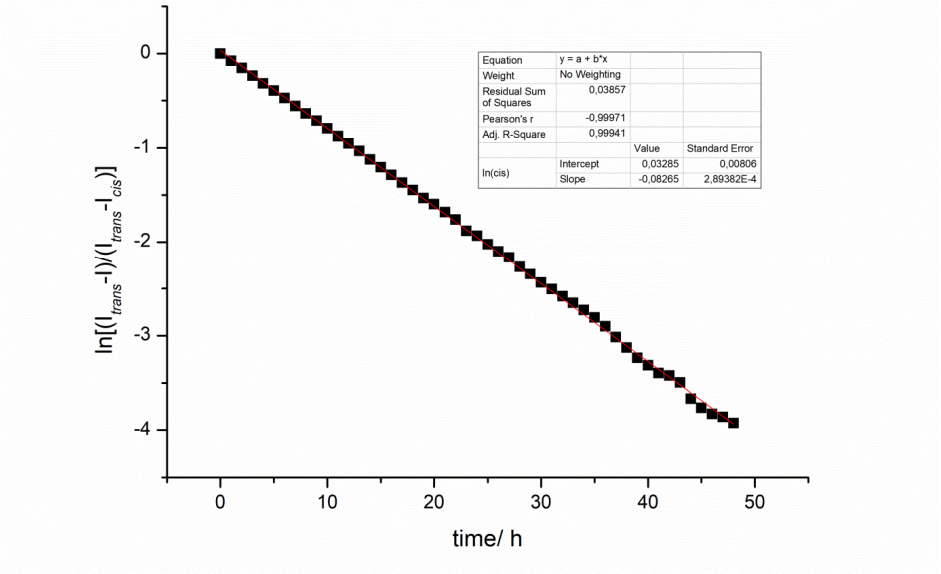

Figure S68. Plot of $\ln[(I_\infty - I)/(I_\infty - I_0)]$ vs. time of compound **2b** in toluene at 297 K, which shows a monoexponential decay of *cis* to *trans* with half-life of 13.4 h.

5.1.5 Compound 3a: (*E*)-12c-(4-(4-(methoxyphenyldiazenyl)-2-methylphenyl)phenyl)ethynyl-4,8,12-tri-*n*-octyl-4,8,12-triazatriangulene

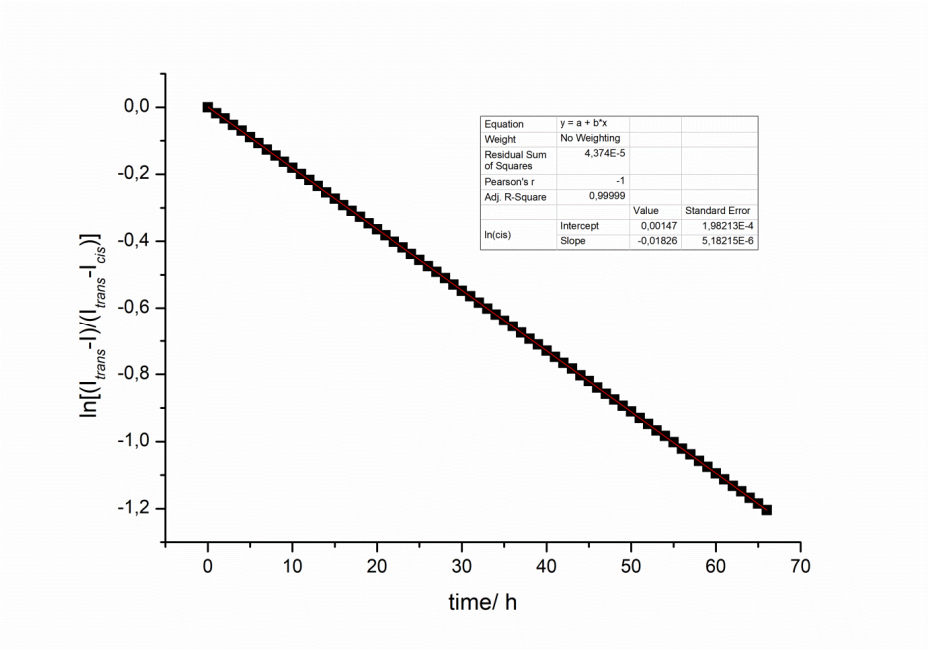

Figure S69. Plot of $\ln[(I_\infty - I)/(I_\infty - I_0)]$ vs. time of compound **3a** in toluene at 290.5 K, which shows a monoexponential decay of *cis* to *trans* with half-life of 37.9 h.

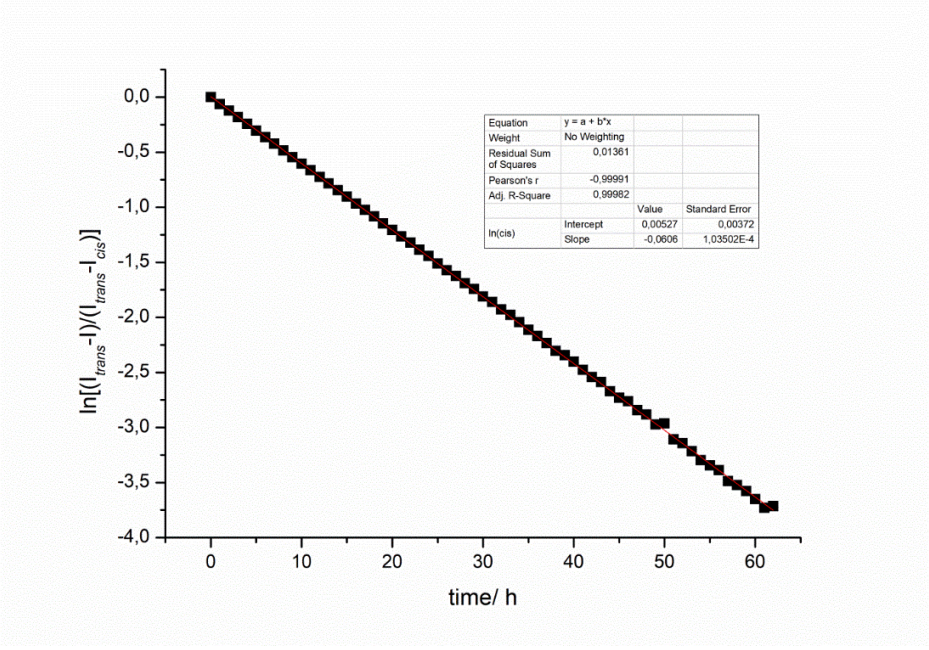

Figure S70. Plot of $\ln[(I_\infty - I)/(I_\infty - I_0)]$ vs. time of compound **3a** in toluene at 300 K, which shows a monoexponential decay of *cis* to *trans* with half-life of 11.4 h.

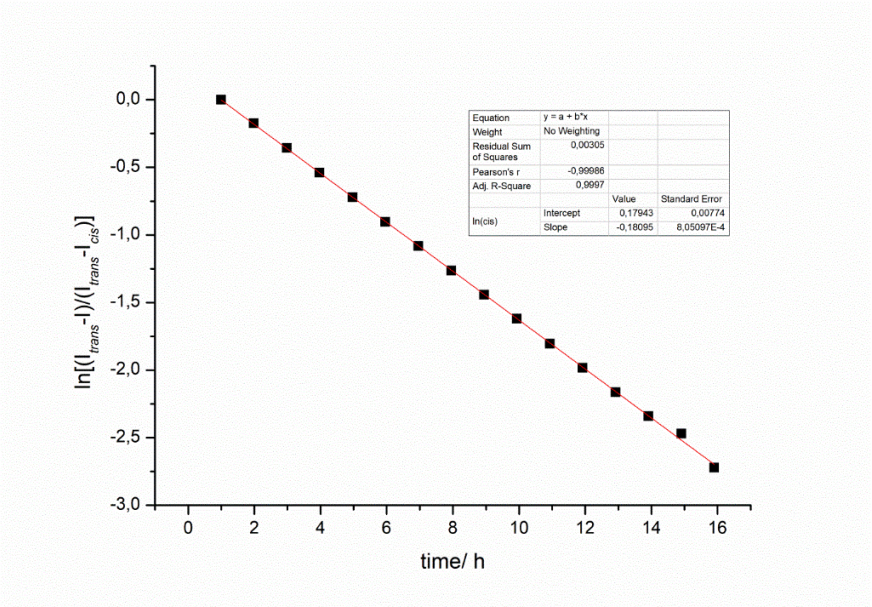

Figure S71. Plot of $\ln[(I_\infty - I)/(I_\infty - I_0)]$ vs. time of compound **3a** in toluene at 309.5 K, which shows a monoexponential decay of *cis* to *trans* with half-life of 3.83 h.

5.1.6 Compound 3b: (*E*)-12c-(4-(4-(methoxyphenyldiazenyl)-2-methylphenyl)phenyl) ethynyl-4,8,12-tri-*n*-propyl-4,8,12-triazatriangulene

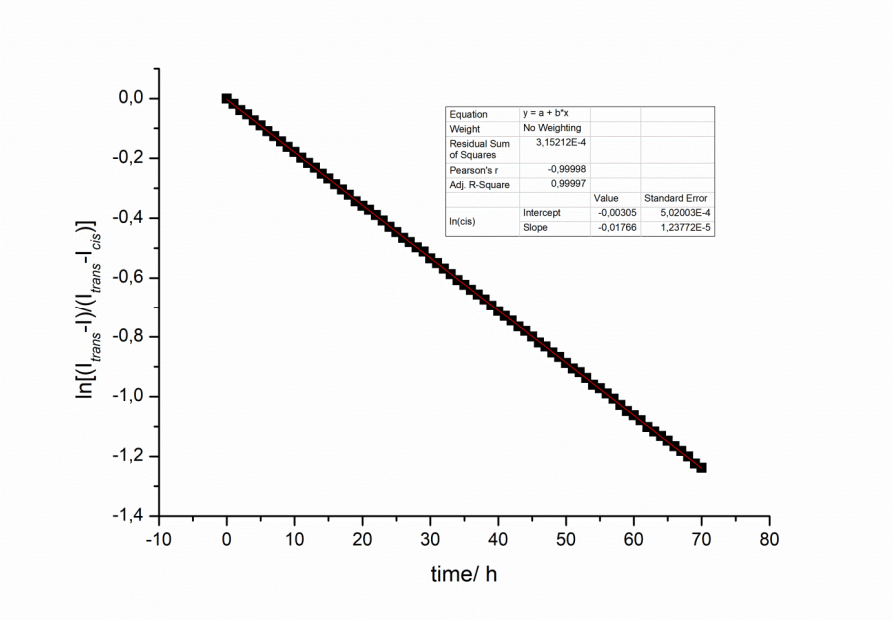

Figure S72. Plot of $\ln[(I_\infty - I)/(I_\infty - I_0)]$ vs. time of compound **3b** in toluene at 297 K, which shows a monoexponential decay of *cis* to *trans* with half-life of 35.7 h.

5.1.7 Compound 4a: (*E*)-12c-(3-methyl-4-(4-(methoxyphenyldiazenyl)-2-methylphenyl) phenyl) ethynyl-4,8,12-tri-*n*-octyl-4,8,12-triazatriangulene

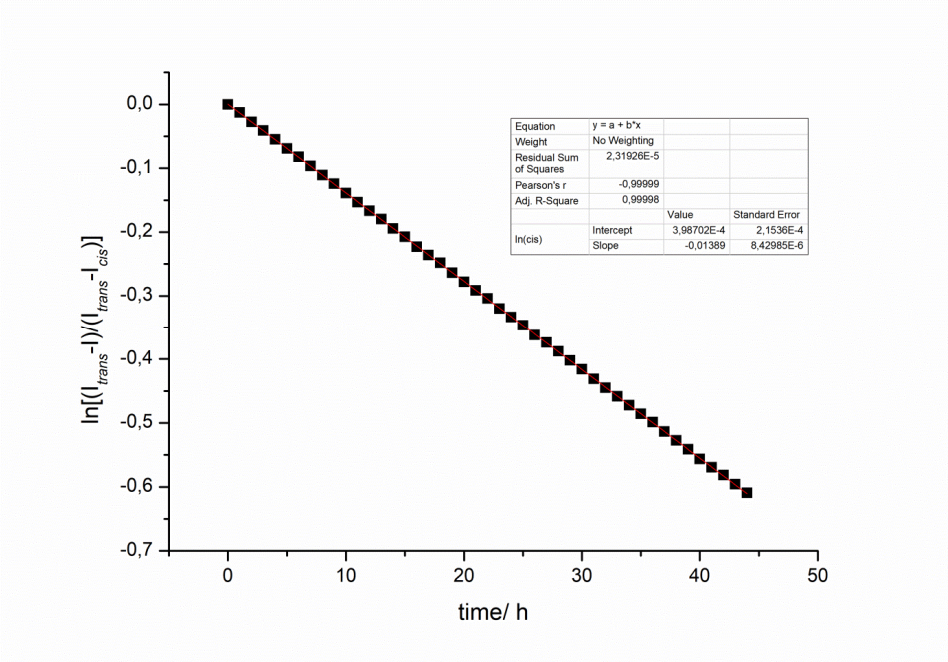

Figure S73. Plot of $\ln[(I_\infty - I)/(I_\infty - I_0)]$ vs. time of compound **4a** in toluene at 290.5 K, which shows a monoexponential decay of *cis* to *trans* with half-life of 49.9 h.

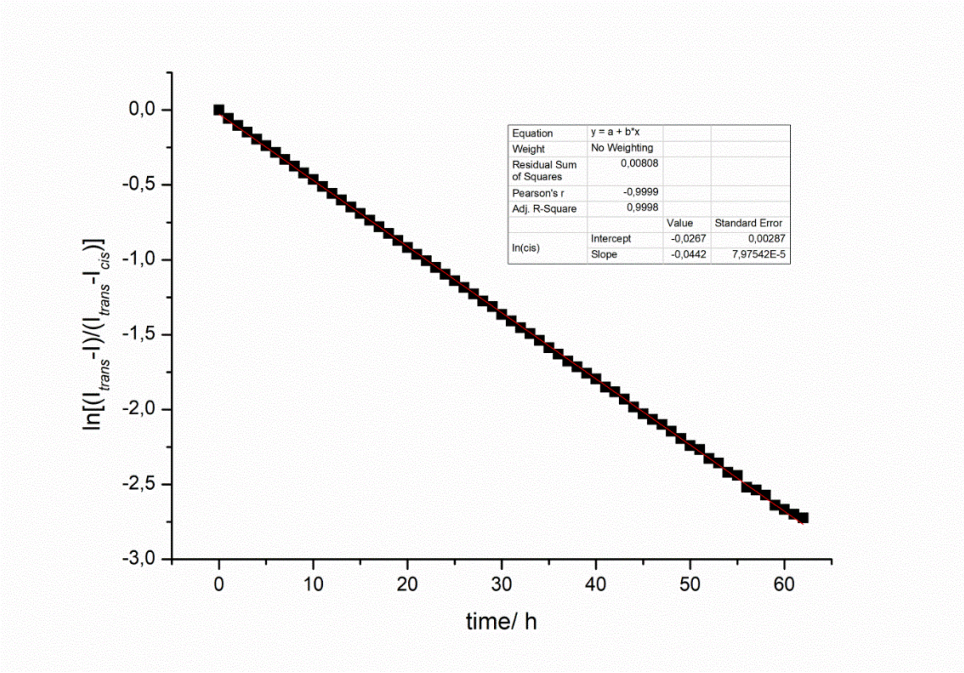

Figure S74. Plot of $\ln[(I_\infty - I)/(I_\infty - I_0)]$ vs. time of compound **4a** in toluene at 300 K, which shows a monoexponential decay of *cis* to *trans* with half-life of 15.7 h.

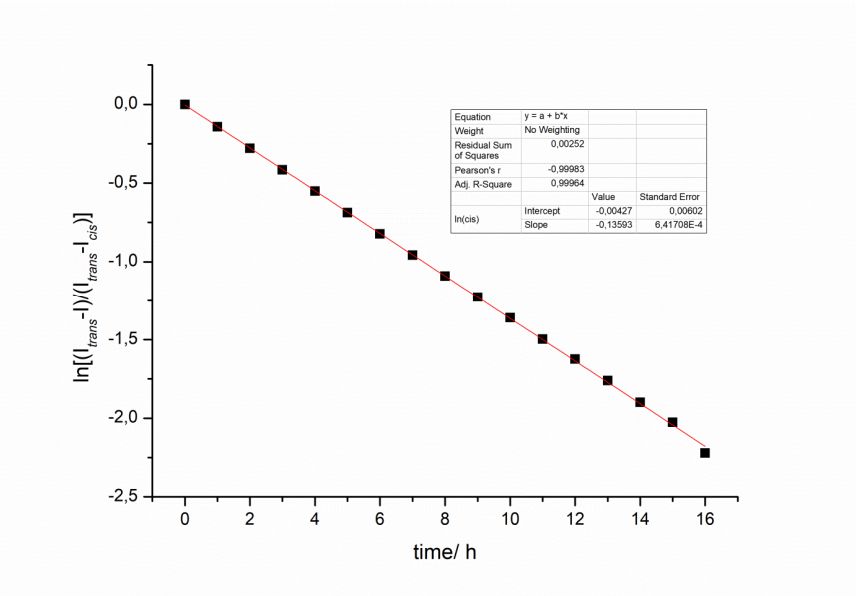

Figure S75. Plot of $\ln[(I_\infty - I)/(I_\infty - I_0)]$ vs. time of compound **4a** in toluene at 309.5 K, which shows a monoexponential decay of *cis* to *trans* with half-life of 5.10 h.

5.1.8 Compound 4b: (*E*)-12c-(3-methyl-4-(4-(methoxyphenyldiazenyl)-2-methylphenyl)phenyl) ethynyl-4,8,12-tri-*n*-propyl-4,8,12-triazatriangulene

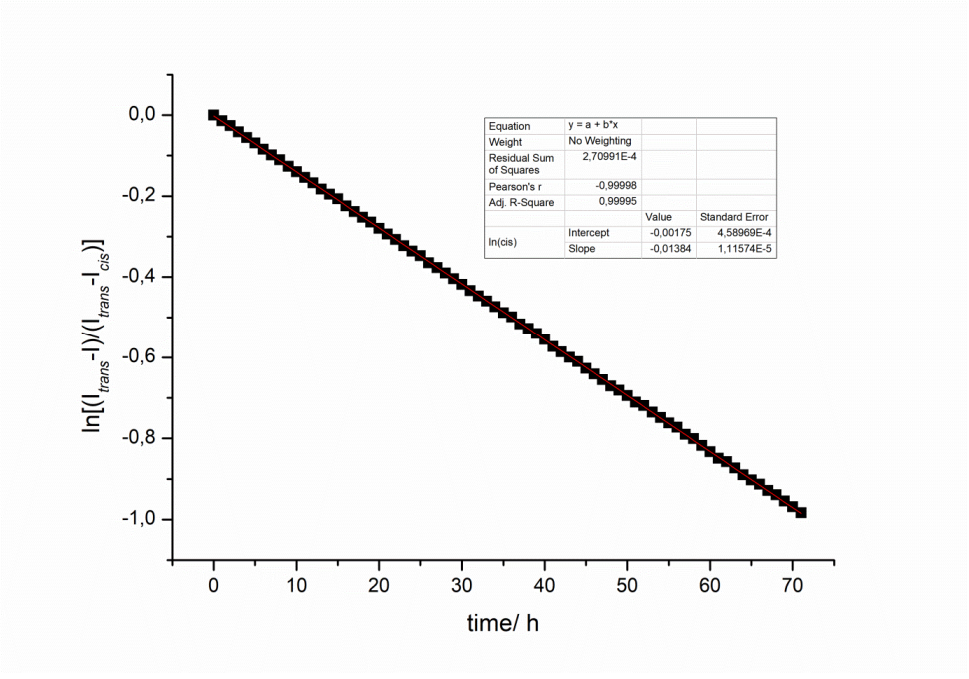

Figure S76. Plot of $\ln[(I_\infty - I)/(I_\infty - I_0)]$ vs. time of compound **4b** in toluene at 297 K, which shows a monoexponential decay of *cis* to *trans* with half-life of 46.2 h.

5.1.9 Compound 5a: (E)-12c-[(4-{4-[(4-methoxyphenyl)diazenyl]phenyl}-2,6,7-trioxabicyclo[2.2.2] octane-1-yl)ethynyl]-4,8,12-tri-n-octyl-4,8,12-triazatriangulene

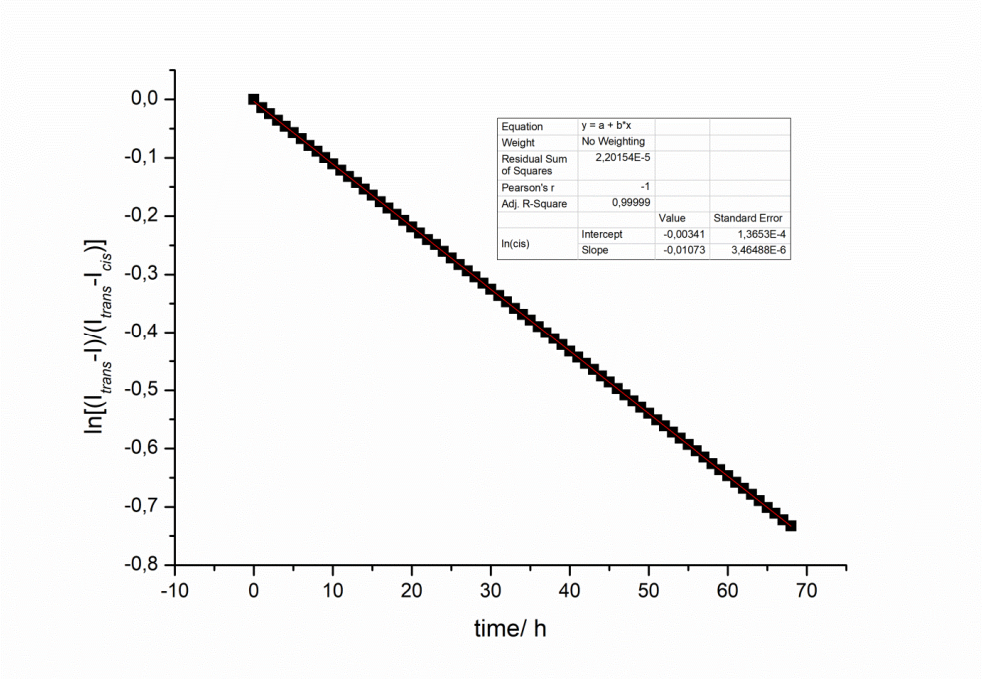

Figure S77. Plot of $\ln[(I_\infty - I)/(I_\infty - I_0)]$ vs. time of compound **5a** in toluene at 290.5 K, which shows a monoexponential decay of *cis* to *trans* with half-life of 64.8 h.

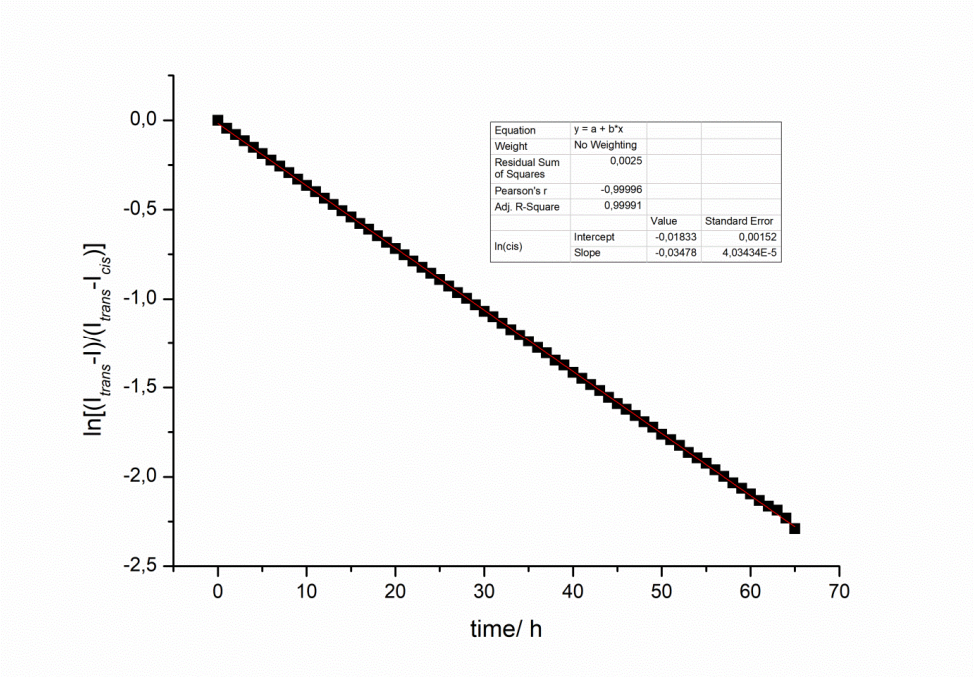

Figure S78. Plot of $\ln[(I_\infty - I)/(I_\infty - I_0)]$ vs. time of compound **5a** in toluene at 300 K, which shows a monoexponential decay of *cis* to *trans* with half-life of 19.9 h.

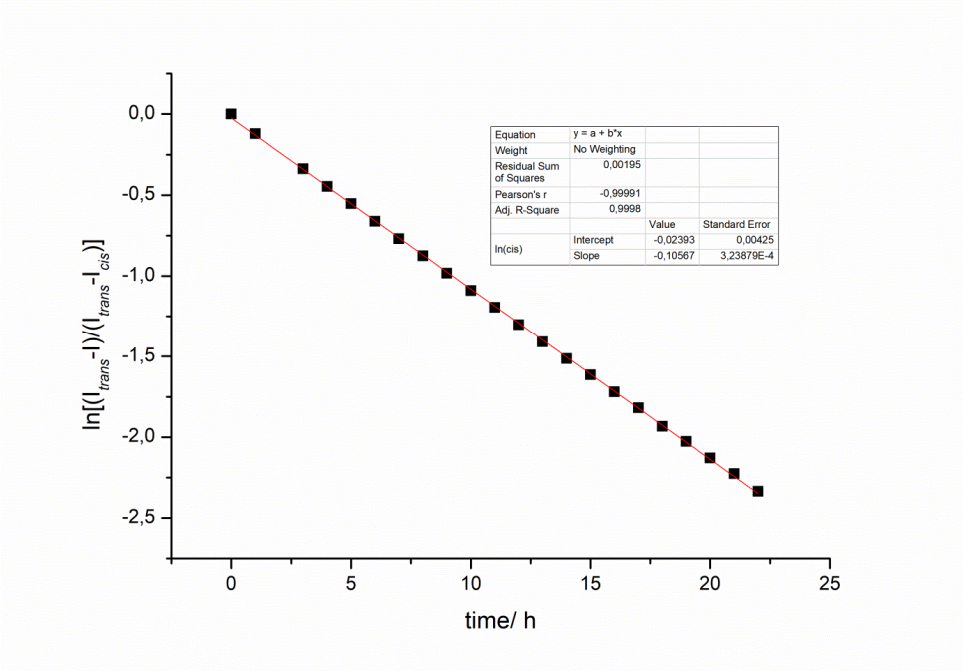

Figure S79. Plot of $\ln[(I_\infty - I)/(I_\infty - I_0)]$ vs. time of compound **5a** in toluene at 309.5 K, which shows a monoexponential decay of *cis* to *trans* with half-life of 6.56 h.

5.1.10 Compound 5b: (*E*)-12c-[(4-{4-[(4-methoxyphenyl)diazenyl]phenyl}-2,6,7-trioxabicyclo[2.2.2]octane-1-yl)ethynyl]-4,8,12-tri-*n*-octyl-4,8,12-triazatriangulene

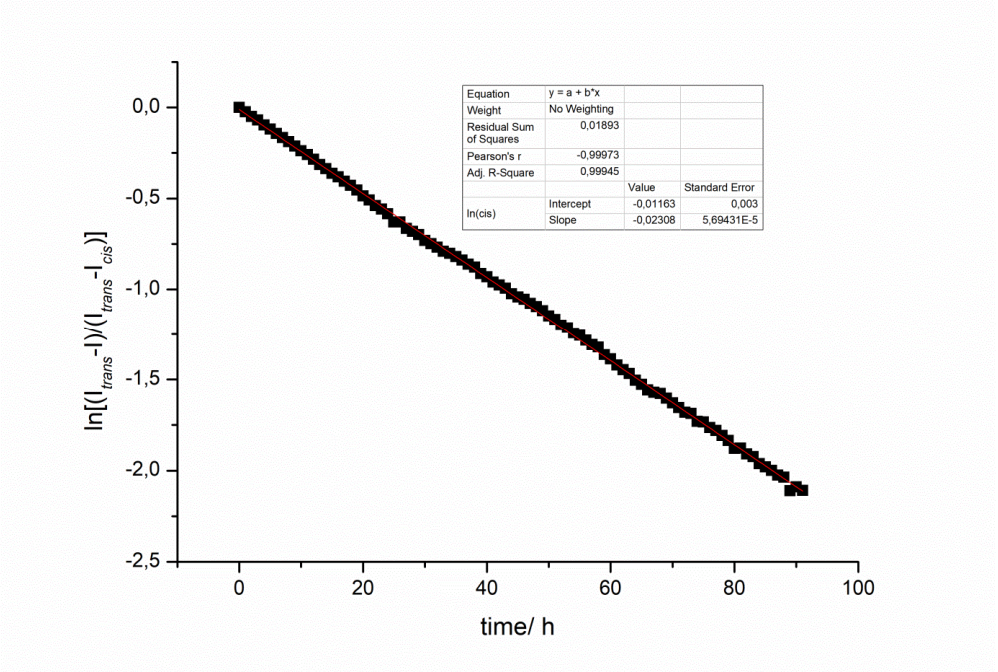

Figure S80. Plot of $\ln[(I_\infty - I)/(I_\infty - I_0)]$ vs. time of compound **5b** in toluene at 297 K, which shows a monoexponential decay of *cis* to *trans* with half-life of 62.5 h.

5.1.11 Compound 30: (*E*)-1-phenyl-2-(4-(2(trimethylsilyl)-ethynyl)phenyl)diazene

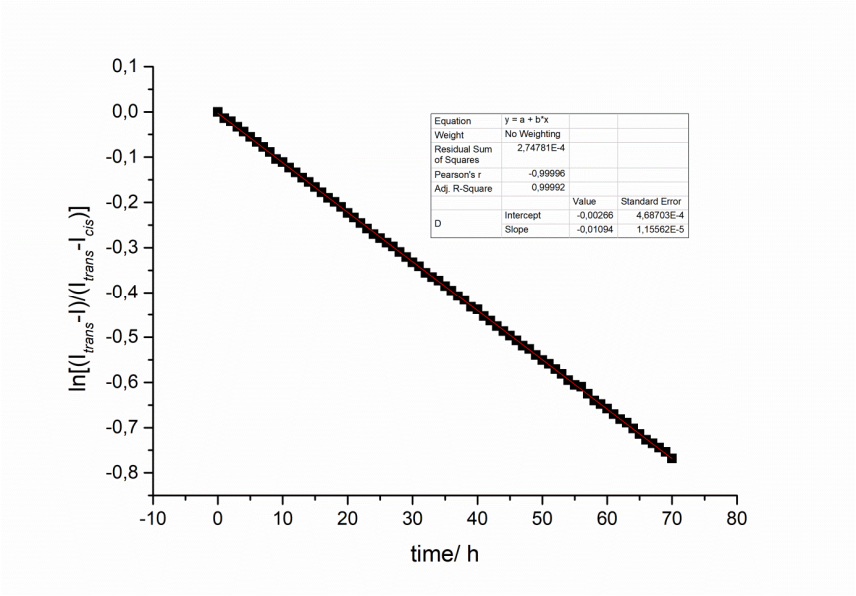

Figure S81. Plot of $\ln[(I_\infty - I)/(I_\infty - I_0)]$ vs. time of compound **30** in toluene at 293 K, which shows a monoexponential decay of *cis* to *trans* with half-life of 63.4 h.

4.1.12 (*E*)-1-phenyl-2-(4-(((tris(2,4,6-trimethylphenyl)-phosphin)-(9Cl)-gold)ethynyl)phenyl)diazene

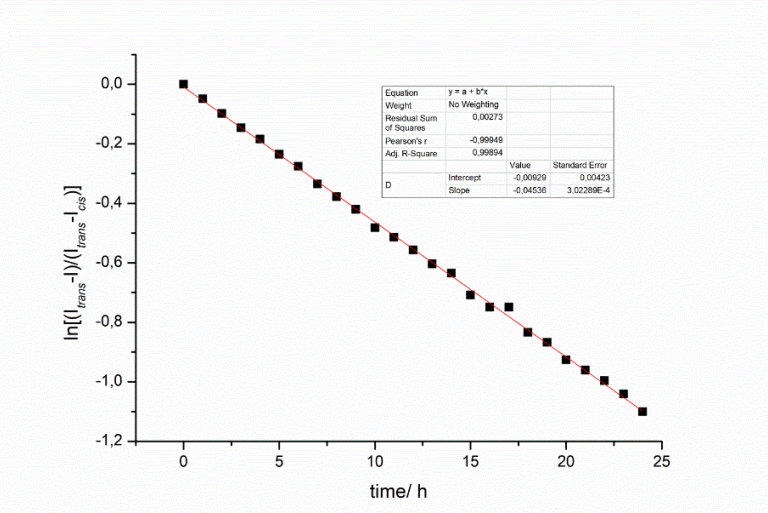

Figure S82. Plot of $\ln[(I_\infty - I)/(I_\infty - I_0)]$ vs. time of compound **6** in toluene at 297 K, which shows a monoexponential decay of *cis* to *trans* with half-life of 15.3 h.

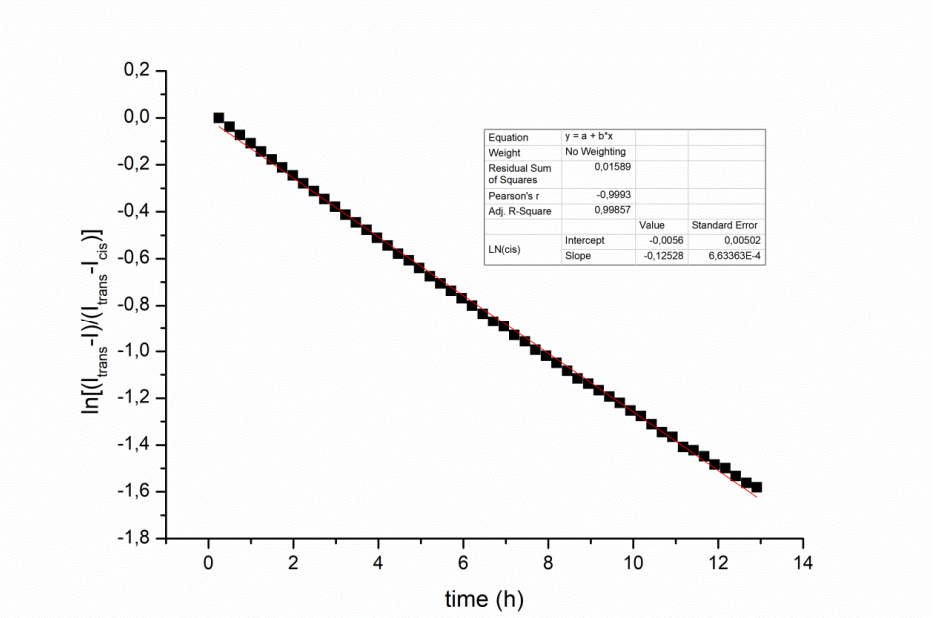

Figure S83. Plot of $\ln[(I_\infty - I)/(I_\infty - I_0)]$ vs. time of compound **6** in toluene at 303.0 K, which shows a monoexponential decay of *cis* to *trans* with half-life of 5.53 h.

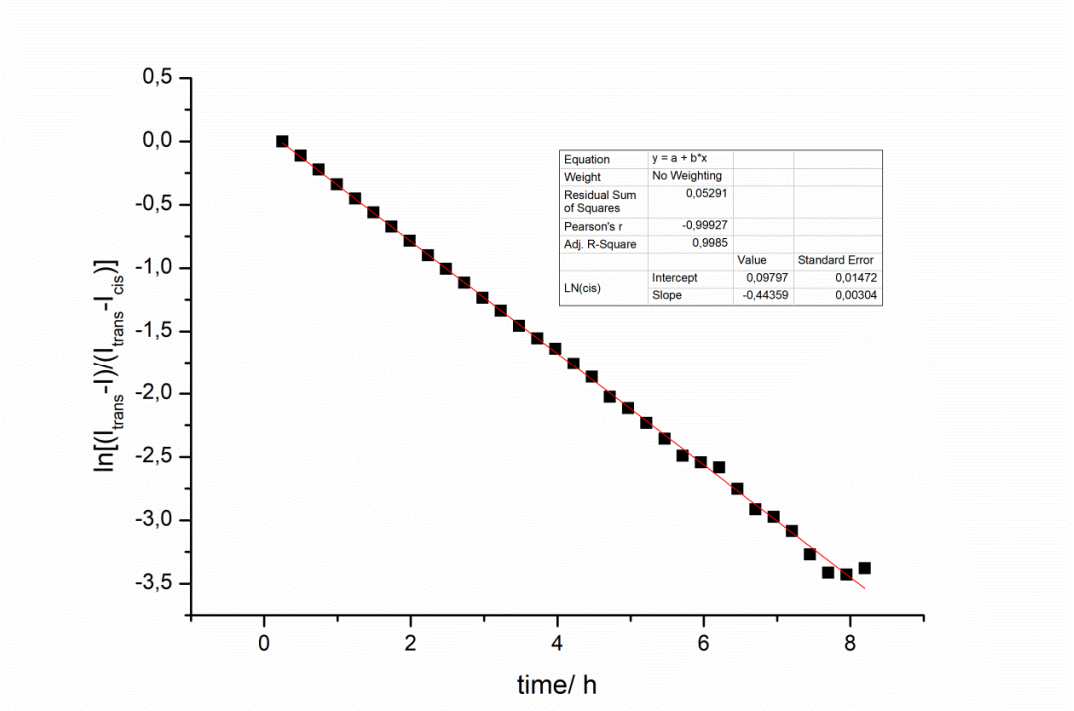

Figure S84. Plot of $\ln[(I_\infty - I)/(I_\infty - I_0)]$ vs. time of compound **6** in toluene at 314.6 K, which shows a monoexponential decay of *cis* to *trans* with half-life of 1.56 h.

5.2 Arrhenius Plots for compound 1-6 in solution

5.2.1 Compound 1a: (*E*)-12*c*-[4-(4-methoxyphenyldiazenyl)phenyl]ethynyl 4,8,12- tri-*n*-octyl-4,8,12-triazatriangulene

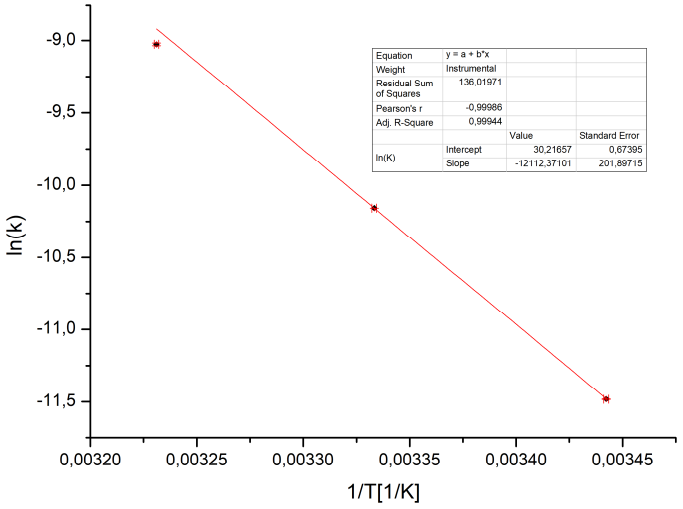

Figure S85. Arrhenius plot of the *cis*-to-*trans* isomerisation of compound **1a** which shows an activation energy of 24.1 kcal/mol.

5.2.2 Compound 2a: (*E*)-12c-(4-(4-(methoxyphenyldiazenyl)phenyl) phenyl)ethynyl-4,8,12-tri-*n*-octyl-4,8,12-triazatriangulene

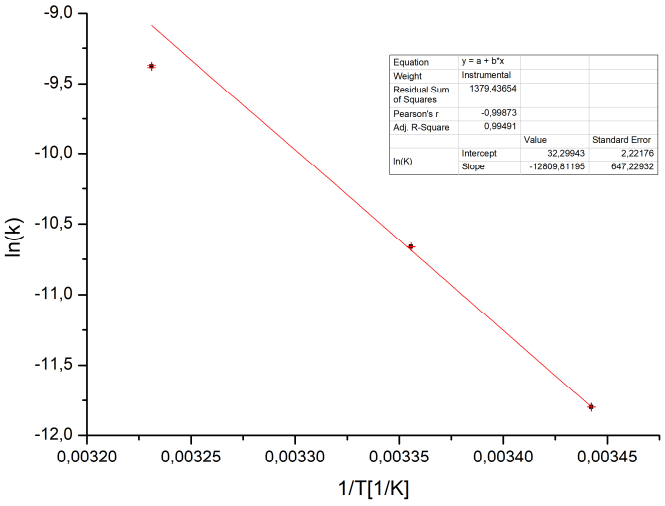

Figure S86. Arrhenius plot of the *cis*-to-*trans* isomerisation of compound **2a** which shows an activation energy of 22.6 kcal/mol.

5.2.3 Compound 3a: (*E*)-12c-(4-(4-(methoxyphenyldiazenyl)-2-ethylphenyl) phenyl)ethynyl-4,8,12-tri-*n*-octyl-4,8,12-triazatriangulene

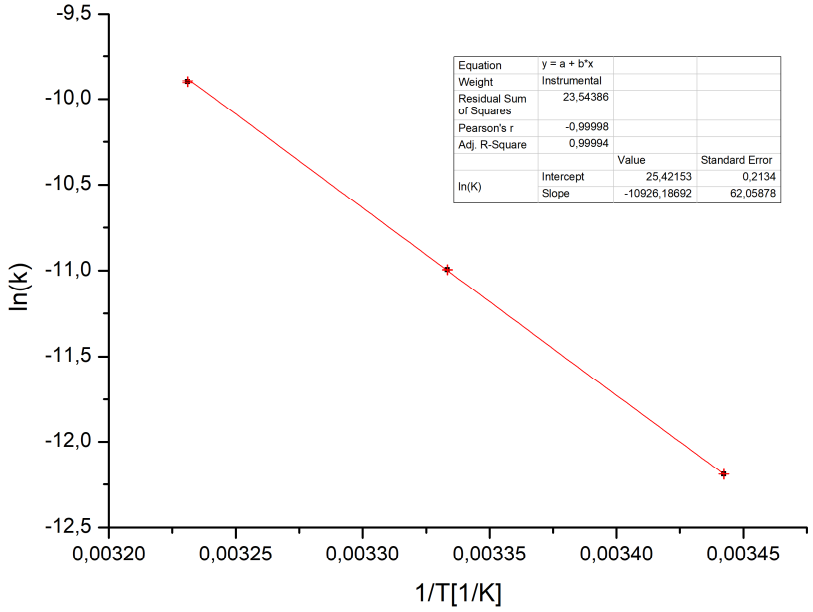

Figure S87. Arrhenius plot of the *cis*-to-*trans* isomerisation of compound **3a** which shows an activation energy of 21.7 kcal/mol.

5.2.4 Compound 4a: (*E*)-12c-(3-methyl-4-(4-(methoxyphenyldiazenyl)-2-methylphenyl) phenyl)ethynyl-4,8,12-tri-*n*-octyl-4,8,12-triazatriangulene

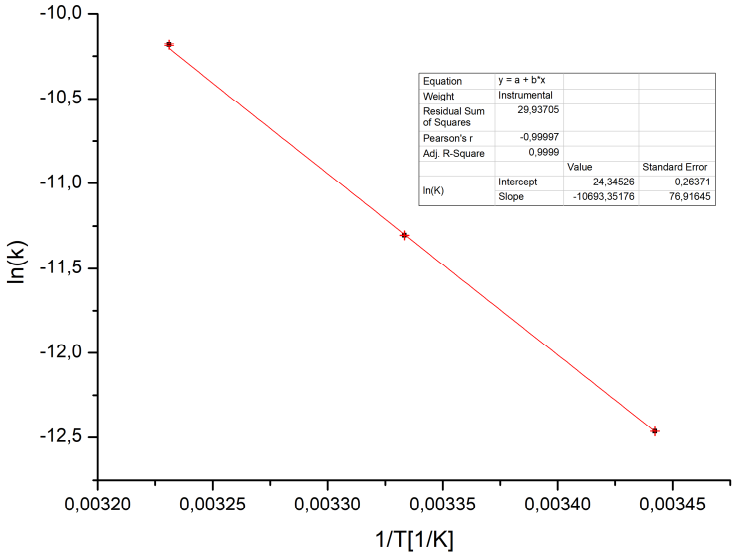

Figure S88. Arrhenius plot of the *cis*-to-*trans* isomerisation of compound **4a** which shows an activation energy of 21.2 kcal/mol.

5.2.5 Compound 5a: (*E*)-12c-[(4-{4-[(4-methoxyphenyl)diazenyl]phenyl}-2,6,7-trioxabi cyclo[2.2.2] octane-1-yl)ethynyl]-4,8,12-tri-*n*-octyl-4,8,12-triazatriangulene

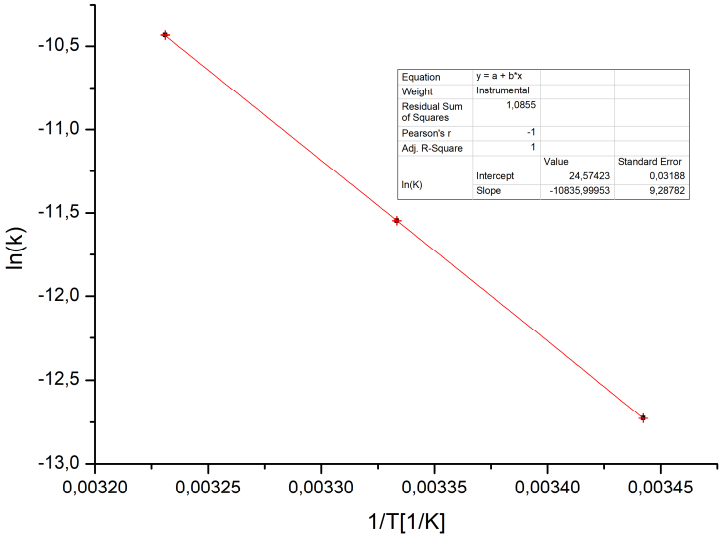

Figure S89. Arrhenius plot of the *cis*-to-*trans* isomerisation of compound **5a** which shows an activation energy of 21.5 kcal/mol.

5.2.6 Compound 6: (*E*)-1-phenyl-2-(4-(((tris(2,4,6-trimethylphenyl)-phosphine)-(9Cl)-gold)ethynyl)phenyl)diazene

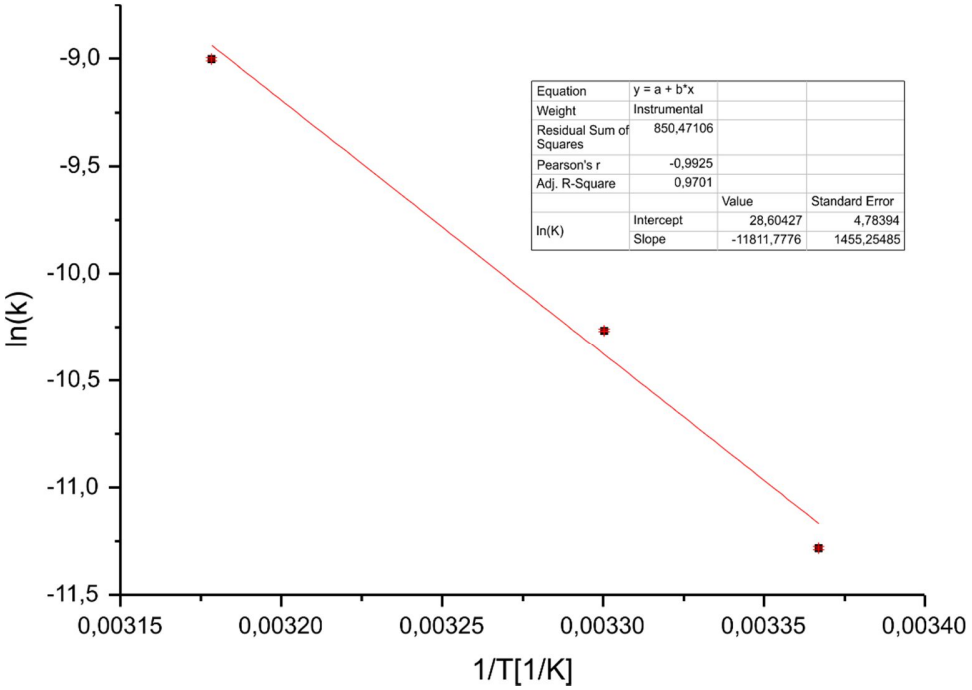

Figure S90. Arrhenius plot of the *cis*-to-*trans* isomerisation of compound **6** which shows an activation energy of 23.5 kcal/mol.

6. Kinetic studies on Au(111) by IRRAS

6.1 Experimental Details

IRRAS. The surface adsorbed molecules were investigated using a Bruker VERTEX 70 FT-IR spectrometer equipped with a Polarization Modulation Accessory (PMA) 50 unit (Bruker Optik GmbH, Ettlingen, Germany). This instrument allows recording IRRAS and PM-IRRAS data with a spectral range from 4000 down to 800 cm^{-1}. IRRAS data were collected with a liquid nitrogen cooled MCT detector in a horizontal reflection unit for grazing incidence (Bruker A518). The sample chamber was purged with dry nitrogen before and during measurements. A deuterated hexadecane-thiol SAM on Au(111) was used as a reference for the background spectrum for conventional IRRA spectra. Each spectrum contains 2048 averaged spectra. A p-polarized beam at an incident angle of 80° to the surface normal was used for the measurements. All spectra were recorded with 4 cm^{-1} resolution. PM-IRRAS data were collected with the PMA 50 accessory using a liquid nitrogen-cooled MCT detector. The PEM maximum efficiency was set for the half-wave at 1750 cm^{-1} for analysis of the C-O stretching mode. All spectra were recorded with 4 cm^{-1} resolution. Processing of IRRAS and PM-IRRAS data was carried out using the OPUS software Version 6.5 (Bruker, Germany). Baseline correction of the resulting IRRAS data was performed by the rubber band method in an interactive mode (estimated intensity error ΔI=0.00005 a. u). PM-IRRAS data were processed by the implicit removal of the Bessel function through manual baseline correction. For the trans-to-cis isomerization of different compounds adsorbed on Au(111) the prepared samples were irradiated within the spectrometer using a LED (Nichia NC4U133(T), peak wavelength: 365 (±9) nm, 1 LEDs, power dissipation: 12 W, luminous flux: 10 lm, distance ~5 cm). For temperature dependent IRRAS measurements the sample holder was modified so that the substrate is attached to an aluminium block which can be temperature-controlled by two peltier elements (ΔT=1 K). The temperature was controlled by a temperature sensor on the aluminum block directly beside the substrate. In this way it was possible to temperature-control the substrate before and during the IRRAS measurements in a certain range (270.0 K -295.0 K, ±1 K).

All Azo-TATA compounds were synthesized with octyl (a) and propyl (b) sidechains, but only the compounds with octyl sidechains were exhaustively investigated adsorbed on a gold surface because the obtained adlayers had a higher reproducibility than for the propyl compound (b). Moreover all octyl compounds (a) showed the same superstructure with higher intermolecular distances than for the propyl compounds (b). Thereby we made sure that the azobenzene has enough space for the *cis*/*trans* isomerization.

Gold Substrates. Glass substrates with a 50 Å titanium adlayer and a 200 nm evaporated gold film from EMF corporation (Ithaca, NY) were used for IRRAS measurements. STM, XPS and NEXAFS measurements were made with sputtered Au(111) single crystals.

Preparation of Monolayers. Monolayers of the different compounds were prepared by immersing Au(111) substrates in 0.5 mM solutions of the respective compound in toluene (Uvasol, Merck) at 80 °C (**1**, **4**, **5**) or 60 °C (**2**, **3**). After 1 h (**1**, **4**, **5**) or 2 h (**2**, **3**) of immersion the sample was removed from the solution, rinsed with toluene and dried in a stream of nitrogen gas.

Bulk IR. IR spectra were recorded on a Bruker Alpha-P ATR-IR Spectrometer.

6.2.1 Compound 1a

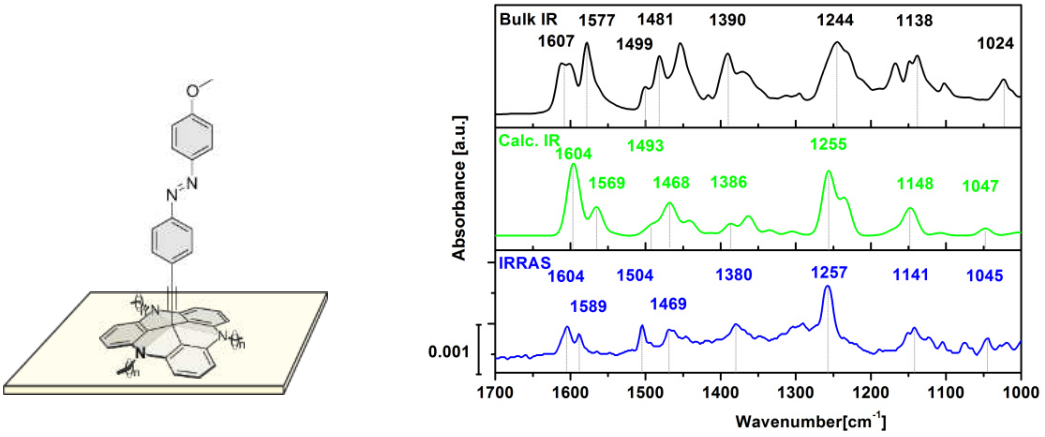

Figure S91. Left: Compound **1a** adsorbed on Au(111); Right: IR fingerprint region. The spectrum in the top panel shows the bulk IR, the spectrum in the middle the calculated IR and the blue spectrum at the bottom the IRRAS data of the surface-adsorbed monolayer.

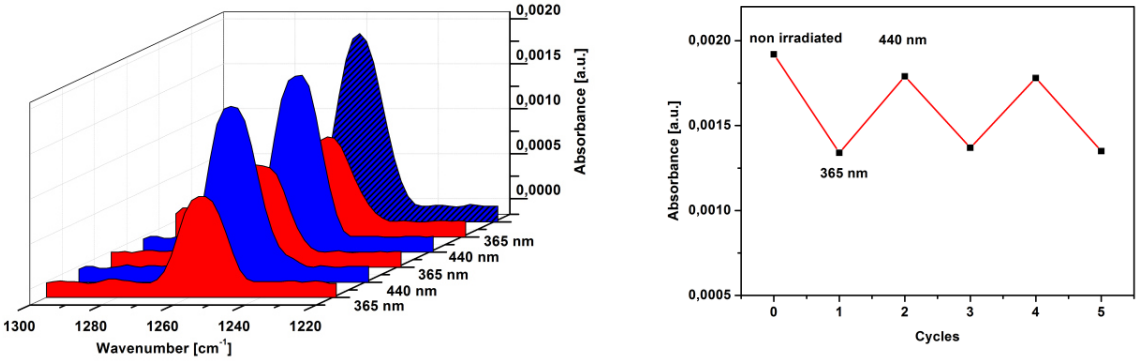

Figure S92. Left: $C_{(phenyl)}$–$O_{(Me)}$ stretching band data of compound **1a** on Au(111) obtained with PM-IRRAS under continuous irradiation with 365 nm (red) or 440 nm (blue). Right: Intensities of the $C_{(phenyl)}$–$O_{(Me)}$ stretching band after irradiation with light of 365 nm or 440 nm.

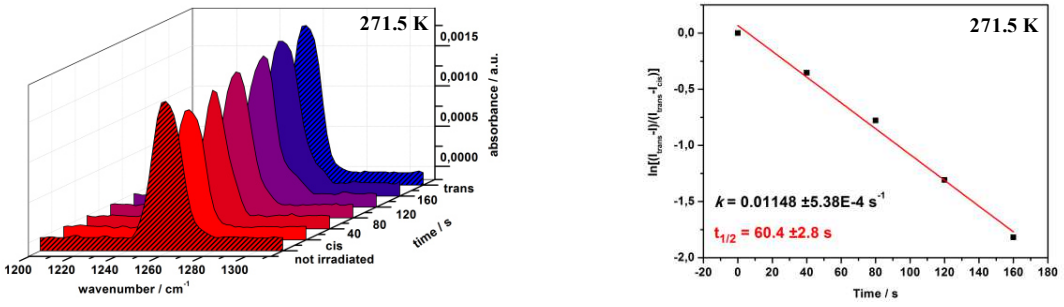

Figure S93. Left: $C_{(phenyl)}$–$O_{(Me)}$ stretching band data of compound **1a** as a monolayer on Au(111) obtained with PM-IRRAS under continuous irradiation with 365 nm (red) and after particular intervals with the LED switched off at 271.5 K. The spectrum of *trans* is shown for comparison (blue, shaded). Right: Plot of $\ln[(I_\infty - I)/(I_\infty - I_0)]$ vs. time, showing a monoexponential decay of *cis* to *trans*.

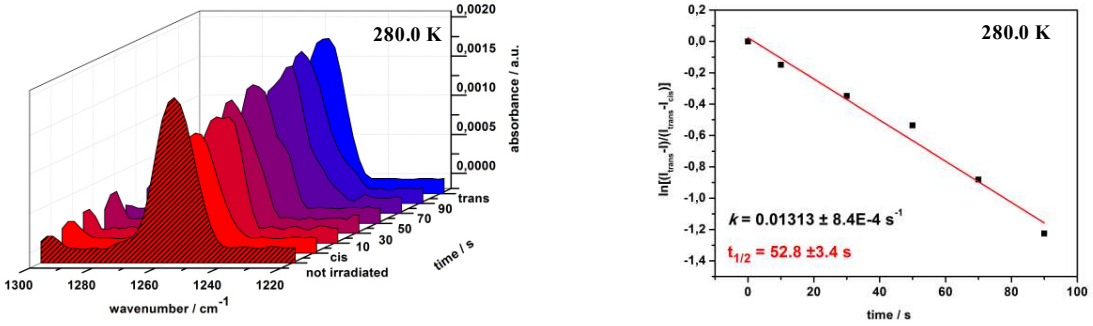

Figure S94. Left: $C_{(phenyl)}$–$O_{(Me)}$ stretching band data of compound **1a** as a monolayer on Au(111) obtained with PM-IRRAS under continuous irradiation with 365 nm (red) and after particular intervals with the LED switched off at 280.0 K. The spectrum of *trans* is shown for comparison (blue, shaded). Right: Plot of $\ln[(I_\infty - I)/(I_\infty - I_0)]$ vs. time, showing a monoexponential decay of *cis* to *trans*.

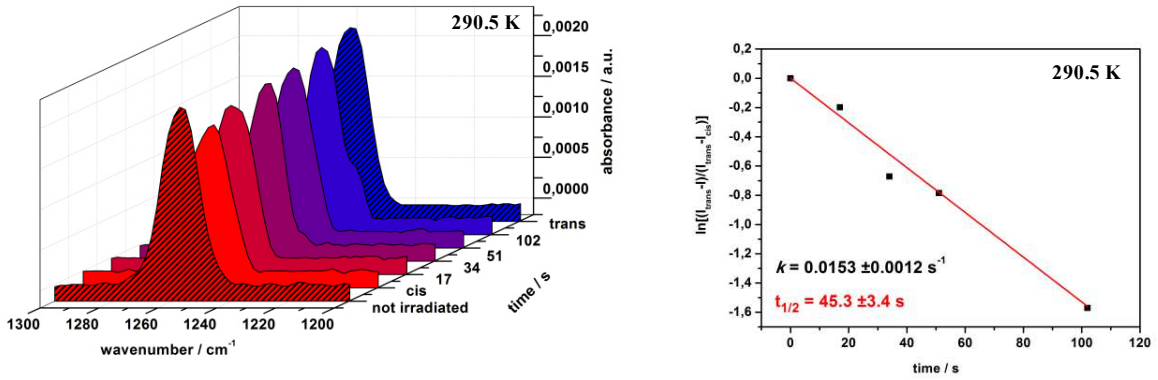

Figure S95. Left: $C_{(phenyl)}$–$O_{(Me)}$ stretching band data of compound **1a** as a monolayer on Au(111) obtained with PM-IRRAS under continuous irradiation with 365 nm (red) and after particular intervals with the LED switched off at 290.5 K. The spectrum of *trans* is shown for comparison (blue, shaded). Right: Plot of $\ln[(I_\infty - I)/(I_\infty - I_0)]$ vs. time, showing a monoexponential decay of *cis* to *trans*.

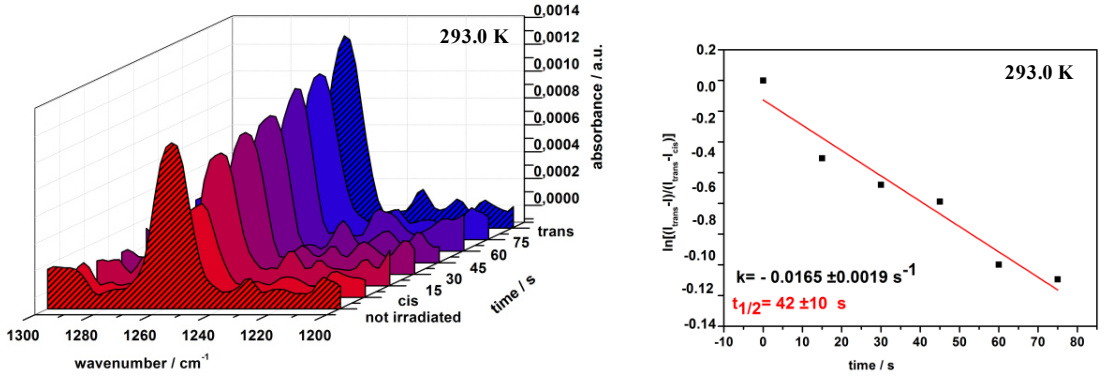

Figure S96. Left: $C_{(phenyl)}$–$O_{(Me)}$ stretching band data of compound **1a** as a monolayer on Au(111) obtained with PM-IRRAS under continuous irradiation with 365 nm (red) and after particular intervals with the LED switched off at 293.0 K. The spectrum of *trans* is shown for comparison (blue, shaded). Right: Plot of $\ln[(I_\infty - I)/(I_\infty - I_0)]$ vs. time, showing a monoexponential decay of *cis* to *trans*.

6.2.2 Compound 2a

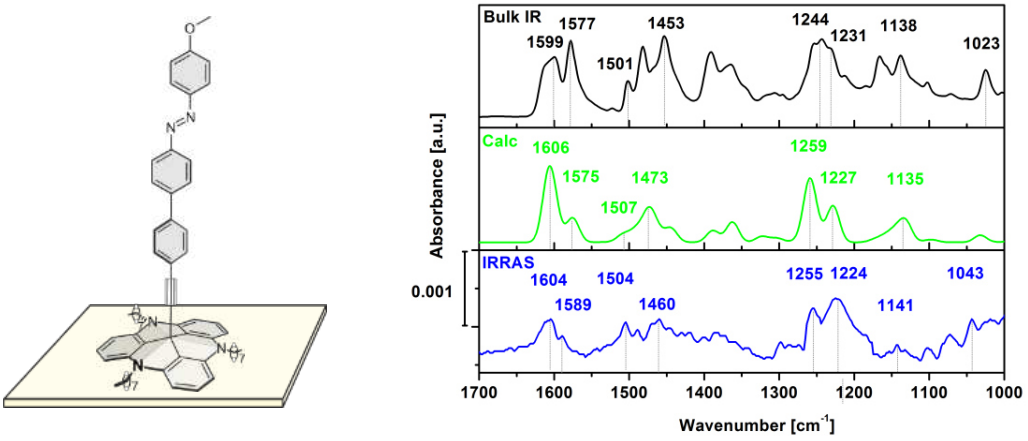

Figure S97. Left: Compound **2a** adsorbed on Au(111); Right: IR fingerprint region. The spectrum in the top panel shows the bulk IR, the spectrum in the middle the calculated IR and the blue spectrum at the bottom the IRRAS data of the surface-adsorbed monolayer.

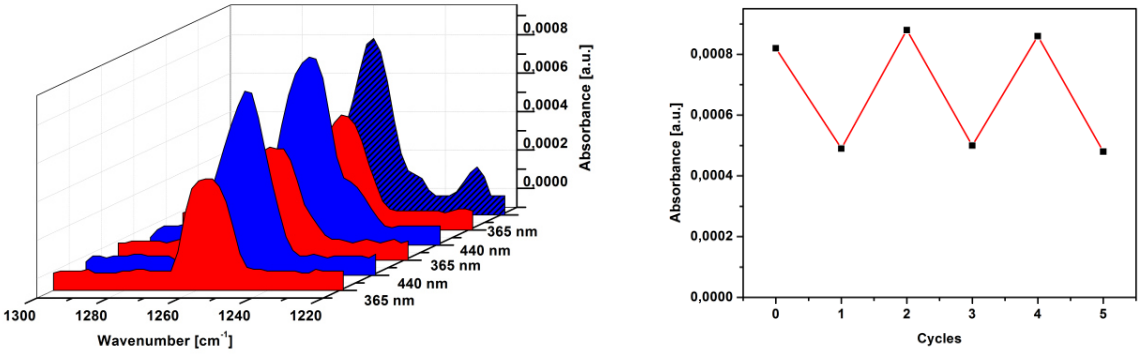

Figure S98. Left: $C_{(phenyl)}$–$O_{(Me)}$ stretching band data of compound **2a** on Au(111) obtained with PM-IRRAS under continuous irradiation with 365 nm (red) or 440 nm (blue). Right: Intensities of the $C_{(phenyl)}$–$O_{(Me)}$ stretching band after irradiation with light of 365 nm or 440 nm.

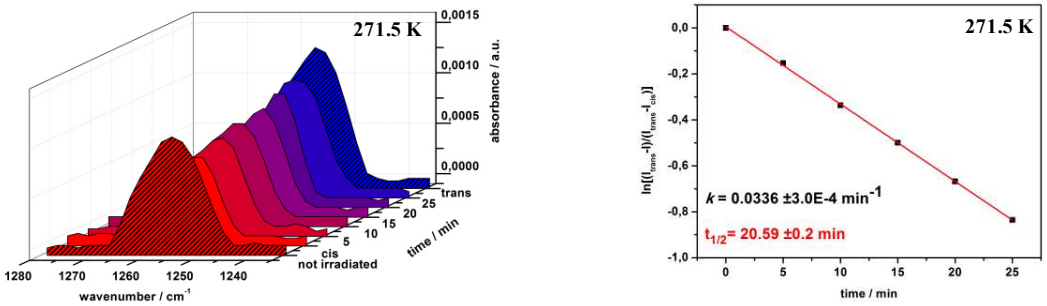

Figure S99. Left: $C_{(phenyl)}$–$O_{(Me)}$ stretching band data of compound **2a** as a monolayer on Au(111) obtained with PM-IRRAS under continuous irradiation with 365 nm (red) and after particular intervals with the LED switched off at 271.5 K. The spectrum of *trans* is shown for comparison (blue, shaded). Right: Plot of $\ln[(I_\infty - I)/(I_\infty - I_0)]$ vs. time, showing a monoexponential decay of *cis* to *trans*.

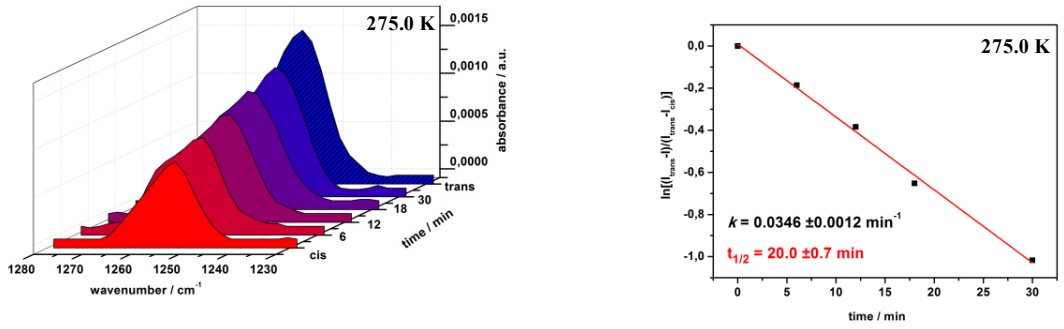

Figure S100. Left: $C_{(phenyl)}$–$O_{(Me)}$ stretching band data of compound **2a** as a monolayer on Au(111) obtained with PM-IRRAS under continuous irradiation with 365 nm (red) and after particular intervals with the LED switched off at 275.0 K. The spectrum of *trans* is shown for comparison (blue, shaded). Right: Plot of $\ln[(I_\infty - I)/(I_\infty - I_0)]$ vs. time, showing a monoexponential decay of *cis* to *trans*.

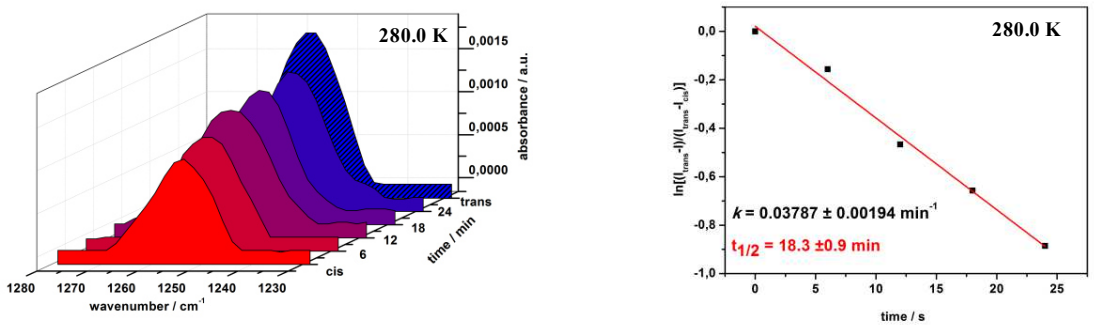

Figure S101. Left: $C_{(phenyl)}$–$O_{(Me)}$ stretching band data of compound **2a** as a monolayer on Au(111) obtained with PM-IRRAS under continuous irradiation with 365 nm (red) and after particular intervals with the LED switched off at 280.0 K. The spectrum of *trans* is shown for comparison (blue, shaded). Right: Plot of $\ln[(I_\infty - I)/(I_\infty - I_0)]$ vs. time, showing a monoexponential decay of *cis* to *trans*.

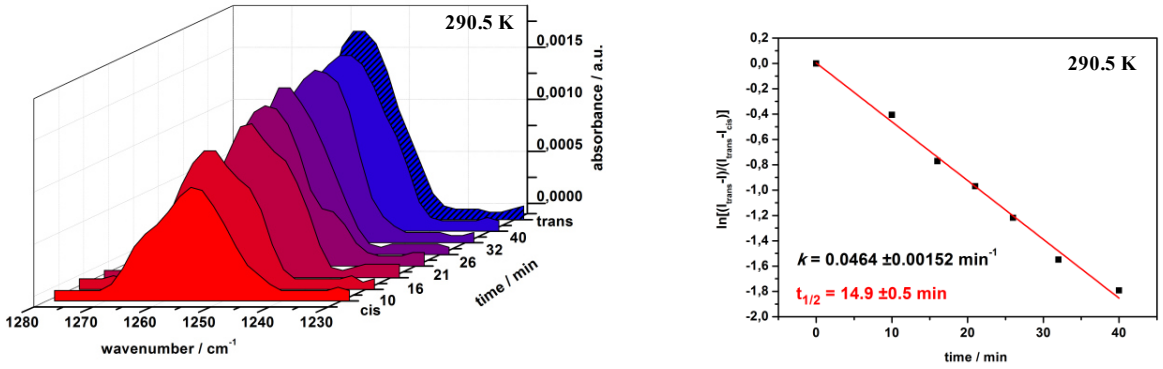

Figure S102. Left: $C_{(phenyl)}$–$O_{(Me)}$ stretching band data of compound **2a** as a monolayer on Au(111) obtained with PM-IRRAS under continuous irradiation with 365 nm (red) and after particular intervals with the LED switched off at 290.5 K. The spectrum of *trans* is shown for comparison (blue, shaded). Right: Plot of $\ln[(I_\infty - I)/(I_\infty - I_0)]$ vs. time, showing a monoexponential decay of *cis* to *trans*.

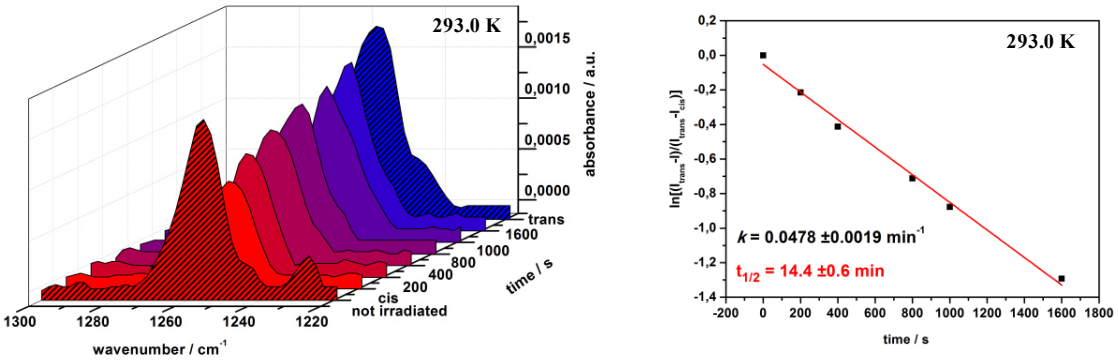

Figure S103. Left: $C_{(phenyl)}$–$O_{(Me)}$ stretching band data of compound **2a** as a monolayer on Au(111) obtained with PM-IRRAS under continuous irradiation with 365 nm (red) and after particular intervals with the LED switched off at 293.0 K. The spectrum of *trans* is shown for comparison (blue, shaded). Right: Plot of $\ln[(I_\infty - I)/(I_\infty - I_0)]$ vs. time, showing a monoexponential decay of *cis* to *trans*.

6.2.3 Compound 3a

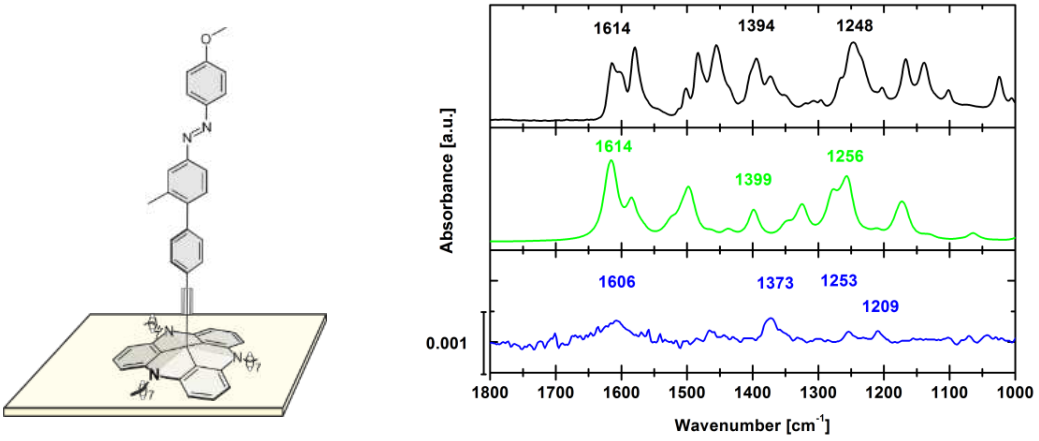

Figure 104. Left: Compound **3a** adsorbed on Au(111); Right: IR fingerprint region. The spectrum in the top panel shows the bulk IR, the spectrum in the middle the calculated IR and the blue spectrum at the bottom the IRRAS data of the surface-adsorbed monolayer.

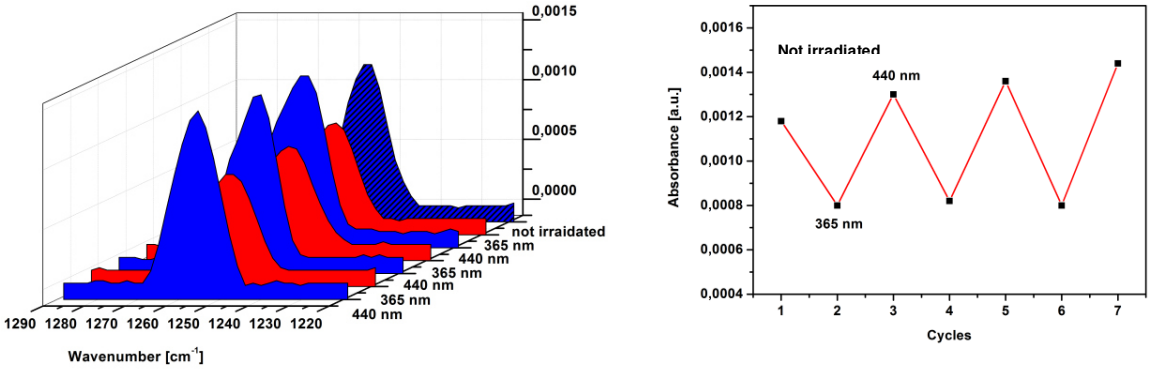

Figure S105. Left: $C_{(phenyl)}$–$O_{(Me)}$ stretching band data of compound **3a** on Au(111) obtained with PM-IRRAS under continuous irradiation with 365 nm (red) or 440 nm (blue). Right: Intensities of the $C_{(phenyl)}$–$O_{(Me)}$ stretching band after irradiation with light of 365 nm or 440 nm.

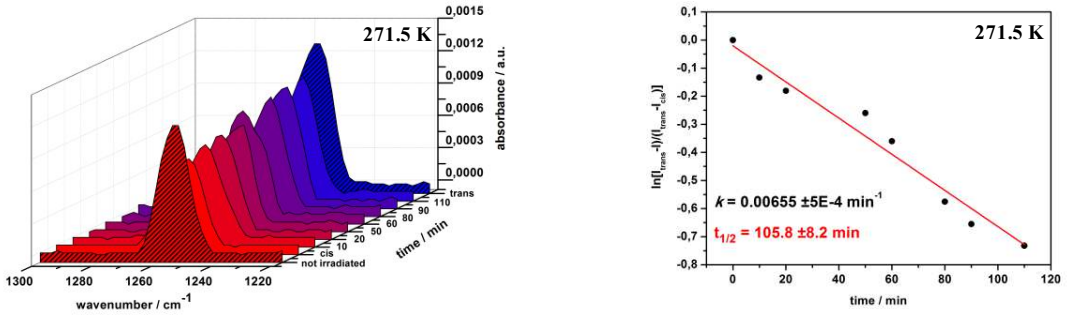

Figure S106. Left: $C_{(phenyl)}$–$O_{(Me)}$ stretching band data of compound **3a** as a monolayer on Au(111) obtained with PM-IRRAS under continuous irradiation with 365 nm (red) and after particular intervals with the LED switched off at 271.5 K. The spectrum of *trans* is shown for comparison (blue, shaded). Right: Plot of $\ln[(I_\infty - I)/(I_\infty - I_0)]$ vs. time, showing a monoexponential decay of *cis* to *trans*.

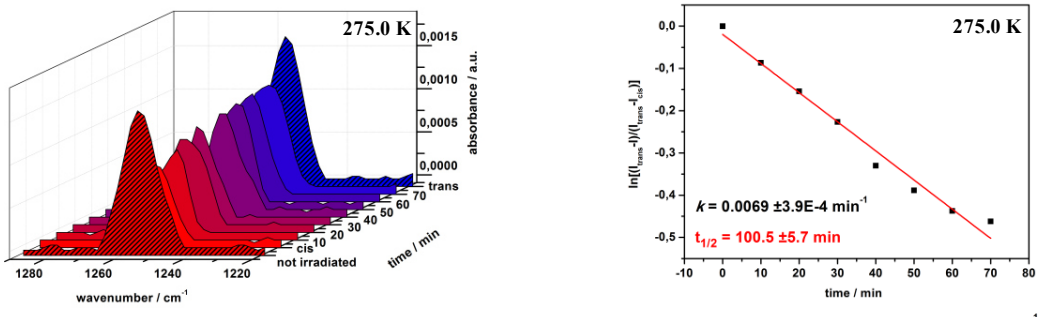

Figure S107. Left: $C_{(phenyl)}$–$O_{(Me)}$ stretching band data of compound **3a** as a monolayer on Au(111) obtained with PM-IRRAS under continuous irradiation with 365 nm (red) and after particular intervals with the LED switched off at 275.0 K. The spectrum of *trans* is shown for comparison (blue, shaded). Right: Plot of $\ln[(I_\infty - I)/(I_\infty - I_0)]$ vs. time, showing a monoexponential decay of *cis* to *trans*.

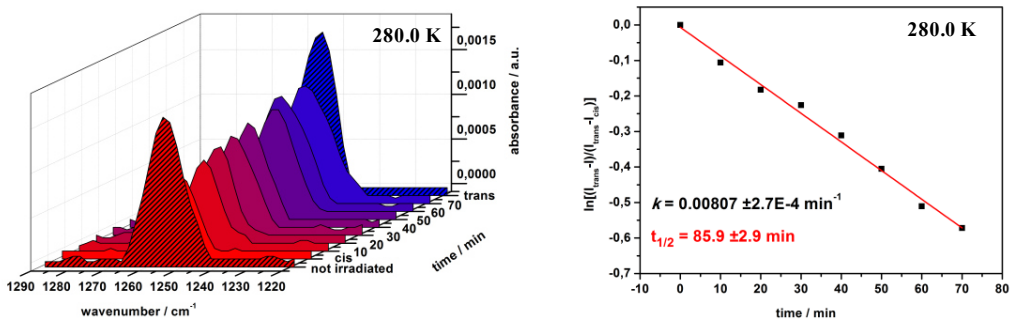

Figure S108. Left: $C_{(phenyl)}$–$O_{(Me)}$ stretching band data of compound **3a** as a monolayer on Au(111) obtained with PM-IRRAS under continuous irradiation with 365 nm (red) and after particular intervals with the LED switched off at 280.0 K. The spectrum of *trans* is shown for comparison (blue, shaded). Right: Plot of $\ln[(I_\infty - I)/(I_\infty - I_0)]$ vs. time, showing a monoexponential decay of *cis* to *trans*.

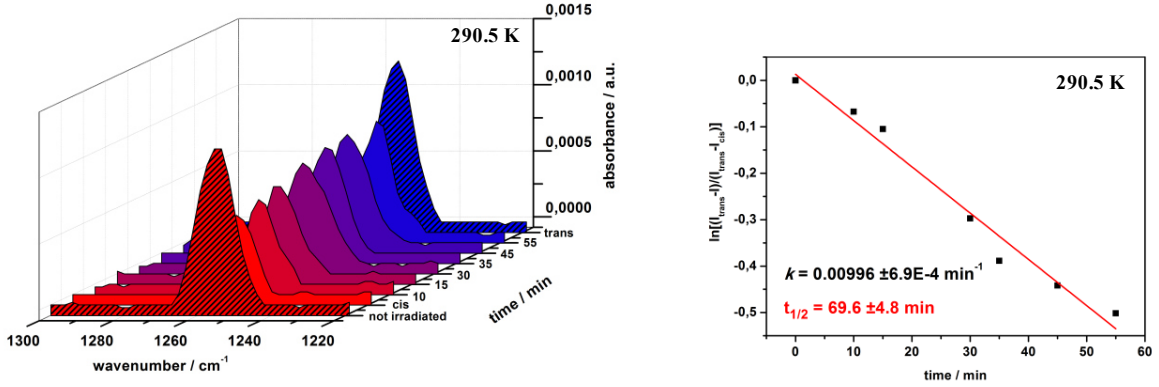

Figure S109. Left: $C_{(phenyl)}$–$O_{(Me)}$ stretching band data of compound **3a** as a monolayer on Au(111) obtained with PM-IRRAS under continuous irradiation with 365 nm (red) and after particular intervals with the LED switched off at 290.5 K. The spectrum of *trans* is shown for comparison (blue, shaded). Right: Plot of $\ln[(I_\infty - I)/(I_\infty - I_0)]$ vs. time, showing a monoexponential decay of *cis* to *trans*.

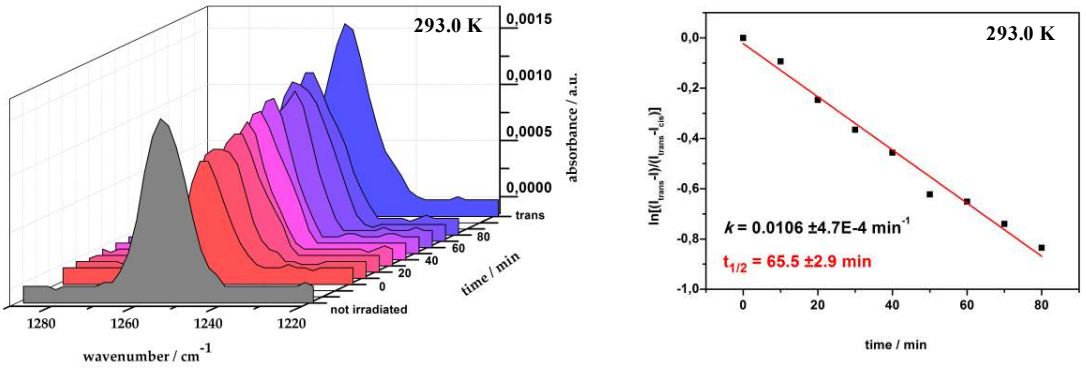

Figure S110. Left: $C_{(phenyl)}$–$O_{(Me)}$ stretching band data of compound **3a** as a monolayer on Au(111) obtained with PM-IRRAS under continuous irradiation with 365 nm (red) and after particular intervals with the LED switched off at 293.0 K. The spectrum of *trans* is shown for comparison (blue, shaded). Right: Plot of $\ln[(I_\infty - I)/(I_\infty - I_0)]$ vs. time, showing a monoexponential decay of *cis* to *trans*.

6.2.4 Compound 4a

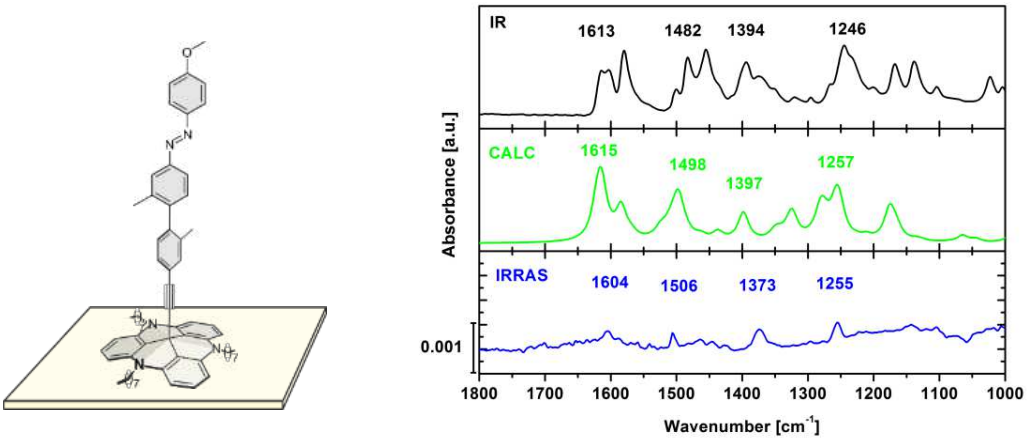

Figure S111. Left: Compound **4a** adsorbed on Au(111); Right: IR fingerprint region. The spectrum in the top panel shows the bulk IR, the spectrum in the middle the calculated IR and the blue spectrum at the bottom the IRRAS data of the surface-adsorbed monolayer.

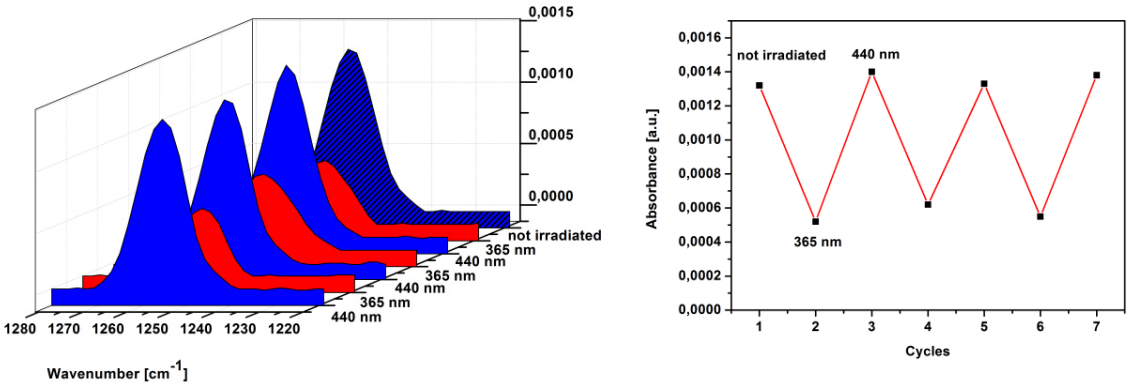

Figure S112. Left: $C_{(phenyl)}$–$O_{(Me)}$ stretching band data of compound **4a** on Au(111) obtained with PM-IRRAS under continuous irradiation with 365 nm (red) or 440 nm (blue). Right: Intensities of the $C_{(phenyl)}$–$O_{(Me)}$ stretching band after irradiation with light of 365 nm or 440 nm.

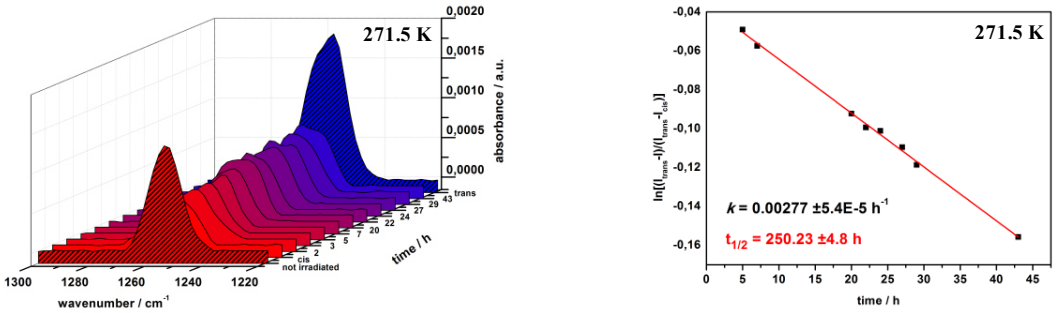

Figure S113. Left: $C_{(phenyl)}$–$O_{(Me)}$ stretching band data of compound **4a** monolayer on Au(111) obtained with PM-IRRAS under continuous irradiation with 365 nm (red) and after particular intervals with the LED switched off at 271.5 K. The spectrum of *trans* is shown for comparison (blue, shaded). Right: Plot of $\ln[(I_\infty - I)/(I_\infty - I_0)]$ vs. time, showing a monoexponential decay of *cis* to *trans*.

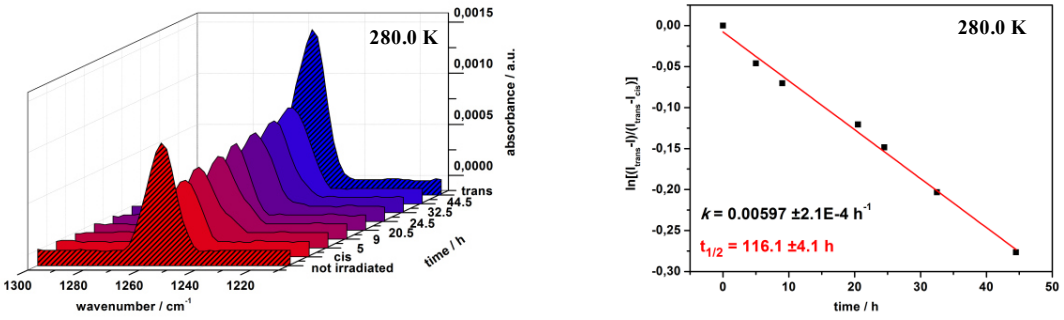

Figure S114. Left: $C_{(phenyl)}$–$O_{(Me)}$ stretching band data of compound **4a** as a monolayer on Au(111) obtained with PM-IRRAS under continuous irradiation with 365 nm (red) and after particular intervals with the LED switched off at 280.0 K. The spectrum of *trans* is shown for comparison (blue, shaded). Right: Plot of $\ln[(I_\infty - I)/(I_\infty - I_0)]$ vs. time, showing a monoexponential decay of *cis* to *trans*.

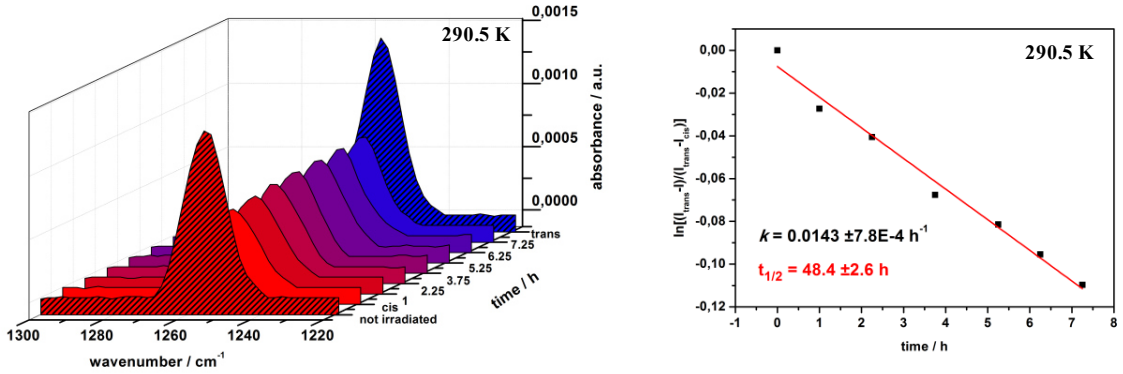

Figure S115. Left: $C_{(phenyl)}$–$O_{(Me)}$ stretching band data of compound **4a** as a monolayer on Au(111) obtained with PM-IRRAS under continuous irradiation with 365 nm (red) and after particular intervals with the LED switched off at 290.5 K. The spectrum of *trans* is shown for comparison (blue, shaded). Right: Plot of $\ln[(I_\infty - I)/(I_\infty - I_0)]$ vs. time, showing a monoexponential decay of *cis* to *trans*.

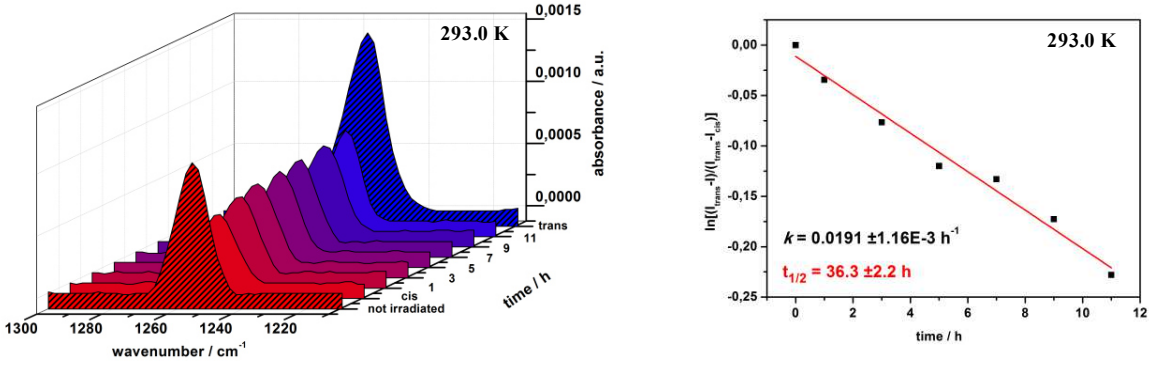

Figure S116. Left: $C_{(phenyl)}$–$O_{(Me)}$ stretching band data of compound **4a** as a monolayer on Au(111) obtained with PM-IRRAS under continuous irradiation with 365 nm (red) and after particular intervals with the LED switched off at 293.0 K. The spectrum of *trans* is shown for comparison (blue, shaded). Right: Plot of $\ln[(I_\infty - I)/(I_\infty - I_0)]$ vs. time, showing a monoexponential decay of *cis* to *trans*.

6.2.5 Compound 5a

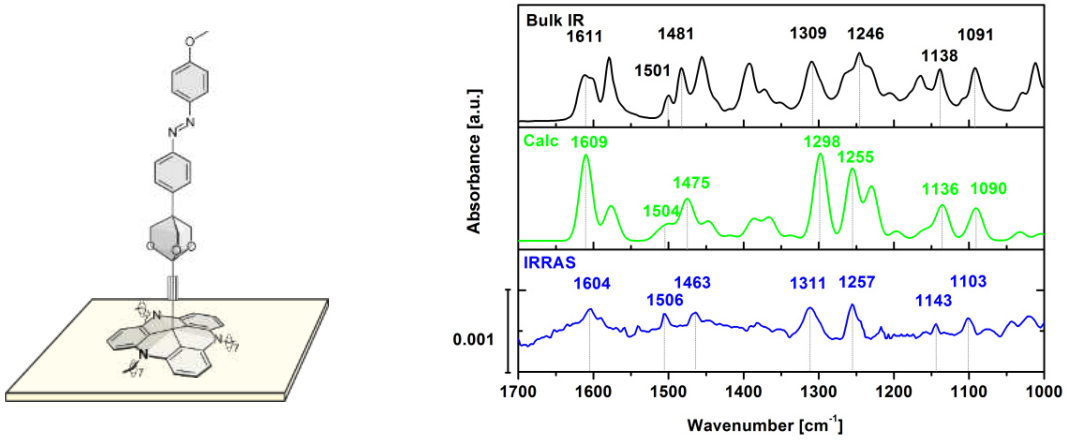

Figure S117. Left: Compound **5a** adsorbed on Au(111); Right: IR fingerprint region. The spectrum in the top panel shows the bulk IR, the spectrum in the middle the calculated IR and the blue spectrum at the bottom the IRRAS data of the surface-adsorbed monolayer.

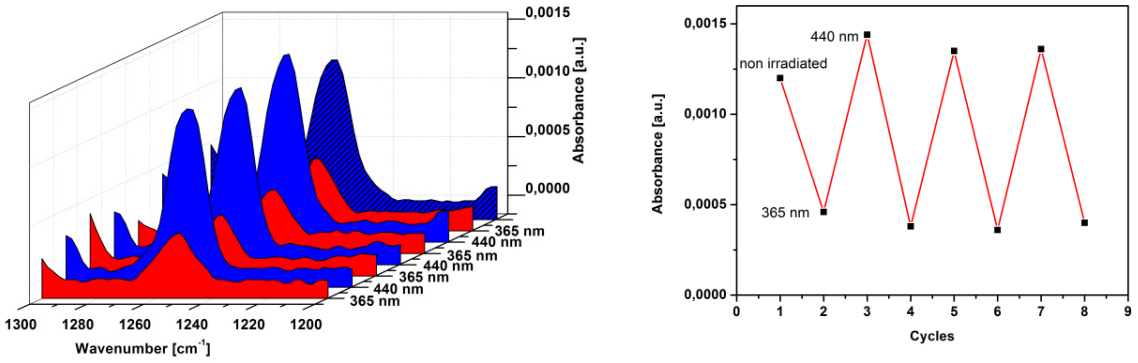

Figure S118. Left: $C_{(phenyl)}$–$O_{(Me)}$ stretching band data of compound **5a** on Au(111) obtained with PM-IRRAS under continuous irradiation with 365 nm (red) or 440 nm (blue). Right: Intensities of the $C_{(phenyl)}$–$O_{(Me)}$ stretching band after irradiation with light of 365 nm or 440 nm.

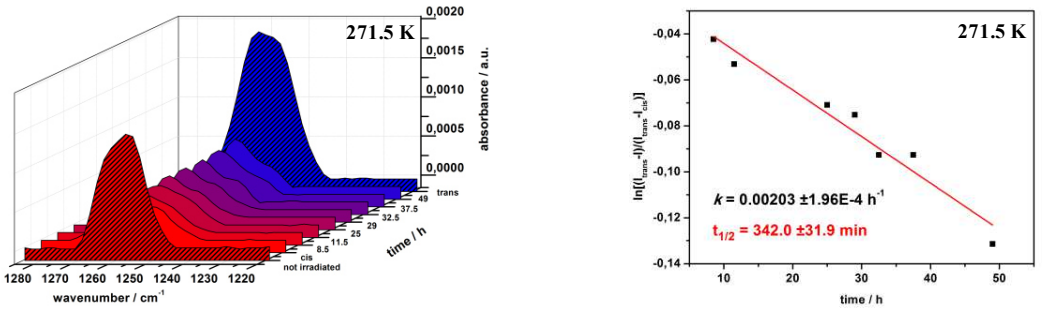

Figure S119. Left: $C_{(phenyl)}$–$O_{(Me)}$ stretching band data of compound **5a** as a monolayer on Au(111) obtained with PM-IRRAS under continuous irradiation with 365 nm (red) and after particular intervals with the LED switched off at 271.5 K. The spectrum of *trans* is shown for comparison (blue, shaded). Right: Plot of $\ln[(I_\infty - I)/(I_\infty - I_0)]$ vs. time, showing a monoexponential decay of *cis* to *trans*.

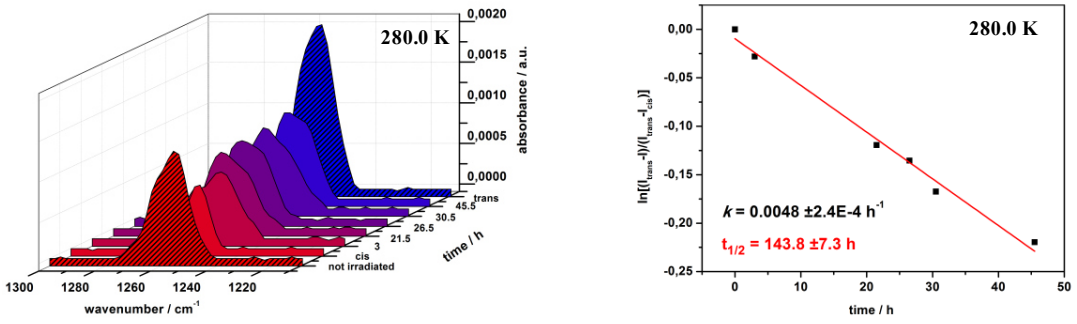

Figure S120. Left: $C_{(phenyl)}$–$O_{(Me)}$ stretching band data of compound **5a** as a monolayer on Au(111) obtained with PM-IRRAS under continuous irradiation with 365 nm (red) and after particular intervals with the LED switched off at 280.0 K. The spectrum of *trans* is shown for comparison (blue, shaded). Right: Plot of $\ln[(I_\infty - I)/(I_\infty - I_0)]$ vs. time, showing a monoexponential decay of *cis* to *trans*.

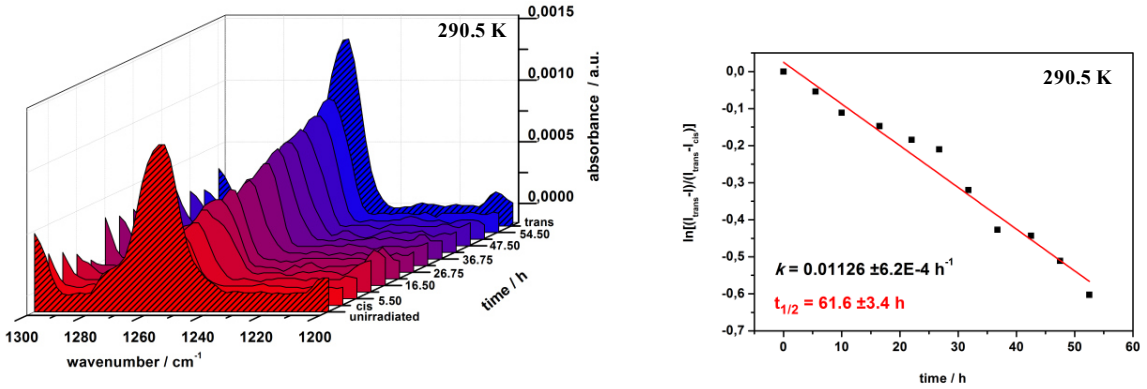

Figure S121. Left: $C_{(phenyl)}$–$O_{(Me)}$ stretching band data of compound **5a** as a monolayer on Au(111) obtained with PM-IRRAS under continuous irradiation with 365 nm (red) and after particular intervals with the LED switched off at 290.5 K. The spectrum of *trans* is shown for comparison (blue, shaded). Right: Plot of $\ln[(I_\infty - I)/(I_\infty - I_0)]$ vs. time, showing a monoexponential decay of *cis* to *trans*.

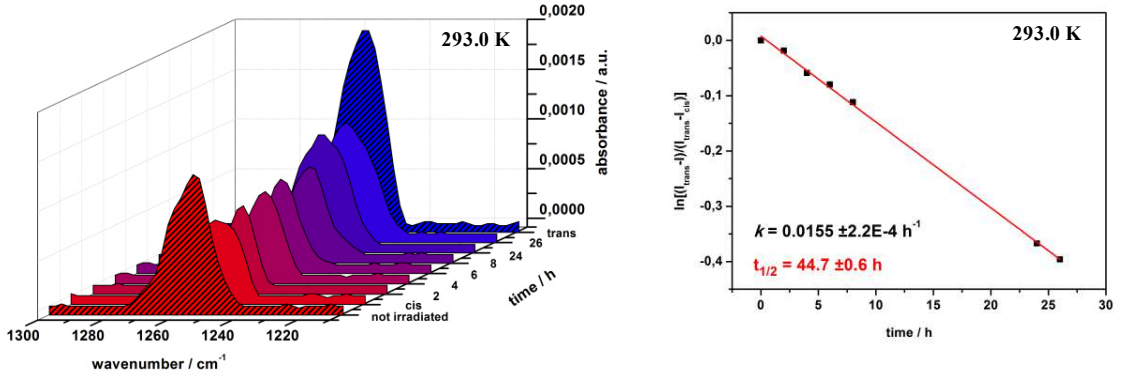

Figure S122. Left: $C_{(phenyl)}$–$O_{(Me)}$ stretching band data of compound **5a** as a monolayer on Au(111) obtained with PM-IRRAS under continuous irradiation with 365 nm (red) and after particular intervals with the LED switched off at 293.0 K. The spectrum of *trans* is shown for comparison (blue, shaded). Right: Plot of $\ln[(I_\infty - I)/(I_\infty - I_0)]$ vs. time, showing a monoexponential decay of *cis* to *trans*.

6.3 IR region of the N=N stretch

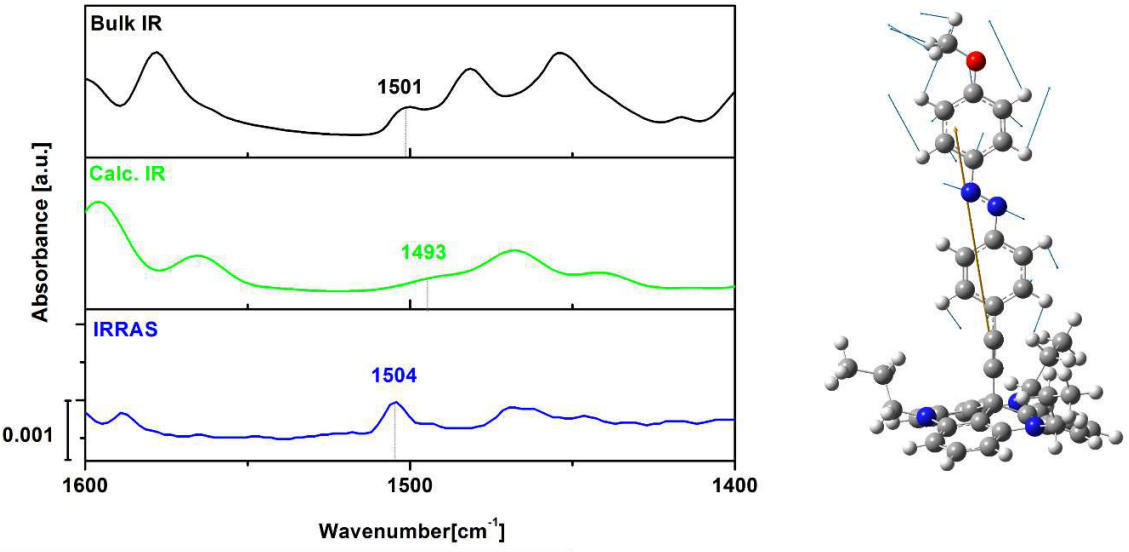

Figure S 123. IR region of the N=N stretch. Region of the N=N-stretch of the vibrational spectra (Bulk IR, Calc. IR and IRRAS)(left) and the displacement vectors of this vibrational mode obtained from calculations. The spectra clearly show that the N=N-stretching vibration of compound **1** does not show any significant shift when it is adsorbed on the gold surface compared to the bulk IR. This fact proves that the azo moiety is not permanently charged. This N=N vibration is observable in the IR spectrum as the vibration is mixed with vibrations of the surrounding phenyl groups.

7. Calculations of spin densities and vibrational spectra

All geometry optimizations were carried out with Turbomole7.2 using.[46] Since the influence of the TATA side chains can largely be neglected for computational treatment of the systems, all calculations have been simplified by substitution of the octyl with propyl groups to save computational costs.

For IR simulation Gaussian09 Rev. D.01[47] with density functional approximation (DFA) B3LYP[48] and a large 6-31++G** basis in combination with a geometry optimization with DFA PBE[49-50] and SVP basis as well as Grimmes D3 dispersion correction[50] was used to simulate vibrations in IR spectra. Preliminary investigations showed that this level of theory could adequately describe experimentally obtained spectra.[12]

Spin densities plots are based on single points from Gaussian16 Rev. A.03[47] using DFA M08HX[51] with def2-TZVP basis. The underlying geometries were obtained with M062X[52]-D3/def2-TZVP, cause these both DFA's performed well in Grimme's latest study for basic properties of small systems.[53]

7.1 Geometry optimizations of compound 1-5

Table S1. Cartesian coordinates of the optimized structure for compound **1a** (propyl side chains) *trans*.

XYZ file

90

Energy=−1893.87779503, Method PBE-D3/SVP, Charge 0, Singlet

C	-3.9471990000	-1.8812930000	-1.2993690000
N	-3.7049260000	-1.1416890000	-2.4704480000
C	-3.7655630000	0.2631040000	-2.4167440000
C	-3.4946940000	0.9064550000	-1.1969780000
C	-3.0431650000	0.0871950000	0.0070750000
C	-3.6913760000	-1.2910670000	-0.0505280000
C	-3.9378840000	-1.9962710000	1.1399160000
N	-3.6679060000	-1.3669360000	2.3693790000
C	-3.7194190000	0.0360740000	2.4446180000
C	-3.4748240000	0.7940570000	1.2873600000

C	-4.1037870000	1.0374770000	-3.5411780000
C	-4.1314330000	2.4241560000	-3.4370520000
C	-3.8581050000	3.0704210000	-2.2363770000
C	-3.5446010000	2.3067850000	-1.0986620000
N	-3.2811290000	2.9171940000	0.1405190000
C	-3.5318860000	2.1978360000	1.3239420000
C	-4.4425230000	-3.1957330000	-1.3561710000
C	-4.6898560000	-3.8825050000	-0.1725670000
C	-4.4597590000	-3.3005610000	1.0697000000
C	-4.0130930000	0.6923250000	3.6526130000
C	-4.0735800000	2.0813820000	3.6769700000
C	-3.8519860000	2.8411090000	2.5329980000
H	-4.3746780000	0.5708300000	-4.4802320000
H	-4.3969160000	3.0153660000	-4.3096290000
H	-3.9102750000	4.1509540000	-2.1832740000
H	-4.6536580000	-3.6688620000	-2.3071380000
H	-5.0957490000	-4.8897790000	-0.2181400000
H	-4.7159850000	-3.8493160000	1.9675430000
H	-4.3238410000	2.5853510000	4.6069000000
H	-3.9604710000	3.9176880000	2.5821650000
C	-1.5643740000	-0.0530130000	-0.0091330000
C	-0.3550470000	-0.1702440000	-0.0180150000
C	1.0640330000	-0.3053360000	-0.0255080000
C	1.8955100000	0.8384220000	-0.0084060000
C	1.6685060000	-1.5779740000	-0.0479120000
C	3.2750230000	0.7168650000	-0.0117940000
C	3.8699590000	-0.5585710000	-0.0328910000
C	3.0522760000	-1.6981160000	-0.0516750000
N	5.2621160000	-0.8038120000	-0.0363060000

N	5.9823320000	0.2356890000	-0.0140590000
C	7.3716700000	-0.0014500000	-0.0162640000
C	8.1842630000	1.1374020000	0.0112430000
C	9.5742840000	1.0343040000	0.0132320000
C	10.1664180000	-0.2349820000	-0.0130300000
C	9.3556830000	-1.3876070000	-0.0414720000
C	7.9787040000	-1.2748040000	-0.0430500000
H	1.4329380000	1.8208410000	0.0076170000
H	1.0392110000	-2.4623060000	-0.0618610000
H	3.9157790000	1.5913550000	0.0021110000
H	3.5311480000	-2.6725550000	-0.0683670000
H	7.7020990000	2.1101390000	0.0315060000
H	10.1780170000	1.9340170000	0.0348870000
H	9.8436550000	-2.3573140000	-0.0616670000
H	7.3451980000	-2.1544250000	-0.0644920000
H	-4.2134910000	0.1297530000	4.5560220000
C	-3.4077390000	-2.1472790000	3.5814280000
H	-4.1966940000	-1.9828730000	4.3294750000
H	-3.4561600000	-3.2020080000	3.3130930000
C	-2.8179850000	4.3060330000	0.1795370000
H	-3.5682050000	4.9824790000	-0.2548730000
H	-2.7175210000	4.5920330000	1.2259270000
C	-3.4593930000	-1.8437190000	-3.7325650000
H	-4.3291620000	-2.4533000000	-4.0169580000
H	-3.3445120000	-1.0918500000	-4.5125690000
O	11.5073280000	-0.4642120000	-0.0135720000
C	12.3846560000	0.6523600000	0.0182180000
H	12.2507190000	1.2937130000	-0.8624330000
H	12.2402530000	1.2506710000	0.9270330000

H	13.3943870000	0.2384980000	0.0140830000
C	-1.4538640000	4.5080230000	-0.4999060000
H	-1.5047960000	4.1870560000	-1.5455740000
H	-0.7264080000	3.8507390000	-0.0070410000
C	-2.1840500000	-2.7015370000	-3.7088910000
H	-2.2489340000	-3.4463030000	-2.9084790000
H	-1.3374380000	-2.0497890000	-3.4606600000
C	-1.9429540000	-3.3999990000	-5.0508340000
H	-1.0276320000	-4.0007290000	-5.0216910000
H	-2.7717690000	-4.0716280000	-5.3078110000
H	-1.8379840000	-2.6757840000	-5.8682890000
C	-0.9899000000	5.9659730000	-0.4239920000
H	-0.0123090000	6.0927350000	-0.9013200000
H	-1.6947080000	6.6372020000	-0.9305030000
H	-0.8983960000	6.3053820000	0.6153810000
C	-2.0221080000	-1.8768960000	4.1897310000
H	-1.9209850000	-0.8147180000	4.4361330000
H	-1.2643570000	-2.0920420000	3.4263690000
C	-1.7746810000	-2.7269800000	5.4399000000
H	-0.7811240000	-2.5311320000	5.8569370000
H	-2.5114250000	-2.5109940000	6.2238730000
H	-1.8347870000	-3.7994190000	5.2158130000

Table S2. Cartesian coordinates of the optimized structure for compound **2a** (propyl side chains) *trans*.

XYZ file

100

Energy= −2124.495009975, Method PBE-D3/SVP, Charge 0, Singlet

C	5.1287040000	2.5067330000	0.1902010000
N	4.9690360000	2.5829320000	-1.2046350000
C	5.2362920000	1.4432580000	-1.9861110000
C	5.0910040000	0.1715810000	-1.4018570000
C	4.5498500000	0.0491310000	0.0181670000
C	4.9884600000	1.2624970000	0.8300570000
C	5.1481870000	1.1488790000	2.2230860000
N	4.9964940000	-0.1157530000	2.8212840000
C	5.2587830000	-1.2674290000	2.0587630000
C	5.1071390000	-1.2156880000	0.6618040000
C	5.6555670000	1.5394650000	-3.3268590000
C	5.8931170000	0.3788260000	-4.0576980000
C	5.7487450000	-0.8834230000	-3.4900360000
C	5.3514780000	-0.9938360000	-2.1445060000
N	5.2056420000	-2.2490830000	-1.5268190000
C	5.3730980000	-2.3464990000	-0.1322590000
C	5.4209620000	3.6507400000	0.9559170000
C	5.5837580000	3.5268620000	2.3325110000
C	5.4639490000	2.2972460000	2.9745170000
C	5.6677160000	-2.4681200000	2.6681900000

C	5.9332790000	-3.5793770000	1.8742520000
C	5.8048480000	-3.5345640000	0.4884160000
H	5.8253850000	2.4998030000	-3.7955760000
H	6.2200420000	0.4615870000	-5.0903710000
H	5.9588980000	-1.7624130000	-4.0849990000
H	5.5379780000	4.6202100000	0.4897690000
H	5.8314370000	4.4074240000	2.9185860000
H	5.6427290000	2.2398650000	4.0402740000
H	6.2698590000	-4.4991620000	2.3442260000
H	6.0656340000	-4.4099640000	-0.0916090000
C	3.0641290000	-0.0163310000	-0.0112730000
C	1.8496500000	-0.0650700000	-0.0249700000
C	0.4219990000	-0.1145650000	-0.0283450000
C	-0.2656290000	-1.2285160000	-0.5502000000
C	-0.3385230000	0.9500840000	0.4961350000
C	-1.6560760000	-1.2737520000	-0.5425990000
C	-2.4201140000	-0.2143170000	-0.0180300000
C	-1.7287620000	0.8979630000	0.4980860000
H	0.3031510000	-2.0527790000	-0.9684000000
H	0.1744720000	1.8118030000	0.9112850000
H	-2.1590810000	-2.1340650000	-0.9738630000
H	-2.2872870000	1.7213670000	0.9331070000
H	5.7956000000	-2.5343270000	3.7406590000
C	4.6793780000	-0.2507010000	4.2458460000
H	5.5012420000	-0.7456270000	4.7818660000
H	4.6001300000	0.7496900000	4.6673060000
C	5.0503750000	-3.4450900000	-2.3589420000
H	5.9101930000	-3.5626780000	-3.0335250000
H	5.0576510000	-4.3136690000	-1.7034480000

C	4.6530910000	3.8726940000	-1.8246280000
H	5.4277360000	4.6160590000	-1.5908270000
H	4.6755520000	3.7406220000	-2.9046480000
C	3.7337790000	-3.4665580000	-3.1530200000
H	3.6433280000	-2.5588310000	-3.7578110000
H	2.9022350000	-3.4504600000	-2.4384930000
C	3.2613570000	4.4027450000	-1.4430690000
H	3.1790320000	4.4917180000	-0.3550410000
H	2.5158660000	3.6612650000	-1.7539660000
C	2.9691690000	5.7566320000	-2.0995780000
H	1.9694230000	6.1143820000	-1.8334230000
H	3.6890600000	6.5202650000	-1.7810920000
H	3.0168930000	5.6916850000	-3.1932980000
C	3.6341950000	-4.7036790000	-4.0526360000
H	2.6836410000	-4.7194560000	-4.5953040000
H	4.4397710000	-4.7223290000	-4.7964170000
H	3.6990510000	-5.6310910000	-3.4708140000
C	3.3495930000	-0.9788140000	4.5021130000
H	3.3681190000	-1.9691850000	4.0362270000
H	2.5494840000	-0.4162650000	4.0066150000
C	3.0555320000	-1.1130010000	6.0002970000
H	2.0976310000	-1.6152340000	6.1687770000
H	3.8302920000	-1.6987930000	6.5096380000
H	3.0059730000	-0.1327210000	6.4897000000
C	-3.9012990000	-0.2702900000	-0.0051640000
C	-4.5803320000	-1.4785140000	0.2348530000
C	-4.6757330000	0.8885690000	-0.2313950000
C	-5.9716340000	-1.5271350000	0.2493600000
H	-4.0135810000	-2.3815950000	0.4393900000

C	-6.0635490000	0.8486010000	-0.2184120000
H	-4.1754960000	1.8283020000	-0.4461440000
C	-6.7281180000	-0.3679820000	0.0239540000
H	-6.4958540000	-2.4574790000	0.4452560000
H	-6.6482820000	1.7423940000	-0.4031110000
N	-8.1334070000	-0.5326710000	0.0635910000
N	-8.8029470000	0.5152910000	-0.1469990000
C	-10.2055080000	0.3593580000	-0.1070320000
C	-10.9599230000	1.5224910000	-0.3448350000
C	-10.8758770000	-0.8483870000	0.1489610000
C	-12.3466740000	1.4855710000	-0.3293180000
H	-10.4315880000	2.4502680000	-0.5411440000
C	-12.2668250000	-0.8952290000	0.1672120000
H	-10.2941530000	-1.7445170000	0.3326510000
C	-13.0103450000	0.2747890000	-0.0728640000
H	-12.9386340000	2.3762340000	-0.5114980000
H	-12.7627360000	-1.8376560000	0.3673540000
O	-14.3713370000	0.3328150000	-0.0768890000
C	-15.1133520000	-0.8568590000	0.1728210000
H	-14.8988520000	-1.2584720000	1.1706250000
H	-16.1630780000	-0.5671330000	0.1167550000
H	-14.9053540000	-1.6225250000	-0.5843760000

Table S3. Cartesian coordinates of the optimized structure for compound **3a** (propyl side chains) *trans*.

XYZ file

103

Energy= −2163.721697638, Method PBE-D3/SVP, Charge 0, Singlet

C	5.3958540000	2.4229740000	0.1912030000
N	5.2411700000	2.5227190000	-1.2035830000
C	5.4046010000	1.3758880000	-2.0041920000
C	5.2040140000	0.1005770000	-1.4243920000
C	4.6862810000	-0.0062280000	0.0071210000
C	5.2049860000	1.1725280000	0.8249690000
C	5.3707790000	1.0338310000	2.2239360000
N	5.1781520000	-0.2313410000	2.8117880000
C	5.3386640000	-1.3906220000	2.0311820000
C	5.1765860000	-1.3114270000	0.6281410000
C	5.7797070000	1.4573600000	-3.3678320000
C	5.9131750000	0.2868460000	-4.1224910000
C	5.7058790000	-0.9768330000	-3.5593540000
C	5.3567410000	-1.0784420000	-2.1911720000
N	5.1587430000	-2.3300710000	-1.5796730000
C	5.3353690000	-2.4564460000	-0.1881950000
C	5.7400760000	3.5517300000	0.9738680000
C	5.9085220000	3.4047380000	2.3546680000
C	5.7421790000	2.1680090000	2.9870390000

C	5.6578750000	-2.6372670000	2.6223510000
C	5.8262010000	-3.7617630000	1.8072880000
C	5.6815890000	-3.6890360000	0.4173120000
H	5.9965200000	2.4249250000	-3.8407600000
H	6.2090470000	0.3627140000	-5.1818660000
H	5.8397180000	-1.8745720000	-4.1775270000
H	5.8992040000	4.5345940000	0.5108360000
H	6.1999790000	4.2807650000	2.9573970000
H	5.9305970000	2.0897150000	4.0662540000
H	6.0988420000	-4.7251110000	2.2688640000
H	5.8666240000	-4.5864470000	-0.1884760000
C	3.2019640000	-0.0002870000	-0.0005910000
C	1.9715980000	-0.0161060000	-0.0035560000
C	0.5444980000	-0.0439980000	-0.0062040000
C	-0.1668060000	-0.9644000000	-0.8188380000
C	-0.2081400000	0.8420440000	0.8073350000
C	-1.5641450000	-0.9934950000	-0.8124520000
C	-2.3196050000	-0.1051710000	-0.0087140000
C	-1.6057750000	0.8111070000	0.8003220000
H	0.3990990000	-1.6576460000	-1.4616520000
H	0.3254990000	1.5550240000	1.4555320000
H	5.7969240000	-2.7294840000	3.7076480000
C	4.8584870000	-0.3674030000	4.2327700000
H	5.6529830000	-0.9443150000	4.7623810000
H	4.8681620000	0.6427180000	4.6825740000
C	4.8217360000	-3.4863140000	-2.4090220000
H	5.6238550000	-3.6836840000	-3.1592550000
H	4.7930550000	-4.3770380000	-1.7542370000
C	4.9587830000	3.8289040000	-1.7984760000

H	5.7708670000	4.5557400000	-1.5584940000
H	4.9723090000	3.7136090000	-2.8980650000
C	3.4554120000	-3.3603380000	-3.1051540000
H	3.4401530000	-2.4471650000	-3.7399530000
H	2.6789470000	-3.2073010000	-2.3210790000
C	3.5877830000	4.3984880000	-1.3948570000
H	3.5288920000	4.4853670000	-0.2875380000
H	2.8051390000	3.6643490000	-1.6921320000
C	3.3147220000	5.7597860000	-2.0401840000
H	2.3151270000	6.1486700000	-1.7482120000
H	4.0705810000	6.5177620000	-1.7322820000
H	3.3378770000	5.6988130000	-3.1519810000
C	3.1234540000	-4.5912440000	-3.9528810000
H	2.1298650000	-4.4871240000	-4.4402320000
H	3.8755110000	-4.7462190000	-4.7595240000
H	3.0989750000	-5.5192870000	-3.3376680000
C	3.4762390000	-0.9926270000	4.4893240000
H	3.4222910000	-1.9947610000	4.0100790000
H	2.7104020000	-0.3648610000	3.9806540000
C	3.1636430000	-1.1102390000	5.9836360000
H	2.1574740000	-1.5526210000	6.1487480000
H	3.9032320000	-1.7583250000	6.5065170000
H	3.1789430000	-0.1161650000	6.4858760000
C	-3.8049860000	-0.1853440000	0.0057430000
C	-4.4069000000	-1.4578120000	0.1597010000
C	-4.6480040000	0.9614980000	-0.1491150000
C	-5.7939530000	-1.6158180000	0.1884240000
C	-6.0388110000	0.7837060000	-0.1265130000
C	-6.6298000000	-0.4883050000	0.0491160000

H	-6.2637200000	-2.6029340000	0.3228860000
H	-6.7157580000	1.6422450000	-0.2609820000
N	-8.0191630000	-0.7303120000	0.0872460000
N	-8.7507470000	0.3012400000	-0.0450000000
C	-10.1354540000	0.0662040000	-0.0071360000
C	-10.9661570000	1.1972700000	-0.1518630000
C	-10.7383330000	-1.2090050000	0.1653590000
C	-12.3617820000	1.0831740000	-0.1279580000
H	-10.4803860000	2.1772000000	-0.2846300000
C	-12.1214680000	-1.3329140000	0.1905750000
H	-10.0786510000	-2.0828390000	0.2764740000
C	-12.9503250000	-0.1892740000	0.0441900000
H	-12.9807190000	1.9847780000	-0.2429080000
H	-12.6111920000	-2.3109790000	0.3232810000
C	-4.0968500000	2.3529580000	-0.3756070000
H	-3.8637780000	2.8699530000	0.5832270000
H	-3.1591370000	2.3398250000	-0.9705260000
H	-4.8412420000	2.9826230000	-0.9077120000
H	-2.1586300000	1.4943330000	1.4638870000
H	-3.7563260000	-2.3384400000	0.2865940000
H	-2.0930370000	-1.7094640000	-1.4629990000
O	-14.2866250000	-0.4224880000	0.0832970000
C	-15.1772620000	0.6692560000	-0.0584530000
H	-15.0514860000	1.1792390000	-1.0429590000
H	-16.1989850000	0.2433540000	0.0020600000
H	-15.0447660000	1.4184280000	0.7578420000

Table S4. Cartesian coordinates of the optimized structure for compound **4a** (propyl side chains) *trans*.

XYZ file

106

Energy= −2202.951028267, Method PBE-D3/SVP, Charge 0, Singlet

C	-5.3522520000	1.6856210000	-1.8798660000
N	-5.1303830000	2.7275100000	-0.9608670000
C	-5.3033880000	2.4866090000	0.4156830000
C	-5.1767260000	1.1632090000	0.9009520000
C	-4.7225610000	0.0528820000	-0.0425750000
C	-5.2337500000	0.3428860000	-1.4505770000
C	-5.4638130000	-0.7289840000	-2.3457720000
N	-5.3390380000	-2.0499030000	-1.8740750000
C	-5.5102200000	-2.3148990000	-0.5030700000
C	-5.2860390000	-1.2820980000	0.4370890000
C	-5.6165040000	3.5243860000	1.3276960000
C	-5.7642970000	3.2321110000	2.6879110000
C	-5.6312340000	1.9281590000	3.1767260000
C	-5.3431250000	0.8747270000	2.2757730000
N	-5.2196640000	-0.4538060000	2.7224710000
C	-5.4555470000	-1.5117830000	1.8232140000
C	-5.6924430000	1.9559440000	-3.2275630000
C	-5.9258500000	0.8908100000	-4.1037630000

C	-5.8285390000	-0.4400960000	-3.6837160000
C	-5.9022860000	-3.5963260000	-0.0455220000
C	-6.0777080000	-3.8126670000	1.3253510000
C	-5.8716850000	-2.7929200000	2.2612100000
H	-5.7744950000	4.5553520000	0.9828070000
H	-6.0122010000	4.0472100000	3.3878180000
H	-5.7753810000	1.7332570000	4.2478120000
H	-5.7988740000	2.9875160000	-3.5884530000
H	-6.2141900000	1.1045980000	-5.1463190000
H	-6.0654660000	-1.2437130000	-4.3941910000
H	-6.4056840000	-4.8049920000	1.6762310000
H	-6.0637440000	-2.9946740000	3.3237930000
C	-3.2397110000	-0.0138540000	-0.0518300000
C	-2.0110620000	-0.0751860000	-0.0544240000
C	-0.5839860000	-0.1476990000	-0.0566810000
C	0.1342370000	-0.3285740000	1.1521290000
C	0.1515330000	-0.0446750000	-1.2627800000
C	1.5367620000	-0.4050660000	1.1857550000
C	2.2591350000	-0.2962460000	-0.0348080000
C	1.5485370000	-0.1189140000	-1.2405630000
H	-0.4341150000	-0.4138830000	2.0931640000
H	-0.3862850000	0.0928480000	-2.2138420000
H	-6.0923450000	-4.4150270000	-0.7522040000
C	-5.0788520000	-3.1617080000	-2.7885720000
H	-5.9160790000	-3.8988720000	-2.7628370000
H	-5.0627330000	-2.7589410000	-3.8183630000
C	-4.8919860000	-0.7090490000	4.1244370000
H	-5.6686340000	-0.2756610000	4.7980680000
H	-4.9246950000	-1.8022780000	4.2880180000

C	-4.7678480000	4.0539230000	-1.4593180000
H	-5.5623400000	4.4534890000	-2.1336810000
H	-4.7290250000	4.7435080000	-0.5959470000
C	-3.4937010000	-0.2069050000	4.5248410000
H	-3.4175790000	0.8858630000	4.3317250000
H	-2.7457630000	-0.6930360000	3.8574750000
C	-3.3984270000	4.0879210000	-2.1601120000
H	-3.3940880000	3.3705590000	-3.0101790000
H	-2.6306730000	3.7232640000	-1.4407850000
C	-3.0389150000	5.4901260000	-2.6590090000
H	-2.0419160000	5.4970670000	-3.1504140000
H	-3.7800260000	5.8622400000	-3.4025730000
H	-3.0055730000	6.2268690000	-1.8243940000
C	-3.1722110000	-0.5016270000	5.9925000000
H	-2.1557240000	-0.1408270000	6.2613610000
H	-3.8949120000	-0.0017550000	6.6765900000
H	-3.2084620000	-1.5933320000	6.2100360000
C	-3.7346090000	-3.8636030000	-2.5277790000
H	-3.7051220000	-4.2429260000	-1.4828840000
H	-2.9244920000	-3.1036480000	-2.6040540000
C	-3.4833430000	-5.0129390000	-3.5078910000
H	-2.5041720000	-5.5004460000	-3.3106840000
H	-4.2691540000	-5.7984010000	-3.4279380000
H	-3.4742640000	-4.6579760000	-4.5635420000
C	3.7537860000	-0.3788460000	-0.0580720000
C	4.3819000000	-1.6317230000	-0.2182010000
C	4.5550470000	0.7957780000	0.0684160000
C	5.7769120000	-1.7432530000	-0.2518600000
C	5.9507940000	0.6702410000	0.0340640000

C	6.5762850000	-0.5889120000	-0.1236090000
H	6.2791630000	-2.7153650000	-0.3782170000
H	6.5997380000	1.5551150000	0.1272060000
N	7.9736240000	-0.7908290000	-0.1674190000
N	8.6750050000	0.2619600000	-0.0465750000
C	10.0664690000	0.0674000000	-0.0912990000
C	10.8643880000	1.2224400000	0.0466560000
C	10.7053000000	-1.1901530000	-0.2634910000
C	12.2627740000	1.1486760000	0.0171040000
H	10.3515390000	2.1884790000	0.1792800000
C	12.0914790000	-1.2741600000	-0.2946950000
H	10.0706630000	-2.0829070000	-0.3702250000
C	12.8875110000	-0.1066080000	-0.1547460000
H	12.8557120000	2.0682170000	0.1277840000
H	12.6083830000	-2.2380680000	-0.4278200000
C	3.9102140000	2.1537210000	0.2282320000
H	3.2640950000	2.4020330000	-0.6429860000
H	3.2500600000	2.1920140000	1.1235860000
H	4.6766690000	2.9502840000	0.3291200000
C	2.2609520000	-0.6082850000	2.4967840000
H	2.8577490000	-1.5472550000	2.4904300000
H	2.9819190000	0.2151850000	2.6999310000
H	1.5485550000	-0.6583380000	3.3472000000
H	2.1133740000	-0.0403270000	-2.1845040000
H	3.7545400000	-2.5327000000	-0.3208240000
O	14.2297920000	-0.3008620000	-0.1996300000
C	15.0892340000	0.8165420000	-0.0658440000
H	14.9552350000	1.3244950000	0.9184500000
H	16.1225070000	0.4202780000	-0.1322870000

H	14.9293830000	1.5598640000	-0.8825540000

Table S5. Cartesian coordinates of the optimized structure for compound **5a** (propyl side chains) *trans*.

XYZ file

106

Energy= −2312.896124127, Method PBE-D3/SVP, Charge 0, Singlet

C	5.35560	2.19990	0.54870
N	5.16900	2.52960	-0.80490
C	5.28110	1.52010	-1.77820
C	5.01670	0.18910	-1.40870
C	4.50940	-0.11840	-0.00490
C	5.09750	0.88650	0.97800
C	5.28330	0.51930	2.32300
N	5.01400	-0.80710	2.70680
C	5.12810	-1.83090	1.75030
C	4.94030	-1.52490	0.39130
C	5.65860	1.80120	-3.10530
C	5.73250	0.76520	-4.03280
C	5.46550	-0.55380	-3.67780
C	5.11290	-0.85170	-2.34860
N	4.85260	-2.17130	-1.94080
C	5.05090	-2.52310	-0.59320
C	5.79160	3.15970	1.48080

C	5.97790	2.78590	2.80850
C	5.74330	1.48310	3.24050
C	5.42290	-3.15400	2.12780
C	5.53830	-4.13370	1.14600
C	5.36860	-3.83860	-0.20430
H	5.91730	2.80570	-3.41410
H	6.02620	0.99030	-5.05430
H	5.54750	-1.33600	-4.42110
H	5.99900	4.17750	1.17710
H	6.33550	3.52320	3.52180
H	5.94400	1.22450	4.27200
H	5.78750	-5.15010	1.43780
H	5.51010	-4.62120	-0.93840
C	3.02480	-0.02200	0.01230
C	1.81930	0.06720	0.01550
C	0.36560	0.19060	0.00620
C	-4.31300	1.73190	0.04140
C	-5.79870	-0.63420	-0.02980
C	-6.46330	0.60430	0.02090
C	-5.70740	1.78170	0.05850
N	-7.87100	0.77300	0.03840
N	-8.53580	-0.29760	-0.00050
C	-9.93750	-0.14390	0.01450
C	-10.68210	-1.32890	-0.02450
C	-12.07760	-1.30590	-0.01540
C	-12.74110	-0.07220	0.03310
C	-11.99840	1.12640	0.07240
C	-10.61610	1.09370	0.06350
H	-3.76200	2.66540	0.07530

H	-6.38180	-1.54750	-0.05600
H	-6.22950	2.73260	0.10060
H	-10.14820	-2.27340	-0.06250
H	-12.62750	-2.23840	-0.04610
H	-12.53970	2.06630	0.10950
H	-10.03930	2.01080	0.09360
H	5.57620	-3.41610	3.16660
C	4.70330	-1.14880	4.09810
H	5.47390	-1.81070	4.51760
H	4.73910	-0.23120	4.68280
C	4.45060	-3.16980	-2.93620
H	5.22250	-3.27830	-3.71080
H	4.38580	-4.13380	-2.43450
C	4.93160	3.92640	-1.18150
H	5.77230	4.56070	-0.86790
H	4.90010	3.97910	-2.26840
O	-14.09340	0.07700	0.04580
C	-14.91370	-1.08740	0.00780
H	-14.74450	-1.66230	-0.91060
H	-14.73580	-1.72680	0.88080
H	-15.94180	-0.72520	0.02580
C	3.08310	-2.87070	-3.57200
H	3.09870	-1.88500	-4.04780
H	2.33500	-2.81740	-2.77250
C	3.60330	4.47910	-0.63940
H	3.58110	4.39740	0.45210
H	2.78880	3.84860	-1.01430
C	3.38360	5.93760	-1.05620
H	2.42940	6.31490	-0.67440

H	4.17570	6.58990	-0.66870
H	3.36920	6.04620	-2.14760
C	2.68890	-3.93790	-4.59910
H	1.70890	-3.71890	-5.03490
H	3.41230	-3.99070	-5.42200
H	2.63300	-4.93390	-4.14300
C	3.30600	-1.76710	4.26980
H	3.21590	-2.66660	3.65260
H	2.56510	-1.05420	3.89000
C	3.01350	-2.11000	5.73470
H	2.01110	-2.53590	5.84470
H	3.72910	-2.84330	6.12620
H	3.06710	-1.22070	6.37450
C	-2.11830	0.41550	-0.01830
C	-3.63520	0.50520	-0.01590
C	-4.41020	-0.67350	-0.04720
H	-3.91970	-1.64190	-0.08550
C	-1.58220	-0.32940	1.22800
H	-1.84190	-1.39500	1.19870
H	-1.97830	0.10870	2.14930
C	-1.56040	-0.34920	-1.24060
H	-1.65530	0.25400	-2.15310
H	-2.06720	-1.30520	-1.39430
C	-1.38840	1.77250	-0.02630
H	-1.50930	2.30060	0.92870
H	-1.73710	2.41610	-0.84000
O	0.01240	1.53700	-0.26670
O	-0.14950	-0.18750	1.27190
O	-0.17320	-0.65280	-0.99850

7.2 Spin densities of Compound 1-5

In order to elucidate the influence of used method onto the spin density calculations, calculations with different methods has been performed. The calculated spin densities for the triplet states of the different compounds differ in dependence on the used method. However, in Figure S 124 it can be shown that the order of the different compounds is except of on case for all methods the same.

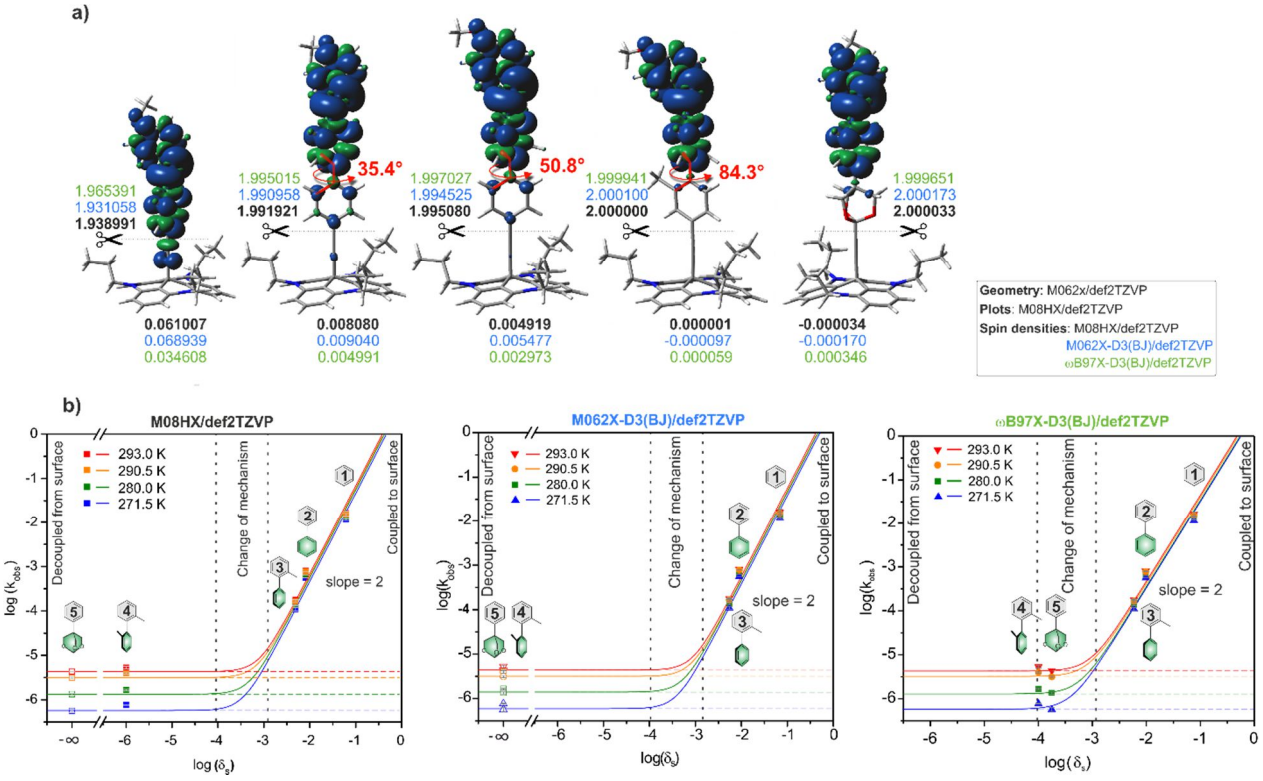

Figure S124. Triplet geometries with calculated spin densities and log(k_{obs}) vs. log(δ_s) plots. a) Spin density plots for the five azobenzene TATA compounds. The compounds are divided into two parts in order to quantify how strong the coupling unit suppresses the πconjugation between platform and azobenzene. The cut for all compounds is placed directly above the ethynyl moiety. The respective spin densities of the platform part and the azobenzene part are shown in coloured numbers.The spin densities were calculated by different methods (M08HX/def2TZVP shown in black, M06X-D3(BJ)/def2TZVP shown in blue and ωB97X-D3(BJ)/def2TZVP shown in green). The numbers in red denote the twist angle between both phenyl units in the coupling unit for compound **2a**, **3a** and **4a**. b) log(k_{obs}) vs. log(δ_s) plots with spin densities calculated by different methods. All plots show the same trend for the five compounds. Negative values for the spin density at the TATA platform shown in a) have been set to zero in b) (unfilled symbols).

8. STM Data

STM measurements were performed with a PicoPlus STM (Agilent, Inc., Santa Clara, USA) at room temperature with mechanically cut Pt/Ir (70:30) tips.

Figure S125. STM images (30 x 30) nm² of self-assembled layers of a) **2a**, b) **3a**, c) **4a** and d) **5a** on Au(111). For the preparation of the SAMs Au(111) single crystals or 200 nm Au wafers

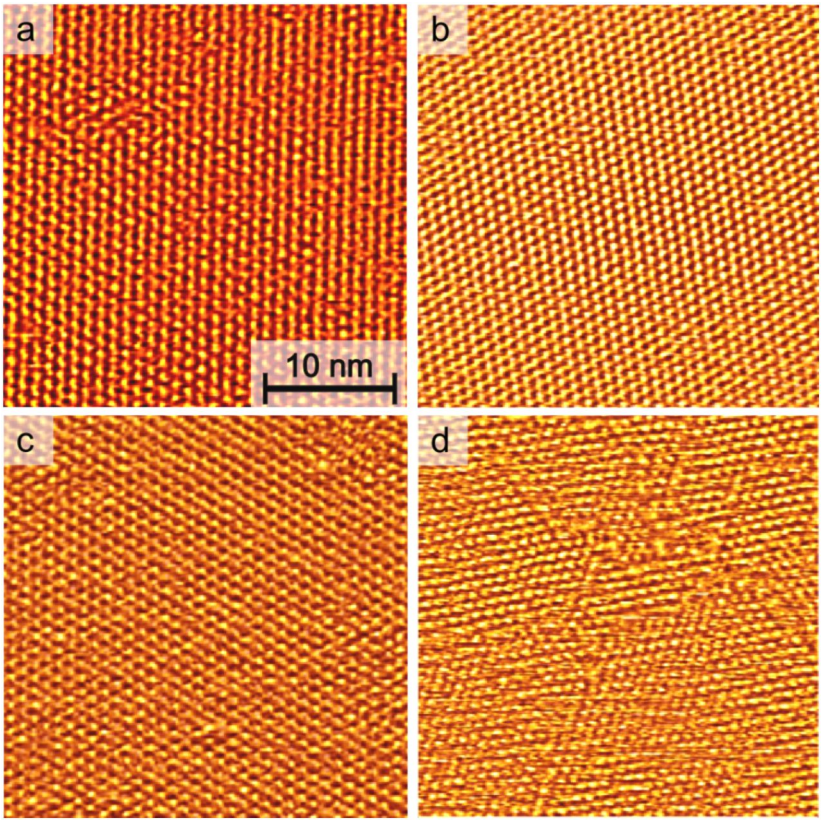

were flame annealed, immersed for 60-120 min. in 1-100 µM solutions of **1**-**5** in toluene at temperatures between 60 and 80 °C. Afterwards, the samples were rinsed with pure toluene. All compounds show a hexagonally ordered superstructure with lattice constants of **1a**:(12.7 ± 0.5) Å, **2a**: (12.4 ± 0.4) Å, **3a**: (12.6 ± 0.7) Å, **4a**: (12.6 ± 0.6) Å and **5a**: (12.5 ± 0.5) Å. Particularly, the intermolecular distances and the angle between the rotational domains are in agreement with a $(\sqrt{19} \times \sqrt{19})$ *R*23.4° superstructure, which was also observed in previous STM investigations of octyl-TATA systems.

9. XPS and NEXAFS Data

The XPS and NEXAFS measurements were performed at the BESSY II synchrotron radiation facility using the PREVAC endstation at the beamline HE-SGM. The experimental station is equipped with a hemispherical VG Scienta R3000 photoelectron analyzer. The energy resolution E/DE of the beamline with 150 mm slits is 800. XP survey spectra were secured at 700 eV photon energy using an analyzer pass energy of 100 eV, whereas for the C 1s spectra the photon energy used was at 350 eV with pass energy of 50 eV. For N 1s spectra the photon energy was at 500 eV with pass energy of 50 eV. All spectra were acquired at normal electron emission. For determination of the relative composition of the TATA adlayers, the XP spectra were energy-corrected using the Au 4f7/2 line at a binding energy of 84.0 eV as reference. Background correction was performed using a combination of a Shirley and a linear background for all signals. Peak fitting was performed using the program CASA XPS. To correct for the photon flux of the NEXAFS measurements, all spectra were divided by the spectrum obtained for a freshly sputtered clean gold substrate and then edge-step normalized (using the average intensities for the C K-edge between 275 ±0.5 eV and 320 ± 0.5 eV and for the N K-edge between 395 ±0.5 eV and 420 ±0.5 eV as pre- and post-edge).

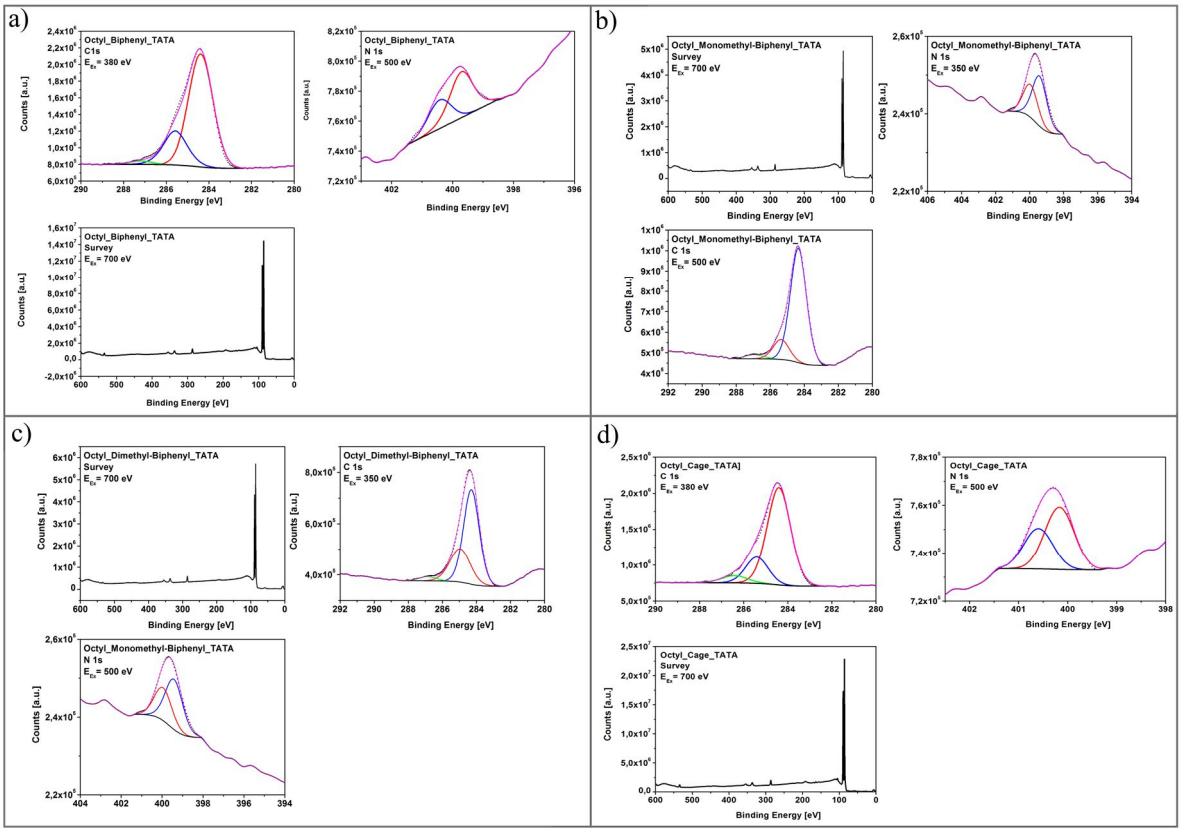

Figure S126. XP spectra of self-assembled layers of a) **2a**, b) **3a**, c) **4a** and d) **5a** on Au(111). a) XP spectra of compound **2a** monolayer. Top, left: C 1s-spectrum along with fit (red: C-C, blue: C-N, green: C-O); Top, right: N 1s-spectrum along with fit (red: amine (TATA), blue: azo moiety); Bottom, left: survey spectrum. b) XP spectra of compound **3a** monolayer. Top, left: survey spectrum; Top, right: N 1s-spectrum along with fit (red: amine (TATA), blue: azo moiety); Bottom, left: C 1s-spectrum along with fit (red: C-C, blue: C-N, green: C-O).c) XP spectra of compound **4a** monolayer. Top, left: survey spectrum; Top, right: C 1s-spectrum along with fit (red: C-C, blue: C-N, green: C-O); Bottom, left: N 1s-spectrum along with fit (red: amine (TATA), blue: azo moiety. d) XP spectra of compound **5a** monolayer. Top, left: C 1s-

spectrum along with fit (red: C-C, blue: C-N, green: C-O); Top, right: N 1s-spectrum along with fit (red: amine (TATA), blue: azo moiety); Bottom, left: survey spectrum.

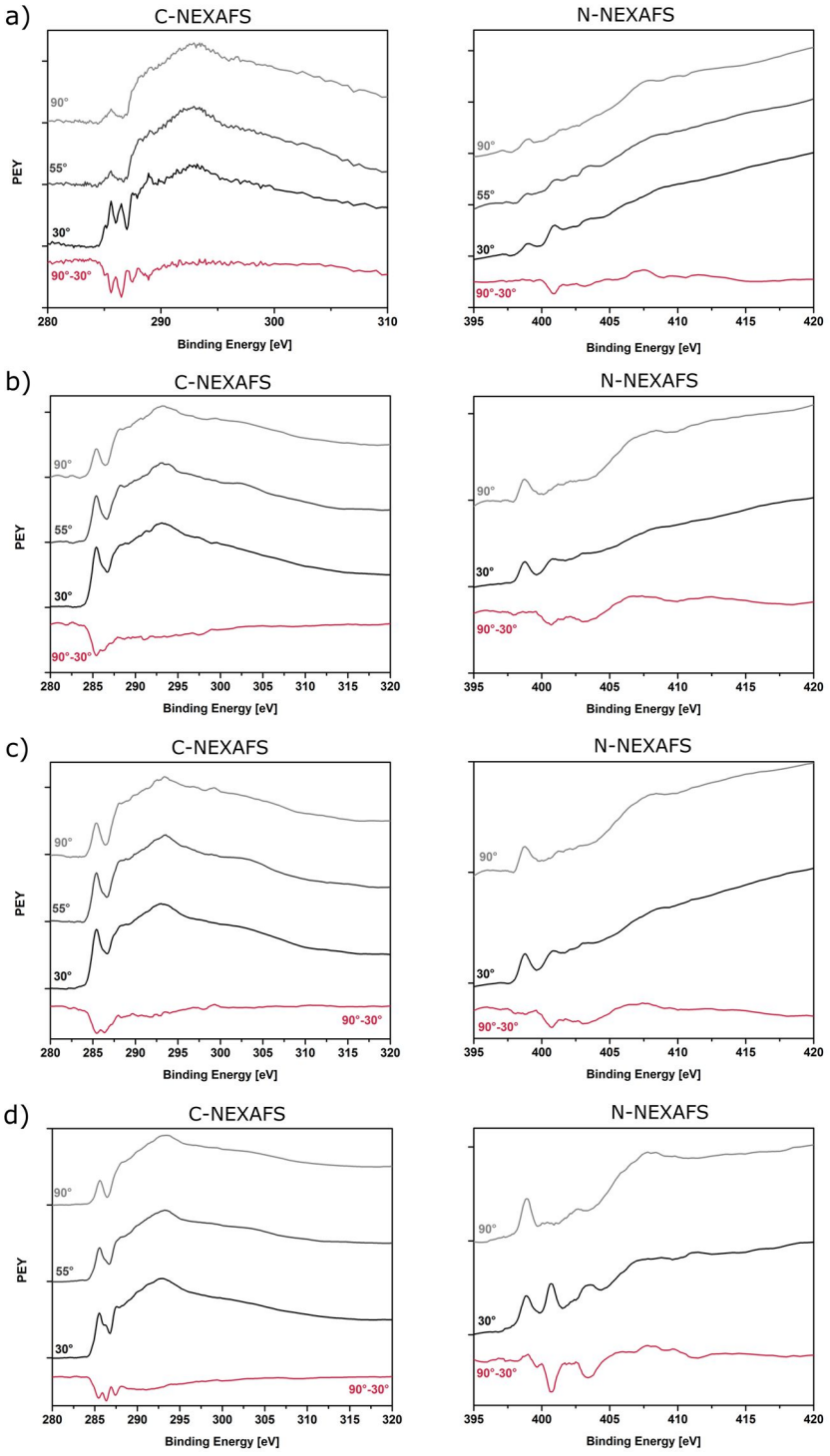

Figure S127. K-edge NEXAFS spectra of self-assembled layers of a) **2a**, b) **3a**, c) **4a** and d) **5a** on Au(111). The NEXAFS spectra were recorded at different angles (grey-black) of incidence. To prove the angular dependence for each compound a difference spectrum (I_{90}-I_{30}) is displayed (red). a) K-edge C-NEXAFS (left) and K-edge N-NEXAFS (right) of compound **2a** are shown. b) K-edge C-NEXAFS (left) and K-edge N-NEXAFS (right) of compound **3a** are shown. c) K-edge C-NEXAFS (left) and K-edge N-NEXAFS (right) of compound **4a** are shown. d) K-edge C-NEXAFS (left) and K-edge N-NEXAFS (right) of compound **5a** are shown.

10. Kinetic Data for Compound **1**-**5**(**6**) in solution and adsorbed on surface

In order to obtain the activation barrier and the frequency factor for compound **1a-5a** adsorbed in Au(111), ln(k) vs T^{-1} has been plotted and fitted. The resulting Arrhenius plots are shown in figure S128. The corresponding errors are also given in figure S 128. A chart with all kinetic data and the corresponding errors is displayed in figure S129. In this chart also the relaxation rates of the compounds **1b**, **2b** and **5b** with propyl sidechains can be found. Due to the shorter sidechains the intermolecular distance on the surface is decreased. The specific rates of the surface adsorbed compounds are a bit lower but nevertheless these compounds show the same rate acceleration as it was observed for the compounds with the octyl sidechains. This fact reinforces our assumption that intermolecular interactions can be neglected in our case for the explanation of the general effect of rate acceleration.
The missing parameters for the relation of equation (1) in the main text were obtained from a $\log(k_{obs}-k)$ vs. $\log(\delta_s)$ plot shown in figure S130. In this way the C(T) values could be determined at different temperatures. Using this C(T) values in a plot of ln(C(T)) vs. T^{-1} the activation barrier and the frequency factor of the part of equation (1) in the main text which depends on the spin density could be obtained (Figure S131).

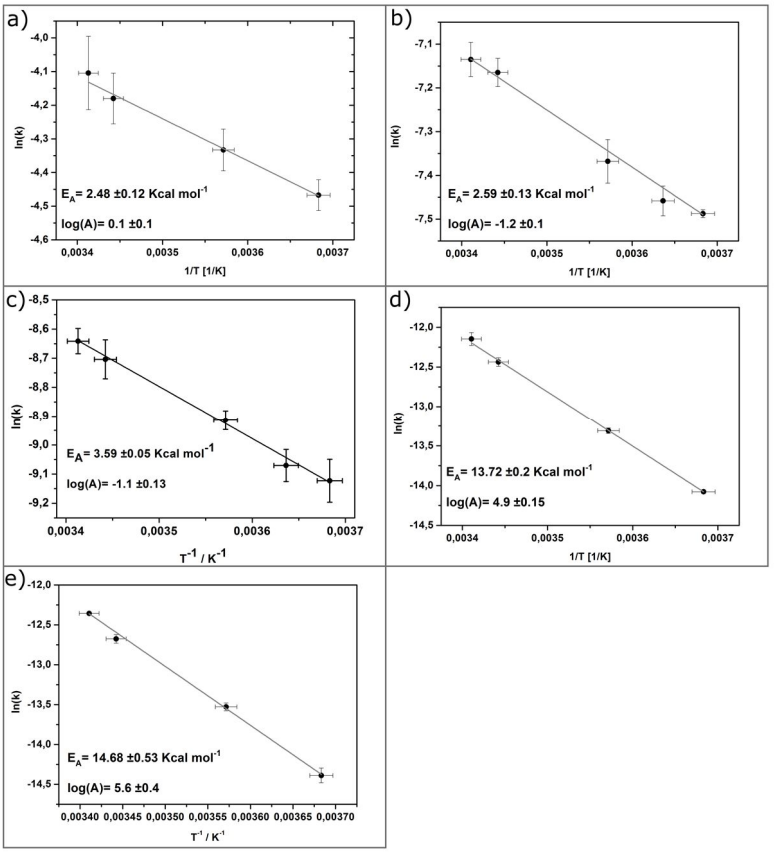

Figure S128. Arrhenius plots for compound **1a, 2a, 3a, 4a and 5a**. a) ln(k) vs. 1/T plot for the determination of activation barrier and frequency factor of compound **1a**. b) ln(k) vs. 1/T plot for the determination of activation barrier and frequency factor of compound **2a**. c) ln(k) vs. 1/T plot for the determination of activation barrier and frequency factor of compound **3a**. d) ln(k) vs. 1/T plot for the determination of activation barrier and frequency factor of compound **4a**. e) ln(k) vs. 1/T plot for the determination of activation barrier and frequency factor of compound **5a**.

Molecule		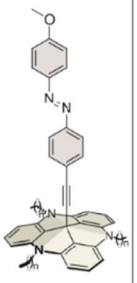 1	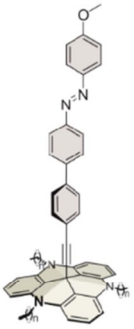 2	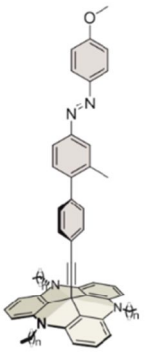 3	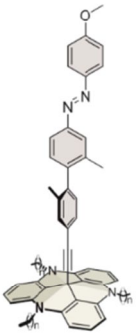 4	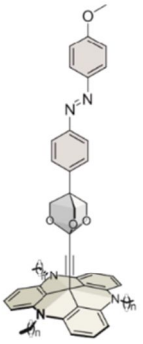 5
In solution (a)	$t_{1/2}$ (290.5 K)	18.7 h ±0.04 h	25.6 h ±0.01 h	37.9 h ±0.02 h	49.9 h ±0.03 h	64.8 h ±0.02 h
	E_A (kcal/mol)	24.1 ±0.4	22.6 ±1.29	21.7 ±0.1	21.2 ±0.2	21.5 ±0.02
	log(A)	13.12 ±0.29	14.02 ±0.97	11.04 ±0.1	10.58 ±0.1	10.67 ±0.01
@Au(111) (a)	$t_{1/2}$ (293.0 K)	42.0 s ±4.8 s	14.4 min ±0.6 min	65.5 min ±2.9 min	36.3 h ±2.2 h	44.7 h ±0.6 h
	$t_{1/2}$ (290.5 K)	45.3 s ±3.4 s	14.9 min ±0.5 min	69.6 min ±4.8 min	48.4 h ±2.6 h	61.6 h ±3.4 h
	$t_{1/2}$ (280.0 K)	52.8 s ±3.4 s	18.3 min ±0.9 min	85.9 min ±2.9 min	116.1 h ±4.1 h	143.8 h ±7.3 h
	$t_{1/2}$ (271.5 K)	60.4 s ±2.8 s	20.6 min ±0.8 min	105.8 min ±8.2 min	250.2 h ±4.8 h	342.0 h ±31.9h
	E_A (kcal/mol)	2.5 ±0.2	2.6 ±0.1	3.6 ±0.1	13.7 ±0.2	14.7 ±0.5
	log(A)	0.1 ±0.1	-1.2 ±0.1	-1.1 ±0.1	4.9 ±0.15	5.6 ±0.4
In solution (b)	$t_{1/2}$ (293 K)	21.1 h ±0.2 h	16.8 h ±0.06 h	39.3 h ±0.03 h	50.1 h ±0.04 h	60.1 h ±0.1 h
@Au(111) (b)	$t_{1/2}$ (293.0 K)	27.5 s ±4 s	10.2 min ±0.5 min	----------	----------	14.4 h ±0.6 h

Figure S129. Kinetic data for the compounds **1a**, **2a**, **3a**, **4a**, **5a, 1b, 2b, 5b** in solution and adsorbed on Au(111) at different temperatures. The half-lives at different temperatures (293.0 K, 290.5 K, 280.0 K, 271.5 K), activation energies and frequency factor values for all systems adsorbed on Au(111) and in solution along with their respective errors are shown

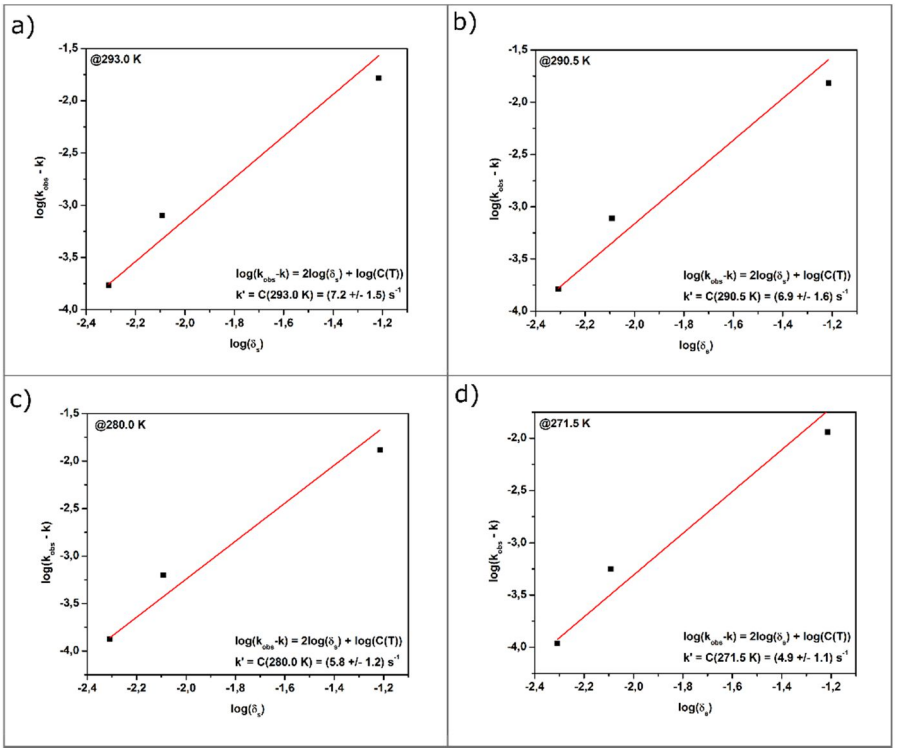

Figure S130. Plots for the determination of C(T) = *A´* exp(-E_A´/RT). a) log(*k_{obs}-k)* vs log(δ_s) plot for the determination of C(T) at 293.0 K. b) log(*k_{obs}-k)* vs log(δ_s) plot for the determination of C(T) at 290.5 K. c) log(*k_{obs}-k)* vs log(δ_s) plot for the determination of C(T) at 280.0 K. d) log(*k_{obs}-k)* vs log(δ_s) plot for the determination of C(T) at 271.5 K. For the linear regression the displayed function equation has been used. C(T) has been determined by the Y-axis intercept.

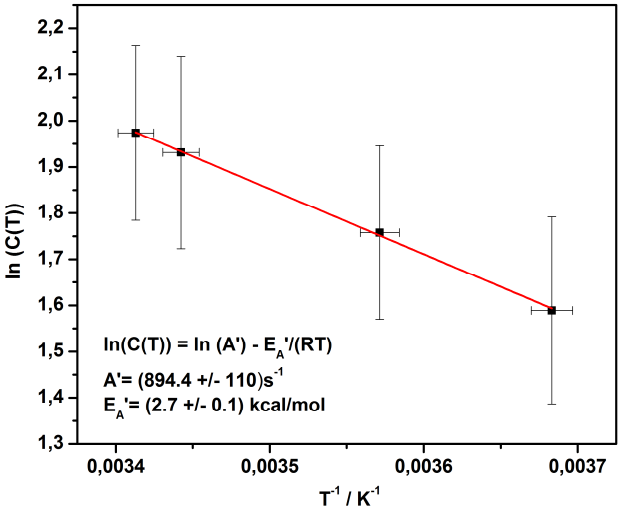

Figure S131. Plots for the determination of *A'* and E_A' from the temperature dependence of C(T). By linear regression analysis of a plot of ln(C(T)) vs. the reciprocal temperature the values of *A'* and E_A' have been determined. Importantly, the E_A´ value fits well to the activation energies determined by standard Arrhenius treatment of compounds **1a**-**3a**.

Table S 6. Comparison of the calculated/determined half-lives (blue, calculated by means of E_A and A) in solution and the determined half-lives of the surface-adsorbed compounds (**1a-5a**).

Molecule		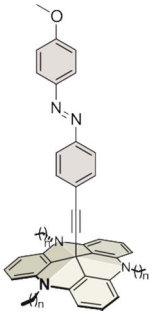 **1a**	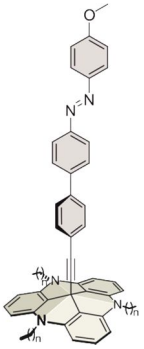 **2a**	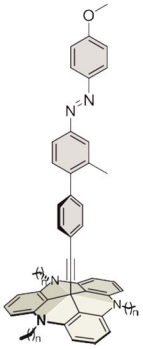 **3a**	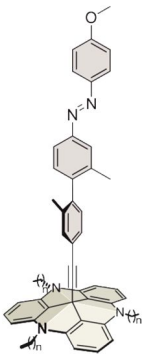 **4a**	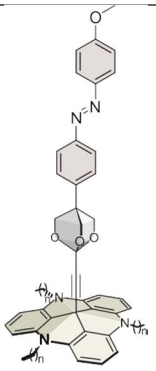 **5a**
In solution (a)	$t_{1/2}$ (309.5 K)	1.6 h	2.3 h	3.8 h	5.1 h	6.6 h
	$t_{1/2}$ (300.0 K)	4.9 h	8.2 h	11.4 h	15.7 h	19.9 h
	$t_{1/2}$ (293.0 K)	14.5 h	17.5 h	29.6 h	39.7 h	41.9 h
	$t_{1/2}$ (290.5 K)	18.7 h	25.6 h	37.9 h	49.9 h	64.8 h
	$t_{1/2}$ (280.0 K)	98.9 h	105.9 h	167.0 h	215.0 h	232.6 h
	$t_{1/2}$ (271.5 K)	383.9 h	377.9 h	566.3 h	708.8 h	779.9 h
	E_A (kcal/mol)	24.1	22.6	21.7	21.2	21.5
	log(A)	13.1	11.9	11.0	10.5	10.7
@Au(111) (b)	$t_{1/2}$ (293.0 K)	42.0 s	14.4 min	65.5 min	36.3 h	44.7 h
	$t_{1/2}$ (290.5 K)	45.3	14.9 min	69.6 min	48.4 h	61.6 h
	$t_{1/2}$ (280.0 K)	52.8 s	18.3 min	85.9 min	116.1 h	143.8 h
	$t_{1/2}$ (271.5 K)	60.4 s	20.6 min	105.8 min	250.2 h	342.0 h
	E_A (kcal/mol)	2.5	2.6	3.6	13.7	14.7
	log(A)	0.1	-1.2	-1.1	4.9	5.6

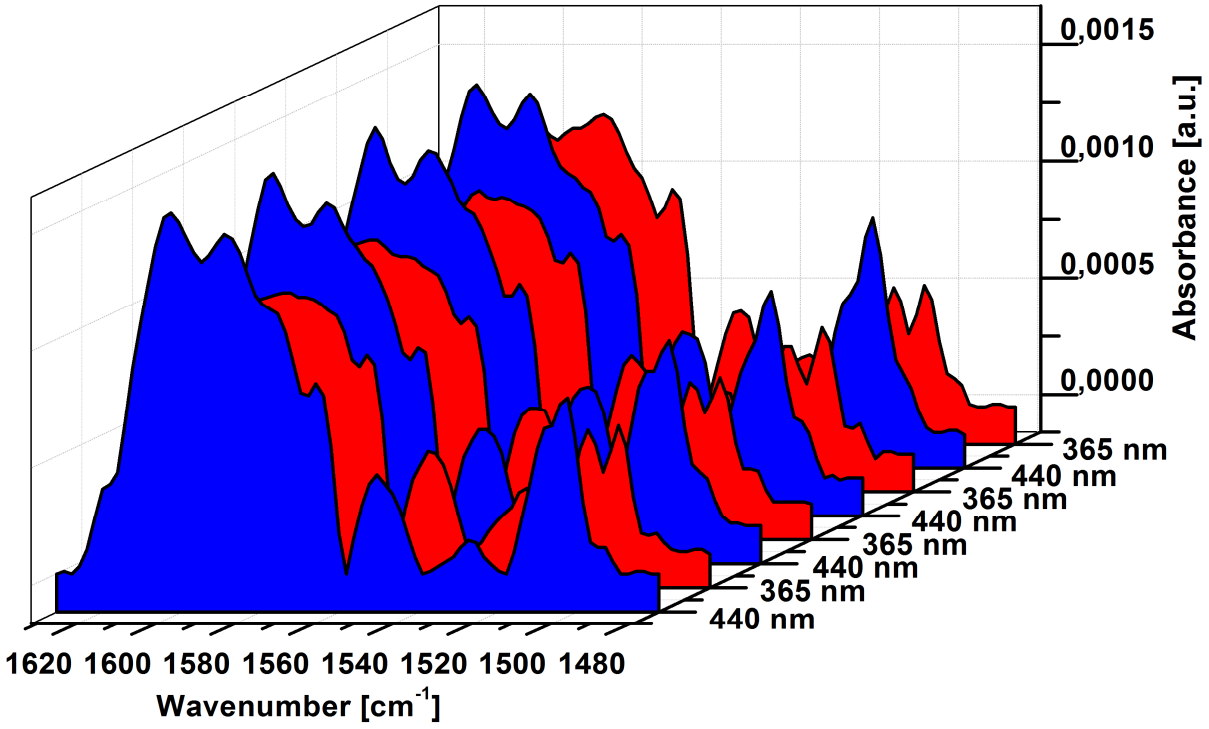

Figure S132. Shown is the region of the IRRA spectrum between 1630 cm^{-1} and 1480 cm^{-1} after irradiation with 365 nm and 440 nm for compound **5a**. Although the C-O stretching vibration well suited to monitore the *cis/trans* isomerization, there are also differences in intensity between *cis* and *trans* isomer for other vibrational modes. The N=N stretching vibration (combined with a ring vibration) at 1530 cm^{-1} decreases after irradiation with light of 440 nm. On the other side the band at 1500 cm^{-1} increases. This bands contains the N=N stretch of *trans* isomer and further ring vibrations of the platform. Interestingly the band at 1550 cm^{-1} shows a constant intensity, because it contains only ring vibrations of the platform.

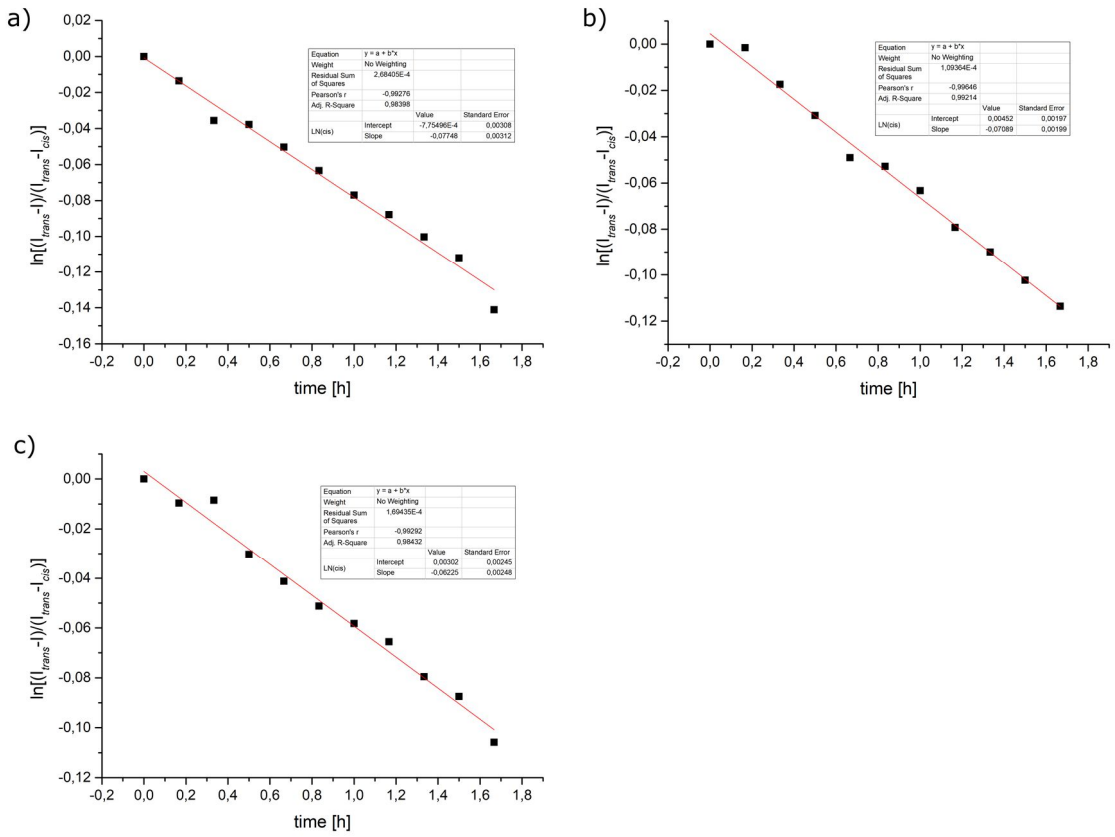

Figure S133. Shown are the relaxation plots of compound **1** in acetone with a certain amount of water at 298 K(a) 0 %, b) 2 %, c) 4 %). The half-lives are not largly effected by the water concentration (0 %: $t_{1/2}$=8.9 h; 2 %: $t_{1/2}$=9.8 h; 4%: $t_{1/2}$= 11.1 h).

References

[1] a) W. H. Miller, S. D. Schwartz, J. W. Tromp, *The Journal of Chemical Physics* **1983**, *79*, 4889; b) W. H. Miller, *The Journal of Chemical Physics* **1974**, *61*, 1823; c) T. Yamamoto, *The Journal of Chemical Physics* **1960**, *33*, 281.

[2] J. O. Richardson, M. Thoss, *The Journal of Chemical Physics* **2013**, *139*, 31102.

[3] J. O. Richardson, R. Bauer, M. Thoss, *The Journal of Chemical Physics* **2015**, *143*, 134115.

[4] G. Berthier, M. J. S. Dewar, H. Fischer, K. Fukui, H. Hartmann, H. H. Jaffé, J. Jortner, W. Kutzelnigg, K. Ruedenberg, E. Scrocco et al., *Charge Transfer Processes in Condensed Media*, Springer Berlin Heidelberg, Berlin, Heidelberg, **1979**.

[5] a) B. W. Laursen, F. C. Krebs, *Chem. Eur. J.* **2001**, *7*, 1773; b) J. Kubitschke, C. Näther, R. Herges, *Eur. J. Org. Chem.* **2010**, *2010*, 5041.

[6] a) A. Smeets, K. van den Bergh, J. de Winter, P. Gerbaux, T. Verbiest, G. Koeckelberghs, *Macromolecules* **2009**, *42*, 7638; b) A. G. Bonn, O. S. Wenger, *The Journal of organic chemistry* **2015**, *80*, 4097; c) J. Xie, C. T. Seto, *Bioorganic & medicinal chemistry* **2007**, *15*, 458.

[7] D. L. Browne, M. Baumann, B. H. Harji, I. R. Baxendale, S. V. Ley, *Organic letters* **2011**, *13*, 3312.

[8] a) A. Mames, S. Stecko, P. Mikołajczyk, M. Soluch, B. Furman, M. Chmielewski, *The Journal of organic chemistry* **2010**, *75*, 7580; b) T. K. Prasad, G. Poneti, L. Sorace, M. J. Rodriguez-Douton, A.-L. Barra, P. Neugebauer, L. Costantino, R. Sessoli, A. Cornia, *Dalton transactions (Cambridge, England : 2003)* **2012**, *41*, 8368.

[9] a) Y. Shirai, T. Sasaki, J. M. Guerrero, B.-C. Yu, P. Hodge, J. M. Tour, *ACS nano* **2008**, *2*, 97; b) W. F. Little, A. K. Clark, *The Journal of organic chemistry* **1960**, *1960*, 1979.

[10] University of Karlsruhe and Forschungszentrum Karlsruhe GmbH, *TURBOMOLE V7.2*, TURBOMOLE GmbH, **2017**.

[11] M. J. Frisch, G. W. Trucks, H. B. Schlegel, G. E. Scuseria, M. A. Robb, J. R. Cheeseman, G. Scalmani, V. Barone, B. Mennucci, G. A. Petersson, H. Nakatsuji, M. Caricato, X. Li, H. P. Hratchian, A. F. Izmaylov, J. Bloino, G. Zheng, J. L. Sonnenberg, M. Hada, M. Ehara, K. Toyota, R. Fukuda, J. Hasegawa, M. Ishida, T. Nakajima, Y. Honda, O. Kitao, H. Nakai, T. Vreven, J. A. Montgomery, Jr., J. E. Peralta, F. Ogliaro, M. Bearpark, J. J. Heyd, E. Brothers, K. N. Kudin, V. N. Staroverov, T. Keith, R. Kobayashi, J. Normand, K. Raghavachari, A. Rendell, J. C. Burant, S. S. Iyengar, J. Tomasi, M. Cossi, N. Rega, J. M. Millam, M. Klene, J. E. Knox, J. B. Cross, V. Bakken, C. Adamo, J. Jaramillo, R. Gomperts, R. E. Stratmann, O. Yazyev, A. J. Austin, R. Cammi, C. Pomelli, J. W. Ochterski, R. L. Martin, K. Morokuma, V. G. Zakrzewski, G. A. Voth, P. Salvador, J. J. Dannenberg, S. Dapprich, A. D. Daniels, O. Farkas, J. B. Foresman, J. V. Ortiz, J. Cioslowski, and D. J. Fox, *Gaussian09 D.01*, Gaussian, Inc., Wallingford CT, **2013**.

[12] A. D. Becke, *The Journal of Chemical Physics* **1993**, *98*, 5648.

[13] Perdew, Burke, Ernzerhof, *Physical review letters* **1996**, *77*, 3865.

[14] S. Grimme, J. Antony, S. Ehrlich, H. Krieg, *The Journal of Chemical Physics* **2010**, *132*, 154104.

[15] H. Jacob, S. Ulrich, U. Jung, S. Lemke, T. Rusch, C. Schütt, F. Petersen, T. Strunskus, O. Magnussen, R. Herges et al., *Physical chemistry chemical physics* **2014**, *16*, 22643.

[16] Y. Zhao, D. G. Truhlar, *Journal of chemical theory and computation* **2008**, *4*, 1849.

[17] Y. Zhao, D. G. Truhlar, *Theor Chem Account* **2008**, *120*, 215.

[18] L. Goerigk, A. Hansen, C. Bauer, S. Ehrlich, A. Najibi, S. Grimme, *Physical chemistry chemical physics : PCCP* **2017**, *19*, 32184.

3.2 Diazocine funktionalisiert auf TATA Plattformen

Der nicht adiabatische Mechanismus, der die thermische *cis*→*trans*-Isomerisierung von Azobenzolen beschleunigt, wurde über den Nachweis der elektronischen Kopplung der Azofunktion zur Goldoberfläche aufgeklärt.[174] Mit der schrittweisen Reduktion der Konjugation zwischen Azofunktion und TATA-Plattform, die über die Variation verschiedener Regulierungseinheiten erreicht wurde, konnte diese elektronische Kopplung nachgewiesen werden. Der nicht adiabatische Mechanismus ermöglicht ein Intersystem-Crossing zwischen Singulett- und Tripletthyperfläche des Azobenzols. Um einen möglichen Anwendungsbereich dieses Mechanismus definieren zu können, ist der Nachweis der thermischen Beschleunigung in weiteren Isomerisierungsreaktionen notwendig. Im Diazocin liegt das *cis*-Isomer aufgrund des Achtrings, der aus der zusätzlichen Ethylenverbrückung gebildet wird, als thermodynamisch stabile Form vor (Abb. 3.3).[169,170] Mit der inversen thermischen Stabilität des Diazocins im Vergleich zu Azobenzol kann der nicht adiabatische Mechanismus auf die thermische *trans*→*cis*-Isomerisierung untersucht werden.

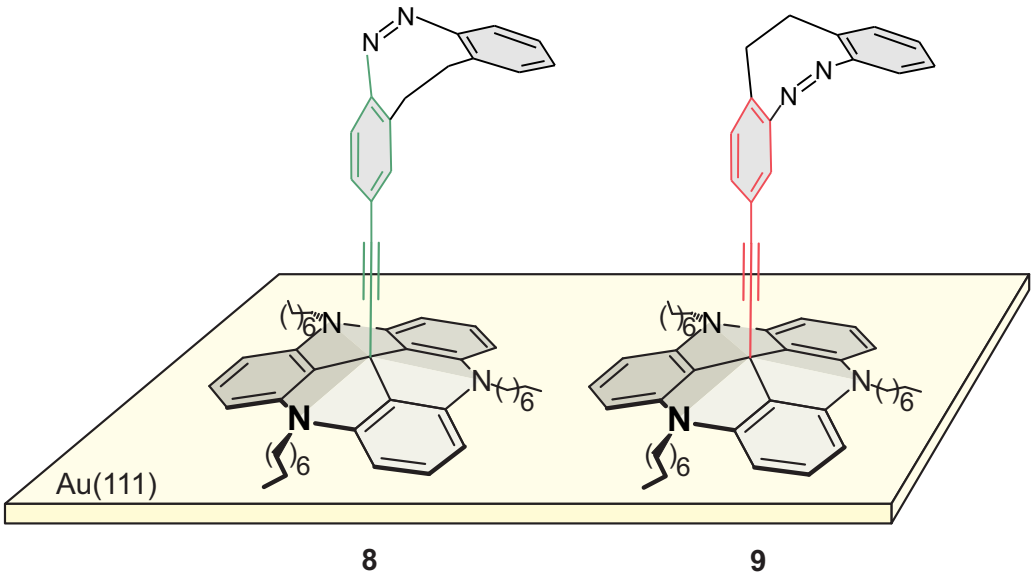

Abb. 3.3: Darstellung des Diazocingrundgerüsts funktionalisiert über ein Acetylen auf einer Octyl-TATA-Plattform und der schematischen Adsorption auf einer Au(111)-Oberfläche. Links ist die *para*- **8** (grün) und rechts die *meta*-Funktionalisierung **9** (rot) des Acetylens zur Azofunktion der Diazocine gezeigt.

Die Ethylenbrücke unterbindet zudem die Rotation um die Azofunktion, wodurch die horizontale Ausrichtung des oberen Phenylrings im *cis*-Isomer bzw. die vertikale Ausrichtung im *trans*-Isomer zur TATA-Plattform bestehen bleibt, wenn das Diazocin, wie in beiden Isomeren (**8**, **9**), in *para*- oder *meta*-Position mit einer Acetyleneinheit funktionalisiert wird. Adsorbiert auf Au(111)-Oberflächen ist diese Ausrichtung essentiell für die Detektion beider Isomere in IRRAS-Messungen. Mit dieser unterschiedlichen Anbringung des Acetylens am Diazocin sollte in der *para*-Funktionalisierung eine hohe elektronische Kopplung zwischen Azofunktion und Goldoberfläche gewährleistet werden, während die *meta*-Funktionalisierung die elektronische Kopplung weitestgehend unterbrechen sollte.

3.2.1 Diazocine functionalized TATA Platforms

Roland Löw, Talina Rusch, Fynn Röhricht, Olaf Magnussen, Rainer Herges

Beilstein J. Org. Chem. **2019**, *15*, 1485-1490.
DOI:10.3762/bxiv.2019.11.v1

Eigenanteil: Synthese, Charakterisierung und photochemische Untersuchungen wurden von Roland Löw durchgeführt. Die DFT-Rechnungen wurden von Fynn Röhricht angefertigt. Die Untersuchungen mittels Rastertunnelmikroskopie wurden von Talina Rusch durchgeführt. Das Manuskript wurde von Roland Löw und Prof. Dr. Rainer Herges verfasst.

3.2.2 Zusammenfassung

In dieser Publikation wird die Synthese von Diazocin-funktionalisierten TATA-Plattformen **10**, **11** und die Untersuchung ihrer photochemischen und thermischen Isomerisierung in Lösung gezeigt. Zusätzlich wird der Nachweis hochgeordneter Monolagen dieser Diazocin-Plattformen auf Au(111)-Oberflächen mittels Rastertunnelmikroskopie erbracht. Diazocine sind durch die Ethylenverbrückung in der freien Rotation um die Azobrücke gehindert. Die Funktionalisierung des Diazocins mit einem Acetylen in *para*- bzw. *meta*-Position zur Azobrücke gewährleistet weiterhin die horizontale Ausrichtung der Methoxykopfgruppe im *cis*-Isomer bzw. die orthogonale Ausrichtung im *trans*-Isomer bezogen zur TATA-Plattform (Abb. 3.4).

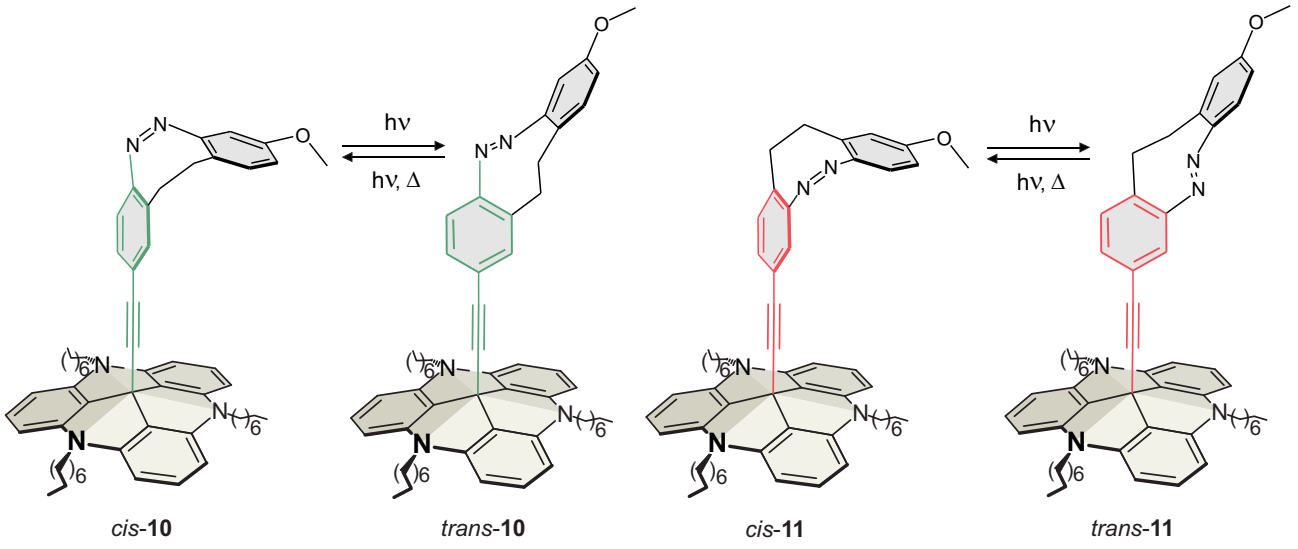

Abb. 3.4: Darstellung der *para*-Diazocin-Plattform **10** (links) und der *meta*-Diazocin-Plattform **11** (rechts) und deren photochemische bzw. thermische Isomerisierung zwischen dem thermodynamisch stabilen *cis*-Isomer in dem metastabilen *trans*-Isomer.

Die Diazocin-Plattform **10** wurde in einer fünfstufigen Syntheseroute mit einer Gesamtausbeute von 1 % erhalten, bei der die Funktionalisierung des Diazocins auf der Plattform mit 99 % nahezu quantitativ verlief. Die Diazocin-Plattform **11** wurde in vier Syntheseschritten mit einer Gesamtausbeute von 3 % gebildet, wobei bei der Funktionalisierung des Diazcoins auf der TATA-Plattform eine Ausbeute von 88 % erhalten wurde. Die hohe Konjugation zwischen Azofunktion und TATA-Plattform in der *para*-Diazocin-Plattform **10** bzw. die Isolation in der *meta*-Diazocin-Plattform **11** resultiert in geringfügig höheren thermischen Isomerisierungszeiten des *meta*-Diazocins **11** verglichen zum *para*-Diazocin **10** in Lösung. Dieses Verhalten gleicht dem der Azobenzol-TATA-Plattformen in Lösung.[174] Weiterhin weisen beide Diazocine nahezu identische Aktivierungsenergien der *trans*→*cis*-Isomerisierung von 86.5 kJ/mol für **10** bzw. 84.7 kJ/mol für **11** in Lösung auf.

BEILSTEIN JOURNAL OF ORGANIC CHEMISTRY

Diazocine-functionalized TATA platforms

Roland Löw[1], Talina Rusch[2], Fynn Röhricht[1], Olaf Magnussen[2] and Rainer Herges[*1]

Full Research Paper

Open Access

Address:
[1]Otto Diels Institute of Organic Chemistry, University of Kiel, Otto-Hahn-Platz 4, 24118 Kiel, Germany and [2]Institute for Experimental and Applied Physics, University of Kiel, Leibnizstraße 19, 24098 Kiel, Germany

Email:
Rainer Herges[*] - rherges@oc.uni-kiel.de

* Corresponding author

Keywords:
cis–trans isomerization; diazocine; molecular switch; photochrome; self-assembled monolayers; TATA platform

Beilstein J. Org. Chem. **2019,** *15,* 1485–1490.
doi:10.3762/bjoc.15.150

Received: 17 April 2019
Accepted: 28 June 2019
Published: 05 July 2019

This article is part of the thematic issue "Molecular switches".

Guest Editor: W. Szymanski

Abstract

Recently, it has been shown that the thermochemical *cis*→*trans* isomerization of azobenzenes is accelerated by a factor of more than 1000 by electronic coupling to a gold surface via a conjugated system with 11 bonds and a distance of 14 Å. The corresponding molecular architecture consists of a platform (triazatriangulenium (TATA)) which adsorbs on the gold surface, with an acetylene spacer standing upright, like a post in the middle of the platform and the azobenzene unit mounted on top. The rate acceleration is due to a very peculiar thermal singlet–triplet–singlet mechanism mediated by bulk gold. To investigate this mechanism further and to examine scope and limitation of the "spin-switch catalysis" we now prepared analogous diazocine systems. Diazocines, in contrast to azobenzenes, are stable in the *cis*-configuration. Upon irradiation with light of 405 nm the *cis*-configuration isomerizes to the *trans*-form, which slowly returns back to the stable *cis*-isomer. To investigate the thermal *trans*→*cis* isomerization as a function of the conjugation to the metal surface, we connected the acetylene spacer in *meta* (weak conjugation) and in *para* (strong conjugation) position. Both isomers form ordered monolayers on Au(111) surfaces.

Introduction

Catalysts increase chemical reaction rates by lowering the activation energies and thus create more favorable reaction pathways [1-4]. However, there are very few reactions which do not follow the classical Eyring theory [5,6]. The rate of these reactions is not dependent on an activation barrier but controlled by quantum mechanical transition probabilities between two quantum states [7-10]. The majority of these quantum chemically forbidden reactions are photochemical processes or transition metal reactions including transitions between spin states or electronic states. We recently discovered a purely organic system in the ground state, whose reaction rate is accelerated from days to seconds by electronic coupling to a bulk gold surface via a conjugated linker over 11 bonds and 14 Å [11]. Thermal *cis*→*trans* isomerizations of azobenzenes are usually slow with half-lives of the *trans*-isomer within the range of hours to days at room temperature (parent azobenzene: 4–5 d at 25 °C) [12]. Rotation around the N=N bond is a symmetry-forbidden process and the slow isomerization proceeds via inversion at the

N atoms [13]. The rate of isomerization is temperature dependent and follows a classical Arrhenius type behavior [12]. However, the rate and the mechanism change dramatically if the azobenzenes are electronically coupled to bulk gold [14-17]. To investigate the *cis*→*trans* isomerizations of azobenzenes as a function of electronic coupling systematically, we used the so-called platform approach [18]. The azobenzenes are not directly adsorbed on the surface, but covalently mounted on "TATA" (triazatriangulenium) platforms which adsorb on Au(111) surfaces. A spacer, such as an ethynyl group is connected to the central carbon atom like a post and the azobenzene is mounted on top of the spacer. After preparation of an ordered self-assembled monolayer on gold, the azobenzene units are freestanding upright on the surface. The platform defines the lateral distance between next neighbors and provides the free volume for unhindered isomerization of the azobenzene units [19,20]. The length and electronic nature of the spacer units control the distance from the surface and define the electronic coupling with the metal surface [11,18]. With increasing π-conjugation from the azobenzene into the platform, and thus coupling to the gold surface, the activation barrier drops to almost zero (≈8 kJ mol^{-1}) and the frequency factors (log A) become negative [11]. Vanishing barriers and low frequency factors are typical for non-adiabatic reactions [9]. The mechanism was elucidated as a singlet–triplet–singlet spin change process, which is forbidden in solution but mediated by coupling to the conduction band of the bulk gold. We are now exploring scope and limitations of this peculiar spin catalysis. To investigate if the reverse isomerization process from the *trans* to the *cis*-configuration would also be accelerated, and to further scrutinize the coupling effects, we prepared analogous diazocine systems. Diazocines are bridged azobenzenes [21]. Imposed by the ring strain of the central eight-membered ring, the *cis*-configuration (boat conformation) is more stable than the *trans*-isomer (twist conformation). Upon irradiation with ≈400 nm the *cis*-form switches to the *trans*-isomer, and irradiation with ≈500 nm or heating leads back to the *cis*-form [22]. Hence, the diazocines are quasi reversed azobenzenes that are more stable in their *trans*-configurations [23].

To investigate the electronic coupling effects, we synthesized two diazocine derivatized TATA platforms with ethynyl spacers (diazocine-TATAs). In compound **1** the diazocine is connected to the platform with the ethynyl group in *para*-position to the azo group, providing a full π-conjugation path of the N=N unit through the ethynyl spacer into the platform. Diazocine-TATA **2** is connected in *meta*-position and thus interrupting conjugation [24,25]. Both diazocine-TATAs are equipped with methoxy groups, which serve as "reporter units" indicating the configuration of the molecules on metal surfaces [15]. In **1** the OMe group is attached *para* and in **2** the methoxy group is *meta* with respect to the azo group. Model calculations predict that the C_{phenyl}–O bonds in the *cis*-isomers thus are parallel, and in the *trans*-isomers orthogonal to the surface (Figure 1). Previous investigations have shown that IRRAS (infrared absorption reflection spectroscopy) in combination with the surface selection rules (stretching mode orthogonal to the surface→high intensity, parallel to the surface→low intensity) is a suitable method to determine the configuration and to measure kinetics on surfaces [15]. The C–O stretching frequencies proved to be ideal reporter signals to determine the configuration and to measure kinetics in monolayers of azo-TATAs on surfaces.

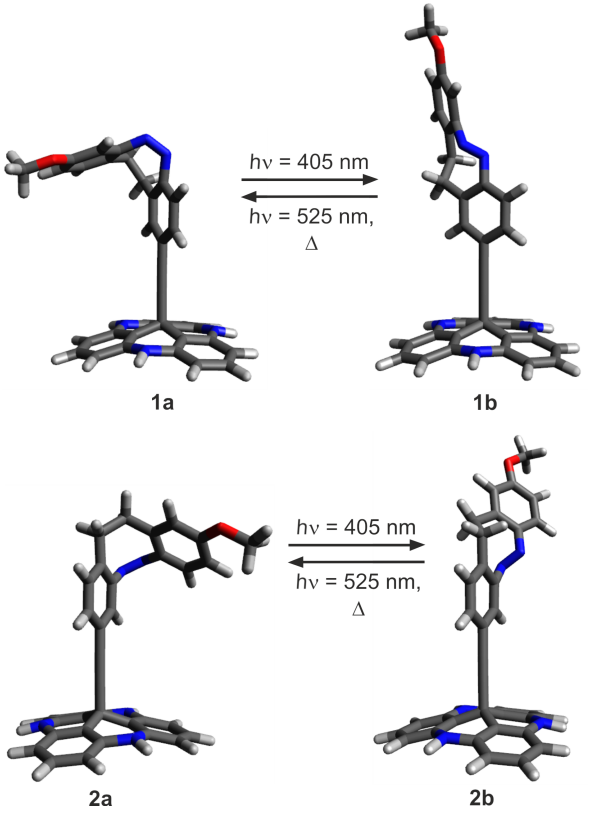

Figure 1: Structures of diazocine platform molecules (diazocine-TATAs) **1** and **2** in *cis* (**1a**, **2a**) and *trans*-configuration (**1b**, **2b**) (octyl side chains are replaced by protons for simplification). The *cis*-diazocines (**1a**, **2a**) isomerize upon irradiation with 405 nm to the metastable *trans*-diazocines (**1b**, **2b**) and with 525 nm or thermally back to the *cis*-diazocines (**1a**, **2a**).

Results and Discussion

To obtain information on preferred conformations of **1** and **2** in their *cis* and *trans*-configurations and to predict thermodynamic and kinetic stabilities, we performed DFT calculations at the M06-2X/def2-TZVP level of theory (Table 1, for details see Supporting Information File 1, chapter VI). As expected for

diazocine-based molecules our calculations predict the *cis* configuration for both compounds as the thermodynamically most stable isomers. For the corresponding *trans*-configuration two different conformations were found: the twist and the chair structures. The twist conformation is about 2.5 kcal mol^{-1} more stable than the chair conformation. Our calculations predict reaction barriers (*trans*-twist→*cis*-boat) for both compounds of approximately 23 kcal mol^{-1} (96 kJ mol^{-1}). Obviously, the TATA platform and the ethynyl spacer have only marginal effects on the isomerization process. Hence, the diazocines **1** and **2** are ideal candidates to investigate the effect of bulk gold as a function of electronic coupling (conjugation) of the azo unit to gold.

Table 1: Calculated quantum chemical energies E_{rel} (M06-2X/def2-TZVP) of the twist and chair conformation of the *trans*-configuration of *para*-ethynyl-substituted diazocine **1b** (*para*-diazocine), and *meta*-diazocine **2b**, relative to the boat conformation of the *cis*-isomers **1a** and **2a**. $\Delta H^{\neq}$ are the calculated reaction barriers (*trans*-twist→*cis*-boat). All energies are given in kcal mol^{-1}.

	E_{rel} *trans* twist	E_{rel} *trans* chair	$\Delta H^{\neq}$
para-diazocine **1**	7.9	10.6	22.6
meta-diazocine **2**	8.0	10.3	23.0

The *para*-diazocine-TATA **1** was synthesized in a 5-step synthesis route (Scheme 1). Bromotoluene **3** was synthesized as described [26]. In a Sonogashira cross-coupling reaction acetylene-substituted toluene **5** was prepared from bromotoluene **3** with TMS-protected acetylene **4** (95%). The C–C bond formation of **5** and **6** to give dibenzoyl **7** was achieved with potassium butoxide and elemental bromine (9%) according to a literature procedure [27]. The *para*-ethynyldiazocine **8** was obtained by reduction of both nitro groups, followed by oxidation of the formed hydrazine (16%). The unprotected ethynyldiazocine **8** was deprotonated with potassium hydroxide and connected to the central carbon atom of the TATA platform **9** (synthesized according to Laursen and Krebs [28]) to obtain target *para*-diazocine mounted on the octyl-substituted TATA platform **1** (99%).

The synthesis of the *meta*-diazocine platform molecule **2** was achieved in a 4-step synthesis route (Scheme 2). Nitrotoluene **10** was synthesized as described in literature [29]. The reaction of ethynyltoluene **10** with methoxytoluene **11** gave dibenzoyl **12** (10%) according to the same procedure as for dibenzoyl **7** (Scheme 1). Diazocine **13** was obtained by reduction and oxidation in moderate yields (22%). The reaction of diazocine **13** with the TATA ion **9** gave the target diazocine **2** (88%, Scheme 2).

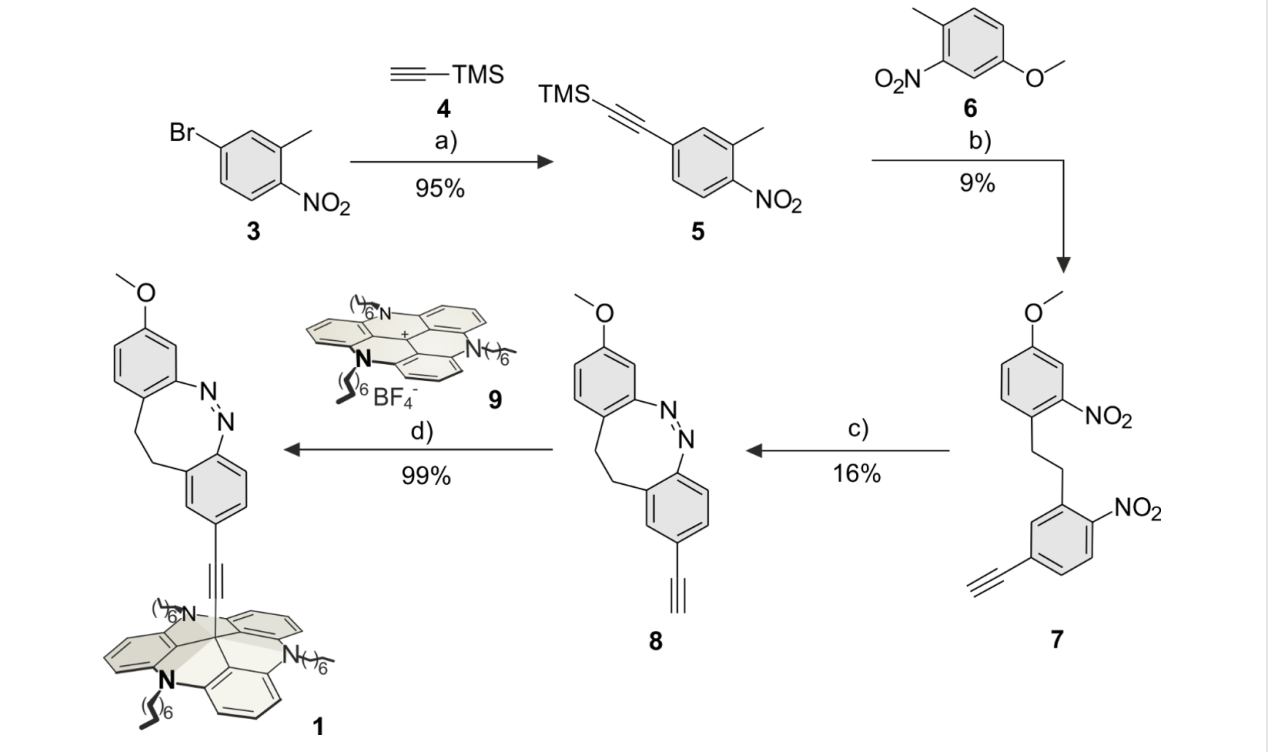

Scheme 1: Synthesis route of *para*-diazocine platform molecule **1**. a) $Pd(dppf)Cl_2$, Cu(I)I, Et_3N, 1 h, 60 °C; b) 1: KO*t*-Bu, THF, 3 min, 0 °C, N_2; 2: Br_2, 5 min, 0 °C; c) 1: $Ba(OH)_2$, Zn, EtOH, H_2O, 4.75 h, reflux; 2: 0.1 M NaOH/MeOH, Cu(II)Cl_2, 6 h, rt; d) KOH, THF, 3.5 h, reflux, N_2.

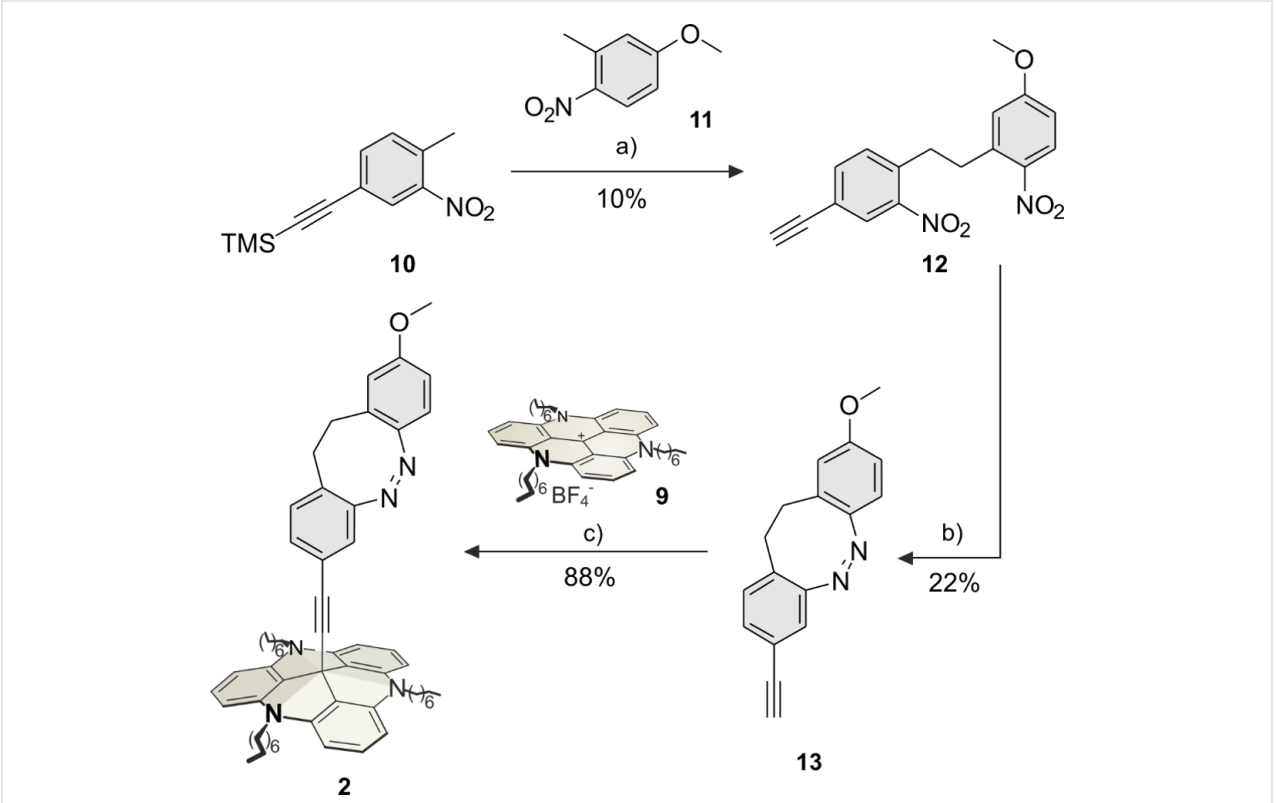

Scheme 2: Synthesis route of *meta*-diazocine platform **2**. a) 1: KO*t*-Bu, THF, 3 min, 0 °C, N_2; 2: Br_2, 5 min, 0 °C, N_2; b) 1: $Ba(OH)_2$, Zn, EtOH, H_2O, 4.75 h, reflux; 2: 0.1 M NaOH/MeOH, Cu(II)Cl_2, 13 h, rt; c) KOH, THF, 2 h, reflux, N_2.

The photophysical properties and the switching behavior of **1** and **2** were determined in solution (THF). The UV–vis spectra of **1** and **2** are shown before and after irradiation with 405 nm and 525 nm. Both diazocine-TATAs **1** and **2** exhibit similar UV spectra. The $n \rightarrow \pi^*$ transition of *cis*-**1** appears at 403 nm and at 494 nm in the *trans*-isomer. The corresponding absorption maxima in diazocine-TATA **2** are 409 nm (*cis*) and 493 nm (*trans*) (Figure 2).

The photostationary states of **1** and **2** were determined in toluene-d_8 by ^{1}H NMR measurements (Table 2). Optimal wavelengths for the *cis*→*trans* isomerization are 405 nm (**1**: 53%

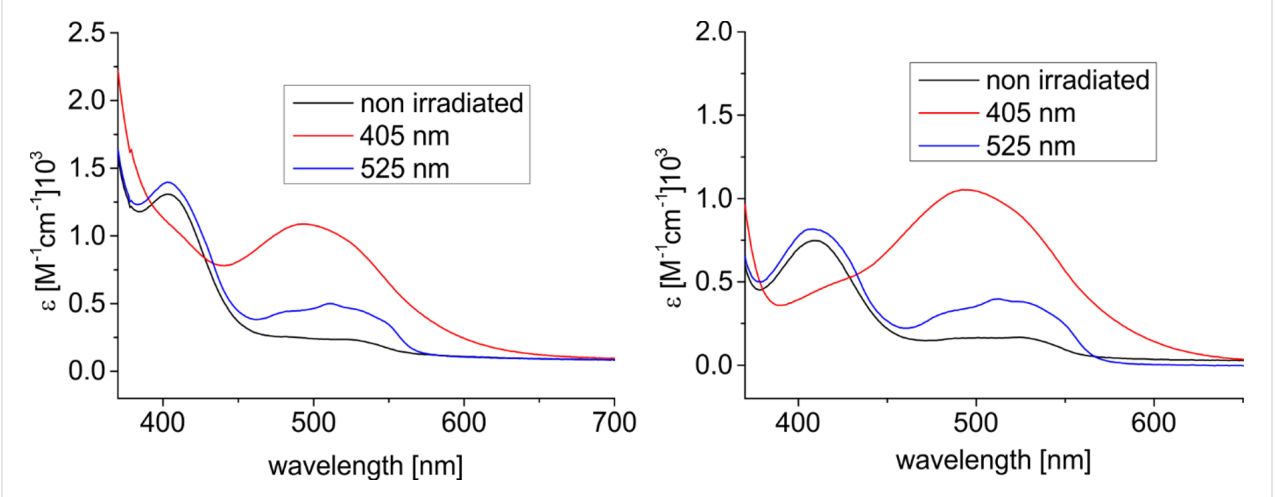

Figure 2: UV–vis spectra of **1** (left) and **2** (right) in THF at room temperature. Black: as synthesized, red: after irradiation with 405 nm, and blue: after irradiation with 525 nm.

trans, **2**: 65% *trans*). Back-isomerization to the *cis*-isomer with 525 nm is nearly quantitative. The half-lives (298 K) are similar for both systems (2.12 h for **1** and 2.32 h for **2**). The lack of conjugation between the azo function and the ethynyl spacer of **2** yields in a slightly higher half-life, which is in agreement with earlier results [11].

Table 2: Photostationary states (PSS) of *para*-diazocine-TATA **1** (2.05 mmol/L) and *meta*-diazocine-TATA **2** (2.27 mmol/L) upon irradiation with light of 405 nm, 525 nm and thermal isomerization half-life ($t_{1/2}$) determined with ^{1}H NMR spectroscopy (in deuterated toluene). The activation energies (E_a) are calculated from the linear fit of an Arrhenius plot.

	para-diazocine **1**	*meta*-diazocine **2**
PSS (405 nm)	53% (*trans*)	65% (*trans*)
PSS (525 nm)	93% (*cis*)	93% (*cis*)
$t_{1/2}$ (290.5 K)	5.27 h	5.76 h
$t_{1/2}$ (298 K)	2.12 h	2.32 h
$t_{1/2}$ (308 K)	0.69 h	0.73 h
E_A (kJ mol^{-1})	86.5	84.7

STM Measurements

The adsorption behavior of the diazocine-TATA molecules on Au(111) surfaces was studied by STM at room temperature (Figure 3). Adlayers of both compounds show a hexagonally ordered superstructure with lattice constants of **1** and **2** being (12.2 ± 0.6) Å and (12.1 ± 0.5) Å, respectively. Additionally, two rotational domains with an angle of (15 ± 4)° are observed. Altogether these parameters are in good agreement with a ($\sqrt{19} \times \sqrt{19}$) *R*23.4° superstructure which has been also observed in previous STM investigations of TATA and azobenzene-TATA molecules with octyl ligands [18,20,30].

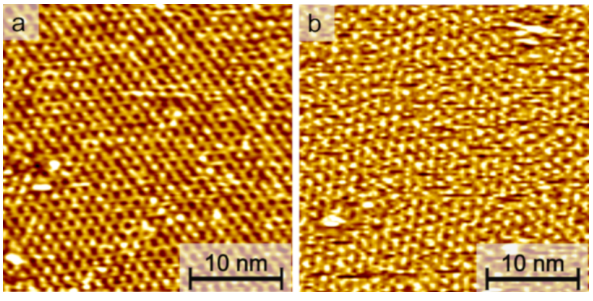

Figure 3: STM images (30 × 30 nm², U_{bias} = 0.3 V, I_t = 40 pA) of self-assembled monolayers of (a) compound **1** and (b) compound **2** on Au(111).

Conclusion

In summary, we present the syntheses of two different diazocines mounted on TATA platforms (**1**, **2**). The photochemical switching between the stable *cis* and metastable *trans*-isomers was investigated. Upon irradiation with light of 405 nm diazocine-TATAs **1** and **2** convert to their *trans*-configurations in moderate to good yields. The metastable *trans*-isomers of **1** and **2** isomerize back to the *cis*-isomer with half-lives of 2.12 h and 2.32 h at 298 K. The *trans*→*cis* activation energies with 86.5 kJ mol^{-1} for **1** and with 84.7 kJ mol^{-1} for **2** are similar to the structurally related azobenzenes [11]. Both diazocine-TATAs form highly ordered monolayers on Au(111) surfaces. Further studies will include IRRAS measurements to determine the *trans*→*cis* isomerization kinetics on Au(111) surfaces.

Experimental

For detailed experimental procedures, including NMR, UV–vis and MS spectra see Supporting Information File 1, chapters I–IV, for kinetic studies see Supporting Information File 1, chapter V.

Supporting Information

Supporting Information File 1

Analytical methods, experimental procedures, NMR and UV spectra, kinetic studies and DFT calculations.
[https://www.beilstein-journals.org/bjoc/content/supplementary/1860-5397-15-150-S1.pdf]

Acknowledgements

The authors gratefully acknowledge financial support by the Deutsche Forschungsgesellschaft within the Sonderforschungsbereich 677, “Function by Switching”.

ORCID® iDs

Roland Löw - https://orcid.org/0000-0002-3051-7831
Talina Rusch - https://orcid.org/0000-0001-8123-6792
Fynn Röhricht - https://orcid.org/0000-0001-9935-9256
Rainer Herges - https://orcid.org/0000-0002-6396-6991

Preprint

A non-peer-reviewed version of this article has been previously published as a preprint doi:10.3762/bxiv.2019.11.v1

References

1. Hauffe, K., Ed. *Katalyse;* DE GRUYTER: Berlin, New York, 1976; p 119. doi:10.1515/9783110829990
2. Ostbald, W. *Z. Phys. Chem.* **1894,** *15,* 705–706.
3. Oyama, S. T.; Somorjai, G. A. *J. Chem. Educ.* **1988,** *65,* 765–769. doi:10.1021/ed065p765
4. Shriver, D. F.; Atkins, P. W.; Langford, C. H. In *Anorganische Chemie,* 2nd ed.; Heck, J.; Kaim, W.; Weidenbruch, M., Eds.; Wiley-VCH: Weinheim, Germany, 1997; p 692.
5. Eyring, H. *J. Chem. Phys.* **1935,** *3,* 107–115. doi:10.1063/1.1749604

6. Gowenlock, B. G. *Q. Rev., Chem. Soc.* **1960,** *14,* 133–145. doi:10.1039/qr9601400133
7. Hauser, A. *Coord. Chem. Rev.* **1991,** *111,* 275–290. doi:10.1016/0010-8545(91)84034-3
8. Xie, C.-L.; Hendrickson, D. N. *J. Am. Chem. Soc.* **1987,** *109,* 6981–6988. doi:10.1021/ja00257a013
9. Harvey, J. N. *Phys. Chem. Chem. Phys.* **2007,** *9,* 331–343. doi:10.1039/b614390c
10. Schreiner, P. R.; Reisenauer, H. P.; Pickard IV, F. C.; Simmonett, A. C.; Allen, W. D.; Mátyus, E.; Császár, A. G. *Nature* **2008,** *453,* 906–909. doi:10.1038/nature07010
11. Schlimm, A.; Löw, R.; Rusch, T.; Röhricht, F.; Strunskus, T.; Tellkamp, T.; Sönnichsen, F.; Manthe, U.; Magnussen, O.; Tuczek, F.; Herges, R. *Angew. Chem., Int. Ed.* **2019,** *58,* 6574–6578. doi:10.1002/anie.201814342
12. Hartley, G. S. *J. Chem. Soc.* **1938,** 633–642. doi:10.1039/jr9380000633
13. Shinkai, S.; Kusano, Y.; Shigematsu, K.; Manabe, O. *Chem. Lett.* **1980,** *9,* 1303–1306. doi:10.1246/cl.1980.1303
14. Jung, U.; Schütt, C.; Filinova, O.; Kubitschke, J.; Herges, R.; Magnussen, O. *J. Phys. Chem. C* **2012,** *116,* 25943–25948. doi:10.1021/jp310451c
15. Jacob, H.; Ulrich, S.; Jung, U.; Lemke, S.; Rusch, T.; Schütt, C.; Petersen, F.; Strunskus, T.; Magnussen, O.; Herges, R.; Tuczek, F. *Phys. Chem. Chem. Phys.* **2014,** *16,* 22643–22650. doi:10.1039/c4cp03438d
16. Krekiehn, N. R.; Müller, M.; Jung, U.; Ulrich, S.; Herges, R.; Magnussen, O. M. *Langmuir* **2015,** *31,* 8362–8370. doi:10.1021/acs.langmuir.5b01645
17. Hagen, S.; Kate, P.; Peters, M. V.; Hecht, S.; Wolf, M.; Tegeder, P. *Appl. Phys. A: Mater. Sci. Process.* **2008,** *93,* 253–260. doi:10.1007/s00339-008-4831-5
18. Baisch, B.; Raffa, D.; Jung, U.; Magnussen, O. M.; Nicolas, C.; Lacour, J.; Kubitschke, J.; Herges, R. *J. Am. Chem. Soc.* **2009,** *131,* 442–443. doi:10.1021/ja807923f
19. Ulrich, S.; Jung, U.; Strunskus, T.; Schütt, C.; Bloedorn, A.; Lemke, S.; Ludwig, E.; Kipp, L.; Faupel, F.; Magnussen, O.; Herges, R. *Phys. Chem. Chem. Phys.* **2015,** *17,* 17053–17062. doi:10.1039/c5cp01447f
20. Kuhn, S.; Baisch, B.; Jung, U.; Johannsen, T.; Kubitschke, J.; Herges, R.; Magnussen, O. *Phys. Chem. Chem. Phys.* **2010,** *12,* 4481. doi:10.1039/b922882a
21. Duval, H. *Bull. Soc. Chim. Fr.* **1910,** *7,* 727.
22. Siewertsen, R.; Neumann, H.; Buchheim-Stehn, B.; Herges, R.; Näther, C.; Renth, F.; Temps, F. *J. Am. Chem. Soc.* **2009,** *131,* 15594–15595. doi:10.1021/ja906547d
23. Hartley, G. S. *Nature* **1937,** *140,* 281. doi:10.1038/140281a0
24. Yaliraki, S. N.; Ratner, M. A. *Ann. N. Y. Acad. Sci.* **2002,** *960,* 153–162. doi:10.1111/j.1749-6632.2002.tb03030.x
25. Mayor, M.; Büschel, M.; Fromm, K. M.; Lehn, J.-M.; Daub, J. *Ann. N. Y. Acad. Sci.* **2002,** *960,* 16–28. doi:10.1111/j.1749-6632.2002.tb03022.x
26. Wahhab, A.; Therrien, E. Small Molecule Inhibitors of Protein Arginine methyltransferases. PCT Pat. Appl. WO2008104077 A1, Feb 28, 2007.
27. Moormann, W.; Langbehn, D.; Herges, R. *Synthesis* **2017,** *49,* 3471–3475. doi:10.1055/s-0036-1590685
28. Laursen, B. W.; Krebs, F. C. *Chem. – Eur. J.* **2001,** *7,* 1773–1783. doi:10.1002/1521-3765(20010417)7:8<1773::aid-chem17730>3.0.co;2-f
29. Park, K.; Lee, B. M. Novel phenylethynyl benzamide glucokinase activator and method for preparing same. PCT Pat. Appl. WO2014112798 A1, Jan 16, 2013.
30. Lemke, S.; Ulrich, S.; Claußen, F.; Bloedorn, A.; Jung, U.; Herges, R.; Magnussen, O. M. *Surf. Sci.* **2015,** *632,* 71–76. doi:10.1016/j.susc.2014.08.028

License and Terms

BEILSTEIN JOURNAL OF ORGANIC CHEMISTRY

Supporting Information

for

Diazocine-functionalized TATA platforms

Roland Löw, Talina Rusch, Fynn Röhricht, Olaf Magnussen and Rainer Herges

Beilstein J. Org. Chem. **2019,** *15,* 1485–1490. doi:10.3762/bjoc.15.150

Analytical methods, experimental procedures, NMR and UV spectra, kinetic studies and DFT calculations

Table of Contents

I. Analytical equipment and methods

NMR Spectroscopy

NMR spectra were measured in deuterated solvents (Deutero). All compounds were characterized using ^{1}H and ^{13}C NMR spectroscopy. The signals were assigned using 2D spectroscopy. For ^{1}H and ^{13}C NMR assignment we performed HSQC and HMBC. The degree of deuteration is given in parentheses. ^{1}H NMR spectra in reference to the following signals:

chloroform-d (99.8%): δ = 7.26 ppm. (s)

acetone-d_6 (99.5%): δ = 2.05 ppm. (quint.)

The signal multiplicities are abbreviated as follows:

s: singlet, d: doublet, dd: double doublet, t: triplet,

Measurements were performed by the following instruments:

Bruker CABAV 500neo (^{1}H NMR: 500 MHz, ^{13}C NMR: 125 MHz, ^{29}Si NMR: 99 MHz)

Bruker AV 600 (^{1}H NMR: 600 MHz, ^{13}C NMR: 150 MHz)

IR spectroscopy

Infrared spectra were measured on a Perkin-Elmer 1600 Series FT-IR spectrometer with an A531-G Golden-Gate-Diamond-ATR-unit. Signals were abbreviated with w, m, s and for weak, medium and strong intensities. Broad signals are additionally labeled with br.

Mass spectrometry

The high resolution (HR) mass spectra were measured with an APEX 3 FT-ICR with a 7.05 T magnet by co. Bruker Daltonics. Electron impact (EI).

Chromatrography stationary phases

For column chromatography purifications silica gel (Merck, particle size 0.040–0.063 mm) was used. R_f values were determined by thin layer chromatography onPolygram® Sil G/UV254 (Macherey-Nagel, 0.2 mm particle size).

II. Experimental procedures

II.1 1-Methyl-2-nitro-5-(2-(trimethylsilyl)ethynyl)benzene (5)

In triethylamine (dry, 80 mL) 4-bromo-2-methyl-1-nitrobenzol [1] **3** (6.00 g, 27.8 mmol), trimethylsilylacetylene (5.21 mL, 36.1 mmol), $Pd(dppf)Cl_2$ (1.02 g, 1.39 mmol, 5%) and cupper(I) iodide (530 mg, 2.78 mmol, 10%) were suspended under nitrogen atmosphere and stirred for 1 h at 60 °C. The reaction solution was filtered over celite and the solvent was removed under reduced pressure. The crude product was purified via column chromatography (silica gel, dichloromethane) to obtain a grey solid (6.14 g, 26.3 mmol, 95%).

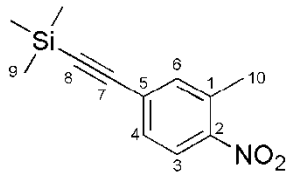

^{1}H NMR (500.1 MHz, $CDCl_3$, 298 K, TMS): δ = 7.93 (d, ^{3}J = 8.4 Hz, 1H, *H*-3), 7.43 (s, 1H, *H*-6), 7.40 (dd, ^{3}J = 8.5 Hz, ^{4}J = 1.6 Hz, 1H, *H*-4), 2.58 (s, 3H, *H*-10), 0.27 (s, 9H, *H*-9) ppm.

^{13}C NMR (125.8 MHz, $CDCl_3$, 298 K, CH_3Cl): δ = 148.43 (s, *C*-2), 136.21 (s, *C*-6), 133.98 (s, *C*-1), 130.30 (s, *C*-4), 128.47 (s, *C*-5), 124.93 (s, *C*-3), 102.91 (s, *C*-7), 99.44 (s, *C*-8), 20.53 (s, *C*-10), -0.12 (s, *C*-9) ppm.

^{29}Si NMR (99.4 MHz, $CDCl_3$, 298 K): δ = -16.99 ppm.

MS (EI, 70eV): m/z = 233.09 $[M]^+$.

IR (ATR): $\tilde{\nu}$ = 2957 (w), 2159 (w), 1601 (w), 1578 (w), 1515 (s), 1479 (w), 1348 (s), 1244 (s), 949 (m), 834 (vs), 756 (s), 698 (m), 663 (s), 450 (m) cm^{-1}.

m.p. = 76.5 °C.

HRMS (EI, 70 eV): m/z $[M]^+$ calcd. for $C_{12}H_{15}NO_2Si$: 233.08720; found: 233.08700.

II.2 4-Ethynyl-2-(4-methoxy-2-nitrophenethyl)-1-nitrobenzene (7)

In tetrahydrofurane (abs., 250 mL) 1-methyl-2-nitro-5-(2-(trimethylsilyl)ethynyl)benzene **5** (5.00 g, 21.4 mmol) and 4-methoxy-1-methyl-2-nitrobenzene (**6**, 2.97 mL, 21.4 mmol) were dissolved under nitrogen atmosphere and the solution was cooled to 0 °C. Potassium butoxide (3.40 g, 27.8 mmol) was added and stirred for 3 min before addition of bromine (1.42 mL, 27.8 mmol). After stirring for 5 min, the reaction was poured onto ice/water (500 mL). The solution was extracted with dichloromethane (3 × 300 mL) and the combined organic layers

were washed with saturated sodium thiosulfate solution and saturated sodium chloride solution and then dried over magnesium sulfate. The solvent was removed under reduced pressure and the crude product was purified via column chromatography (silica gel, cyclohexane/ethyl acetate, 2:1) to obtain a beige solid (615 mg, 1.89 mmol, 9%).

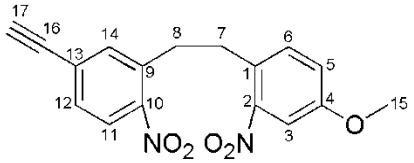

^{1}H NMR (500.1 MHz, $CDCl_3$, 298 K, TMS): δ = 7.92 (d, ^{3}J = 8.5 Hz, 1H, *H*-11), 7.55 (d, ^{4}J = 1.8 Hz, 1H, *H*-14), 7.50 (d, ^{4}J = 2.7 Hz, 1H, *H*-3), 7.47 (dd, ^{3}J = 8.4 Hz, ^{4}J = 1.8 Hz, 1H, *H*-12), 7.31 (d, ^{3}J = 8.5 Hz, 1H, *H*-6), 7.11 (dd, ^{3}J = 8.5 Hz, ^{4}J = 2.7 Hz, 1H, *H*-5), 3.87 (s, 3H, *H*-15), 3.30 (s, 1H, *H*-17), 3.23-3.13 (m, 4H, *H*-7, *H*-8) ppm.

^{13}C NMR (125.8 MHz, $CDCl_3$, 300 K, TMS): δ = 158.61 (s, *C*-4), 149.43 (s, *C*-2), 148.63 (s, *C*-10), 136.49 (s, *C*-9), 136.01 (s, *C*-14), 133.27 (s, *C*-6), 130.94 (s, *C*-12), 127.76 (s, *C*-1), 127.59 (s, *C*-13), 124.98 (s, *C*-11), 120.28 (s, *C*-5), 109.35 (s, *C*-3), 81.55 (s, *C*-17), 55.85 (s, *C*-15), 34.36 (s, *C*-8), 33.79 (s, *C*-7) ppm.

MS (EI, 70eV): m/z = 326.08 $[M]^+$.

IR (ATR): $\tilde{\nu}$ = 3286 (m), 2939 (br. w), 1602 (s), 1573 (w), 1485 (vs), 1461 (m), 1309 (w), 1278 (s), 1245 (vs), 1156 (w), 1107 (w), 1037 (m), 898 (w), 865 (w), 812 (m), 658 (w), 616 (w) cm^{-1}.

m.p. = 104.1 °C.

HRMS (EI, 70 eV): m/z $[M]^+$ calcd. for $C_{17}H_{14}N_2O_5$: 326.09027; found: 326.09052.

II.3 (*Z*)-2-Ethynyl-8-methoxy-11,12-dihydrodibenzo[*c*,*g*][1,2]-diazocine (8)

In ethanol (100 mL) 4-ethynyl-2-(4-methoxy-2-nitrophenethyl)-1-nitrobenzene (**7**, 400 mg, 1.23 mmol) was dissolved, an aqueous solution of barium hydroxide $[Ba(OH)_2{\cdot}8H_2O]$ (1.16 g, 3.68 mmol) in H_2O (40 mL) and zinc powder (1.29 g, 19.7 mmol) were added. The reaction was refluxed for 4.75 h. The reaction mixture was filtered through celite and the solvent was removed under reduced pressure. The crude product was dissolved in dichloromethane, filtered through celite and the solvent was removed under reduced pressure. The crude product was dissolved in 0.1 M methanolic NaOH solution (120 mL), $CuCl_2$ (6.60 mg, 49.1 µmol) was added and air was bubbled through the solution for 6 h at room temperature. The reaction was neutralized with 1 M hydrogen chloride solution and saturated sodium bicarbonate solution

(150 mL) was added. The aqueous layer was extracted with dichloromethane (3 × 150 mL) and the solvent was removed under reduced pressure. The crude product was purified via column chromatography (silica gel, cyclohexane/ethyl acetate, 2/1) to obtain an orange solid (51.0 mg, 194 µmol, 16%).

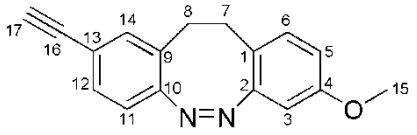

^{1}H NMR (500.1 MHz, acetone-d_6, 298 K, TMS): δ = 7.28 (dd, ^{3}J = 8.1 Hz, ^{4}J = 1.7 Hz, 1H, *H*-12), 7.20 (d, ^{4}J = 1.6 Hz, 1H, *H*-14), 6.97 (d, ^{3}J = 8.4 Hz, 1H, *H*-6), 6.83 (d, ^{3}J = 8.1 Hz, 1H, *H*-11), 6.61 (dd, ^{3}J = 8.4 Hz, ^{4}J = 2.6 Hz, 1H, *H*-5), 6.39 (d, ^{4}J = 2.7 Hz, 1H, *H*-3), 3.71 (s, 3H, *H*-15), 3.59 (s, 1H, *H*-17), 2.87-2.81 (m, 4H, *H*-7, *H*-8) ppm.

^{13}C NMR (125.8 MHz, acetone-d_6, 298 K, acetone): δ = 159.44 (s, *C*-4), 157.41 (s, *C*-2), 156.85 (s, *C*-10), 134.12 (s, *C*-14), 131.82 (s, *C*-6), 131.10 (s, *C*-12), 130.21 (s, *C*-9), 121.72 (s, *C*-13), 120.61 (s, *C*-1), 119.68 (s, *C*-11), 113.61 (s, *C*-5), 104.60 (s, *C*-3), 83.52 (s, *C*-16), 79.25 (s, *C*-17), 55.66 (s, *C*-15), 31.86 (s, *C*-8), 31.10 (s, *C*-7) ppm.

MS (EI, 70eV): m/z = 262.11 $[M]^{+}$.

IR (ATR)**:** $\tilde{\nu}$ = 3275 (m), 1605 (w), 1493 (s), 1393 (w), 1251 (m), 1143 (w), 1065 (w), 1030 (vs), 999 (s), 899 (w), 811 (vs), 671 (s), 616 (s), 509 (s) cm^{-1}.

m.p. = 133.8 °C.

HRMS (EI, 70 eV): m/z [M]+ calcd. for $C_{17}H_{14}N_2O$: 262.11061; found: 262.11019.

II.4 (*Z*)-12c-(8-Methoxy-11,12-dihydrodibenzo[c,g][(1,2]diazocin-2-yl)ethynyl-4,8,12-tri-*n*-octyl-4,8,12-triazatriangulene (1)

In tetrahydrofurane (abs., 30 mL) (*Z*)-2-ethynyl-8-methoxy-11,12-dihydrodibenzo(*c*,*g*)(1,2)-diazocine (**8**, 46.0 mg, 175 µmol), octyl-TATA-BF_4 [2] **9** (161 mg, 228 µmol) and powdered potassium hydroxide (105 mg, 1.87 mmol) were suspended under nitrogen atmosphere and refluxed for 3.5 h. The reaction was poured onto saturated sodium chloride solution (20 mL) and the aqueous layer was extracted with diethyl ether (3 × 30 mL). The combined organic layers were dried over magnesium sulfate and the solvent was removed under reduced pressure. The crude product was purified via column chromatography (aluminium oxide, basic, diethylether) to obtain an orange solid (153 mg, 174 µmol, 99%).

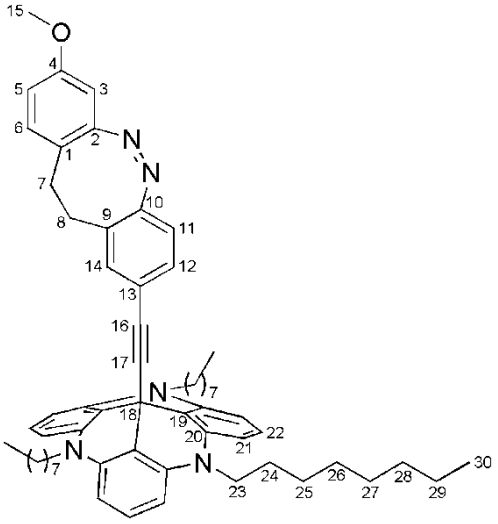

^{1}H NMR (500.1 MHz, acetone-d_6, 298 K, TMS): δ = 7.18 (t, ^{3}J = 8.3 Hz, 3H, *H*-22), 6.85-6.80 (m, 2H, *H*-6, *H*-12), 6.72 (d, ^{4}J = 1.6 Hz, 1H, *H*-14), 6.65-6.60 (m, 7H, *H*-11, *H*-21), 6.47 (dd, ^{3}J = 8.4 Hz, ^{4}J = 2.7 Hz, 1H, *H*-5), 6.26 (d, ^{4}J = 2.6 Hz, 1H, *H*-3), 3.99-3.93 (ps. t, 6H, *H*-23), 3.63 (s, 3H, *H*-15), 2.76-2.62 (m, 4H, *H*-7, *H*-8), 1.84-1.77 (ps. sechst., 6H, *H*-24), 1.52-1.45 (ps. pent., 6H, *H*-25), 1.41-1.21 (m, 24H, *H*-26, *H*-27, *H*-28, *H*-29), 0.90-0.85 (ps. t, 9H, *H*-30) ppm.

^{13}C NMR (125.8 MHz, acetone-d_6, 298 K, acetone): δ = 159.31 (s, *C*-4), 157.40 (s, *C*-2), 156.04 (s, *C*-10), 141.34 (s, *C*-20), 133.14 (s, *C*-14), 131.61 (s, *C*-6), 130.32 (s, *C*-12), 129.81 (s, *C*-9), 129.38 (s, *C*-22), 123.01 (s, *C*-13), 120.62 (s, *C*-1), 119.25 (s, *C*-11), 113.28 (s, *C*-5), 110.82 (s, *C*-19), 106.03 (s, *C*-21), 104.50 (s, *C*-3), 94.77 (s, *C*-17), 83.72 (s, *C*-16), 55.56 (s, *C*-15), 46.72 (s, *C*-23), 32.58 (s, *C*-29), 31.77 (s, *C*-8), 31.01 (s, *C*-7), 30.11 (s, C-26), 30.06 (s, C-27), 27.43 (s, *C*-25), 26.62 (s, *C*-24), 23.33 (s, *C*-28), 14.40 (s, *C*-30) ppm.

MS (MALDI-TOF, Cl-CCA): m/z = 879.6 $[M]^{+}$.

IR (ATR)**:** $\tilde{\nu}$ = 2924 (m), 2852 (m), 1614 (vs), 1579 (vs), 1482 (vs), 1457 (vs), 1393 (vs), 1267 (m), 1242 (s), 1167 (s), 1145 (m), 1036 (w), 895 (w), 809 (w), 772 (m), 748 (m), 726 (s), 657 (w) cm^{-1}.

II.5 4-Ethynyl-1-(5-methoxy-2-nitrophenethyl)-2-nitrobenzene (12)

In tetrahydrofurane (abs., 280 mL) 1-methyl-2-nitro-4-(2-(trimethylsilyl)ethynyl)-benzene (**10**) [3] (6.00 g, 25.7 mmol) and 4-methoxy-2-methyl-1-nitrobenzene (**11**, 6.45 g, 30.9 mmol) were dissolved under nitrogen atmosphere and cooled to 0 °C. Potassium butoxide (4.40 g, 36.0 mmol) was added and stirred for 3 min before addition of bromine (1.84 mL, 36.0 mmol). After stirring for 5 min, the reaction was poured onto ice/water (500 mL). The solution was

extracted with dichloromethane (3 × 300 mL) and the combined organic layers were washed with saturated sodium thiosulfate solution and saturated sodium chloride solution and then dried over magnesium sulfate. The solvent was removed under reduced pressure and the crude product was purified via column chromatography (silica gel, cyclohexane/ethyl acetate, 2/1) to obtain a beige solid (817 mg, 2.50 mmol, 10%).

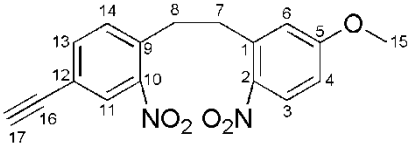

^{1}H NMR (600.1 MHz, $CDCl_3$, 298 K, TMS): δ = 8.10 (d, ^{3}J = 9.0 Hz, 1H, *H*-3), 8.06 (d, ^{4}J = 1.6 Hz, 1H, *H*-11), 7.63 (dd, ^{3}J = 8.0 Hz, 1H, *H*-13), 7.44 (d, ^{3}J = 7.9 Hz, 1H, *H*-14), 6.85 (dd, ^{3}J = 9.1 Hz, ^{4}J = 2.8 Hz, 1H, *H*-4), 6.83 (d, ^{4}J = 2.8 Hz, 1H, *H*-6), 3.88 (s, 3H, *H*-15), 3.30-3.21 (m, 4H, *H*-7, *H*-8), 3.18 (s, 1H, *H*-17) ppm.

^{13}C NMR (150.9 MHz, $CDCl_3$, 298 K, TMS): δ = 163.40 (s, *C*-5), 149.01 (s, *C*-10), 141.85 (s, *C*-2), 139.20 (s, *C*-1), 136.67 (s, *C*-9), 136.38 (s, *C*-13), 132.67 (s, *C*-14), 128.24 (s, *C*-11), 127.97 (s, *C*-3), 121.96 (s, *C*-12), 116.85 (s, *C*-4), 112.97 (s, *C*-6), 81.00 (s, *C*-16), 79.56 (s, *C*-17), 55.89 (s, *C*-15), 35.37 (s, *C*-7), 34.14 (s, *C*-8) ppm.

MS (EI, 70eV): m/z = 326.06 $[M]^+$.

$]^+$. **IR** (ATR): $\tilde{\nu}$ = 3274 (m), 1601 (m), 1586 (m), 1548 (w), 1521 (s), 1500 (s), 1455 (w), 1343 (m), 1327 (vs), 1298 (w), 1258 (vs), 1211 (m), 1077 /m), 1069 (m), 1030 (m), 896 (m), 870 (m), 831 (m), 804 (m), 762 (m), 699 (m) cm^{-1}.

m.p. = 127.1 °C.

HRMS (EI, 70 eV): m/z $[M]^+$ calcd. for $C_{17}H_{14}N_2O_5$: 326.09027; found: 326.09068.

II.6 (*Z*)-8-Ethynyl-2-methoxy-11,12-dihydrodibenzo[*c*,*g*][1,2]-diazocine (13)

In ethanol (80 mL) 4-Ethynyl-1-(5-methoxy-2-nitrophenethyl)-2-nitrobenzene (**12**, 396 mg, 1.21 mmol) was dissolved, an aqueous solution of barium hydroxide $[Ba(OH)_2{\cdot}8H_2O]$ (1.15 g, 3.64 mmol) in H_2O (34 mL) and zinc powder (1.27 g, 19.4 mmol) were added. The reaction was refluxed for 4.75 h. The reaction mixture was filtered through celite and the solvent was removed under reduced pressure. The crude product was dissolved in dichloromethane (50 mL), filtered through celite and the solvent was removed under reduced pressure. The crude product was dissolved in 0.1 M sodium hydroxide solution in methanol (120 mL), $CuCl_2$ (6.5 mg, 48 µmol) was added and air was bubbled through the solution for 13 h at room

temperature. The reaction was neutralized with 1 M hydrogen chloride solution and saturated sodium bicarbonate solution (200 mL) was added. The aqueous layer was extracted with dichloromethane and the solvent was removed under reduced pressure. The crude product was purified via column chromatography (silica gel, cyclohexane/ethyl acetate, 2:1) to obtain an orange solid (69.0 mg, 263 µmol, 22%).

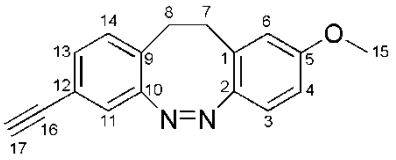

^{1}H NMR (500.1 MHz, $CDCl_3$, 298 K, TMS): δ = 7.15 (dd, ^{3}J = 7.9 Hz, ^{4}J = 1.6 Hz, 1H, *H*-13), 6.96 (d, ^{3}J = 7.8 Hz, 1H, *H*-14), 6.94 (d, ^{4}J = 1.6 Hz, 1H, *H*-11), 6.83 (d, ^{3}J = 8.7 Hz, 1H, *H*-3), 6.69 (dd, ^{3}J = 8.6 Hz, ^{4}J = 2.6 Hz, 1H, *H*-4), 6.49 (d, ^{4}J = 2.6 Hz, 1H, *H*-6), 3.71 (s, 3H, *H*-15), 3.03 (s, 1H, *H*-17), 2.85 (m, 4H, *H*-7, *H*-8) ppm.

^{13}C NMR (125.8 MHz, $CDCl_3$, 298 K, TMS): δ = 158.36 (s, *C*-5), 155.27 (s, *C*-10), 148.95 (s, *C*-2), 130.61 (s, *C*-13), 129.64 (s, *C*-14), 129.46 (s, *C*-9), 129.15 (s, *C*-1), 122.37 (s, *C*-11), 120.94 (s, *C*-3), 120.54 (s, *C*-12), 114.77 (s, *C*-6), 111.98 (s, *C*-4), 82.71 (s, *C*-16), 77.62 (s, C-17), 55.27 (s, *C*-15), 32.08 (s, *C*-7), 31.47 (s, *C*-8) ppm.

MS (EI, 70eV): m/z = 262.11 $[M]^+$.

IR (ATR): $\tilde{\nu}$ = 3265 (m), 2919 (br. w), 2851 (w), 1609 (w), 1575 (m), 1483 (s), 1464 (m), 1427 (m), 1308 (m), 1259 (vs), 1154 (m), 1110 (m), 1040 (m), 864 (m), 819 (m), 798 (vs), 703 (m), 613 (s), 586 (s) cm^{-1}.

m.p. = 112.1 °C.

HRMS (EI, 70 eV): m/z [M]+ calcd. for $C_{17}H_{14}N_2O$: 262.11061; found: 262.11016.

II.7 (*Z*)-12c-(9-Methoxy-11,12-dihydrodibenzo[c,g][1,2]diazocin-3-yl)ethynyl-4,8,12-tri-*n*-octyl-4,8,12-triazatriangulene (2)

In tetrahydrofurane (abs., 10 mL) (*Z*)-8-Ethynyl-2-methoxy-11,12-dihydrodibenzo(*c*,*g*)(1,2)-diazocine (**13**, 20.0 mg, 76.2 µmol), octyl-TATA-BF_4 [2] **9** (64.6 mg, 91.5 µmol) and powdered potassium hydroxide (34.2 mg, 610 µmol) were suspended under nitrogen atmosphere and refluxed for 2 h. The reaction was poured onto saturated sodium chloride solution (30 mL) and extracted with diethylether (3 × 25 mL). The combined organic layers were dried over magnesium sulfate and the solvent was removed under reduced pressure. The crude product

was purified via column chromatography (aluminium oxide, basic, diethylether) to obtain an orange solid (59.0 mg, 67.0 µmol, 88%).

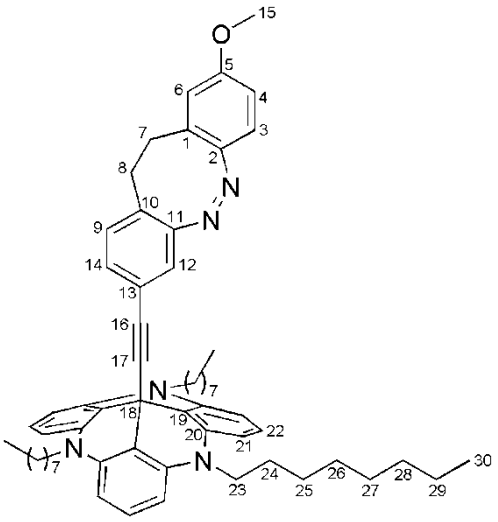

^{1}H NMR (500.1 MHz, acetone-d_6, 298 K, TMS): δ = 7.18 (t, ^{3}J = 8.24 Hz, 3H, *H*-22), 6.89 (d, ^{3}J = 8.0 Hz, 1H, *H*-9), 6.71 (dd, ^{3}J = 8.0 Hz, ^{4}J= 1.7 Hz, 1H, *H*-14), 6.68 (d, ^{3}J = 8.5 Hz, 1H, *H*-3), 6.65-6.60 (m, 7H, *H*-4, *H*-21), 6.52 (d, ^{4}J = 2.6 Hz, 1H, *H*-6), 6.44 (d, ^{4}J = 1.6 Hz, 1H, *H*-12), 3.99-3.93 (ps. t, 6H, *H*-23), 3.63 (s, 3H, *H*-15), 2.78-2.69 (m, 4H, *H*-7, *H*-8), 1.85-1.76 (ps. pent., 6H, *H*-24), 1.52-1.44 (ps. pent., 6H, *H*-25), 1.41-1.22 (m, 24H, *H*-26, *H*-27, *H*-28, *H*-29), 0.90-0.85 (ps. t, 9H, *H*-30) ppm.

^{13}C NMR (125.8 MHz, acetone-d_6, 298 K, acetone): δ = 159.25 (s, *C*-5), 156.54 (s, *C*-11), 150.00 (s, *C*-2), 141.36 (s, *C*-20), 130.52 (s, *C*-9), 130.38 (s, *C*-14), 130.27 (s, *C*-1), 129.44 (s, *C*-10), 129.38 (s, *C*-22), 122.89 (s, *C*-13), 121.52 (s, *C*-12), 121.15 (s, *C*-3), 115.65 (s, *C*-6), 112.54 (s, *C*-4), 110.86 (s, *C*-19), 106.05 (s, *C*-21), 95.09 (s, *C*-17), 83.45 (s, *C*-16), 55.48 (s, *C*-15), 46.67 (s, *C*-23), 32.57 (s, *C*-29), 32.38 (s, *C*-7), 31.73 (s, *C*-8), 30.10 (s, *C*-26), 30.05 (s, *C*-27), 27.43 (s, *C*-25), 26.65 (s, *C*-24), 23.32 (s, *C*-28), 14.40 (s, *C*-30) ppm.

MS (MALDI-TOF): m/z = 879.6 $[M]^{+}$.

IR (ATR): $\tilde{\nu}$ = 2924 (s), 2852 (m), 1614 (s), 1579 (vs), 1482 (vs), 1457 (vs), 1393 (vs), 1374 (m), 1243 (s), 1167 (s), 1039 (w), 911 (w), 807 (w), 772 (m), 750 (s), 724 (s), 657 (w) cm^{-1}.

III. NMR Spectra

III.1 1-Methyl-2-nitro-5-(2-(trimethylsilyl)ethynyl)benzene

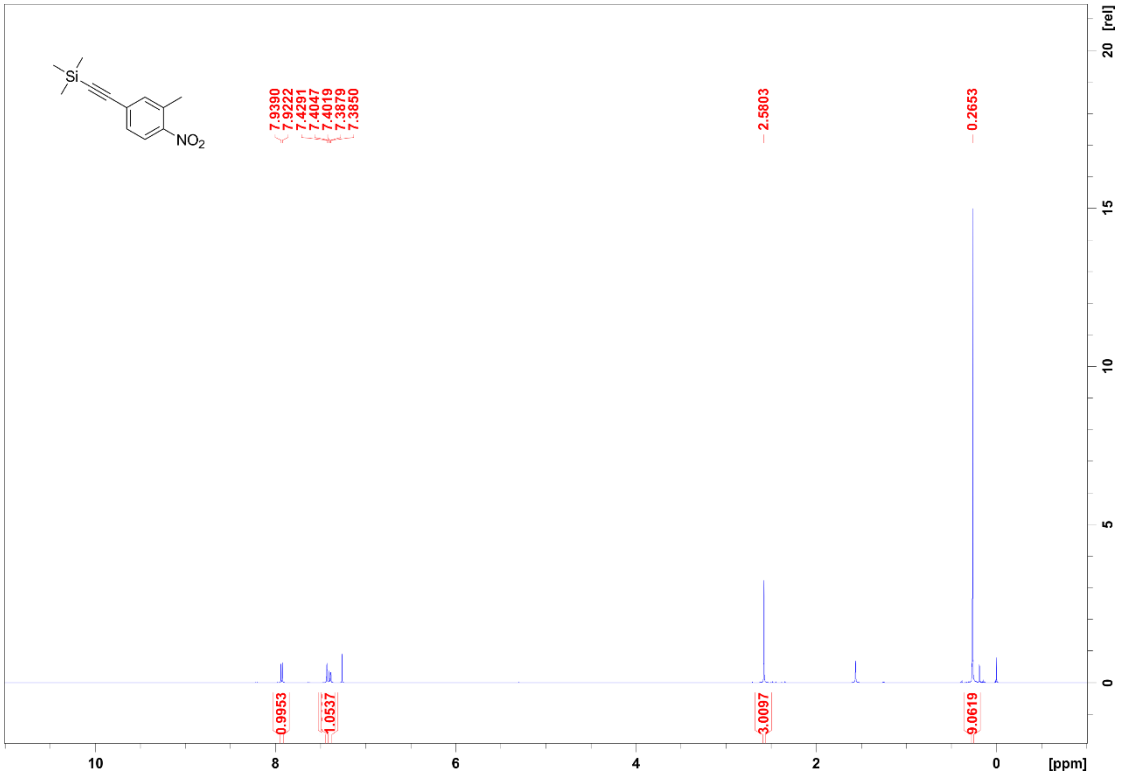

Figure S1. ^{1}H NMR spectrum (500.1 MHz, $CDCl_3$) of compound **5**.

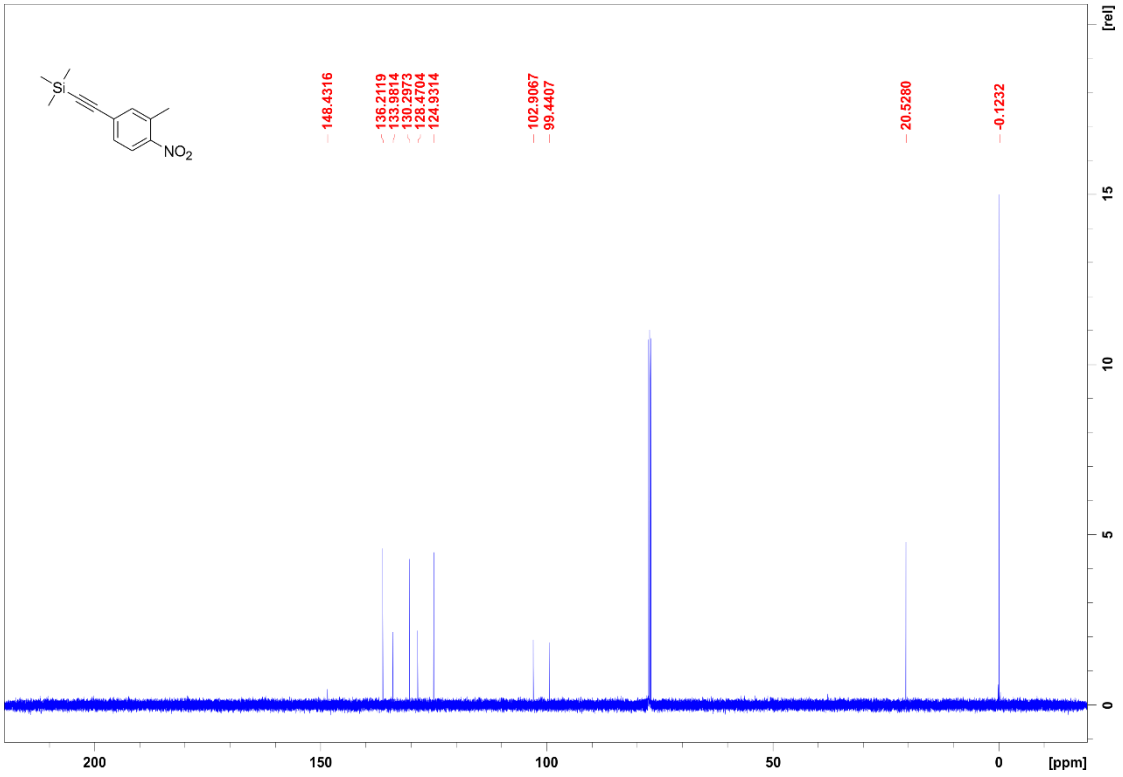

Figure S2. ^{13}C NMR spectrum (125.8 MHz, $CDCl_3$) of compound **5**.

III.2 4-Ethynyl-2-(4-methoxy-2-nitrophenethyl)-1-nitrobenzene

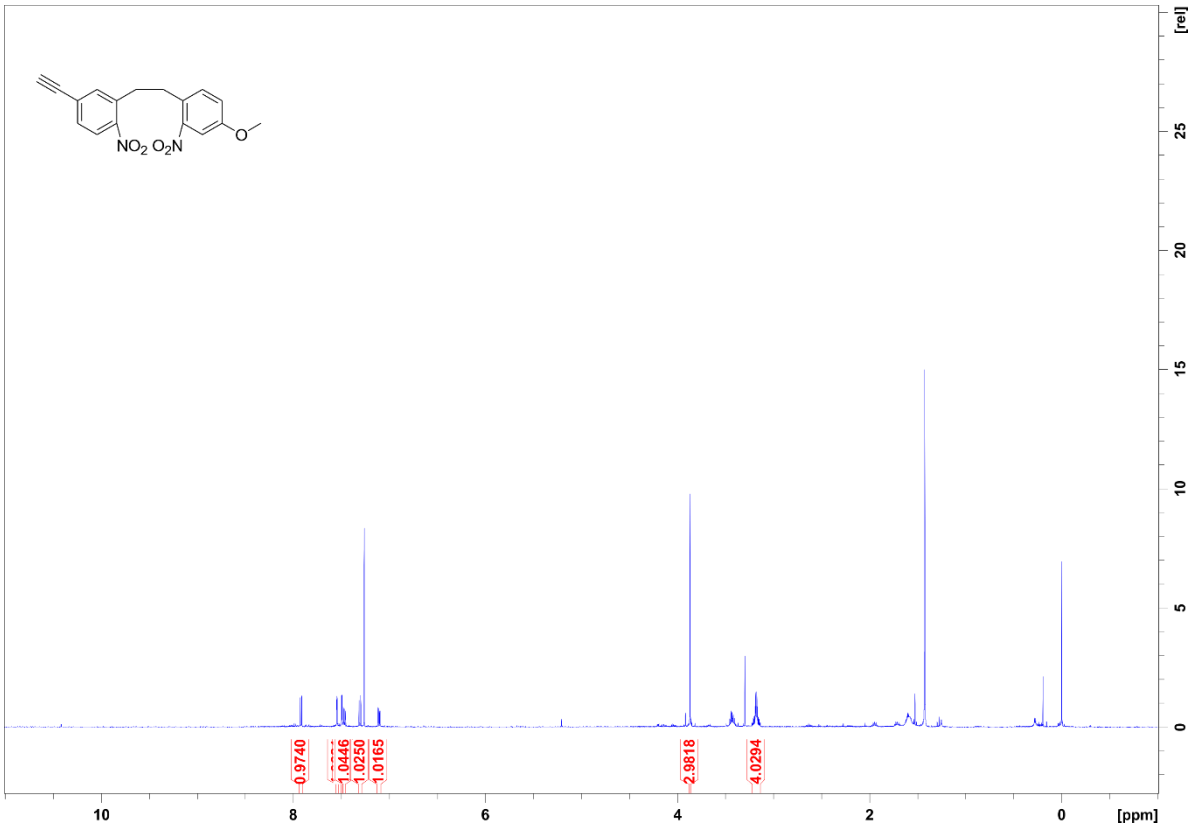

Figure S3. ^{1}H NMR spectrum (500.1 MHz, $CDCl_3$) of compound **7**.

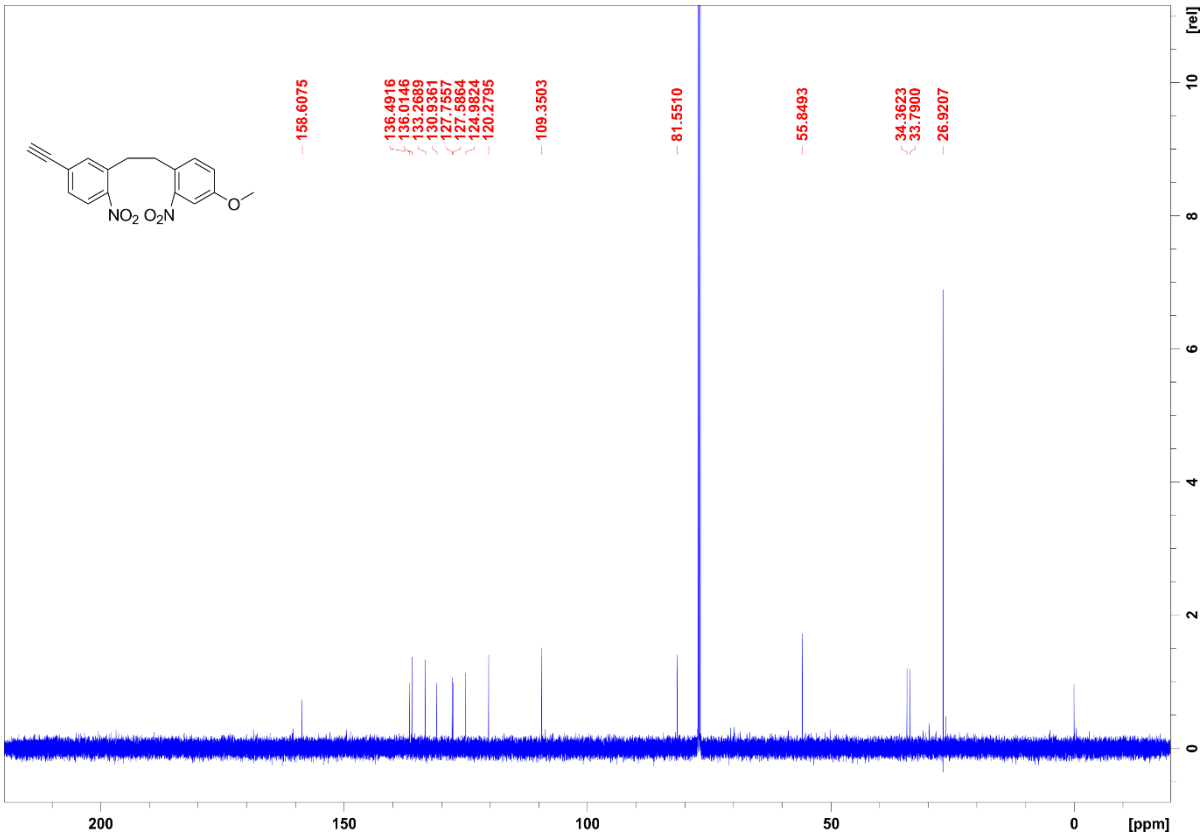

Figure S4. ^{13}C NMR spectrum (125.8 MHz, $CDCl_3$) of compound **7**.

III.3 (*Z*)-2-Ethynyl-8-methoxy-11,12-dihydrodibenzo[*c*,*g*][1,2]-diazocine

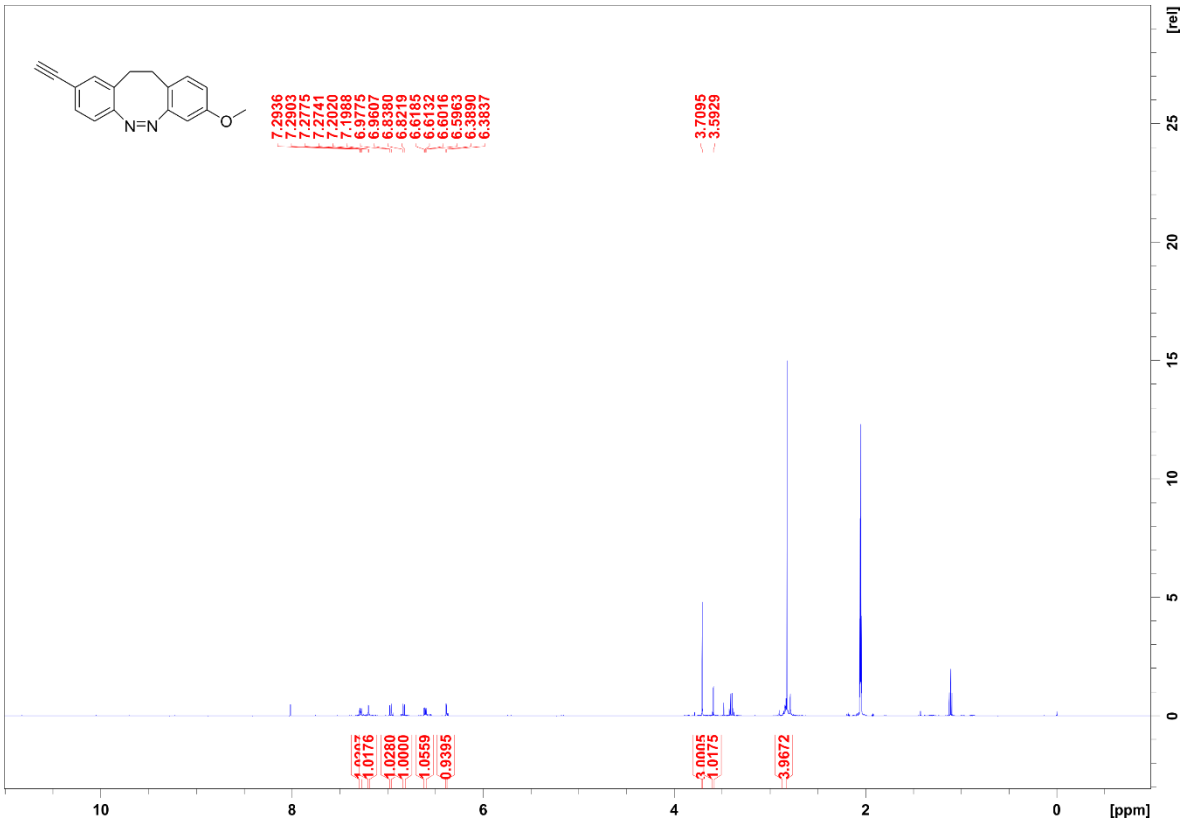

Figure S5. ^{1}H NMR spectrum (500.1 MHz, acetone-d_6) of compound **8**.

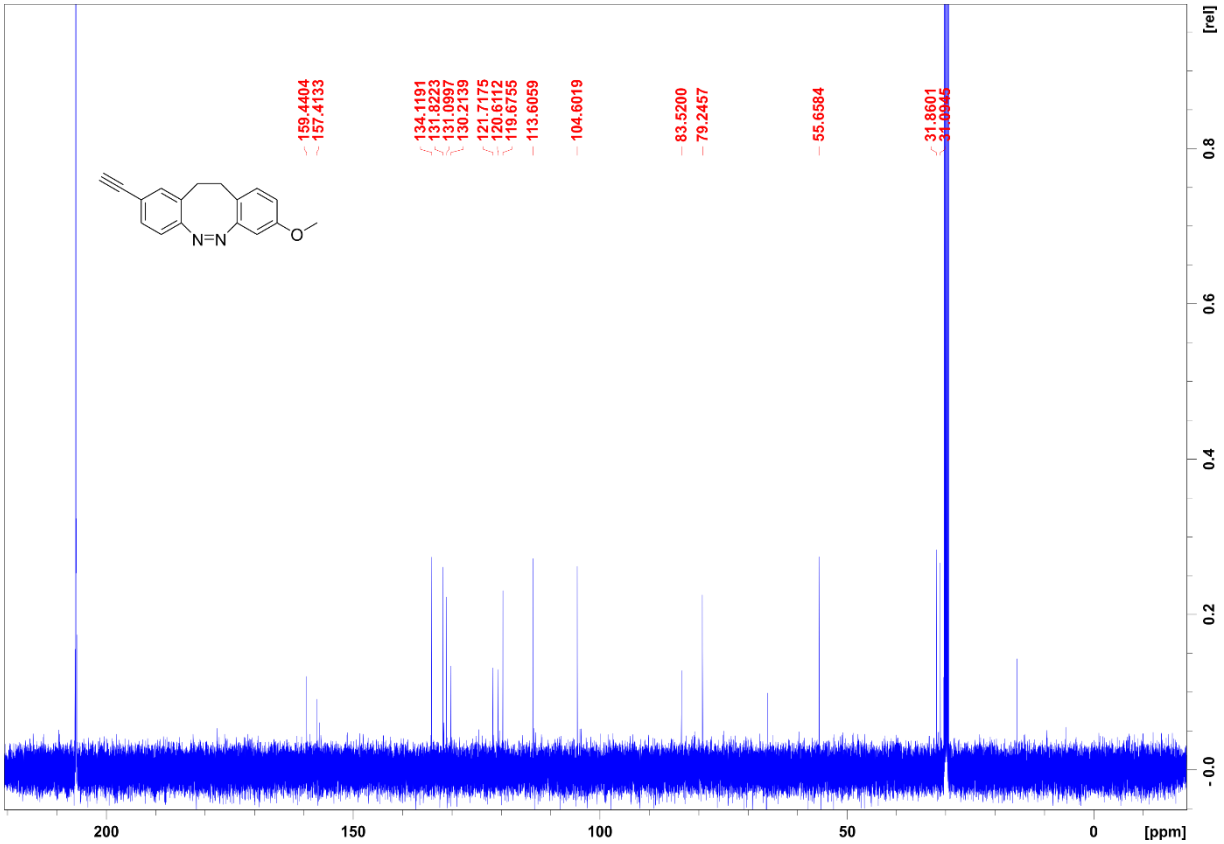

Figure S6. ^{13}C NMR spectrum (125.8 MHz, acetone-d_6) of compound **8**.

III.4 (*Z*)-12c-(8-Methoxy-11,12-dihydrodibenzo[c,g][1,2]diazocin-2-yl)ethynyl-4,8,12-tri-*n*-octyl-4,8,12-triazatriangulene

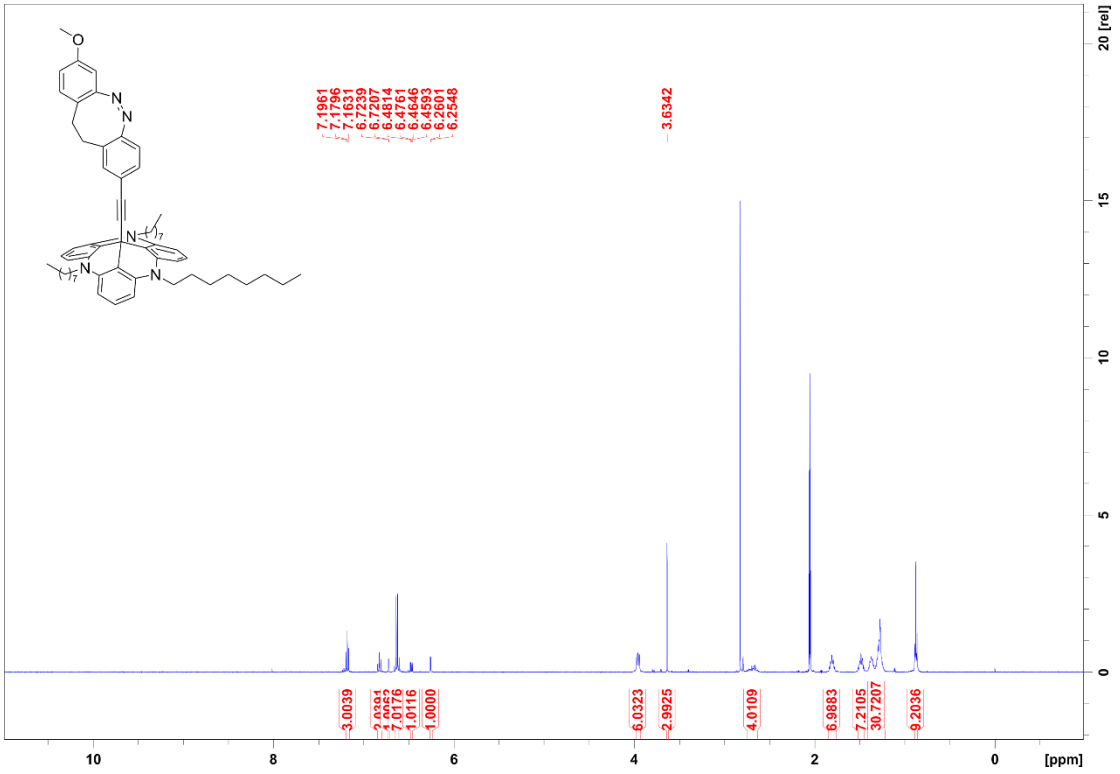

Figure S7. ^{1}H NMR spectrum (500.1 MHz, acetone-d_6) of compound **1**.

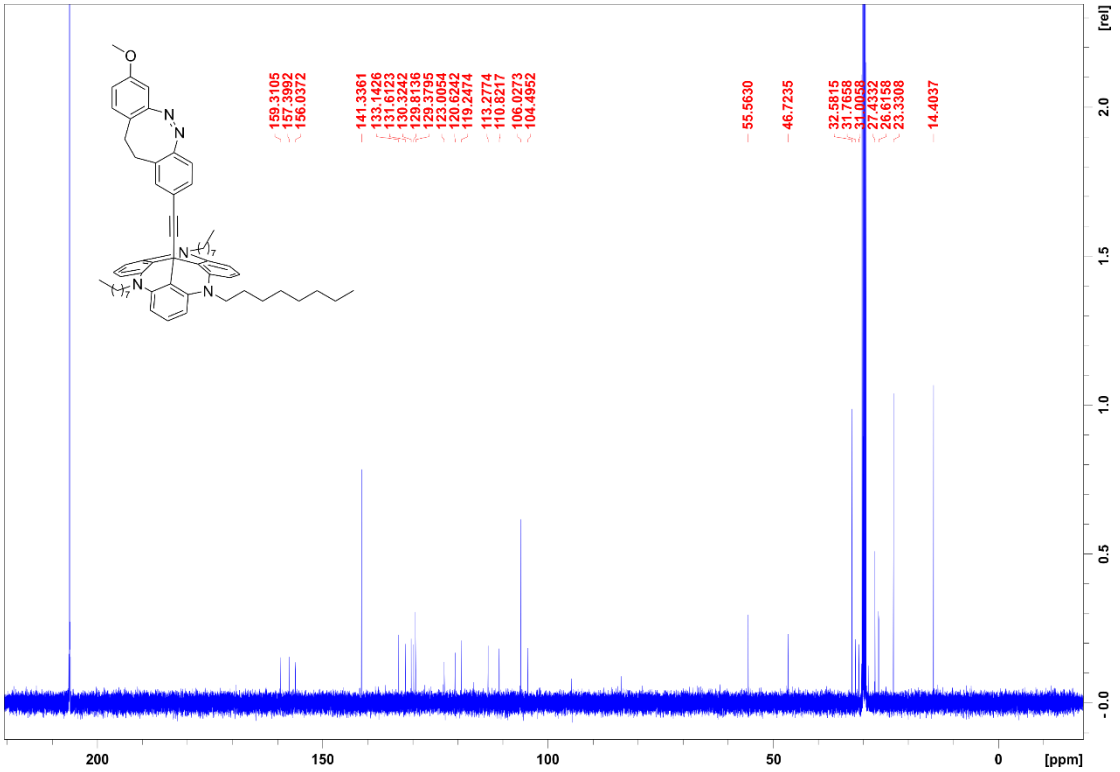

Figure S8. ^{13}C NMR spectrum (125.8 MHz, acetone-d_6) of compound **1**.

III.5 4-Ethynyl-1-(5-methoxy-2-nitrophenethyl)-2-nitrobenzene

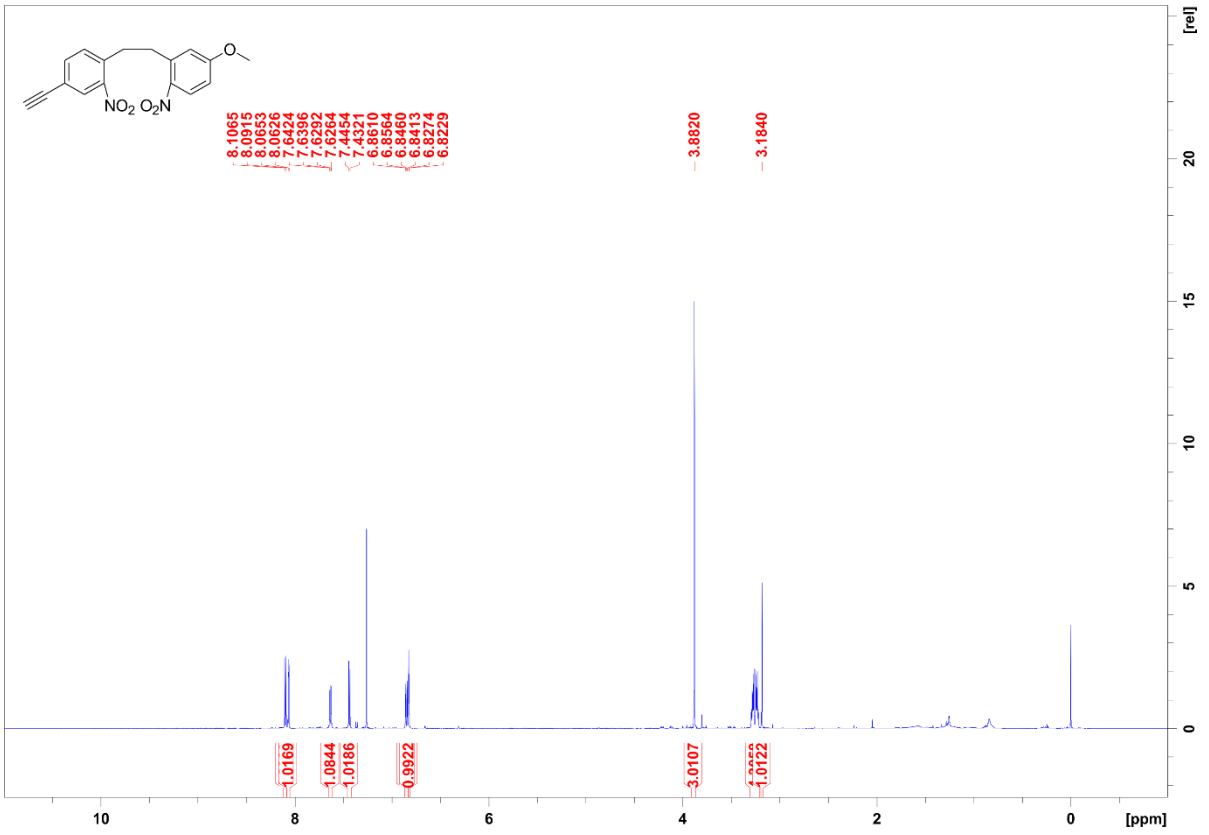

Figure S9. ^{1}H NMR spectrum (600.1 MHz, $CDCl_3$) of compound **12**.

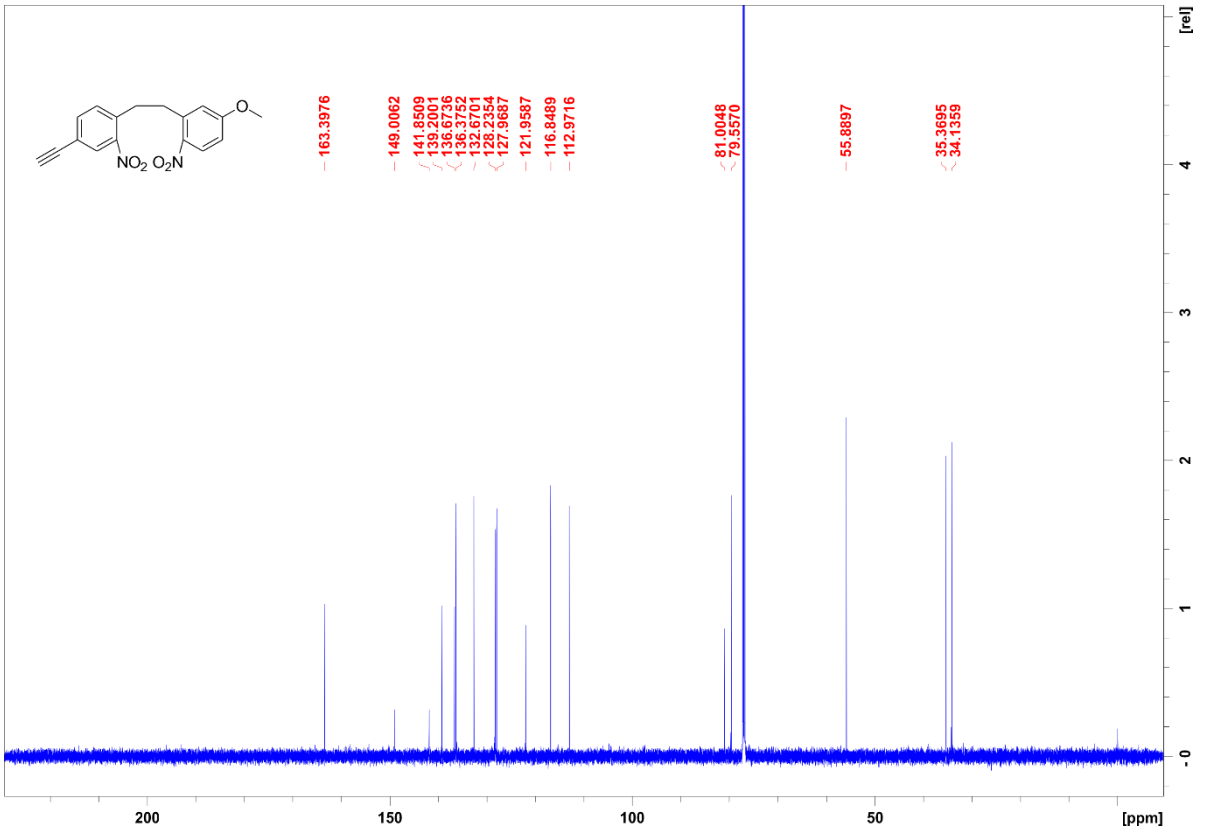

Figure S10. ^{13}C NMR spectrum (150.9 MHz, $CDCl_3$) of compound **12**.

III.6 (*Z*)-8-Ethynyl-2-methoxy-11,12-dihydrodibenzo[*c*,*g*][1,2]diazocine

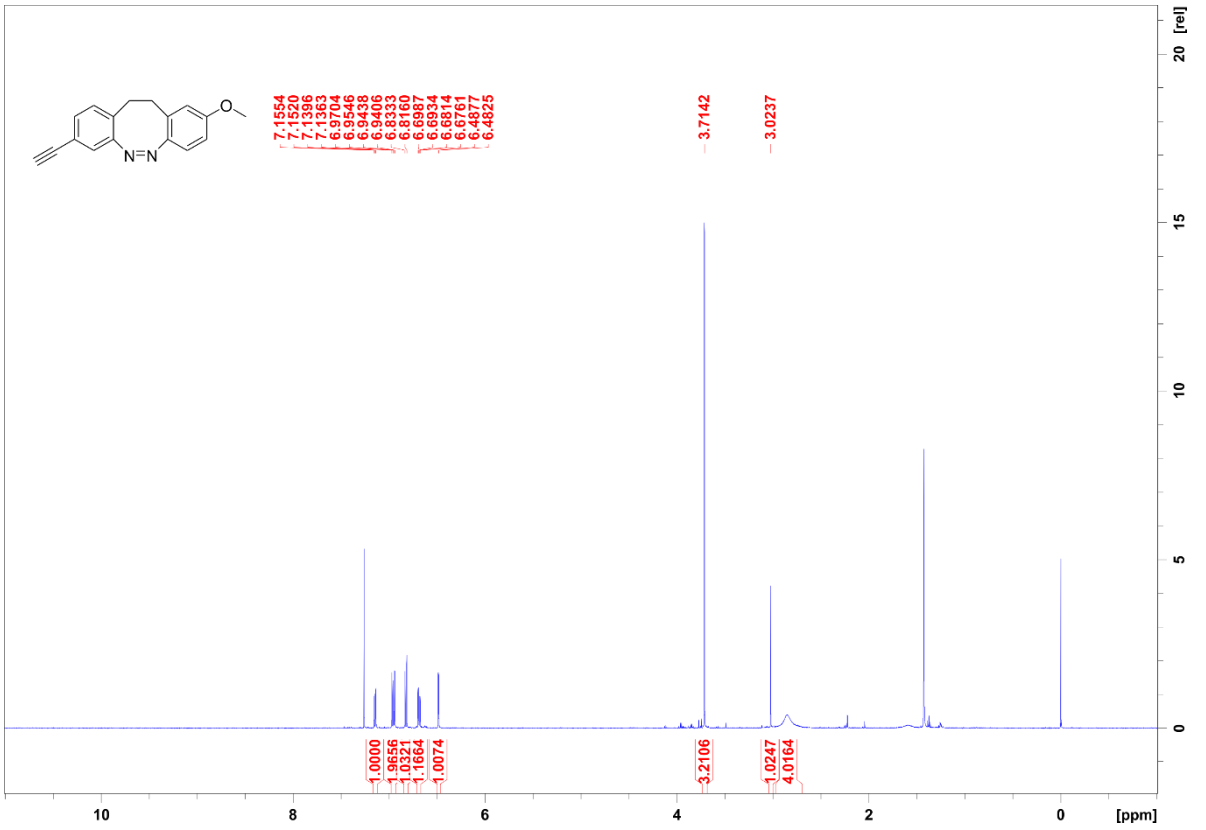

Figure S11. ^{1}H NMR spectrum (500.1 MHz, $CDCl_3$) of compound **13**.

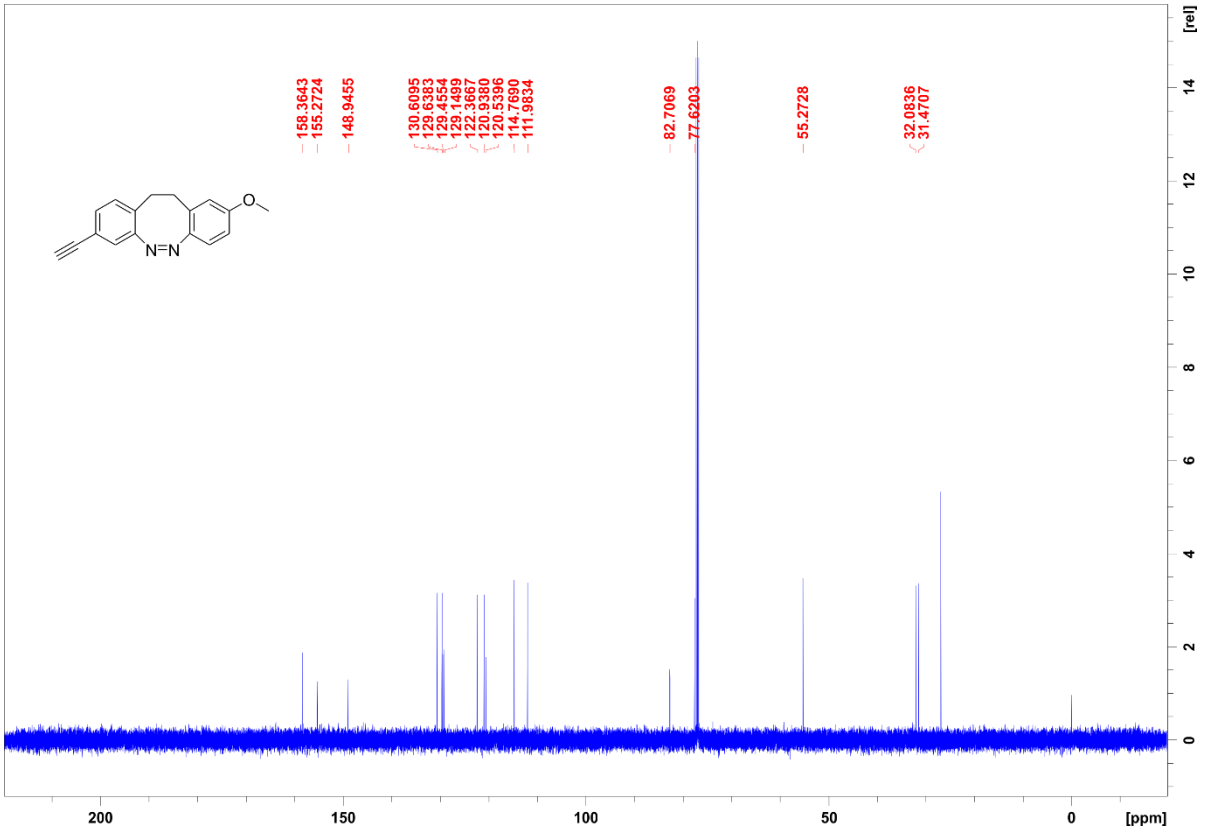

Figure S12. ^{13}C NMR spectrum (125.8 MHz, $CDCl_3$) of compound **13**.

III.7 (*Z*)-12c-(9-Methoxy-11,12-dihydrodibenzo[c,g][1,2]diazocin-3-yl)ethynyl-4,8,12-tri-*n*-octyl-4,8,12-triazatriangulene

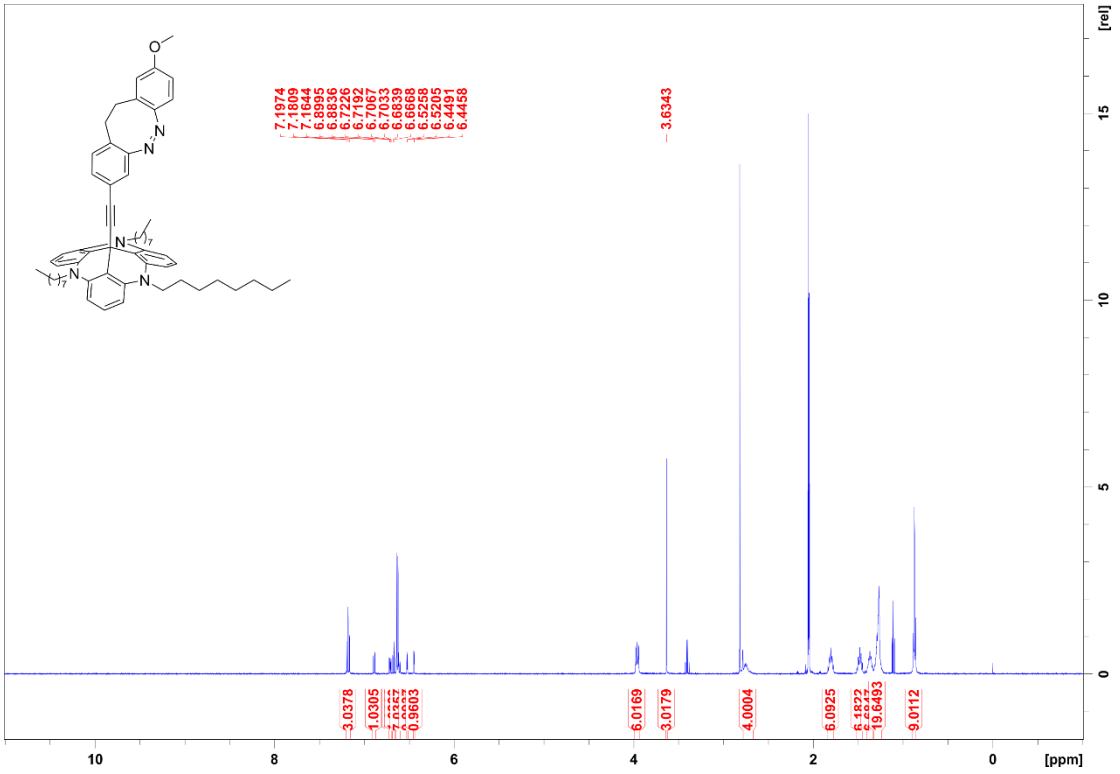

Figure S13. ^{1}H NMR spectrum (500.1 MHz, acetone-d_6) of compound **2**.

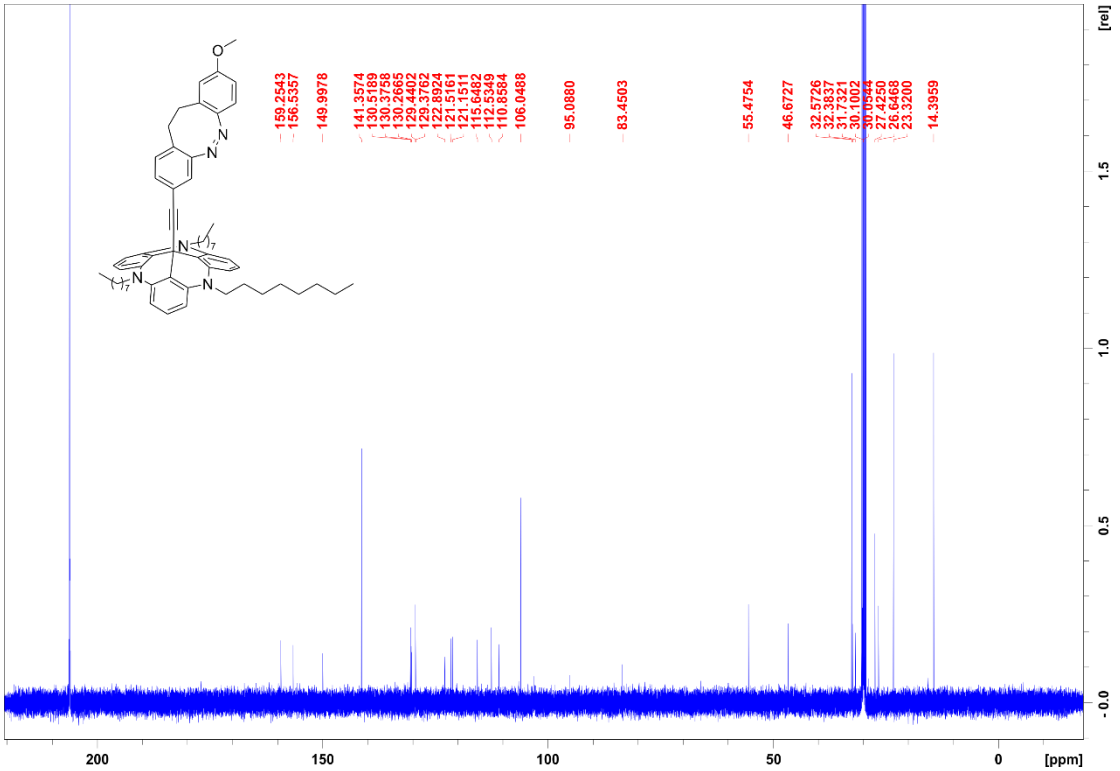

Figure S14. ^{13}C NMR spectrum (125.8 MHz, acetone-d_6) of compound **2**.

IV. UV–vis absorption spectra

IV.1 Methods

UV-Vis spectra were recorded on a PerkinElmer Lambda 650 Photospectrometer in a 1 cm path length quartz cuvette. Irradiation of UV–vis samples were carried out at 25 °C using a custom-made LED positioned at a distance of 1 cm from the sample.

IV.2 UV–vis spectra

Compound 1:

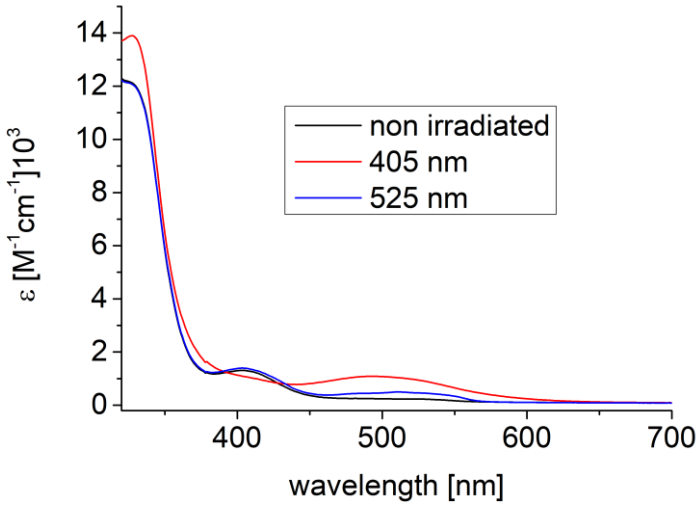

Figure S15. UV–vis spectra of compound **1** in tetrahydrofuran at room temperature (68 μmol/L). Upon irradiation with 405 nm and 525 nm.

Compound 2:

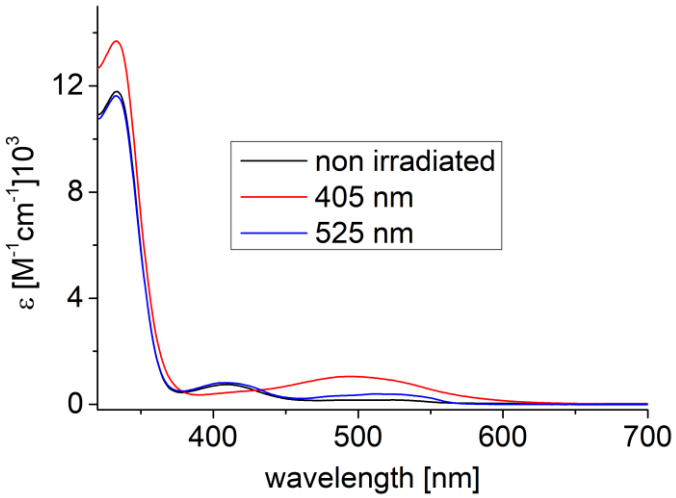

Figure S16. UV–vis spectra of compound **2** in tetrahydrofuran at room temperature (68 μmol/L). Upon irradiation with 405 nm and 525 nm.

V. Kinetic studies in solution by ^{1}H NMR spectroscopy

V.1 Thermal isomerization measurements by ^{1}H NMR

V.1.1 Compound 1: (*Z*)-12c-(8-methoxy-11,12-dihydrodibenzo[c,g][1,2]diazocin-2-yl)ethynyl-4,8,12-tri-*n*-octyl-4,8,12-triazatriangulene

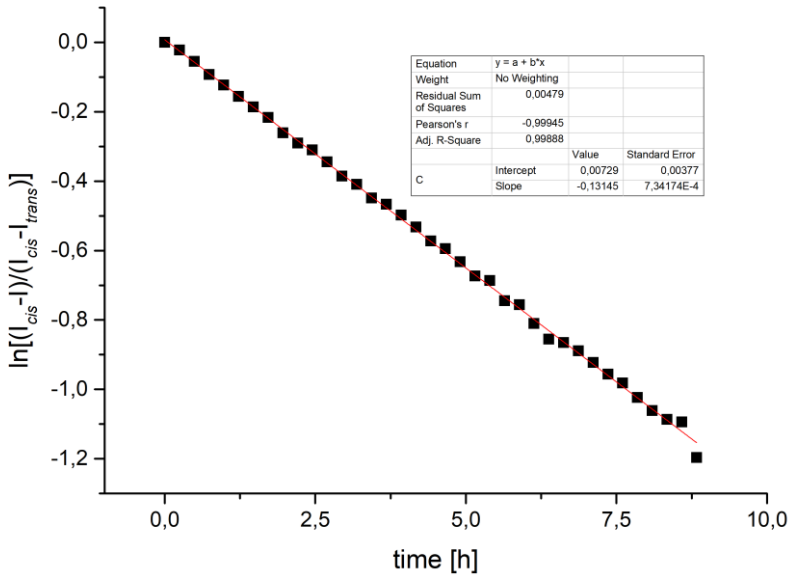

Figure S17. Determination of the thermal isomerization rate *k* of **1b**→**1a** by ^{1}H NMR spectroscopy (deuterated toluene, 290.5 K, 2.05 mmol/L). (I_{cis}-I): ^{1}H NMR integral of the CH_3 signal of the methoxy group at time *t*, (I_{cis}-I_{trans}) corresponding ^{1}H integral at *t* = 0. A rate constant of *k* = 0.131 [s^{-1}] was determined from a linear fit of the ln[(I_{cis}-I)/(I_{cis}-I_{trans})]/*t* curve. The half-life of **1** at 290.5 K in toluene was determined as 5.27 h.

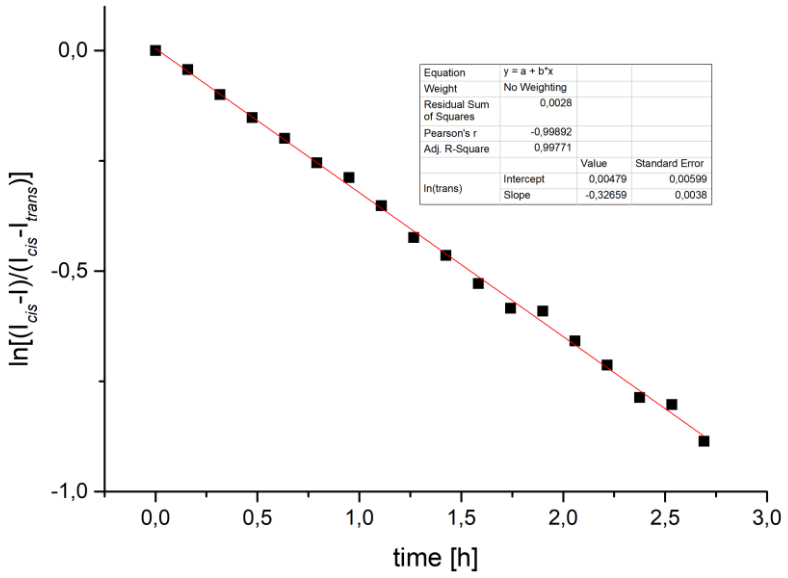

Figure S18. Determination of the thermal isomerization rate k of **1b**→**1a** by ^{1}H NMR spectroscopy (deuterated toluene, 298 K, 2.05 mmol/L). (I_{cis}-I): ^{1}H NMR integral of the CH_3 signal of the methoxy group at time *t*, (I_{cis}-I_{trans}) corresponding ^{1}H integral at *t* = 0. A rate constant of *k* = 0.327 [s^{-1}] was determined from a linear fit of the ln[(I_{cis}-I)/(I_{cis}-I_{trans})]/*t* curve. The half-life of **1** at 298 K in toluene was determined as 2.12 h.

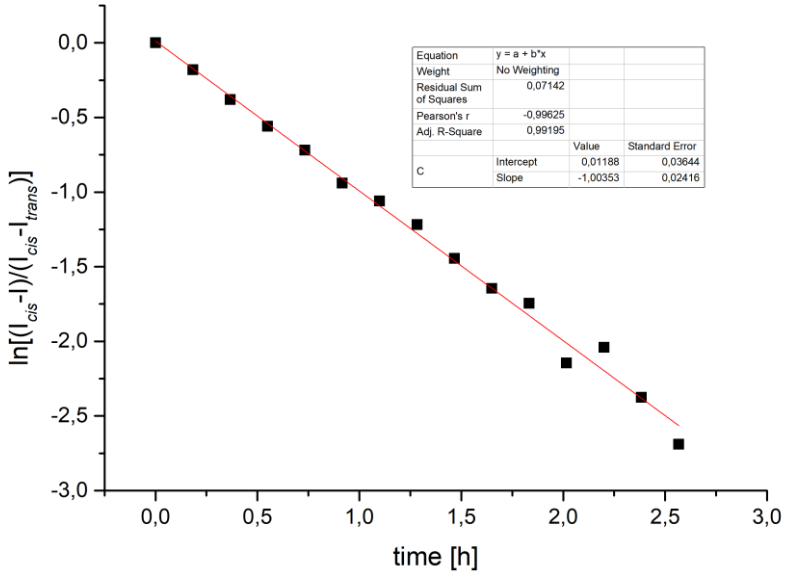

Figure S19. Determination of the thermal isomerization rate *k* of **1b**→**1a** by ^{1}H NMR spectroscopy (deuterated toluene, 308 K, 2.05 mmol/L). (I_{cis}-I): ^{1}H NMR integral of the CH_3 signal of the methoxy group at time *t*, (I_{cis}-I_{trans}) corresponding ^{1}H integral at *t* = 0. A rate constant of *k* = 1.00 [s^{-1}] was determined from a linear fit of the ln[(I_{cis}-I)/(I_{cis}-I_{trans})]/*t* curve. The half-life of **1** at 308 K in toluene was determined as 0.69 h.

V.1.2 Compound 2: (*Z*)-12c-(9-methoxy-11,12-dihydrodibenzo(c,g)(1,2)diazocin-3-yl)ethynyl-4,8,12-tri-*n*-octyl-4,8,12-triazatriangulene

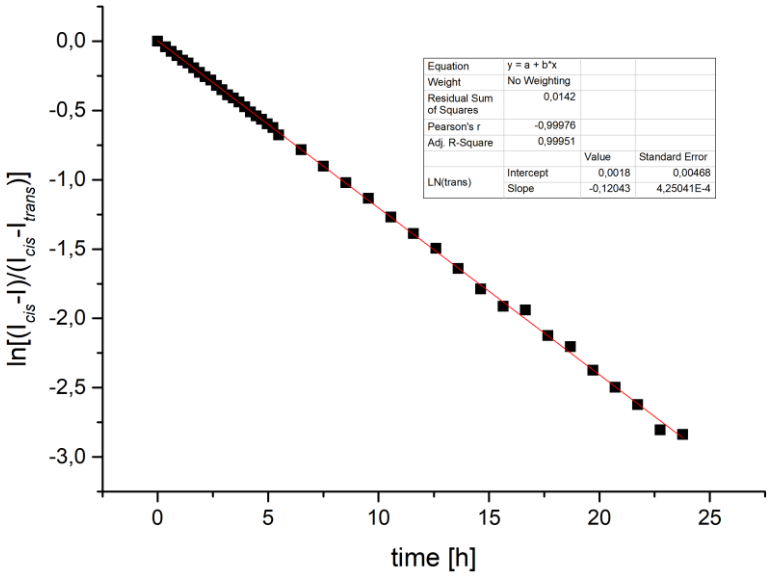

Figure S20. Determination of the thermal isomerization rate *k* of **2b**→**2a** by ^{1}H NMR spectroscopy (deuterated toluene, 290.5 K, 2.27 mmol/L). (I_{cis}-I): ^{1}H NMR integral of the CH_3 signal of the methoxy group at time *t*, (I_{cis}-I_{trans}) corresponding ^{1}H integral at *t* = 0. A rate constant of *k* = 0.120 [s^{-1}] was determined from a linear fit of the ln[(I_{cis}-I)/(I_{cis}-I_{trans})]/*t* curve. The half-life of **2** at 290.5 K in toluene was determined as 5.76 h.

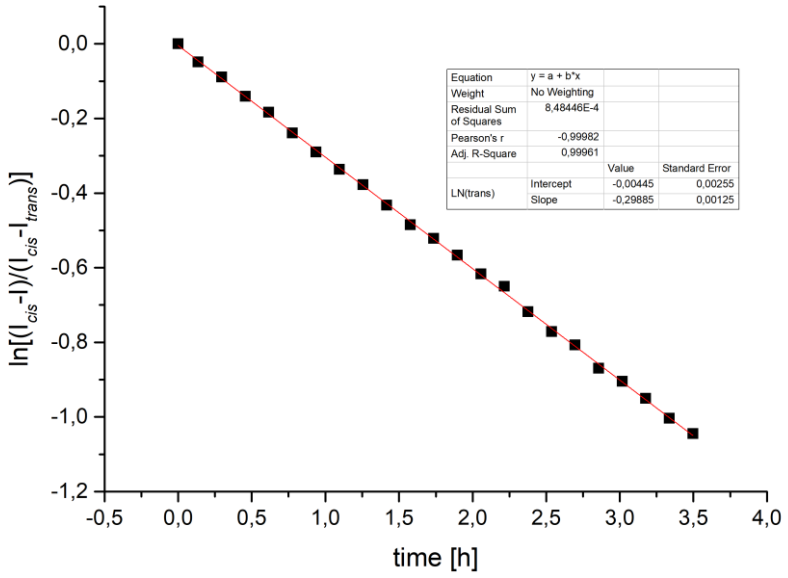

Figure S21. Determination of the thermal isomerization rate *k* of **2b**→**2a** by ^{1}H NMR spectroscopy (deuterated toluene, 298 K, 2.27 mmol/L). (I_{cis}-I): ^{1}H NMR integral of the CH_3 signal of the methoxy group at time *t*, (I_{cis}-I_{trans}) corresponding ^{1}H integral at *t* = 0. A rate constant of *k* = 0.299 [s^{-1}] was determined from a linear fit of the ln[(I_{cis}-I)/(I_{cis}-I_{trans})]/*t* curve. The half-life of **2** at 298 K in toluene was determined as 2.32 h.

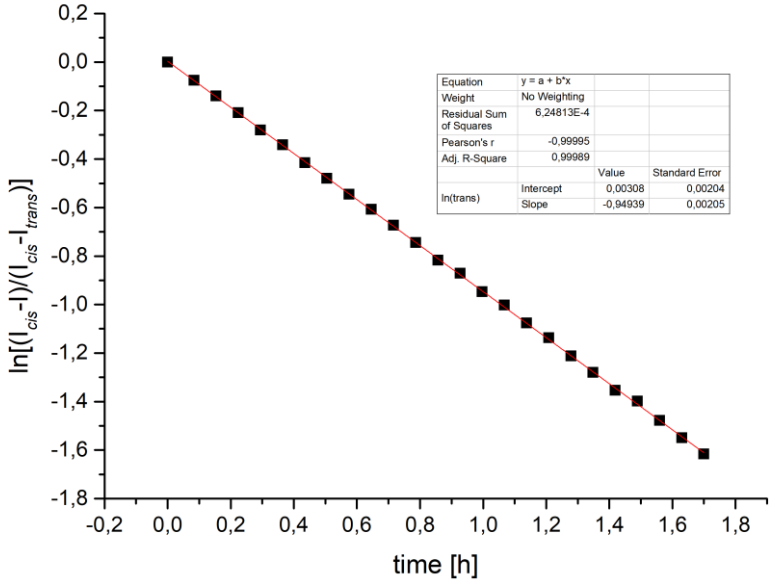

Figure S22. Determination of the thermal isomerization rate *k* of **2b**→**2a** by ^{1}H NMR spectroscopy (deuterated toluene, 308 K, 2.27 mmol/L). (I_{cis}-I): ^{1}H NMR integral of the CH_3 signal of the methoxy group at time *t*, (I_{cis}-I_{trans}) corresponding ^{1}H integral at *t* = 0. A rate constant of *k* = 0.949 [s^{-1}] was determined from a linear fit of the ln[(I_{cis}-I)/(I_{cis}-I_{trans})]/*t* curve. The half-life of **2** at 308 K in toluene was determined as 0.73 h.

V.2 Arrhenius Plots in solution

V.2.1 Compound 1: (*Z*)-12c-(8-methoxy-11,12-dihydrodibenzo[c,g][1,2]diazocin-2-yl)ethynyl-4,8,12-tri-*n*-octyl-4,8,12-triazatriangulene

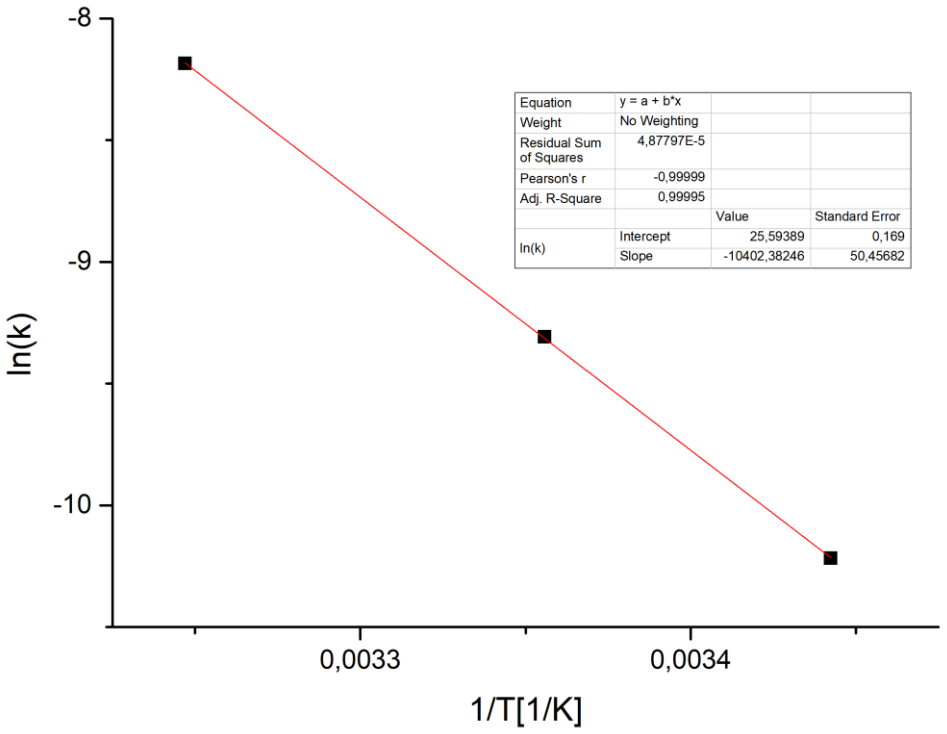

Figure S23. Arrhenius plot of the thermal isomerization of diazocine-TATA **1** in toluene-d_8 (2.05 mmol/L). An activation energy of 86.5 kJ/mol was determined from the linear fit.

V.2.2 Compound 2: (*Z*)-12c-(9-methoxy-11,12-dihydrodibenzo[c,g][1,2]diazocin-3-yl)ethynyl-4,8,12-tri-*n*-octyl-4,8,12-triazatriangulene

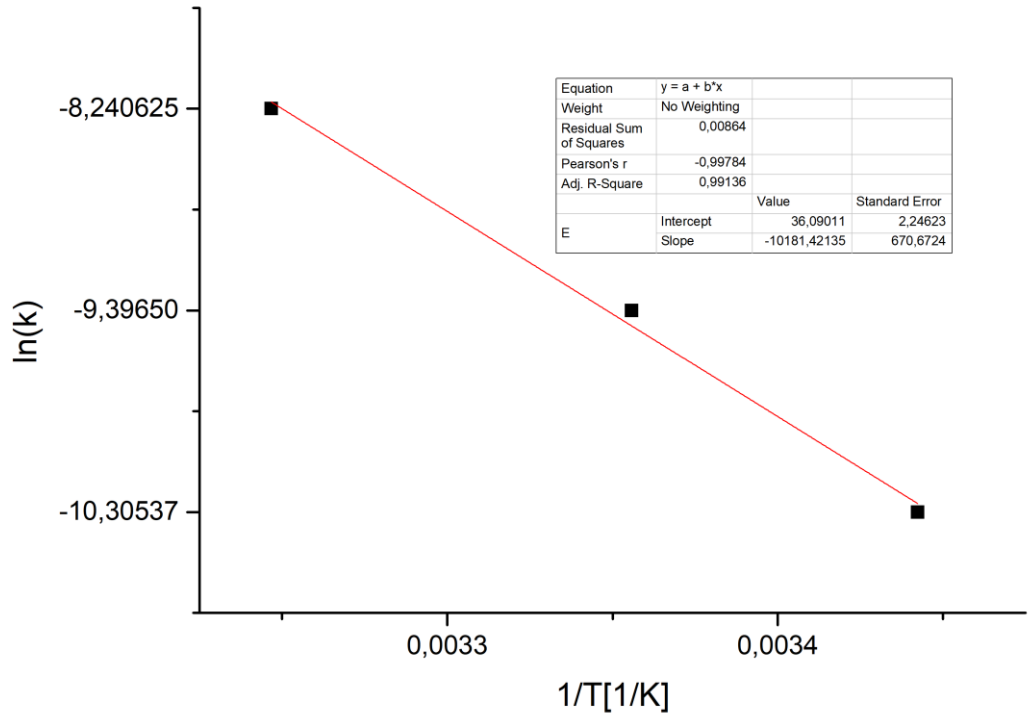

Figure S24. Arrhenius plot of the thermal isomerization of diazocine-TATA **1** in toluene-d_8 (2.27 mmol/L). An activation energy of 84.7 kJ/mol was determined from the linear fit.

VI. Calculations

The geometry optimizations were carried out using density functional theory with the Minnesota functional M06-2X [4] including Grimmes D3 [5] dispersion correction and the large triple zeta basis def2-TZVP [6]. This theoretical level performed well in Grimme's latest study on basic properties of a large set of organic molecules [7]. The calculations were performed with Turbomole7.2 [8], including the m4 grid (in Turbomole nomenclature) and resolution-of-identity (RI) with multipole accelerated RI-J (marij) to speed up the calculations. All stationary points are characterized by frequency calculations.

Coordinates

1a *cis para*-diazocine platform molecule

$E_{M062X\text{-}D3/def2TZVP}$ = -1735.7479869

Nimag = 0

C	0.8423706	1.1888220	-0.6747150	H	-3.5272321	4.6583588	1.1749579	C	-1.7241891	-4.1607832	2.4452278
C	-0.1996660	2.0068443	-1.1074483	C	3.9125498	-4.1448213	0.3982673	C	-0.3444466	-4.0889102	2.5578823
C	-0.1398925	3.3967441	-1.0422542	C	4.6345339	-4.2440201	-0.7810573	C	0.4109032	-3.7338574	1.4403335
C	1.0223796	3.9601501	-0.5091298	C	4.0471275	-4.0005035	-2.0127256	H	-3.4428446	-3.9956847	1.1611128
C	2.0852794	3.1594786	-0.1005557	C	2.7057736	-3.6212184	-2.0624485	N	1.7986504	-3.6621140	1.4954364
C	1.9973550	1.7838344	-0.1632224	C	1.9807273	-3.4750703	-0.8830149	H	2.2277130	-3.9774921	2.3498833
H	-1.0914091	1.5383759	-1.5056817	C	2.5715400	-3.7649591	0.3435754	N	2.0648118	-3.3781377	-3.2723777
H	2.9819589	3.6400909	0.2693096	H	4.3769412	-4.3609439	1.3520549	H	2.5885516	-3.5904101	-4.1056892
C	-1.3105728	4.1869891	-1.5808886	H	5.6758958	-4.5362731	-0.7404083	N	-2.2006654	-3.3137539	-1.1070004
C	-1.7461674	5.4307277	-0.7760201	H	4.6160706	-4.1032279	-2.9281033	H	-3.1844787	-3.5174147	-1.1741062
H	-1.0924538	4.4946436	-2.6076251	C	0.5801611	-2.9076635	-0.9274357	H	-2.3115962	-4.4356067	3.3117727
H	-2.1542639	3.4983177	-1.6405533	C	-0.0865050	-3.2926499	-2.2284278	H	0.1467189	-4.3085544	3.4973437
C	-1.5420640	5.2802242	0.7041029	C	-0.2242457	-3.4401278	0.2368146	H	-3.1193570	4.3721736	3.5712556
H	-1.1986834	6.3052325	-1.1276249	C	0.6802168	-3.4448358	-3.3805660	H	2.8166211	1.1625062	0.1714491
H	-2.8003327	5.6183047	-0.9827574	C	0.0558928	-3.6574386	-4.6095389	C	0.7345624	-0.2343858	-0.7608235
C	-0.2844198	5.5415248	1.2574631	C	-1.3272498	-3.7326336	-4.6601775	C	0.6573516	-1.4322857	-0.8353981
N	0.7413389	6.0835543	0.4087727	C	-2.1007592	-3.6268692	-3.5146184	O	-0.7193084	4.8615394	4.7621776
N	1.2900393	5.3763382	-0.4349021	C	-1.4719191	-3.4135487	-2.2880545	C	-1.7112975	4.4038811	5.6523843
C	-2.5394135	4.8649177	1.5709273	H	0.6499490	-3.7641717	-5.5083383	H	-2.5641030	5.0876124	5.6803824
C	-2.3125004	4.7020769	2.9341852	H	-1.8132084	-3.8967404	-5.6133066	H	-1.2455211	4.3680744	6.6333135
C	-1.0516817	4.9786282	3.4537246	H	-3.1789158	-3.7116775	-3.5641797	H	-2.0578418	3.4040073	5.3772583
C	-0.0360076	5.4225193	2.6090289	C	-1.6068547	-3.5584966	0.1271758				
H	0.9345117	5.6637019	3.0215445	C	-2.3664292	-3.9129133	1.2420571				

1b *trans-twist para*-diazocine platform molecule

$E_{M062x\text{-}D3/def2TZVP}$ = -1735.735229021

Nimag = 0

C	0.8401254	0.1948635	0.0360794	H	1.1741032	7.6128466	1.0894853	C	-1.8939926	-4.2381829	1.3740998
C	-0.2729335	1.0400154	-0.0243101	H	-2.6574324	6.7748141	-1.9084151	C	-2.6704482	-4.4080346	2.5200733
C	-0.1386510	2.4177595	-0.1184809	C	3.5638146	-5.2305087	1.7091597	C	-2.0402677	-4.5761731	3.7433375
C	1.1692801	2.9299883	-0.1589074	C	4.2663082	-5.5114055	0.5476077	C	-0.6584129	-4.6055172	3.8483196
C	2.2860807	2.1127853	-0.1424469	C	3.6905641	-5.3535140	-0.7035748	C	0.1139022	-4.4345541	2.6994767
C	2.1232416	0.7436426	-0.0203797	C	2.3831539	-4.8759661	-0.7939827	H	-3.7506721	-4.4106999	2.4483676
H	-1.2612185	0.5966497	-0.0038849	C	1.6815291	-4.5471477	0.3626292	N	1.5031637	-4.4697177	2.7472178
H	3.2718125	2.5534381	-0.2131845	C	2.2567143	-4.7528786	1.6135244	H	1.9131286	-4.7240231	3.6308465
C	-1.3762462	3.3088971	-0.2078395	H	4.0166120	-5.3816756	2.6808333	N	1.7533543	-4.7140140	-2.0231881
C	-1.3958483	4.4404894	-1.2796657	H	5.2813791	-5.8800634	0.6200090	H	2.2519580	-5.0547658	-2.8288416
H	-1.5828978	3.7407077	0.7731500	H	4.2410387	-5.6009943	-1.6023805	N	-2.4760349	-4.0792681	0.1203924
H	-2.2121142	2.6432411	-0.4262808	C	0.3289959	-3.8804263	0.2572901	H	-3.4736538	-4.2078232	0.0747186
C	-1.0454856	5.8625000	-0.8489445	C	-0.3762696	-4.3491317	-0.9954210	H	-2.6411549	-4.7051841	4.6343589
H	-2.4099923	4.4858328	-1.6793384	C	-0.5054668	-4.2208910	1.4711478	H	-0.1789633	-4.7616051	4.8063518
H	-0.7578972	4.1453934	-2.1157176	C	0.3668245	-4.6830394	-2.1244616	H	-2.1184867	9.0621580	-1.2483986
C	0.0446053	6.1544622	-0.0072817	C	-0.2819383	-4.9747604	-3.3241070	H	2.9820643	0.0874583	0.0154085
N	0.6676551	4.9751295	0.4861435	C	-1.6670613	-4.9435670	-3.3672287	C	0.6625517	-1.2214745	0.1247796
N	1.2069869	4.3266472	-0.4148385	C	-2.4206648	-4.6546030	-2.2400173	C	0.5137014	-2.4133541	0.1878260
C	-1.8014483	6.9456693	-1.2654587	C	-1.7673524	-4.3637036	-1.0426123	O	-0.0431878	9.7250870	0.3812710
C	-1.4995793	8.2533712	-0.8897991	H	0.2940887	-5.2256625	-4.2058178	C	-0.7941606	10.8319233	-0.0627180
C	-0.4193272	8.4956810	-0.0487556	H	-2.1720674	-5.1679745	-4.2978623	H	-0.7673156	10.9161225	-1.1524606
C	0.3481191	7.4278275	0.4164893	H	-3.5024669	-4.6564358	-2.2814871	H	-0.3318585	11.7103496	0.3792683

H -1.8338887 10.7629892 0.2688271

1c *trans-chair para*-diazocine platform molecule

$E_{M062x\text{-}D3/def2TZVP}$ = -1735.731545735

Nimag = 0

C	0.7082396	0.2261391	0.3888250	H	-3.0801986	6.7293631	-0.9492613	C	-2.0940015	-4.9238661	3.6041398
C	-0.4046217	1.0614675	0.2314074	C	3.5743751	-5.1778347	1.6618947	C	-0.7147348	-4.8982802	3.7399250
C	-0.2849941	2.4414148	0.2850565	C	4.3126377	-5.3407285	0.4998894	C	0.0722537	-4.6091744	2.6252323
C	1.0007728	2.9625528	0.4950667	C	3.7562225	-5.1153072	-0.7495741	H	-3.7829147	-4.7398869	2.2837639
C	2.1123435	2.1672652	0.6774918	C	2.4308280	-4.6891601	-0.8360845	N	1.4605433	-4.5859946	2.7037064
C	1.9642902	0.7891610	0.6158220	C	1.6909782	-4.4801618	0.3245306	H	1.8630241	-4.8885180	3.5755163
H	-1.3765155	0.6102457	0.0722836	C	2.2491018	-4.7524653	1.5704019	N	1.8207175	-4.4604832	-2.0646164
H	3.0803611	2.6185564	0.8488864	H	4.0140529	-5.3795116	2.6304364	H	2.3506686	-4.7175443	-2.8812164
C	-1.5061101	3.3514154	0.2289882	H	5.3414802	-5.6696257	0.5691698	N	-2.4773722	-4.1802558	0.0176199
C	-1.6607090	4.3745881	-0.9415195	H	4.3367669	-5.2682985	-1.6506197	H	-3.4666843	-4.3500615	-0.0617535
H	-1.5656470	3.8990432	1.1732130	C	0.3127289	-3.8653812	0.2367203	H	-2.7062303	-5.1471152	4.4684313
H	-2.3764585	2.6950228	0.1951461	C	-0.3442793	-4.2665333	-1.0642772	H	-0.2482327	-5.1022131	4.6953042
C	-1.1663037	5.8043388	-0.7656366	C	-0.5305801	-4.3325596	1.4012316	H	-2.2460488	9.0242121	-0.8319690
H	-2.7274781	4.4439738	-1.1594537	C	0.4365903	-4.4806247	-2.1968641	H	2.8198825	0.1391608	0.7391279
H	-1.1907471	3.9507376	-1.8329601	C	-0.1730496	-4.7078390	-3.4304774	C	0.5573863	-1.1953463	0.3306599
C	0.2023232	6.0942363	-0.6210724	C	-1.5569448	-4.7354486	-3.5047030	C	0.4404436	-2.3915078	0.2864734
N	0.9487146	4.8766153	-0.5838408	C	-2.3461503	-4.5684054	-2.3773795	O	0.3839256	9.6744167	-0.5924437
N	0.9462892	4.3884030	0.5463486	C	-1.7319121	-4.3403067	-1.1460741	C	-0.4759518	10.7901697	-0.6398201
C	-2.0148260	6.8953695	-0.8368125	H	0.4325221	-4.8623801	-4.3146005	H	-1.0379749	10.8166874	-1.5770790
C	-1.5428375	8.2069148	-0.7754406	H	-2.0316730	-4.9100628	-4.4615777	H	0.1608989	11.6680495	-0.5756017
C	-0.1791626	8.4431141	-0.6536034	H	-3.4256106	-4.6166721	-2.4445513	H	-1.1750720	10.7851469	0.2009318
C	0.7104348	7.3675658	-0.5800397	C	-1.9144591	-4.4048704	1.2698584				
H	1.7703948	7.5530838	-0.4742390	C	-2.7057063	-4.6940063	2.3816618				

1 TS *twist2cis para*-diazocine platform molecule

$E_{M062x\text{-}D3/def2TZVP}$ = -1735.699182956

Nimag = 1 (XXX)

C	0.3680808	3.0635202	-1.7967020	H	-0.9593991	4.0757152	-3.1961138	C	-3.3844571	-4.3688074	-1.3786551
H	1.4206581	3.3321159	-1.9122578	H	-1.3122196	4.4290282	-1.5196740	C	-2.7635184	-4.0658609	-0.1670248
H	0.1870829	2.2465766	-2.4948836	O	3.2142652	8.5378853	-2.4446310	H	-0.6182965	-4.9748522	-3.2610530
C	1.5150269	7.2471821	-3.6040155	C	3.4409836	9.2685310	-3.6271398	H	-3.0810260	-4.9079900	-3.4220505
C	0.5711058	6.2222035	-3.5199735	H	4.2160590	9.9932868	-3.3929059	H	-4.4646521	-4.3669946	-1.4502161
C	0.3483589	5.5219119	-2.3548531	H	3.7849098	8.6185118	-4.4362434	C	-2.9554900	-3.9053726	2.2436902
C	1.0645587	5.9255925	-1.1951874	H	2.5370770	9.7939634	-3.9469266	C	-3.7626836	-4.0525310	3.3715127
C	2.0245940	6.9382330	-1.2563942	C	-0.2002532	0.5049472	0.9612639	C	-3.1657951	-4.2001418	4.6138920
C	2.2557916	7.5756926	-2.4706701	C	2.4895026	-4.8998917	2.7418355	C	-1.7871955	-4.2313172	4.7567481
C	0.1568622	2.5000834	-0.4078982	C	3.2222827	-5.2009076	1.6042425	C	-0.9839561	-4.0828977	3.6262269
N	0.7453893	5.2639332	-0.0846180	C	2.6809430	-5.0620322	0.3356202	H	-4.8406042	-4.0527639	3.2711848
N	0.1954972	4.6962046	0.8387140	C	1.3783239	-4.5821830	0.2022019	N	0.4038289	-4.1172850	3.7118856
C	0.1274746	3.2532519	0.7772774	C	0.6465310	-4.2344514	1.3341981	H	0.7889869	-4.3607933	4.6097254
C	-0.0218188	1.1277480	-0.2776612	C	1.1870723	-4.4209895	2.6034216	N	0.7827099	-4.4360360	-1.0463831
C	-0.2307323	1.2843465	2.1192757	H	2.9158329	-5.0356485	3.7276160	H	1.3015911	-4.7930127	-1.8320117
C	-0.0876462	2.6528749	2.0121935	H	4.2340577	-5.5703028	1.7098117	N	-3.5022211	-3.7674134	0.9725318
H	1.6748239	7.7496302	-4.5452462	H	3.2553655	-5.3243057	-0.5437306	H	-4.4998958	-3.8822935	0.9006233
H	0.0278154	5.9351164	-4.4133732	C	-0.7029324	-3.5698917	1.1822805	H	-3.7906782	-4.3115957	5.4905843
H	2.5754089	7.2395767	-0.3776367	C	-1.3739700	-4.0543798	-0.0824149	H	-1.3342079	-4.3717034	5.7299641
H	-0.0246564	0.5086138	-1.1662823	C	-1.5699436	-3.8903029	2.3782215	C	-0.3696216	-0.9118524	1.0349016
H	-0.3831785	0.8111169	3.0794798	C	-0.6008122	-4.4047363	-1.1858380	C	-0.5157470	-2.1039058	1.0999901
H	-0.1375282	3.2948706	2.8825064	C	-1.2174065	-4.7100340	-2.3990481				
C	-0.4954302	4.2871743	-2.2331561	C	-2.6008789	-4.6739611	-2.4807512				

2a *cis meta*-diazocine platform molecule

$E_{M062x\text{-}D3/def2TZVP}$ = -1735.747650270

Nimag = 0

C	0.1005678	2.0463851	-1.6611740	N	2.0108712	3.5881256	1.7613586	C	0.0353231	-3.2679406	-2.4425163
C	0.1244073	3.4153545	-1.4781007	C	-1.8264152	5.6321308	2.0079822	C	-0.0786814	-3.4833737	0.0191137
C	0.7130306	4.0163742	-0.3630355	C	-2.6969736	4.8639713	2.7811628	C	0.8015296	-3.3523428	-3.6018550
C	1.2868067	3.1637902	0.5831543	C	-2.2029403	3.8069115	3.5385827	C	0.1811351	-3.5685847	-4.8323503
C	1.2988344	1.7871428	0.3978979	C	-0.8410511	3.5297002	3.5119781	C	-1.1965427	-3.7149123	-4.8774026
C	0.6918946	1.2092155	-0.7130393	H	-0.4364720	2.7266271	4.1144295	C	-1.9670395	-3.6775307	-3.7255399
H	-0.3378961	4.0541600	-2.2213399	H	-2.2356606	6.4635855	1.4468042	C	-1.3422967	-3.4604759	-2.4974708
H	1.7871697	1.1619962	1.1338705	C	4.0897990	-3.9732270	0.1421640	H	0.7740172	-3.6230725	-5.7365064
C	0.7099925	5.5242194	-0.2786540	C	4.8082534	-4.0066847	-1.0429093	H	-1.6794983	-3.8821422	-5.8315473
C	0.4815875	6.1424476	1.1150637	C	4.2012367	-3.7644020	-2.2653270	H	-3.0395489	-3.8177913	-3.7713730
H	1.6510426	5.9104667	-0.6810430	C	2.8420994	-3.4536913	-2.2988122	C	-1.4543099	-3.6684836	-0.0855904
H	-0.0769943	5.8768182	-0.9470539	C	2.1181236	-3.3737001	-1.1125317	C	-2.1878228	-4.0825863	1.0260646
C	-0.4742917	5.3447437	1.9565171	C	2.7309982	-3.6613529	0.1036630	C	-1.5260397	-4.3208304	2.2205889
H	1.4327406	6.2320394	1.6393818	H	4.5710484	-4.1868645	1.0881025	C	-0.1507140	-4.1830826	2.3270657
H	0.0967099	7.1536497	0.9821977	H	5.8635872	-4.2451046	-1.0148008	C	0.5786095	-3.7681373	1.2128009
C	0.0059671	4.2661577	2.7064472	H	4.7690474	-3.8147211	-3.1856659	H	-3.2594800	-4.2162373	0.9499809
N	1.4213897	4.0190734	2.7520312	C	0.6889933	-2.8809961	-1.1359764	N	1.9610137	-3.6247413	1.2618042

H	2.4118516	-3.9345560	2.1070827
N	2.1813889	-3.2148393	-3.4994084
H	2.7099417	-3.3819104	-4.3399593
N	-2.0670041	-3.4282827	-1.3108427
H	-3.0412989	-3.6733052	-1.3771396
H	-2.0935535	-4.6405729	3.0848896
H	0.3566416	-4.3956912	3.2595875
C	0.6842865	-1.4072352	-0.9999765
C	0.6860142	-0.2113059	-0.8745509
H	-0.3703190	1.6143836	-2.5337616
H	-2.8539400	3.2060591	4.1558922
O	-4.0021655	5.2313538	2.7416285
C	-4.9167402	4.4812763	3.5077115
H	-5.8942076	4.9215863	3.3313237
H	-4.6799219	4.5375812	4.5736596
H	-4.9281323	3.4333820	3.1952714

2b *trans-twist meta*-diazocine platform molecule

$E_{M062x\text{-}D3/def2TZVP}$ = -1735.735003400

Nimag = 0

C	-2.1201189	1.1640095	0.3349273
C	-2.0441739	2.5472550	0.4061257
C	-0.8270935	3.2145272	0.3230141
C	0.3189743	2.4198439	0.1554423
C	0.2658510	1.0463880	0.0392032
C	-0.9668891	0.3987491	0.1512976
H	-3.0763636	0.6637760	0.4063100
H	-2.9545174	3.1229730	0.5277103
H	1.1706741	0.4763477	-0.1233989
C	-0.7594651	4.7373026	0.3952480
C	0.1419966	5.4914029	-0.6287705
H	-0.4746584	5.0371531	1.4064247
H	-1.7796641	5.0957765	0.2527965
C	1.5341116	5.9330840	-0.1804562
H	-0.3872137	6.4014109	-0.9138505
H	0.2279727	4.8943782	-1.5385119
C	2.3922304	5.1013830	0.5657239
N	1.7936363	3.8652328	0.9362226
N	1.4842046	3.2043174	-0.0606603
C	1.9837288	7.2076388	-0.4741841
C	3.2415142	7.6509661	-0.0576418
C	4.0608894	6.8208816	0.6990162
C	3.6115521	5.5463920	1.0289074
H	4.2233081	4.8903872	1.6343800
H	5.0296099	7.1500063	1.0441630
H	1.3632781	7.8987385	-1.0316748
O	3.5663912	8.9162750	-0.4230688
C	4.8167397	9.4175165	-0.0094065
H	4.8900513	9.4457824	1.0812618
H	4.8849324	10.4283219	-0.4021967
H	5.6368064	8.8160132	-0.4108599
C	-1.0401240	-1.0267811	0.0648989
C	-1.0894704	-2.2260766	-0.0088607
C	2.2092428	-4.8554828	1.2801515
C	2.9515644	-4.9384196	0.1123476
C	2.3773709	-4.7119779	-1.1288916
C	1.0278230	-4.3666047	-1.1999369
C	0.2812975	-4.2368301	-0.0321556
C	0.8599973	-4.5097456	1.2041016
H	2.6643420	-5.0572791	2.2415058
H	3.9993015	-5.2037807	0.1696615
H	2.9628532	-4.8018011	-2.0351253
C	-1.1313215	-3.7028733	-0.0990262
C	-1.7688725	-4.1052817	-1.4094306
C	-1.9409540	-4.2514505	1.0537321
C	-0.9812203	-4.2412175	-2.5492410
C	-1.5813166	-4.4709512	-3.7870490
C	-2.9614729	-4.5783564	-3.8587020
C	-3.7547439	-4.4885414	-2.7254234
C	-3.1500815	-4.2583607	-1.4899072
H	-0.9712587	-4.5650708	-4.6764685
H	-3.4288887	-4.7549405	-4.8188167
H	-4.8298392	-4.5975954	-2.7915149
C	-3.3186930	-4.4013471	0.9233912
C	-4.0870360	-4.7693676	2.0277829
C	-3.4577002	-4.9987404	3.2414473
C	-2.0817637	-4.8958517	3.3747525
C	-1.3176054	-4.5274066	2.2675762
H	-5.1600369	-4.8761676	1.9309700
N	0.0670082	-4.4247611	2.3431776
H	0.4907396	-4.7235177	3.2061270
N	0.3998080	-4.1403675	-2.4200155
H	0.9408966	-4.3425779	-3.2447035
N	-3.8988187	-4.1731661	-0.3203735
H	-4.8770293	-4.3974894	-0.4020633
H	-4.0520136	-5.2831363	4.1001247
H	-1.6002797	-5.1009146	4.3224631

2c *trans-chair meta*-diazocine platform molecule

$E_{M062x\text{-}D3/def2TZVP}$ = -1735.731545735

Nimag = 0

C	0.7082396	0.2261391	0.3888250
C	-0.4046217	1.0614675	0.2314074
C	-0.2849941	2.4414148	0.2850565
C	1.0007728	2.9625528	0.4950667
C	2.1123435	2.1672652	0.6774918
C	1.9642902	0.7891610	0.6158220
H	-1.3765155	0.6102457	0.0722836
H	3.0803611	2.6185564	0.8488864
C	-1.5061101	3.3514154	0.2289882
C	-1.6607090	4.3745881	-0.9415195
H	-1.5656470	3.8990432	1.1732130
H	-2.3764585	2.6950228	0.1951461
C	-1.1663037	5.8043388	-0.7656366
H	-2.7274781	4.4439738	-1.1594537
H	-1.1907471	3.9507376	-1.8329601
C	0.2023232	6.0942363	-0.6210724
N	0.9487146	4.8766153	-0.5838408
N	0.9462892	4.3884030	0.5463486
C	-2.0148260	6.8953695	-0.8368125
C	-1.5428375	8.2069148	-0.7754406
C	-0.1791626	8.4431141	-0.6536034
C	0.7104348	7.3675658	-0.5800397
H	1.7703948	7.5530838	-0.4742390
H	-3.0801986	6.7293631	-0.9492613
C	3.5743751	-5.1778347	1.6618947
C	4.3126377	-5.3407285	0.4998894
C	3.7562225	-5.1153072	-0.7495741
C	2.4308280	-4.6891601	-0.8360845
C	1.6909782	-4.4801618	0.3245306
C	2.2491018	-4.7524653	1.5704019
H	4.0140529	-5.3795116	2.6304364
H	5.3414802	-5.6696257	0.5691698
H	4.3367669	-5.2682985	-1.6506197
C	0.3127289	-3.8653812	0.2367203
C	-0.3442793	-4.2665333	-1.0642772
C	-0.5305801	-4.3325596	1.4012316
C	0.4365903	-4.4806247	-2.1968641
C	-0.1730496	-4.7078390	-3.4304774
C	-1.5569448	-4.7354486	-3.5047030
C	-2.3461503	-4.5684054	-2.3773795
C	-1.7319121	-4.3403067	-1.1460741
H	0.4325221	-4.8623801	-4.3146005
H	-2.0316730	-4.9100628	-4.4615777
H	-3.4256106	-4.6166721	-2.4445513
C	-1.9144591	-4.4048704	1.2698584
C	-2.7057063	-4.6940063	2.3816618
C	-2.0940015	-4.9238661	3.6041398
C	-0.7147348	-4.8982802	3.7399250
C	0.0722537	-4.6091744	2.6252323
H	-3.7829147	-4.7398869	2.2837639
N	1.4605433	-4.5859946	2.7037064
H	1.8630241	-4.8885180	3.5755163
N	1.8207175	-4.4604832	-2.0646164
H	2.3506686	-4.7175443	-2.8812164
N	-2.4773722	-4.1802558	0.0176199
H	-3.4666843	-4.3500615	-0.0617535
H	-2.7062303	-5.1471152	4.4684313
H	-0.2482327	-5.1022131	4.6953042
H	-2.2460488	9.0242121	-0.8319690
H	2.8198825	0.1391608	0.7391279
C	0.5573863	-1.1953463	0.3306599
C	0.4404436	-2.3915078	0.2864734
O	0.3839256	9.6744167	-0.5924437
C	-0.4759518	10.7901697	-0.6398201
H	-1.0379749	10.8166874	-1.5770790
H	0.1608989	11.6680495	-0.5756017
H	-1.1750720	10.7851469	0.2009318

TS *twist2cis meta*-diazocine platform molecule

$E_{M062x\text{-}D3/def2TZVP}$ = -1735.698417078

Nimag = 3 (-463.03; -18.65; -2.32 cm^{-1})

C	0.4799215	4.6077299	-1.0428513
H	1.5222966	4.8365489	-0.8076583
H	0.3519139	4.8427689	-2.0994513
C	1.4973969	8.1459795	1.8710647
C	0.5952935	7.6009605	0.9560476
C	0.3644579	6.2456689	0.8695926
C	1.0246275	5.4037812	1.8052373
C	1.9419284	5.9222488	2.7217206
C	2.1865545	7.2913146	2.7289713
C	0.2627984	3.1169252	-0.9037511
N	0.6974296	4.1155555	1.7230108
N	0.1460550	3.0388924	1.6188545
C	0.1601110	2.4172185	0.3088229
C	0.1568715	2.3517604	-2.0646549
C	-0.1240261	0.3010979	-0.8239645
C	-0.0531469	1.0479938	0.3489530
H	1.6660685	9.2113567	1.8840302
H	0.0947795	8.2612853	0.2566753
H	2.4496623	5.2811995	3.4271215
H	0.2131162	2.8546373	-3.0228562
H	-0.1643234	0.5727886	1.3150540
C	-0.4253919	5.5679075	-0.2110369
H	-0.8493481	6.3246529	-0.8705902
H	-1.2692739	5.0063543	0.2002082
O	3.1040306	7.7095069	3.6390832
C	3.3534692	9.0928038	3.7289544
H	4.0990851	9.2172372	4.5095784
H	3.7446132	9.4875180	2.7873006
H	2.4475795	9.6415438	4.0009548
C	-0.0172281	0.9777680	-2.0401502
C	2.4232220	-5.1695126	0.9080849
C	3.1714259	-5.4707343	-0.2193676
C	2.6552021	-5.3103711	-1.4958937

C	1.3632179	-4.8074844	-1.6473329
C	0.6170237	-4.4589826	-0.5251350
C	1.1312007	-4.6682404	0.7515975
H	2.8296724	-5.3219104	1.8997767
H	4.1752428	-5.8571539	-0.0996717
H	3.2408962	-5.5730393	-2.3676682
C	-0.7162267	-3.7662612	-0.6934121
C	-1.3729216	-4.2227615	-1.9759393
C	-1.6112999	-4.0850220	0.4822614
C	-0.5867566	-4.5777178	-3.0686879
C	-1.1868169	-4.8599145	-4.2958372
C	-2.5676338	-4.7971328	-4.4021645
C	-3.3651688	-4.4876107	-3.3113904
C	-2.7607848	-4.2079487	-2.0858075
H	-0.5771265	-5.1283003	-5.1492822
H	-3.0349356	-5.0137972	-5.3540457
H	-4.4437291	-4.4654312	-3.4020525
C	-2.9941002	-4.0714820	0.3226532
C	-3.8245367	-4.2152921	1.4337832
C	-3.2534891	-4.3874558	2.6851476
C	-1.8786421	-4.4466038	2.8526059
C	-1.0521531	-4.3019687	1.7385257
H	-4.9002516	-4.1930909	1.3138813
N	0.3328030	-4.3642201	1.8486167
H	0.6983818	-4.6185056	2.7515772
N	0.7929774	-4.6382656	-2.9048351
H	1.3189669	-4.9971936	-3.6847541
N	-3.5146759	-3.9085644	-0.9567422
H	-4.5128435	-4.0034988	-1.0481155
H	-3.8962065	-4.4955385	3.5492407
H	-1.4462945	-4.6047040	3.8324077
C	-0.3249636	-1.1136338	-0.7831670
C	-0.4987671	-2.3029686	-0.7490388
H	-0.0872305	0.4193083	-2.9640899

References

[1] Wahhab, A.; Therrien, E.; inventor; Methylgene Inc., assignee. Small Molecule Inhibitors of Protein Arginine methyltransferases. WO 2008104077 (A1). 2007-02-28.

[2] Laursen, B. W.; Krebs, F. C. *Chem. Eur. J.* **2001**, *7*, 1773-1783.

[3] Park, K.; Lee, B. M. inventor; Yuhan Corp., assignee. Novel phenylethynyl benzamide glucokinase activator and method for preparing same. WO 2014112798 (A1). 2013-01-16.

[4] Zhao, Y.; Truhlar, D. G. *Theor. Chem. Account* **2008**, *120*, 215-241. https://doi.org/10.1007/s00214-007-0310-x.

[5] Grimme, S.; Antony, J.; Ehrlich, S.; Krieg, H. *J. Chem. Phys.* **2010**, *132*, 154104. DOI: 10.1063/1.3382344

[6] Weigend, F.; Häser, M.; Patzelt, H.; Ahlrichs, R. *Chem. Phys. Lett.* **1998**, *294*, 143-152.

[7] Goerigk, L.; Hansen, A.; Bauer, C.; Ehrlich, S.; Najibi, A.; Grimme, S. *Phys. Chem. Chem. Phys.* **2017**, *19*, 32184–32215.

[8] Turbomole7.2: TURBOMOLE V7.2 2017, a development of University of Karlsruhe and Forschungszentrum Karlsruhe GmbH, 1989-2007, TURBOMOLE GmbH, since 2007; available from http://www.turbomole.com.

3.3 Norbornadien-funktionalisierte TATA- und TOTA-Plattformen

Mit dem Nachweis der thermischen Isomerisierungsbeschleunigung von Azobenzolen auf Goldoberflächen über die Aufhebung des verbotenen Intersystem-Crossing zwischen der Singulett- und Tripletthyperfläche[174] gilt es, diesen Prozess in weiteren Reaktionen nachzuweisen. Sowohl die [2+2]-Cycloaddition als auch die [2+2]-Cycloreversion sind im Norbornadienstammsystem photochemisch erlaubt und thermisch verboten.[119,175–177] Diese Reaktionen werden im Norbornadien für die photochemische Isomerisierung zwischen dem thermodynamisch stabilen Norbornadien (NBD) und metastabilen Quadricyclan (QC) genutzt.[136,137] Bei einer optimalen Funktionalisierung des Norbornadiengrundgerüsts mit elektronenziehenden bzw. elektronschiebenden Substituenten kann die Topografie der Tripletthyperfläche so verändert werden, dass ein in den Triplettzustand angeregtes Quadricyclan bevorzugt in das Norbornadien isomerisiert.[139,144] Auf Goldoberflächen sollte der aufgeklärte nicht adiabatische Mechanismus das Intersystem-Crossing in den Triplettzustand im Quadricyclan begünstigen, wodurch die thermische [2+2]-Cycloreversion zum Norbornadien ermöglicht wird. In den Arbeiten von BAUER wurde die spontane [2+2]-Cycloreversion vom Quadricyclan zum Norbornadien bereits auf atomar flachen Nickel- und Platinoberflächen bei tiefen Temperaturen nachgewiesen (Abb. 3.5).[178,179] Das gebildete Norbornadien fragmentiert allerdings bei etwas höheren Temperaturen von 200 K weiter zu Benzol auf Nickel- bzw. zu undefinierten Substanzen auf Platinoberflächen.

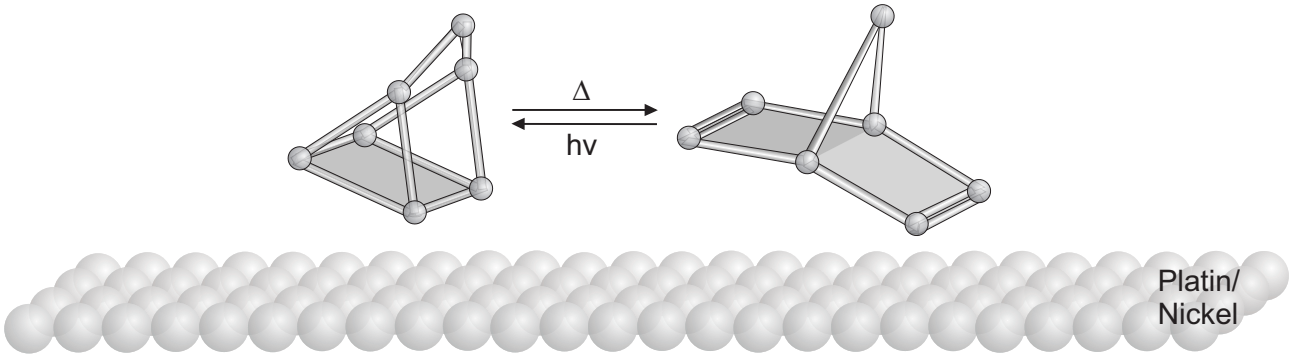

Abb. 3.5: Katalytische Isomerisierung von Quadricyclan zu Norbornadien auf Nickel- und Platinoberflächen.[178,179]

Mit dem Wechsel auf klassisch inerte Goldoberflächen und durch die räumliche Entfernung des Quadricyclans über die Funktionalisierung auf TATA- bzw. TOTA-Plattformen soll geprüft werden, ob die Zersetzung vermieden werden kann und ausschließlich die elektronische Kopplung zum Quadricyclan die thermische [2+2]-Cycloreversion beschleunigt.

3.3.1 Norbornadiene functionalized triaza-triangulenium and trioxa-triangulenium platforms

Roland Löw, Talina Rusch, Tobias Moje, Fynn Röhricht, Olaf Magnussen, Rainer Herges

Beilstein J. Org. Chem. **2019**, *15*, 1815-1821.
DOI:10.3762/bxiv.2019.5.v1

Eigenanteil: Die Synthese und Charakterisierung aller Moleküle außer des TOTA-BArF-Ions wurden von Roland Löw durchgeführt. Die Synthese des TOTA-BArF-Ions wurde von Tobias Moje durchgeführt. Die Untersuchungen der Zielmoleküle in Lösung wurden von Roland Löw durchgeführt. Die DFT-Rechnungen wurden von Fynn Röhricht angefertigt. Die Untersuchungen mittels Rastertunnelmikroskopie wurden von Talina Rusch durchgeführt. Das Manuskript wurde von Roland Löw und Prof. Dr. Rainer Herges verfasst.

3.3.2 Zusammenfassung

In dieser Publikation wird die Synthese von Cyanonorbornadienen funktionalisiert über verschiedene Verknüpfungseinheiten auf TATA- **12**, **13** bzw. direkt auf einer TOTA-Plattform **14** beschrieben. Zudem wurde die photochemische sowie thermische Isomerisierung dieser Norbornadien-Plattformen in Lösung untersucht. Die Norbornadien-Plattformen **12**, **13** und **14** sind mit einer Cyanogruppe in Nachbarschaft zur Verknüpfungseinheit bzw. zur TOTA-Plattform funktionalisiert (Abb. 3.6). Durch diese elektronenziehende Gruppe wird die Topografie der Singuletthyperflächen der Norbornadiene so verändert, dass die direkten photochemischen Anregungen in hohem Maße zu den Quadricyclanen führen. Folgend kann angenommen werden, dass die Minima der Tripletthyperflächen auf die Seite der Norbornadiene verschoben sind. Dieses Verhalten ist essentiell für eine Untersuchung des nicht adiabatischen Mechanismus ausgehend von Goldoberflächen über ein Intersystem-Crossing.

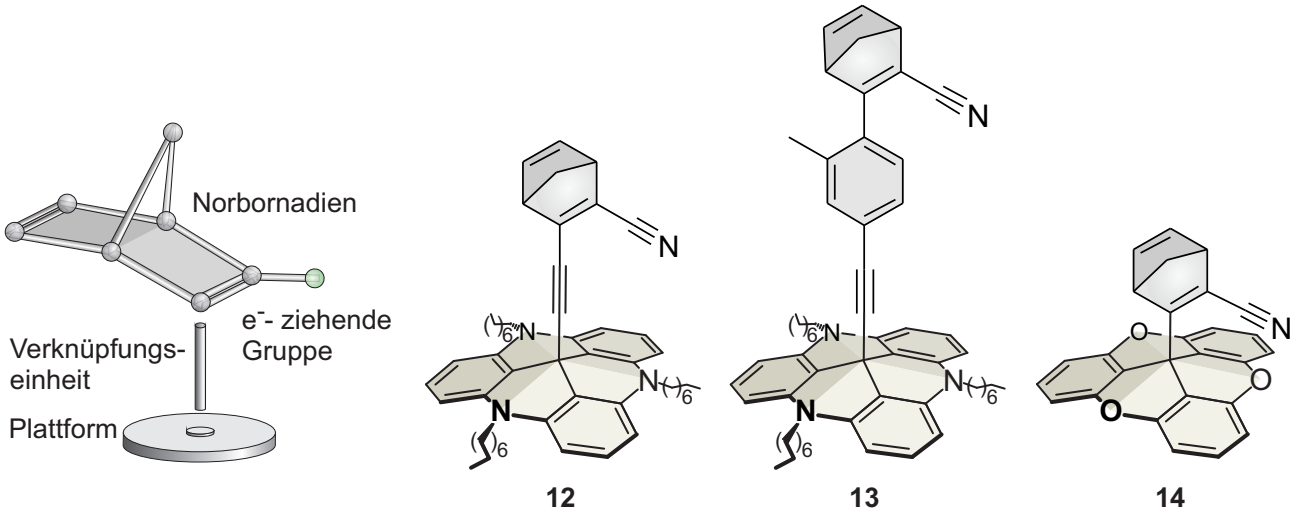

Abb. 3.6: Schematische Darstellung des Norbornadien-Plattformkonzepts (links) und die Norbornadien-TATA-Plattformen **12** und **13** bzw. -TOTA-Plattform **14**.

Durch die elektronenziehenden Cyano- und Acetylengruppe im Norbornadien **12** wird die Energiebarriere der thermischen [2+2]-Cycloreversion soweit herab gesetzt, dass eine Halbwertszeit bei Raumtemperatur (30 Tage) beobachtet werden kann. Mit der Einführung eines methylsubstituierten Phenylrings in die Verknüpfungseinheit in Plattform **13** wird die Konjugation zwischen Plattform und Norbornadien reduziert. Über die direkte Funktionalisierung des Norbornadiens auf der TOTA-Plattform in **14** wird eine stabile kovalente Bindung zwischen Plattform und Norbornadien erhalten. Diese beiden Norbornadien-Plattformen **13** und **14** weisen keine thermische Isomerisierung innerhalb von 30 Tagen bei Raumtemperatur auf. Es ist davon auszugehen, dass durch die Abwesenheit der elektronenziehenden Ethinylgruppe die Höhe der Aktivierungsenergien weniger reduziert werden. Die Wellenlängen, mit denen die Norbornadiene photochemisch isomerisieren können, sind ebenfalls von den Substituenten abhängig. Aufgrund der bathochromen Verschiebungen der Absorptionen von **12** und **13** isomerisieren diese mit 385 nm (NBD→QC) bzw. 311 nm (QC→NBD), während in **14** 311 nm (NBD→QC) und 254 nm (QC→NBD) benötigt werden. Die Norbornadien-Plattform **12** wurde

bereits auf Au(111) adsorbiert, wobei zwei unterschiedliche relative Höhen in STM-Messungen nachgewiesen wurden. Es besteht die Möglichkeit, dass bei der Präparation Umgebungsbeleuchtung das Norbornadien teilweise zum Quadricyclan isomerisiert hat oder der Aufbau teilweise von der Plattform abgespalten wurde. Das gebildete Quadricyclan oder das TATA-ion könnten die zweite relative Höhe in den Monolagen darstellen.

BEILSTEIN JOURNAL OF ORGANIC CHEMISTRY

Norbornadiene-functionalized triazatriangulenium and trioxatriangulenium platforms

Roland Löw[1], Talina Rusch[2], Tobias Moje[1], Fynn Röhricht[1], Olaf M. Magnussen[*2] and Rainer Herges[*1]

Full Research Paper

Open Access

Address:
[1]Otto Diels Institute for Organic Chemistry, University of Kiel, Otto-Hahn-Platz 4, 24118 Kiel, Germany and [2]Institute for Experimental and Applied Physics, University of Kiel, Leibnizstraße 19, 24098 Kiel, Germany

Email:
Olaf M. Magnussen[*] - magnussen@physik.uni-kiel.de;
Rainer Herges[*] - rherges@oc.uni-kiel.de

* Corresponding author

Keywords:
[2 + 2] cycloaddition; [2 + 2] cycloreversion; norbornadiene; photochemical isomerization; quadricyclane; self-assembled monolayers; TATA platform; thermal isomerization; TOTA platform

Beilstein J. Org. Chem. **2019,** *15,* 1815–1821.
doi:10.3762/bjoc.15.175

Received: 11 April 2019
Accepted: 17 July 2019
Published: 30 July 2019

This article is part of the thematic issue "Molecular switches".

Guest Editor: W. Szymanski

Abstract

Triazatriangulenium (TATA) and trioxatriangulenium (TOTA) ions are particularly suited systems to mount functional molecules onto atomically flat surfaces such as Au(111). The TATA and TOTA units serve as platforms that absorb onto the surface and form ordered monolayers, while the functional groups are protruding upright and freestanding from the central carbon atoms. Azobenzene derivatized TATA's are known to exhibit extremely fast *cis*→*trans* isomerization on metal surfaces, via a peculiar non-adiabatic singlet→triplet→singlet mechanism. We now prepared norbornadienes (NBD) and quadricyclanes (QC) attached to TATA and TOTA platforms which can be used to check if these accelerated rates and the spin change mechanism also apply to [2 + 2] cycloreversions (QC→NBD).

Introduction

Recently, we discovered that the thermochemically forbidden *cis–trans* isomerization of azobenzenes can be efficiently catalysed by a very peculiar mechanism on bulk gold [1]. In heterogeneous catalysis, the surface is chemically involved in bond making and breaking. In contrast to this conventional surface catalysis the new mechanism does not involve direct contact with the surface. Electronic coupling via a conjugated π-system to the conducting band of a bulk metal is sufficient to accelerate the rate of isomerization by three orders of magnitude [2-4]. To keep the reacting azobenzene molecule at a distance of about 14 Å from the surface, it is not directly absorbed onto the surface but mounted on a carefully designed molecular framework. This approach was named the platform approach [5]. Three molecular units are combined in a modular way to achieve a controlled adsorption on the surface: the platform, a spacer and the functional molecule. Triazatriangulenium

(TATA) and trioxatriangulenium (TOTA) units are used as molecular platforms. They adsorb on the surface and form ordered monolayers. A linear, π-conjugated spacer (e.g., an ethynyl unit) is attached to the central carbon atom and the functional molecule is mounted on top. This architecture allows investigating molecules on surfaces under controlled conditions. The size of the platforms determines the intermolecular distances and enforces an upright orientation of the free standing functional groups [6]. The length and the nature of the spacer is used to tune the distance and electronic coupling of the functional system on top [1].

Preliminary experiments proved that the electronic coupling to the surface is the decisive parameter controlling the *cis–trans* rate acceleration of azobenzenes and not the length of the spacer [1]. A full conjugation path from the azobenzene on top through the ethynyl spacer and the platform to a bulk gold surface shortens the half-life of the metastable *cis*-isomer from days to seconds even though the azo N=N group is 11 bonds and 14 Å away from the surface. A singlet→triplet→singlet pathway was suggested to explain the dramatic rate acceleration.

To obtain further insight into this unusual mechanism and to explore the scope and limitation of the general concept, we are aiming at the extension from simple *cis*→*trans* isomerization to other thermochemically forbidden reactions such as [2 + 2] cycloreversions. Moreover, a deeper understanding of the non-adiabatic, catalytic process and successful application of the concept to the QC→NBD isomerization could contribute to the elucidation of the mechanisms of bulk metal catalysis and open new ways to design new catalytic systems.

Towards this end, and following the "platform concept", we designed a cyano-substituted norbornadiene, which is functionalized with an acetylene spacer on a TATA platform to investigate an eventual "spin-catalysed" [2 + 2] cycloreversion on bulk gold of quadricyclane **1b** to norbornadiene **1a** (Figure 1).

The cycloreversion of most quadricyclane systems proceeds smoothly in solution upon irradiation in the presence of triplet sensitizers [7]. If **1b** is adsorbed on a gold surface the bulk gold could take the role of a triplet sensitizer, mediate the spin change (which otherwise is forbidden) and accelerate the cycloreversion. Substitution in the 2 and 3 positions shifts the bathochromic absorption to 375 nm which is in agreement with similar systems [8]. Furthermore, the cyano and ethynyl groups provide a complete conjugation path across the double bond of norbornadiene to the metal. Additionally, it is known that electron-withdrawing groups in 2 or 3 position change the triplet energy hypersurface in such a way that a triplet excited quadricyclane **1b** decays into the ground state of the norbornadiene **1a** [9], which is a precondition for an efficient QC→NBD isomerization via our postulated non-adiabatic singlet→triplet→singlet mechanism.

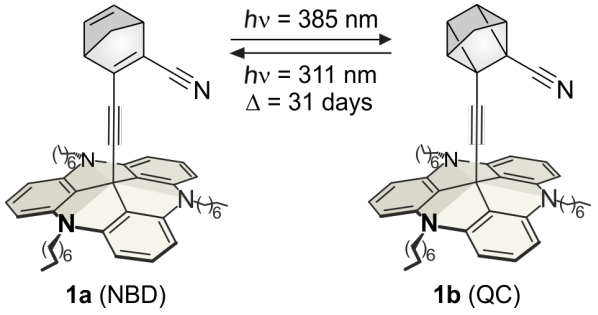

Figure 1: Structures of the norbornadiene platform **1a** and the quadricyclane platform **1b** (for geometry coordinates and further details see Supporting Information File 1). The norbornadiene isomerizes upon irradiation with 385 nm to the quadricyclane **1b**. Back-isomerization to the norbornadiene **1a** is achieved upon irradiation with 311 nm or thermochemically with a half-life of 31 days.

Results and Discussion

If our proposed spin change mechanism, mediated by the conducting electrons in bulk gold were correct, interruption of the conjugation path and decoupling from the surface should restore the properties of the system (half-life of the metastable quadricyclane) in solution. According to this line of thought, we synthesized molecule **2** with a 2-methylphenyl group inserted into the spacer unit (see below Scheme 2). The methyl group prevents a planar arrangement of the phenyl group and the double bond of the NBD unit and thus lowers the conjugation.

We also synthesized the corresponding system directly connected to a TOTA platform **3**. Functionalized TOTA molecules are more stable than the corresponding TATA systems and usually can be sublimed without decomposition, which is a necessary precondition for ultra-high vacuum STM investigations.

The 3-bromo-2-cyano-substituted norbornadiene **4** was synthesized as described in the literature (Scheme 1) [10-12].

4 was converted to **5** with trimethylsilylacetylene (72%) in a Sonogashira cross-coupling reaction. The triazatriangulenium ion **6** was synthesized according to a procedure of Laursen and Krebs [13]. The platform **6** was functionalized with norbornadiene **5** by deprotection of the acetylene with potassium hydroxide and in situ formation of the C–C bond between the acetylene and the central C atom of the platform **6** to yield the norbornadiene-substituted platform **1** (62%).

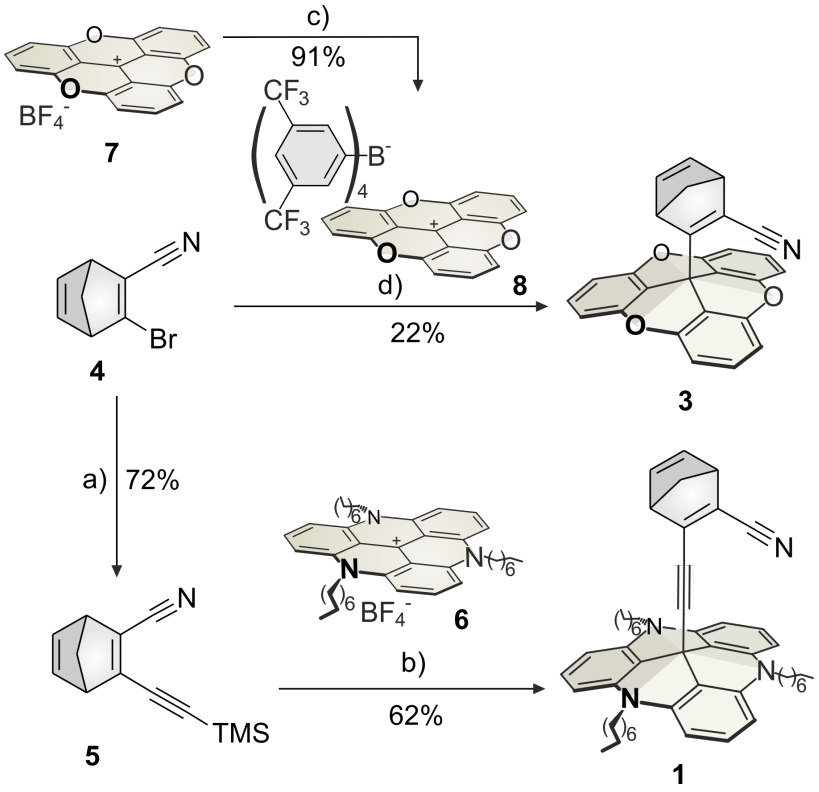

Scheme 1: Syntheses of the norbornadiene TATA platform **1** and TOTA platform **3**. a) TMS-acetylene, $Pd(PPh_3)_4$, Cu(I)I, Et_3N, toluene, N_2, 60 °C, 1.3 h; b) KOH, THF, N_2, reflux, 5 h; c) sodium tetrakis[3,5-bis(trifluoromethyl)phenyl]borate ($NaBAr^F{}_4$), DCM, rt, 2 h; d) *n*-BuLi, THF, N_2, −78 °C to rt, 20 h.

The TOTA cation with the tetrakis(3,5-bis(trifluoromethyl)phenyl)borate anion ($TOTA^+$ $[BAr^F{}_4]^-$, **8**) was obtained by ion exchange of the TOTA tetrafluoroborate **7** ($TOTA^+$ BF_4^-) to achieve a high solubility in organic solvents [14]. 3-Bromo-2-cyanonorbornadiene (**4**) was subjected to halogen–metal exchange with *n*-BuLi and coupled with the central atom of the TOTA platform **8** to obtain the norbornadiene-functionalized TOTA platform **3** (22%, Scheme 1). The synthesis of the corresponding TATA platform including an additional 2-methylphenyl group (**2**) was obtained in a convergent synthesis (Scheme 2). Boronic ester **9** was synthesized as described in the literature [15]. In a Suzuki cross-coupling reaction norborna-

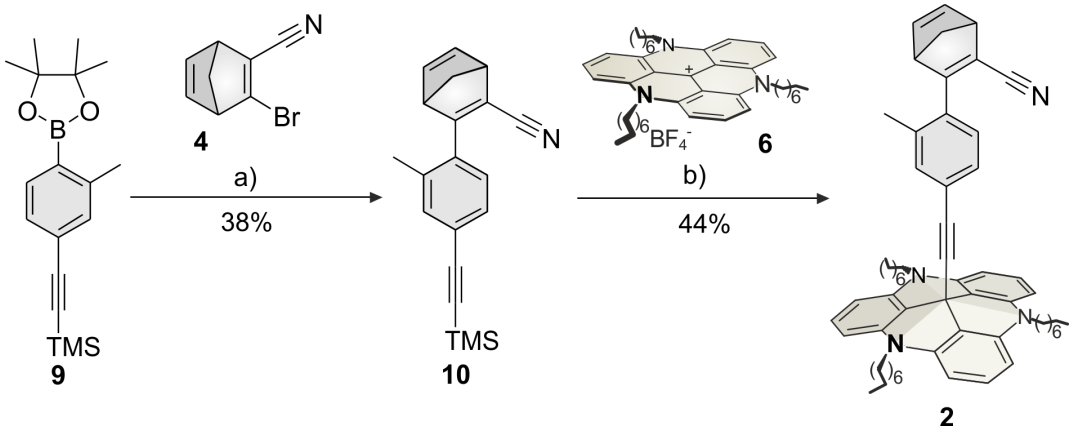

Scheme 2: Synthesis of methylphenylnorbornadiene platform **2**. a) $Pd(PPh_3)_4$, Na_2CO_3, toluene, EtOH, H_2O, N_2, reflux, 12 h; b) KOH, THF, N_2, reflux, 1 h.

diene **4** was coupled with **9** to the extended norbornadiene **10** (38%), which was attached to the TATA platform **6** to yield the extended norbornadiene platform **2** (44%).

The photophysical properties and the switching behaviour of **1**, **2** and **3** were determined in solution (THF). The UV–vis spectra of the norbornadienes (NBD, black, **1a**, **2a**, **3a**) and quadricylanes (QC, red, **1b**, **2b**, **3b**) and the spectra of the QCs after irradiation with 311 nm for **1b** and **2b** or 254 nm for **3b** (blue) are shown in Figure 2. The bathochromic absorption maximum of norbornadiene **1a** is at 375 nm (as compared to <300 nm in parent norbornadiene) [16,17]. The absorption maximum of quadricyclane **1b** is at 336 nm (as compared to 187 nm in parent quadricyclane) [18]. The weak and broad absorption band with a maximum at 524 nm is due to the TATA cation generated by decomposition during irradiation with 311 nm.

The photostationary states were determined in deuterated oxygen containing deuterated benzene and degassed deuterated benzene by ^{1}H NMR measurements (Figure 3). Norbornadiene **1a** isomerizes quantitatively to quadricyclane **1b** by irradiation with 385 nm. Upon irradiation of **1b** under nitrogen with 311 nm, the cycloreversion yields 28% norbornadiene (Table 1).

The efficiency of the cycloreversion is higher under air (52%), however, slow decomposition was observed (cleavage of the $TATA^+$ platform). Obviously, in the presence of oxygen, the photochemical cycloreversion proceeds via a triplet radical mechanism. This agrees with observations described in the literature [16]. In degassed benzene neither **1a** nor **1b** exhibits decomposition upon repeated irradiation with 385 nm and 311 nm.

The thermal isomerization of QC **1b** back to NBD **1a** was investigated by ^{1}H NMR measurements (Figure 4).

The cycloreversion follows a first order reaction, the rate constant could be determined by logarithmic fitting of the integrals of the CH_2 signals next to the nitrogen atoms of the platform as

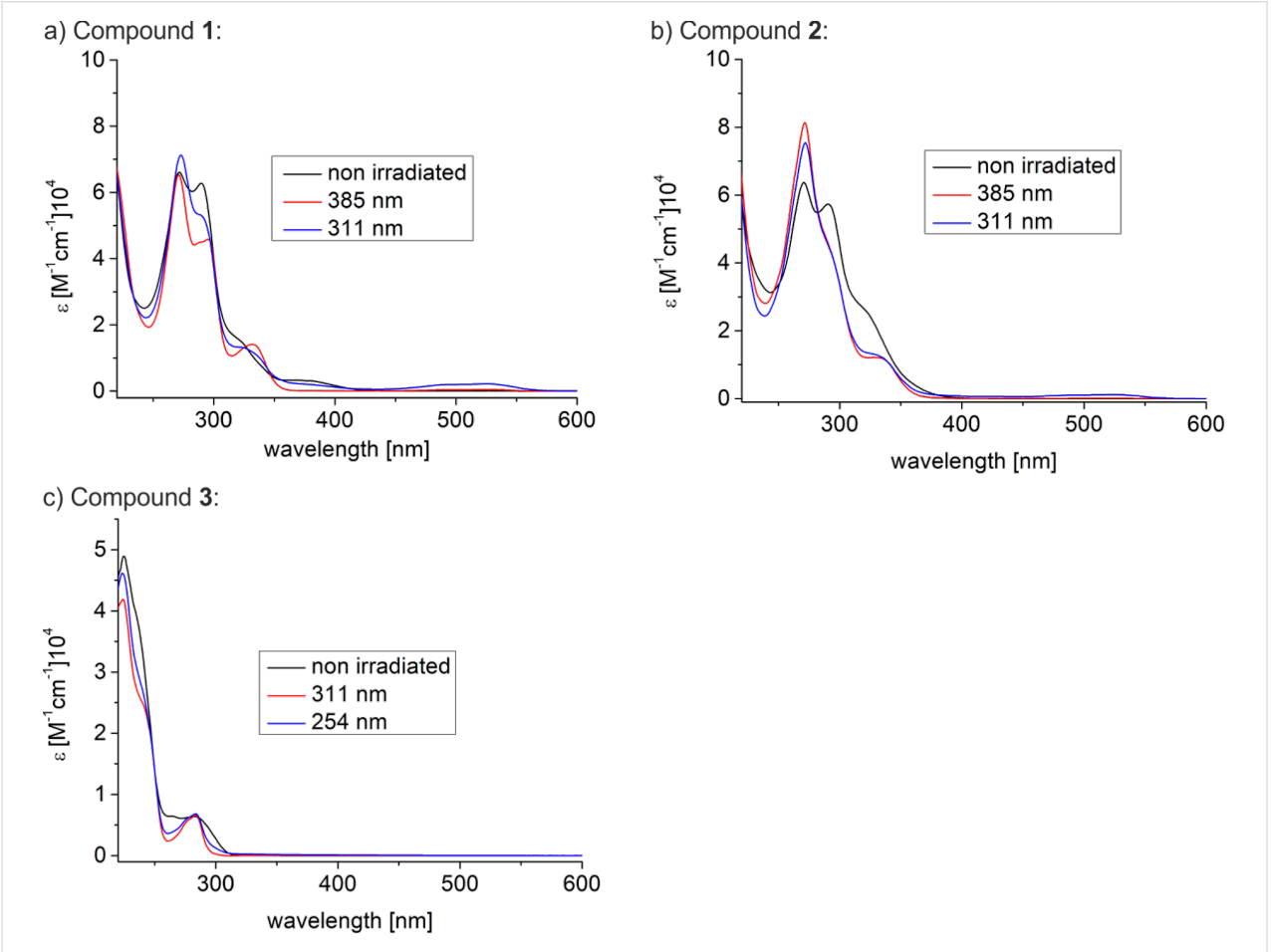

Figure 2: UV–vis spectra of platform molecules **1** (a), **2** (b) and **3** (c) (in THF at rt): Norbornadiene (black), quadricyclane (red) and after irradiation with 311 nm (compound **1b** and **2b**) or 254 nm (compound **3b**) for 2.5 min (blue).

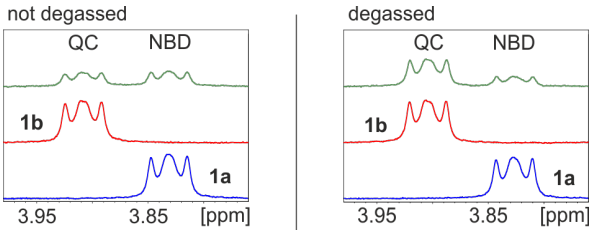

Figure 3: ^{1}H NMR spectra of **1** in deuterated oxygen containing deuterated benzene (left) and degassed deuterated benzene (right). Shown are the signals of the CH_2 groups of the alkyl side chains next to the nitrogen atoms in the TATA platforms, which are indicative of the isomerization. Left bottom (blue): non-irradiated NBD **1a**; left middle (red): pure QC **1b** obtained after irradiation of **1b** with 385 nm for one minute; and left top (green): photostationary state of **1a** and **1b** after 1 h irradiation with 311 nm under air (52% **1a**/48% **1b**). Right bottom (blue): pure NBD **1a**; right middle (red): pure QC **1b** obtained after irradiation of **1a** with 385 nm for one minute and right top (green): photostationary state of **1a** and **1b** after 2 h irradiation with 311 nm under nitrogen atmosphere (28% **1a**/72% **1b**).

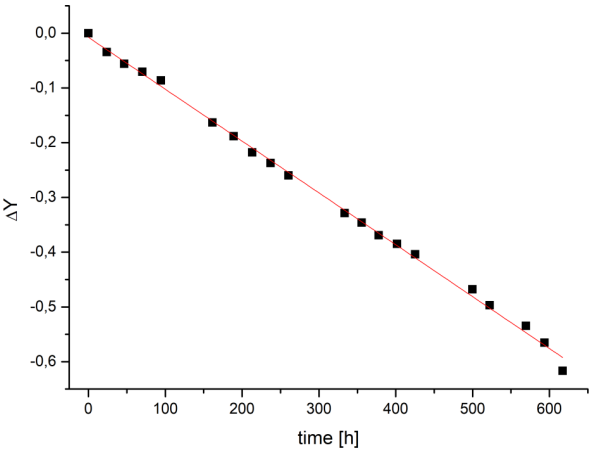

Figure 4: Determination of the thermal isomerization rate k of **1b** (QC) by ^{1}H NMR spectroscopy (toluene, 293.5 K, 800 µmol/L, under nitrogen). ΔY: ln {$[QC]_t/[QC]_0$}, $[QC]_t$: ^{1}H NMR integral of the CH_2 group neighbouring the N bridge atom of the TATA platform in QC **1b** at time t, $[QC]_0$ corresponding ^{1}H integral at t = 0. A rate constant of $k = 0.95 \cdot 10^{-3}$ s^{-1} was determined from a linear fit of the ΔY/t curve.

$k = 1.06 \cdot 10^{-3}$ s^{-1} under air and $0.95 \cdot 10^{-3}$ s^{-1} under nitrogen. Hence, the thermal reaction (in contrast to the photochemical reaction) is not largely affected by oxygen. The half-life of the metastable quadricyclane is $t_{1/2}$ = 655 h in benzene under air at 293 K (Table 1). Minor amounts of degradation products (<1%) after following the cycloreversion within a period of one month are visible in the ^{1}H NMR spectrum. Under nitrogen atmosphere the half-life of the cycloreversion is $t_{1/2}$ = 732 h (294 K).

The rate constant as a function of the temperature follows an Arrhenius-type relationship. The activation energy for the cycloreversion was determined by linear fit of ln (k) as a function of 1/T. The cycloreversion of QC **1b** to NBD **1a** has an activation energy of 111 kJ mol^{-1} (degassed deuterated benzene). The switching efficiency of NBD **2a** to QC **2b** is quantitative (≈100%) after irradiation with 385 nm, whereas the photostationary state of NBD **3a** to QC **3b** is lower with 91%.

No thermal cycloreversion of the quadricyclanes **2b** and **3b** was observed at room temperature within a period of one month. Obviously, a cyano as well as a neighbouring ethynyl substituent are necessary to induce the back-isomerisation at ambient conditions as realized in compound **1**. Consequently, future surface chemistry investigations will be performed with compound **1** including the TATA platform and an ethynyl spacer.

STM Measurements

The adsorption behaviour of the NBD **1a** on Au(111) surfaces was studied by scanning tunnelling microscopy (STM) at room temperature (Figure 5a). The molecules form a hexagonally ordered self-assembled monolayer (SAM) with an intermolecular distance of (1.23 ± 0.07) nm. This is in agreement with a ($\sqrt{19} \times \sqrt{19}$) R23.4° superstructure, which was observed in our previous investigations of adlayers of octyl-TATA derivatives [1,6,19-21]. Two types of molecules with a distinct difference in apparent height of ≈1 Å were observed in the STM images (Figure 5b). Both types of molecules are located at identical positions of the ($\sqrt{19} \times \sqrt{19}$) R23.4° lattice and seem to be distri-

Table 1: Photostationary states (PSS) of norbornadiene platforms **1**, **2** and **3** upon irradiation with light of the wavelengths λ_{irrad} = 385 nm (**1a**, **2a**) or 311 nm (**3a**) and 311 nm (**1b**, **2b**) or 254 nm (**3b**) and the thermal isomerization half-life $t_{1/2}$ determined by ^{1}H NMR spectroscopy (deuterated benzene under air/degassed deuterated benzene).

Compound	atmosphere	PSS % QC (λ_{irrad})	PSS % NBD (λ_{irrad})	$t_{1/2}$ (h)	EA kJ/mol
1	air	≈100 (385 nm)	52 (311 nm)	655 (293 K)	/
1	N_2	≈100 (385 nm)	28 (311 nm)	732 (294 K)	111
2	N_2	≈100 (385 nm)	48 (311 nm)	>1 year	/
3	N_2	91 (311 nm)	33 (254 nm)	>1 year	/

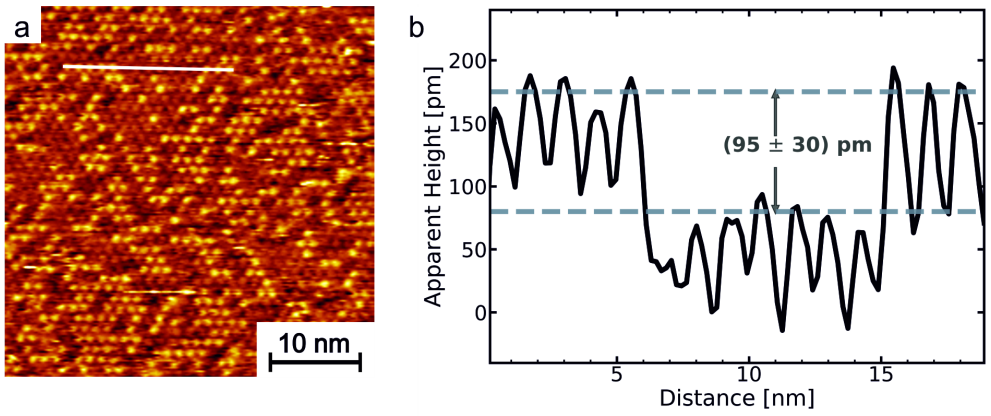

Figure 5: (a) STM image of self-assembled monolayers of compound **1** on Au(111) (40 × 40 nm^2, I_t = 0.05 nA, U_{bias} = 0.40 V) and (b) crossection along the white line in (a).

buted rather randomly on the surface. Two explanations are possible to account for the presence of these two species: Either they correspond to a mixture of adsorbed NBD-TATA **1a** and QC-TATAs **1b** or to coadsorption of **1a** and the pure octyl-TATA **6**. The first case may be possible, because the molecules are able to switch to the **1b** state at a wavelength of 385 nm and the substance was exposed to daylight during preparation and incorporation into the STM. However, since the ratio on the surface is 42% for molecules with a greater apparent height and 58% for molecules with a lower apparent height, this assumption is unlikely as at least 42% of the molecules would have to be in the switched state **1b**. The second explanation, i.e., that the mixed monolayer consists of octyl-TATA **6** and the NBD-TATA **1a**, seems to be more likely, since molecule **1** decays slowly under irradiation in contact with oxygen. Previous measurements have shown that self-assembly from solutions containing pure and vertically functionalized TATA molecules leads to the formation of stochastically mixed monolayers with a highly ordered ($\sqrt{19} \times \sqrt{19}$) R23.4° superstructure [22]. This would be also expected for self-assembly from solution containing **1a** and **6**. The composition of the adlayer on the surface does not necessarily have to be identical to the ratio of the two species in solution. In fact, in our previous study the fraction of adsorbed octyl-TATA **6** as compared to that of the functionalized TATA was found to be much higher than the ratio in solution. We attributed this to the smaller size of **6** and its correspondingly higher diffusion coefficient, which results in faster transport to the Au surface and accordingly enhanced surface coverages. Thus, even low decay rates of **1a** may lead to sufficiently high concentrations of **6** for obtaining mixed adlayers. By varying the preparation conditions, e.g., performing the preparation in a nitrogen atmosphere, decomposition might be avoided and monolayers of better quality could be achievable.

Conclusion

In summary, we present the syntheses of three different norbornadiene functionalized platform molecules **1**–**3**. The photochemical switching between the norbornadiene and quadricyclane isomers with two different wavelengths was investigated. Norbornadienes **1** and **2** are quantitatively converted to the corresponding quadricyclanes upon irradiation with light of 385 nm. Back-isomerization with 311 nm to the norbornadiene isomer **1a** is less efficient (52%). The high-energy quadricyclane isomer **1b** is thermochemically unstable at room temperature (half-life 31 d at 21 °C in benzene) only if a cyano as well as an ethynyl substituent are present. No thermal conversion under ambient conditions was observed for **2** and **3**, which are lacking ethynyl substitution. Further studies will be devoted to the surface chemistry of these compounds. Norbornadiene **1** forms highly ordered monolayers on Au(111) surfaces with two different apparent heights. It is not clear if a mixture of norbornadiene **1a** and quadricyclane **1b** or norbornadiene **1a** and octyl-TATA **6** form these mixed monolayers.

Experimental

For detailed experimental procedures, including NMR, UV–vis, MS spectra and STM measurements see Supporting Information File 1, chapters I–IV, and for kinetic studies see chapter V.

Supporting Information

Supporting Information File 1

Experimental and analytical data.
[https://www.beilstein-journals.org/bjoc/content/supplementary/1860-5397-15-175-S1.pdf]

Acknowledgements

The authors gratefully acknowledge financial support by the Deutsche Forschungsgesellschaft within the Sonderforschungsbereich 677, “Function by Switching”.

ORCID® iDs

Roland Löw - https://orcid.org/0000-0002-3051-7831
Fynn Röhricht - https://orcid.org/0000-0001-9935-9256
Rainer Herges - https://orcid.org/0000-0002-6396-6991

Preprint

A non-peer-reviewed version of this article has been previously published as a preprint doi:10.3762/bxiv.2019.5.v1

References

1. Schlimm, A.; Löw, R.; Rusch, T.; Röhricht, F.; Strunskus, T.; Tellkamp, T.; Sönnichsen, F.; Manthe, U.; Magnussen, O.; Tuczek, F.; Herges, R. *Angew. Chem., Int. Ed.* **2019,** *58,* 6574–6578. doi:10.1002/anie.201814342
2. Jung, U.; Schütt, C.; Filinova, O.; Kubitschke, J.; Herges, R.; Magnussen, O. *J. Phys. Chem. C* **2012,** *116,* 25943–25948. doi:10.1021/jp310451c
3. Jacob, H.; Ulrich, S.; Jung, U.; Lemke, S.; Rusch, T.; Schütt, C.; Petersen, F.; Strunskus, T.; Magnussen, O.; Herges, R.; Tuczek, F. *Phys. Chem. Chem. Phys.* **2014,** *16,* 22643–22650. doi:10.1039/c4cp03438d
4. Bronner, C.; Tegeder, P. *New J. Phys.* **2014,** *16,* 053004. doi:10.1088/1367-2630/16/5/053004
5. Baisch, B.; Raffa, D.; Jung, U.; Magnussen, O. M.; Nicolas, C.; Lacour, J.; Kubitschke, J.; Herges, R. *J. Am. Chem. Soc.* **2009,** *131,* 442–443. doi:10.1021/ja807923f
6. Ulrich, S.; Jung, U.; Strunskus, T.; Schütt, C.; Bloedorn, A.; Lemke, S.; Ludwig, E.; Kipp, L.; Faupel, F.; Magnussen, O.; Herges, R. *Phys. Chem. Chem. Phys.* **2015,** *17,* 17053–17062. doi:10.1039/c5cp01447f
7. Nishino, H.; Toki, S.; Takamuku, S. *J. Am. Chem. Soc.* **1986,** *108,* 5030–5032. doi:10.1021/ja00276a067
8. Quant, M.; Lennartson, A.; Dreos, A.; Kuisma, M.; Erhart, P.; Börjesson, K.; Moth-Poulsen, K. *Chem. – Eur. J.* **2016,** *22,* 13265–13274. doi:10.1002/chem.201602530
9. Ikezawa, H.; Kutal, C.; Yasufuku, K.; Yamazaki, H. *J. Am. Chem. Soc.* **1986,** *108,* 1589–1594. doi:10.1021/ja00267a032
10. Kenndoff, J.; Polborn, K.; Szeimies, G. *J. Am. Chem. Soc.* **1990,** *112,* 6117–6118. doi:10.1021/ja00172a031
11. Tranmer, G. K.; Yip, C.; Handerson, S.; Jordan, R. W.; Tam, W. *Can. J. Chem.* **2000,** *78,* 527–535. doi:10.1139/v00-047
12. Gunes, Y.; Arcelik, N.; Sahin, E.; Fleming, F. F.; Altundas, R. *Eur. J. Org. Chem.* **2015,** 6679–6686. doi:10.1002/ejoc.201500895
13. Laursen, B. W.; Krebs, F. C. *Chem. – Eur. J.* **2001,** *7,* 1773–1783. doi:10.1002/1521-3765(20010417)7:8<1773::aid-chem17730>3.0.co;2-f
14. Martin, J. C.; Smith, R. G. *J. Am. Chem. Soc.* **1964,** *86,* 2252–2256. doi:10.1021/ja01065a030
15. Browne, D. L.; Baumann, M.; Harji, B. H.; Baxendale, I. R.; Ley, S. V. *Org. Lett.* **2011,** *13,* 3312–3315. doi:10.1021/ol2010006
16. Gray, V.; Lennartson, A.; Ratanalert, P.; Börjesson, K.; Moth-Poulsen, K. *Chem. Commun.* **2014,** *50,* 5330–5332. doi:10.1039/c3cc47517d
17. Dilling, W. L. *Chem. Rev.* **1966,** *66,* 373–393. doi:10.1021/cr60242a002
18. Srinivasan, R.; Baum, T.; Epling, G. *J. Chem. Soc., Chem. Commun.* **1982,** 437–438. doi:10.1039/c39820000437
19. Hammerich, M.; Rusch, T.; Krekiehn, N. R.; Bloedorn, A.; Magnussen, O. M.; Herges, R. *ChemPhysChem* **2016,** *17,* 1870–1874. doi:10.1002/cphc.201600147
20. Schlimm, A.; Stucke, N.; Flöser, B. M.; Rusch, T.; Krahmer, J.; Näther, C.; Strunskus, T.; Magnussen, O. M.; Tuczek, F. *Chem. – Eur. J.* **2018,** *24,* 10732–10744. doi:10.1002/chem.201800911
21. Lemke, S.; Ulrich, S.; Claußen, F.; Bloedorn, A.; Jung, U.; Herges, R.; Magnussen, O. M. *Surf. Sci.* **2015,** *632,* 71–76. doi:10.1016/j.susc.2014.08.028
22. Rusch, T. R.; Hammerich, M.; Herges, R.; Magnussen, O. M. submitted for publication.

BEILSTEIN JOURNAL OF ORGANIC CHEMISTRY

Supporting Information

for

Norbornadiene-functionalized triazatriangulenium and trioxatriangulenium platforms

Roland Löw, Talina Rusch, Tobias Moje, Fynn Röhricht, Olaf M. Magnussen and Rainer Herges

Beilstein J. Org. Chem. **2019,** *15,* 1815–1821. doi:10.3762/bjoc.15.175

Experimental and analytical data

Table of Contents

I. Analytical equipment and methods

Materials

Solvents for extraction and chromatography were technical grade. Most solvents used in reactions were extra dried (abs.) or used as received. Analytical TLC was performed with Polygeram® SilG/UV254 (Macherey Nagel, 0.2 mm particle size) and visualization was accomplished by UV light. Flash chromatography was carried out using 0.040–0.063 nm silica gel (Merck). Reactions were carried out inert atmosphere using nitrogen (N_2) as gas.

NMR Spectroscopy

NMR spectra were measured in deuterated solvents (Deutero). All compounds were characterized using ^{1}H and ^{13}C NMR spectroscopy. The signals were assigned using 2D spectroscopy. For ^{1}H and ^{13}C NMR assignment we performed HSQC and HMBC experiments. The degree of deuteration is given in parentheses. ^{1}H NMR spectra are referenced to the following signals:

chloroform-*d* (99.8%): δ = 7.26 ppm. (s)

benzene-d_6 (99.8%): δ = 7.16 ppm. (s)

acetone-d_6 (99.5%): δ = 2.05 ppm. (quint.)

The signal multiplicities are abbreviated as follows:

s: singlet, d: doublet, t: triplet, m: multiplet, dt: double triplet, ps. t: pseudo triplet, dd: double dublet, td: trible dublet.

Measurements were performed by the following instruments:

Bruker CABAV 500neo (^{1}H NMR: 500 MHz, ^{13}C NMR: 125 MHz, ^{11}B NMR: 160 MHz, ^{19}F NMR: 470 MHz, ^{29}Si NMR: 99 MHz)

Bruker AV 600 (^{1}H NMR: 600 MHz, ^{13}C NMR: 150 MHz)

IR spectroscopy

Infrared spectra were measured on a Perkin-Elmer 1600 Series FT-IR spectrometer with an A531-G Golden-Gate-Diamond-ATR-unit. Signals were abbreviated with w, m, s and for weak, medium and strong intensities. Broad signals are additionally labeled with br.

Mass spectrometry

The high resolution (HR) mass spectra were measured with an APEX 3 FT-ICR with a 7.05 T magnet by co. Bruker Daltonics. Electron impact (EI). Electrospray ionization (ESI) mass spectra were measured with a Thermo Scientific Q EXACTIVE.

Chromatrography stationary phases

For column chromatography purifications silica gel (Merck, particle size 0.040–0.063 mm) was used. R_f values were determined by thin layer chromatography onPolygram® Sil G/UV254 (Macherey-Nagel, 0.2 mm particle size).

II. Experimental procedures

II.1 3-[2-(Trimethylsilyl)ethynyl]bicyclo[2.2.1]hepta-2,5-diene-2-carbonitrile (5).

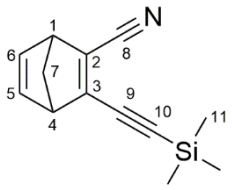

In toluene (24 mL), 3-bromobicyclo[2.2.1]hepta-2,5-diene-2-carbonitrile (**4** [1], 600 mg, 3.06 mmol) was dissolved under nitrogen atmosphere, trimethylsilylacetylene (522 µL, 3.67 mmol), $Pd(PPh_3)_4$ (106 mg, 91.8 µmol), copper(I) iodide (58.3 mg, 306 µmol) and triethylamine (1.06 mL, 7.65 mmol) were added and the mixture was stirred for 80 min at 60 °C. The mixture was filtered through celite and the solvent was removed under reduced pressure. The crude product was purified via column chromatography (silica gel, cyclohexane/ ethyl acetate, 4:1) to obtain a yellow liquid (468 mg, 2.19 mmol, 72%).

^{1}H NMR (500.1 MHz, $CDCl_3$, 298 K, TMS): δ = 6.85-6.81 (m, 2H, *H*-5, *H*-6), 3.86-3.83 (m, 1H, *H*-1), 3.77-3.73 (m, 1H, *H*-4), 2.27 (dt, ^3J = 7.0 Hz, ^4J = 1.6 Hz, 1H, *H*-7_a), 2.18 (dt, ^3J = 7.0 Hz, ^4J = 1.6 Hz, 1H, *H*-7_b), 0.24 (s, 9H, *H*-11) ppm.

^{13}C NMR (125.8 MHz, $CDCl_3$, 298 K, $CHCl_3$): δ = 154.1 (s, *C*-2), 142.0 (s, *C*-5), 141.5 (s, *C*-6), 129.8 (s, *C*-3), 115.0 (s, *C*-9), 97.6 (s, *C*-8), 73.1 (s, *C*-7), 57.3 (s, *C*-4), 54.2 (s, *C*-1), -0.2 (s, *C*-11) ppm.

^{29}Si NMR (99.4 MHz, $CDCl_3$, 298 K, TMS): δ = -16.23 ppm.

MS (EI, 70eV): m/z = 213.1 $[M]^+$.

IR (ATR)**:** $\tilde{\nu}$ = 2927 (w), 2852 (w), 2207 (m), 2139 (w), 1576 (w), 1557 (w), 1450 (w), 1302 (m), 1251 (m), 1132 (w), 1068 (w), 1019 (w), 840 (vs), 760 (m), 733 (s), 702 (w), 626 (m), 534 (m) cm^{-1}.

HRMS (EI, 70 eV): m/z $[M]^+$ calcd. for $C_{13}H_{15}NSi$: 213.09738, found: 213.09724.

II.2 12c-(2-(2-Cyanobicyclo[2.2.1]hepta-2,5-diene-3-yl)ethynyl)-4,8,12-tri-*n*-octyl-4,8,12-triazatriangulene (1).

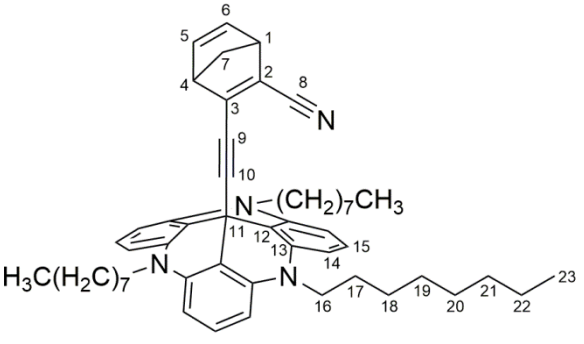

In THF (abs., 60 mL) 3-[2-(trimethylsilyl)ethynyl]bicyclo[2.2.1]hepta-2,5-diene-2-carbonitrile (**5**, 100 mg, 469 µmol) was dissolved under nitrogen atmosphere, octyl-TATA-BF_4 **6** [2] (397 mg, 562 µmol) and powdered potassium hydroxide (263 mg, 3.69 mmol) were added and the mixture was refluxed for 5 h. The mixture was poured onto saturated sodium chloride solution (50 mL) and the aqueous phase extracted with diethyl ether (3 × 50 mL). The combined organic layers were dried over magnesium sulfate and the solvent was removed under reduced pressure. The crude product was purified via column chromatography (aluminium oxide basic, diethyl ether) and recrystallized from ethanol to obtain an orange solid (222 mg, 292 µmol, 62%).

^{1}H NMR (600.1 MHz, C_6D_6, 298 K, TMS): δ = 7.21 (t, ^3J = 8.2 Hz, 3H, *H*-15), 6.61 (m, 6H, *H*-14), 5.91-5.86 (m, 1H, *H*-5), 5.76-5.73 (m, 1H, *H*-6), 3.86-3.80 (ps. t, 6H, *H*-16), 2.89-2.86 (m, 1H, *H*-4), 2.82-2.79 (m, 1H, *H*-1), 1.86-1.77 (m, 6H, *H*-17), 1.34-1.20 (m, 32H, *H*-7_a, *H*-7_b, *H*-18, *H*-19, *H*-20, *H*-21, *H*-22), 0.94-0.90 (ps. t, 9H, *H*-23) ppm.

^{13}C NMR (150.9 MHz, C_6D_6, 298 K, TMS): δ = 153.8 (s, *C*-2), 141.3 (s, *C*-5), 141.1 (s *C*-13), 140.8 (s, *C*-6), 129.4 (s, *C*-3), 129.1 (s, *C*-15), 109.4 (s, *C*-12), 105.6 (s, *C*-14), 79.5 (s, *C*-10), 72.2 (s, *C*), 56.4 (s, *C*-1), 53.6 (s, *C*-4), 47.1 (s, *C*-16), 32.2 (s, *C*), 30.2 (s, *C*-11), 29.8 (s, *C*), 29.7 (s, *C*-7), 27.2 (s, *C*), 25.9 (s, *C*-17), 23.1 (s, *C*-18), 14.4 (s, *C*-22) ppm.

MS (MALDI-TOF): m/z = 759.1 $[M]^+$.

IR (ATR): $\tilde{\nu}$ = 2953 (m), 2922 (m), 2851 (m), 2207 (w), 1617 (s), 1579 (vs), 1481 (s), 1456 (vs), 1394 (vs), 1372 (m), 1267 (m), 1246 (m), 1207 (w), 1167 (s), 1147 (m), 908 (w), 766 (vs), 731 (vs), 657 (w), 637 (m), 609 (w) cm^{-1}.

m.p. = 101.7 °C.

Elemental analysis calcd. (%) for $C_{53}H_{66}N_4$: C 83.86; H 8.76; N 7.38; found: C 83.53; H 8.65; N 7.32.

II.3 3-[2-Methyl-4-(trimethylsilylethynyl)phenyl]bicyclo[2.2.1]hepta-2,5-diene-2-carbonitrile (10).

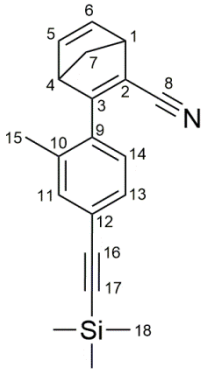

In a solution of toluene (13 mL), ethanol (3.75 mL) and H_2O (750 µL) 2-[2-methyl-4-[2-(trimethylsilyl)ethynyl]phenyl]-4,4,5,5-tetramethyl-1,3,2-dioxaborolane (**9** [3], 321 mg, 1.02 mmol), 3-bromo-bicyclo[2.2.1]hepta-2,5-diene-2-carbonitrile (**4** [1], 100 mg, 510 µmol), $Pd(PPh_3)_4$ (29.5 mg, 25.5 µmol) and sodium carbonate (136 mg, 1.28 mmol) were suspended under nitrogen atmosphere and refluxed for 12 h. To the mixture H_2O (10 mL) was added and the layers were separated. The water layer was extracted with dichloromethane (3 × 30 mL)

and the combined organic layers were dried over magnesium sulfate. The solvent was removed under reduced pressure and the crude product was purified via column chromatography (silica gel, cyclohexane/ethyl acetate, 4:1) to obtain a yellow oil (59.0 mg, 194 μmol, 38%).

^{1}H NMR (500.1 MHz, acetone-d_6, 298 K, TMS): δ = 7.39 (s, 1H, *H*-11), 7.33 (dd, ^{3}J = 8.0 Hz, ^{4}J = 1.0 Hz, 1H, *H*-13), 7.19 (d, ^{3}J = 8.0 Hz, 1H, *H*-14), 7.11-7.04 (m, 2H, *H*-5, *H*-6), 3.99-3.96 (m, 2H, *H*-1, *H*-4), 2.45 (td, ^{3}J = 6.9 Hz, ^{4}J = 1.6 Hz, 1H, *H*-7_a), 2.32 (s, 3H, *H*-9), 2.21 (td, ^{3}J = 6.9 Hz, ^{4}J = 1.6 Hz, 1H, *H*-7_b), 0.24 (s, 9H, *H*-18) ppm.

^{13}C NMR (125.8 MHz, acetone-d_6, 298 K, TMS): δ = 174.1 (s, *C*-3), 144.0 (s, *C*), 142.6 (s, *C*), 137.0 (s, C-10), 135.9 (s, *C*-9), 134.8 (s, *C*-11), 130.0 (s, *C*-13), 128.2 (s, *C*-14), 124.7 (s, *C*-12), 123.6 (s, *C*-2), 105.5 (s, *C*-16), 95.7 (s, *C*-17), 73.7 (s, *C*-7), 58.3 (s, *C*), 55.4 (s, *C*), 20.4 (s, *C*-9), 0.0 (s, *C*-18) ppm.

^{29}Si NMR (99.4 MHz, acetone-d_6, 298 K, TMS): δ = -17.48 ppm.

MS (EI, 70eV): m/z = 303.14 $[M]^+$.

IR: $\tilde{\nu}$ = 2958 (br, w), 2204 (m), 2151 (w), 1606 (w), 1560 (w), 1493 (w), 1450 (w), 1310 (w), 1295 (m), 1233 (w), 1004 (w), 949 (w), 899 (w), 834 (vs), 814 (s), 759 (m), 723 (vs), 658 (m) cm^{-1}.

HRMS (EI, 70 eV): m/z $[M]^+$ calcd. for $C_{20}H_{21}NSi$: 303.14433, found: 303.14410.

II.4 12c-(4-(2-Cyanobicyclo[2.2.1]hepta-2,5-diene-3-yl)-3-methylphenyl)ethynyl-4,8,12-tri-*n*-octyl-4,8,12-triazatriangulene (2).

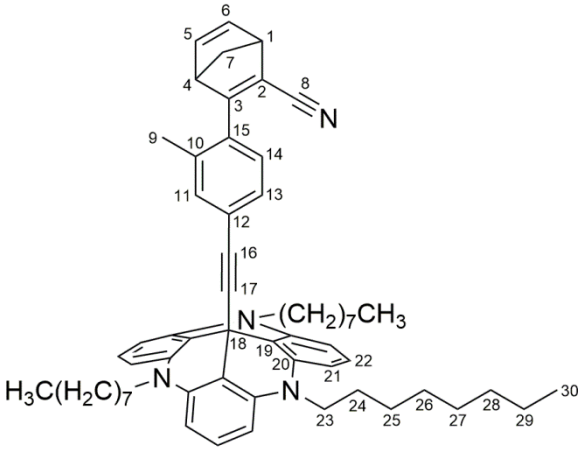

In THF (abs., 40 mL) 3-[2-methyl-4-(trimethylsilylethynyl)phenyl]bicyclo[2.2.1]hepta-2,5-diene-2-carbonitrile (**10**, 65.0 mg, 214 μmol) was dissolved under nitrogen atmosphere and octyl-TATA-BF_4 **6** [2] (181 mg, 257 μmol) and powdered potassium hydroxide (95.9 mg, 1.71 mmol) were added and the mixture and was refluxed for 1 h. The mixture was poured onto sat. sodium chloride solution (30 mL) and extracted with diethyl ether (3 × 50 mL). The combined organic layers were dried over magnesium sulfate and the solvent was removed under reduced pressure. The crude product was purified via column chromatography (aluminium oxide basic, diethyl ether) and recrystallized from ethanol to obtain a grey solid (80.0 mg, 94.2 μmol, 44%).

^{1}H NMR (500.1 MHz, C_6D_6, 298 K, TMS): δ = 7.25 (t, ^3J = 8.3 Hz, 3H, *H*-22), 6.85 (dd, ^3J = 8.1 Hz, ^4J = 1.1 Hz, 1H, *H*-13), 6.82 (s, 1H, *H*-11), 6.66-6.61 (m, 7H, *H*-21, H-14), 6.33 (dd, ^3J = 5.1 Hz, ^3J = 3.0 Hz, 1H, *H*-5), 6.19 (dd, ^3J = 5.1 Hz, ^3J = 3.0 Hz, 1H, *H*-6), 3.84-3.78 (ps. t, 6H, *H*-23), 3.24-3.21 (m, 1H, *H*-4), 3.02-2.99 (m, 1H, *H*-1), 1.85-1.77 (m, 6H, *H*-24), 1.76 (s, 3H, *H*-9), 1.64 (td, ^3J = 6.8 Hz, ^4J = 1.5 Hz, 1H, *H*-7_a), 1.54 (td, ^3J = 6.8 Hz, ^4J = 1.5 Hz, 1H, *H*-7_b), 1.31-1.15 (m, 30H, *H*-25, *H*-26, *H*-27, *H*-28, *H*-29), 0.91 (ps. t, 9H, *H*-30) ppm.

^{13}C NMR (125.8 MHz, C_6D_6, 298 K, TMS): δ = 172.3 (s, *C*-3), 142.9 (s, *C*-5), 141.2 (s, *C*-20), 141.0 (s, *C*-6), 135.0 (s, *C*-10), 134.5 (s, *C*-11), 133.5 (s, *C*-15), 129.4 (s, *C*-13), 128.7 (s, *C*-22) 126.7 (s, *C*-14), 125.0 (s, *C*-12), 122.2 (s, *C*-2), 111.1 (s, *C*-19), 105.7 (s, *C*-21), 95.6 (s, *C*-16), 84.1 (s, *C*-17), 72.4 (s, *C*-7), 57.2 (s, *C*-1), 54.5 (s, *C*-4), 46.7 (s, *C*-23), 32.2 (s, *C*-27), 29.7 (s, *C*-28), 29.7 (s, *C*-29), 29.1 (s, *C*-18), 27.2 (s, *C*-25), 26.2 (s, *C*-24), 23.0 (s, *C*-26), 20.0 (s, *C*-9), 14.4 (s, *C*-30) ppm.

MS (MALDI-TOF): m/z = 849.4 $[M]^+$.

IR: $\tilde{\nu}$ = 2922 (s), 2852 (m), 2204 (w), 1615 (s), 1579 (vs), 1482 (vs), 1456 (vs), 1393 (cs), 1373 (m), 1293 (w), 1267 (m), 1244 (m), 1167 (s), 1022 (w), 911 (w), 886 (w), 828 (w),, 816 (w), 789 (w), 772 (m), 748 (m), 724 (s), 696 (vs), 657 (w), 608 (w) cm^{-1}.

m.p. = 73.6 °C.

Elemental analysis calcd. (%) for $C_{60}H_{72}N_4$: C 84.86; H 8.55; N 6.60; found: C 84.63; H 8.48; N 6.57.

II.5 Synthesis of 4,8,12-Trioxatriangulenium tetrakis[3,5-bis(trifluoromethyl)phenyl]-borate (8)

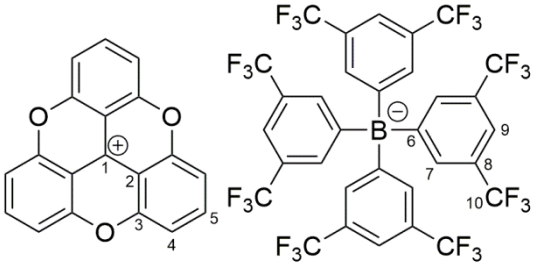

In dichloromethane (200 mL) 4,8,12-trioxatriangulenium tetrafluoroborate (**7** [4], 636 mg, 1.71 mmol) and sodium tetrakis[3,5-bis(trifluoromethyl)phenyl]borate (1.89 g, 2.10 mmol) were suspended and stirred at room temperature for 2 h. The mixture was filtered and the solution was washed with water (3 × 150 mL) and dried over magnesium sulfate. The solvent was removed under reduced pressure and the crude product was dissolved in 25 mL ethyl acetate and precipitated by adding 400 mL cyclohexane. Filtration gave 1.77 g (1.54 mmol, 91%) of a yellowish solid.

^{1}H NMR (500.1 MHz, acetone-d_6, 298 K, TMS): δ = 8.66 (t, ^3J = 8.5 Hz, 3H, *H*-5), 7.99 (d, ^3J = 8.5 Hz, 6H, *H*-4), 7.79 (t, ^4J = 2.5 Hz, 8H, *H*-7), 7.67 (s, 4H, *H*-9) ppm.

^{13}C NMR (125.8 MHz, acetone-d_6, 298 K, TMS): δ = 162.6 (q, *C*-6), 154.7 (s, *C*-3), 144.7 (m, *C*-5), 135.5 (m, *C*-7), 130.0 (m, *C*-10), 125.4 (d, *C*-8), 118.4 (m, *C*-9), 113.6 (s, *C*-4), 107.3 (s, *C*-2) ppm.

^{19}F NMR (470 MHz, acetone-d_6, 298 K, TMS): δ = -62.2 ppm.
^{11}B NMR (160 MHz, acetone-d_6, 298 K, TMS): δ = -5.86 ppm.

IR (ATR): $\tilde{\nu}$ = 2311 (w), 2164 (w), 1635 (s), 1552 (m), 1467 (m), 1355 (s), 1275 (s), 1143 (s), 1112 (s), 1063 (s), 1021 (s), 900 (m), 887 (m), 776 (s), 681 (s), 558 (s), 412 (m) cm^{-1}.

MS (ESI, pos): m/z = 285.05 $[C_{19}H_9O_3]^+$.

MS (ESI, neg): m/z = 863.07 $[C_{32}H_{12}BF_{24}]^-$.

m.p. = 202 °C.

HRMS (ESI, pos): m/z $[M]^+$ calc. for $C_{19}H_9O_3$: 285.05462, found: 285.05428.
(ESI, neg): m/z $[M]^-$ calc. for $C_{32}H_{12}BF_{24}$: 862.06906, found: 862.06892.

II.6 12c-(2-Cyanobicyclo[2.2.1]hepta-2,5-diene-3-yl)-4,8,12-trioxatriangulene (3).

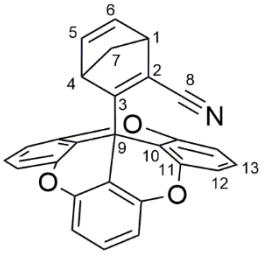

In THF (abs., 15 mL), 3-bromobicyclo[2.2.1]hepta-2,5-diene-2-carbonitrile (**4** [5-7], 213 mg, 1.09 mmol) was dissolved under nitrogen atmosphere und the solution was cooled to −78 °C. To the solution *n*-BuLi (436 µL, 1.09 mmol, 2.5 M in *n*-hexane) was added slowly and stirred for 45 min. 4,8,12-Trioxatriangulenium tetrakis[3,5-bis(trifluormethyl)phenyl]borate (**8**, 1.38 g, 1.20 mmol), dissolved in THF (abs., 30 mL), was added slowly and stirred for 45 min at −78 °C and further for 20 h at room temperature. To the solution, diethyl ether (30 mL) was added and the solution was washed with water (3 × 50 mL). The combined organic layers were dried over magnesium sulfate and the solvent was removed under reduced pressure. The crude product was purified via column chromatography (alox basic, diethyl ether) and recrystallized from methanol to obtain a colorless solid (147 mg, 367 µmol, 22%).

^{1}H NMR (500.1 MHz, C_6D_6, 298 K, TMS): δ = 6.93 (t, ^3J = 8.3 Hz, 3H, *H*-13), 6.87-6.81 (m, 6H, *H*-12), 6.01 (dd, ^3J = 5.0 Hz, ^3J = 3.1 Hz, 1H, *H*-5), 5.83 (dd, ^3J = 5.0 Hz, ^3J = 3.1 Hz, 1H, *H*-6), 3.55-3.53 (m, 1H, *H*-4), 3.03-3.00 (m, 1H, *H*-1), 1.25-1.20 (m, 2H, *H*-7) ppm.

^{13}C NMR (125.8 MHz, C_6D_6, 298 K, TMS): δ = 173.7 (s, *C*-3), 153.3 (d, *C*-11), 142.3 (s, *C*-5), 140.3 (s, *C*-6), 129.9 (s, *C*-13), 120.4 (s, *C*-2), 111.9 (d, *C*-12), 109.9 (s, *C*-10), 70.7 (s, *C*-7), 55.4 (s, *C*-1), 52.6 (s, *C*-4), 31.3 (s, *C*-9) ppm.

MS (EI, 70eV): m/z = 401.07 $[M]^+$.

IR (ATR): $\tilde{\nu}$ = 2946 (w), 2202 (w), 1743 (w), 1612 (s), 1481 (m), 1456 (s), 1306 (w), 1260 (vs), 1065 (m), 1041 (m), 1010 (vs), 934 (w), 903 (m), 877 (m), 786 (m), 773 (m), 688 (m), 597 (w), 576 (w) cm^{-1}.

HRMS (EI, 70 eV): m/z $[M]^+$ calcd. for $C_{27}H_{15}NO_3$: 401.10519, found: 401.10515.

III. NMR spectra

III.1 3-[2-(Trimethylsilyl)ethynyl]bicyclo[2.2.1]hepta-2,5-diene-2-carbonitrile (5).

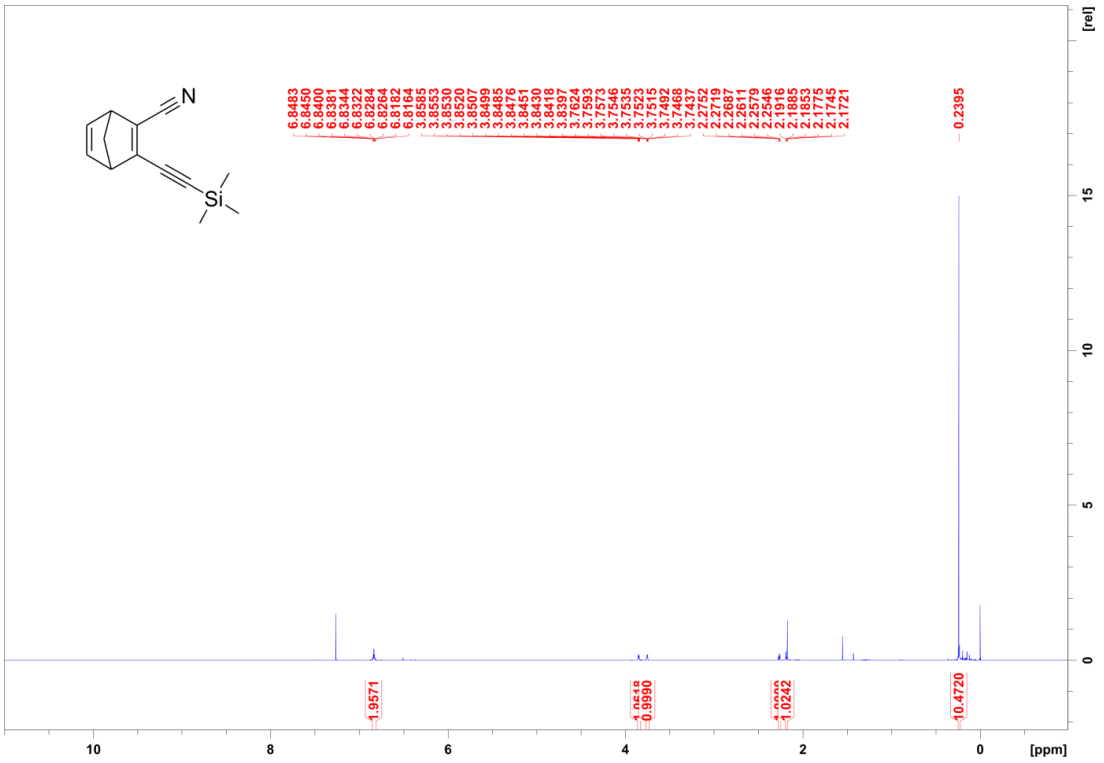

Figure S1. ^{1}H NMR spectrum (500.1 MHz, $CDCl_3$) of compound **5**.

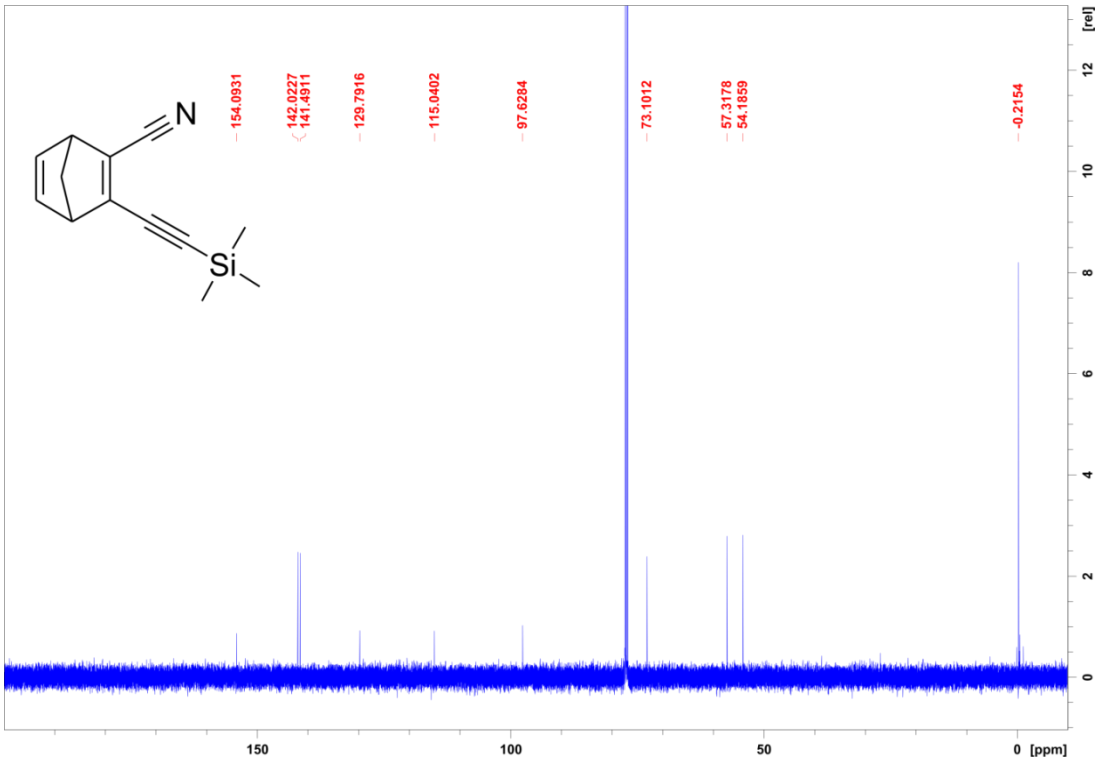

Figure S2. ^{13}C NMR spectrum (125.8 MHz, $CDCl_3$) of compound **5**.

III.2 12c-(2-(2-Cyanobicyclo[2.2.1]hepta-2,5-diene-3-yl)ethynyl)-4,8,12-tri-*n*-octyl-4,8,12-triazatriangulene (1).

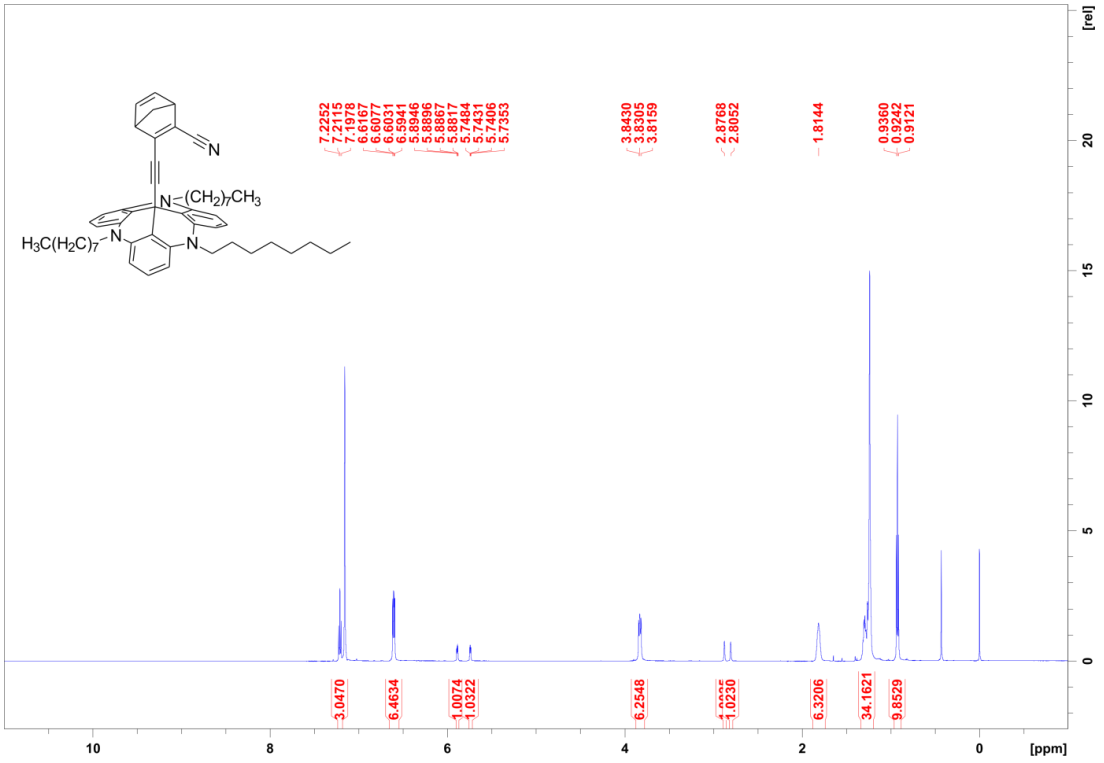

Figure S3. ^{1}H NMR spectrum (600.1 MHz, C_6D_6) of compound **1**.

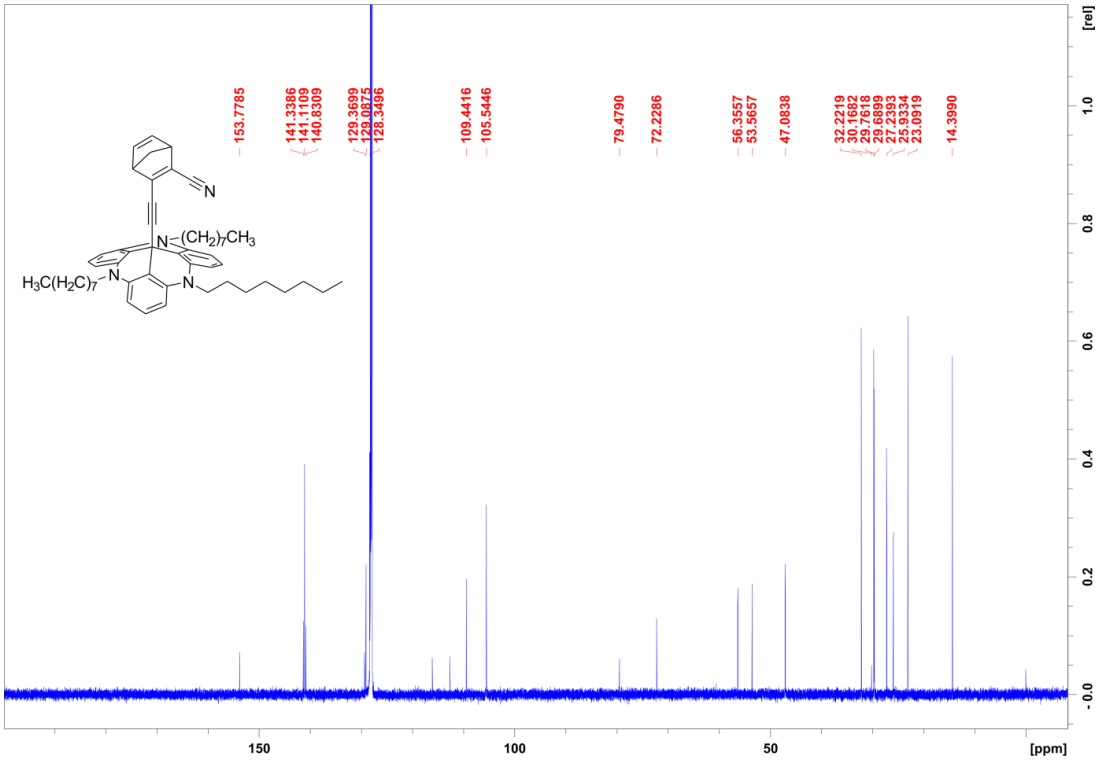

Figure S4. ^{13}C NMR spectrum (150.9 MHz, C_6D_6) of compound **1**.

III.3 3-[2-Methyl-4-(trimethylsilylethynyl)phenyl]bicyclo[2.2.1]hepta-2,5-diene-2-carbonitrile (10).

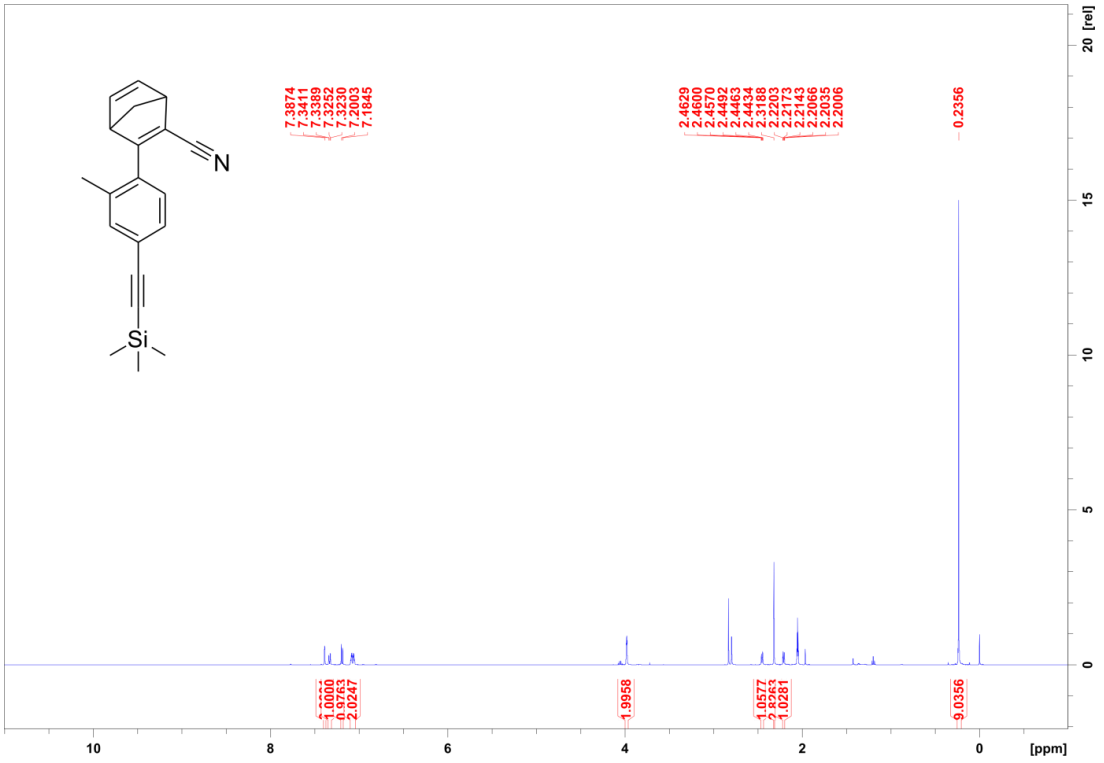

Figure S5. ^{1}H NMR spectrum (500.1 MHz, acetone-d_6) of compound **10**.

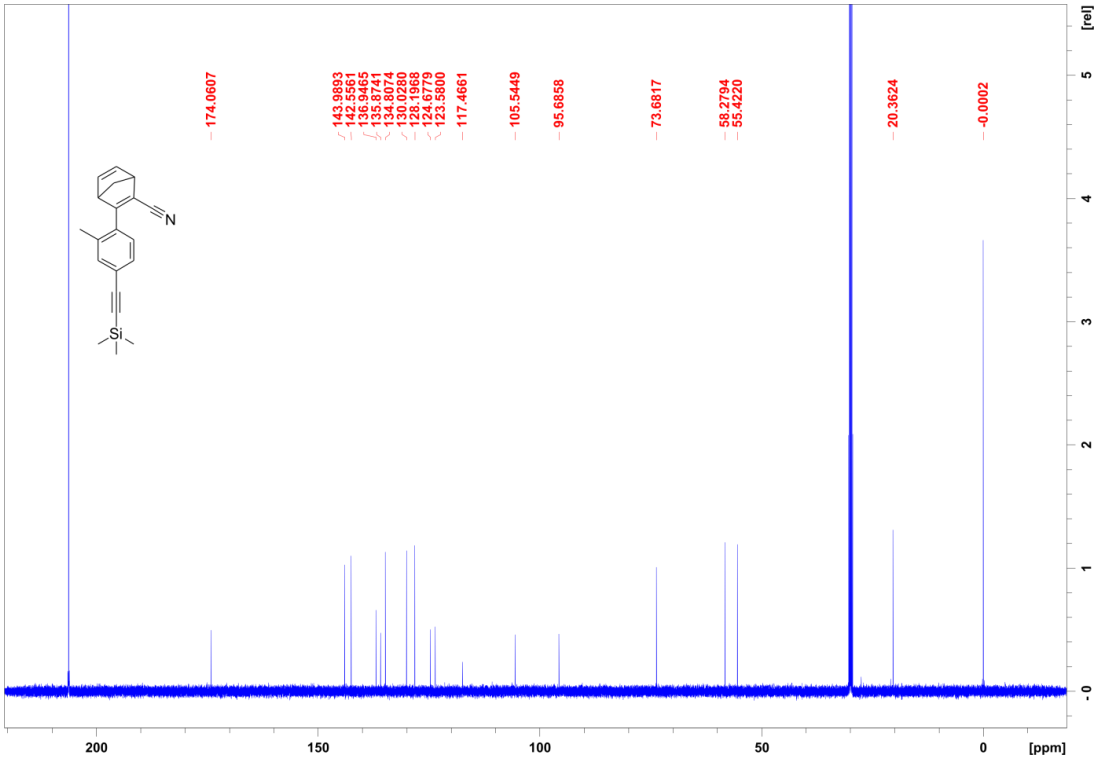

Figure S6. ^{13}C NMR spectrum (125.8 MHz, acetone-d_6) of compound **10**.

III.4 12c-(4-(2-Cyanobicyclo[2.2.1]hepta-2,5-diene-3-yl)-3-methylphenyl)ethynyl-4,8,12-tri-*n*-octyl-4,8,12-triazatriangulene (2).

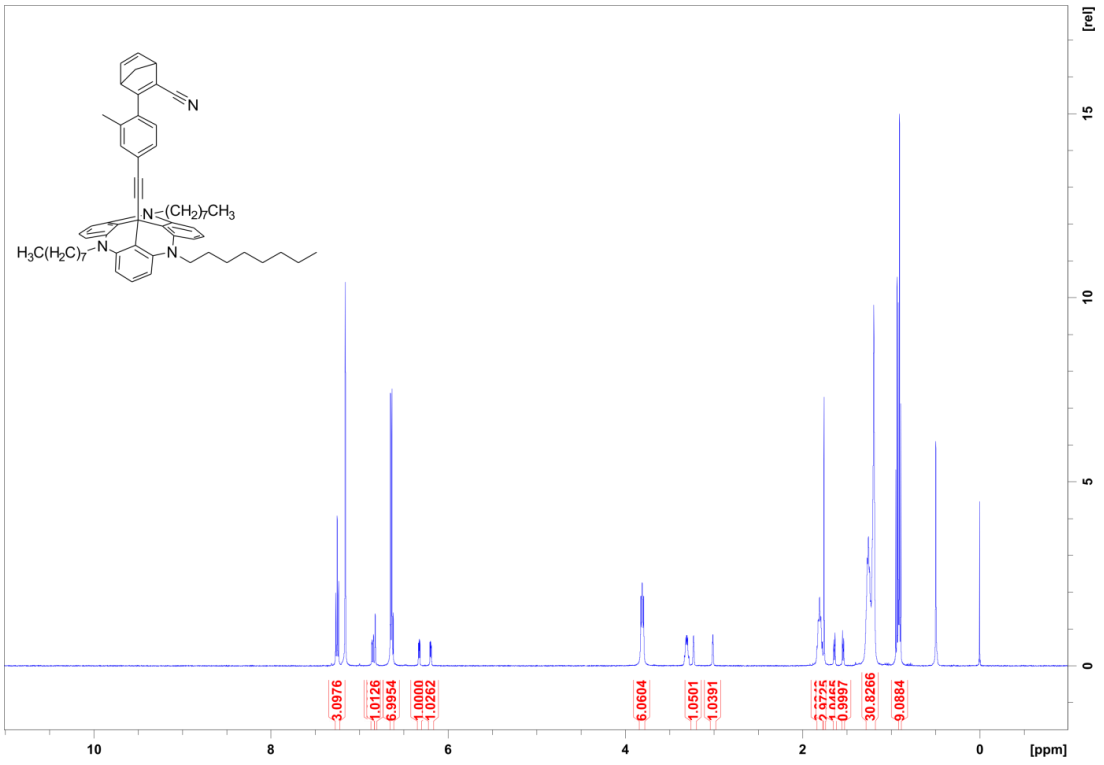

Figure S7. ^{1}H NMR spectrum (500.1 MHz, C_6D_6) of compound **2**.

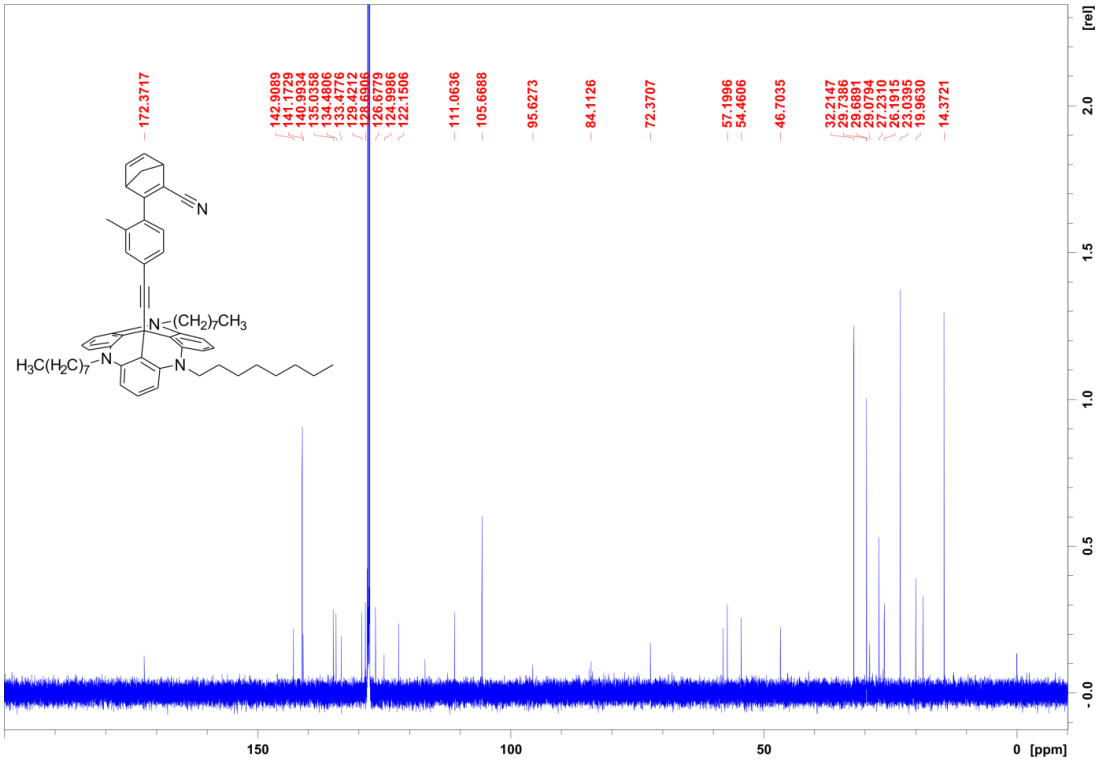

Figure S8. ^{13}C NMR spectrum (125.8 MHz, C_6D_6) of compound **2**.

III.5 Synthesis of 4,8,12-trioxatriangulenium tetrakis[3,5-bis(trifluoromethyl)phenyl]-borate (8)

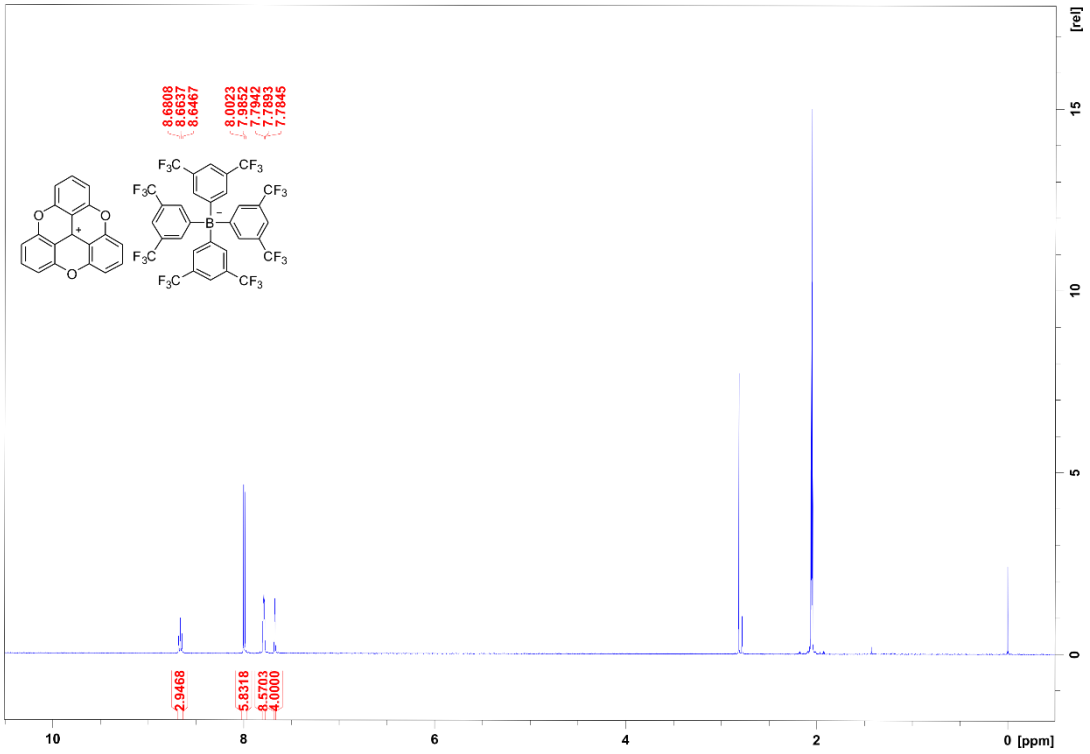

Figure S9. ^{1}H NMR spectrum (500.1 MHz, acetone-d_6) of compound **8**.

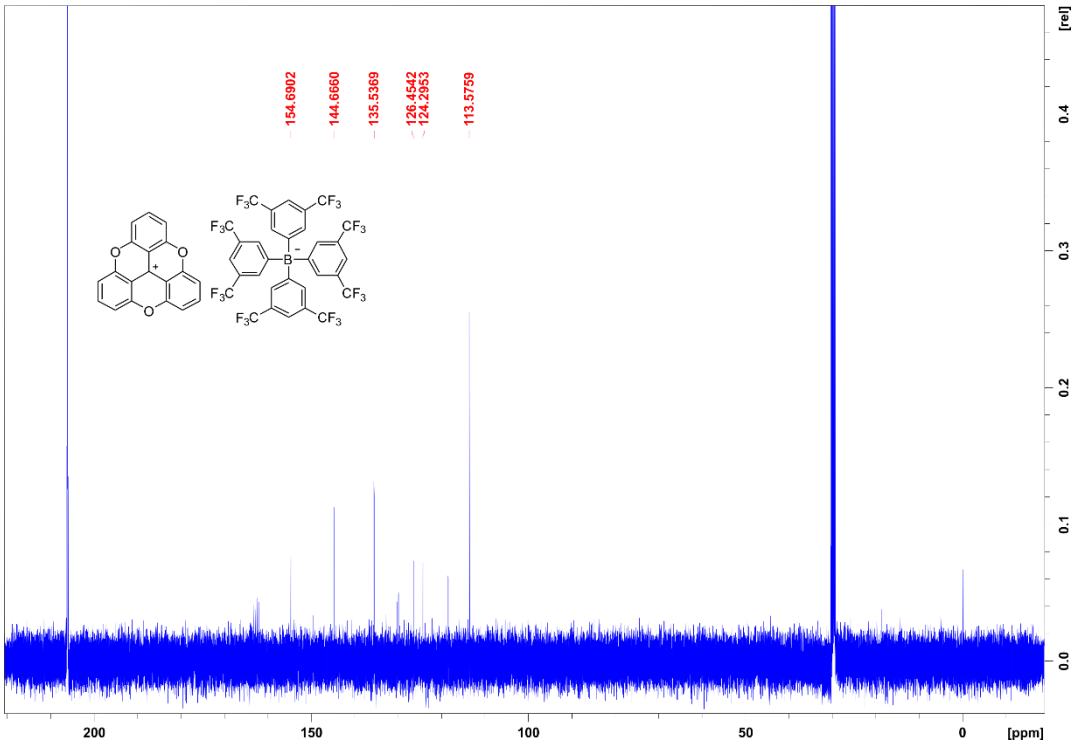

Figure S10. ^{13}C NMR spectrum (125.8 MHz, acetone-d_6) of compound **8**.

III.6 12c-(2-Cyanobicyclo[2.2.1]hepta-2,5-diene-3-yl)-4,8,12-trioxatriangulene (3).

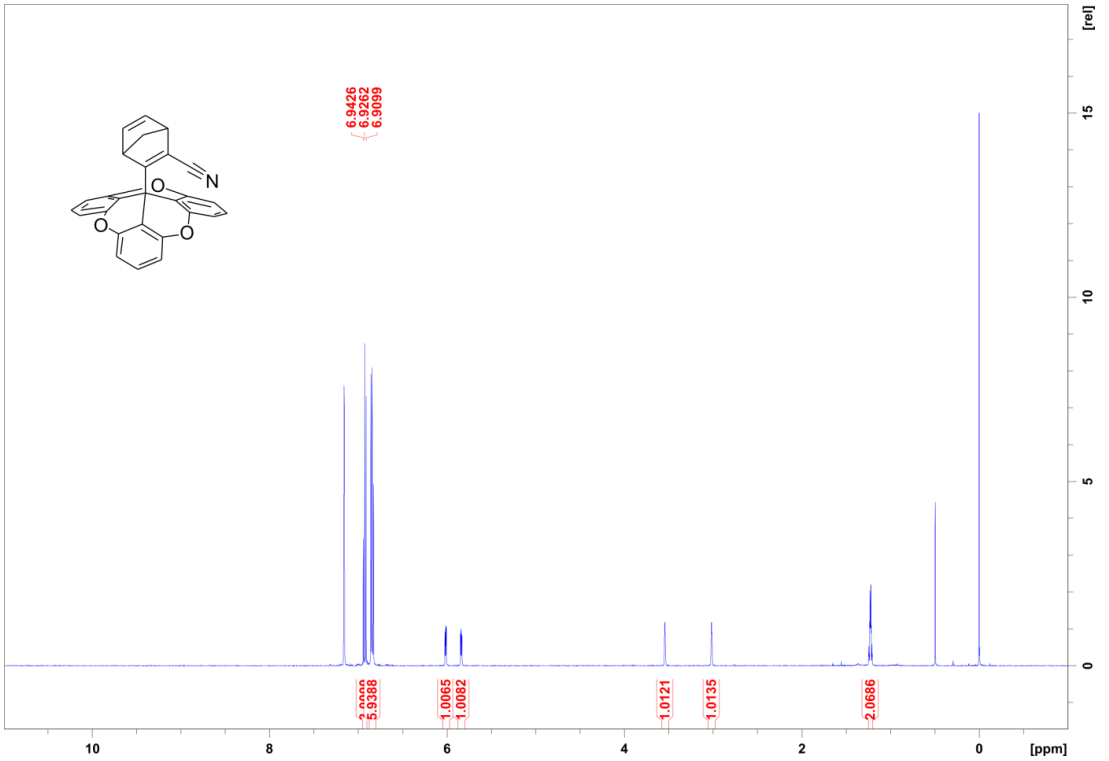

Figure S11. ^{1}H NMR spectrum (500.1 MHz, acetone-d_6) of compound **3**.

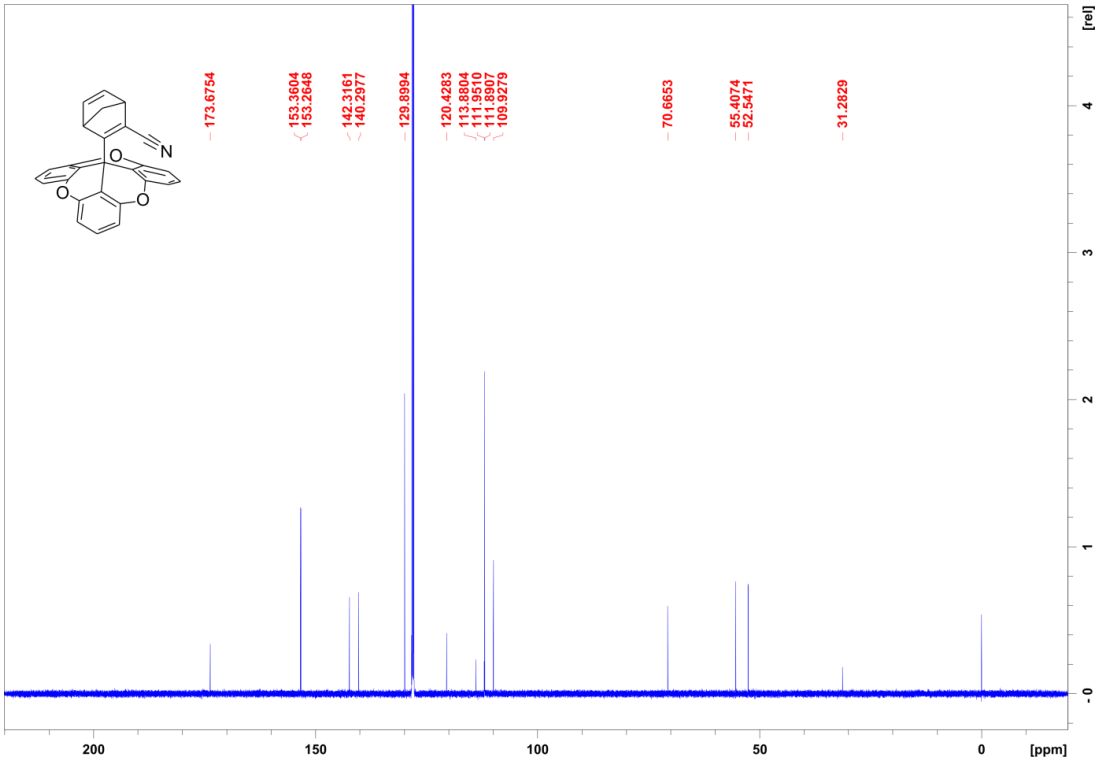

Figure S12. ^{13}C NMR spectrum (125.8 MHz, acetone-d_6) of compound **3**.

IV. UV–vis absorption spectra

IV.1 Methods

UV–vis spectra were recorded on a PerkinElmer Lambda 650 Photospectrometer in a 1 cm path length quartz cuvette. Irradiation of UV–vis samples were carried out at 25 °C using a self-built LED positioned at a distance of 1 cm from the sample.

IV.2 UV/Vis spectra

Compound **1**:

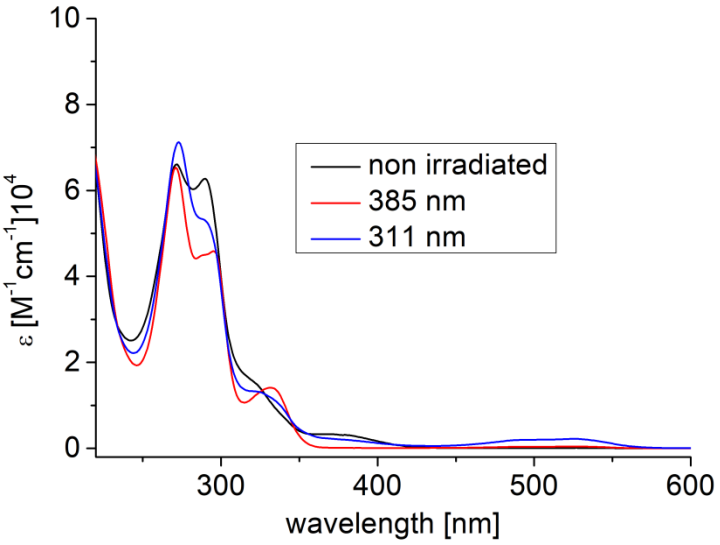

Figure S13. UV–vis spectra of compound **1** in THF at rt (31.6 μmol/L). Upon irradiation with 385 nm the [2 + 2] cycloaddition and with 311 nm the [2 + 2] cycloreversion take place with partly decomposition of **1**.

Compound **2**:

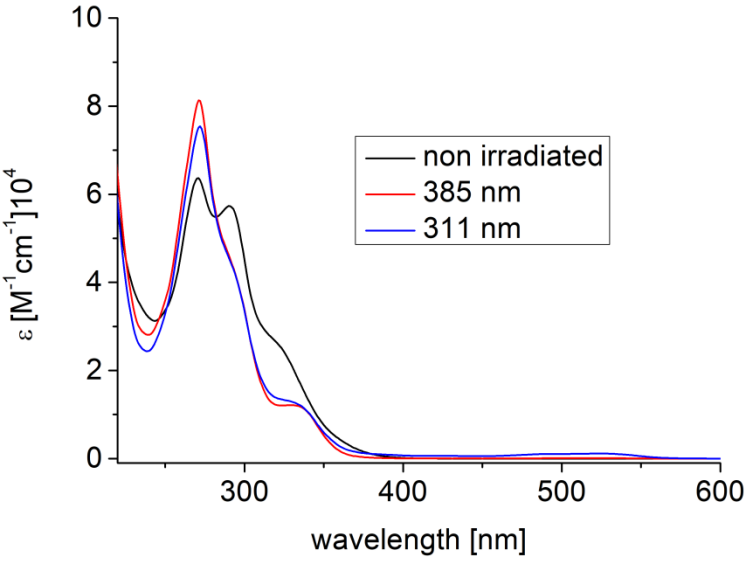

Figure S14. UV–vis spectra of compound **2** in THF at rt (30.6 μmol/L). Upon irradiation with 385 nm the [2 + 2] cycloaddition and with 311 nm the [2 + 2] cycloreversion take place with partly decomposition of **2**.

Compound **3**:

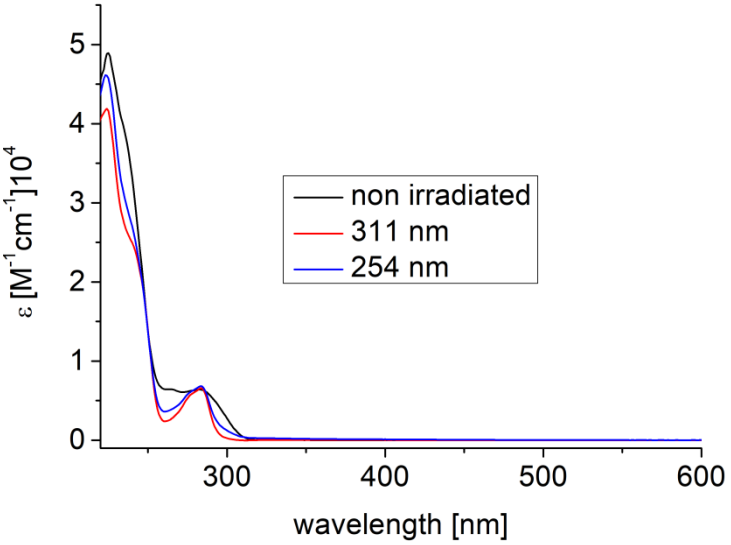

Figure S15. UV–vis spectra of compound **3** in THF at rt (79.7 μmol/L). Upon irradiation with 311 nm the [2 + 2] cycloaddition and with 254 nm the [2 + 2] cycloreversion take place.

V. Kinetic studies in solution by ^{1}H NMR spectroscopy

V.1 Thermal isomerization rate measurements by ^{1}H NMR

V.1.1 Compound 1: 12c-(2-(2-cyanobicyclo[2.2.1]hepta-2,5-diene-3-yl)ethynyl)-4,8,12-tri-*n*-octyl-4,8,12-triazatriangulene

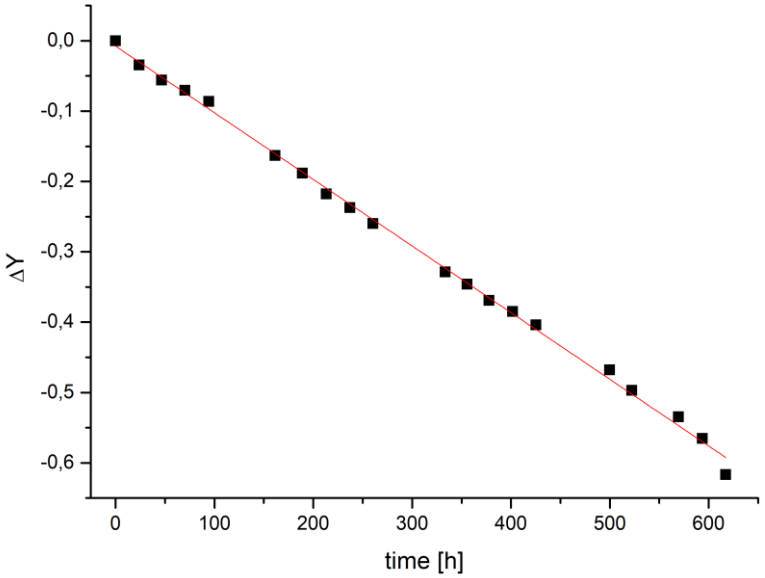

Figure S16. Determination of the thermal isomerization rate *k* of **1b** (QC) by ^{1}H NMR spectroscopy (toluene, 294.5 K, 800 µmol/L, under nitrogen). ΔY: ln { $[QC]_t/[QC]_0$ }, $[QC]_t$: ^{1}H NMR integral of the CH_2 group neighbouring the N bridge atom of the TATA platform in QC **1b** at time *t*, $[QC]_0$ corresponding ^{1}H integral at $t = 0$. A rate constant of $k = 0.95 \cdot 10^{-3}$ s^{-1} was determined from a linear fit of the Δ*Y*/*t* curve. The half-life of **1b** at 293.5 K in toluene was determined as 742.7 h.

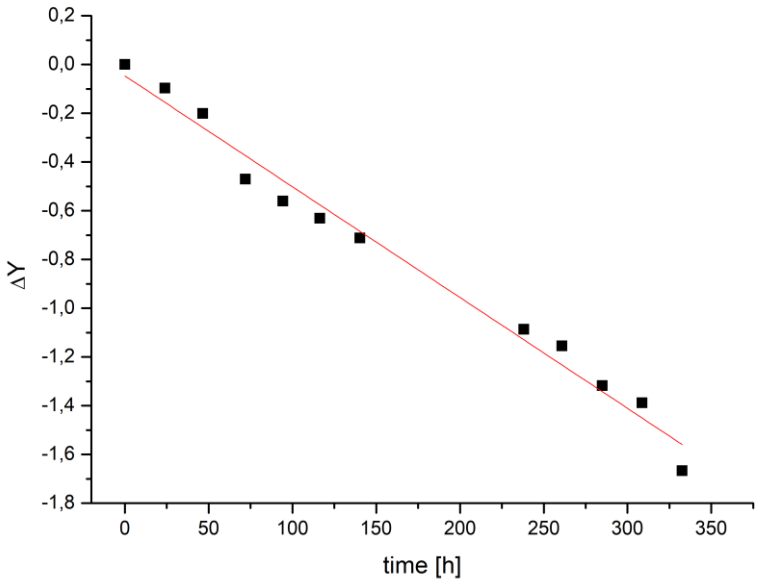

Figure S17. Determination of the thermal isomerization rate *k* of **1b** (QC) by ^{1}H NMR spectroscopy (toluene, 306 K, 800 µmol/L, under nitrogen). ΔY: ln { $[QC]_t/[QC]_0$ }, $[QC]_t$: ^{1}H NMR integral of the CH_2 group neighbouring the N bridge atom of the TATA platform in QC **1b** at time *t*, $[QC]_0$ corresponding ^{1}H integral at *t* = 0. A rate constant of $k = 4.55 \cdot 10^{-3}$ s^{-1} was determined from a linear fit of the ΔY/*t* curve. The half-life of **1b** at 305 K in toluene was determined as 152.3 h.

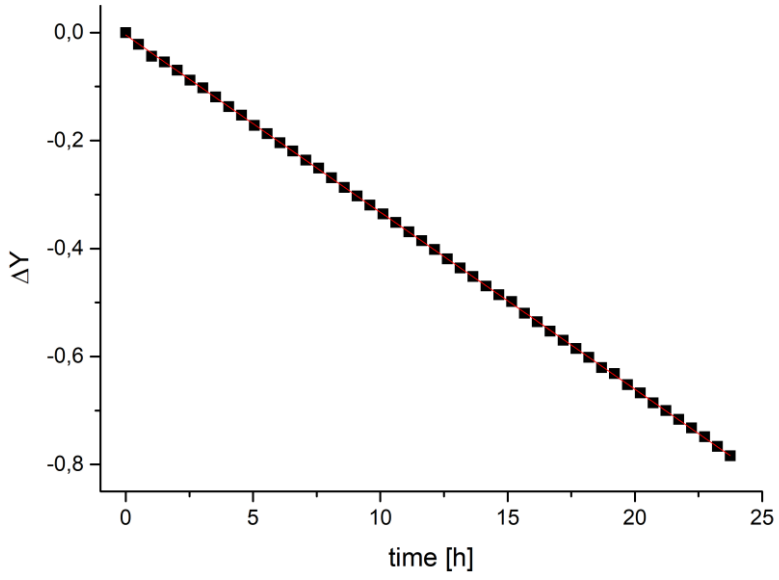

Figure S18. Determination of the thermal isomerization rate *k* of **1b** (QC) by ^{1}H NMR spectroscopy (toluene, 318 K, 800 µmol/L, under nitrogen). ΔY: ln { $[QC]_t/[QC]_0$ }, $[QC]_t$: ^{1}H NMR integral of the CH_2 group neighbouring the N bridge atom of the TATA platform in QC **1b** at time *t*, $[QC]_0$ corresponding ^{1}H integral at *t* = 0. A rate constant of $k = 3.28 \cdot 10^{-2}$ s^{-1} was determined from a linear fit of the ΔY/*t* curve. The half-life of **1b** at 316 K in toluene was determined as 21.1 h.

V.2 Arrhenius Plots for compound 1 in solution

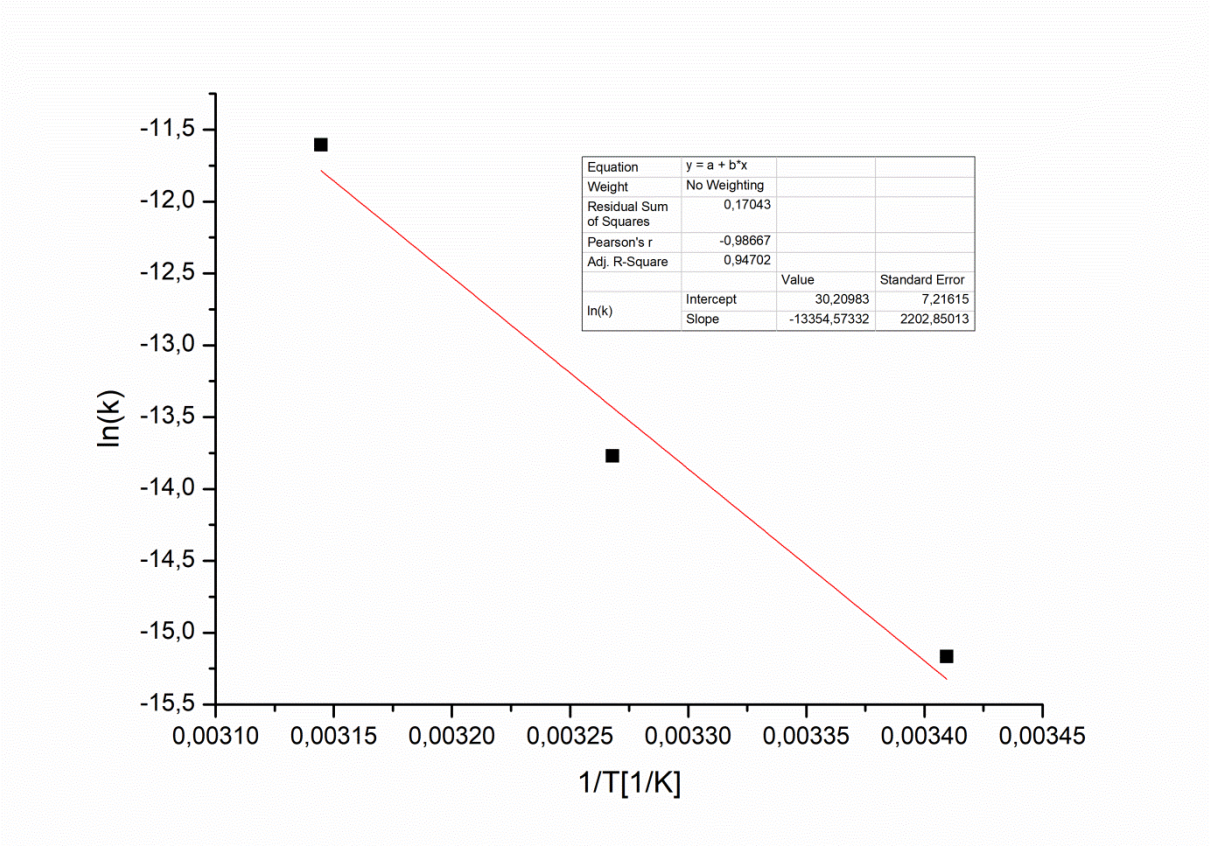

Figure S19. Arrhenius plot of the QC→NB isomerization of compound **1** which shows an activation energy of 111 kJ/mol.

VI. STM measurements

SAMs were prepared by immersing an Au(111) single crystal 3 hours in a 1–100 µM solution of **1** in toluene at room temperature. Afterwards the samples were rinsed with toluene and dried in the air. STM measurements were performed under ambient conditions, using a PicoPlus SPM (Agilent) and Pt/Ir tips.

VII. Calculations

General

All geometry optimizations were carried out using density functional theory with the Minnesota functional M06-2X [8] in cooperation with Grimmes D3 [9] dispersion correction and the large triple zeta basis def2-TZVP [10]. This level performed well in Grimme's study on basic properties of a selected data base of structures [11]. The calculations were carried out with Turbomole7.2 [12], the m4 grid (in Turbomole nomenclature) and resolution-of-identity (RI) with multipole accelerated RI-J (marij). All stationary points were characterized by frequency calculations.

Coordinates

1a Norbornadiene-ethinyl-TATA

$E_{M062x\text{-}D3/def2TZVPP}$ = -1334.818694137

Nimag = 2 (-17.61 cm^{-1}; -6.98 cm^{-1})

C	0.2951221	-0.0928872	-0.1011107	H	-1.9156187	-0.2236005	4.6214454	H	-1.9634605	-2.0799268	3.0960594
C	-1.1704890	0.0583325	0.0307701	H	-1.8804372	4.2837995	-1.7919981	C	5.1902861	0.1449561	-0.3944998
C	-1.8459803	-1.2871414	-0.0863013	H	-2.5840991	0.8914577	-4.3295204	C	3.7945606	0.7798825	-0.2757764
C	-1.4660755	0.6715255	1.3802029	H	-2.4584959	3.3342520	-3.9952168	C	2.8939936	-0.2162297	-0.3304604
C	-1.6505093	0.9771099	-1.0692086	C	-2.2135302	-1.7702573	-1.3397407	C	3.6995631	-1.5188465	-0.4949560
C	-2.0166023	0.4470018	-2.3024972	C	-2.7092283	-3.0680069	-1.4664217	C	4.4984532	-1.7012154	0.8018948
C	-2.3089692	1.2999839	-3.3661180	C	-2.8470960	-3.8518472	-0.3315202	C	5.3851804	-0.7160310	0.8609508
C	-2.2386146	2.6708262	-3.1696166	C	-2.5305116	-3.3665867	0.9278284	C	4.8322591	-0.9762285	-1.4018125
C	-1.9128988	3.2121107	-1.9358891	C	-2.0351589	-2.0682900	1.0509749	H	3.1192811	-2.3681946	-0.8372177
C	-1.6242241	2.3558268	-0.8734252	H	-2.9850852	-3.4502756	-2.4404461	H	4.4734997	-0.5956125	-2.3564633
C	-1.6581455	-0.1500244	2.4865432	H	-3.2290342	-4.8592200	-0.4288256	H	5.6385924	-1.6930174	-1.5405454
C	-1.4436158	2.0566046	1.5252156	H	-2.6682762	-3.9798697	1.8085969	C	3.5404447	2.1563930	-0.0592153
C	-1.5573038	2.6223135	2.7950065	N	-1.7190682	-1.5269515	2.2918696	N	3.3664019	3.2799138	0.1124753
C	-1.7095793	1.7905484	3.8931360	N	-2.0723133	-0.9366409	-2.4432285	C	1.4937530	-0.1463250	-0.2039334
C	-1.7761609	0.4122027	3.7570676	N	-1.3062321	2.8403748	0.3878158	H	4.2997123	-2.4654899	1.5367172
H	-1.5258145	3.6970613	2.9141541	H	-1.3325165	3.8377176	0.5145511	H	6.0798673	-0.4901947	1.6549143
H	-1.7950422	2.2281439	4.8787235	H	-2.4407027	-1.2816335	-3.3135604	H	5.9899191	0.8322061	-0.6473880

1b Quadricyclane-ethinyl-TATA

$E_{M062x\text{-}D3/def2TZVPP}$ = -1334.790048271

Nimag = 2 (-17.69 cm^{-1}; -16.54 cm^{-1})

C	0.3054503	0.3034247	-0.0945918	H	-2.3276835	-1.0302136	-4.3946707	H	-2.5118600	1.1332272	-3.3628401
C	-1.1302770	-0.0443125	-0.0006913	H	-1.0336213	-3.7179672	2.8571254	C	5.2248477	0.2524714	0.3025426
C	-1.9801978	1.1980518	-0.1257588	H	-2.0094006	0.0955646	4.5736198	C	3.9342807	-0.4616393	-0.0379931
C	-1.4616538	-1.0110023	-1.1140504	H	-1.5490045	-2.3171390	4.8222897	C	2.8957731	0.6715019	-0.2368182
C	-1.3719566	-0.7026080	1.3381671	C	-2.3001572	1.9364283	1.0109498	C	3.6884847	1.9334865	0.0194105
C	-1.6973779	0.0753641	2.4446918	C	-2.9682718	3.1546828	0.8838703	C	3.7715013	1.2663363	-1.3237662
C	-1.7628444	-0.5075456	3.7096545	C	-3.3237891	3.6014334	-0.3792977	C	4.7973406	0.1400815	-1.1295429
C	-1.5059887	-1.8641665	3.8408492	C	-3.0562099	2.8526103	-1.5147241	C	4.9144361	1.6269682	0.8459516
C	-1.2152576	-2.6576889	2.7424688	C	-2.3876446	1.6349595	-1.3835984	H	3.1346661	2.8545877	0.1149901
C	-1.1582689	-2.0717652	1.4776801	H	-3.2091368	3.7351609	1.7648138	H	4.6984026	1.6082974	1.9136120
C	-1.8709972	-0.5278849	-2.3527081	H	-3.8403526	4.5467600	-0.4793723	H	5.7259757	2.3295061	0.6541510
C	-1.2454623	-2.3740050	-0.9257332	H	-3.3640005	3.1992886	-2.4925361	C	3.6513980	-1.8297003	0.2286013
C	-1.3857235	-3.2533699	-1.9996441	N	-2.1129522	0.8365935	-2.4881291	N	3.4231702	-2.9358321	0.4371242
C	-1.7589621	-2.7531021	-3.2371711	N	-1.9403505	1.4332685	2.2557890	C	1.4871371	0.5111329	-0.1655574
C	-2.0180939	-1.4040318	-3.4274294	N	-0.8904824	-2.8190303	0.3395901	H	6.0527536	-0.3436335	0.6547414
H	-1.2041283	-4.3108295	-1.8608406	H	-0.7586756	-3.8087064	0.4598547	H	5.3362125	-0.3924080	-1.8947861
H	-1.8658301	-3.4336704	-4.0711709	H	-2.2768692	1.9408163	3.0566112	H	3.4516521	1.7002478	-2.2557280

2a Norbornadiene-me-phenyl-ethinyl-TATA

$E_{M062x\text{-}D3/def2TZVPP}$ = -1605.175260624

Nimag = 2 (-14.49 cm^{-1}; -5.84 cm^{-1})

C	-0.2457023	-1.4876625	0.6394580	C	-3.5806782	-3.9147659	-0.9130747	H	-3.0871473	-2.2969734	5.7594210
C	-0.5345119	-2.8676838	1.0900366	C	-2.7862046	-3.4233285	0.1223341	H	-0.6348968	-2.5765825	5.7403275
C	0.7645750	-3.6248130	1.2443716	C	-0.5378466	-2.7990450	3.6024283	H	-4.6567694	-3.8121724	-0.8663231
C	-1.2622650	-2.8201868	2.4137094	C	-2.6503133	-2.7136067	2.4365560	H	-1.1383084	-5.2010861	-2.8979447
C	-1.4012621	-3.5439317	0.0519411	C	-3.3135472	-2.5177101	3.6480923	H	-3.5872371	-4.9109227	-2.8011110
C	-0.8075457	-4.2041110	-1.0202745	C	-2.5748045	-2.4519134	4.8192594	C	1.3142258	-4.2850416	0.1485604
C	-1.5980179	-4.6969740	-2.0579207	C	-1.1970648	-2.6040793	4.8162472	C	2.5813256	-4.8598954	0.2459864
C	-2.9730723	-4.5329856	-1.9949587	H	-4.3912342	-2.4230832	3.6670754	C	3.2679201	-4.7802511	1.4476407

C	2.7135300	-4.1658290	2.5597123
C	1.4471049	-3.5902321	2.4571918
H	3.0149114	-5.3643891	-0.6075029
H	4.2514598	-5.2240593	1.5249284
H	3.2498093	-4.1324687	3.4988770
N	0.8404326	-2.9726842	3.5454905
N	0.5756259	-4.3506219	-1.0278267
N	-3.3446155	-2.8032974	1.2353062
H	-4.3483933	-2.8206550	1.2995923
H	0.9607517	-4.9145682	-1.7666791
H	1.3179713	-3.0511334	4.4274931
C	0.9680124	6.9793596	-2.7339705
C	0.9649280	5.4453064	-2.8762942
C	0.8816211	4.9176407	-1.6438303
C	0.8239345	6.1198949	-0.6802712
C	-0.4940389	6.8555527	-0.9575329
C	-0.4094463	7.3661454	-2.1793393
C	1.7903035	7.0708631	-1.4275572
H	1.0396913	5.8789458	0.3557012
H	2.7982860	6.6717841	-1.5273003
H	1.8036216	8.0725182	-1.0031535
C	0.8718669	4.7838203	-4.1256252
N	0.7937828	4.2809286	-5.1570715
C	-0.0232352	-0.3705807	0.2531119
H	1.3146740	7.5238232	-3.6054905
C	1.4605920	2.4533002	-1.6987746
C	0.7241607	3.5368517	-1.1888772
C	-0.2146732	3.3100529	-0.1731754
C	0.2309185	0.9542328	-0.2180916
C	-0.4770424	2.0426037	0.3000452
C	1.1963954	1.1829498	-1.1961089
H	1.7625446	0.3398852	-1.5707817
C	2.5472956	2.6035233	-2.7274277
H	-0.7652839	4.1514835	0.2292815
H	-1.2197137	1.8793297	1.0678276
H	2.1558548	2.4738581	-3.7366770
H	3.3158407	1.8496040	-2.5663322
H	3.0121400	3.5871838	-2.6845659
H	-1.1656789	7.8992154	-2.7341704
H	-1.3355569	6.8786681	-0.2819695

2b Quadricyclane-ethinyl-TATA

$E_{M062x\text{-}D3/def2TZVPP}$ = -1605.149206215

Nimag = 2 (-20.93 cm^{-1}; -9.38 cm^{-1})

C	-0.4920794	-1.4529178	0.5637063
C	-0.6497178	-2.8474594	1.0339735
C	0.6905283	-3.5411787	0.9486421
C	-1.1341775	-2.8431952	2.4661788
C	-1.6521433	-3.5606216	0.1557829
C	-1.2252173	-4.1886762	-1.0113497
C	-2.1615047	-4.7197010	-1.8983923
C	-3.5100246	-4.6290828	-1.5908788
C	-3.9465520	-4.0463391	-0.4111764
C	-3.0068563	-3.5154283	0.4722432
C	-0.2122939	-2.7884330	3.5081096
C	-2.4994852	-2.8126794	2.7361005
C	-2.9466326	-2.6632881	4.0488097
C	-2.0164256	-2.5644119	5.0717509
C	-0.6548805	-2.6381868	4.8222882
H	-4.0073038	-2.6289898	4.2599392
H	-2.3616269	-2.4451470	6.0899393
H	0.0604890	-2.5835176	5.6323330
H	-5.0008288	-4.0033645	-0.1714096
H	-1.8328189	-5.1984179	-2.8113169
H	-4.2372912	-5.0393975	-2.2786082
C	1.0710642	-4.1663107	-0.2357381
C	2.3648607	-4.6692074	-0.3724295
C	3.2503876	-4.5512686	0.6874022
C	2.8711554	-3.9696366	1.8874712
C	1.5764238	-3.4681948	2.0196116
H	2.6662243	-5.1455667	-1.2959930
H	4.2552340	-4.9375438	0.5814181
H	3.5650125	-3.9040339	2.7151366
N	1.1413604	-2.8839265	3.2047149
N	0.1395976	-4.2686432	-1.2623338
N	-3.3908861	-2.9311621	1.6751103
H	-4.3640119	-3.0099840	1.9180068
H	0.4174890	-4.7994281	-2.0704374
H	1.7711986	-2.9396377	3.9871547
C	1.7019674	6.8108616	-2.8178765
C	1.2703154	5.3728702	-3.0219623
C	0.5161198	4.9838844	-1.7199147
C	0.6297525	6.2324134	-0.8755158
C	-0.4356858	6.1274493	-1.9385272
C	0.2938146	6.5132441	-3.2347611
C	1.7652195	7.1124688	-1.3402804
H	0.3357150	6.1603382	0.1610384
H	2.7217615	6.8264237	-0.9024730
H	1.5803935	8.1676805	-1.1365444
C	1.8153984	4.4849070	-3.9889471
N	2.2584441	3.7623320	-4.7646901
C	-0.3406944	-0.3260744	0.1716934
H	2.3854789	7.2403303	-3.5344409
H	-0.1472328	6.8140257	-4.1701537
H	-1.4960300	6.1783506	-1.7529481
C	1.3828491	2.8335390	-0.8097147
C	0.2912287	3.6098636	-1.2288832
C	-0.9923770	3.0768596	-1.1789070
C	-0.1392530	1.0086375	-0.3004507
C	-1.2157592	1.7910799	-0.7147000
C	1.1510065	1.5448698	-0.3551056
H	1.9824647	0.9340598	-0.0279695
C	2.7767330	3.3963533	-0.8425132
H	-1.8260071	3.6794573	-1.5156086
H	-2.2159864	1.3829082	-0.6769466
H	3.1174578	3.5506670	-1.8680076
H	3.4785479	2.7231449	-0.3551211
H	2.8160902	4.3620323	-0.3355287

3a Norbornadiene-TOTA

$E_{M062x\text{-}D3/def2TZVPP}$ = -1318.251824257

Nimag = 0

C	0.0303869	-0.3511217	0.0093937
C	1.3420349	-1.0221292	0.2740226
C	-0.7457136	-0.3070325	1.2894456
C	-0.7297440	-1.1668789	-0.9776950
C	-0.0526605	-1.8771252	-1.9544285
C	-0.7483791	-2.5153255	-2.9666958
C	-2.1361776	-2.4470080	-2.9580989
C	-2.8358062	-1.7987171	-1.9477594
C	-2.1144738	-1.1678017	-0.9497075
C	-0.0882837	-0.2360257	2.5078261
C	-2.1323889	-0.3281868	1.2480166
C	-2.8704806	-0.1641679	2.4103500
C	-2.1904889	-0.0186140	3.6133187
C	-0.8033025	-0.0741643	3.6843094
H	-3.9495247	-0.1672460	2.3630357
H	-2.7577960	0.1083719	4.5251978
H	-0.2781967	-0.0107475	4.6261669
H	-3.9151937	-1.7686390	-1.9316991
H	-0.2096073	-3.0428432	-3.7398128
H	-2.6892449	-2.9282005	-3.7525818
C	1.9566344	-1.7459952	-0.7380835
C	3.2168738	-2.2907561	-0.5446882
C	3.8271663	-2.1296525	0.6931762
C	3.1928158	-1.4785037	1.7444906
C	1.9342613	-0.9413044	1.5248404
H	3.6902777	-2.8390446	-1.3460414
H	4.8098448	-2.5512750	0.8532533
H	3.6472956	-1.3961991	2.7209928
C	0.2441183	3.1763812	-1.4434643
C	-0.1432466	1.6879500	-1.5909415
C	0.2480325	1.0660811	-0.4730302
C	0.9069482	2.1357278	0.4133587
C	-0.2121972	3.1072510	0.8141606
C	-0.6039523	3.7295868	-0.2906174
C	1.5817329	2.9810505	-0.6931381
H	1.5267044	1.7560412	1.2190608
H	2.3195066	2.4244061	-1.2685206
H	1.9969285	3.9128835	-0.3156694
C	-0.8639888	1.2073038	-2.7175994
N	-1.4372901	0.9026812	-3.6666912
H	0.2450549	3.7415778	-2.3689055
H	-1.4054541	4.4419521	-0.4081380
H	-0.6177832	3.1861946	1.8113661
O	1.2824772	-0.3324287	2.5730844
O	1.3227328	-1.9451889	-1.9370433
O	-2.7904529	-0.5231175	0.0621837

3b Quadricyclane-TOTA

$E_{M062x\text{-}D3/def2TZVPP}$ = -1318.226393475

Nimag = 0

C	0.0061829	-0.2663180	0.1019546
C	1.2952103	-0.9497219	0.4240347
C	-0.8673625	-0.3232148	1.3141530
C	-0.6628669	-1.0177742	-1.0034119
C	0.1051800	-1.6523562	-1.9689094
C	-0.4891891	-2.2507742	-3.0667525
C	-1.8772693	-2.2367703	-3.1552149
C	-2.6681507	-1.6908088	-2.1538345
C	-2.0459605	-1.1015356	-1.0619001
C	-0.2948222	-0.2693854	2.5765276
C	-2.2430847	-0.4371384	1.1872189
C	-3.0602172	-0.3620850	2.3051467
C	-2.4677453	-0.2226779	3.5521713
C	-1.0856375	-0.2002219	3.7100225
H	-4.1321166	-0.4116404	2.1839295
H	-3.0974024	-0.1590752	4.4287937
H	-0.6238301	-0.1446450	4.6850072
H	-3.7468299	-1.7257810	-2.1963387
H	0.1249975	-2.7274976	-3.8165603
H	-2.3541478	-2.6964228	-4.0101575
C	1.9987600	-1.6096470	-0.5709343
C	3.2481389	-2.1504571	-0.3092725
C	3.7637243	-2.0336771	0.9764523
C	3.0509072	-1.4226615	2.0010432
C	1.8019465	-0.8927239	1.7130851
H	3.7898972	-2.6541903	-1.0965201
H	4.7372488	-2.4523368	1.1912893
H	3.4391516	-1.3622045	3.0073400
O	1.0759732	-0.3068098	2.7199027
O	1.4751725	-1.7192327	-1.8361984
O	-2.8247284	-0.6292435	-0.0395596
C	-0.0171503	3.3606456	-1.3172645
C	-0.7139158	2.3431798	-0.4315860

C	0.2990561	1.1706492	-0.3030867
C	1.4564655	1.6131371	-1.1602513
C	1.3228780	2.1242525	0.2541833
C	1.0279293	2.6658945	-2.1535188
H	2.2380206	0.9017713	-1.3801845
C	-2.1144788	2.3768862	-0.1845161
N	-3.2436121	2.4471762	0.0161454
C	0.3298704	3.2887176	0.1368149
H	-0.6051590	4.1896293	-1.6807240
H	0.6067968	2.2307517	-3.0597319
H	1.8444056	3.3368115	-2.4216740
H	0.1556229	4.0733537	0.8535434
H	2.0421408	1.9561725	1.0393432

References

[1] Gunes, Y.; Arcelik, N.; Sahin, E.; Fleming, F. F.; Altundas, R. *Eur. J. Org. Chem.* **2015**, 6679-6686.

[2] Laursen, B. W.; Krebs, F. C. *Chem. Eur. J.* **2001**, *7*, 1773-1783.

[3] Browne, D. L.; Baumann, M.; Harji, B. H.; Baxendale, I. R.; Ley, S. V. *Org. Lett.* **2011**, *13*, 3312-3315.

[4] Martin, J. C.; Smith, R. G. *J. Am. Chem. Soc.* **1964**, *11*, 2252-2256.

[5] Kenndoff, J.; Polborn, K.; Szeimies, G. *J. Am. Chem. Soc.* **1990**, *112*, 6117-6118.

[6] Tranmer, G. K.; Yip, C.; Handerson, S.; Jordan, R. W.; Tam, W. *Can. J. Chem.* **2000**, *78*, 527-535.

[7] Gunes, Y.; Arcelik, N.; Sahin, E.; Fleming, F. F.; Altundas, R. *Eur. J. Org. Chem.* 2015, 6679-6686.

[8] Zhao, Y.; Truhlar, D. G., *Theor. Chem. Account* **2008**, *120*, 215-241.

[9] Grimme, S.; Antony, J.; Ehrlich, S.; Krieg, H., *J. Chem. Phys.* **2010**, *132*, 154104.

[10] Weigend, F.; Häser, M.; Patzelt, H.; Ahlrichs, R., *Chem. Phys. Lett.* **1998**, *294*, 143.

[11] Goerigk, L.; Hansen, A.; Bauer, C.; Ehrlich, S.; Najibi, A.; Grimme, S., *Phys. Chem. Chem. Phys.* **2017**, *19*, 32184-32215.

[12] Turbomole7.2: TURBOMOLE V7.2 2017, a development of University of Karlsruhe and Forschungszentrum Karlsruhe GmbH, 1989-2007, TURBOMOLE GmbH, since 2007; available from http://www.turbomole.com.

3.4 Konjugierte und nichtkonjugierte Referenz-Plattformen

Im von der Arbeitsgruppe HERGES etablierten Plattformkonzept adsorbieren TATA- bzw. TOTA-Plattformen mit einem definierten Abstand zueinander auf Au(111)-Oberflächen.[29,31] Dieses Verhalten garantiert den auf den Plattformen funktionalisierten Aufbauten in der Regel ausreichend Freiraum, sodass intermolekulare Wechselwirkungen in den SAMs unterbunden werden. Photoschalter besitzen durch diesen Freiraum ähnliche Isomerisierungseigenschaften wie in Lösung.[48] Dieser ausreichende Abstand kann bei selbstorganisierenden Monolagen (SAMs), die über die kovalente Bindung von Thiolen auf einzelne Goldatome gebildet werden, unter anderem durch die Bildung von gemischten SAMs erreicht werden.[6,19,23] Dabei enthalten die SAMs neben den Photoschaltern eine weitere Spezies, die den intermolekularen lateralen Abstand der Photoschalter ausreichend ermöglicht. Vorteil dieser Abstandshalter ist zudem, dass Isomerisierungen von photoschaltbaren Molekülen über die Änderung der relativen Höhe mithilfe des Rastertunnelmikroskops untersucht werden können, wobei der Abstandshalter mit einer definierten relativen Höhe als Referenz dient.[23,180] Dieses Konzept der gemischten Monolagen mit Referenzen kann auf das Plattformkonzept erweitert werden, wodurch Referenz-TATA-Plattformen die Untersuchung der Isomerisierung von Photoschaltern auf TATA-Plattformen in STM Messungen ermöglichen könnten (Abb. 3.7).

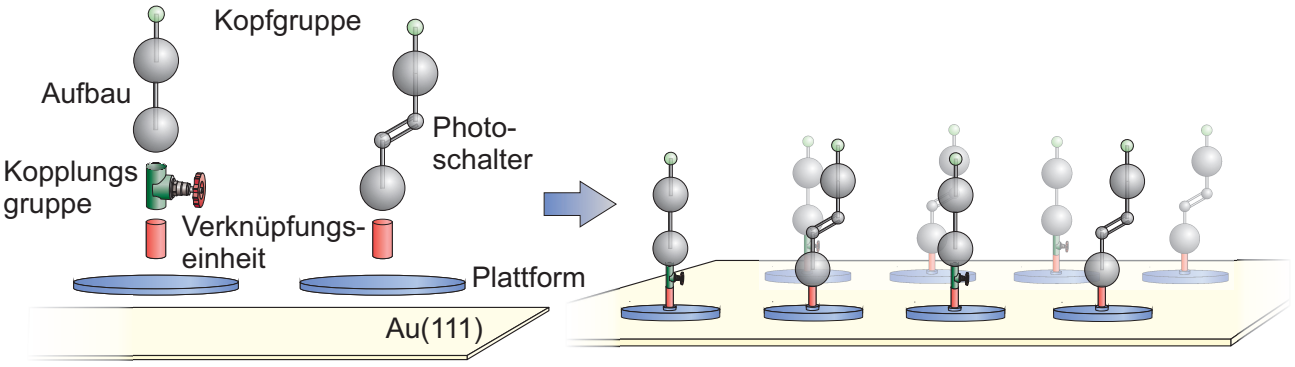

Abb. 3.7: Links ist das schematische Design der Referenzplattform und das Plattformkonzept mit Photoschalter dargestellt. Die Veranschaulichung der gemischten Monolagen auf Goldoberflächen mit Plattformen, die mit Photoschalter oder Referenzaufbauten funktionalisiert sind, ist rechts dargestellt.

Für ein variables Konzept können mehrere Referenz-Plattformen etabliert werden, die in ihrer relativen Höhe variieren. Diese kann durch unterschiedliche Höhen und Leitfähigkeiten der Aufbauten erreicht werden. Dabei können die Leitfähigkeiten durch unterschiedliche Konjugationen einer Kopplungsgruppe gesteuert werden.

3.4.1 Conjugated and non-conjugated reference TATA Platforms

Roland Löw, Talina Rusch, Fynn Röhricht, Olaf Magnussen, Rainer Herges

Manuskript für
Beilstein of Organic Chemistry

Eigenanteil: Die Synthese und Charakterisierung aller Moleküle wurden von Roland Löw durchgeführt. Die DFT-Rechnungen wurden von Fynn Röhricht angefertigt. Die Untersuchungen mittels Rastertunnelmikroskopie wurden von Talina Rusch durchgeführt. Das Manuskript wurde von Roland Löw und Prof. Dr. Rainer Herges verfasst.

3.4.2 Zusammenfassung

In dieser Publikation wird die Synthese von drei verschiedenen Referenz-TATA-Plattformen **15**, **16** und **17** gezeigt (Abb. 3.8). Die Aufbauten unterscheiden sich in ihrer Höhe und der Konjugation auf TATA-Plattformen. Hohe Konjugationen wurden durch die Verwendung von Phenyl- bzw. Acetyleneinheiten erreicht, während mit der Einführung eines isolierenden cyclischen Orthoesters die Konjugation unterbrochen wurde. Die Referenz-Plattform **15** wurde in einer vierstufigen Syntheseroute mit einer Gesamtausbeute von 28 % erhalten. Die fünfstufigen konvergenten Syntheserouten von **16** und **17** starteten von Bromiodbenzol und Phenylacetylen für **16** bzw. Fluorphenylacetylen für **17**. Daraus aufbauend verliefen die Syntheseschritte identisch, wobei für **16** eine Gesamtausbeute von 53 % und für **16** von 18 % erreicht wurde. Die Funktionalisierung der Aufbauten auf den TATA-Plattformen verliefen in guten Ausbeuten von 87 % für **15** und jeweils von 75 % für **16** und **17**. Nach der Adsorption von einer Referenz-Plattform **15** ohne Kopfgruppe auf Au(111)-Oberflächen konnten zwei unterschiedliche relative Höhen nachgewiesen werden, was auf die Ausbildung von Mono- und Bilagen hindeutet. Mit der Einführung von Fluor- **16** bzw. Iodkopfgruppen **17** konnte die Bilagenbildung unterbunden werden.

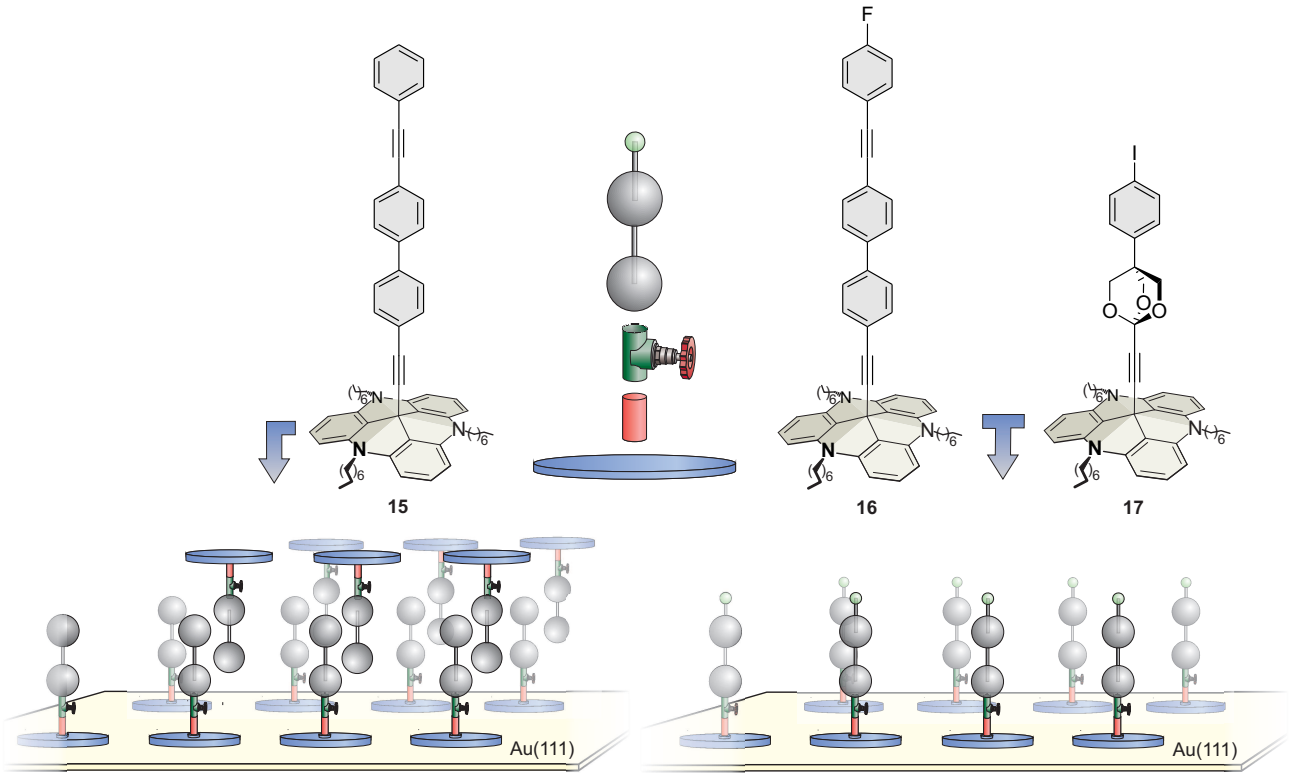

Abb. 3.8: Strukturen der Referenz-Plattformen mit hoher Konjugation **15**, **16** und der nichtkonjugierten Referenzplattform **17**. Die schematische Bilagenbildung auf Au(111) ist links und die reine Monolagenbildung rechts dargestellt.

Es kann davon ausgegangen werden, dass die voluminösen bzw. polaren Kopfgruppen die π-π-Wechselwirkungen der Phenylringe mindern und somit die Bilagenbildung durch Stacking verhindert wird.

Conjugated and non-conjugated reference TATA platforms

Roland Löw, Talina Rusch, Fynn Röhricht, Olaf Magnussen[2] and Rainer Herges[1]

[1]Otto Diels Institute for Organic Chemistry, University of Kiel, Otto-Hahn-Platz 4, 24118 Kiel, Germany
Email: rherges@oc.uni-kiel.de
[2]Institute for experimental and Applied Physics, University of Kiel, Leibnizstraße 19, 24098 Kiel, Germany
Email: magnussen@physik.uni-kiel.de

Abstract

Triazatriangulenium ions are used to adsorb a variety of functional photochromic molecules. We have now calculated and synthesized a conjugated and non-conjugated structure on TATA platform as reference for the analysis of functional units on TATA platforms in mixed self-assembled monolayers on Au(111) surfaces. For this advantage highly ordered self-assembled monolayers of these reference platforms were prepared. These are the first reference TATA platforms and are consummate systems for the analysis of the isomerization of azobenzene functionalized TATA platforms in mixed self-assembled monolayers on Au(111) surfaces.

Keywords

self-assembled monolayers, TATA platform, conjugated reference molecule, non-conjugated reference molecule,

Introduction

An interesting research field for self-assembled monolayers on metal surfaces is the investigation of switchable molecules like azobenzenes on surfaces. The azobenzene isomerizes between the *cis* and *trans* isomer as two different states[1,2]. Interestingly, thiol-functionalized azobenzenes on gold surfaces only exhibit poor isomerisation behaviour due to steric hindrance of the densely packed monolayers.

Isomerisation could be only observed at the edges of these monolayers or in loosely packed regions[3,4]. The decrease of lateral density between these chromophores by installing the monolayers on curved surfaces[5] or by the incorporation of shorter alkyl thiols in the SAMs lead to a significantly improved switching behaviour[6-8]. The photo isomerization was observed by surface plasmon resonance spectroscopy[8], photo electrochemical measurements[8], vibrational sum-frequency generation[9], surface-enhanced raman spectroscopy[10] and scanning tunnelling microscopy (STM)[11]. In STM *cis* and *trans* isomers are distinguishable by the apparent height which is affected by the resistance of the molecules in the monolayer and their actual height[11-18]. The alkyl thiolates are used additionally as reference for the observation of the isomerization in mixed SAMs in STM[11]. However, mixed SAMs tend to form separated regions of the pure components, with switching only detectable at the edges[19-21]. In the HERGES group the platform approach was designed to arrange the functional units perpendicular to the surface with an adequate distance to each other as well as to the surface itself, giving each molecule enough space for the isomerisation process. The triazatriangulenium (TATA) ions serve as a pedestal and the functional units are connected with ethynyl or phenyl units as spacers by the polar C-C bond formation at the central C atom of the platform[22]. The large π system has a high affinity to atomically flat gold surfaces similar to the affinity of a thiol group[23]. In monolayers the distance of the platforms can be controlled by the size of the side chains at the nitrogen atoms[24]. Vertically ordered, free-standing azobenzenes on surfaces have the same extinction and quantum yield efficiency as in solution[25]. Due to the lack of a reference, the investigation of azobenzenes on platforms by comparing the apparent height of the *trans* and *cis* isomers in STM measurements at ambient conditions is problematic. Therefore, it is required to establish a reference TATA platform system for mixed SAMs. Requirements of these systems are stability and inactivity towards irradiation of the mixed SAMs as well as an appropriate defined apparent height for the investigation of the photochromic compound. To meet these prerequisites, a non-conjugated reference platform **1** and a conjugated reference platform **2** were designed (Figure 1).

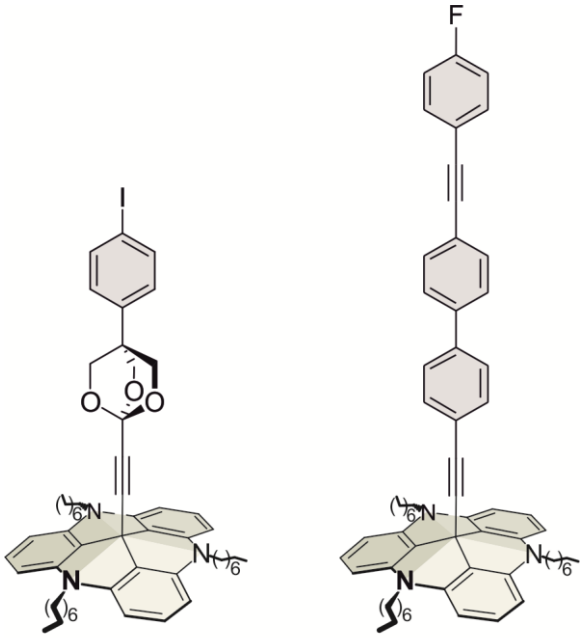

Figure 1: The non-conjugated (left) **1** and conjugated (right) **2** reference platform system.

Results and Discussion

The preparation of the non-conjugated iodophenyl TATA platform **1** was achieved in a five-step synthesis route (Figure 2). Aniline **4** was synthesized as described[26]. In a SANDMEYER reaction the iodobenzene **5** was synthesized. In ether condensations with ortho ester **6** gave the closed cage of **7**. The functionalization of the octyl TATA platform **8**, which was synthesized according to a procedure of LAURSEN and KREBS[27], was acomplished by deprotection of the terminal silyl-protected alkyne group of **7** with potassium hydroxide and in situ coupling at the central carbon atom of the octyl TATA ion **8** to get the final isolated target platform **1**.

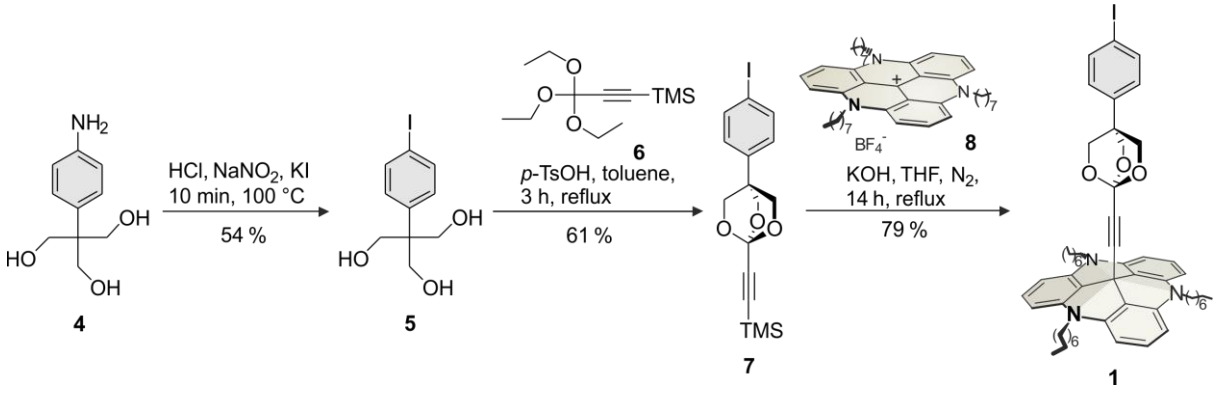

Figure 2: Synthesis route to form the non-conjugated reference TATA platform **1**.

The conjugated reference TATA platform **2** was obtained in a convergent synthesis route over five steps (Figure 3). The ethynediylbisbenzene **11** was achieved by SONOGASHIRA cross coupling reaction out of 4-bromo-iodobenzene **10** and fluorophenyl acetylene **9**. In a SUZUKI cross coupling reaction the pinacol ester **12**, which was synthesized according to literature[28], and the ethynediylbisbenzene **11** were converted to the final target molecule **13**. The trimethylsilyl protected acetylene **13** was deprotected and connected with the central atom of the octyl TATA ion **8** to get the conjugated TATA platform **2**.

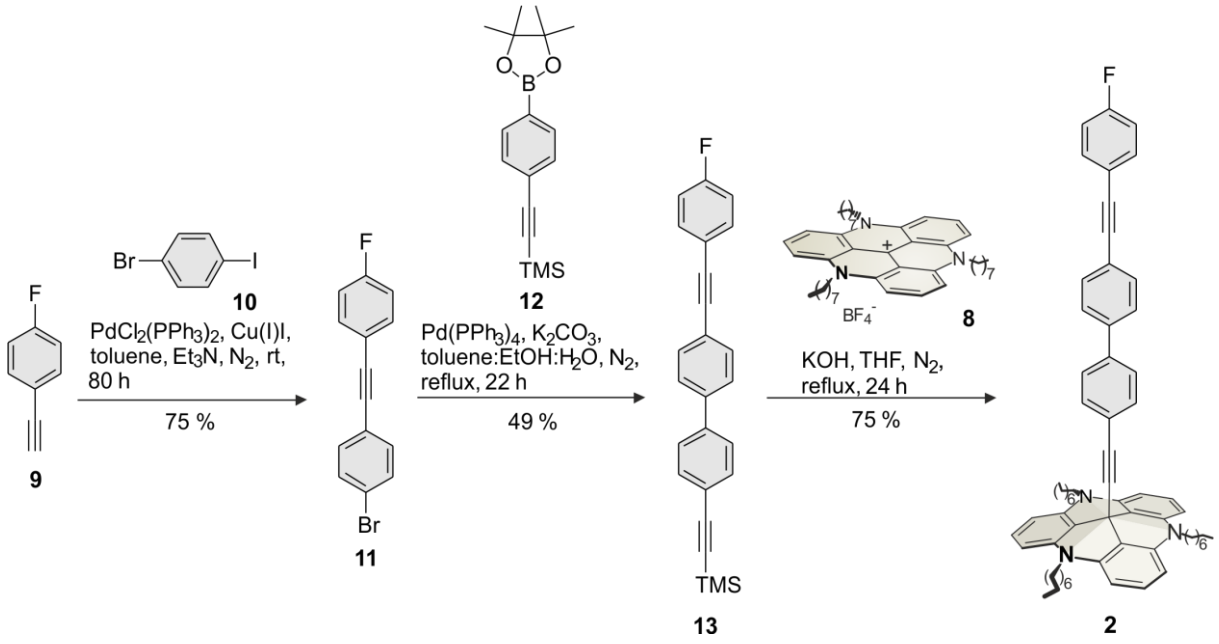

Figure 3: Synthesis route to form the conjugated reference TATA platforms **2**.

The conjugated TATA platform **3** without headgroup was obtained in a convergent sysnthesis route (Figure 4). The bromo-ethynediylbisbenzene **14** and pinacol ester **12** were synthesized according to literature[28,29], which formed in a SUZUKI cross coupling reaction the Biphenyl **15**. The formation of the final reference TATA platform **3** was obtained by deprotection of **15** and functionalization at the central atom of TATA ion **8**.

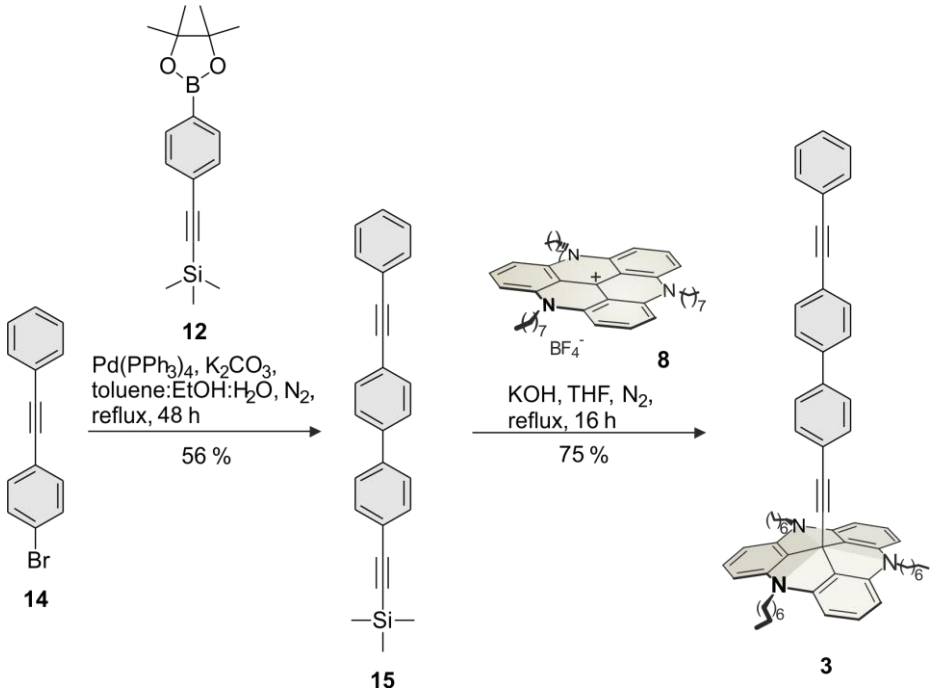

Figure 4: Synthesis route to form the conjugated reference TATA platform **3**.

STM measurements

For the preparation of the self-assembled monolayers (SAMs) Au(111) single crystals were flame annealed, immersed for 60 to 80 min. in 1-100 µM solutions of compound ***(1-3)*** in toluene at 80 °C. Afterwards, the samples were rinsed with pure toluene. The resulting SAMs were then investigated by scanning tunneling microscopy (STM) at room temperature (Figure 5). Adlayers of all compounds reveal a hexagonally ordered superstructure with a lattice constant of d_1 = (12.8 ± 0.3) Å, d_x = (12.8 ± 0.4) Å and d_2 = (12.3 ± 0.4) Å. Particularly, the intermolecular distances d and the angle between the rotational domains α_1 = 15.4° ± 3, are in agreement with a (√19 x √19) *R*23.4° superstructure, which was also observed in previous STM investigations of octyl-TATA systems[22,24,30,31].

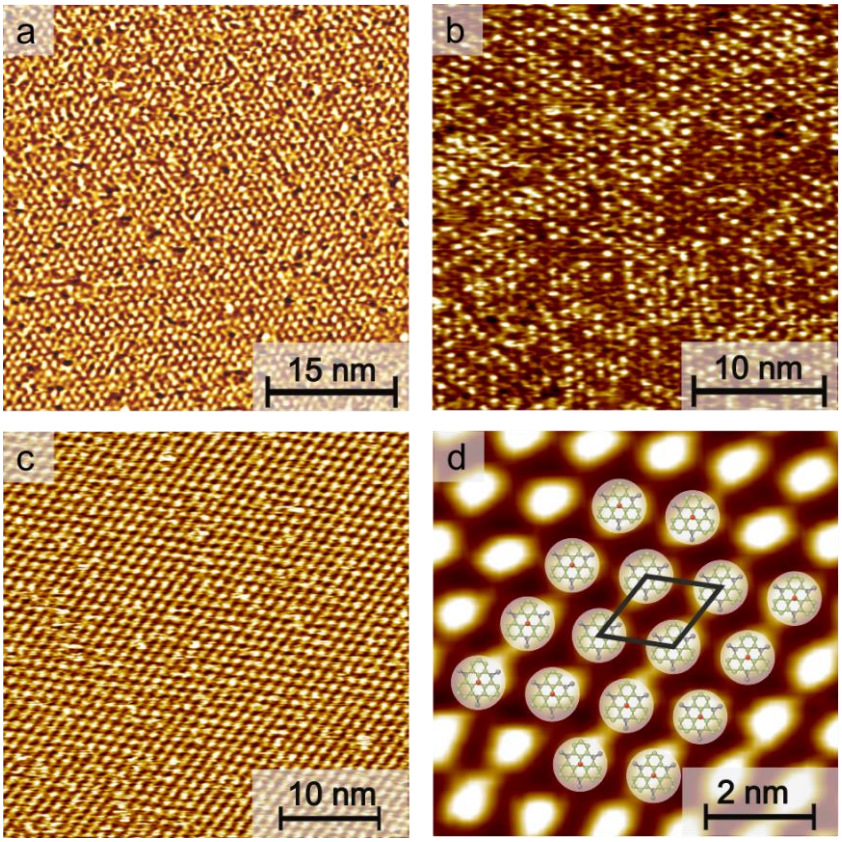

Figure 5: STM images of self-assembled layers of a) non-conjugated platform molecule **1** (50 x 50) nm², b) conjugated platform molecule **3** (15 x 15) nm², c) conjugated platform molecule **2** (40x40) nm² and d) **2** (7x7) nm² with an overlaying schematic model of a (√19 x √19) *R*23.4° superstructure on Au(111).

The platform molecules **1** and **2** form highly ordered monolayers whereby platform **3** forms on Au(111) monolayers with two different species verifable by their different apparent heights (Figure 5b). It is obvious that the phenylrings of 3 interact by π- π-stacking and form bilayers. These bilayers can't be formed with the conjugated reference platform **1** because of the polar fluorine head group. Out of this perception it is advisable to avoid bilayers by addition of polar head groups for the TATA platform concept.

Conclusion

In summary, we present the synthesis of a non-conjugated **1** and conjugated reference TATA platforms **2**. The calculated actual heights are 13.103 Å for **1** and 19.372 Å for **2**. Both platforms were analysed in STM measurements under ambient conditions and form highly ordered SAMs on Au(111) surfaces, whereby the fluorine

head group in **2** is necessary to avoid the instruction of bilayers because of $\pi-\pi$ stacking. These reference platforms can be used for the investigation of switchable structures on platforms in mixed self-assembled monolayers.

Acknowledgements

The authors gratefully acknowledge financial support by the Deutsche Forschungsgesellschaft within the Sonderforschungsbereich 677, “Function by Switching”.

References

[1] Hartley, G. S. *nature* **1937**, *140*, 281.

[2] Satzger, H.; Root, C.; Braun, M. *J. Phys. Chem. A* **2004**, *108*, 6265-6271.

[3] Siemelilng, U.; Bruhn, C.; Bretthauer, F.; Borg, M.; Träger, F.; Vogel, F.; Azzam, W.; Badin, M.; Strunskus, T.; Wöll, C. *Dalton Trans.* **2009**, 8593-8604.

[4] Heinemann, N.; Grunau, J.; Leißner, T.; Andreyev, O.; Kuhn, S.; Jung, U.; Zargarani, D.; Herges, R.; Magnussen, O.; Bauer, M. *Chemical Physics* **2012**, *402*, 22-28.

[5] Moldt, T.; Brete, D.; Przyrembel, D.; Das, S.; Goldman, J. R.; Kundu, P. K.; Gahl, C.; Klajn, R.; Weinelt, M. *Langmuir* **2015**, *31*, 1048-1057.

[6] Ahonen, R.; Laaksonen, T.; Schiffrin, D. J.; Kontturi, K. *Phys. Chem. Chem. Phys.* **2007**, *9*, 4898-4901.

[7] Yasuda, S.; Nakamura, T.; Matsumoto, M.; Shigekawa, H. *J. Am. Chem. Soc.* **2003**, *125*, 16430-16433.

[8] Jung., U.; Filinova, O.; Kuhn, S.; Zargarani, D.; Bornholdt, C.; Herges, R.; Magnussen, O. *Langmuir* **2010**, *26* (17), 13913-13923.

[9] Valley, D. T.; Onstott, M.; Malyk, S.; Benderskii, A. V. *Langmuir* **2013**, *29*, 11623-11631.

[10] Zheng, Y. B.; Payton, J. L.; Chung, C.-H.; Liu, R.; Cheunkar, S.; Pathem, B. K.; Yang, Y.; Jensen, L.; Weiss, P. S. *Nano Lett.* **2011**, *11*, 3447-3452.

[11] Kumar, A. S.; Ye, T.; Takami, T.; Yu, B.-C.; Flatt, A. K.; Tour, J. M.; Weiss, P. S. *Nano Lett.* **2008**, *8*, 1644-1648.

[12] Mativetsky, J. M.; Pace, G.; Elbing, M.; Rampi, M. A.; Mayor, M.; Samori, P. *J. Am. Chem. Soc.* **2008**, *130*, 9192-9193.

[13] Comstock, M. J.; Levy, N.; Kirakosian, A.; Cho, J.; Lauterwasser, F.; Harvey, J. H.; Strubbe, D. A.; Fréchet, J. M. J.; Trauner, D.; Louie, S. G.; Crommie, M. F. *Phys. Rev. Lett.* **2007**, *99*, 038301.

[14] Henzl, J.; Mehlhorn, M.; Gawronski, H.; Rieder, K.-H.; Morgenstern, K. *Angew. Chem. Int. Ed.* **2006**, *45*, 603-606.

[15] Alemani, M.; Selvanathan, S.; Ample, F.; Peters, M. V.; Rieder K.-H.; Moresco, F.; Joachim, C.; Hecht, S.; Grill., L. *J. Phys. Chem. C* **2008**, *112*, 10509-10514.

[16] Henningsen, N.; Rurali, R.; Franke, K. J.; Fernández-Torrentee, I.; Pascual, J. I. *Appl. Phys. A* **2008**, *93*, 241-246.

[17] Alemani, M.; Peters, M. V.; Hecht, S.; Rieder, K.-H.; Moresco, F.; Grill, L. *J. Am. Chem. Soc.* **2006**, *128*, 14446-14447.

[18] Scheil, K.; Gopakumar, T. G.; Bahrenburg, J.; Temps, F.; Maurer, R. J.; Reuter, K.; Berndt, R. *J. Phys. Chem. Lett.* **2016**, *7*, 2080-2084.

[19] Stranick, S. J.; Parikh, A. N.; Tao, Y. T.; Allara, D. L.; Weiss, P. S. *J. Phys. Chem.* **1994**, *98*, 7636-7646.

[20] Tamada, K.; Hara, K.; Sasabe, H.; Knoll, W. *Langmuir* **1997**, *13*, 1558-1566.

[21] Lüssem, B.; Müller-Meskamp, L.; Karthäuser, S.; Waser, R.; Homberger, M.; Simon, U. *Langmuir* **2006**, *22*, 3021-3027.

[22] Baisch, B.; Raffa, D.; Jung, U.; Magnussen, O. M.; Nicolas, C.; Lacour, J.; Kubitschke, J.; Herges, R. *J. Am. Chem. Soc.* **2009**, *131*, 442–443.

[23] Otto, F. L.; Schütt, C.; Krekiehn, N. R.; Jung, U.; Magnussen, O.; Herges R. *J. Am. Chem. Soc.* **2014**, *136*, 11248-11251.

[24] Ulrich, S.; Jung, U.; Strunskus, T.; Schütt, C.; Bloedorn, A.; Lemke, S.; Ludwig, E.; Kipp, L.; Faupel, F.; Magnussen, O. M.; Herges, R. *Phys. Chem. Chem. Phys.* **2015**, *17*, 17053–17062.

[25] Kuhn, S.; Baisch, B.; Jung, U.; Johannsen, T.; Kubitschke, J.; Herges, R.; Magnussen, O. M. *Phys. Chem. Chem. Phys.* **2010**, *12*, 4481–4487.

[26] Prasad, T. K.; Poneti, G.; Sorace, L.; Rodrigue-Douton, M. J.; Barra, A.-L.; Neugebauer, P.; Costantino, L.; Sessolib, R.; Cornia, A. *Dalton Trans*. **2012**, *41*, 8368.

[27] Laursen, B. W.; Krebs, F. C. *Chem. Eur. J.* **2001**, *7*, 1773-1783.

[28] Browne, D. L.; Baumann, M.; Harji, B. H.; Baxendale, I. R.; Ley, S. V. *Org. Lett.* **2011**, *13*, 3312-3315.

[29] Hassaneen, H. M.; Dawood, K. M.; Ahmed, M. S. M. Abdelhadi, H. A.; Mohamed, M. A.-M. *ARKIVOC* **2015**, *5*, 334-349.
[30] Jacob, H.; Ulrich, S.; Jung, U.; Lemke, S.; Rusch, T.; Schütt, C.; Petersen, F.; Strunskus, F.; Magnussen, O.; Herges, R.; Tuczek F. *Phys. Chem. Chem. Phys.* **2014**, *16*, 22643.
[31] Lemke, S.; Ulrich, S.; Claußen, F.; Bloedorn, A.; Jung, U.; Herges, R.; Magnussen, O. M. *Surface Science*, **2015**, *632*, 71-76.

Supporting Information

For

Conductive and non-conductive reference TATA platforms

Roland Löw, Talina Rusch, Fynn Röhricht, Olaf Magnussen[2] and Rainer Herges[1]

[1]Otto Diels Institute for Organic Chemistry, University of Kiel, Otto-Hahn-Platz 4, 24118 Kiel, Germany
Email: rherges@oc.uni-kiel.de
[2]Institute for experimental and Applied Physics, University of Kiel, Leibnizstraße 19, 24098 Kiel, Germany
Email: magnussen@physik.uni-kiel.de

Analytial equipment and methods, experimental procedures and NMR spectra

Table of Contents

I. Analytical equipment and methods

NMR Spectroscopy

NMR spectra were measured in deuterated solvents (Deutero). All compounds were characterized using ^{1}H and ^{13}C NMR spectroscopy. The signals were assigned using 2D spectroscopy. For ^{1}H and ^{13}C NMR assignment we performed HSQC and HMBC. The degree of deuteration is given in parentheses. ^{1}H NMR spectra in reference to the following signals:

chloroform-d (99.8%): δ = 7.26 ppm. (s)

benzene-d_6 (99.8%): δ = 7.16 ppm. (s)

acetone-d_6 (99.5%): δ = 2.05 ppm. (s)

The signal multiplicities are abbreviated as follows:

s: singlet, d: doublet, t: triplet, m: multiplet

Measurements were performed by the following instruments:

Bruker CABAV 500neo (^{1}H NMR: 500 MHz, ^{13}C NMR: 125 MHz)

Bruker AV 600 (^{1}H NMR: 600 MHz, ^{13}C NMR: 150 MHz)

IR spectroscopy

Infrared spectra were measured on a Perkin-Elmer 1600 Series FT-IR spectrometer with an A531-G Golden-Gate-Diamond-ATR-unit. Signals were abbreviated with w, m, s and for weak, medium and strong intensities. Broad signals are additionally labeled with br.

Mass spectrometry

The high resolution (HR) mass spectra were measured with an APEX 3 FT-ICR with a 7.05 T magnet by co. Bruker Daltonics. Electron impact (EI). Electrospray ionization (ESI) mass spectra were measured with a Thermo Scientific Q EXACTIVE.

Chromatrography stationary phases

For column chromatography purifications silica gel (Merck, particle size 0.040–0.063 mm) was used. R_f values were determined by thin layer chromatography onPolygram® Sil G/UV254 (Macherey-Nagel, 0.2 mm particle size).

Elemental analysis

The amount of carbon, hydrogen and nitrogen in a compound was determined with a CHNSO-Elemental analyser Euro EA 3000 Series by co. Euro Vector.

II. Experimental procedures

II.1 Synthesis of 2-(hydroxymethyl)-2-(4-iodophenyl)propan-1,3-diol (5)

In 3 M hydrochloric acid 2-(hydroxymethyl)-2-(4-aminophenyl)propan-1,3-diol[1] **4** (3.00 g, 15.2 mmol) was dissolved and cooled to 0 °C. Sodium nitrite (1.07 g, 15.5 mmol), dissolved in H_2O (10 mL), was added slowly and stirred for 5 min. Then potassium iodide (7.58 g, 45.7 mmol), dissolved in H_2O (10 mL), was added slowly and stirred additional for 10 min at 100 °C. The solution was cooled down to room temperature, extracted with ethyl acetate (3x 150 mL) and the organic layer was washed with saturated sodium thiosulfate solution and dried over magnesium sulfate. The solvent was removed under reduced pressure and the crude product was purified *via* column chromatography (silica gel, ethyl acetate) to obtain a white solid (2.54 g, 8.25 mmol, 54%).

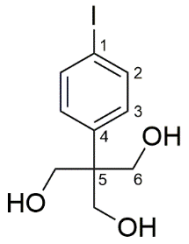

^{1}H NMR (500.1 MHz, acetone-d_6, 298 K, TMS): δ = 7.65 (d, ^3J = 8.7 Hz, 2H, *H*-3), 7.35 (d, ^3J = 8.7 Hz, 2H, *H*-2), 3.96 (d, ^3J = 5.4 Hz, 6H, *H*-6) ppm. **^{13}C NMR** (125.8 MHz, $CDCl_3$, 298 K, TMS): δ = 143.3 (s, *C*-1), 137.7 (s, *C*-3), 131.3 (s, *C*-2), 91.8 (s, *C*-4), 66.0 (s, *C*-6), 50.2 (s, *C*-5) ppm. **MS** (EI, 70eV): m/z = 307.99 $[M]^+$. **IR** (ATR): $\tilde{\nu}$ = 3234 (br., m), 2859 (w), 1583 (w), 1490 (w), 1458 (w), 1411 (w), 1389 (w), 1370 (w), 1298 (w), 1281 (w), 1243 (w), 1200 (w), 1145 (w), 1127 (w), 1064 (m), 1040 (vs), 1027 (vs), 999 (vs), 955 (w), 880 (w), 819 (m), 812 (m), 735 (m), 672 (m), 655 (m), 568 (m), 509 (m), 492 (m), 451 (w), 408 (w) cm^{-1}. **m.p.** = 96.7 °C.

II.2 Synthesis of 1-iodo-4-(1-((trimethylsilyl)ethynyl)-2,6,7-trioxa-bicyclo[2.2.2]octan-4-yl)benzene (7)

In toluene (350 mL) 2-(hydroxymethyl)-2-(4-iodophenyl)propan-1,3-diol **5** (2.00 g, 6.49 mmol) was dissolved and trimethyl(3,3,3-triethoxyprop-1-in-1-yl)silane **6** (1.59 g, 6.49 mmol) and catalytic amount of *p*-toluene sulfonic acid were added. Toluene was distilled for 3 h in order to remove arised ethanol. The solution was cooled down to room temperature and triethylamine (3 mL) was added and washed with saturated sodium carbonate solution (200 mL) and H_2O (200 mL). The solvent was removed under reduced pressure and the crude product was purified *via* column chromatography (silica gel, cyclohexane/ethyl acetate, 1/1) to obtain a white solid (1.65 g, 3.99 mmol, 61%).

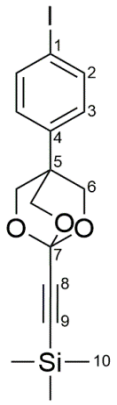

^{1}H NMR (500.1 MHz, acetone-d_6, 298 K, acetone): δ = 7.78 (d, ^{3}J = 8.7 Hz, 2H, *H*-2), 7.15 (d, ^{3}J = 8.7 Hz, 2H, *H*-3), 4.34 (s, 6H, *H*-6), 0.19 (s, 9H, *H*-10) ppm. **^{13}C NMR** (125.8 MHz, acetone-d_6, 298 K, acetone): δ = 139.0 (s, *C*-2), 136.7 (s, *C*-4), 128.81 (s, *C*-3), 102.5 (s, *C*-7), 94.1 (s, *C*-1), 87.0 (s, *C*-9), 72.0 (s, *C*-6), 37.2 (s, *C*-5), -0.6 (s, *C*-10) ppm. **^{29}Si NMR** (99.4 MHz, acetone-d_6, 298 K, acetone): δ = -16.28 ppm. **MS** (EI, 70eV): m/z = 413.99 $[M]^+$. **IR** (ATR): $\tilde{\nu}$ = 3228 (br., w), 2961 (w), 2893 (w), 2183 (w), 1697 (s), 1491 (w), 1397 (w), 1238 (vs), 1177 (w), 1124 (m), 1069 (w), 1052 (w), 1032 (m), 1002 (vs), 936 (m), 842 (vs), 812 (s), 754 (vs), 721 (m), 703 (m), 612 (m), 587 (m), 410 (w) cm^{-1}. **m.p.** = 98.8 °C.

II.3 Synthesis of 12c-((4-(4-iodophenyl)-2,6,7-trioxabicyclo-[2.2.2]octan-1-yl)ethynyl)-4,8,12-triazatriangulene (1)

In tetrahydrofuran (abs., 150 mL) 1-iodo-4-(1-((trimethylsilyl)ethynyl)-2,6,7-trioxa-bicyclo[2.2.2]octan-4-yl)benzene **7** (250 mg, 603 µmol) was dissolved under nitrogen atmosphere, octyl-TATA-BF_4[2] **8** (511 mg, 724 µmol) and crushed potassium hydroxide (398 mg, 6.03 mmol) were added and refluxed for 14 h. The solution was poured onto H_2O (100 mL) and extracted with diethyl ether (3x 200 mL). The combined organic layers were dried over magnesium sulfate and the solvent was removed under reduced pressure. The crude product was purified *via* column chromatography (alox basic, diethyl ether) to obtain a white solid (456 mg, 475 µmol, 79%).

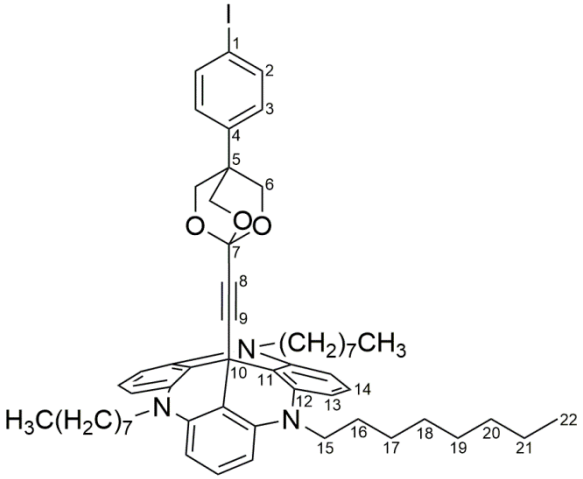

[1]H NMR (500 MHz, acetone-d_6, 298 K, acetone): δ = 7.71 (d, ^3J = 8.7 Hz, 2H, *H*-2), 7.21 (t, ^3J = 8.2 Hz, 3H, *H*-14), 7.01 (d, ^3J = 8.7 Hz, 2H, *H*-3), 6.65 (d, ^3J = 8.3 Hz, 6H, *H*-13), 4.10 (s, 6H, *H*-6), 3.99-3.94 (ps. t, 6H, *H*-15), 1.87-1.79 (ps. quint., 6H, *H*-16), 1.56-1.49 (ps. quint., 6H, *H*-17), 1.47-1.27 (m, 24H, *H*-18, *H*-19, *H*-20, *H*-21), 0.91-0.87 (ps. t, 9H, *H*-22) ppm. **[13]C NMR** (150.9 MHz, acetone-d_6, 298 K, acetone): δ = 141.3 (s, *C*-12), 138.9 (s, *C*-2), 136.8 (s, *C*-4), 129.6 (s, *C*-14), 128.6 (s, *C*-3), 109.5 (s, *C*-11), 106.0 (s, *C*-13), 103.3 (s, *C*-7), 94.0 (s, *C*-1), 85.7 (s, *C*-9), 78.9 (s, *C*-8), 71.7 (s, *C*-6), 47.0 (s, *C*-15), 37.0 (s, *C*-5), 32.6 (s, *C*-21), 30.2 (s, *C*-18), 30.1 (s, *C*-19), 28.3 (s, *C*-10), 27.5 (s, *C*-17), 26.4 (s, *C*-16), 23.4 (s, *C*-20), 14.4 (s, *C*-22) ppm. **IR** (ATR): $\tilde{\nu}$ = 2932 (w), 2847 (w), 1616 (w), 1597 (w), 1556 (w), 1510 (vs), 1440 (s), 1375 (m), 1338 (vs), 1279 (m), 1268 (m), 1202 (m), 1162 (m), 1089 (m), 1031 (m), 996 (w), 970 (w), 872 (vs), 829 (vs), 751 (vs), 691 (m) cm^{-1}. **m.p.** = 108 °C. **MS** (MALDI-TOF, Cl-CCA): m/z = 959.1 $[M]^+$.

II.4 Synthesis of 4-(2-phenylethynyl)-4'-((trimethylsilyl)ethynyl)-biphenyl (15)

In toluene (30 mL), ethanol (7.5 mL) and H_2O (1.5 mL) 1-bromo-4-(2-phenylethynyl)benzene[4] **14** (393 mg, 1.53 mmol), 4,4,5,5-tetramethyl-2[-4-[2-(trimethylsilyl)ethynyl]phenyl]-1,3,2-dioxaborolane[3] **12** (459 mg, 1.53 mmol), $Pd(PPh_3)_4$ (88.4 mg, 76.5 µmol) and potassium carbonate (529 mg, 3.83 mmol) were dissolved under nitrogen atmosphere and stirred for 48 h at 90 °C. H_2O (30 mL) was added and the aqueous layer was extracted with dichloromethane (3x 50 mL). The combined organic layers were dried over magnesium sulfate and the solvent was removed under reduced pressure. The crude product was purified *via* column chromatography (silica gel, cyclohexane/ethyl acetate, 4/1) to obtain a white solid (300 mg, 856 µmol, 56%).

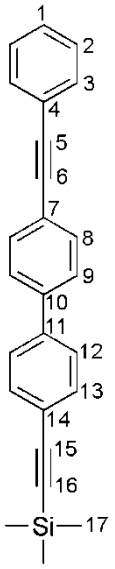

^{1}H NMR (500.1 MHz, $CDCl_3$, 298 K, TMS): δ = 7.62-7.52 (m, 10H, H-3, H-8, *H*-9, *H*-12, *H*-13,), 7.39-7.32 (m, 3H, *H*-1, *H*-2), 0.27 (s, 9H, H-17) ppm. **^{13}C NMR** (125.8 MHz, $CDCl_3$, 298 K, $CHCl_3$): δ = 140.4 (s, *C*), 140.1 (s, *C*), 132.6 (s, *C*-13), 132.2 (s, *C*-8), 131.8 (s, *C*-3), 128.5 (s, *C*-2), 128.5 (s, *C*-1), 127.0 (s, *C*), 126.9 (s, *C*), 123.4 (s, *C*-4), 122.8 (s, *C*), 122.6 (s, *C*), 105.0 (s, *C*-15), 95.4 (s, *C*-16), 90.5 (s, *C*-5), 89.3 (s, *C*-6), 0.1 (s, *C*) ppm. **^{29}Si NMR** (99.4 MHz, $CDCl_3$, 298 K, TMS): δ = -17.67 ppm. **MS** (EI, 70eV): m/z = 326.14 $[M]^+$. **IR** (ATR): $\tilde{\nu}$ = 2955 (w), 2154 (w), 1494 (w), 1245 (w), 839 (s), 820 (vs), 753 (s), 689 (s), 664 (m), 621 (w), 539 (w), 522 (m) cm^{-1}. **m.p.** = 189.4 °C. **Elemental analysis** calcd. (%) for $C_{25}H_{22}Si$: C 85.66; H 6.33; found C 85.919; H 6.284.

II.5 Synthesis of 12c-((4-phenylethynyl)phenylphenyl)-ethynyl-4,8,12-tri-n-octyl-4,8,12-triazatriangulene (3)

In tetrahydrofuran (abs., 60 mL) 4-(2-phenylethynyl)-4'-((trimethylsilyl)ethynyl)-biphenyl **15** (100 mg, 285 µmol) was dissolved under nitrogen atmosphere and octyl-TATA-BF_4 **8** (242 mg, 342 µmol) and crushed potassium hydroxide (128 mg, 2.28 mmol) were added and refluxed for 16 h. The mixture was poured onto H_2O (60 mL) and extracted with diethyl ether (3x 60 mL). The combined organic layers were dried over magnesium sulfate and the solvent was removed under reduced pressure. The crude product was purified *via* column chromatography (alox basic, diethyl ether) to obtain a white solid (191 mg, 213 µmol, 75%).

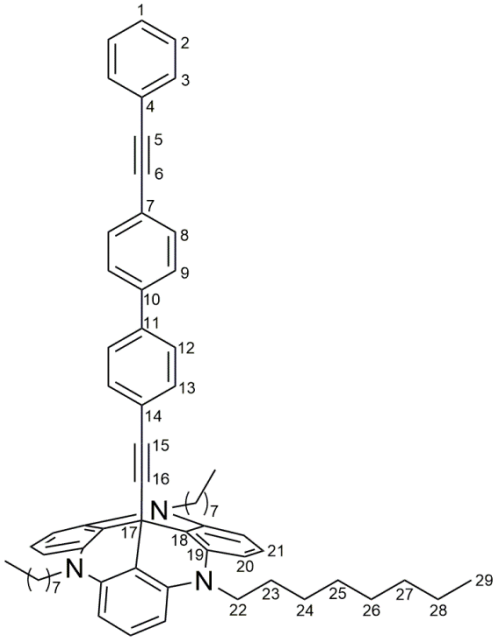

^{1}H NMR (500.1 MHz, C_6D_6, 298 K, TMS): δ = 7.53-7.49 (m, 2 H, *H*-3), 7.44 (d, ^{3}J = 8.6 Hz, 2 H, *H*-8), 7.25 (t, ^{3}J = 8.3 Hz, 3 H, *H*-21), 7.10 (d, ^{3}J = 8.6 Hz, 2 H, *H*-13), 7.03-6.92 (m, 7 H, *H*-1, *H*-2, *H*-9, *H*-12), 6.64 (d, ^{3}J = 8.3 Hz, 6 H, *H*-20), 3.82 (m, 6 H, *H*-22), 1.86-1.76 (m, 6 H, *H*-23), 1.32-1.15 (m, 30 H, *H*-24, *H*-25, *H*-26, *H*-27, *H*-28), 0.91-0.86 (ps. t, 9 H, *H*-29) ppm. **^{13}C NMR** (125.8 MHz, C_6D_6, 298 K, TMS): δ = 141.2 (s, *C*-19), 140.4 (s, *C*-10), 139.2 (s, *C*-11), 132.5 (s, *C*-13), 132.2 (s, *C*-8), 131.9 (s, *C*-3), 128.7 (s, *C*-2), 128.6 (s, *C*-21), 128.4 (s, *C*-1), 127.1 (s, *C*-9), 126.5 (s, *C*-12), 123.9 (s, *C*-4), 123.6 (s, *C*-14), 122.6 (s, *C*-7), 111.1 (s, *C*-18), 105.7 (s, *C*-20), 95.6 (s, *C*-16), 90.8 (s, *C*-5), 90.2 (s, *C*-6), 84.2 (s, *C*-15), 46.7 (s, *C*-22), 32.2 (s, *C*-28), 29.7 (s, *C*-26), 29.7 (s, *C*-27), 27.3 (s, *C*-24), 26.2 (s, *C*-23), 23.1 (s, *C*-25), 14.4 (s, *C*-29) ppm. **MS** (MALDI-TOF, Cl-CCA): m/z = 895.1 $[M]^{+}$. **IR** (ATR): $\tilde{\nu}$ = 2921 (s), 2851 (m), 1614 (s), 1580 (vs), 1483 (vs), 1456 (vs), 1393 (s), 1372 (m), 1244 (s), 1165 (s), 992 (w), 915 (w), 818 (vs), 763 (s), 729 (m), 701 (s), 689 (s) cm^{-1}. **m.p.** = 166.1 °C.

II.6 Synthesis of 1-bromo-4-[(4-fluorophenyl)ethynyl]benzene (11)

In triethylamine (dry, 15 mL) and toluene (15 mL) 1-ethynyl-4-fluorobenzene **9** (1.00 g, 8.32 mmol), 1-bromo-4-iodobenzene **10** (2.35 g, 8.32 mmol), $PdCl_2(PPh_3)_2$ (117 mg, 166 μmol) and copper(I)iodide (44.6 mg, 234 μmol) were suspended under nitrogen atmosphere and stirred for 80 h at 100 °C. To the mixture water (15 mL) was added and the layers were separated. The aqueous layer was extracted with dichloromethane (3x 20 mL) and the combined organic layers were dried over magnesium sulfate. The solvent was removed under reduced pressure and the crude product was purified *via* column chromatography (silica gel, cyclohexane/ethyl acetate, 4/1) and recrystallized out of ethanol to obtain a yellow solid (1.72 g, 6.25 mmol, 75%).

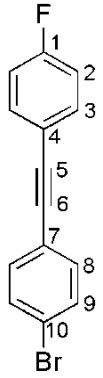

^{1}H NMR (500.1 MHz, $CDCl_3$, 298 K, TMS): δ = 7.52-7.46 (m, 4 H, *H*-3, *H*-9), 7.37 (d, ^{3}J = 8.6 Hz, 2 H, *H*-8), 7.08-7.02 (m, 2 H, *H*-2) ppm. **^{13}C NMR** (125.8 MHz, $CDCl_3$, 298 K, acetone): δ = 162.8 (d, ^{1}J = 250.2 Hz, *C*-1), 133.6 (d, ^{3}J = 8.4 Hz, *C*-3), 133.1 (d, ^{8}J = 0.4 Hz, *C*-8), 131.8 (s, *C*-9), 122.7 (s, *C*-10), 122.2 (s, ^{7}J = 0.5 Hz, *C*-7), 119.2 (d, ^{4}J = 3.5 Hz, *C*-4), 115.9 (d, ^{2}J = 22.1 Hz, *C*-2), 89.6 (d, ^{5}J = 0.6 Hz, *C*-5), 88.1 (d, ^{6}J = 1.5 Hz, *C*-6) ppm. **^{19}F NMR** (470.6 MHz, acetone-d_6, 298 K, acetone): δ = -110.91 – -110.99 ppm. **MS** (EI, 70eV): m/z = 273.96 $[M]^+$. **IR** (ATR): $\tilde{\nu}$ = 1908 (w), 1774 (w), 1657 (w), 1599 (m), 1586 (w), 1508 (vs), 1480 (m), 1394 (w), 1296 (w), 1224 (s), 1153 (m), 1071 (m), 1007 (v), 837 (vs), 822 (vs), 796 (m), 683 (s), 635 (w) cm^{-1}. **m.p.** = 104.7 °C. **Elemental analysis** calcd. (%) for $C_{14}H_8BrF$: C 61.12; H 2.93; found C 61.465; H 2.951.

II.7 Synthesis of 4-(4-fluorophenylethynyl)-4'-((trimethylsilyl)ethynyl)-biphenyl (13)

In toluene (72 mL), ethanol (17.8 mL), and H_2O (3.6 mL) 1-bromo-4-[(4-fluorophenyl)ethynyl]benzene **11** (1.00 g, 3.63 mmol), 4,4,5,5-tetramethyl-2[-4-[2-(trimethylsilyl)ethynyl]phenyl]-1,3,2-dioxaborolane[3] **12** (1.09 g, 3.63 mmol), $Pd(PPh_3)_4$ (210 mg, 182 μmol) and potassium carbonate (1.26 g, 9.12 mmol) were dissolved under nitrogen atmosphere and refluxed for 22 h. To the mixture water (200 mL) was added and the layers were separated. The aqueous layer was extracted with dichloromethane (3x 150 mL) and the combined organic layers were dried over magnesium sulfate. The solvent was removed under reduced pressure and the crude product was purified *via* column chromatography (silica gel, dichloromethane) and recrystallization out of acetone to obtain a grey solid (647 mg, 1.78 mmol, 49%).

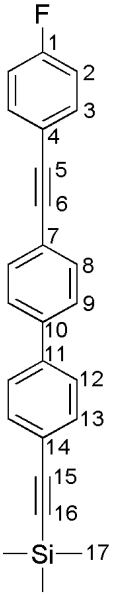

^{1}H NMR (500.1 MHz, $CDCl_3$, 298 K, TMS): δ = 7.59-7.50 (m, 10 H, *H*-3, *H*-8, *H*-9, *H*-12, *H*-13), 7.08-7.03 (m, 2 H, *H*-2) ppm. **^{13}C NMR** (125.8 MHz, $CDCl_3$, 298 K, TMS): δ = 162.6 (d, ^{1}J = 249.8 Hz, *C*-1), 140.2 (s, *C*), 140.1 (s, *C*), 133.5 (d, ^{3}J = 8.4 Hz, *C*-3), 132.5 (s, *C*), 132.1 (d, *J* = 0.4 Hz, *C*), 126.9 (s, *C*), 126.7 (s, *C*), 122.5 (s, *C*), 122.4 (d, *J* = 0.4 Hz, *C*), 119.3 (d, ^{4}J = 3.5 Hz, *C*-4), 115.7 (d, ^{2}J = 22.1 Hz, *C*-2), 104.8 (s, *C*-15), 95.3 (s, *C*-16), 89.3 (d, ^{6}J = 0.6 Hz, *C*-6), 88.9 (d, ^{5}J = 1.5 Hz, *C*-5), 0.0 (s, *C*-17) ppm. **^{19}F NMR** (470.6 MHz, acetone-d_6, 298 K): δ = -110.22 – -111.30 ppm. **^{29}Si NMR** (99.4 MHz, $CDCl_3$, 298 K): δ = -17.64 ppm. **MS** (EI, 70eV): m/z = 368.14 $[M]^+$. **IR** (ATR): $\tilde{\nu}$ = 2963 (w), 2904 (w), 2157 (m), 1595 (w), 1505 (m), 1400 (w), 1256 (m), 1220 (m), 1154 (w), 1093 (w), 1003 (w), 833 (vs), 819 (vs), 759 (m), 716 (w), 701 (w), 648 (m) cm^{-1}. **m.p.** = 220.6 °C. **Elemental analysis** calcd. (%) for $C_{25}H_{21}FSi$: C 81.48; H 5.74; found: C 81.277; H 5.747.

II.8 Synthesis of 12c-((4-fluorophenylethynyl)phenylphenyl)-ethynyl-4,8,12-tri-*n*-octyl-4,8,12-triazatriangulene (2)

In tetrahydrofuran (abs., 64 mL) 4-(4-fluorophenylethynyl)-4'-((trimethylsilyl)ethynyl)-biphenyl **13** (150 mg, 407 μmol), *n*-octyl-TATA-BF_4 **8** (575 mg, 814 μmol) and crushed potassium hydroxide (183 mg, 3.26 mmol) were suspended under nitrogen atmosphere and refluxed for 24 h. The mixture was poured onto sat. sodium chloride solution (20 mL) and the layers were separated. The aqueous layer was extracted with diethyl ether (3x 20 mL) and the combined organic layers were dried over magnesium sulfate. The solvent was removed under reduced pressure and the crude product was purified *via* column chromatography (aluminium oxide, basic, diethylether) to obtain a white solid (279 mg, 305 μmol, 75%).

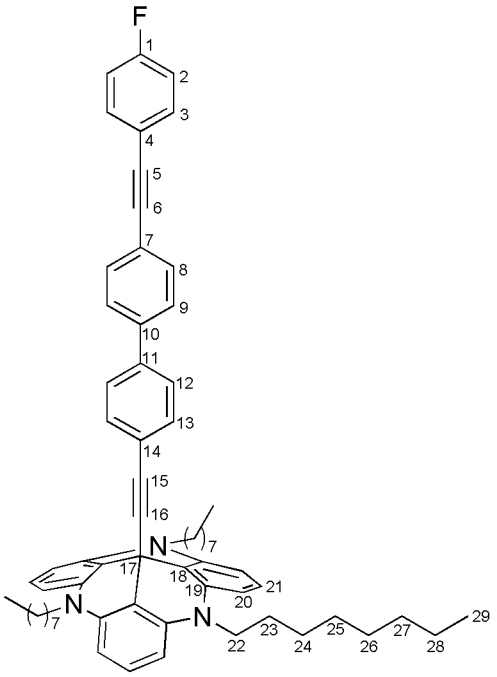

^{1}H NMR (600.1 MHz, acetone-d_6, 298 K, TMS): δ = 7.65-7.56 (m, 6H, *H*-3, *H*-8, *H*-9), 7.53 (d, ^{3}J = 8.4 Hz, 2H, *H*-12), 7.24-7.17 (m, 5H, *H*-2, *H*-21), 7.16 (d, ^{3}J = 8.4 Hz, 2H, *H*-13), 6.68 (d, ^{3}J = 8.3 Hz, 6H, *H*-20), 4.04-4.00 (ps. t, 6H, *H*-22), 1.88-1.81 (ps. quint., 6H, *H*-23), 1.55-1.48 (ps. quint., 6H, *H*-24), 1.42-1.21 (m, 24H, *H*-25, *H*-26, *H*-27, *H*-28), 0.86-0.82 (ps. t, 9H, *H*-29) ppm. **^{13}C NMR** (150.9 MHz, acetone-d_6, 298 K, TMS): δ = 163.5 (d, ^{1}J = 248.2 Hz, *C*-1), 141.5 (s, *C*-19), 140.8 (s, *C*-10), 139.9 (s, *C*-11), 134.5 (d, ^{3}J = 8.5 Hz, *C*-3), 132.8 (s, *C*-8), 132.7 (s, *C*-13), 129.4 (s, *C*-21), 127.6 (s, *C*-9), 127.3 (s, *C*-12), 124.0 (s, *C*-14), 123.1 (s, *C*-7), 120.4 (s, *C*-4), 116.6 (d, ^{2}J = 22.4 Hz, *C*-2), 111.2 (s, *C*-18), 106.1 (s, *C*-20), 95.9 (s, *C*-16), 89.8 (s, *C*-6), 89.6 (s, *C*-5), 84.1 (s, *C*-15), 46.7 (s, *C*-22), 32.6 (s, *C-27*), 30.2 (s, *C*-25), 30.1 (s, *C*-26), 27.5 (s, *C*-24), 26.8 (s, *C*-23), 23.3 (s, *C*-28), 14.4 (s, *C*-29) ppm. **^{19}F NMR** (470.6 MHz, acetone-d_6, 298 K): δ = -111.22 - -111.30 ppm. **MS** (MALDI-TOF, Cl-CCA): m/z = 913.6 $[M]^+$. **IR** (ATR): $\tilde{\nu}$ = 2920 (m), 2851 (m), 1614 (s), 1581 (vs), 1506 (m), 1484 (vs), 1456 (vs), 1393 (s), 1371 (m), 1267 (m), 1245 (s), 1233 (s), 1167 (m), 992 (w), 916 (w), 836 (s), 818 (vs), 761 (vs), 721 (s), 685 (m), 660 (w) cm^{-1}. **m.p.** = 134.9 °C. **Elemental analysis** calcd. (%) for $C_{65}H_{72}FN_3$: C 85.39; H 7.94; N 4.60; found: C 85.301; H 8.083; N 4.613.

III. NMR spectra

III.1 2-(hydroxymethyl)-2-(4-iodophenyl)propan-1,3-diol

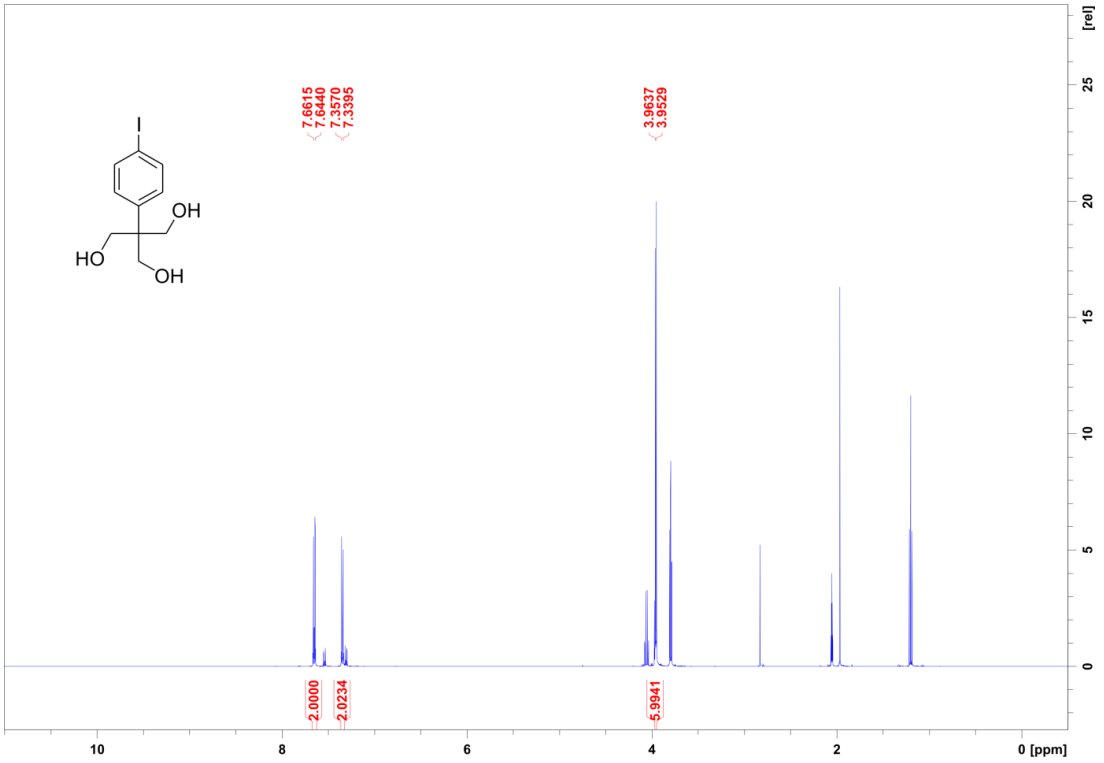

Figure S1. ^{1}H NMR spectrum (500.1 MHz, acetone-d_6) of compound **5**.

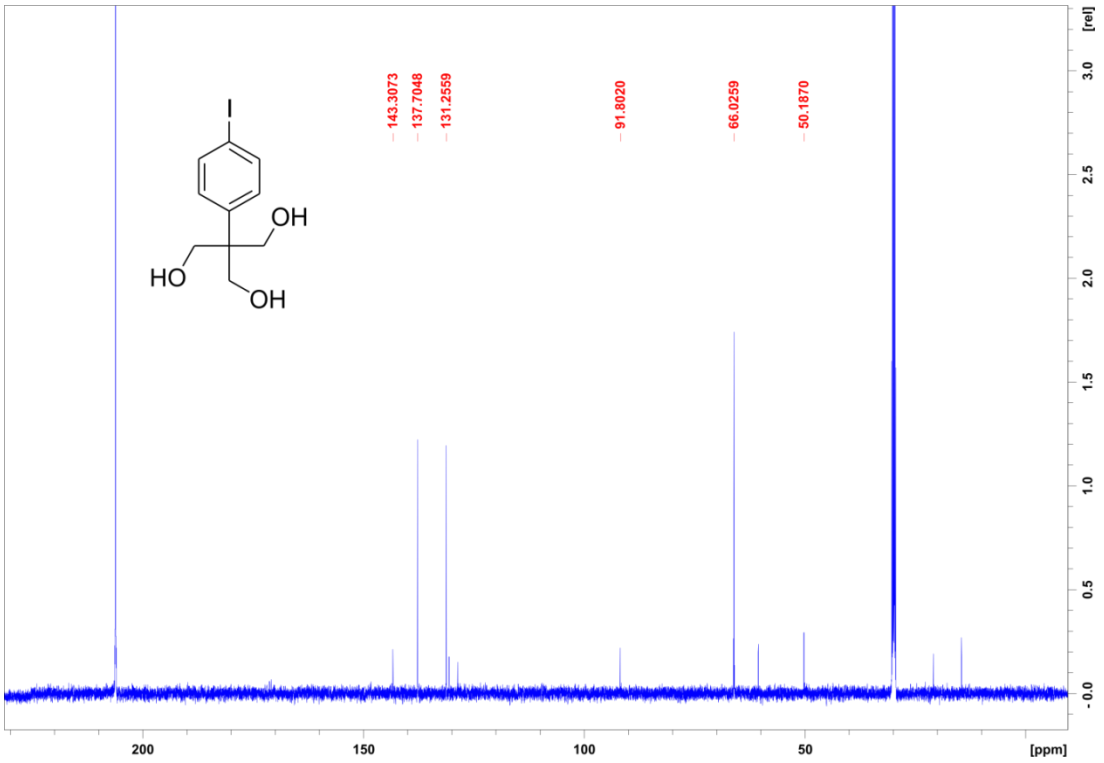

Figure S2. ^{13}C NMR spectrum (125.8 MHz, acetone-d_6) of compound **5**.

III.2 1-iodo-4-(1-((trimethylsilyl)ethynyl)-2,6,7-trioxa-bicyclo[2.2.2]octan-4-yl)benzene

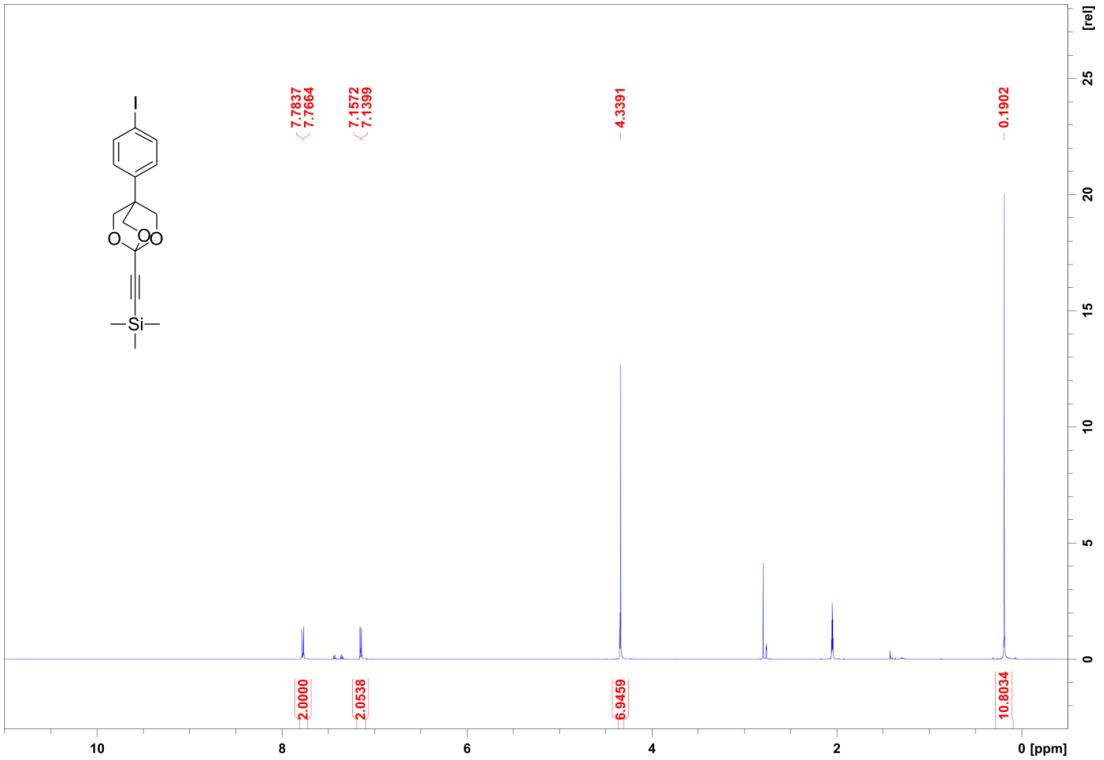

Figure S3. ^{1}H NMR spectrum (500.1 MHz, acetone-d_6) of compound **7**.

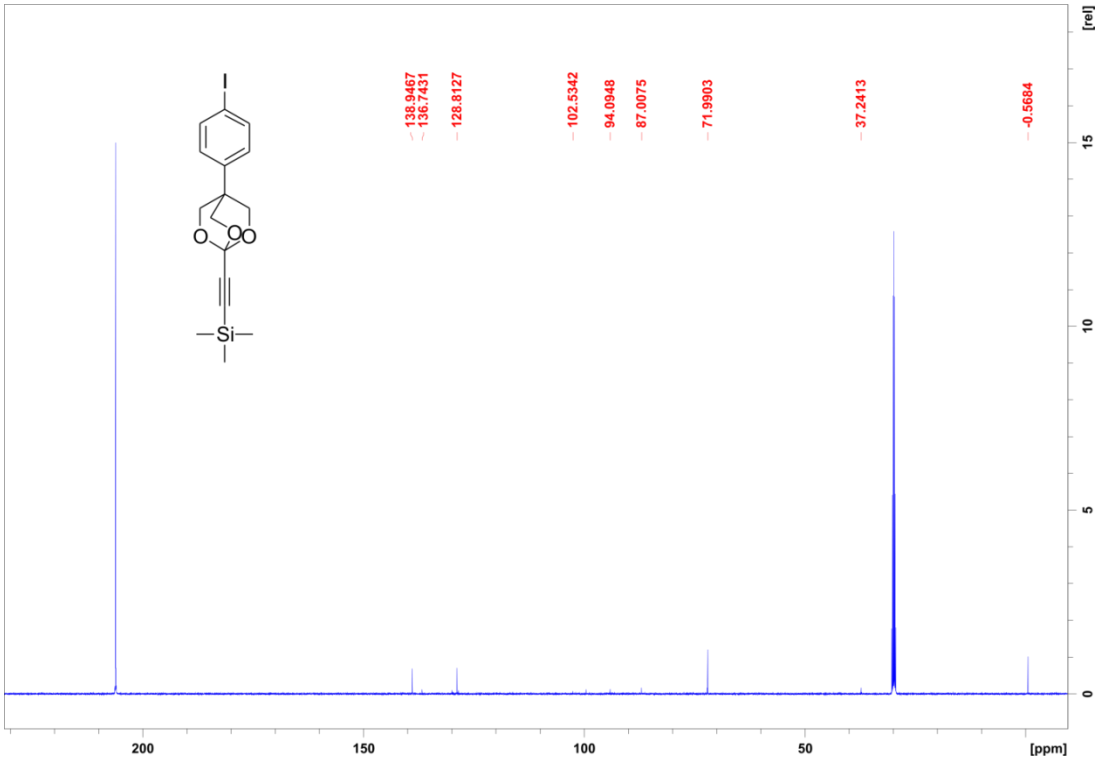

Figure S4. ^{13}C NMR spectrum (125.8 MHz, acetone-d_6) of compound **7**.

III.3 12c-((4-(4-iodophenyl)-2,6,7-trioxabicyclo-[2.2.2]octan-1-yl)ethynyl)-4,8,12-triazatriangulene

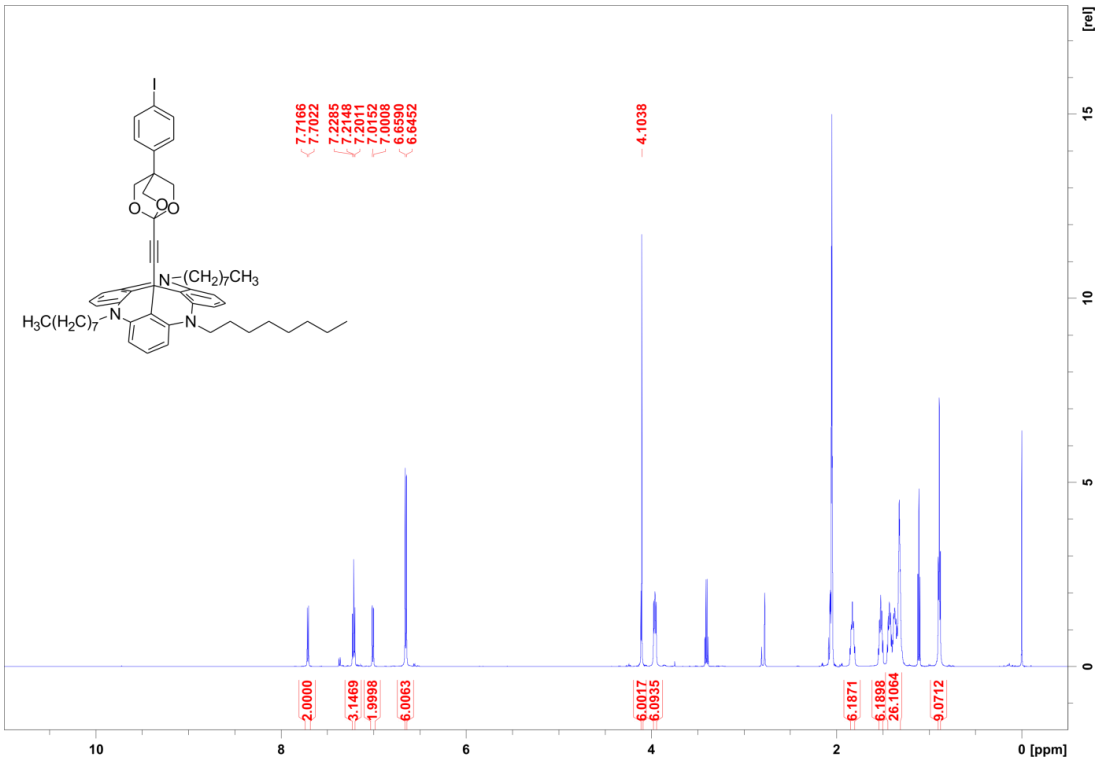

Figure S5. ^{1}H NMR spectrum (500.1 MHz, acetone-d_6) of compound **1**.

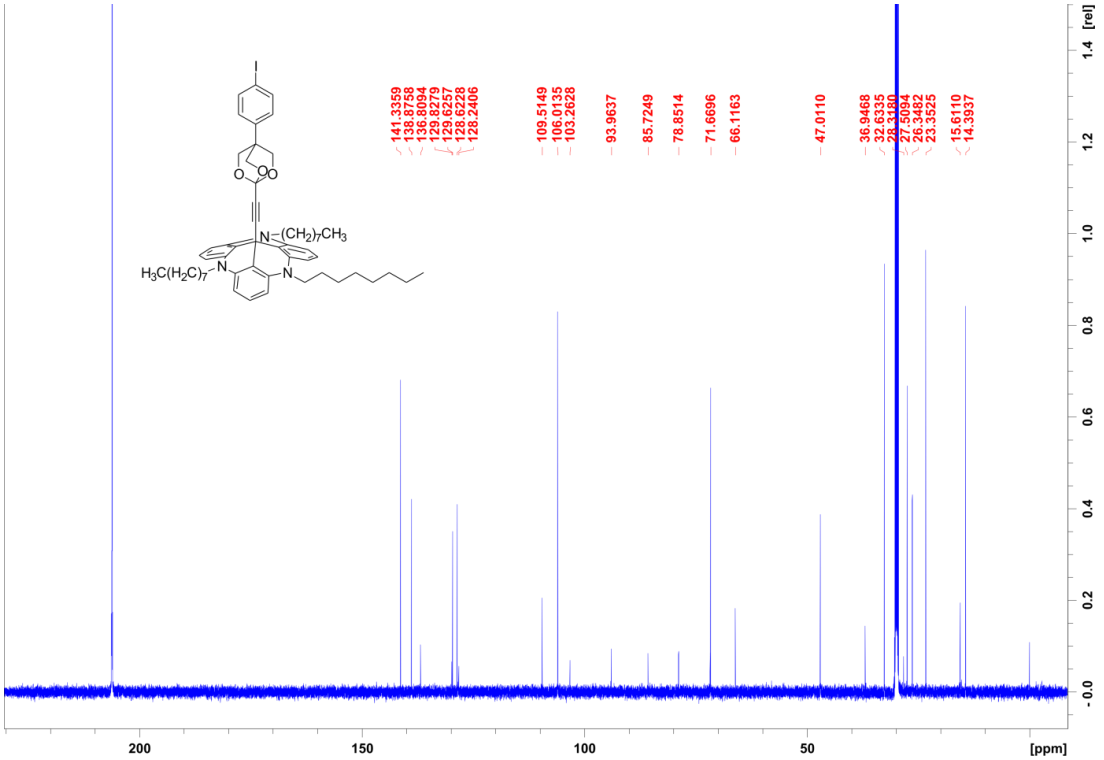

Figure S6. ^{13}C NMR spectrum (150.9 MHz, acetone-d_6) of compound **1**.

III.4 4-(2-phenylethynyl)-4‘-((trimethylsilyl)ethynyl)-biphenyl

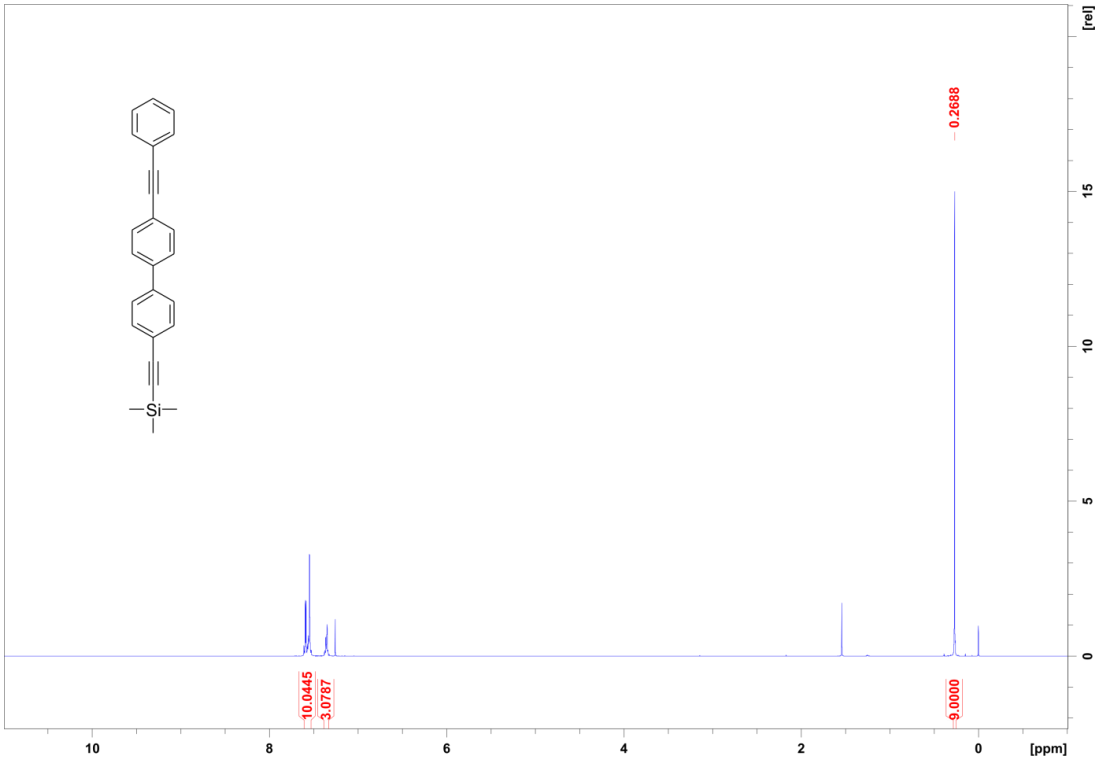

Figure S9. ^{1}H NMR spectrum (500.1 MHz, $CDCl_3$) of compound **15**.

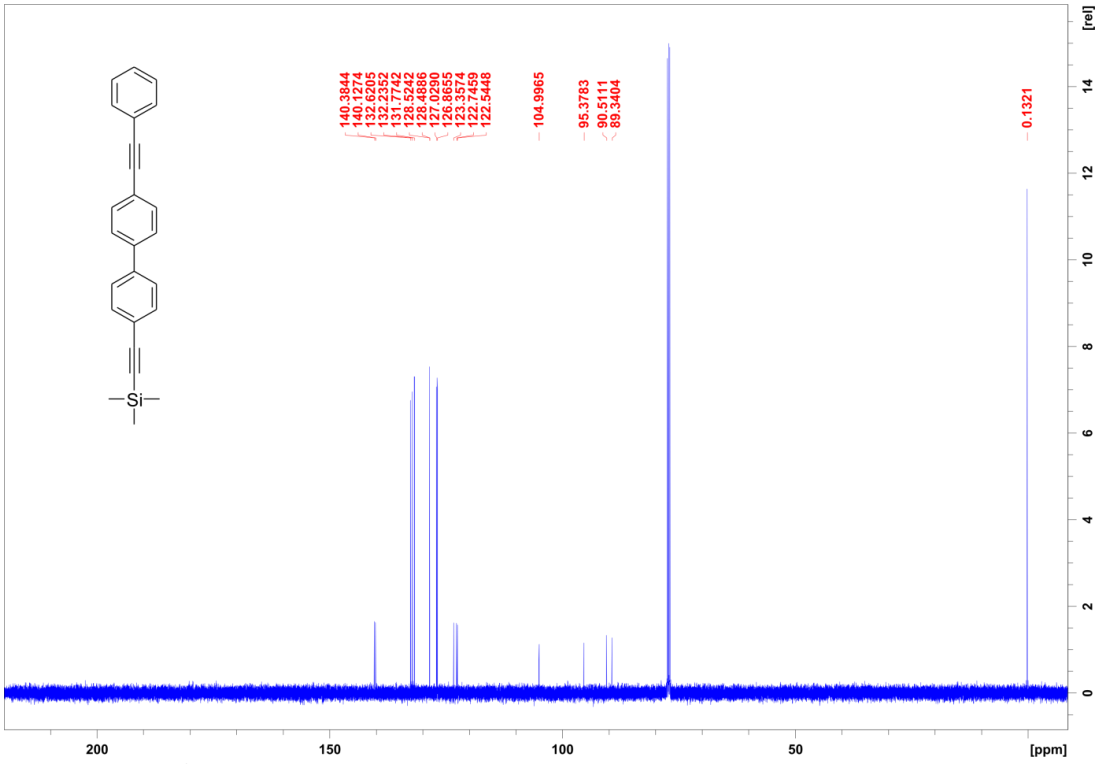

Figure S10. ^{13}C NMR spectrum (125.8 MHz, $CDCl_3$) of compound **15**.

III.5 12c-((4-phenylethynyl)phenylphenyl)-ethynyl-4,8,12-tri-n-octyl-4,8,12-triazatri-angulene

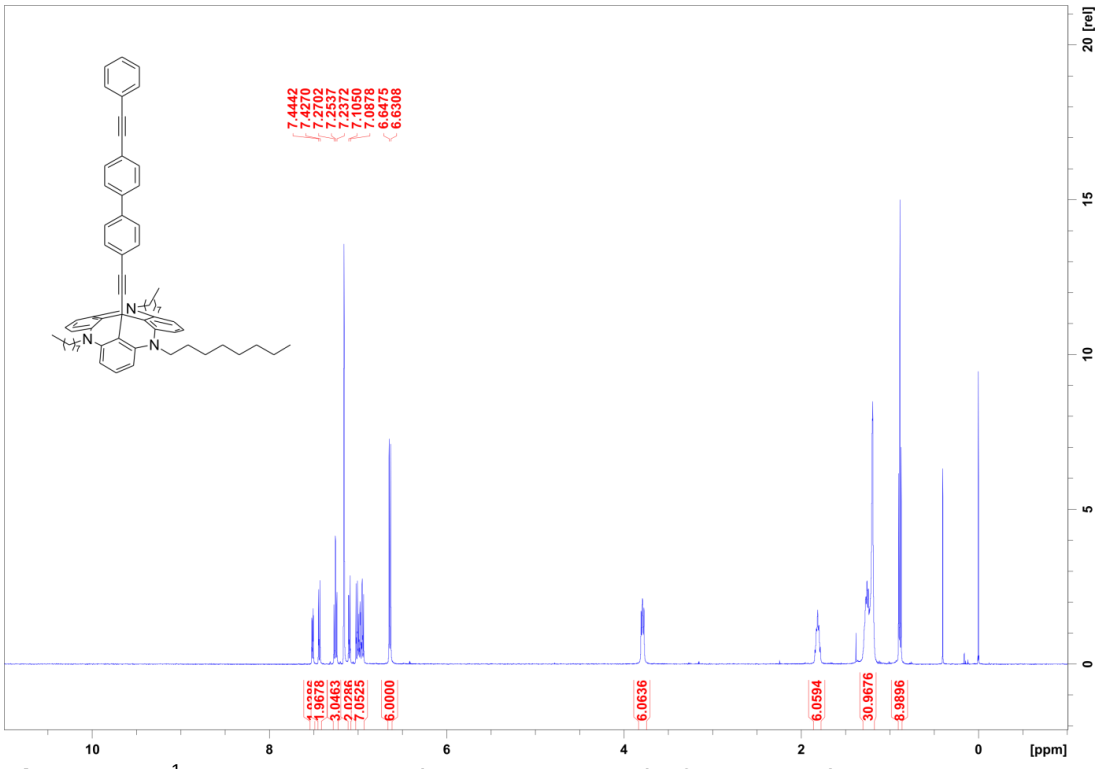

Figure S11. ^{1}H NMR spectrum (500.1 MHz, C_6D_6) of compound **3**.

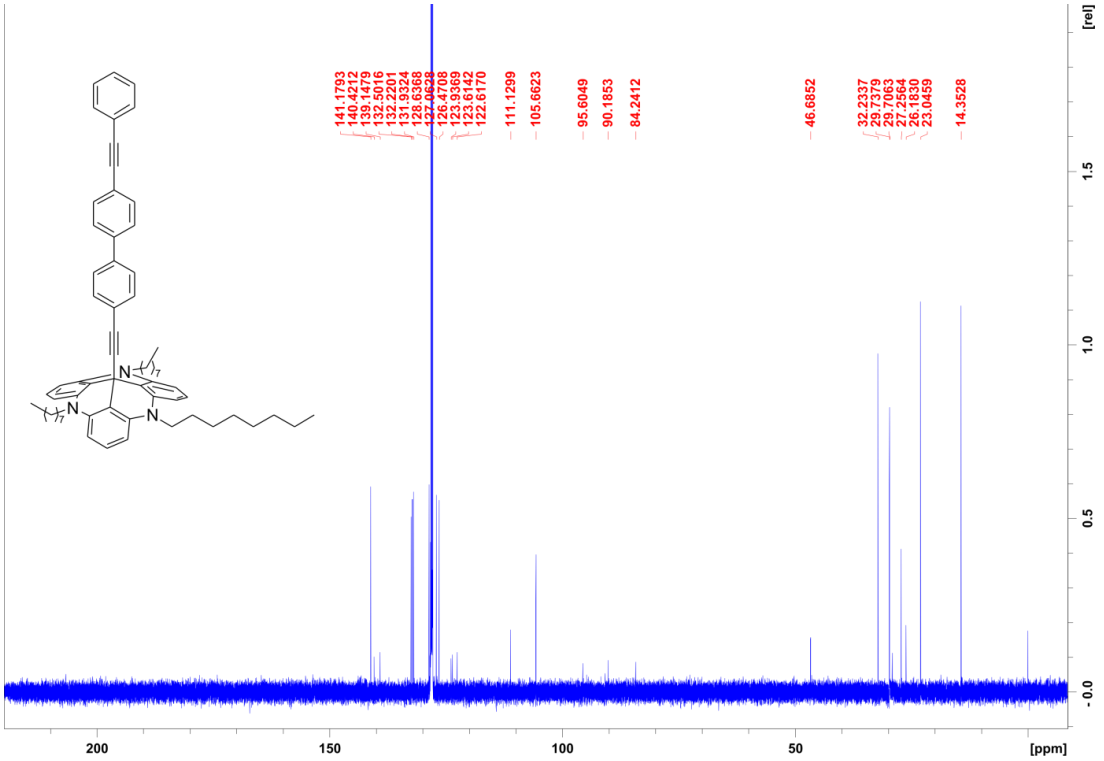

Figure S12. ^{13}C NMR spectrum (125.8 MHz, C_6D_6) of compound **3**.

III.6 1-bromo-4-[(4-fluorophenyl)ethynyl]benzene

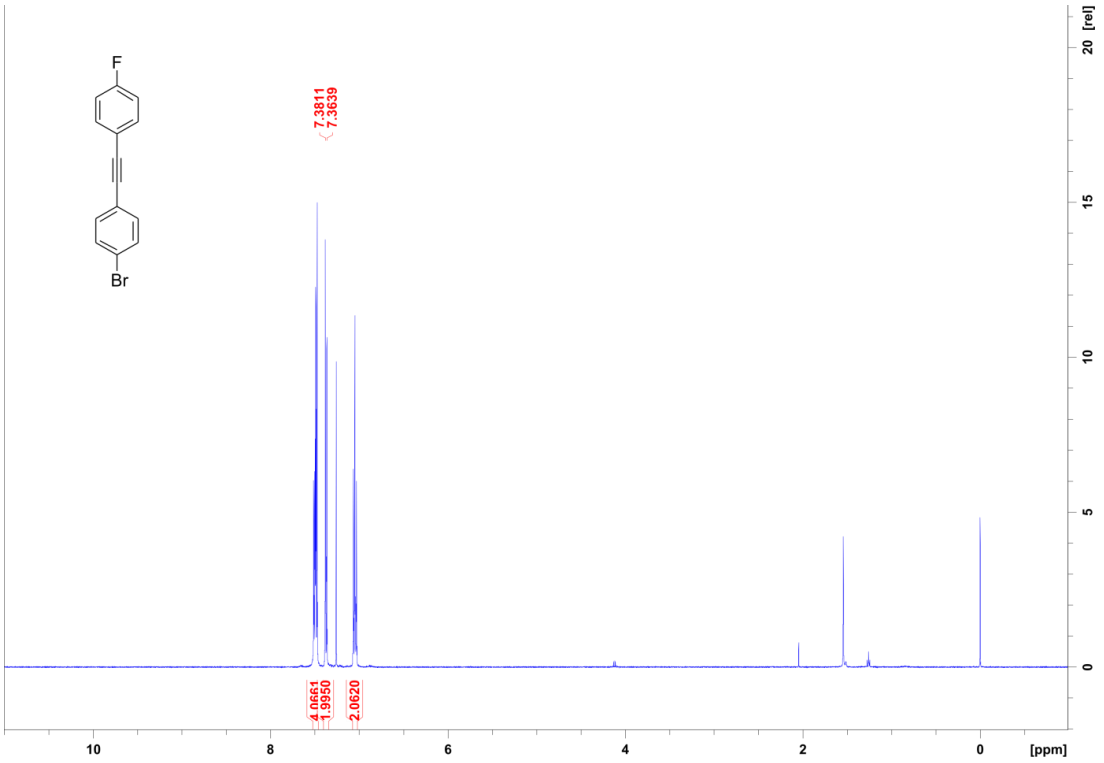

Figure S13. ^{1}H NMR spectrum (500.1 MHz, $CDCl_3$) of compound **11**.

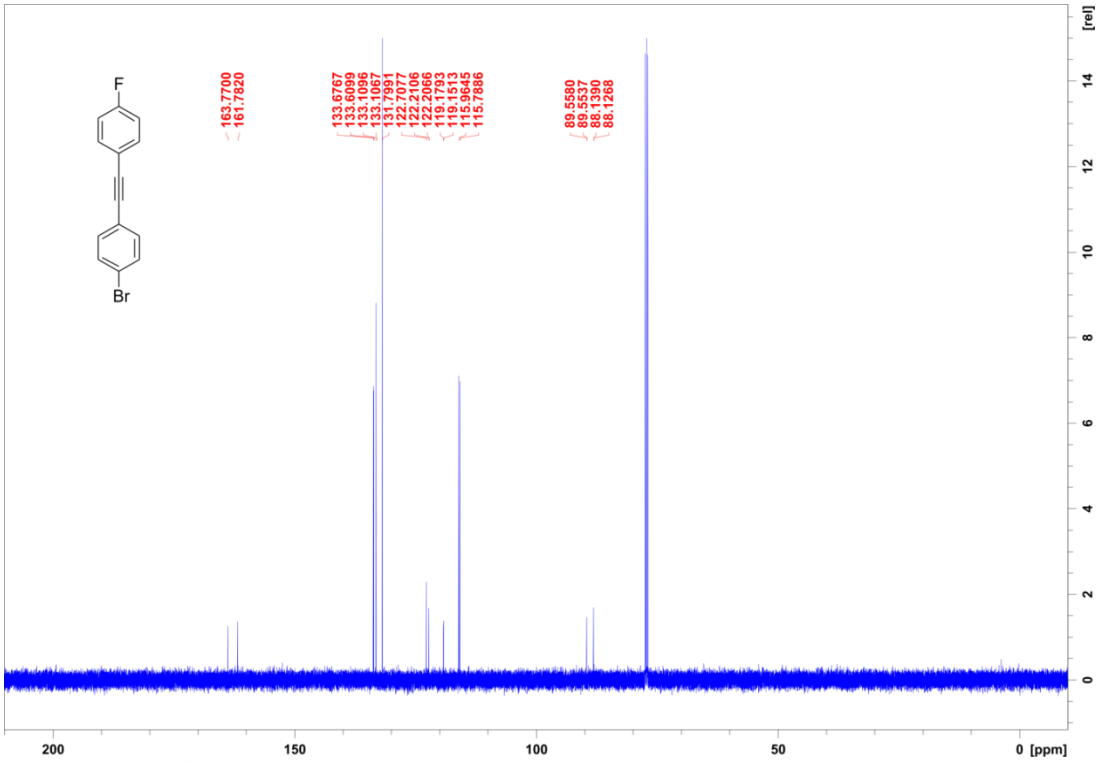

Figure S14. ^{13}C NMR spectrum (125.8 MHz, $CDCl_3$) of compound **11**.

III.7 4-(4-fluorophenylethynyl)-4‘-((trimethylsilyl)ethynyl)-biphenyl

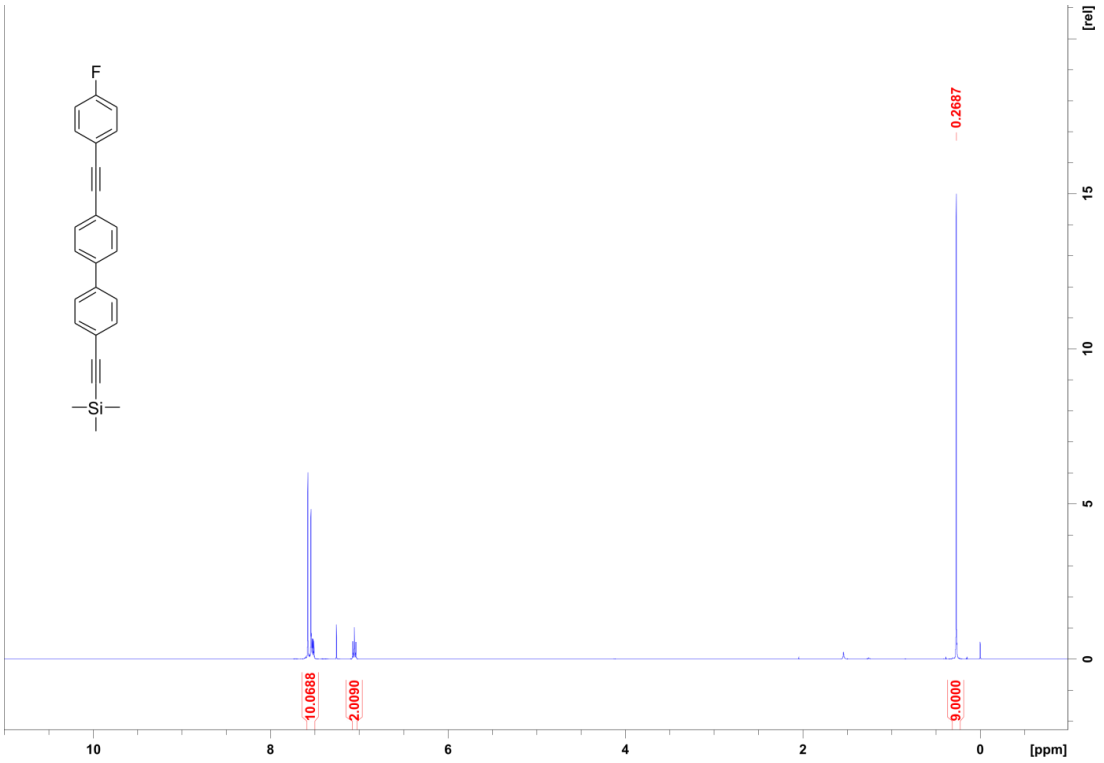

Figure S15. ^{1}H NMR spectrum (500.1 MHz, $CDCl_3$) of compound **13**.

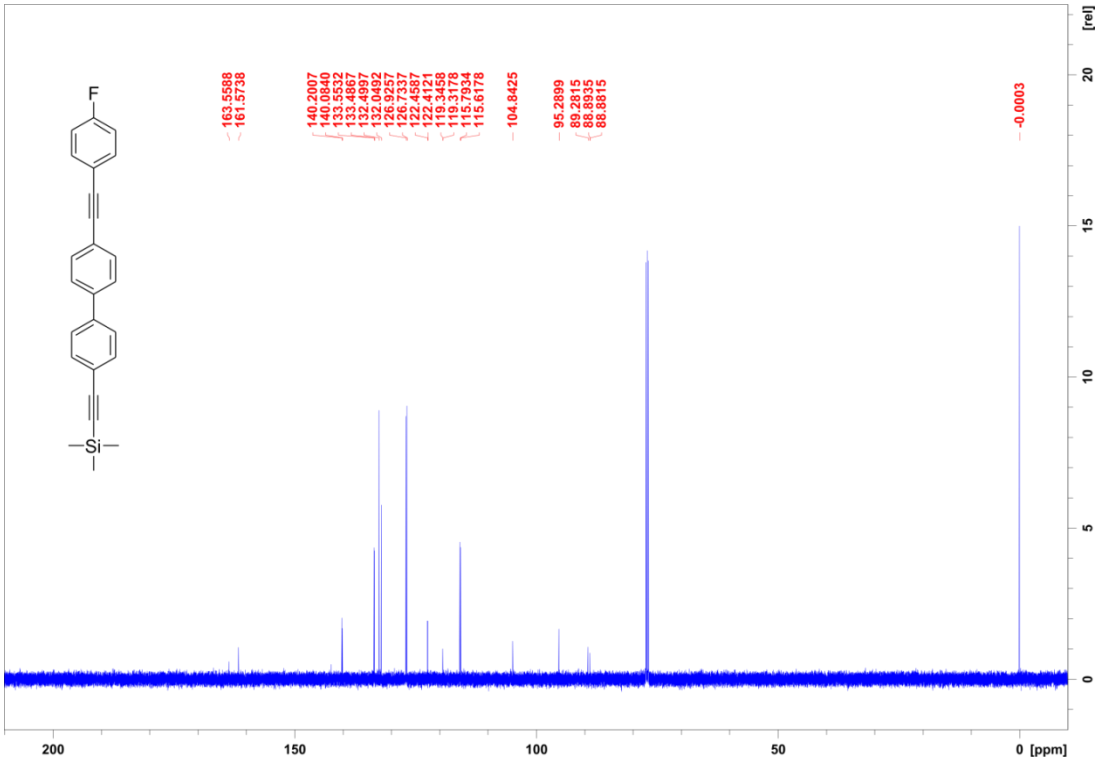

Figure S16. ^{13}C NMR spectrum (125.8 MHz, $CDCl_3$) of compound **13**.

III.8 12c-((4-fluorophenylethynyl)phenylphenyl)-ethynyl-4,8,12-tri-n-octyl-4,8,12-triaza-triangulene

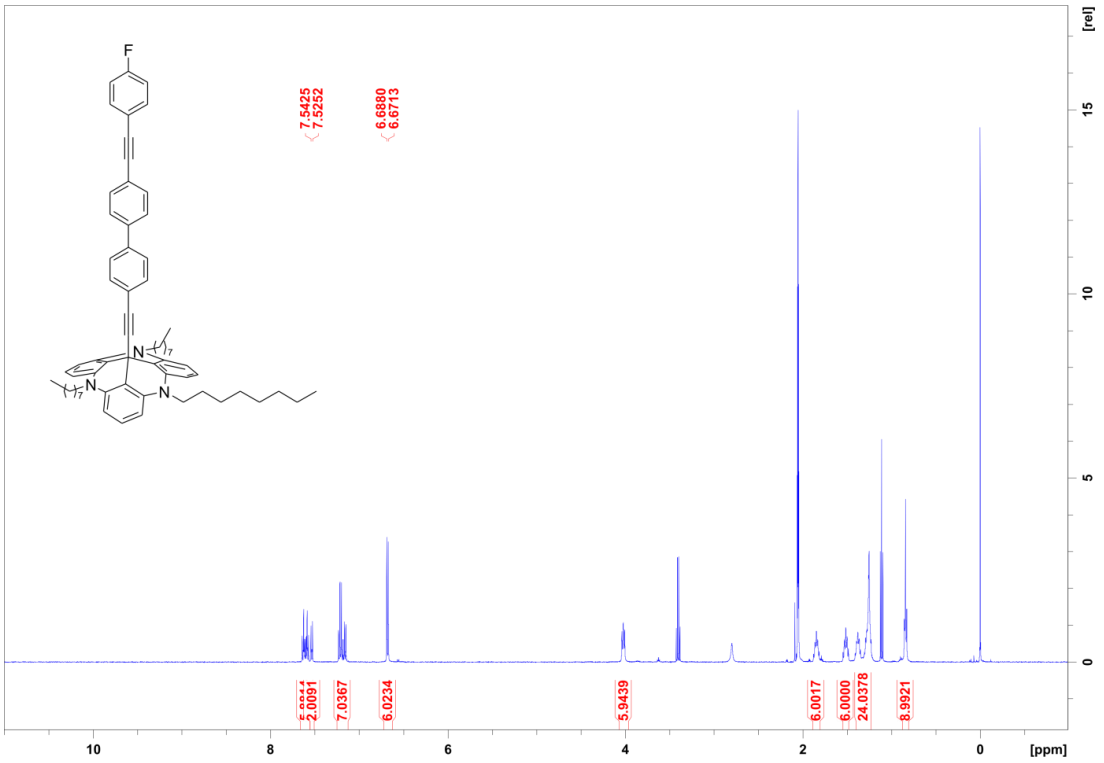

Figure S17. ^{1}H NMR spectrum (600.1 MHz, acetone-d_6) of compound **2**.

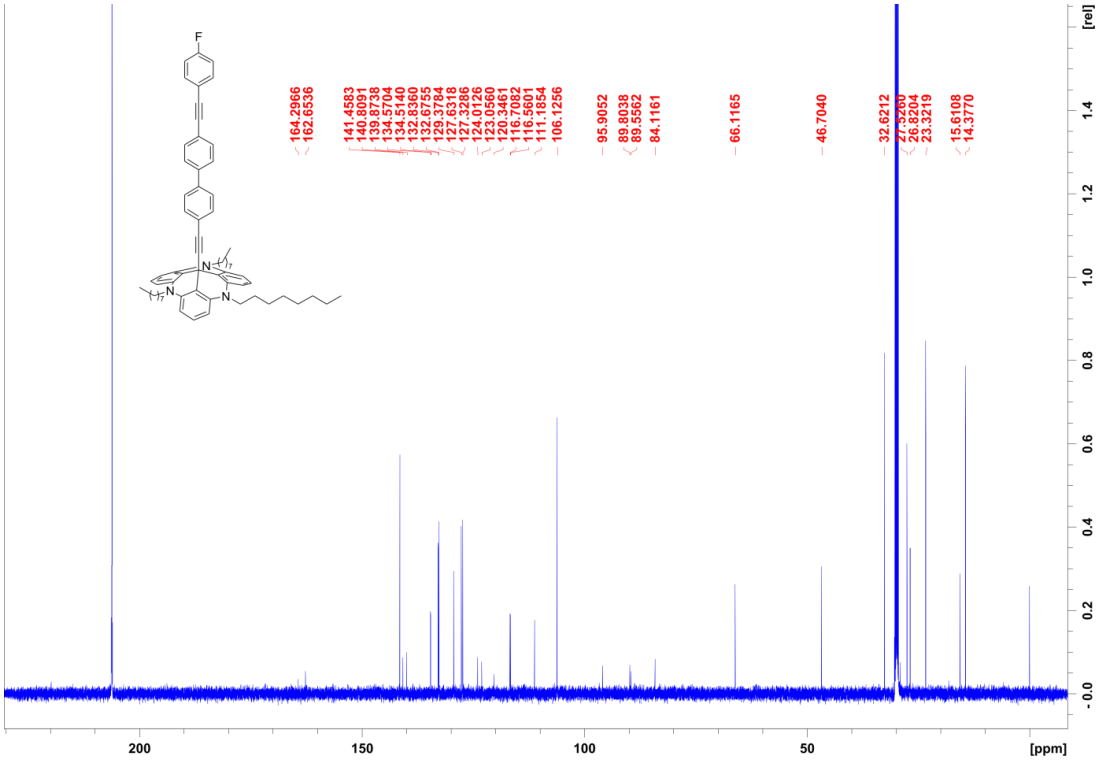

Figure S18. ^{13}C NMR spectrum (150.9 MHz, acetone-d_6) of compound **2**.

IV STM measurements

For the preparation of the self-assembled monolayers (SAMs) Au(111) single crystals were flame annealed, immersed for 60 to 80 min. in 1-100 µM solutions of compound **1**, **2** and **3** in toluene at 80 °C. Afterwards, the samples were rinsed with pure toluene. The resulting SAMs were then investigated by scanning tunneling microscopy (STM) at room temperature.

Adlayers of all compounds reveal a hexagonally ordered superstructure with a lattice constant of d_1 = (12.8 ± 0.3) Å, d_3 = (12.8 ± 0.4) Å and d_2 = (12.3 ± 0.4) Å. Particularly, the intermolecular distances d and the angle between the rotational domains α_1 = 15.4° ± 3, are in agreement with a (√19 x √19) *R*23.4° superstructure, which was also observed in previous STM investigations of octyl-TATA systems.[5-8]

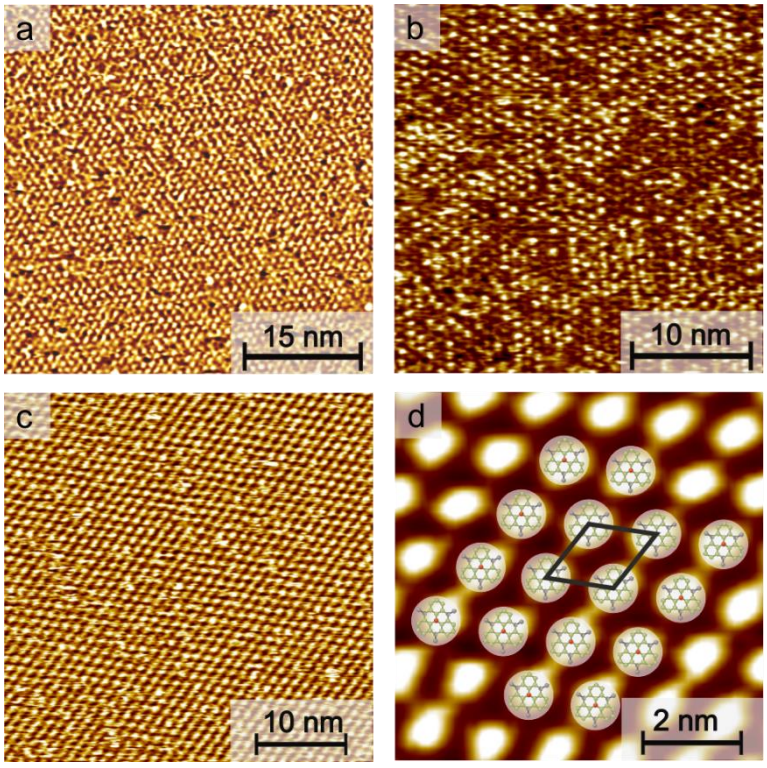

Figure 19: STM images of self-assembled layers of a) **1** (50 x 50) nm², b) **3** (15 x 15) nm², c) **2** (40x40) nm² and d) **2** (7x7) nm² with an overlaying schematic model of a (√19 x √19) *R*23.4° superstructure on Au(111).

References

[1] Prasad, T. K.; Poneti, G.; Sorace, L.; Rodrigue-Douton, M. J.; Barra, A.-L.; Neugebauer, P.; Costantino, L.; Sessolib, R.; Cornia, A. *Dalton Trans*. **2012**, *41*, 8368.

[2] Laursen, B. W.; Krebs, F. C. *Chem. Eur. J.* **2001**, *7*, 1773-1783.

[3] Browne, D. L.; Baumann, M.; Harji, B. H.; Baxendale, I. R.; Ley, S. V. *Org. Lett.* 2011, *13*, 3312-3315.

[4] Hassaneen, H. M.; Dawood, K. M.; Ahmed, M. S. M. Abdelhadi, H. A.; Mohamed, M. A.-M. *ARKIVOC* **2015**, *5*, 334-349.
[5] Baisch, B.; Raffa, D.; Jung, U.; Magnussen, O. M.; Nicolas, C.; Lacour, J.; Kubitschke, J.; Herges, R. *J. Am. Chem. Soc.* **2009**, *131*, 442–443.
[6] Ulrich, S.; Jung, U.; Strunskus, T.; Schütt, C.; Bloedorn, A.; Lemke, S.; Ludwig, E.; Kipp, L.; Faupel, F.; Magnussen, O. M.; Herges, R. *Phys. Chem. Chem. Phys.* **2015**, *17*, 17053–17062.
[7] Jacob, H.; Ulrich, S.; Jung, U.; Lemke, S.; Rusch, T.; Schütt, C.; Petersen, F.; Strunskus, F.; Magnussen, O.; Herges, R.; Tuczek F. *Phys. Chem. Chem. Phys.* **2014**, *16*, 22643.
[8] Lemke, S.; Ulrich, S.; Claußen, F.; Bloedorn, A.; Jung, U.; Herges, R.; Magnussen, O. M. *Surface Science*, **2015**, *632*, 71-76.

4 Zusammenfassung

Das in der Arbeitsgruppe HERGES entwickelte Plattformkonzept bietet die Möglichkeit, Moleküle mit einem definierten Abstand auf atomar flachen Metalloberflächen zu adsorbieren und die sich bildenden selbstorganisierten Monolagen zu untersuchen.[29,34,35] Die von LAURSEN und KREBS entwickelten TATA-Ionen bilden den Sockel, an dessen zentralem Kohlenstoffatom funktionelle Moleküle über Verknüpfungseinheiten wie Ethinyl- oder Phenylgruppen angebracht werden können.[29,181] Seit der Etablierung des Plattformkonzepts konnten bereits eine Vielzahl verschiedener Moleküle auf TATA-Plattformen funktionalisiert werden.[29,30,36–42] In verschiedenen oberflächensensitiven Messtechniken, wie zum Beispiel der Rastertunnelmikroskopie (STM) oder der Infrarot-Reflektions-Absorptions-Spektroskopie (IRRAS), können die Monolagen der auf atomar flachen Oberflächen adsorbierten TATA-Plattformen untersucht werden.[29,47] Mit der Erweiterung des Plattformkonzepts auf die TOTA-Plattformen, wird die Bindung zwischen Aufbau und Plattform stabilisiert, sodass funktionalisierte TOTA-Plattformen auf Metalloberflächen mittels Elektrosprayverfahren deponiert und im Ultrahochvakuum untersucht werden können.[31–33]
In dieser Arbeit wurden verschiedene photoschaltbare Moleküle synthetisiert und auf TATA- und TOTA-Plattformen funktionalisiert, die für die Untersuchung der nicht adiabatischen Isomerisierungsbeschleunigung verschiedener chemischer Reaktionen dienen. In früheren Arbeiten wurde bereits eine Beschleunigung der thermischen Isomerisierung von Azobenzolen auf Au(111)-Oberflächen beobachtet, deren mechanistische Wirkungsweise allerdings nicht aufgeklärt werden konnte.[47] Mithilfe der in dieser Arbeit synthetisierten und charakterisierten Azobenzol-funktionalisierten TATA-Plattformen ist der Mechanismus der thermischen Isomerisierungsbeschleunigung aufgeklärt worden. Der bisher im Plattformkonzept verwendete Ethinylspacer, der eine hohe Konjugation zwischen Azofunktion und TATA-Plattform bzw. hohe elektronische Kopplung zwischen Azoeinheit und Goldoberfläche gewährleistet, wurde mit verschiedenen Phenylringen bzw. einem isolierenden cyclischen Orthoester erweitert (Abbildung 4.1). Mit diesen designten Regulierungseinheiten konnte die elektronische Kopplung der Goldoberfläche mit der Azofunktion schrittweise reduziert werden und somit die Stärke der nicht adiabatischen Beschleunigung auf die thermische *cis*→*trans*-Isomerisierung reguliert werden. Mit der logarithmischen Auftragung der Ratenkonstante der thermischen Isomerisierung und der Spindichte des Orbitals der Azofunktion unterhalb der Regulierungseinheit wird die Temperaturabhängigkeit der Isomerisierung der Azobenzol-TATA-Plattformen graphisch verglichen. Mit Einheiten, die eine hohe Konjugation aufweisen und somit eine hohe elektronische Kopplung zwischen Azofunktion und Gold zulassen, wird der Isomerisierungsprozess vom goldvermittelten Singulett→Triplett→Singulett-Mechanismus dominiert. Die Temperaturabhängigkeit dieses Isomerisierungsmechanismus ist vernachlässigbar und hängt nur von der Spindichte des Orbitals der Azofunktion im Gold ab. Dem gegenüber verläuft bei Regulierungseinheiten, die die Konjugation vollständig unterbrechen und somit den Einfluss des Goldes nahezu unterbinden, die thermische Isomerisierung hauptsächlich nach den Gesetzen

der klassischen Thermodynamik. Zwischen diesen Mechanismen wurde ein Bereich postuliert, in dem die thermische Isomerisierung von beiden Mechanismen abhängig ist. Mit der Auswertung der kinetischen Daten dieser Isomerisierungen konnte die Aufhebung des quantenmechanischen Verbots des Intersystem-Crossings zwischen der Singulett- und Tripletthyperfläche nachgewiesen werden, wodurch die Reaktionsgeschwindigkeit der thermischen *cis*→*trans*-Isomerisierung ausschließlich von der quantenmechanischen Übergangswahrscheinlichkeit abhängt.

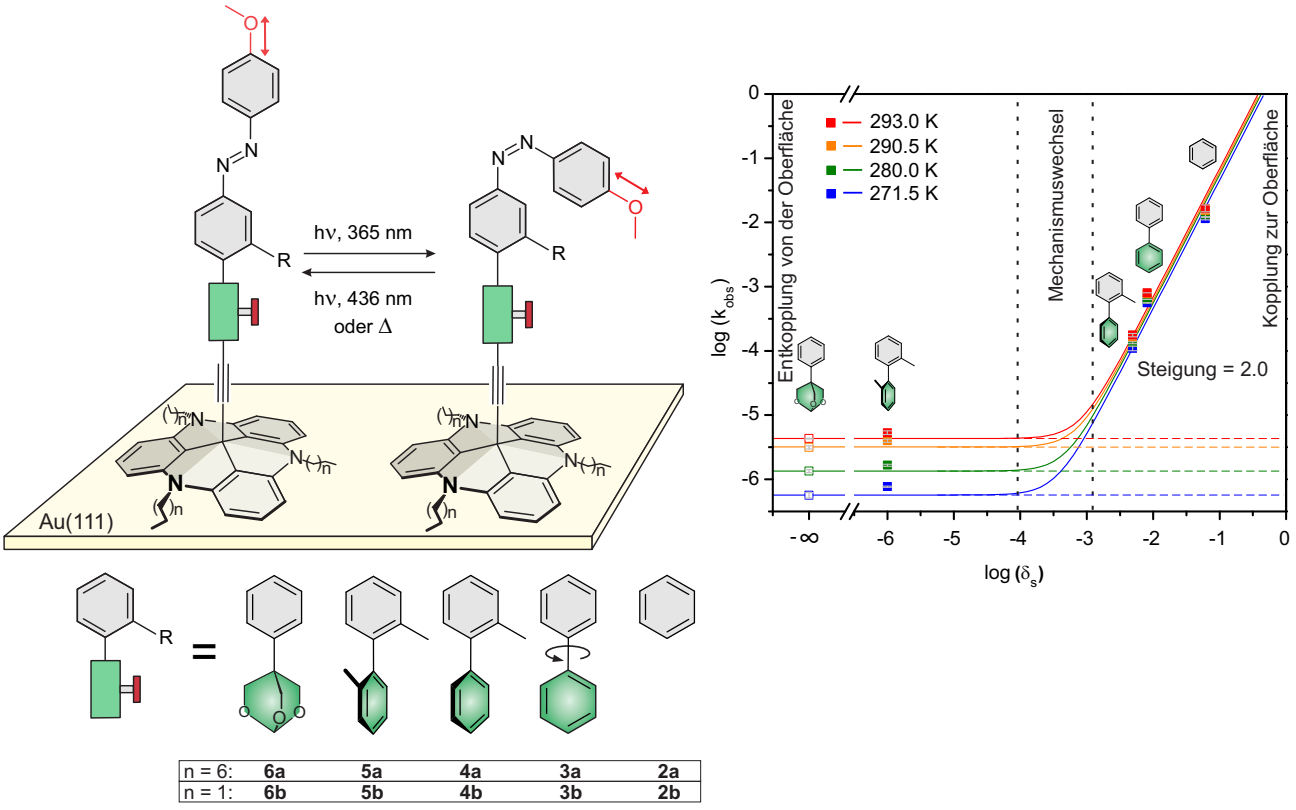

Abb. 4.1: Darstellung der Azo-TATA-Plattform im *trans*- und *cis*-Isomer mit der schematisch dargestellten Regulierungseinheit (grün), die den gezeigten Strukturen entspricht (links). Die Auftragung von $\log(k_{obs})$ als Funktion von $\log(\delta_s)$ ist graphisch aufgezeigt (rechts). Dabei ist k_{obs} die Ratenkonstante der thermischen *cis*→*trans*-Isomerisierung der jeweiligen Azo-TATA-Plattform und δ_s die Spindichte des Orbitals der Azofunktion unterhalb der Regulierungseinheit.

Die Ratenkonstanten dieser Azobenzole auf Octyl- und Propyl-TATA-Plattformen, adsorbiert auf Au(111)-Oberflächen, wurden in Abhängigkeit zu den intermolekularen Abständen in den Monolagen verglichen, um den sterischen Einfluss auf die thermische *cis*→*trans*-Isomerisierung zu untersuchen. Die Ergebnisse zeigten, dass der geringere Freiraum im Fall der Propyl-TATA-Plattformen die Isomerisierung geringfügig beeinflusst und im Fall der Octyl-TATA-Plattformen eine intermolekulare sterische Beeinflussung auf die Isomerisierung vernachlässigbar ist.

Mit der Etablierung von methoxyfunktionalisierten Diazocinen auf TATA-Plattformen wird die Möglichkeit zur Untersuchung des nicht adiabatischen Mechanismus auf die thermische *trans*→*cis*-Isomerisierung geboten. Aufgrund der Ethylenverbrückung der Phenylringe im Diazocin liegt ein

Achtring vor, wodurch die Rotation um die Azofunktion unterbunden wird. Daraus ergeben sich variable Funktionalisierungen der Diazocine mit der Methoxykopfgruppe und der Verknüpfungseinheit verglichen zum Azobenzol und weiterhin können beide Isomere in der IRRA-Spektroskopie unterschieden werden. Folglich konnten zwei unterschiedlich funktionalisierte Diazocine auf TATA-Plattformen etabliert werden (Abb. 4.2). Erstere Diazocin-Plattform **10** wurde in *para*-Position zur Azofunktion mit einer Acetyleneinheit ausgestattet, um eine hohe Konjugation zwischen Azofunktion und TATA-Plattform zu gewährleisten. In der zweiten Diazocin-Plattform **11** wurde das Acetylen in *meta*-Position zur Azobrücke etabliert, wodurch die Azofunktion von der TATA-Plattform weitestgehend elektronisch isoliert vorliegt. Die Methoxygruppe, die als Markereinheit in IRRAS-Messungen dienen soll, ist in beiden Strukturisomeren **10** und **11** im *cis*-Isomer parallel und im *trans*-Isomer orthogonal zur TATA-Plattform ausgerichtet. Die kinetischen Daten der Isomerisierung in Lösung konnten ermittelt und mittels STM-Messungen die hochgeordneten Monolagen beider Diazocine auf Au(111) nachgewiesen werden.

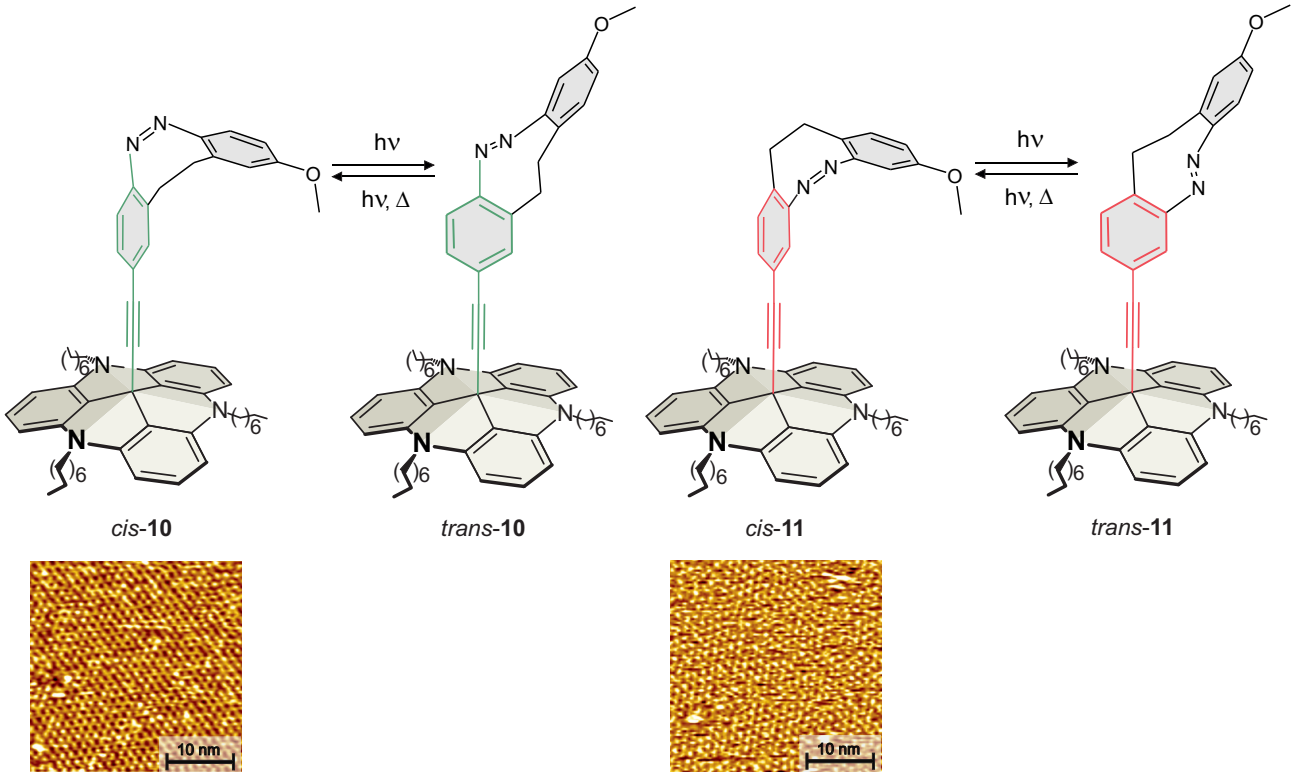

Abb. 4.2: Dargestellt sind die Diazocin-TATA-Plattform mit hoher Konjugation **10** (links) und unterbrochener Konjugation **11** (rechts) zwischen Azofunktion und TATA-Plattform und deren Isomerisierungen zwischen dem *cis*- und *trans*-Isomer. Zusätzlich sind die per STM aufgenommenen Monolagen beider Diazocin-Plattformen auf Au(111) gezeigt.

Um die Anwendungsmöglichkeiten dieses aufgeklärten Mechanismus definieren zu können, ist die Untersuchung in einer weiteren Reaktion neben der thermischen *cis*→*trans*- bzw. *trans*→*cis*-Isomerisierung azobenzolbasierter Photoschalter essentiell. Aus diesem Grund wurden Norbornadiene auf TATA- und TOTA-Plattformen funktionalisiert (Abb. 4.3), die photochemisch in einer [2+2]-

Cycloaddition in das metastabile Quadricyclan überführt werden können und photochemisch oder thermisch in einer [2+2]-Cycloreversion in das Norbornadien zurückisomerisieren. Das Substitutionsdesign der Norbornadien-TATA-Plattform **12** wurde so gewählt, dass mit einer elektronenziehenden Cyanoeinheit und der Acetyleneinheit eine thermische [2+2]-Cycloreversion bei Raumtemperatur beobachtet werden kann. Eine Reduktion der Konjugation zwischen TATA-Plattform und Norbornadien wurde mit einer methylsubstituierten Phenyleinheit in **13** erreicht.

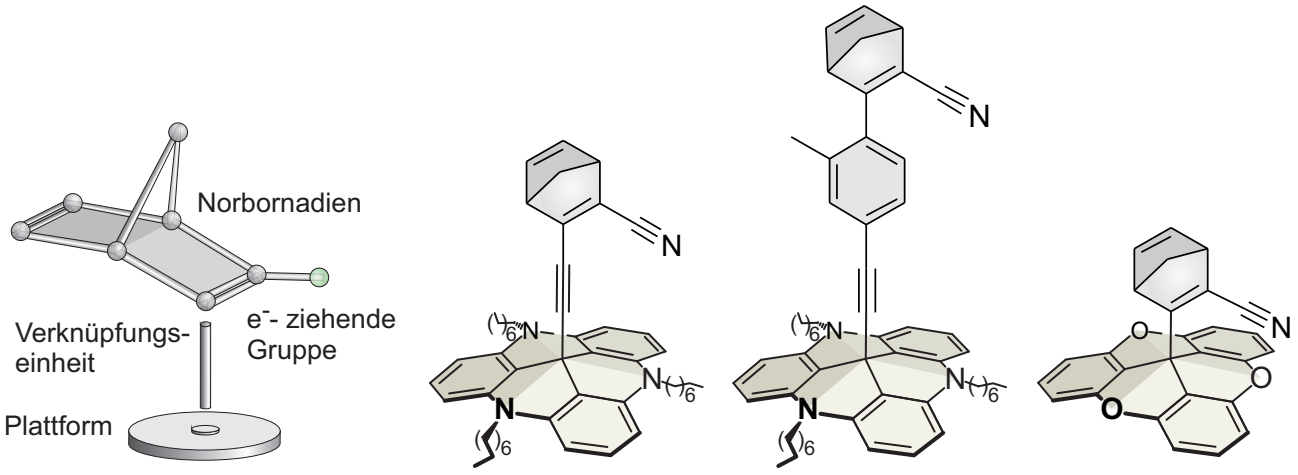

	Atmos-phäre	PSS (% QC)	PSS (% NBD)	$t_{1/2}$ (h)	EA kJ/mol
12	Luft	~100 (385 nm)	52 (311 nm)	655 (293 K)	/
12	N_2	~100 (385 nm)	28 (311 nm)	732 (294 K)	111
13	N_2	~100 (385 nm)	52 (311 nm)	/	/
14	N_2	91 (311 nm)	33 (254 nm)	/	/

Abb. 4.3: Schematische Darstellung des Norbornadien-Plattformkonzepts und den ensprechenden Norbornadien-TATA-Plattformen **12**, **13** und Norbornadien-TOTA-Plattform **14**. Die photostationären Zustände, die Halbwertszeiten und die entsprechende Aktivierungsenergie sind tabellarisch zusammengefasst.

Zusätzlich wurde ein Norbornadien mit Cyanogruppe direkt auf TOTA-Plattform **14** funktionalisiert, um eine stabile Verbindung zwischen Plattform und Norbornadien zu erhalten. In Untersuchungen der adsorbierten Norbornadien-Plattformen von **12** auf Goldoberflächen in STM-Messungen wurden zwei unterschiedliche relative Höhen nachgewiesen. Es besteht die Möglichkeit, dass bei der Präparation der Monolagen von **12** bei einem gewissen Anteil der Norbornadienaufbau von der Plattform abgebrochen ist und das TATA-Plattformion als zweite relative Höhe detektiert wurde. Eine weitere Möglichkeit ist, dass die umgebende Laborbeleuchtung zur Isomierisierung des Norbornadiens geführt hat und die entsprechende Quadricyclan-Plattform eine unterschiedliche relative Höhe verglichen zur Norbornadien-Plattform aufweisen könnte.

Das Moleküldesign der Azobenzole, Diazocine und Norbornadiene ist jeweils für die Untersuchung mit verschiedenen oberflächensensitiven Methoden optimiert. Die Rastertunnelmikroskopie hat sich in

bisherigen Forschungsarbeiten vor allem für den Nachweis der hochgeordneten Monolagen bewährt. Die Isomerisierung der photoschaltbaren Moleküle auf Plattformen könnte in STM-Messungen über die Änderung der relativen Höhe untersucht werden, wobei ein Vergleich zu einer Referenz nötig ist. Aus diesem Grund wurden verschiedene Referenz-TATA-Plattformen **15**, **16**, **17** synthetisiert und zusätzlich auf deren Verhalten zur Monolagenbildung auf Au(111)-Oberflächen in STM-Messungen untersucht (Abb. 4.4). Diese Aufbauten auf den TATA-Plattformen variieren in ihrer Höhe und dem Grad der Konjugation.

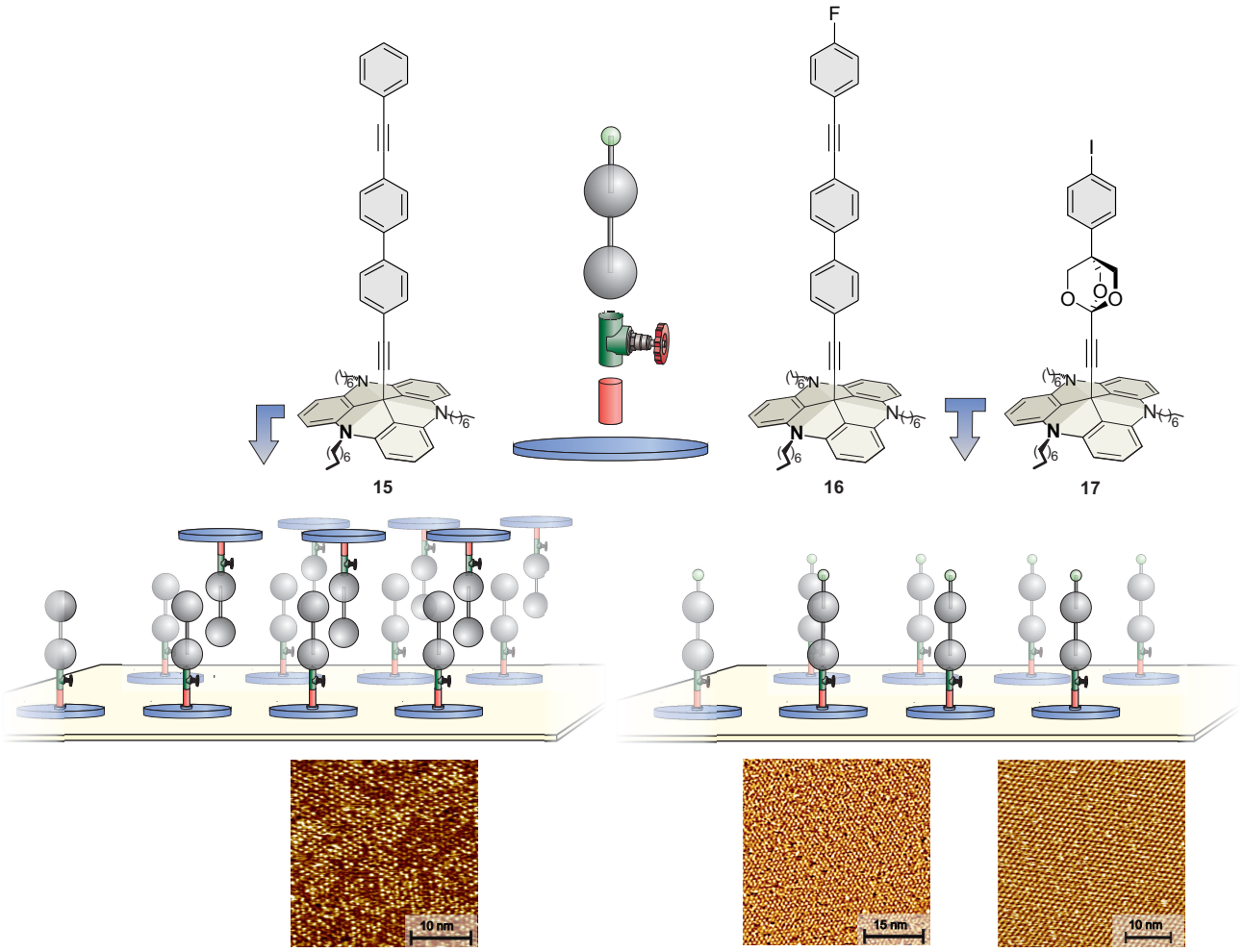

Abb. 4.4: Strukturen der Referenzplattformen mit hoher Konjugation **15**, **16** und der nicht konjugierten Referenzplattform **17**. Die schematische postulierte Bilagenbildung auf Au(111) ist links und die reine Monolagenbildung rechts dargestellt.

Zusätzlich wurde bei den leitfähigen Referenzplattformen **15**, **16** der Einfluss einer Kopfgruppe auf die Eigenschaften der Monolagenbildung auf Au(111)-Oberflächen verglichen. Beim Verzicht einer Fluorkopfgruppe in **17** wurden zwei unterschiedliche relative Höhen nachgewiesen, was auf eine Bilagenbildung hindeutet. Im Vergleich dazu wurde eine mögliche Bilagenbildung mit Verwendung der Fluorkopfgruppe in **16** bzw. der Iodkopfgruppe in **17** unterbunden. Aufgrund der drei Phenylringe in der Referenzplattform **15** können π-π-Wechselwirkungen zur Bilagenbildung führen, während die Bilagenbildung mit der Fluor- bzw. Iodkopfgruppe unterbunden werden.

5 Ausblick

Für den Nachweis des nicht adiabatischen Singulett→Triplett→Singulett-Mechanismus in weiteren Reaktionen könnten in zukünftigen Arbeiten die Diazocine **10** und **11** und Norbornadiene **12**, **13** und **14** auf Goldoberflächen auf eine thermische Isomerisierungsbeschleunigung untersucht werden. Adsorbiert auf Goldoberflächen sollte im Fall der Diazocin-TATA-Plattformen die elektronische Kopplung der Goldoberfläche mit der Azofunktion des Diazocins **10** zur Beschleunigung der thermischen Isomerisierung führen, während im Diazocin **11** die Azofunktion von der Goldoberfläche weitestgehend isoliert vorliegen sollte und die Ratenkonstante der thermischen Isomerisierung der Ratenkonstante in Lösung annähernd gleichen sollte. Die Norbornadien-TATA-Plattform **12** könnte ebenfalls auf Goldoberflächen auf eine thermische Isomerisierungsbeschleunigung überprüft und mit den bereits erhaltenen Ratenkonstanten und Aktivierungsenergien der thermischen [2+2]-Cycloreversion in Lösung verglichen werden. Aufgrund der niedrigeren Konjugation der Verbrückungseinheit in der Norbornadien-TATA-Plattform **13** sollte eine geringere Beschleunigung der thermischen Isomerisierung auf Gold im Vergleich zu **12** vorliegen. Die Norbornadien-TOTA-Plattform **14** sollte aufgrund der höheren Stabilität zwischen Plattform und Aufbau über ein Elektrosprayverfahren auf Goldoberflächen adsorbiert und die Isomerisierungseigenschaften im Ultrahochvakuum unter Tieftemperaturbedingungen sowie milden Bedingungen untersucht werden können.
Die Untersuchung der Kinetik von Azobenzolen auf Goldoberflächen hat den katalytischen Mechanismus als nicht adiabatischen Singulett→Triplett→Sinuglett-Mechanismus aufgeklärt. Allerdings werden mit den verschiedenen Regulierungseinheiten zwei getrennt voneinander beobachtete Isomerisierungsmechanismen beobachtet. Bei diesen fünf Regulierungseinheiten wird beim Azobenzol keine thermische Isomerisierung beobachtet, die nach beiden Mechanismen, dem klassischen und dem nicht-adiabatischen Mechanismus, abläuft. Um den fließenden Wechsel beider Mechanismen zusammen in der thermischen Isomerisierung beobachten zu können, muss der Verdrillungswinkel der Biphenyleinheit zwischen 51-84 ° gebracht werden. In diesem Bereich wird die Spindichte der Azofunktion im Gold soweit herabgesetzt, dass der nicht adiabatische Mechanismus einen vergleichenbaren Einfluss auf die thermische Isomerisierung wie die klassische Thermodynamik haben sollte. Mit neu designten Regulierungseinheiten, die die Methylgruppe der Methylbiphenyleinheit substituieren, kann der Verdrillungswinkel leicht erhöht werden. Dafür bietet sich eine Isopropylgruppe an, die einen Verdrillungswinkel von 54.6 ° ergibt, bzw. eine Butylenbrücke mit einem Verdrillungswinkel von 58.4 ° (Abb. 5.1).[182]

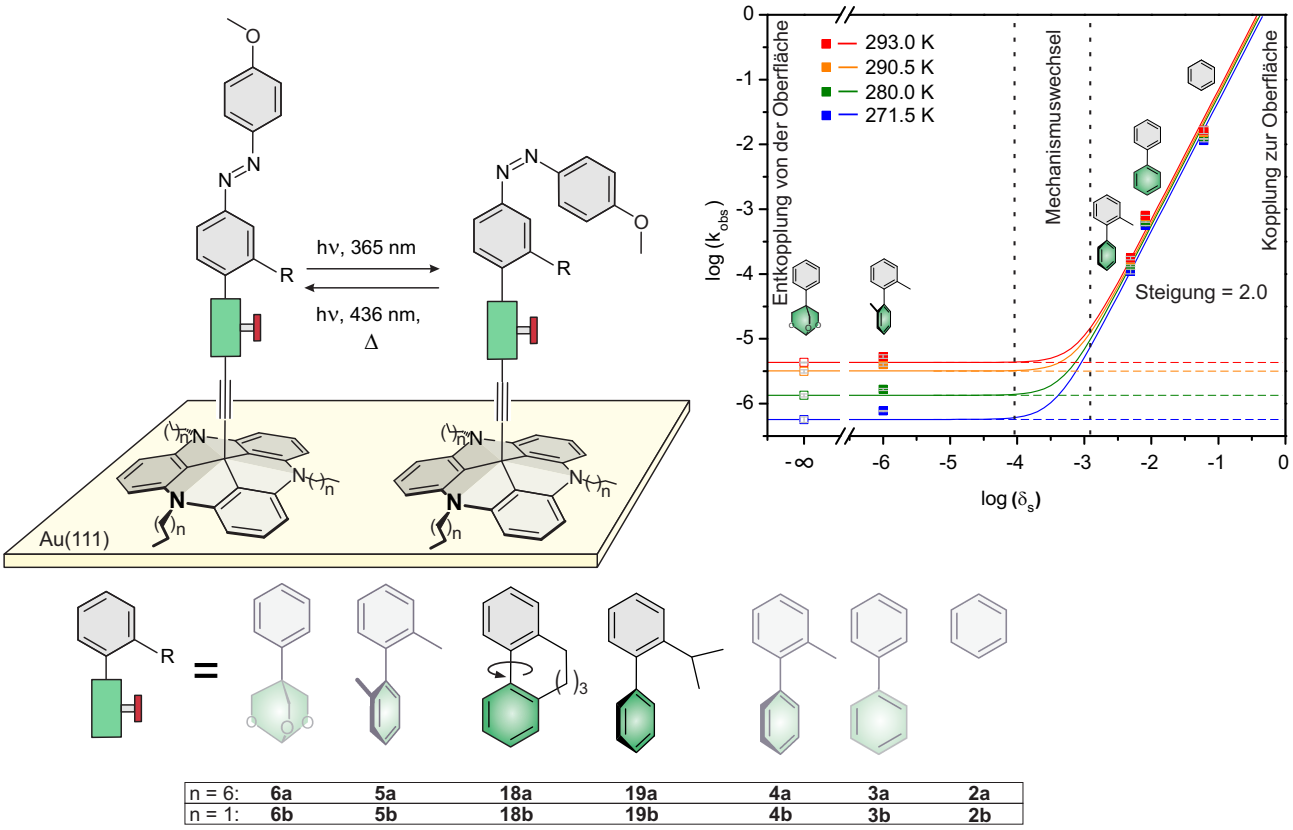

Abb. 5.1: Schematische Darstellung der Azo-TATA-Plattform im *trans*- und *cis*-Isomer (links) mit den bisherigen Regulierungseinheiten (unten, grau) und der graphischen Darstellung ihrer thermischen Isomerisierung auf Bulk-Gold (rechts). Mit den neu vorgeschlagenen Substituenten in der Biphenyleinheit in **18** und **19** (Isopropyl, Butylbrücke) soll der Verdrillungswinkel der Biphenyleinheit zwischen 51-84 ° gebracht werden, um den Wechsel des Isomerisierungsmechanismus genauer zu verstehen. Der Verdrillungswinkel mit Isopropylbiphenyleinheit liegt bei 54.6 ° bzw. mit Butylenbrücke bei 58.4 °.[182]

Der nicht adiabatische Mechanismus wurde intensiv mithilfe der thermischen Isomerisierung des Azobenzols auf Au(111)-Oberflächen untersucht. Weiterhin sind mit auf Plattform funktionalisierte Diazocinen und Norbornadienen weitere Photoschalter etabliert worden, mit denen der nicht adiabatische Mechanismus untersucht werden könnte. Zusätzlich zu diesen bereits designten und synthetisierten Photoschalter-Plattformen könnten mit Stilbenen und molekularen Motoren weitere photoschaltbare Moleküle auf Plattformen funktionalisiert und auf Gold untersucht werden (Abb. 5.2).[183] Die thermische Isomerisierung des *cis*-Stilben zum *trans*-Stilben findet bei Raumtemperatur aufgrund der hohen Aktivierungsbarriere nicht statt.[126,127] Sollte das Gold das quantenmechanische Verbot des Intersystem-Crossings zwischen Singulett- und Tripletthyperfläche aufheben, könnte eine thermische Isomerisierung bei Raumtemperatur auf Goldoberflächen nachweisbar sein. Dieses Verhalten würde den Mechanismus über ein Intersystem-Crossing bestätigen. Bei den molekularen Motoren könnte ein Design gewählt werden, das eine Isomerisierung im Stundenbereich aufweist, um die mögliche Beschleunigung der Rotation um die Doppelbindung genau bestimmen zu können.[183]

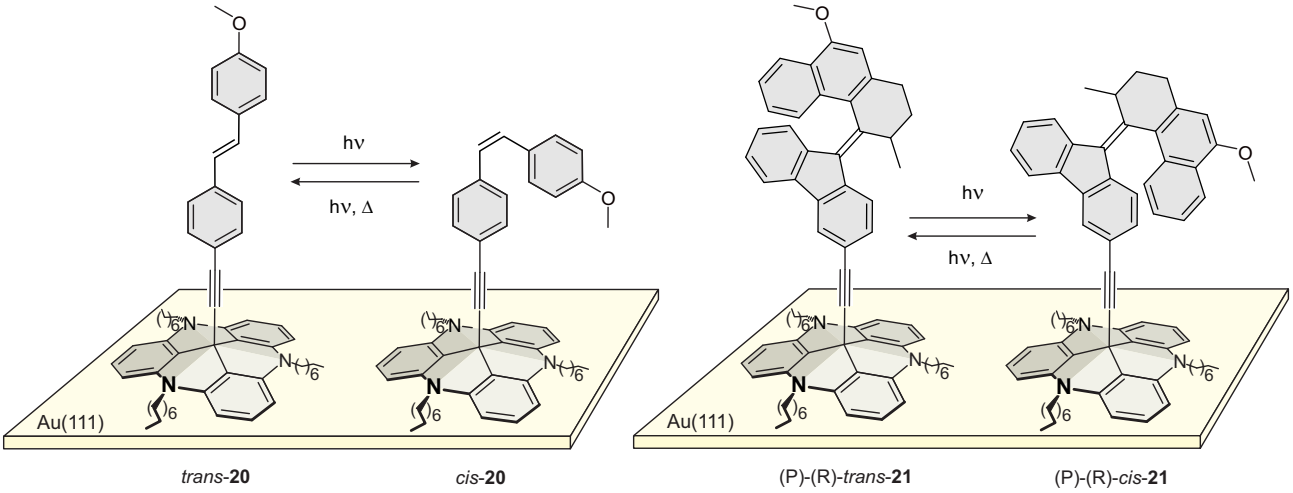

Abb. 5.2: Schematische Darstellung von Octyl-TATA-Plattformen funktionialisiert mit Stilben **20** bzw. molekularem Motor **21** adsorbiert auf Au(111). Beide Photoschalter sind über ein Acetylen auf der Plattform angebracht und enthalten eine Methoxygruppe die orthogonal zur Oberfläche (*trans*-**20**, (P)-(R)-*trans*-**21**) bzw. parallel ausgerichtet sein sollten (*cis*-**20**, (P)-(R)-*cis*-**21**).

In den bisherigen Untersuchungen von Azobenzolen funktionalisiert auf Octyl- und Propyl-TATA-Plattformen konnte festgestellt werden, dass durch die geringeren intermolekularen Abstände der Propyl-TATA-Plattformen in Monolagen die *cis*-Azobenzole miteinander interagieren. Daraus resultieren sowohl geringfügig beschleunigte thermische Isomerisierungen als auch erniedrigte photostationäre Gleichgewichte der *cis*-Isomere in Monolagen. Diese Annäherung der *cis*-Azobenzole und deren Wechselwirkungen untereinander könnten ebenfalls mit verlängerten Kopfgruppen bei Octyl-TATA-Plattformen erreicht werden und somit die Rotation im *cis*-Isomer gezielt eingeschränkt werden. Mit dem Austausch des oberen Phenylrings des Azobenzols durch ein Biphenyl in **22** bzw. einer Terphenyleinheit in **23** ist die horizontale Ausrichtung der *cis*-Azobenzole größer als der Abstand zwischen dem zentralen Kohlenstoffatomen der Plattformen (Abb. 5.3).[182]

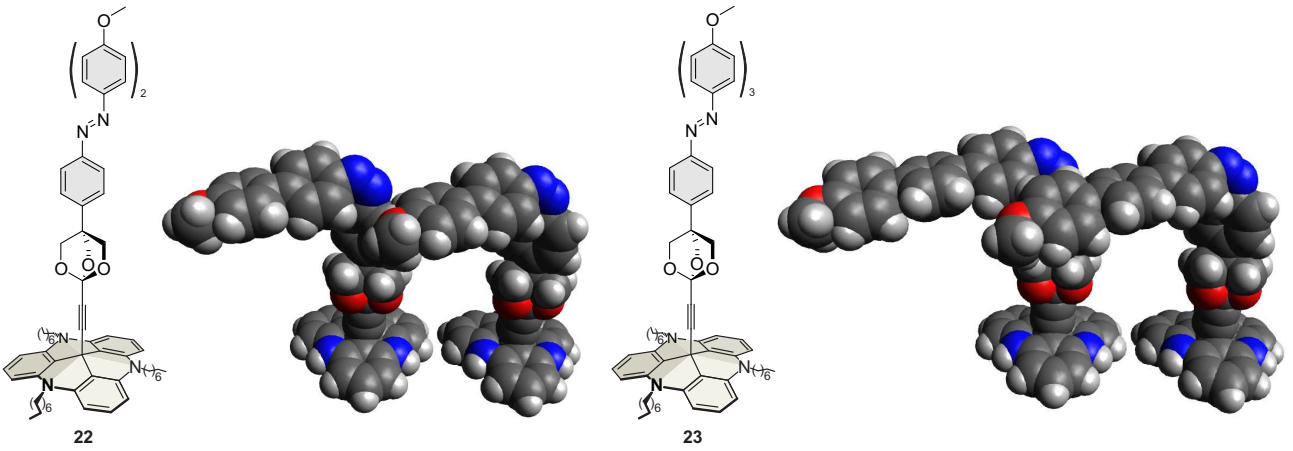

Abb. 5.3: Verschiedene Azobenzol-TATA-Plattformen mit verlängerten Kopfgruppen. Realisiert wird die Verlängerung über die Einführung eines Phenylrings **21** bzw. zweier Phenylringe **22**. Die sterische Hinderung wurde theoretisch kalkuliert.[182]

Werden diese Azobenzol-TATA-Monolagen mit polarisiertem Licht bestrahlt, sollte die photochemische *trans*→*cis*-Isomerisierung ausschließlich in eine definierte Richtung erfolgen und die Ausrichtung der *cis*-Isomere sollte durch die sterische Hinderung fixiert sein. Dieses Verhalten könnte in STM-Messungen analysiert werden. Für eine hohe Ordnung dieser *cis*-Azobenzole in Monolagen ist ein hoher *cis*-Anteil über mehrere Stunden essentiell, weswegen die goldvermittelte thermische Isomerisierungsbeschleunigung unterbunden werden muss. Mit der Einführung des cyclischen Orthoesters in die Verknüpfungseinheit wird die elektronische Isolation des Azobenzols von der Oberfläche gewährleistet. Zusätzlich zur Einschränkung der Rotation sollten ebenfalls die Ratenkonstanten der thermischen Isomerisierung beeinflusst sein, die mithilfe der Methoxygruppe in IRRAS-Messungen untersucht werden könnten.

Literaturverzeichnis

[1] V. Balzani, A. Credi, F. M. Raymo, J. F. Stoddart, *Angew. Chem. Int. Ed.* **2000**, *39*, 3348–3391.

[2] T. Kudernac, N. Ruangsupapichat, M. Parschau, B. Maciá, N. Katsonis, S. R. Harutyunyan, K.-H. Ernst, B. L. Feringa, *Nature* **2011**, *479*, 208–211.

[3] A. S. Shah, Y. Ben-Shahar, T. O. Moninger, J. N. Kline, M. J. Welsh, *Science* **2009**, *325*, 1131–1134.

[4] G. Füchsel, T. Klamroth, J. Dokić, P. Saalfrank, *J Phys. Chem. B* **2006**, *110*, 16337–16345.

[5] E. Merino, M. Ribagorda, *Beilstein J. Org. Chem.* **2012**, *8*, 1071–1090.

[6] S. D. Evans, S. R. Johnson, H. Ringsdorf, L. M. Williams, H. Wolf, *Langmuir* **1998**, *14*, 6436–6440.

[7] A. Ulman, *Chem. Rev.* **1996**, *96*, 1533–1554.

[8] R. G. Nuzzo, D. L. Allara, *J. Am. Chem. Soc.* **1983**, *105*, 4481–4483.

[9] M. D. Porter, T. B. Bright, D. L. Allara, C. E. D. Chidsey, *J. Am. Chem. Soc.* **1987**, *109*, 3559–3568.

[10] C. D. Bain, E. B. Troughton, Y.-T. Tao, J. Evall, G. M. Whitesides, R. G. Nuzzo, *J. Am. Chem. Soc.* **1989**, *111*, 321–335.

[11] R. G. Nuzzo, L. H. Dubios, D. L. Allara, *J. Am. Chem. Soc.* **1990**, *112*, 558–569.

[12] P. E. Laibinis, G. M. Whitesides, D. L. Allara, Y.-T. Tao, A. N. Parikh, R. G. Nuzzo, *J. Am. Chem. Soc.* **1991**, *113*, 7152–7167.

[13] C. D. Bain, H. A. Biebuyck, G. M. Whitesides, *Langmuir* **1989**, *5*, 723–727.

[14] N. Katsonis, T. Kudernac, M. Walko, S. J. van der Molen, B. J. van Wees, B. L. Feringa, *Adv. Mater.* **2006**, *18*, 1397–1400.

[15] L. Strong, G. M. Whitesides, *Langmuir* **1988**, *4*, 546–558.

[16] P. E. Laibinis, C. D. Bain, R. G. Nuzzo, G. M. Whitesides, *J. Phys. Chem.* **1995**, *99*, 7663–7676.

[17] L. Häussling, B. Michel, H. Ringsdorf, H. Rohrer, *Angew. Chem. Int. Ed.* **1991**, *30*, 569–572.

[18] N. Heinemann, J. Grunau, T. Leißner, O. Andreyev, S. Kuhn, U. Jung, D. Zargarani, R. Herges, O. Magnussen, M. Bauer, *Chem. Phys.* **2012**, *402*, 22–28.

[19] U. Siemeling, C. Bruhn, F. Bretthauer, M. Borg, F. Träger, F. Vogel, W. Azzam, M. Badin, T. Strunskus, C. Wöll, *Dalton Trans.* **2009**, *0*, 8593–8604.

[20] T. Weidner, F. Bretthauer, N. Ballav, H. Motschmann, H. Orendi, C. Bruhn, U. Siemeling, M. Zharnikov, *Langmuir* **2008**, *24*, 11691–11700.

[21] G. Pace, V. Ferri, C. Grave, M. Elbing, C. v. Hänisch, M. Zharnikov, M. Mayor, M. A. Rampi, P. Samori, *Proc. Nat. Acad. Sci.* **2007**, *104*, 9937–9942.

[22] T. Moldt, D. Brete, D. Przyrembel, S. Das, J. R. Goldman, P. K. Kundu, C. Gahl, R. Klajn, M. Weinelt, *Langmuir* **2015**, *31*, 1048–1057.

[23] A. S. Kumar, T. Ye, T. Takami, B.-C. Yu, A. K. Flatt, J. M. Tour, P. S. Weiss, *Nano Lett.* **2008**, *8*, 1644–1648.

[24] K. Tamada, M. Hara, H. Sasabe, W. Knoll, *Langmuir* **1997**, *13*, 1558–1566.

[25] B. Lüssem, L. Müller-Meskamp, S. Karthäuser, R. Waser, M. Homberger, U. Simon, *Langmuir* **2006**, *22*, 3021–3027.

[26] S. J. Stranick, A. N. Parikh, Y.-T. Tao, D. L. Allara, P. S. Weiss, *J. Phys. Chem.* **1994**, *98*, 7636–7646.

[27] D. Takamatsu, Y. Yamakoshi, K. i. Fukui, *J. Phys. Chem. B* **2006**, *110*, 1968–1970.

[28] S. Wagner, F. Leyssner, C. Kördel, S. Zarwell, R. Schmidt, M. Weinelt, K. Rück-Braun, M. Wolf, P. Tegeder, *Phys. Chem. Chem. Phys.* **2009**, *11*, 6242–6248.

[29] B. Baisch, D. Raffa, U. Jung, O. M. Magnussen, C. Nicolas, J. Lacour, J. Kubitschke, R. Herges, *J. Am. Chem. Soc.* **2009**, *131*, 442–443.

[30] J. Kubitschke, C. Näther, R. Herges, *Eur. J. Org. Chem.* **2010**, *26*, 5041–5055.

[31] S. Kuhn, U. Jung, S. Ulrich, R. Herges, O. Magnussen, *Chem. Commun.* **2011**, *47*, 8880–8882.

[32] T. Jasper-Tönnies, A. Garcia-Lekue, T. Frederiksen, S. Ulrich, R. Herges, R. Berndt, *Phys. Rev. Lett.* **2017**, *119*, 0066801.

[33] T. Jasper-Tönnies, I. Poltavsky, S. Ulrich, T. Moje, A. Tkatchenko, R. Herges, R. Berndt, *J. Chem. Phys.* **2018**, *149*, 244705.

[34] S. Lemke, S. Ulrich, F. Claußen, A. Bloedorn, U. Jung, R. Herges, O. M. Magnussen, *Surf. Sci.* **2015**, *632*, 71–76.

[35] S. Kuhn, B. Baisch, U. Jung, T. Johannsen, J. Kubitschke, R. Herges, O. Magnussen, *Phys. Chem. Chem. Phys.* **2010**, *12*, 4481–4487.

[36] M. Hammerich, R. Herges, *J. Org. Chem.* **2015**, *80*, 11233–11236.

[37] F. L. Otte, S. Lemke, C. Schütt, N. R. Krekiehn, U. Jung, O. M. Magnussen, R. Herges, *J. Am. Chem. Soc.* **2014**, *136*, 11248–11251.

[38] N. Hauptmann, L. Groß, K. Buchmann, K. Scheil, C. Schütt, F. L. Otto, R. Herges, C. Herrmann, R. Berndt, *New J. Phys.* **2015**, *17*, 1–8.

[39] T. Tellkamp, J. Shen, Y. Okamoto, R. Herges, *Eur. J. Org. Chem.* **2014**, 5456–5461.

[40] M. Hammerich, T. Rusch, N. R. Krekiehn, A. Bloedorn, O. M. Magnussen, R. Herges, *ChemPhysChem* **2016**, *17*, 1870–1874.

[41] A. Schlimm, N. Stucke, B. M. Flöser, T. Rusch, J. Krahmer, C. Näther, T. Strunskus, O. M. Magnussen, F. Tuczek, *Chem. Eur. J.* **2018**, *24*, 10732–10744.

[42] Z. Wei, X. Wang, A. Borges, M. Santella, T. Li, J. K. Sørensen, M. Vanin, W. Hu, Y. Liu, J. Ulstrup, G. C. Solomon, Q. Chi, T. Bjørnholm, K. Nørgaard, B. W. Laursen, *Langmuir* **2014**, *30*, 14868–14876.

[43] T. R. Rusch, A. Schlimm, N. R. Krekiehn, B. M. Flöser, F. Röhricht, M. Hammerich, I. Lautenschläger, T. Strunskus, R. Herges, F. Tuczek, O. M. Magnussen, *J. Phys. Chem. C* **2019**, *123*, 13720–13730.

[44] U. Jung, S. Kuhn, U. Cornelissen, F. Tuczek, T. Strunskus, V. Zaporojtchenko, J. Kubitschke, R. Herges, O. Magnussen, *Langmuir* **2011**, *27*, 5899–5908.

[45] S. Ulrich, U. Jung, T. Strunskus, C. Schütt, A. Bloedorn, S. Lemke, E. Ludwig, L. Kipp, F. Faupel, O. Magnussen, R. Herges, *Phys. Chem. Chem. Phys.* **2015**, *17*, 17053–17062.

[46] N. R. Krekiehn, M. Müller, U. Jung, S. Ulrich, R. Herges, O. M. Magnussen, *Langmuir* **2015**, *31*, 8362–8370.

[47] H. Jacob, S. Ulrich, U. Jung, S. Lemke, T. Rusch, C. Schütt, F. Petersen, T. Strunskus, O. Magnussen, R. Herges, F. Tuczek, *Phys. Chem. Chem. Phys.* **2014**, *16*, 22643–22650.

[48] U. Jung, C. Schütt, O. Filinova, J. Kubitschke, R. Herges, O. Magnussen, *J. Phys. Chem. C* **2012**, *116*, 25943–25948.

[49] J. Kubitschke, *Dissertation*, Christian-Albrechts-Universität zu Kiel, Kiel **2010**.

[50] S. Hagen, P. Kate, M. V. Peters, S. Hecht, M. Wolf, P. Tegeder, *Appl. Phys. A* **2008**, *93*, 253–260.

[51] M. Wolf, P. Tegeder, *Surf. Sci.* **2009**, *603*, 1506–1517.

[52] R. Meyer, C. Lemire, S. K. Shaikhutdinov, H.-J. Freund, *Gold Bull.* **2004**, *37*, 72–124.

[53] J. Schwank, *Gold Bull.* **1983**, *16*, 103–110.

[54] M. Haruta, N. Yamada, T. K. K. Iijima, *J. Catal.* **1989**, *115*, 301–309.

[55] T. Hayashi, K. Tanaka, M. Haruta, *J. Catal.* **1998**, *178*, 566–575.

[56] D. Andreeva, V. Idakiev, T. Tabakova, A. Andreev, R. Giovanoli, *Appl. Catal. A: General* **1996**, *134*, 275–283.

[57] A. Ueda, M. Haruta, *Gold Bull.* **1999**, *32*, 3–11.

[58] G. C. Bond, P. A. Sermon, G. Webb, D. A. Buchanan, P. B. Wells, *J. Chem. Soc., Chem. Commun.* **1973**, 444–445.

[59] G. J. Hutchings, *Catal. Today* **2002**, *72*, 11–17.

[60] T. Aida, R. Higuchi, H. Niiyama, *Chem. Lett.* **1990**, 2247–2250.

[61] H. Sakurai, M. Haruta, *Catal. Today* **1996**, *29*, 361–365.

[62] D. A. Outka, R. J. Madix, *Surf. Sci.* **1987**, *179*, 351–360.

[63] J. M. Gottfried, K. J. Schmidt, S. L. M. Schroeder, K. Christmann, *Surf. Sci.* **2003**, *525*, 197–206.

[64] D. A. Outka, R. J. Madix, *Surf. Sci.* **1987**, *179*, 361–376.

[65] A. M. Paul, B. E. Bent, *J. Catal.* **1994**, *147*, 264–271.

[66] A. Paul, M. X. Yang, B. E. Bent, *Surf. Sci.* **1993**, *297*, 327–344.

[67] M. X. Yang, S. K. Jo, A. Paul, L. Avila, B. E. Bent, K. Nishikida, *Surf. Sci.* **1995**, *325*, 102–120.

[68] D. Syomin, B. E. Koel, *Surf. Sci.* **2001**, *490*, 265–273.

[69] D. F. Shriver, P. W. Atkins, C. H. Langford, *Anorganische Chemie*, Bd. 2, Wiley-VCH, Weinheim **1997**.

[70] B. Binnig, C. F. Quate, C. Gerber, *Phys. Rev. Lett.* **1986**, *56*, 930.

[71] F. J. Giessibl, *Science* **1995**, *267*, 68–71.

[72] G. Meyer, N. M. Amer, *Appl. Phys. Lett.* **1990**, *56*, 2100–2101.

[73] M. Fleischmann, P. J. Hendra, A. J. McQuillan, *Chem. Phys. Lett.* **1974**, *26*, 163–166.

[74] D. L. Jeanmaire, R. P. van Duyne, *J. Electroanal. Chem.* **1977**, *84*, 1–20.

[75] H. Kwart, T. J. George, *J. Am. Chem. Soc.* **1977**, *99*, 5214–5215.

[76] J. Stöhr, D. A. Outka, *Phys. Rev. B* **1987**, *36*, 7891–7905.

[77] G. Hähner, *Chem. Soc. Rev.* **2006**, *35*, 1244–1255.

[78] J. Haase, *Chem. unserer Zeit* **1992**, *26*, 219–231.

[79] G. Binnig, H. Rohrer, *Physica B+C* **1984**, *127*, 37–45.

[80] G. Binnig, H. Rohrer, C. Gerber, E. Weibel, *Phys. Rev. Lett.* **1982**, *49*, 57–61.

[81] F. Besenbacher, *Prog. Phys.* **1996**, *59*, 1737.

[82] T. R. Rusch, M. Hammerich, R. Herges, O. M. Magnussen, *Chem. Commun.* **2019**, *55*, 9511–9514.

[83] S. Kano, T. Tada, Y. Majima, *Chem. Soc. Rev.* **2015**, *44*, 970–987.

[84] R. G. Greenler, *J. Chem. Phys.* **1966**, *44*, 310.

[85] R. F. Baddour, M. Modell, R. L. Goldsmith, *J. Phys. Chem.* **1970**, *74*, 1787–1796.

[86] F. M. Hoffmann, *Surf. Sci. Rep.* **1983**, *3*, 109–192.

[87] P. Hollins, *Infrared Reflection-Absorption Spectroscopy*, John Wiley & Sons **2000**.

[88] T. Buffeteau, B. Desbat, J. M. Turlet, *Appl. Spectrosc.* **1991**, *45*, 380–389.

[89] R. Aroca, *Surface-Enhanced Vibrational Spectroscopy*, 65, John Wiley & Sons **2006**.

[90] P. R. Griffiths, J. A. D. Haseth, J. D. Winefordner, *Fourier Transform Infrared Spectrometry*, Bd. 2, Wiley & Sons **2007**.

[91] W. G. Golden, D. S. Dunn, J. Overend, *J. Catal.* **1981**, *71*, 395–404.

[92] A. E. Dowrey, C. Marcott, *Appl. Spectrosc.* **1982**, *36*, 414–416.

[93] T. Buffeteau, B. Desbat, J.-M. Turlet, *Microchim. Acta* **1988**, *95*, 23–26.

[94] W. G. Golden, K. Kunimatsu, H. Seki, *J. Phys. Chem.* **1984**, *88*, 1275–1277.

[95] A. H. Kycia, K. Koczkur, J. J. Leitch, J. Lipkowski, V. Zamlynny, M. W. P. Petryk, *Anal. Bioanal. Chem.* **2013**, *405*, 1537–1546.

[96] H. A. Pearce, N. Sheppard, *Surf. Sci.* **1976**, *59*, 205–217.

[97] P. Tegeder, *J. Phys.: Condens. Matter* **2012**, *24*, 394001.

[98] P. Hollins, J. Pritchard, *Prog. Surf. Sci.* **1985**, *19*, 275–349.

[99] A. Mishchenko, L. A. Zotti, D. Vonlanthen, M. Bürkle, F. Pauly, J. C. Cuevas, M. Mayor, T. Wandlowski, *J. Am. Chem. Soc.* **2011**, *133*, 184–187.

[100] A. Mishchenko, D. Vonlanthen, V. Meded, M. Bürkle, C. Li, I. V. Pobelov, A. Bagrets, J. K. Viljas, F. Pauly, F. Evers, M. Mayor, T. Wandlowski, *Nano Lett.* **2010**, *10*, 156–163.

[101] D. Bléger, J. Dokić, M. V. Peters, L. Grubert, P. Saalfrank, S. Hecht, *J. Phys. Chem. B* **2011**, *115*, 9930–9940.

[102] J. N. Harvey, *Phys. Chem. Chem. Phys.* **2007**, *9*, 331–343.

[103] M. Aschi, J. N. Harvey, C. A. Schalley, D. Schröder, H. Schwarz, *Chem. Commun.* **1998**, 531–533.

[104] J. N. Harvey, *Faraday Discuss.* **2004**, *127*, 165–177.

[105] J. M. L. Martin, P. R. Taylor, *Chem. Phys. Lett.* **1993**, *209*, 143–150.

[106] Q. Cui, K. Morokuma, *Theor. Chem. Acc.* **1999**, *102*, 127–133.

[107] P. T. Snee, C. K. Payne, S. D. Mebane, K. T. Kotz, C. B. Harris, *J. Am. Chem. Soc.* **2001**, *123*, 6909–6915.

[108] T. A. Seder, A. J. Ouderkirk, E. Weitz, *J. Chem. Phys.* **1986**, *85*, 1977–1986.

[109] A. Hauser, *J. Chem. Phys.* **1991**, *94*, 2741–2748.

[110] A. Hauser, *Coord. Chem. Rev.* **1991**, *111*, 275–290.

[111] Y. Hirshberg, E. Fischer, *J. Chem. Soc.* **1954**, *297*, 3129–3137.

[112] A. Tork, F. Boudreault, M. Roberge, A. M. Ritcey, R. A. Lessard, T. V. Galstian, *Appl. Opt.* **2001**, *40*, 1180–1186.

[113] Y. Hirshberg, *J. Am. Chem. Soc.* **1956**, *78*, 2304–2312.

[114] T. Bercovici, E. Fischer, *J. Am. Chem. Soc.* **1964**, *86*, 5687–5688.

[115] N. W. Tyer, R. S. Becker, *J. Am. Chem. Soc.* **1970**, *92*, 1289–1302.

[116] J. B. Flannery, *J. Am. Chem. Soc.* **1968**, *90*, 5660–5671.

[117] H. Bach, J. G. Calvert, *J. Am. Chem. Soc.* **1970**, *92*, 2608–2614.

[118] J. T. C. Wojtyk, A. Wasey, P. M. Kazmaier, S. Hoz, E. Buncel, *J. Phys. Chem. A* **2000**, *104*, 9046–9055.

[119] H. Dürr, H. Bouas-Laurent, Hg., *Photochromism Molecules and Systems*, Bd. 40, Elsevier, New York **1990**.

[120] D. H. Waldeck, *Chem. Rev.* **1991**, *91*, 415–436.

[121] J. L. Magee, W. Shand, Jr., H. Eyring, *J. Am. Chem. Soc.* **1941**, *63*, 677–688.

[122] M. C. Lin, K. J. Laidler, *Can. J. Chem.* **1967**, *46*, 973–978.

[123] W. M. Horspool, *CRC Handbook of Organic Photochemistry and Photobiology*, Bd. 2, CRC Press, Boca Rota, London, New York, Wahsington DC **1994**.

[124] J. Saltiel, A. Marinari, D. W.-L. Chang, J. C. Mitchener, E. D. Megarity, *J. Am. Chem. Soc.* **1979**, *101*, 2982–2996.

[125] J. Saltiel, J. L. Charlton, *Rearrangements in Ground and Excited States*, Bd. 42.3, Academic Press, New York **1980**.

[126] F. W. J. Taylor, A. R. Murray, *J. Am. Chem. Soc.* **1938**, *60*, 2078–2086.

[127] A. V. Santoro, E. J. Barrett, H. H. Hoyer, *J. Am. Chem. Soc.* **1967**, *89*, 4545.

[128] G. B. Kistiakowsky, W. R. Smith, *J. Am. Chem. Soc.* **1934**, *56*, 638–642.

[129] M. Irie, M. Mohri, *J. Org. Chem.* **1988**, *53*, 803–808.

[130] M. Irie, K. Sayo, *J. Phys. Chem.* **1992**, *96*, 7671–7674.

[131] H.-G. Cho, B.-S. Cheong, *Bull. Korean Chem. Soc.* **1998**, *19*, 308–313.

[132] M. Irie, T. Lifka, S. Kobatake, N. Kato, *J. Am. Chem. Soc.* **2000**, *122*, 4871–4876.

[133] S. Nakamura, M. Irie, *J. Org. Chem.* **1988**, *53*, 6136–6138.

[134] S. L. Gilat, S. H. Kawai, J.-M. Lehn, *Chem. Eur. J.* **1995**, *1*, 275–284.

[135] S. Kobatake, K. Uchida, E. Tsuchida, M. Irie, *Chem. Lett.* **2000**, *29*, 1340–1341.

[136] S. J. Cristol, J. E. Leffler, *J. Am. Chem. Soc.* **1954**, *76*, 4468–4469.

[137] W. G. Dauben, R. L. Cargill, *Tetrahedron* **1961**, *15*, 197–201.

[138] G. S. Hammond, P. Wyatt, C. D. DeBoer, N. J. Turro, *J. Am. Chem. Soc.* **1964**, *86*, 3110.

[139] H. Ikezawa, C. Kutal, K. Yasufuku, H. Yamazaki, *J. Am. Chem. Soc.* **1986**, *108*, 1589–1594.

[140] K. Raghavachari, R. C. Haddon, H. D. Roth, *J. Am. Chem. Soc.* **1983**, *105*, 3110–3114.

[141] K. Maruyama, K. Terada, Y. Yamamoto, *J. Org. Chem.* **1981**, *46*, 5294–5300.

[142] Z.-I. Yoshida, *J. Photochem.* **1985**, *29*, 27–40.

[143] K. Hirao, A. Ando, T. Hamada, O. Yonemitsu, *J. Chem. Soc., Chem. Commun.* **1984**, 300–302.

[144] N. J. Turro, W. R. Cherry, M. F. Mirbach, M. J. Mirbach, *J. Am. Chem. Soc.* **1977**, *99*, 7388–7390.

[145] R. Herges, F. Starck, T. Winkler, M. Schmittel, *Chem. Eur. J.* **1999**, *5*, 2965–2970.

[146] K. Maruyama, H. Tamiaki, *Chem. Lett.* **1987**, *16*, 683–686.

[147] K. Maruyama, H. Tamiaki, T. Yanai, *Bull. Chem. Soc. Jpn.* **1985**, *58*, 781–782.

[148] H. Hogeveen, B. J. Nusse, *Tetrahedron Lett.* **1974**, *15*, 159–162.

[149] H. Nishino, S. Toki, S. Takamuku, *J. Am. Chem. Soc.* **1986**, *108*, 5030–5032.

[150] K. Nakabayashi, H. Nishino, S. Toki, S. Takamuku, *Radiat. Phys. Chem.* **1989**, *34*, 809–815.

[151] G. J. II, S.-H. Chiang, P. T. Xuan, *J. Photochem.* **1979**, *10*, 1–18.

[152] H.-D. Scharf, J. Fleischhauer, H. Leismann, I. Ressler, W. Schleker, R. Weitz, *Angew. Chem. Int. Ed.* **1979**, *18*, 652–662.

[153] E. Mitscherlich, *Ann. Pharm.* **1834**, *12*, 311–314.

[154] G. S. Hartley, *Nature* **1937**, *140*, 281–282.

[155] T. Schultz, J. Quenneville, B. Levine, A. Toniolo, T. J. Martínez, S. Lochbrunner, M. Schmitt, J. P. Shaffer, M. Z. Zgierski, A. Stolow, *J. Am. Chem. Soc.* **2003**, *125*, 8098–8099.

[156] T. Sueyoshi, N. Nishimura, S. Yamamoto, S. Hasegawa, *Chem. Lett.* **1974**, *3*, 1131–1134.

[157] T. Ishikawa, T. Noro, T. Shoda, *J. Chem. Phys.* **2001**, *115*, 7503–7512.

[158] P. Cattaneo, M. Persico, *Phys. Chem. Chem. Phys.* **1999**, *1*, 4739–4743.

[159] H. Rau, E. Lüddecke, *J. Am. Chem. Soc.* **1982**, *104*, 1616–1620.

[160] S. Loudwig, H. Bayley, *J. Am. Chem. Soc.* **2006**, *128*, 12404–12405.

[161] A. Cembran, F. Bernardi, M. Garavelli, L. Gagliardi, G. Orlandi, *J. Am. Chem. Soc.* **2004**, *126*, 3234–3243.

[162] E. Miller, Hg., *Neuere Anschauungen der organischen Chemie*, Springer-Verlag **1957**.

[163] J. Halpern, G. W. Brady, C. A. Winkler, *Can. J. Res., Sect. B* **1950**, *28*, 140.

[164] R. J. W. L. Fevre, J. Northcott, *J. Chem. Soc.* **1953**, 867–870.

[165] G. S. Hartley, *J. Chem. Soc.* **1938**, *0*, 633–642.

[166] M. Tsuda, K. Kuratani, *Bull. Chem. Soc. Japan* **1964**, *37*, 1284–1288.

[167] S. Ljunggren, G. Wettermark, *Acta. Chem. Scand.* **1971**, *25*, 1599–1606.

[168] G. C. Hampson, J. M. Robertson, *J. Chem. Soc.* **1941**, 409.

[169] H. Duval, *Bull. Soc. Chim. Fr.* **1910**, *7*, 727–732.

[170] R. Sievertsen, H. Neumann, B. Buchheim-Stehn, R. Herges, C. Näther, F. Renth, F. Temps, *J. Am. Chem. Soc.* **2009**, *131*, 15594–15595.

[171] N. O. Carstensen, *Phys. Chem. Chem. Phys.* **2013**, *15*, 15017–15026.

[172] H. Rau, *J. Photochem.* **1984**, *26*, 221–225.

[173] F. Gerson, E. Heilbronner, A. van Veen, B. M. Wepster, *Helv. Chim. Acta* **1960**, *43*, 1889–1898.

[174] A. Schlimm, R. Löw, T. Rusch, F. Röhricht, T. Strunskus, T. Tellkamp, F. Sönnichsen, U. Manthe, O. Magnussen, F. Tuczek, R. Herges, *Angew. Chem. Int. Ed.* **2019**, *58*, 6574–6578.

[175] R. B. Woodward, R. Hoffmann, *Angew. Chem. Int. Ed.*. **1969**, *8*, 781–853.

[176] F. Bernardi, M. Olivucci, M. A. Robb, *Acc. Chem. Res.* **1990**, *23*, 405–412.

[177] N. J. Turro, V. Ramamurthy, J. C. Scaiano, Hg., *Modern Molecular Photochemistry of Organic Molecules* **2010**.

[178] U. Bauer, S. Mohr, T. Döpper, P. Bachmann, F. Späth, F. Düll, M. Schwarz, O. Brummel, L. Fromm, U. Pinkert, A. Görling, A. Hirsch, J. Bachmann, H.-P. Steinrück, J. Libuda, C. Papp, *Chem. Eur. J.* **2017**, *23*, 1613–1622.

[179] U. Bauer, L. Fromm, C. Weiß, P. Bachmann, F. Späth, F. Düll, J. Steinhauer, W. Hieringer, A. Görling, A. Hirsch, H.-P. Steinrück, , C. Papp, *J. Phys. Chem. C* **2019**, *123*, 7654–7664.

[180] S. Yasuda, T. Nakamura, M. Matsumoto, H. Shigekawa, *J. Am. Chem. Soc.* **2003**, *125*, 16430–16433.

[181] B. W. Laursen, F. C. Krebs, *Chem. Eur. J.* **2001**, *7*, 1773–1783.

[182] F. Röhricht, aktuelle Arbeiten **2019**, Christian-Albrechts-Universität zu Kiel.

[183] J. Vicario, A. Meetsma, B. L. Feringa, *Chem. Commun.* **2005**, 5910–5912.